AGARD-CP-221

AGARD

ADVISORY GROUP FOR AEROSPACE RESEARCH & DEVELOPMENT

7 RUE ANCELLE 92200 NEUILLY SUR SEINE FRANCE

AGARD CONFERENCE PROCEEDINGS No. 221

on

Fracture Mechanics Design Methodology

NORTH ATLANTIC TREATY ORGANIZATION

DISTRIBUTION AND AVAILABILITY
ON BACK COVER

DISCLAIMER NOTICE

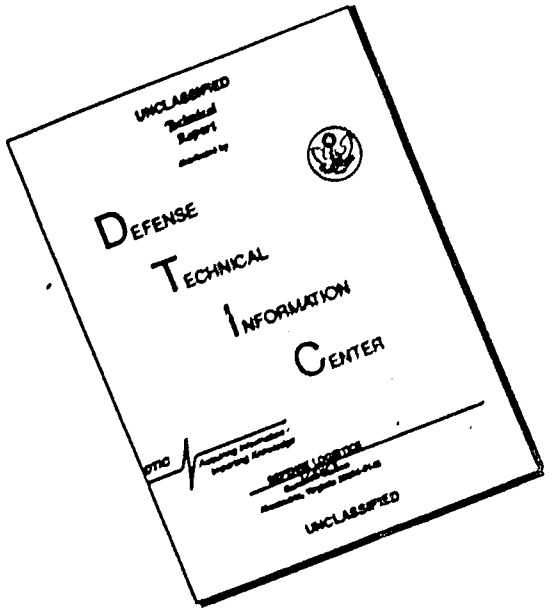

THIS DOCUMENT IS BEST QUALITY AVAILABLE. THE COPY FURNISHED TO DTIC CONTAINED A SIGNIFICANT NUMBER OF PAGES WHICH DO NOT REPRODUCE LEGIBLY.

NORTH ATLANTIC TREATY ORGANIZATION

ADVISORY GROUP FOR AEROSPACE RESEARCH AND DEVELOPMENT

(ORGANISATION DU TRAITE DE L'ATLANTIQUE NORD)

AGARD Conference Proceedings No.221

FRACTURE MECHANICS DESIGN METHODOLOGY

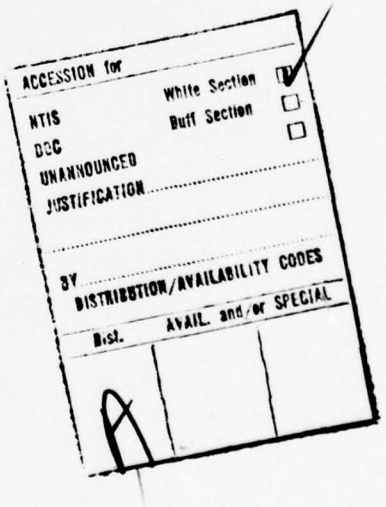

Papers and other contributions presented at the 43rd Meeting of the AGARD Structures and Materials Panel held in London, UK on 28–29 September 1976.

THE MISSION OF AGARD

The mission of AGARD is to bring together the leading personalities of the NATO nations in the fields of science and technology relating to aerospace for the following purposes:

- Exchanging of scientific and technical information;
- Continuously stimulating advances in the aerospace sciences relevant to strengthening the common defence posture;
- Improving the co-operation among member nations in aerospace research and development;
- Providing scientific and technical advice and assistance to the North Atlantic Military Committee in the field of aerospace research and development;
- Rendering scientific and technical assistance, as requested, to other NATO bodies and to member nations in connection with research and development problems in the aerospace field;
- Providing assistance to member nations for the purpose of increasing their scientific and technical potential;
- Recommending effective ways for the member nations to use their research and development capabilities for the common benefit of the NATO community.

The highest authority within AGARD is the National Delegates Board consisting of officially appointed senior representatives from each member nation. The mission of AGARD is carried out through the Panels which are composed of experts appointed by the National Delegates, the Consultant and Exchange Program and the Aerospace Applications Studies Program. The results of AGARD work are reported to the member nations and the NATO Authorities through the AGARD series of publications of which this is one.

Participation in AGARD activities is by invitation only and is normally limited to citizens of the NATO nations.

Published February 1977

ISBN 92-835-1090-X

Printed by Technical Editing and Reproduction Ltd
Harford House, 7–9 Charlotte St, London, W1P 1HD

PREFACE

In recent years Fracture Mechanics has become an important and necessary tool for the aircraft designer in his endeavour for more durable aircraft structures. In addition to his job of meeting the usual requirements for static strength, stiffness, structural stability and fatigue resistance he now has to account for the presence of cracks or similar defects. Therefore crack propagation and residual strength of cracked structure have to be investigated by analysis and testing. Safe and economic operation of aircraft depend heavily on the designer's ability to design and demonstrate a damage tolerant and durable structure.

The Structures and Materials Panel has realized this many years ago and initiated projects in fatigue damage accumulation and related fields such as stress corrosion cracking, non-destructive inspection, fractography and other materials topics. In 1969 a Working Group on Fracture Mechanics was created. This work culminated in AGARDograph No.176 "Fracture Mechanics in Aircraft Structures" which gives a detailed survey of the principal tools available to the engineer and designer: analytical tools, testing methods and materials data.

Following this publication the panel decided to continue its activities with a focus on Fracture Mechanics Design Methodology. In spite of the large amount of literature existing on the subject and the various methods described, the varied and complicated processes involved in fracture mechanics of aircraft materials permit today only approximate analytical treatment. Consequently in practical application to aircraft design the agreement between analytical results and experiment is still unsatisfactory in many cases. Therefore testing will play an important role for many years to come. On the other hand it is important to increase the number of available analytical solutions for the numerous practical problems in structural elements such as in lugs, integral structures or the problems of skin stringer interactions in built-up structures.

It is important now to synthesize the present information and to highlight the important aspects between both analysis and testing, so that an appropriate design methodology will continue to evolve.

The panel felt that it could assist the evolution of a Fracture Mechanics Design Methodology by compiling and selecting typical examples of the application of fracture mechanics to the design of aircraft. This specialists meeting was set up to get a comprehensive survey of available examples. The following areas were addressed:

- practical applications of fracture mechanics in the design of new aircraft
- durability and damage tolerance assessment in aircraft in service
- design methodology for built-up sheet structures
- selection of aircraft structural materials using fracture mechanics
- special problems (with forgings; lugs; manufactory influences etc.) .

In prepared discussions a critical review of each paper was given.

The conference results present an important step towards the final goal of this AGARD project to prepare a design guide indicating various approaches in Fracture Mechanics Design Methodology by giving practical examples of analysis and testing.

The panel wishes to express its gratitude to all the groups and individuals who contributed to the success of the specialists meeting; to the UK National Delegation who hosted the meeting; to the authors, discussors and session chairmen and to Dean Harold Liebowitz, the technical coordinator who took the main burden of organizing this meeting into a coherent whole and editing the discussion. Finally our thanks go to our Panel Executive, Mr John Willis, for his excellent assistance in organizing the meeting and preparing these proceedings.

T.GAYMANN
Chairman, Fracture Mechanics
Design Methodology Working Group
AGARD Structures and Materials Panel
Ottobrunn, Germany
November 1976

CONTENTS

SUMMARY

Highlights

The papers at the Conference on Fracture Mechanics Design Methodology were chiefly concerned with the application of fracture mechanics to the design of aircraft. Many of the papers dealt with analyses for obtaining safe-life and fail-safe aircraft structures. For structures containing cracks, it was necessary to determine the appropriate steps to avoid catastrophic failure of a primary component. Design concepts were highlighted in achieving a damage-tolerant structure. Certainly, load spectra drew attention because of its importance on life expectancy. There was a consensus that fracture mechanics analyses and testing were important tools in designing aircraft and in assessing damage tolerance.

To consider real life situations, two papers, making extensive use of fracture mechanics were presented which dealt with specific aircraft such as F-111 and F-5E/F. In both cases, the use was after the fact, to characterize the damage tolerance of the previous designs. Both designs later dealt considerably in complying with USAF Military Standards 1530 and Military Specifications A83344. In the past, fatigue tests have been believed to tell us everything about crack initiation, crack propagation and residual strength. Certainly, this belief has been shattered particularly as pointed out in the F-111 paper.

Fatigue test specimens were used to complete tests of four life-times and were assumed to be typical of the rest of the fleet, as is assumed in all fatigue test specimens. And yet, a unique flaw slipped through the nondestructive inspection, during production, and a catastrophic failure occurred. Perhaps, as Mr. Heath suggested, the answer to how we deal with the initial flaw problem lies in Mr. Murname's paper, where the full-scale fatigue test was supported by a fatigue analysis using both the cumulative damage hypothesis and the residual-strength method based on fracture mechanics. As the test progressed, damage tolerance analysis was conducted on each area shown to be critical, and in this way, damage tolerance analysis provided the basis for defining inspection methods in service, assuming a structure with initial flaws.

A particular approach suggested by Mr. Murname on future aircraft would be to achieve as good a job as one can in obtaining a realistic spectrum, including proper balance loads in the airplane, and then running a real good flight-by-flight fatigue test. Then after the test is completed, perform a very extensive tear-down inspection to find the actual quality one has.

There was a concern when introducing flaws into components for testing as to the appropriate size of the component. For the F-111, the size referred to by Mr. Buntin would be a specimen large enough, such as the center fuselage with a good part of the wing on either side. General Dynamics Corporation had three components like this in addition to the full-scale fatigue test of the F-111. It was felt that the component has to be big enough such that the boundary conditions for the area were being simulated.

Significant progress had been made in predicting crack-propagation rates in panels subjected to a fatigue environment. Two methods, one termed the stress concentration factor and the other the lap-joint approach, utilize a mixture of theory and experiment, stress-intensity computations, appropriate SN curves, combined with Miner's rule in attempting to provide insight into this complex problem. The primary difference between the two methods is that the stress concentration approach utilizes the maximum stress as a precursor to crack initiation at the rivet-hole of the stiffener of a cracked panel, whereas the lap-joint method presumes an analogy between the fatigue behaviour in the stringer and a dry riveted lap-joint. A statistical treatment of both methods was also accomplished. Also included in Professor Salvetti's paper was a brief address aimed at minimum weight-design methodologies for fail-safe structures.

Stretching has a strong beneficial effect on crack-propagation rate, but a small detrimental effect on facture toughness. The bending cycle has a small detrimental effect on crack propagation rates and no effect on the fracture toughness, whereas a combination of the stretching and the bending cycle has a reduced positive effect on the crack propagation rate and virtually no effect on fracture toughness, although it is a bit detrimental to it. There was a feeling that the 10% pre-stretch was perhaps too high and a lower pre-stretch should be used; the optimum process suggested was a pre-stretch of 6% and a post-stretch of 3%.

In determining crack propagation, inclusion of retardation models could lead to results on the unsafe side. Investigations were performed using very different load specifications, for example, including fighter and transport load specifications as well as those in very different mean stresses. Mathematical tools are available to optimize designs for crack propagation and for damage-tolerance, whether bonded or riveted stringers are used. Evidence exists that crack growth under flight service loading may be predicted consistently within reasonable factors.

Test results on stiffened panels show that there may be considerable scatter in crack growth. Inspection programs based on crack growth analyses can save considerable cost.

Sentiment was expressed that proof loading is a sound procedure. However, questions were posed such as: On how high a value should the proof load be, compared with the statistically known service loads? How long should the proof load be maintained? What will the effect of the proof load be on the subsequent fatigue life? And how large a crack can still be present after the proof load, considering the scatter in fracture toughness? It was felt that the one or a few

locations of main interest should be identified and then one should apply the proof load philosophy to only these locations. Consideration needs to be given to tests on other alloys, different designs, different stress levels, cyclic rate of stressing, and environmental effects.

There was a question posed whether by using flight-simulation testing there was less effect of corrosion than in a constant amplitude test. Several explanations were offered. There was a plea for the designer to know the properties of the material used and not rely only on the figures contained in a handbook as there is more to a material than just the figures quoted in the text. Also, materials chosen for aircraft, where fracture mechanics is employed in the design, must have crack growth characteristics which preclude reaching critical flaw size in less than one lifetime. Materials which are selected for use should be screened for toughness, weight, and strength.

Computer programs are available for evaluating stress intensity factors of corner cracks growing from the hole. When cracking occurs at a fastener hole or out of a lug, cracking will usually occur on both sides of the hole. In the USAF damage-tolerance specifications for slow crack growth, the assumption is made that there is only a single worse initial flaw of the 0.05 in. type defect. Some experience has shown that this may not be all that conservative. In reality the USAF does not assume only a single initial flaw; within the damage-tolerance specification requirement for continuing damage it is stated that a single worse flaw grows out to a free edge, but it must immediately be assumed that there is a flaw on the other side of the hole, grown inboard. It is expected that the next revision of the damage-tolerance specifications will include a Δ growth of the very small defect that might have existed in the diametrically opposite side of the hole that would have occurred up to the point when the big flaw grew out to the free edge.

Large amounts of scatter was experienced in determining the fracture toughness of steel forgings. Test results varied by as much as a factor of 5 for specimens taken from the same prototype landing gear. Consequently, a full scale fatigue test would give unsafe life data if, as is usual, only one or two test specimens are used. NLR's tests on forgings showed that scatter was much higher for maneuver load spectrums than gust load. General Dynamics found faster propagation rates in forged aluminium alloys than unforged specimens; life expectancy in forged specimens was less.

There was some sentiment expressed that fail-safe and damage tolerance were largely equivalent and that the subdivision into three different types of structures, as in MIL-A83444, like crack growth structure, multiple load path structure, and crack arrest structure, is basically sound. Prediction of the static strength of an aircraft part, wing or whole airplane, is not less than 10%. Consequently, this amount may act as a guide in striving for a number in designing for damage tolerance.

The problems concerning the use of fracture mechanics were identified by Macchi. One of the reasons for going to a fail-safe approach from safe-life is the extreme variation in the service loading between different operations to the extent that some of the load spectra varied with a factor of 20 to 1. The inspection periods which are necessary to establish fail-safe conditions for the aircraft will also be so comparatively short, since the inspection period obviously goes with the rate of propagation; and obviously the rates of propagation must be very much higher on these aircraft which are subject to the various severe spectra.

Work on stiffened panels indicates encouraging progress in including the configuration details of typical stringer wing-panels, using closed form solutions. We are now in a stage that damage tolerance is a very useful tool and can be used in the design stage. There was some concern expressed, however, of applications of fracture mechanics to civil airplanes where more ductile fracturing may be predominant. Interest was expressed in how the new fracture criteria should be applied to existing service aircraft. Certainly the airplanes are not going to be redesigned. Basically there is an effort to define the critical areas of the airframe, determine inspection requirements for these areas to maintain safety of the airplane, and define or predict the modification requirements to determine the monetary obligations for these airplanes in the future. A decision would have to be made to retire and replace or keep them in service. Lastly effort should be made to update the tracking programs of these aircraft.

Future Efforts

Work which has been proposed for the future included some of the following: effects of curvature in pressure cabin design; methods of predicting approach to crack instability in residual strength tests; variability in crack propagation rates and associated scatter factors; standard solutions for stress intensity factor prediction relating to pin-loaded holes, feather-edge holes, interference fit-pins, and others; fastener flexibility effects on stiffened panels; prediction of stress intensity factors in nonuniform stress fields requiring attention of cracks extending both in wing spar web, and in wing-skin, simultaneously; materials data, particularly on K_c and on crack propagation rates; improved models for estimating crack growth retardation effect and methods of obtaining simplified stress intensity factors; effects of the onset of yielding which are likely to occur before failure of a multi-element structure. There is a lack of published test data on the failure of real aircraft wing structures containing cracks to help in developing new methods of analyses.

It was also pointed out that the designer needs such data as fracture toughness of typical components in structures under uniaxial and biaxial stresses; crack propagation under realistic flight-by-flight load sequences of such components and structures; stress intensity solutions for such components in structures with service-like crack shapes, for example, multiple cracks under riveted heads of a pressure cabin.

Further development is needed to: increase the accuracy of load analysis through the use of flight test measured loads for all major structural components and flight conditions; integrate these loads with current operating roles to predict accurate loads and stress spectra; obtain a final damage tolerant analyses of the critical areas to define the safety limits accurately; perform a program of individual aircraft tracking and fleet monitoring to determine the economic life and safety limits for each aircraft.

Further work is also needed to achieve methodologies to compute the crack growth in stiffened structures; and for the further development of design methodologies for minimum-weight fail-safe structures.

There have been requests for the application of fracture mechanics to various types of forgings. Large amounts of scatter was experienced by IABG in steel forgings. General Dynamics Corporation found faster propagation rates in forged aluminium alloys than unforged specimens. There is an interest in performing fracture mechanics tests on different forgings made of alloys subjected to various heat treatments. An experimental approach is advocated for future research in studying crack growth behaviour in lugs. There is some concern about not applying Mode II to the Mode I failure for the analysis of corner crack growth in lugs.

There is a lack of published data on the failure of real aircraft wing structures containing cracks to help in developing new methods of analyses; the effect of curvature on crack propagation should be assessed; there is a need to predict whether a crack is going to pass between rivets or turn and go into one of them, bonded stiffeners appear to be better than riveted ones but the validity for widely spaced stiffeners should be determined; the optimum properties for adhesives in bonded joints should be determined; while statistical analysis of the data on stringer fatigue endurance and its correlation with crack-length in the sheet cover can be confidently predicted, the stress concentration approach needs to be further developed; the analytical correction factor methods presently available, are inadequate to represent realistic cracks in fuselage structures. The absence of an analytically based design procedure and the consequent limits in the basic understanding of fracture mechanics of pressure cabins limits the efficiency of the damage-tolerance design process; in utilizing COD methods, there are problems in interpreting readings from real complex structures in relation to control data from test specimens; also, there is more difficulty in applying the COD approach to determine critical crack growth on military airplanes than on Trident; in simplified testing of pressure-cabin structure, which will give more severe results, there has been an omission of hoop loading and mechanical application of both pressure-induced and thermal-induced longitudinal stresses; fracture mechanics analysis of built-up structures has great versatility for parametric studies at the design stage, but it may be a bit limited in the case of heavy skin-stringer combinations as used in wing structures, where stringer eccentricities may be very significant.

As copper-containing alloys are prone to be very sensitive to corrosion for materials in the condition between naturally and artificially aged in the bending heat-treatment cycle, corrosive studies are recommended.

Suggestions were made that other alloys should be investigated under pre-stretch and post-stretch conditions. Corrosion-fatigue tests should be performed as well as flight simulation tests. Also it was pointed out that realistic materials tests of maneuver-type loadings of fighter aircraft should be in terms of 2, 3, 6 cycles per minute rather than in cycles per second.

The objectives of this meeting were met in presenting examples of how fracture mechanics is used in the design of aircraft structures and their components. In addition to the practical examples being emphasized, gaps of knowledge required by the designer have been identified. The presentations and subsequent discussions should provide a significant contribution to the design manual on "Fracture Mechanics Design of Aircraft Structures" being prepared by AGARD.

Acknowledgements

The Technical Coordinator, Dean Harold Liebowitz, expresses his gratitude and appreciation to the following who gave so graciously of their time, advice, and expertise to this meeting: Dr. T.Gaymann, Chairman of the Fracture Mechanics Design Methodology Working Group; Mr. John Willis, Executive, Structures and Materials Panel; T.F.Kearns, Panel Chairman; M.F.Harpur, Deputy Panel Chairman; Dr. Brian P.Mullins, former Acting Chairman of Working Group; F.L.Ripley and G.C.Deutsch, Panel Members; authors, discussors, session chairmen and panelists; Members of Working Group; U.K. National Delegation who hosted this meeting; and Miss A.Guerillot, staff of Structures and Materials Panel. Without their invaluable assistance and participation, it would not have been possible to achieve the success experienced in this specialists meeting.

H.LIEBOWITZ
Technical Coordinator
Washington, D.C.
December 10, 1976

PRACTICAL APPLICATIONS OF FRACTURE MECHANICS TECHNIQUES TO AIRCRAFT STRUCTURAL PROBLEMS

W. G. Heath*

L. F. Nicholls**

W. T. Kirkby†

SUMMARY

The paper outlines some experience gained in the UK in the application of fracture mechanics techniques to problems arising in the design, testing and operation of aircraft. Design examples are taken from studies of crack behaviour in stiffened wing panels and also from pressure cabin design, including areas subject to combined mechanical and thermal stresses. Problems of testing are illustrated by reference to the use of COD, and other measurements, in residual strength tests to predict approach to unstable crack growth. Test data are given which illustrate scatter in crack growth in stiffened panels. The paper concludes with a discussion of the nature of the difficulties that have been encountered in applying fracture mechanics analysis to failures arising in aircraft in service.

1. INTRODUCTION

Fracture mechanics analysis has been used to an increasing extent in the United Kingdom over the past five years for the analysis of crack growth and residual strength problems which have arisen in the design, testing and operation of civil and military aircraft. The object of this paper is to give examples of the way in which fracture mechanics analysis has been used to assist in the solution of such problems and to indicate, where possible, the success that has attended such applications. From such considerations it becomes apparent where further development in analytical capability, and sounder knowledge of material behaviour, is desirable. Space does not permit a review of all applications of fracture mechanics which have taken place in recent years, but a selection of examples have been chosen which give a fair representation of the overall picture.

In the first part of the paper attention is directed to problems which have arisen in the design of aircraft structure and examples are taken from two radically different types of structure - firstly, stiffened wing panels for a large transport aircraft and, secondly, problems are discussed which relate to the design of pressure cabins, including consideration of behaviour under combined mechanically and thermally induced stresses. This part of the paper is followed by examples of applications of fracture mechanics which have arisen in the planning and analysis of structural test work related to the development and certification of structures. The examples chosen illustrate the use of fracture mechanics concepts to predict approach to critical crack growth in residual strength tests. This is followed by an example of the use of fracture mechanics analysis to evolve a simplified, but valid, representation of a combination of pressurisation, bending and thermal loading in a pressure cabin test. This section concludes with some observations on scatter in crack growth rate in nominally identical integrally machined panel specimens.

The final section of the paper discusses the analysis of some of the problems which have arisen when fatigue cracks have been detected in aircraft in service. A variety of problems are discussed, which have been chosen to highlight limitations in our current analytical capabilities or inadequacies in available knowledge of materials behaviour.

2. DESIGN PROBLEMS

2.1 Stiffened wing panels

2.1.1 General

Aircraft 'fail-safe' structures are designed to enable the aircraft to tolerate the presence of fatigue cracks or other similar damage and still have adequate strength until such damage is found during normal routine inspection of the structure. The period during which the damage has to be 'safe' ranges from just a single flight, when the damage is suddenly inflicted and immediately obvious, to possibly years of service when the initial damage is small or easy to overlook. Fracture mechanics is now a widely used method for estimating the residual strength of a cracked structure, and the time for a crack to propagate from a 'minimum detectable' length, to the maximum acceptable (or critical) length, from which the maximum safe inspection period is determined.

The fracture mechanics work on stiffened wing panels at HSA, Hatfield has been based mainly on the original work by C.C. Poe[1]. Poe presented the analytical solutions for the stress intensity at the crack tip (K) for a crack symmetrical about a stringer and symmetrical about a point mid-way between two stringers, in a panel stiffened by an infinite array of equally pitched stringers. In Poe's model each stringer is considered as another 'skin' attached to the skin at a single line of equally spaced locations, representing the stringer fasteners. To avoid problems of singularity, each attachment is a small circular

---

* Hawker Siddeley Aviation Ltd.

** British Aircraft Corporation Ltd.

† Royal Aircraft Establishment.

ring equal to the fastener diameter which does not deform, rather than a point. The fasteners are therefore assumed to be rigid in this model.

Various assumptions had to be made when applying this model to real structures. For example, when a 'mid-bay' crack is being considered but the stringers adjacent to the crack tips are unequal in size, the analysis is based on the smaller stringer area; or, if the stringer pitch is locally unequal too, the lower value of μ is used. The problem of a crack symmetrical under a failed stringer is treated by assuming that the effective bay width (b) is the sum of the bay widths on each side of the failed stringer; using the lower value of μ of the two adjacent (intact) stringers; and assuming that the stress in the skin is increased due to the load in the failed stringer carried by the skin between the two adjacent stringers.

More recently, note is being taken of Swift's work[2] which is based on a slightly different model. The stringer is considered as a simple prismatic bar, still attached to the skin at a single line of discrete equal spaced points. However, Swift has taken into account fastener flexibility, out-of-plane bending of the stringer, and bi-axial stresses. Inserting a realistic fastener stiffness instead of the rigid fastener into the analysis results in an increased value of K for a given crack length (i.e. a reduced estimate of the residual strength). The effect of out-of-plane bending on the value of K is not very marked for conventionally stiffened wing panels. The influence of bi-axial stresses is important in pressure cabin design; it is unlikely to be significant in wings, except perhaps in regions where an engine pylon joins the wing, for example.

2.1.2 Stringers with two rows of fasteners

Poe's solutions, in conjunction with the assumptions stated above, were used to predict the failing strength of the Trident test wing, for a series of 'fail-safe' tests in which several long artificial cracks were made in the lower skin panels. The intention was to load the wing finally until failure occurred.

The stringers in the Trident wing are of a closed 'top-hat' section i.e. attached to the skin by two closely spaced flanges. Nevertheless, this was still simulated in the analytical model by a single line attachment down the stringer centre-line. The stringers are also redux-bonded to the skin; a condition not catered for by Poe. As a skin crack propagates under a bonded stringer flange, local failure of the bonding would be expected to occur in the region of the crack tip. It follows that it is not right to assume that the equivalent fastener 'pitch' is zero for a bonded joint; in fact the equivalent pitch probably increases as the crack propagates and the local de-bonding spreads away from the crack. In the Trident estimates a fastener pitch : stringer pitch ratio (p/b) = 1/12 was used, this being the lowest value given in Ref.1.

However, the test results far exceeded expectations, which was the more surprising as no allowance had been made for out-of-plane bending of the stringer. The crack did extend (stable growth) under the stringer flange, so any error arising from using an inappropriate value of p/b was not considered to be significant.

The conclusion drawn was that to represent a 'top-hat' stringer as a stringer attached by a single line of fasteners led to an over-estimate of the value of K, particularly when the crack tip is near or under the stringer flange.

Both Cartwright (Southampton University) and Williams and Cash (HSA) have been working to obtain a satisfactory solution for K for the condition when stringers are attached to the skin by two lines of fasteners.

Cartwright has obtained the solution[3] for an arbitrary array of stringers perpendicular to the skin crack, symmetric about the line of the crack, and attached by a single line of fasteners. It is an easy step from this model to call up an array of stringers, at alternately close and wide pitch, to represent stringers attached by two lines of fasteners. The stringer area is divided into two equal 'sub-stringers' of half the area each, separated by the distance between the fastener lines in the stringer. The effect of out-of-plane bending of the stringer is still not included, but fastener flexibility can be allowed for. The effect of in-plane bending of the stringer could be significant in the '2-line' case, and this is being studied at the moment by considering the two extremes, (a) 'uncoupled' stringers, i.e. no interaction between one sub-stringer and the other, implying that the stringer has zero shear stiffness in the plane of the skin; (b) 'coupled' stringers, in which the fasteners in each *row* in the two sub-stringers are constrained to deflect the same amount perpendicular to the crack in the skin, implying that the stringer has infinite shear stiffness in the plane of the skin.

Williams and Cash have extended[4] Swift's work to include the effect of a stringer attached by two lines of fasteners. The difference between this model and that of Cartwright is that the stringer is still considered to be one element but loaded by two lines of fasteners.

As the skin deflects different amounts at each line of fasteners, the load in each fastener is different, but the stringer is loaded at each row by the sum of the loads in the two fasteners in each row. This therefore results in a solution which is compatible with that of Cartwright for a 'coupled' stringer, but includes the effect of out-of-plane stringer bending if required. Fastener flexibility can also be allowed for, as in Swift's work.

In order to study the practical implications of these new solutions, a typical stiffened wing panel example has been taken from the A.300B lower wing structure and analysed by all the available methods.

The example chosen has the following geometry ratios:

$$\mu = (AE)_{st} / (AE)_{st} + (AE)_{sk} = 0.338 ;$$

$$h/p = 2.2 ; \quad p/b = 0.217 ; \quad d/p = 0.208$$

where $(AE)_{st}$ = area × E of stringer adjacent to crack tip

$(AE)_{sk}$ = area × E of skin associated with stringer (mid-bay to mid-bay)

b = stringer pitch

d = fastener diameter

h = fastener pitch between the two lines of fasteners in a stringer (assumed to be symmetrical about stringer centre-line)

p = fastener pitch along stringer, i.e. between rows of fasteners.

In Fig.1 the residual strength, expressed as S_{crit}/K_c, is plotted against a/b, where a = ½ crack length. The crack considered is a 'mid-bay' crack propagating equally towards two adjacent stringers. The estimated strengths when the stringer is attached by a single line or two lines of fasteners may be compared. The effect of the 'zero stiffness' and 'infinite stiffness' limits of the in-plane shear stiffness of the stringer on the residual strength of the panel are as shown; the solution therefore lies in the hatched area.

The height of the 'hump' in these curves gives a guide to the effectiveness of the stringer as a 'crack-stopper', and quite clearly a stringer of a given area (μ) attached by two lines of fasteners is more effective in this role than one attached by a single line, particularly if the in-plane shear stiffness is high. From this it may be deduced that an 'I' section or inverted 'T' section stringer would probably be a more effective 'crack-stopper' than a 'top-hat' stringer, (although of course there are other factors to be taken into account than just crack-stopping when designing the stringer shape).

Note however, that the height of the 'hump' in the Scrit v. a/b curve is reduced when the effect of the fastener flexibility is included. Further work is in hand to determine the fastener flexibility coefficient so that this may be included in the analyses.

The solution for the K at the ends of an asymmetric skin crack with respect to the stringers cannot be obtained from Ref.1. Within the limitations of the solutions in Ref.1 such a crack can either be assumed to be symmetrical about the stringer or 'mid-bay'; and with either the tip in the right location but of the wrong length, or of the right length but with the tip in the wrong location! Of these four possibilities the 'mid-bay' crack of the right length (with the tip in the wrong location) was considered to be the best compromise for cracks up to one stringer pitch in length. However, in Fig.2 Cartwright's solution for an asymmetric crack is compared with the 'mid-bay' solution, for stringers attached by two lines of fasteners.

First it may be seen that (in this example) the early approximate solution obtained by assuming the crack is a mid-bay crack of the correct length was acceptably accurate for short crack lengths, up to a/b = 0.2, but for longer cracks could over-estimate the strength by almost 15%. It is also interesting to note that although the curve for tip 'B' does not strictly apply in this example, as the 'tip' is a fastener hole, if that had been a crack, or if a crack suddenly started from the other side of the hole, at certain crack lengths tip 'B' is more critical than tip 'A'. Note that all three curves meet at a/b = 0.52, corresponding to a crack which is symmetrical between the fastener holes of adjacent stringers.

The effect of out-of-plane bending of the stringer as the crack in the skin extends was studied by Williams and Cash. In this example, with a low value of μ and a stringer profile that has its centroid fairly near the skin, S_{crit}/K_c only drops by about 3.5% in the region of the 'hump' of the S_{crit}/K_c v. a/b curve in Fig.1, when the out-of-plane bending is taken into account. However, the reduction could be greater in panels having a high μ and/or when the stringer centroid is far away from the skin.

2.2 Pressure cabin design

2.2.1 Effects of curvature - background

The investigation, both theoretical and experimental, of cracks propagating under the loads found in pressurised fuselage structure remains incomplete. As a result, correlation with flat panel data has not been widely reported. Design of new lightweight fuselage structures demands increasing attention to detail thus increasing the need for a greater effort on this topic.

Two types of damage are most frequently considered when evaluating the crack propagation and residual strength of pressurised fuselage structures. These are longitudinal cracks, in general subject to high hoop stresses induced by cabin pressurisation, and circumferential cracks where the greatest stresses derive from overall fuselage vertical bending. Of the two types, the correction to the stress intensity factor required to account for curvature is greater for the longitudinal crack.

Two main approaches to the solution of this problem on unstiffened cylinders have so far been employed. The first is an analytic approach using thin shell theory to characterise the stress and displacement in the pressure vessel[5-9]. This suffers from the limitation that the boundary conditions along the crack surface cannot be satisfied exactly, use being made of the Kirchoff equivalent shear to satisfy conditions of twisting and transverse shear. Solutions are usually presented in terms of a shell parameter λ, where

$$\lambda = \left[12(1 - \nu^2)\right]^{\frac{1}{4}} \frac{a}{\sqrt{R_c t}} \qquad (1)$$

where a crack of length 2a is in a cylinder of radius R_c and skin thickness t and ν is Poisson's ratio. The limitations of thin shell theory tend to be emphasised with increasing λ. Thus for any cylinder, the theoretical model becomes less accurate with increasing crack length.

The second approach is empirical and involves the measurement of crack growth or residual strength of a test cylinder[10,11]. The results are then compared with equivalent results obtained in a flat sheet.

Most researchers using this approach have found for large diameter cylinders, say R_c/t greater than 100, that the correction to the stress intensity factor is of the form

$$C = 1 + \beta \frac{a}{R_c} \quad , \tag{2}$$

where β is an empirical constant. Other researchers[12] have preferred to model their empirical relationship on the theoretical shell parameter λ. Hahn *et al*[13] however empirically adjusted the theoretical function derived by Folias[5] for a longitudinal crack to give for $(R_c/t) > 50$

$$C = \left\{1 + 1.61 \frac{a^2}{R_c^2} \left(50 \tanh \frac{R_c}{50t}\right)\right\}^{\frac{1}{2}} \quad . \tag{3}$$

Work, both theoretical and empirical, on cracked cylinders reinforced by stiffeners has been approached along similar lines but has attracted fewer researchers. As far as is known, published theoretical analyses are restricted to the solution for a longitudinal crack approaching a ring stiffener[14]. This evaluation shows that the stiffener has more effect in a curved than in a flat panel subjected to an in-plane stress equal to the hoop stress in the curved panel, since it alleviates bulging.

Tests have been carried out for Concorde certification purposes. These tests have involved the measurement of crack propagation rates and the demonstration of residual strength of stiffened fuselage shells containing circumferential and longitudinal cracks.

(a) Circumferential crack behaviour

In the majority of residual stength tests, loading has been applied to simulate a design limit load case. In essence, the structure has been designed to be able to withstand such a load in the presence of a crack. Therefore, the residual strength data can only give an upper bound to the curvature correction factor.

Writing

$$K_I = \sigma C_1 C \sqrt{\pi a} \quad , \tag{4}$$

where C_1 is a correction to the stress intensity factor to account for stringers, etc., and assuming that failure occurs if $K_I > K_c$ where K_c is the appropriate plane stress fracture toughness for the material, it follows that

$$C \leqslant \frac{K_c}{\sigma C_1 \sqrt{\pi a}} \quad , \tag{5}$$

for a successful residual strength test. In each of the tests discussed here, the crack extended to stringers. Although, in some cases, the crack initially lay short of the stringers, slow stable growth took place during the loading phase. In all cases, the stringer pitch was about 5.25in.

The first set of tests was used to demonstrate residual strength in the presence of a long circumferential cut representing damage due to a disc burst. The tests consisted of loading a cracked stiffened cylinder under pressure only. The crack was extended following each test. The ratio R_c/t was 800, with values λ (Eq.(1)) ranging from 13.1 to 32.9. The first point to notice is that λ is very much larger than the range for which theoretical solutions are available. Thus at λ of 32.9 it was found that for a successful test, $C \leqslant 3.6$. At shorter lengths, the applied load was too small to demonstrate values of C lower than 3.6.

The second set of tests was used to demonstrate the residual strength of the fuselage top surface under combined pressure and bending in the presence of cracks. In these cases, the crack lay across two stringer bays to a length of some 10in. In one case only did the crack run rapidly to be arrested at an adjacent panel joint. Values of λ ranged from 4.7 to 5.5 with R_c/t ranging from 800 to 1000. The test to failure gave a value of $C = 1.095$, at $\lambda = 4.9$. Other tests gave limiting values of C below 1.24. In comparison, Erdogan and Ratwani[8] gave a membrane curvature correction factor C in an unstiffened cylinder of 1.55 at $\lambda = 4.9$.

(b) Longitudinal crack behaviour

Rather more data is available on longitudinal crack growth. Fatigue crack propagation tests have been conducted under pressure loading giving an easily definable stress cycle - most propagation tests on circumferential cracks have been carried out under spectrum loading. The crack growth data can be reduced to stress intensity factors using Forman's equation[15], namely

$$\frac{da}{dN} = \frac{C_f(\Delta K)^m}{(1 - R)K_c - \Delta K} \quad , \tag{6}$$

in which the coefficients C_f and m have been derived from tests on flat panels.

Eq.(6) can be rewritten as

$$C_f(\Delta K)^m + \frac{da}{dN}(\Delta K) - (1 - R)K_c \frac{da}{dN} = 0 \quad , \tag{7}$$

which is a polynominal in ΔK. For any given da/dN and R this may be solved for ΔK using

Newton's approximate method. Knowing $\Delta\sigma$ and a, it is a simple task to isolate the correction factor

$$C_1 C \left(= \frac{\Delta K}{\Delta\sigma \sqrt{\pi a}} \right).$$

On Fig.3, a number of results have been shown for an axial crack midway between two frames. Test 6.1 was conducted at a radius of 50.1in with a skin thickness t = 0.063in. The remaining tests were conducted at R_c = 56.7in with t ranging from 0.055in to 0.071in. Except where stated, the data represent the total correction factor and include contributions from the frame and from the curvature. The solid and broken lines show Hahn's correction factor for an unstiffened sheet at R_c = 50.1in and R_c = 56.7in respectively. At $\lambda < 6$, i.e. a crack of length less than 11in, the correction factor is similar to Hahns. Beyond this λ, the influence of the frame reduced the correction factor giving a divergence from Hahn's solution. This difference cannot totally be accounted for by C_1, the component of the correction factor derived from a flat plate analysis of the effect of the frame. On Fig.3, the correction factor C, accounting for curvature only, is shown for test 6.1. On Fig.4, the results of residual strength tests on similar configurations are shown. The crack extended in most cases from frame to frame and was about 20in in length. Radius of curvature R_c ranged from 44.8in to 56.7in and thickness t from 0.055in to 0.071in. Where the crack commenced to grow rapidly, the data point is shown with an F. Other tests not pursued to failure give an upper limit to the total correction factor (see Eqs.(4) and (5)).

On Fig.5, the results of a fatigue test on cracks growing away from completely failed frames are shown. Here R_c ranges from 50 to 56.7in and t from 0.055 to 0.071in. It can be seen that the total correction factor is close to unity at short lengths indicating that the broken frame does not increase the stress intensity factor as much as does a similar frame in a flat sheet. At longer crack lengths, the correction factor tends to increase.

(c) Concluding remarks

To summarise, it is considered that present knowledge of the effect of curvature and pressure on crack propagation and residual strength of stiffened cylinders in inadequate. Hahn's empirical adjustment to Folias' correction factor gives a good approximation to the present results for axial cracks at short lengths but increasingly diverges as the influence of the frame is felt. The crack growing away from the completely failed frame did not apparently experience much acceleration due to the failure. This is a topic which requires further investigation.

2.2.2 Crack growth under mechanical and thermal stress cycling

(a) Background

During climb, when Concorde accelerates to supersonic speeds, the exposed surfaces are subjected to kinetic heating but deep structure such as the area masked by the fin or wing remains relatively cool. This induces axial tension stresses in the masked region. During descent, on the other hand, the masked region retains its heat longer than the exposed structure to give axial compression stress in this area.

(b) Design/development work

A crack propagation test was performed on an integrally machined flat panel representative of the top surface of the Concorde fuselage beneath the fin. The test panel consisted of a representative region of the upper surface panel between stringer 5 (LH) to stringer 5 (RH), see Fig.6, and carried the fin-fuselage sealing members but no other representation of the bridging effect of the fin in the longitudinal sense. Outside of stringers 5 (LH and RH side) the panel was not representative of the production aircraft, but consisted of back-to-back machined panels to provide the cross sectional area necessary to induce the correct thermal climb stresses. The test panel was subjected to cyclic thermal and mechanical loading to simulate a typical once per flight stress cycle for this region, see Fig.7. The specimen, which carried frame members, was suspended in the test rig at four points per frame, on swinging links, such that no restraint was imposed on the panel during thermal and mechanical loading.

The mechanical load was applied by three hydraulic jacks through a whiffle-tree arrangement to give a uniform stress distribution. A similar arrangement at the opposite end of the specimen reacted the load through a common loading frame. The specimen was partially enclosed in a duct such that alternate heating and cooling of appropriate areas, by circulating hot air or ambient air, could be achieved. The thermal stress cycle was controlled automatically by thermocouples sensing the required temperature differential. The time at which the mechanical loads were applied was also controlled automatically by measured temperature differentials.

Strain gauges and thermocouples were attached to the panel to measure the stress and temperature distribution over the panel, particularly in the area selected for insertion of the initial damage. Pre-damage measurement of the stress distribution across the panel showed that a uniform mechanical stress was achieved by the loading arrangement and that representative thermal stress distributions were achieved. The peak thermal tension stresses generated agreed closely with the required design values. The required compressive stresses representing the descent phase could not be achieved, since the area ratio (masked/unmasked) and the temperature differentials had been chosen to give the correct climb stresses.

The initial damage consisted of a sawcut in the centre of the panel through and perpendicular to the centre stringer and 0.8in long in the skin. Under cyclic mechanical and thermal loading the crack propagated steadily as shown in Fig.7. The thermal stress distribution across the specimen, measured at various crack lengths, is shown in Fig.8. Insufficient strain data was available to

determine stress intensity factors. However, it was observed that the stress at a constant distance ahead of the crack tip did not increase by load diffusion round the crack to the same extent as it would under mechanical loading. Thus the crack acts to relieve the thermal stress, the action being somewhat similar to the effect of constant displacement boundary conditions.

Six development tests have been conducted on similar machined panels under cyclic thermal stresses only. From the crack propagation results on these panels it was found the crack growth data could be related to the stress intensity factor using an equation of the Paris form:

$$\frac{da}{dN} = C_f \Delta K^m \quad , \tag{8}$$

where the stress intensity factors were derived from stress measurements in the uncracked panels. In this equation, ΔK represents the stress intensity range where 60% of the compressive stress is considered to be effective. This value of 60% was chosen to give the best equivalence between tests conducted under tension thermal loading only and tests conducted under tension - compression thermal loading.

For the mechanical loading cycle, Forman's Eq.(6) for the material at room temperature was used. Summing the crack growth in a linear sense, using Eq.(8) for the combined thermal and mechanical cycle and Eq.(6) for the mechanical only cycle (neglecting crack growth retardation effects) a prediction of crack growth behaviour can be made. By far the largest contribution to crack extension is the thermal cycle, which at the centre of the uncracked panel reaches a maximum tension stress of 11400 lbf/in^2 during the climb phase and falls to -11400 lbf/in^2 in the descent phase. Close agreement was obtained between the calculated crack growth and that determined by test. By comparison, calculation of the crack growth rate based on a zero to peak tension stress cycle for a quasi-mechanical stress equal in magnitude to the combined test thermal and mechanical stress and using Eq.(6) predicted a life 50% less than test achievement. The test thus demonstrated that crack growth under a thermally generated stress was less than that produced by mechanically applied stress.

The crack propagation behaviour under thermally generated stresses has been shown to be different to that which occurs under mechanically applied stresses. Strain gauge measurements ahead of the crack tip would indicate that the presence of the crack reduces the thermal loading due to the strain relieving effect which it has. To determine a correction factor to be applied for the case of thermally generated stress levels, the calculated stress intensities for thermal and mechanical loadings respectively were compared for given crack growth rates using Eqs. (8) and (6) respectively. A constant correction factor, $C_T = 0.8$ emerged which, if applied to the calculated stress intensity factor for the test geometry and loading and using the room temperature crack growth rate Eq.(6) for the material, gave good correlation with the test results, that is, the effective stress intensity range ΔK was taken to be

$$\Delta K = \Delta\sigma \sqrt{\pi a}\, C_1 C_T \tag{9}$$

where $\Delta\sigma$ is the stress range measured in the uncracked panel, 60% compression assumed effective; C_1 is a correction factor to account for the effect of broken and intact stiffeners, etc. and C_T is the factor to account for the thermally generated stress.

(c) Concluding remarks

To summarise, crack propagation rates under thermally generated stresses were reduced compared with rates under an equivalent mechanical loading. Over the range of testing it was found that a constant correction factor applied to the calculated stress intensity factor for the thermal loading situation, could be used to correlate crack growth rates, using the room temperature crack growth rate equation for the material.

3. TESTING

3.1 The use of crack opening displacement methods to monitor approach to failure in residual strength tests

Residual strength tests on 'fail-safe' aircraft structures which contain cracks are normally included in the programme of tests which are carried out to ensure that the structure will meet the associated airworthiness requirements. Such work may entail the exploration of the effect on residual strength of a number of differing crack locations and configurations which are usually considered independently. It is important to ensure that the structure shall not be lost, inadvertently, by any one crack being loaded to critical conditions with consequent catastrophic structural damage before the behaviour of the other cracks has been established. It is therefore essential to employ an experimental technique which may be used to monitor the approach of each individual crack to critical conditions as the load on the structure is increased. Should it then become apparent that any crack is approaching critical conditions, remedial action may be taken - generally by applying a 'patch' repair to the crack concerned - before continuing the tests to higher levels to establish the behaviour of the remaining cracks.

In this section two examples of such work are presented. In both cases crack opening displacement (COD) measurements were used to monitor approach to criticality. The first example (3.1.1) is taken from work on a large military aircraft and the second example (3.1.2) relates to a research programme on residual strength of structures, which was conducted on a civil transport aircraft after it had successfully completed airworthiness clearance tests.

3.1.1 *'COD' applied to residual strength tests on a large military aircraft*

During residual strength testing of a large military aircraft predictions of skin crack behaviour were required. This was in order to avoid, in the early stages of testing, failure of the tension panels

on the wing under-surface which might produce catastrophic structural failure. Crack opening displacement (COD) measurements were used to monitor crack behaviour and to predict the onset of unstable crack growth. In the final stages of residual strength testing the accuracy of the failure predictions was investigated. The replica technique due to Hickson[16], in which a replica of the crack tip area is made using a small heated platen faced with a low melting point alloy, was used to record COD and other crack tip phenomena. Measurements of COD were then made using a comparator microscope.

To provide a basis for assessment of the approach to critical crack growth in the full-scale structure a series of pre-cracked coupon specimens were tested to destruction whilst taking replicas of the crack tip areas at increments of load. The coupon specimens were made from sheets of aluminium alloy, Specification DTD 687A, as used in the aircraft skin. The coupon tests covered several crack lengths and specimen sizes. They were loaded in various ways, including representation of different aspects of the fatigue and residual strength testing of the structure. The loads conditions covered single loading to failure (Coupon 1), repeated loading to 40% ultimate load then single loading to failure (Coupon 2), and also load cycles to progressively higher loads, then final loading to failure (Coupon 3).

Some indication of the nature of the results obtained on the coupons and on the wing may be obtained from Figs.9a and 9b. Curves of COD against $\sigma/\sigma_{fract.}$ are shown for a single load cycle (close to failure) and for final loading to failure.

From the replicas taken during coupon testing a number of stages in crack development could be observed. Firstly, elastic deformation in the maximum COD range 0 to 15 microns occurred. This was followed by plastic deformation in the maximum COD range 15 to 90 microns with hysteresis in the COD against $\sigma/\sigma_{fract.}$ curve and visible 'dimpling' at the crack tip. Further increase in loading induced stable crack growth in the maximum COD range 90 to 150 microns with gross hysteresis and residual COD in the COD against $\sigma/\sigma_{fract.}$ curve and visible movement of the crack tip into the plastic region. This stage is shown in Fig.9a. Finally unstable crack growth initiated at a COD between 150 and 250 microns and gave abrupt tensile failure, as shown in Fig.9b.

Initially it had been anticipated that a single value of COD would result from the coupon testing which would define the onset of unstable crack growth. It was found however, particularly on the aircraft structure, that no single parameter fitted all observed crack behaviour. Thus for prediction of skin crack behaviour a consensus of the following parameters was used:

(i) COD from the coupon testing approximately 150 microns represented $0.97\sigma/\sigma_{fract}$;

(ii) shape of COD against $\sigma/\sigma_{fract.}$ curve. A marked flattening in the curve occurred above $0.9\sigma/\sigma_{fract}$;

(iii) gross stress field. (The gross stress field in each cracked wing skin, having been previously determined from strain gauges, was compared with the gross value of 155MPa approximately at which the coupon specimens failed.);

(iv) crack growth per load cycle. A crack growth of 0.04in represented a load cycle to approximately $0.96\sigma/\sigma_{fract}$;

(v) residual COD (i.e. hysteresis at zero load). An hysteresis of 15 microns represented the crack having been loaded to $0.97\sigma/\sigma_{fract}$;

(vi) mean cyclic COD. This parameter was the mean hysteresis over a full loading and unloading cycle and a value of 30 microns indicated a load cycle to $0.97\sigma/\sigma_{fract}$.

(a) Tests on aircraft structure

The test programme on the aircraft structure was lengthy and complex and is beyond the scope of this paper. From the many hundreds of replicas taken predictions of crack behaviour were made. Initially panels containing cracks approaching criticality were repaired and the structure survived the full residual strength testing programme. Subsequent tests were concerned with the 'fail-safe' testing of 'as-cracked' skin panels. For these tests the crack behaviour predictions were followed by testing to high loads to produce failure. The results were that, of the 8 cracks investigated:-

2 failed at the predicted load.
1 failed well above the predicted load.
3 gave every evidence (except unstable crack growth) of failure somewhat above the predicted load.
1 predicted failure did not occur in any form.
1 survived as predicted.

The result was therefore that predictions generally erred on the conservative side. There were no cases of cracks failing before the predicted load.

(b) Comparison of structure and coupons

Since the crack behaviour predictions were, on the whole, less accurate than was hoped for, the areas of non-equivalence between the aircraft structure and the coupon specimens are worthy of mention though none was investigated.

Loading: The coupon specimens were tested in uniaxial tension whereas the wing skins were generally loaded biaxially.

Stress gradients: On the structure crack propagation could be inhibited by low-stress regions or rivet holes.

Supporting structure: The skins on the aircraft were reinforced by stringers, spars, etc., whilst the coupon specimens were simple unreinforced sheet.

Strain-governed load sharing: Extension of the skins under cracking could tend to shed the load to the supporting structure. This effect was not reproduced in the coupon loading.

(c) Conclusions

The main conclusion from the work was that the predictions of behaviour for the structure skin cracks using COD measurements were generally conservative with an overall tendency for the cracks to survive the predicted failing load. The accuracy of prediction may have been influenced by areas of non-equivalence between the coupon specimens and the aircraft structure, with respect both to geometrical detail and applied loading. The use of the replica technique was found to be a most useful tool for recording COD and other crack tip phenomena.

3.1.2 'COD' applied to tests on a civil transport aircraft

After satisfactorily completing a long programme of airworthiness clearance tests, which covered fatigue and 'fail-safe' aspects, the Trident 1 full-scale test specimen was subjected to a series of residual strength tests as part of a fracture mechanics research programme. The objective of the research was to demonstrate a 'fast-fracture and crack-arrest' condition, in a part of the wing lower surface that was reasonably amenable to simple fracture mechanics analysis.

(a) Crack locations

The choice of locations for new cuts was therefore restrained by the need to be:

(i) where the structure was relatively simple and uniform to ease the problems of analysis;

(ii) far enough apart to avoid interactions between two cuts;

(iii) far enough away from repairs or large reinforcings to avoid large stress gradients near the cuts.

Within these restraints four locations were selected (see Fig.10):

(a) Two examples of a chordwise skin crack under a failed (i.e. cut) stringer. The pitch and area of the stringers in these two examples were very similar, but the skin thickness in one example was twice that in the other.

These cuts were labelled 'D' and 'F', 'F' having the thicker skin.

(b) Two examples of a skin crack from the edge of the panel under a spar cap. Cut 'C' was under the rear spar cap near the wing roof, where the spar cap area is large. Cut 'E' was under the front spar cap at the same spanwise location as cut 'D' above (but in the other wing), so that a comparison could be made between the residual strengths of similar structures containing either an edge-crack or a '2 ended' crack.

The predicted strength of the structure at these four locations was based on analytical solution by C.C. Poe to account for the effect of equally spaced stiffeners on the stress intensity of a crack in a panel, for a crack either midway between two stiffeners or symmetrically under a stiffener. The effect of the failed stiffener at cuts 'D' and 'F' was allowed for by considering the bay width as '2b', i.e. the distance between the intact stringers on either side of the 'failed' stiffener, assuming a reduced value of μ, and increasing the skin stress as a result of putting the 'failed' stiffener end load into the skin over a width 2b. When considering the edge cuts 'C' and 'E' the panel model was assumed to be a symmetric crack under a stiffener (i.e. the spar cap) of twice the actual crack length with a stiffener pitch 'b' equal to the pitch between the spar cap and the adjacent stiffener in the wing panel. The resulting stress intensity estimate was increased by 1.1 (if $a/b < 0.8$) or 1.2 ($0.8 \leqslant a/b < 1.4$), which is an empirical factor based on previous tests on panels containing edge cracks. These calculations resulted in characteristic 'humped' residual strength v. crack length curves, indicating that the strength of the structure increases as the crack tip approaches a stiffener, before falling away again once the crack has propagated under the stiffener. It is this behaviour that enables the stiffeners on a panel to act as 'crack-stoppers', provided the stiffeners and their attachments are strong enough.

(c) Test procedure

It was required to load the specimen until each crack or cut was brought as near as possible to its failing strength. (Note that there were also two natural cracks which were being studied at the same time, which occurred during the 'fail-safe' part of the previous test programme). To achieve this aim the cuts were introduced into the specimen one at a time, in descending order of predicted failing strength, and the specimen was re-loaded after each cut to a load no higher than had been achieved already in previous tests. In this way the risk of a failure originating from an earlier crack or cut was minimised.

During each test run, the behaviour of each crack or cut of main interest in that test (i.e. generally the 'new' cut that had been made for that test), was monitored continuously by observing the crack opening displacements (COD). These COD measurements were recorded using strain-gauged double cantilever beam gauges; more commonly called 'clip-gauges'. Each gauge was mounted between two light alloy 'vee-blocks' (approximately 28mm × 16mm × 3.2mm), bonded to the panel adjacent to the crack tip, with the bevelled edges paralled to, and 2.5mm each side of the crack.

The COD readings were compared during each run with a 'reference envelope' COD curve, which had been derived from several Airbus wing bottom skin panel tests. Some details of these tests are summarised in the table below. It was found that, in spite of the wide variation of structural feature surrounding the crack, when COD is plotted against percentage of failing load the curves were all very similar. The curves for the three panels which failed and one which evidently was nearly loaded to failure are given in Fig.11. In two of the tests is evidence of some 'fast-fracture and crack-arrest' occurring between 80-90% of the failing load, as indicated by the flattish part of the COD curves in tests 1 and 6. Nevertheless, the curves all finally converge to give a very small variation in the maximum COD at the instant of failure, regardless of crack length or stress level attained.

It was therefore concluded that, as the Trident wing bottom skin was made in the same material as the Airbus, provided the COD reading was kept within the 'reference envelope' in Fig.11 the wing could be loaded safely without failure until the final test.

(d) Results of tests

The results of the COD measurements on the Airbus wing panels are given in Table 1 below and in Fig.11:-

Table 1

Test	Type of panel	Skin t (mm)	Initial crack ℓ (mm)	Stable crack growth (mm)	COD at onset of stable growth (mm)	Final COD (mm)	Remarks
1	1 bay skin crack + stringer failed	15.7	103	18	0.76	1.78	Crack ran into rivet hole.
2	1 bay skin crack + stringer failed	18.4	95	20	0.63	2.11	Failure
3	Crack from one edge of manhole	13.5	400*	32	1.27	1.27	Test stopped
4	Crack from one edge of manhole	11.2	360*	11	1.0	1.00	Test stopped
5	Cracks from bolt edges of manhole	13.5	540*	20	1.02	2.01	Failure
6	2 bay skin crack under failed stringer	7.1	178	38	0.84	2.01	Failure
7	Skin edge crack + spar flange failed	4.7	139	18	1.37	1.37	Spar failed

* Including width of manhole = 254mm

[Note that the final COD includes the extra increment which occurs when the crack tip moves away from the clip gauge location; hence the final COD values are slightly larger than the true COD at the crack tip at the instant of failure. No correction for this was made when drawing the curves in Fig.11 and hence no allowance was made for this increment in the Trident testing either. This procedure is quite acceptable provided the amount of stable crack growth is about the same. In thinner skins the amount of stable crack growth might be expected to be greater (excluding the influence of stringers which may be effective as 'crack-stopper'), but the use of an uncorrected 'reference envelope' COD would be conservative in that event.]

The results of the Trident COD measurements are given in Fig.12. The earlier test runs with less than the final number of cuts are not shown, but it can be seen that even at about 75% of the final applied load the ranking order of the strengths of the four locations is clearly recognisable, as the relative values of the COD at the four locations remain about constant during the last 20-25% of the loading. The COD readings therefore give a reliable indication of the location which should be watched most closely during the final stages of a test.

Regrettably, as the strength of the wing containing these cuts was much higher than predicted, final failure of the wing occurred away from any of the locations being studied. However, from the final COD values it may be estimated that location 'D' reached about 94% of its failing strength, and the ranking order of strengths was 'D', 'C', 'F' and 'E'. The ranking order of the calculated residual strengths at the four locations was 'E', 'C', 'F' and 'D'. This lack of agreement between the calculated strengths and estimated strengths from the COD readings is disappointing, and further work is going on to try and improve the analytical methods for predicting the strength of cracked structure. However, to put the discrepancies in perspective, the ranking orders would be in agreement if the calculated strength of cut 'D' and cut 'E' had been 17% less and 15% more respectively.

3.2 Simplified representation of combined pressurisation, thermal and bending loading in tests on fuselage top surface panels

3.2.1 Objective

In many cases, residual strength testing of a cracked structure is carried out near the limit of the structure's tolerance to that damage. The possibility therefore arises that such a crack may begin to propagate rapidly. If the test loading includes a contribution from pressure, the energy stored within the structure is usually considerable particularly if air is used as the pressurising medium. Crack instability could thus lead to an explosive decompression causing considerable damage not only to the specimen but also to the test facility. A residual strength test was carried out on a curved, integrally machined panel forming part of the top surface of the forward fuselage of Concorde, which in practice would be subjected to a combination of cabin pressurisation loads, thermal loads and fuselage bending loads. This test was conducted to determine whether it was possible to replace pressure and, for economy reasons, thermal loads by an additional overall bending moment.

3.2.2 Test procedure and associated analysis

The crack was circumferential in direction and was 10.1in in length. Each of the tips extended to the fillet radius of an integrally machined stringer. The centre of the crack ran across a broken stringer. The crack had been grown from an 8in jeweller's saw cut under a ground-air-ground simulated flight spectrum to a length of 9.34in. Two additional bending moments were applied during which the crack extended firstly to 9.97in and finally to 10.1in. Note that during the present test the crack further extended to 10.31in.

The test specimen was instrumented to measure radial deflections, crack opening, strains ahead of the crack tip in both skin and stringer as well as the general strains at the test location. The test was conducted in three parts. Parts 1 and 2 enabled the contributions to stresses and displacements from unit loads of pressure and overall bending to be determined. The final part of the test consisted of the application of a limit load, which represented a peak gust experienced during descent, for certification purposes.

Prior to the insertion of the damage a comprehensive range of strain gauge measurements was made to determine the general levels of stress at the site of the proposed test under pressure, thermal and bending loads applied separately. Equivalence of applied loads was determined by equating the axial stress, that is the stress normal to the crack, due to pressure and thermal loads to the axial stress induced by the additional bending moment. For this particular test location and limit load case, it was found that axial stresses derived by pressure and thermal loadings could be simulated by a 46% increase in the limit bending moment. No attempt was made to apply a hoop loading to simulate the hoop stresses induced by pressure and thermal gradients. The modified loading arrangement results in strains normal to the crack being greater under augmented bending than under the combined loading of bending, pressure and thermal gradients.

Miniature strain gauges, consisting of a block of ten end load gauges, were adhered to the specimen ahead of the crack on both the inside and outside skins and along the integral stiffener on the side adjacent to the crack. The gauges were aligned to measure axial strains.

From Westergaard's stress function the equation for an unstiffened sheet can be derived:-

$$K_I = \frac{E\varepsilon_{x_0}\sqrt{\pi a}}{\frac{y(1-\nu)}{\sqrt{y^2 - a^2}} + \nu(1-\alpha)} \qquad (11)$$

where α is the ratio of the stress parallel to the crack to the stress normal to the crack

E, ν are Young's modulus and Poisson's ratio respectively,

and ε_{x_0} is the measured strain at distance y from the centre of a crack of length $2a$, $y > a$.

It is thus possible to determine the stress intensity factor. Care needs to be exercised since strain gauges close to the crack tip show evidence of plastic deformation in the specimen. The equation, being for an unstiffened sheet does not, accurately, take into account the influence on the stress intensity factor of a stress normal to the stringer, (i.e. parallel to the crack). Further, local bending of the stringer itself tend to induce variations in ε_{x_0} and hence scatter in the estimates of K_I. In practice, it was found that the estimates of K_I from the strain gauges gave stress intensity factors midway between predictions which (a) neglected, and (b) included the curvature correction factor proposed by Erdogan and Ratwani[8]. It was however, possible to make a comparative assessment of the results. It was found that values of K_I obtained for the combined loadings tended to be less than the values of K_I obtained from the case with the limit bending moment augmented by 46%.

No attempt was made to measure the crack opening displacement at the crack tip itself. Use was however made of the equation, derived from linear elastic fracture mechanics, which may be written as

$$K_I = \frac{\delta_{int} E \sqrt{\pi a}}{4\sqrt{a^2 - y^2}} \qquad (12)$$

where δ_{int} is the total separation of the crack surfaces at a distance y from the centre of a crack of length 2a, $y < a$. This equation suffers similar limitations to Eq.(1), since it is assumed that a stress normal to the stringer, i.e. parallel to the crack, has no influence on the stress intensity factor. Crack opening displacements were made some 4.3in from the crack centre-line (i.e. 1 in from the tip). This approach gave stress intensity factors which were slightly lower than those using the previous method but with less variation between the two crack tips. It confirmed the findings that the displacements and hence stress intensity factors tended to be lower under combined loading than under an augmented bending moment. Note that this particular set of measurements gave some indication of crack closure due to the previous load history. Positive crack openings were not recorded until the applied pressure loading was about 10% of the maximum and the applied bending moment was about 5% of the limit bending moment.

Radial deflection measurements showed that the greatest absolute movements of the crack lips were produced by bending stresses. For both pressure and bending, the relative movement between the forward and aft lips took on an antisymmetric pattern, that is, the relative deflections reached a maximum between stringers, passed through zero at the broken central stringer and reached a maximum in the opposite sense the next stringer bay. Relative deflections under pressure tended to be greater mid-bay but lower near the crack tip. However the sensitivity of the instrumentation precluded a quantitative assessment of the effect of the deflections on stress intensity factor and hence on residual strength.

3.2.3 Final observations

In conclusion, it was considered that there was no evidence to show that pressure and thermal loading could not be replaced by an additional bending moment to give equivalent axial stress. If anything the augmented bending was more severe due to the absence of restraint in the hoop direction.

3.3 Observations of scatter in fatigue crack growth in large integrally machined panels

The determination of Concorde fuselage damage tolerance was supported by a number of tests on various structural configurations. Full-scale fuselage panels were tested in a fuselage section which could be cyclically pressurised in a water tank. Tests were also made on a forward fuselage section which could be pressurised with air and also subjected to flight loadings and temperature variations with time.

The tests performed were both expensive and time consuming. Although information on scatter in crack propagation was required, additional tests with this degree of complexity could not be justified. Scant published data was available, although there was some evidence that for coupon specimens scatter in propagation time was similar to that in total life to failure[17-20]. To investigate whether this was the case for full-scale production components an investigation into scatter was included in a research programme at RAE, Farnborough.

3.3.1 Specimen

The specimens were structurally typical of Concorde fuselage panels but were flat. They were machined from slabs of BAC M76 aluminium alloy (a modified RR 58) and had integral stiffeners and separate frames. The test area comprised three bays between frames (approximately 160cm) and six bays between stiffeners (approximately 80cm). The edges of the specimens each contained six spherical bearings through which loads were applied. The edges were thickened to support the bearings and slotted to reduce the effect of increased edge stiffness on transverse loads. The overall specimen size was approximately 225cm in both width and length.

The objective of the investigation was to determine the scatter in crack propagation rate which might be expected in typical Concorde panels. To this end five nominally identical panels were tested. The material for the specimens was taken from the production stock-pile for the aeroplane and production methods and tolerance were requested for manufacture.

3.3.2 Test conditions

The specimen and test rig were designed for biaxial tests with various loading wave forms. However the initial scatter investigation was planned for uniaxial sinusoidal constant amplitude loading. The load level chosen represented a gust loading superimposed upon the longitudinal stress due to fuselage pressurisation.

The test rig was purpose built for the test programme. It comprised six hydraulic jacks each independently controlled by an electro hydraulic servo value. Each jack was attached to two of the load input points on the specimen. Two adjacent sides of the specimen were loaded while the other two sides were restrained. For the scatter investigation only three jacks were pressurised to produce uniaxial tension in the stiffness and the panel.

The loads for the first specimen were balanced between the three jacks to achieve a strain distribution across the specimen as near uniform as possible. After recording the strain distribution the load was removed and a 4in crack starter notch cut into the specimen centred on and across the central stiffener. The specimen was then cycled at the loads previously determined for the uncut condition. Since the test condition was a load controlled situation, (i.e. pressurisation plus bending moment) the subsequent four specimens were all loaded to the same load cell readings as for the first test (within the 1% accuracy of the system).

3.3.3 Data collection

Each specimen was extensively strain gauged to enable a strain survey to be completed both before and after the crack starter notch was introduced. Selected strain gauges were monitored during the crack growth phase to record stress changes in the skin and stiffeners during crack growth.

Crack growth gauges were used to measure crack length. The gauge outputs were continuously monitored together with a number of load cycles to give a record of crack length with load cycles. Crack growth was recorded in both the skin and stiffeners. Plots of crack length v. number of cycles are shown for each of the five panels in Fig.13. (The two tips of each crack are designated /1 and /2.)

3.3.4 Analysis

The standard deviation of the logarithmic life required to grow the crack for each 25mm increment was calculated. The standard deviations for growth from the notch to just before and just after the stiffener were also calculated.

A polynomial equation was fitted to the crack growth curve plotted for each crack tip. This equation was differentiated to obtain crack growth rate. From tests on plain panels in this material BAC have derived the crack growth rate equation, in the Forman, Kerney and Engles[15] format. Using this equation and the observed crack growth rates in the stiffened panels estimates were made of the values of stress intensity factors as the cracks progressed. The values of stress intensity factor so derived have been plotted against crack length for each panel. The theoretical stress intensity range was calculated using the compounding technique proposed by Rooke, Cartwright and Davis[21]. The results were plotted for comparison with the experimentally derived values. Fig.14 shows a comparison between the envelope of the experimentally derived values of K and the corresponding theoretical predictions.

3.3.5 Discussion

The standard deviation of log time for an increment of crack growth is shown below in Table 2.

Table 2

STANDARD DEVIATIONS OF CRACK GROWTH RATES

Crack growth increment (mm)	Increment cycles (average)	Standard deviation (log cycles)	'Typical' standard deviation
50 to 75	3027	0.1239	0.15
75 to 100	1452	0.1664	
100 to 125	1010	0.1726	
125 to 150	2033	0.1412	
50 to 125	5490	0.1350	
50 to 150	7786	0.1289	

AvP 970 standard deviation for total life to failure from first loading is 0.176.

NB: Stringer centre line is at crack length 135mm.

The data is too limited to allow conclusions to be drawn on the variation of standard deviation with crack length. However a typical value of (say) 0.15 would be equivalent to a scatter factor of about 2.8 on the mean propagation time obtained from an infinite number of specimens. This compares to a scatter factor of 3.33 for an infinite number of specimens tested to establish 'safe life'[22]. The standard deviation for propagation from the starter notch to beyond the stiffener is 0.1289, equivalent to a scatter factor of about 2.5.

The results obtained are for monolithic structure. For multi-element structures, variables such as load transfer between elements, crack delay in holes and crack initiation in attached load-carrying elements would all be expected to increase the variations in crack growth. Thus it appears that the minimum scatter factor for monolithic structure should be at least 2.5 based on mean life and that 2.8 would be more appropriate. In the absence of test evidence the retention of the 3.33 factor accepted for safe life specimens would appear prudent for multi-element structure.

The variation in both the theoretically and experimentally determined stress intensities with crack length is shown in Fig.14. There is an apparent 20% variation in the experimentally deduced stress intensity range. The theoretical predictions agree well with the highest experimentally derived values. It suggests that if predictions of stress intensity are required for crack propagation calculations then it is debatable whether great accuracy is required. Certainly errors of a few per cent can be tolerated if this allows the use of a simpler solution or more speedy computation.

4. PROBLEMS IN SERVICE

4.1 General

In the preceding sections of this paper applications of fracture mechanics have been discussed which relate to problems arising in design and testing of aircraft structures. Generally, in the associated analytical work, attention is focussed on problems where analysis can be attempted with some confidence because appropriate stress intensity factor solutions exist. Also the general stress field is known, or may be established by measurements during test, and materials data on crack growth rates and fracture toughness are available or may be obtained within an adequate time scale.

The situation is usually very different when cracks are discovered in aircraft in service and questions must be answered, within a relatively short time scale, regarding anticipated crack growth rates and residual strength of the structure. Broadly speaking, the main problems which arise fall under three headings: firstly, inability to derive rapidly and with confidence a solution for the stress intensity factor, secondly, difficulty in establishing the general stress field in the area of structure concerned and, thirdly, lack of adequate materials data. These shortcomings may occur together and lead, overall, to a low level of confidence in the accuracy of the associated analysis.

A number of fracture mechanics studies associated with service failures have been made over the past few years and have highlighted the above three problem areas. In the paragraphs which follow the three areas are discussed in turn in some detail. In some cases the observations made are based on general experience - in other cases the comments are illustrated by specific problems which have occurred in service.

4.2 Solutions for stress intensity factors

It will be appreciated that when cracks are detected in aircraft in service the associated analysis is generally conducted as quickly as possible. In many cases the structural geometry is very complex in the vicinity of the crack and, because of the time constraint, recourse is made to the use of standard solutions[23-25] to give as good an approximation as possible to the real crack/structural geometry. Superposition or compounding[26] of two or more standard solutions may be used to improve the representation of the real situation: time does not generally permit the use of complex finite-element models to obtain a solution. The use of standard solutions has contributed in no small measure to success in handling service problems but, nevertheless, situations have arisen in which they prove to be inadequate. Some of the more commonly occurring cases are illustrated and discussed below.

4.2.1 Pin loaded holes

There are a number of solutions for cracks at or near holes in various stress fields. However there is little published work on pin loaded holes and problems on such geometries have arisen on several occasions. In one particular case two references which were available due to Ratcliffe and Cartwright[27] and Shah[28] were used to analyse a failure which occurred to an attachment lug of a hydraulic jack. The stress intensity factors which were obtained from the application of these references differed by a factor of 2. While it may well be possible that these solutions were unwittingly used in conditions to which they did not strictly apply it was not possible to cross refer them, since the former was obtained by experimental compliance and the latter by elasticity theory. Nor was a third solution available to provide guidance.

There is a need for a standard solution which will take into account finite width of the lug, relative to pin diameter, and the width of material above the pin (in the loading direction). Additionally, solutions for asymmetry of the cracking about the hole are required.

4.2.2 Feather edge holes

Although feather edges are clearly undesirable there are a number of situations in which they can and do occur. Recent examples are oblique drilled holes in a high strength steel jack body and over-deep counter sunk holes in zinc rich aluminium alloy wing skins (Fig.15). There are no solutions known to the authors for this geometry. An approximation which has been used is the standard solution for a hole with a through crack, modified to take account of the stress gradient around an oblique hole, instead of the stress gradient around a normal drilled hole. The accuracy of this modified solution cannot be checked and the results obtained must be treated with caution. A proven standard solution for this case could show an easing of the inspection requirements for this geometry arising from an increased confidence in the result.

4.2.3 Interference-fit pins

Interference fits can take a number of forms ranging from bushes and oversize fasteners to the techniques of pre-deformation of the hole with mandrels and split bushes. In service varying combinations of applied load and field stress around the hole occur. It follows that since these holes are subjected to special treatments because they are likely to sustain fatigue damage, then they are also the areas which the engineer will be called upon to analyse. Although much attention is being given to this problem we are a long way from a well proven analytical method which accounts for the residual stress field.

The importance of the interference stress has been demonstrated by Petrak and Stewart[29] who have shown that increased interference leads to decreased crack propagation. An analytical method has been developed by Grandt[30] from which the stress intensity factor can be calculated for a given stress distribution around the fastener. The possible combinations of interference stress and applied stress are formidable, but even so this appears to be the most promising approach currently available.

4.3 Difficulties associated with the general stress field in the vicinity of the crack

4.3.1 Establishing the general stress field

In many cases it is difficult to establish the general nature of the stress field in the vicinity of the crack component and, for example, in a wing skin with a chordwise crack detailed knowledge of the stress distribution across the wing cross section (in the uncracked state) may not be available, and it may be necessary to assume an average gross or net section stress. This can clearly be a significant source of error. Another area of uncertainty arises when dealing with cracks from covered inspection holes. Large differences in predicted stress intensity factor result from differing assumptions concerning the load carried by the cover plate. The use of the most pessimistic assumption that the cover plate takes no load may be unduly conservative.

4.3.2 Analysis in the presence of a non-uniform stress field

There are a number of solutions available in the handbooks which describe particular crack configurations in linearly varying stress fields. The general case of a crack in an infinite sheet with an arbitrary stress field can be handled without undue difficulty using a Green's Function. However difficulties arise if boundaries are present in the vicinity of the crack. It would be of great value if some modification of the Green's Function approach could be developed to handle such situations, accepting that the solutions might be approximate.

4.3.3 Combined bending and tension

Very few stress conditions which occur in real structures are simple uniaxial uniform tension. In many cases tension is combined with bending. This can occur in a number of ways and can result in a range of combinations from very simple to complex.

Of the examples of combined stress conditions which have been considered, possibly the most simple is the rail mounting of a small lifting surface. The load was applied to a shoulder and resulted in both tension and bending in the shoulder support (Fig.16). Superposition was used to combine bending and tension, with reasonable correlation between experiment and theory. A similar problem occurred with a pressurised vessel with a screwed end cap (Fig.16). Here the situation was complicated by the deformation of the vessel body and the curvature in the plane of the crack. The authors are not aware of any solution for a part through crack of a curved surface subject to bending. Although calculations were made for this component the correlation with a known failure condition was poor. A second pressure vessel problem worthy of attention occurred with an undercarriage oleo which was required to resist bending while pressurised. Here the bending stress varied from tension to compression radially around the section. Calculations could not be checked with a failure condition but, based upon the experience of the previous case, inspection requirements were set which were aimed to err on the side of caution, and could have been over severe.

The above should illustrate the present lack of understanding of how to combine stressing cases. However a further example presents even greater difficulties. The helicopter rotor blade section shown in Fig.17 is subjected to tension due to centrifugal acceleration and also to flap and lag bending. Both bending moments vary with the angle of the blade to the flight direction and are also usually out of phase with each other due to differences in flap and lag damping. Further the flap bending moment decreases as the crack grows since for a given flight condition the blade is at a given deflection and hence the reduced stiffness of the blade leads to a reduced moment. There appears to be no way in which a theoretical prediction can be made for the stress intensity at the tip of the crack. Present efforts are being directed at obtaining an effective stress intensity based upon correlation of crack propagation rate with materials data.

4.3.4 Fastener flexibility

Fastener flexibility can result in substantially increased stress intensity in stringer panels[2]. As yet there is no readily available method for quickly assessing the effects of fastener flexibility for any general stiffened panel. Very little data is available on the degree of flexibility which occurs in practice and the studies which have been published are based on what appear to be arbitrary assumptions. More readily available data on the degree of flexibility which occurs with various fasteners in various situations could lead to a better appreciation of the importance of this problem and hence to better methods of analysis.

4.4 Materials data

4.4.1 Introduction

Turning now to the third area of difficulty in analysis, the type of data required will depend upon the purpose of the analysis. Whether we are interested in strength, propagation or environmental effects, the available materials data will be the decisive factor in application of the analysis. Such data as becomes available is collected in various handbooks[31-33]. However the number of variables which have to be covered is prohibitive and much of the data which is required is not available. There are however particular problems in interpretation of data in both the strength and crack propagation fields.

4.4.2 Fracture strength K_c - K_{Ic}

Methods of determining K_{Ic} are now well defined but there are still doubts about the determination of K_c. This value depends not only upon specimen thickness but upon width as well. While it may well be possible to determine the variation of K_c with panel width it is by no means clear what specimen width equates with a stiffened panel.

Many of the cracks which occur in aeroplane structures and components are neither pure plane strain nor pure plane stress but are part way between these two extremes. Most data is for K_{Ic}, usually obtained from compact tension test pieces, and for K_c, often for centre cracked panels. There is a need for some means, as yet undefined, of combining these two sets of data which are not strictly comparable, to give an indication of fracture toughness at any thickness desired.

4.4.3 Crack propagation

Given a set of data describing crack propagation rate variation with stress intensity at a constant stress amplitude, the calculation of crack propagation for specified constant stress amplitude cycles can be attempted with reasonable confidence. This is not necessarily true where the stress amplitude varies from cycle to cycle. Broek has discussed the various theories which predict crack propagation under varying stress cycles[34]. No one method consistently predicts life reliably, but all appear to be accurate under particular, but different, conditions. Compressive loads in the spectrum are not accounted for although these can be detrimental for some materials.

Analysis of the propagation of the crack shown in Fig.15 has emphasised the problem in life prediction when the crack propagates in steps due to what appears to be static failure contained within the volume of the material. This has been examined by Forsyth[35] who has concluded that the jumping of the crack front is associated with a critical ratio of length of crack front to the length between the crack tip and the origin. This type of crack propagation has also been observed under constant amplitude loading (Fig.18).

The reasons for this behaviour are not understood and the implications to fracture strength and critical crack length under a variable amplitude spectrum give rise to concern. In the absence of a better understanding there is a strong emphasis on finding cracks which occur in service aeroplanes before crack front jumping occurs. In the case of the countersunk hole in Fig.15 this requires that the crack be found while still under the rivet head.

4.5 Conclusions

The problems discussed are a few of those which have proved the most difficult to resolve with the objective of keeping service aeroplanes flying safely. Those which have been mentioned are by no means exhaustive. While fracture mechanics techniques are undoubtedly helping to keep aeroplanes in service, where uncertainties in analysis occur flying restrictions or inspection requirements are based on pessimistic assumptions. Advances in resolution of these problems would lead to more efficient operation.

5. CONCLUDING OBSERVATIONS

In this paper a broad indication has been given of the part that fracture mechanics analysis has played in recent years in relation to the design testing and operation of aircraft in the United Kingdom. The objectives of writing this paper were two-fold. Firstly, to share with others our general experience in this field and, secondly, to identify areas where our knowledge is inadequate and further work is required. Areas which have been highlighted as requiring further attention include the following:

(a) effects of curvature in pressure cabin design

(b) methods of predicting approach to crack instability in residual strength tests

(c) variability in crack propagation rates and associated scatter factors

(d) standard solutions for stress intensity factor predictions relating to: pin-loaded holes (including lugs), feather-edge holes, interference fit pins

(e) fastener flexibility effects in stiffened panels

(f) prediction of stress intensity factors in non-uniform stress fields

(g) materials data - particularly on K_c and on crack propagation rates

(h) improved models for estimating crack growth retardation effects.

It is evident that whilst fracture mechanics analysis has contributed greatly to our capability of handling the overall fatigue problem in aircraft structures, the full potential has not yet been realised and much remains to be done to improve our analytical capability.

SYMBOLS

a	half crack length
A	cross sectional area
b	stringer pitch
C	curvature correction factor
C_l	correction to the stress intensity factor to account for stringers, cutouts etc.
C_f	coefficient in crack propagation equation
C_T	correction factor to account for thermal loading
d	fastener diameter
E	Young's modulus of elasticity
h	fastener pitch between two lines of fasteners in a stringer
K	stress intensity factor
K_c	plane stress fracture toughness
K_I	opening mode stress intensity factor
ΔK	range of stress intensity factor
m	exponent in crack propagation equation
N	number of cycles
p	fastener pitch along length of stringer
R	ratio, minimum to maximum stress in cycle
R_c	radius of curvature
S	stress (gross)
t	thickness
x,y	cartesian coordinates
α	ratio of stress parallel and normal to crack
β	empirical constant
δ_{int}	total separation of crack surfaces at distance y from crack tip
ε_{x0}	strain ahead of crack along $x = 0$
λ	shell parameter
μ	$\frac{A_{st}}{A_{sk} + A_{st}}$
ν	Poisson's ratio
σ	stress (gross)
$\Delta\sigma$	stress range

Suffices

sk	skin	crit	critical
st	stringer	fract	fracture

Acknowledgments

The authors wish to thank their colleagues in Industry, and elsewhere, who have contributed to the preparation of the paper. In particular their thanks are due to:-

R.F.W. Anstee - RAE, Farnborough
D.J. Cartwright - University of Southampton
D.F.G. Cash - HSA, Kingston
A. Jefferson - BAC, Filton
J.A.B. Lambert - HSA, Hatfield
M. Miller - BAC, Filton
A.K. Redfern - HSA, Woodford
J.S. Williams - HSA, Kingston

REFERENCES

1 Poe, C.C.: "Stress-intensity factors for a cracked sheet with rivetted and uniformly spaced stringers", NASA Tech. Rep. R-358 (1971)

2 Swift, T.: "The effects of fastener flexibility and stiffener geometry of the stress intensity in stiffened cracked sheet", Douglas Paper 6211, presented at Conference on Prospects of Fracture Mechanics, Delft, June 1974

3 Cartwright, D.J.: Private communication, May 1976

4 Cash, D.G.F.: "Fracture analysis of stiffened aircraft structures using closed form solutions", HSA-KGT-N-GEN-00443, November 1975

5 Folias, E.S.: "The stresses in a cylindrical shell containing an axial crack", Report No. ARL 64-174, Aerospace Research Laboratories, Wright-Patterson Air Force Base, Dayton, Ohio (1964)

6 Folias, E.S.: "A circumferential crack in a pressurised cylindrical shell", Int. J. Fracture Mechanics, Vol.3, pp.1-12 (1967)

7 Erdogan, F., Kibler, J.: "Cylindrical and spherical shells with cracks", Report under grant No. NGR-39-007011, Lehigh University, Bethlehem, Pa (1968)

8 Erdogan, F., Ratwani, M.: "Fatigue and fracture of cylindrical shells", Int. J. Fracture Mechanics, Vol.6, pp.379-392 (1970)

9 Copley, L.G., Sanders, J.L. Jr.: "A longitudinal crack in a cylindrical shell under internal pressure", Int. J. Fracture Mechanics, Vol.5, pp.117-131 (1969)

10 Kuhn, P.: "The prediction of notch and crack strength under static or fatigue loading", Preprint No.843C, presented at the SAE - ASME Air Transport and Space Meeting, New York, April 1964

11 Anderson, R.B., Sullivan, T.L.: "Fracture mechanics of through-cracked cylindrical pressure vessels", NASA TN D3252 (1966)

12 Crichlow, W.J., Wells, R.H.: "Crack propagation and residual static strength of fatigue cracked titanium and steel cylinders", Fatigue Crack Propgation, ASTM STP415, Am.Soc.Testing, Materials, pp.25-70 (1967)

13 Hahn, G.T., Sarrate, M., Rosenfield, A.R.: "Criteria for crack extension in cylindrical pressure vessels", Int. J. Fracture Mechanics, Vol.5, pp.187-210 (1969)

14 Duncan, M.E., Sanders, J.L. Jr.: "The effect of a ring stiffener on the stress in a cylindrical shell with a longitudinal crack", Harvard University Report No.SM-13 (1967)

15 Forman, R.G., Kearney, V.E., Engle, R.M.: "Numerical analysis of crack propagation in cyclic loaded structures", Trans. ASME, J. Basic Engineering, Vol.89, p.459 (1967)

16 Hickson, V.M.: "A replica technique for measuring static strains", Journal of Mechanical Engineering Science, Vol.1, No.2, p.171 (1959)

17 Schijve, T., de Rijk, P.: "The fatigue crack propagation in 2024-T3 Alclad sheet materials from seven different manufacturers", NLR-TR M2162 (1966)

18 Mukherjee, B., Burns, D.J.: "Regression models for the effect of stress ratio on fatigue crack growth rate", (ASTM 74 Annual Meeting 1971) ASTM STP 511

19 Jacoby, G.H., Nowack, H.: "Comparison of scatter under program and random loading and influencing factors" (ASTM 74 Annual Meeting 1971) ASTM STP 511

20 Jost, G.S., Esson, C.P.: "Fatigue of D6ac steel specimens - means and variables under programmed loading", ARL Materials and Structures Report 349 (1974)

21 Rooke, D.P., Cartwright, D.J., Davis, Elizabeth: "Stress intensity factors for cracks in stiffened sheets", RAE Technical Report 75072 (1975)

22 Anon: "Design requirements for service aircraft", AvP 970

23 Sih, G.C.: "Handbook of stress intensity factors for researchers and engineers", Institute of Fracture and Solid Mechanics, Lehigh University, Bethlehem, Pennsylvania (1975)

REFERENCES (concluded)

24 Tada, H., Paris, P., Irwin, G.: "The stress analysis of cracks handbook", Del Research Corporation, Hellertown, Pennsylvania (1973)

25 Rooke, D.P., Cartwright, D.J.: "Compendium of stress intensity factors", Her Majesty's Stationery Office, London (1976)

26 Cartwright, D.J., Rooke, D.P.: "Approximate stress intensity factors compounded from known solutions", Engng. Fracture Mechs., 6, pp.563-571 (1974)

27 Cartwright, D.J., Ratcliffe, G.A.: "Strain energy release rate for radial cracks emanating from a pin loaded hole", International Journal of Fracture, Vol.8, No.2 (1972)

28 Shah, R.C.: "Stress intensity factors for through and part through cracks originating at fastener holes", 8th National Symposium on Fracture Mechanics, Brown University, Providence, RI (1974)

29 Petrak, G.J., Stewart, R.P.: "Retardation of cracks emanating from fastener holes", Engineering Fracture Mechanics, Vol.6, pp.275-282 (1974)

30 Grandt, A.F.: "Stress intensity factors for some through cracked fastener holes", International Journal of Fracture, Vol.11, No.2 (1975)

31 "Damage tolerant design handbook", MCIC-HB-01 Air Force Materials Laboratory, Wright Patterson Air Force Base, Dayton, Ohio (1972)

32 "Fatigue data series, Vol.4", Engineering Sciences Data Unit, London (1976)

33 Liebowitz, H. (Ed.): "Agardograph No.176, Fracture Mechanics of Aircraft Structures

34 Broek, D.: *Ibid.*

35 Forsyth, P.J.E.: "The causes of mixed fatigue/tensile crack growth and the significance of microscopic crack behaviour", RAE Technical Report 75143 (1976)

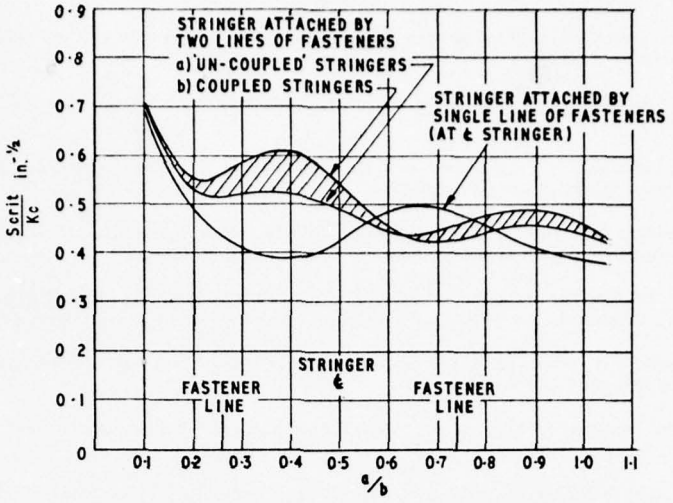

Fig.1 Influence of stringers attached by two lines of fasteners on the residual strength of panel with 'mid-bay' crack

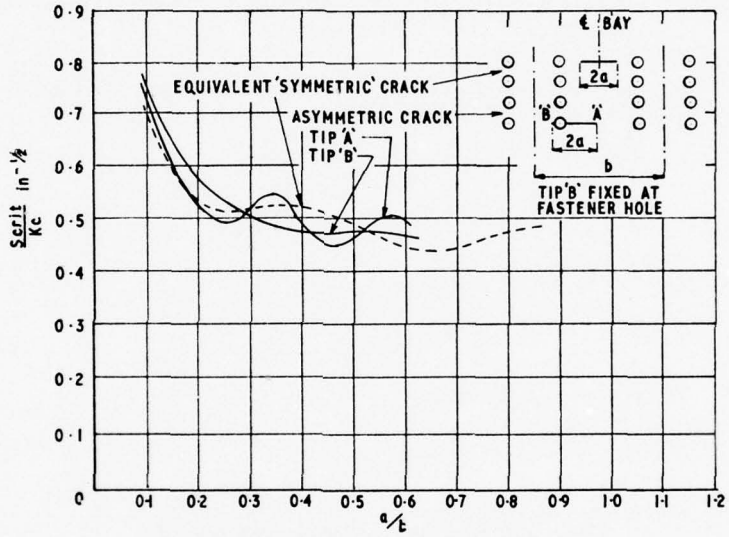

Fig.2 Residual strength of panel containing an asymmetrical crack relative to the stringers

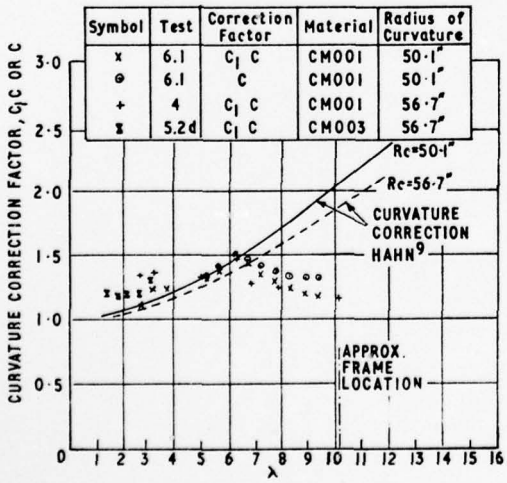

Fig.3 Curvature correction factor for an axial crack midway between frames based on fatigue crack propagation data

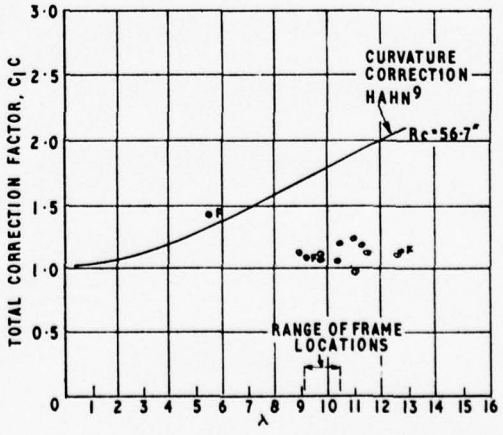

Fig.4 Curvature correction factor for an axial crack midway between frames based on residual strength data

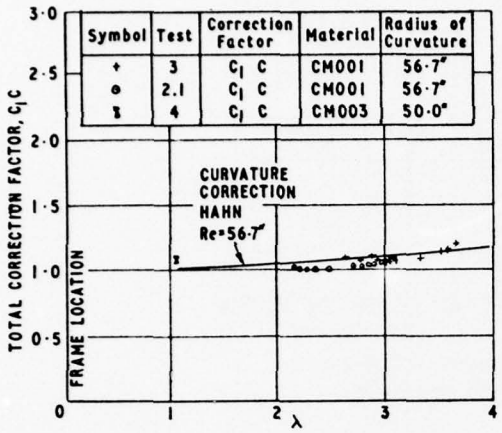

Fig.5 Curvature correction factor for an axial crack growing away from a broken frame based on fatigue crack propagation data

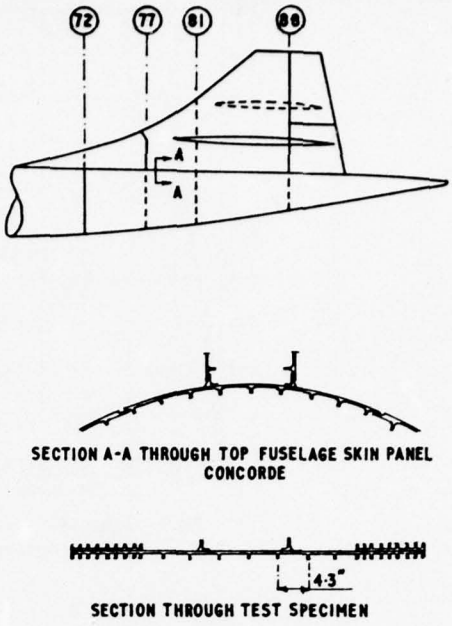

Fig.6 Comparison between Concorde and test specimen

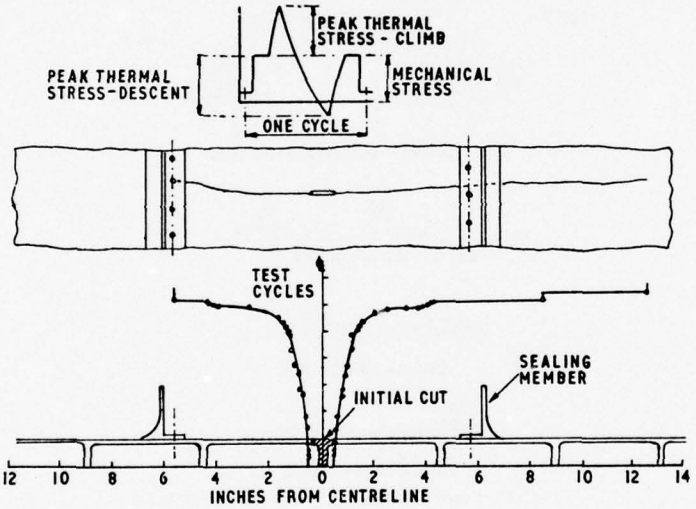

Fig.7 Details of crack propagation

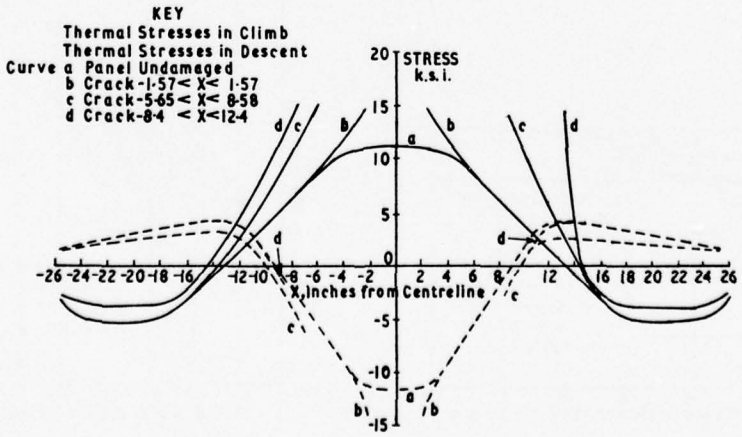

Fig.8 Distribution of peak thermal stresses across test panel

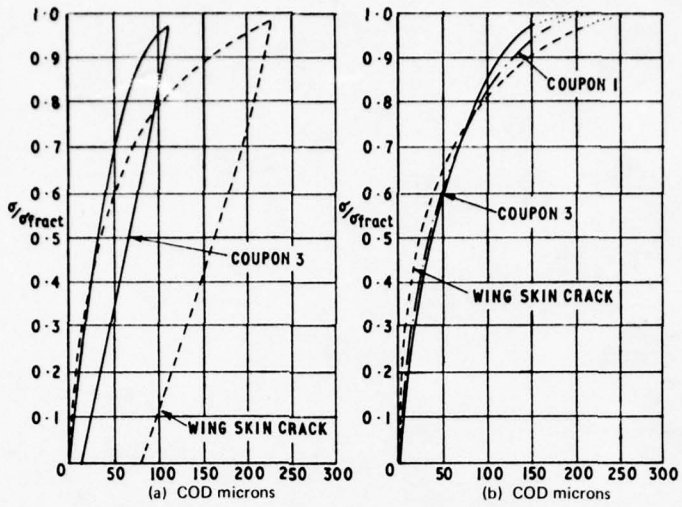

Fig.9 Curves of crack opening displacement (COD) against σ/σ_{fract} for coupon and aircraft wing skin tests

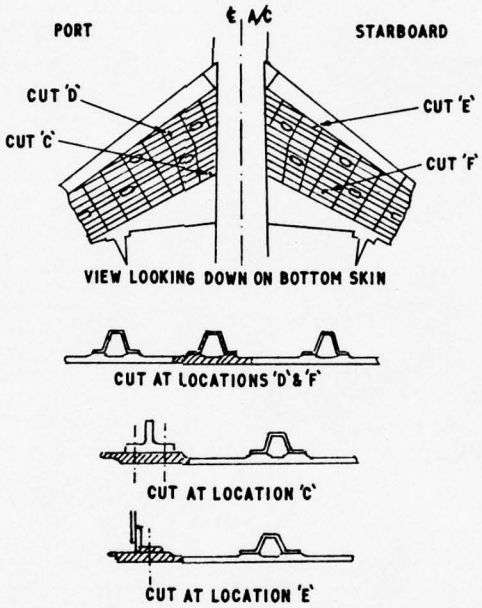

Fig.10 Location of cuts in lower surface of wing

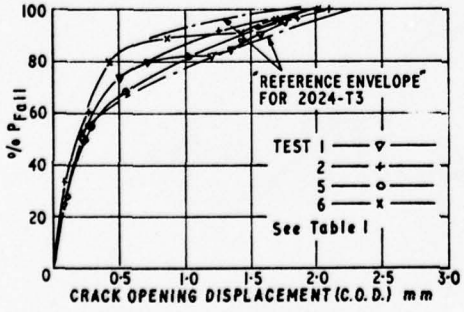

Fig.11 COD values from Airbus test panels

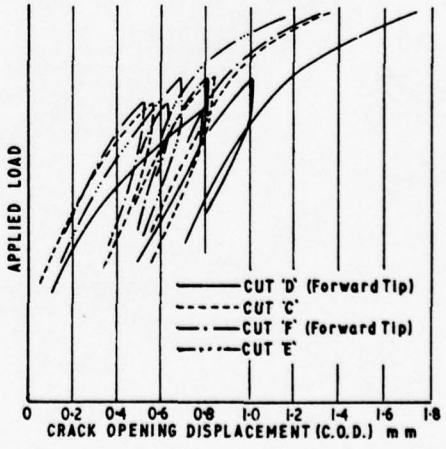

Fig.12 COD values from Trident wing tests

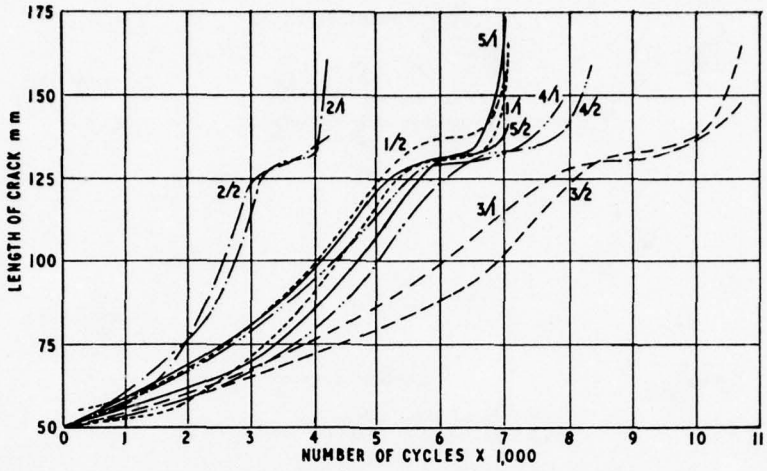

Fig.13 Crack propagation in Concorde machined panels

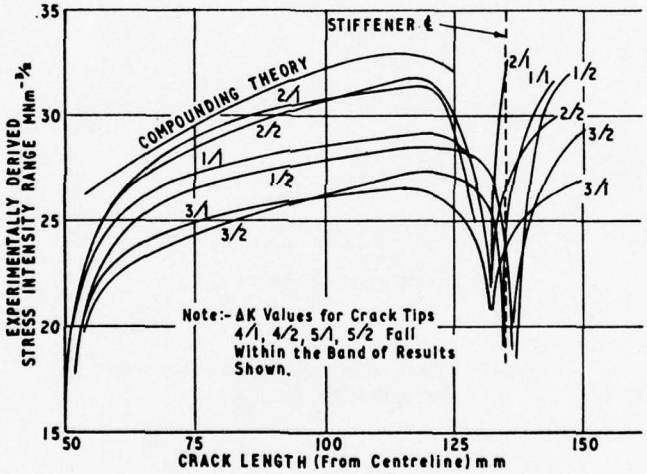

Fig.14 Variation of experimentally derived ΔK with crack length

Fig.15 Crack growth from feather edge

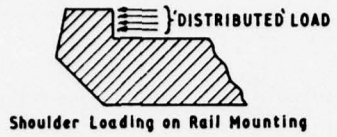

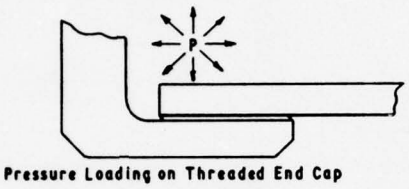

Fig.16 Examples of combined bending and tension loadings

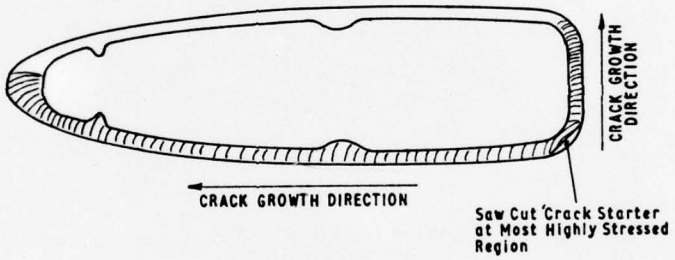

Fig.17 Typical helicopter rotor blade cross section after fatigue test

Fig.18 Crack 'jumping' -- constant amplitude loading

CONTRIBUTED DISCUSSION

by

John W.Bristow
Civil Aviation Authority – Airworthiness Division
Brabazon House
Redhill, Surrey RH1 1SQ
England

The Paper covers a wide range of topics, some of the key points are reviewed under three headings:

1. TEST AND ANALYSIS OF WING STRUCTURE
2. TEST AND ANALYSIS OF FUSELAGE STRUCTURE
3. MATERIALS BEHAVIOUR

The views expressed below are those of the author personally and are not of necessity those of the Civil Aviation Authority.

1. TEST AND ANALYSIS OF WING STRUCTURE

The refinements to the original stiffened sheet model of, crack assymetry, fastener flexibility, stiffener offset and allowance for unequal space fastener rows are encouraging. However, there remains the difficulties of correlation with the wing structure tested which appear to lie in three areas

(i) the analysis used
(ii) the final failure mode and loads
(iii) materials toughness data.

Item (i) appears to be covered by the refinements cited. Item (ii) and (iii) could be resolved if some way could be found to continue the test to failure, perhaps just in the localised areas of the test cuts, and also to establish materials data from those areas. There is a lack of published test data on the failure of real aircraft wing structures containing cracks to provide a yardstick for new methods of analysis. It will be a pity if no way can be found to establish the missing links in this case.

The two different methods of crack tip measurements (COD) presented both show promise as a useful testing tool to predict conservatively the onset of failure. Their empirical nature appears to preclude the read-across of actual COD values from one structure type to another.

2. TEST AND ANALYSIS OF FUSELAGE STRUCTURE

Several analytical predictions of the effect of curvature imply even greater correction factors than the empirical correction due to Hahn shown in this Paper. This supports the claim that analytical correction methods at present available are inadequate to represent realistic cracks in fuselage structures.

It is interesting to note that some published test results by Swift (ref. 1) for longitudinal crack in fuselage shells indicate correction factors around 1.4, at values about 7, which are very similar to the results presented as in the Paper figures 3 and 4.

Two cases are made in the Paper for simplified representation of pressurization, thermal and bending loads. Two notes of caution are raised in this context as points for discussion -

(i) For crack propagation analysis, 60% of the compression loading was considered to be effective; whereas crack closure up to significant tension loading was reported in another test.

(ii) In the static situation equivalence of an overall increased bending moment to pressurization, thermal and bending loads is demonstrated. However, should crack growth occur during such a test it is not clear whether such equivalence could be read-across to the dynamic situation.

3. MATERIALS BEHAVIOUR

There are several references in the Paper to the presence of yielding in the vicinity of the crack tip. Refinement in analysis techniques to predict failure will of necessity include such effects and materials data and will be required in parallel with this. There is little to be gained from chasing valid toughness values, if failure occurs by a yielding mechanism.

The results of the crack propagation tests on full scale aircraft panels show that the known, but little publicised, scatter found in small scale materials test coupons occurs in full size structure also. At a first glance the scatter appears to be wider than observed previously. Typically for aluminium alloys, e.g. data from reference 2 show maximum to minimum scatter factors of between 3 and 5 compared with a factor in excess of 6 proposed here. These results are significant because the establishment of reliable crack propagation rates, to determine inspection periods, is a fundamental part of modern "fail safe" design.

4. CONCLUSIONS

The items for further attention highlighted at the end of the Paper are all certainly worthy of further study. Two points are suggested as an augmentation to the list.

Item (b) might usefully include the effects of the onset of yielding which are likely to occur before failure of multi-element structures, built in high toughness materials.

Item (f). A specific case of non-uniform stress field requiring attention is the crack extending both in wing spar web and in wing skin simultaneously.

The latter type of cracking is known to have been the cause of aircraft structural failure in service, reference 3, and the prevention of such failure is surely the motivation behind the use of applied fracture mechanics in aircraft design.

It is of comfort to note that whereas complete correlation between test and analysis has not always been achieved, conservative predictions of the behaviour are made by the methods employed.

REFERENCES :

1. SWIFT T. ASTM. STP. 486 pp. 164-214 (1971)
2. HAHN C.T. and SIMON R. Eng. Fract. Mech. Vol. 5, p. 530 (1973)
3. NTSB - AAR - 75-5.

CONTRIBUTED DISCUSSION

by

Dr.-Ing. Walter Schütz
Industrieanlagen-Betriebsgesellschaft mbH
Einsteinstrasse, 8012 Ottobrunn, Germany

1. INTRODUCTION

Looking through the enormous amount of literature on fracture mechanics one almost exclusively finds the following:

- Materials data in the form of K_{Ic} or K_c, determined with standardized specimens
- Constant amplitude crack propagation data, mostly on small, unstiffened uncurved sheet specimens with center cracks, some on thick specimens with half-elliptical cracks or on standardized (CT-) specimens
- Theoretical or experimental K-solutions for simple crack shapes.

Not all questions have been solved for these relatively simple problems. For example, the scatter of fracture toughness within one heat of material and expecially between different heats can only be determined by a large number of fracture toughness tests and not by calculations or metallurgical investigations. However, the real test for fracture mechanics is: Will it correctly predict the residual static strength of cracked structure as well as its crack propagation behaviour under the more or less random service loads? So the designer actually needs the following data:

- Fracture toughness of typical components and structures, be they integrally or differentially stiffened curved shells or machined and unmachined forgings and a comparison with the fracture toughness of standardized small specimens of the same material.
- As above, under bi-axial stresses
- Crack propagation under realistic flight-by-flight load sequences of such components and structures
- K-solutions for such components and structures with service like crack shapes (for example, multiple cracks under the rivet heads of a pressure cabin).

On these problems, very few data are available in the literature, partly because of theoretical difficulties, partly because of the enormous costs involved.
What is more, some of these data are contradictory or even demonstrably wrong.

2. RESULTS AND DISCUSSION

The paper discussed here fills a gap in our knwoledge because it sums up the experience of two aircraft firms and one government agency on the applications of fracture mechanics to aircraft structural problems, that is, it attacks the actual problems as discussed in the introduction:

The many practical problems facing the designer who tries to apply, for example, one of the models for stiffened structure to his peculiar structure which always differs from the model one, are first discussed, then the assumptions used to make the real structure fit the model one are presented, subsequently the results of the test(s) and the reasons for the departure (if any) from the prediction are given. Finally, work in the U.K. and elsewhere to correct these deficiencies is described. To this discussant, the last two points alone already make this paper a "bonanza" for any engineer applying fracture mechanics to real structure.

Another subject treated in the paper is crack growth under mechanical and thermal stress cycling. It was shown (by test) that a thermally generated stress is less damaging than a mechanically applied stress.

The many other topics covered in the paper cannot be discussed here, they are, for example:

- COD-measurements for measuring the onset of unstable crack growth
- scatter of crack propagation in large integrally machined panels
- problems in service
- materials data (K_{Ic} - K_c)

The paper concludes with an enumeration of the many problems which are still unsolved.

3. CONCLUSIONS

This discussant considers the paper at very important contribution to the meeting (and to the planned AGARDograph as well)

- for the many practical problems discussed
- for the analytical and experimental solutions to these problems and, last not least,
- the clear and easily understandable way in which they have been presented.

CONTRIBUTED DISCUSSION

by

Derek Eccles
Deputy Company Co-ordinating Engineer
(Structures Research)
Hawker Siddeley Aviation Ltd
Kingston-upon-Thames
Surrey, UK

1. INTRODUCTION

The joint BAC/HSA/RAE contribution reports on UK applications of Fracture Mechanics on three fronts, viz. in damage tolerance design, in verification testing and in service damage analysis. This discussion reviews the progress and problems in applied Fracture Mechanics revealed by the various papers and highlights the research implications.

2. DESIGN PROBLEMS

2.1 Wing panels

The HSA paper on stiffened wing panels indicates encouraging progress in extending the method of direct closed-form solution (as distinct from FEM analysis) to include the configurational detail of typical skin/stringer wing panels. Whilst significant advances have been made and further developments are in hand there is clearly a need for test substantiation, either of the K solutions themselves or of associated predictions of panel residual strength

The verification of K solutions by the correlation of stiffened panel and plain panel crack propagation results (ΔK v. $^{da}/dN$) is a recognised method. However, as regards residual strength prediction, the problems introduced by the slow stable tear characteristics of the high-toughness aluminium alloys typically used in wing tension skins remain unresolved. An appropriate, test-substantiated analysis is required (possibly the "energy balance" approach, using material R-curve data and panel G-curves derived from the elastic K solutions). It should be noted that the curves of "residual strength" in Figs. 1 and 2, expressed as S_{crit}/K_c, only strictly apply to a material exhibiting no pre-fracture ductility.

To sum up it is suggested that the reported progress in deriving K solutions for practical wing panels should be complemented by a corresponding effort on the problems of residual strength prediction. In view of the general complexities of stiffened panel analysis and the problems of scatter in material properties it would seem advisable to proceed by a systematic step-by-step analysis/test programme in order to clearly disassociate the various effects.

2.2 Pressure cabin design

The section on pressure cabin fracture problems clearly indicates the limitations of available stress intensity solutions for pressurised cylinders in relation to typical aircraft pressure cabins with frames and stringers.

BAC presents test-derived "total correction factors" which relate values of K deduced from stiffened cylinder test results to analytical K solutions for uniaxially-loaded, plain, flat panels. These "total" factors are compared with Hahn's curvature correction factors for unreinforced pressure cylinders, revealing both significant disparities and unexplained correlations. The problem with this approach is that no rational interpretation of the "total" effect is possible in terms of its constituent parts since so many geometric, loading and materials effects are simultaneously involved. It is therefore impossible to derive K solutions for other cylinder geometries.

The value of the above exercise is that it re-emphasises the inadequacies in our detail knowledge of the fracture mechanics of pressure cabin structures, as distinct from the working knowledge of the performance of the total structure gained from test experience.

It is evident that the absence of an analytically-founded design procedure and the consequent limitations in detail understanding of the fracture mechanics of pressure cabins must limit the efficiency of the damage tolerance design process. Research to remedy this situation would appear essential to the refinement and evolution of pressure cabin design.

The complexities in pressure cabin fracture mechanics introduced by the frames and stringers suggest the merit of an indirect attack on the problem via the analysis and test of flat panels (of fuselage-type skin/stringer/frame construction) in conjunction with the testing of actual cylindrical structures. This three-pronged attack commends itself as a near-term approach to the development of

a design rationale. The development and substantiation of a direct analysis of the stiffened cylinder problem (possibly by FEM analysis) would appear to be a much longer term possibility.

3. TESTING

3.1 COD monitoring

HSA presents two examples of the application of COD methods to monitor the imminence of fast fracture in full-scale aircraft structures. These examples, relating to Vulcan and Trident wings respectively (with reference also to A300B wing panel tests), illustrate the problems in interpreting COD readings from complex structures in relation to control data from coupon specimens.

An interesting difference between the work on Vulcan and on A300B is that on the Vulcan it was found necessary to base the fast fracture predictions on numerous parameters from the COD tests, whereas in the A300B work a single parameter, (maximum pre-failure COD), reportedly gave a good indication of crack instability for a wide variety of crack locations, crack lengths and stress levels. A speculative interpretation of this might well include the differences in materials (DTD 687 in Vulcan, 2024-T351 in A300B), in test techniques (replicas in Vulcan, clip gauges in A300B) and in crack sizes (significantly longer in A300B). Further basic work is needed to resolve these points.

The COD applications in the Trident wing tests demonstrated the value of this technique in indicating the relative criticality of several co-existent cracks by reference to the COD ranking order, which stabilises at higher loadings. These Trident tests served incidentally to re-emphasise the inadequacy of existing analytical methods of residual strength prediction for wing panels.

The overall conclusion from the reported work is that the COD technique provides a very useful means of monitoring crack behaviour during full-scale testing. The recorded data may be used to give a generally conservative prediction of residual strength and to indicate the relative criticality of damage. Further investigation is recommended to resolve problems of interpretation and thereby increase the value of the method.

3.2 Simplified testing of pressure cabin structure

The BAC paper on the use of a simplified, mechanically-loaded test panel as an economic alternative to a fully representative, cylindrical test specimen raises the obvious question of the validity of such a procedure. BAC acknowledges that the mechanical application of an additional longitudinal stress to the panel specimen (to simulate the pressure-induced and thermally-induced longitudinal stresses in the cylinder) and the omission of applied hoop loadings results in greater longitudinal strain and greater crack tip K values than in the cylinder. The K values are however deduced from equations which take no account of the relieving effect of hoop stresses and hence the panel test will be more conservative (more severe) than indicated by the calculated K ratio.

A further point, stemming from the BAC work on crack growth under mechanical and thermal cycling (Section 2.2.2 of this paper), is that the simulation of thermal stresses (derived from intact cylinder strain gauging) by mechanically applied stresses in the saw-cut panel ignores the phenomenon of the relieving effect of a crack under thermally generated stress conditions. This introduces a further element of severity into the simplified test.

The absence of differential pressure and the associated crack bulging action in the panel test is an element of difference from the cylinder test which might have been anticipated to be less significant for circumferential cracks than longitudinal. However the reported antisymmetric relative deflection mode between the crack lips in a cylinder under combined pressure and bending (implying a Mode III tearing effect) suggests a significant deficiency in the panel test.

The above arguments suggest the inadequacy of an evaluation of the proposed simplified test method based on the derived K values alone. Despite the apparent conservatism of the panel test a demonstration of the relative crack propagation performance and/or residual strength of the two systems would appear essential for a reliable judgement.

3.3 Scatter in panel crack growth rates

The RAE work on crack propagation in integrally machined panels in the Concorde programme gives a useful appreciation of the scatter effect under uniaxial loading conditions. The distribution of results shown in Fig. 13, three sets in a close band and two sets more remotely spaced, illustrates the importance of adequate sampling.

A comparison of the theoretically-derived curve of ΔK v. a and the scatter band of test-derived values in Fig. 14 indicates the problem of verifying calculated stress intensity solutions in absolute terms via crack propagation testing, but also shows that the general shape of the predicted curve is confirmed in this instance.

It would be interesting to see the results of equivalent tests under biaxial loading to determine the effect on crack propagation scatter of the fuselage hoop tension loading. Furthermore, in the light of the foregoing comments on simplified testing procedures (see 3.2), a comparison of crack propagation rates from the flat panel test and the cylinder test work would be instructive.

4. PROBLEMS IN SERVICE

The final paper discusses the various "unknowns" which inhibit the application of fracture mechanics to the solution of many problems arising in service. The following comments are offered:-

4.1 Stress intensity solutions

The paper emphasises the inadequacy of available K solutions for practical hole/pin problems, which may be further complicated by the presence of interference-induced stresses. A fundamental requirement in the derivation of such solutions is the shape of the crack front during crack growth, an important case being the transition from a hole-edge, corner crack to a "through-the-thickness" crack. In the treatment of such problems, as found in lugs, plates and fittings, it would appear essential to determine the typical crack front morphology by experimental means, e.g. by *fractographic analysis*.

4.2 Residual strength analysis of part-through, hole-edge fractures

Having determined a range of K solutions corresponding to practical crack geometries in the "part-through" crack regime, there remains the problem of predicting residual strength when there is a variation in K around the fracture surface boundary, i.e. of determining the failure criterion in terms of some reference K value and some material toughness property (K_c appropriate to section thickness and crack front orientation). This problem, which appears to have received little attention, is clearly in need of research effort.

CONTRIBUTED DISCUSSION

by

H.E.Parish
British Aircraft Corporation Limited,
Military Aircraft Division,
Warton Aerodrome,
Preston PR4 1AX,
Lancashire,
England.

1. INTRODUCTION

The paper deals with fracture mechanics problems under three headings, namely, design, testing and service problems. A topic has been selected in each category and commented upon, location in the main paper being shown after the subject heading.

2. DESIGN

2.1. Effect of compression (para. 2.2.2.)

It is not unusual for the compressive cycle to be neglected in crack propagation predictions although work has been reported which shows that compressive overload nullifies the retarding effect of tensile overload. This assumption may be more appropriate for the military combat aircraft than to a civil transport, largely because the military spectrum is in the positive g regime with little overshoot on returning to level flight. On the other hand the civil transport is more influenced by its symmetric gust spectrum.

The paper reports the results of six panels tested under thermal cyclic loading only and concludes that the results conform with an equation of the Paris form,

$$\frac{da}{dN} = C_f \Delta K^m$$

in which ΔK represents the stress intensity range where only 60% of the compressive stress is considered effective.

Since it is stated that the thermal cycle is the largest contributor to crack propagation why was an equivalence sought between thermal tension cycling and thermal tension-compression cycling? This has apparently led to a stress intensity range in which 60% of compression is considered effective. Without seeing the test results, one wonders why coefficients could not be derived in the Paris equation that would account for the true stress range.

2.2. Combination of Mechanical and Thermal Cycling (para. 2.2.2.)

Comparisons have been made using Forman's Equation (6) derived at room temperature for mechanically applied stresses and Equation (8), derived from test panels subjected to thermal loading only, but used for combined mechanical and thermal stresses. The good agreement between prediction and test confirms the statement that the thermal cycle is the dominant term.

However, further work is reported using Equation (6) to predict the life, whilst subjected to a peak stress, equal in magnitude to the combined thermal and mechanical stresses and with R = 0. This prediction showed only half the life of the thermally cycled test panels but it used a crack growth equation that was derived at room temperature. Would the comparison of crack growth life be so different if Equation (6) had been produced at constant elevated temperature?

3. TESTING

3.1. Simplification of combined loading (para. 3.2)

The objective of trying to simplify complex loading is sound, when one considers the economics of testing.

In this case measurements were made to equate axial stresses due to pressure and thermal loading with that for a simple bending condition. It would appear that a 46% bending increment fulfilled this purpose but the simplified loading resulted in strains normal to the crack being greater under augmented bending than under combined loading, presumably because the effects of hoop loading were not represented in the bending measurement.

It is stated that after deriving K_1 from measurement and Westergards stress function, it was found that K_1 under augmented bending was greater than under combined loading, which follows the same pattern as the strain measurements.

Has any attempt been made to apply a correction to the simplified bending case to allow for hoop effects?

As a second point in this section, radial deflections were measured at the crack lips and apparently followed an antisymmetric pattern which is rather surprising since the loading is symmetrical and one would expect the pressure loading to maintain symmetry. However, since asymmetry took place did this result in a mixed mode failure combining Modes 1 and 3?

3.2. Scatter in fatigue crack growth (para. 3.3)

The results in Table 2 show that the scatter in crack growth is largest when the crack tip is in the mid bay position but the value of most interest would be the scatter when propagating from the starter position to the next stringer. On this basis a factor of 2.5 appears reasonable. The quoted standard deviation of 0.176 in Av.P.970 is, I believe, more relevant to the crack initiation phase than to propagation.

The proposition that multi-element structures should retain a factor of 3.33 raises an interesting point. Each of the factors is derived on the basis that 3 standard deviations is the accepted probability of failure. If however, the monolithic structure is not fail safe but the multi element one is, then should not these structural concepts have different acceptable probability levels in which case the factor for multi-element may not require to be larger than monolithic structure.

4. SOLUTIONS FOR STRESS INTENSITY FACTORS

4.1. Pin loaded holes (para. 4.2.1)

Section 4.2.1. notes that stress intensity factors due to Shah (1) and Cartwright (3) for pin loaded holes differ by a factor of 2. These solutions are plotted graphically in figure 1 together with a third published solution for an attachment lug. The solutions have been re-arranged and plotted in a common (bearing stress) format. It would appear from the figure that the authors have compared Shah with Cartwright's solution for $2R/W = 0.5$, a typical lug geometry, where in fact a difference of at least 2 exists between them. However, Cartwright's solution for $2R/W = 0.25$ is much closer to Shah's solution. A further point is that the solution by Aberson (2) for a lug is approximately 50% greater than Cartwright's ($2R/W = 0.5$) solution. B.A.C. have pointed out these variations in the three solutions to Dr. Cartwright of Southampton University (4). Cartwright has suggested (5) reasons for the differences which were amplified in (6). The following is a summary of references (4 - 6).

(1) Differences between Shah's (1) solution and Cartwright's solutions for $2R/W = 0.25$ and 0.5 are caused by differences in $2R/W$ ratios used in each solution. Note that Shah's value of $2R/W$ was $\simeq 0.1$.

For small cracks :-

$$K_1 \simeq K_B \sigma \sqrt{\pi a}$$

where K_B = Bearing stress concentration factor.

for $\frac{2R}{W} \simeq 0.1$ $K_B \simeq 1$
$\frac{2R}{W} \simeq 0.25$ $K_B \simeq 1.2$
$\frac{2R}{W} \simeq 0.5$ $K_B \simeq 2.5$
} From ESDU Data Sheet 65004

Therefore, one would expect K_{Shah} to be 2.5 x less than $K_{Cartwright}$ ($2R/W = 0.5$) and K_{Shah} to be 1.2 x less than $K_{Cartwright}$ ($2R/W = 0.25$) for small crack lengths. This is approximately the behaviour shown in figure 1. The same effect is also to be expected at longer crack lengths since the edges of the strip (or lug) will increase K sooner in the structures with higher $2R/W$ ratios.

(2) Differences between Aberson's (2) and Cartwright's K solution for $2R/W = 0.5$ may be attributed to two further variables. Firstly, Aberson considered a lug ($H/W = 1$) whereas Cartwright considered an infinite strip ($H/W = \infty$). Reduction of H/W from ∞ to 1 will cause a significant increase in stress intensity factor.

Secondly, Aberson assumed an arc of contact of 170° and Cartwright considered an arc of contact of 180°. Reduction of the arc of contact from 180° to 170° will cause a significant increase in stress intensity. Cartwright suggests (5) that the difference in stress intensity between the two solutions is of the same order as the increase in stress intensity due to the variation of H/W and arc of contact.

COMMENT

The above discussion has gone some way to explaining the differences between three published stress intensity factor solutions for pin loaded holes containing through cracks. Since $2R/W$ ratios for lugs are usually about 0.5, the most appropriate stress intensity solution for lugs would seem to be Aberson's (2), however, comparison of the stress intensity factor solutions in figure 1 with published residual static strength data for lugs suggests that Aberson's solution may be excessively pessimistic.

A further problem yet to be solved in lugs concerns actual cracks in service. Since lugs tend to be thick sections, cracks grow as corner flaws rather than through cracks. No stress intensity solution is available for this geometry.

REFERENCES.

(1) R.C. Shah — Stress Intensity Factors for Through and Part-Through Cracks at Fastener Holes. 8th National Symposium on Fracture Mechanics, Brown University, Providence 1974. Also in ASTM STP 590.

(2) J.A. Aberson and J.M. Anderson — Cracked Finite Elements Proposed for Nastran NASA TM X-2893 (1973)

(3) D.J. Cartwright and D.A. Ratcliffe. — Strain Energy Release Rate for Radial Cracks Emanating from a Pin Loaded Hole. Int. J. Fracture Vol.8 p.175 (1972)

(4) R.S. Whitehead — Private communication to D.J. Cartwright. 10.12. 1975.

(5) D.J. Cartwright — Private communication to R.S. Whitehead. 5.1. 1976.

(6) R.S. Whitehead and D.J. Sanderson — An Investigation into the Implications of MIL-A-83444 'Airplane Damage Tolerance Design Requirements'. B.A.C. Report Number SON(P)148. 1976.

COMPARISON OF STRESS INTENSITY FACTOR SOLUTIONS FOR CRACKS AT PIN LOADED HOLES.

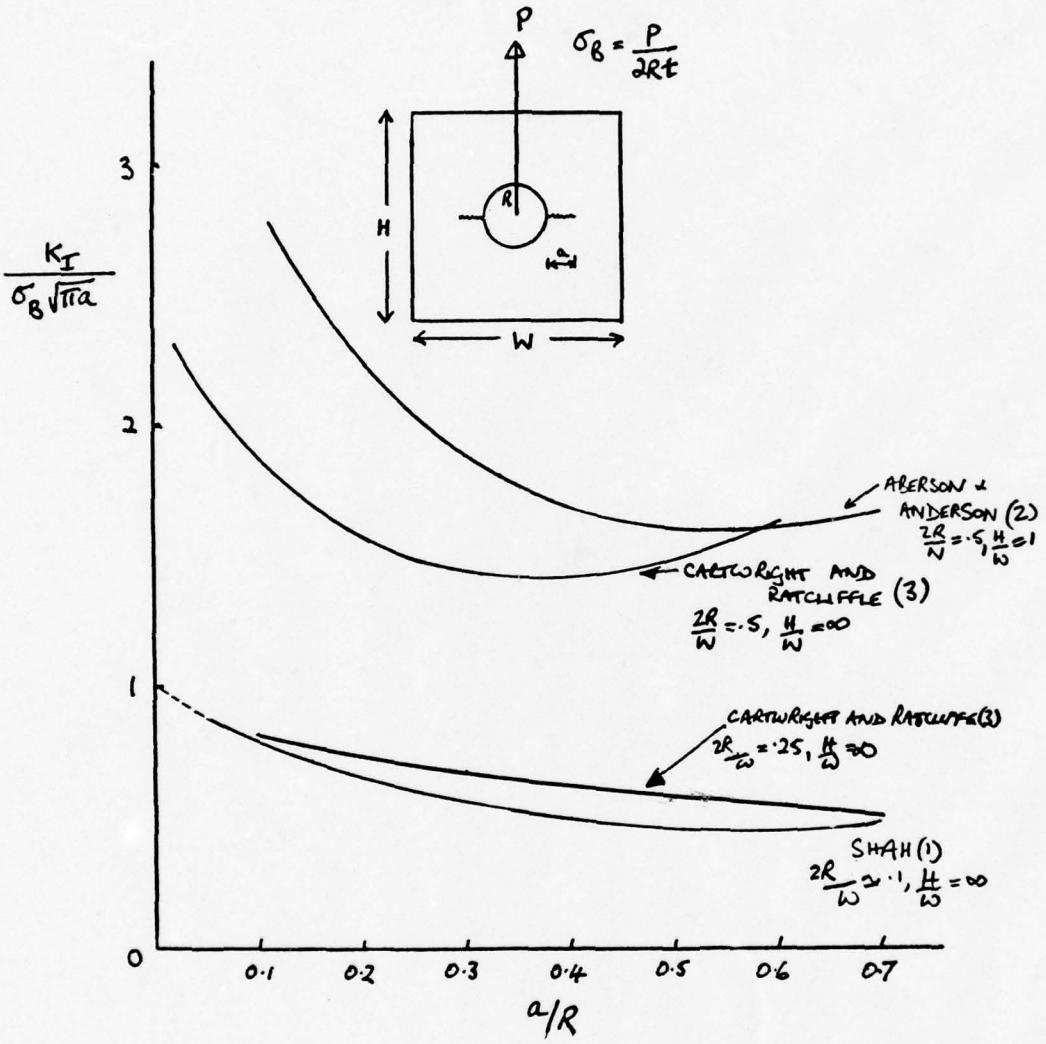

FIGURE 1.

CRACK PROPAGATION AND RESIDUAL STATIC STRENGTH OF TYPICAL AIRCRAFT FORGINGS

by

Dr.-Ing. Walter Schütz

Industrieanlagen-Betriebsgesellschaft mbH
Einsteinstraße, 8012 Ottobrunn, Germany

SUMMARY

Many highly loaded airframe components are dieforgings, whose fatigue, crack propagation and residual static strength properties are therefore of interest to the designer, the certification agency and the operator. Intuitively one might expect that due to, for example, grain flow differences between individual forgings difficulties in predicting the above properties could arise.

So a test program was carried out by the IABG using nose landing gear struts of 7075-T6, manufactured to the same drawings, but forged by several forges in different countries. Cracks were introduced in various sections of the forgings and crack propagation and residual static strength determined by test and compared with calculations:

It was not possible to predict residual static strength with any accuracy even if an ASTM-CT-specimen was taken out of the same forging near the failure location. Crack propagation under two realistic load sequences was highly irregular and could not be correctly predicted using the Willenborg retardation model. Also, scatter of the above properties was much larger than for the sheet and plate specimens normally used for such tests.

The conclusions to be drawn from these results are shortly discussed and the urgent need for further work is stressed.

1. INTRODUCTION

The structure of modern aircraft contains a large number of aluminum forgings. Such forged components usually have a single load path and are designed to the "safe life" or (more modern) the "safe crack growth" philosophy. Therefore properties such as fracture toughness, residual static strength crack propagation and fatigue life of forgings should be especially important to the designer, the certification agency and the operator: failure of a single load path structure usually results in an accident.

In the literature, however, there is an almost complete lack of corresponding data, probably due to the high cost of forgings. By chance, some years ago the nose landing gear strut of a certain tactical aircraft type was replaced throughout the fleet because of suspected stress corrosion cracks; a large number of (originally) expensive forgings thus became available for test purposes.

The material was 7075-T6, which is no longer used in modern aircraft due to its wellknown disadvantages. However, it was (and still is) felt by the author that the results of fatigue and fracture tests still would be generally representative of typical aluminum aircraft forgings: The nose landing gear strut would nowadays probably be manufactured of 7075-T73; it is not at all likely that this small change in heat treatment would fundamentally alter the behavior of the forgings in question in the cracked condition under static or repeated loading, especially the associated scatter. Another, more serious, objection was the fact that the various nose landing gear struts had been in service for different, but unknown numbers of flying hours. However, during flying service different sections were highly stressed than in the tests carried out in the laboratory.

2. PURPOSE AND SCOPE OF THE TEST PROGRAM

One purpose of this test program was to provide reliable data on the behavior of typical aluminum forgings in the cracked condition under static and repeated loading. A second purpose was the use of fracture mechanics to predict this behavior; in other words: Is fracture mechanics able to predict the residual static strength of and the fatigue crack propagation in the aluminum forgings?

To this end, a large number of nose landing gear struts was obtained, enabling us to determine the scatter of residual static strength. The forgings (see Figure 1) had been manufactured to identical drawings by four different forges in three different countries. Thus, the influence of manufacturing on the above properties also was determined. The forgings were first notched by sawcuts in three locations, see Figure 2. Fatigue cracks were then grown in locations, 1, 2 and 3 by applying constant load amplitudes at the points shown in Figure 2 until a predetermined crack length was reached. The nose landing gear strut was then broken by increasing the load until failure occurred, the COD being registered. The failing load and stress (computed as M/W (bending moment / section modulus) were determined. Finally the fracture toughness of the forging was computed, using the formula of Irwin [1] which is based on [2]. The limited width of the component was accounted for according to [3], bending according to [4].
It was then determined if the thus calculated value K_Q could be considered a valid K_{Ic}, using the following criteria:

- $K_{fmax} < 0{,}6 \cdot K_Q$ [5]
- $\frac{F_{max}}{F_Q} \leq 1{,}1$ (5-per cent secant) [5] and
- $\frac{\text{crack depth}}{\text{component width}} < 0{,}5$ [1]

Near location 1 and 2 CT-specimens according to ASTM-E 399-72 [5] were then cut from the forgings (see Figure 1) and the fracture toughness determined after [5]. Near location 2 C-shaped specimens (see figure 3) were machined from the forging. This specimen type was originally developed by the Watervliet Arsenal of the US Army /6 to 8/. For the dimensions shown in Figure 3 the calibration formulae given in [8] were not applicable; therefore the compliance of the specimen was measured and the formula for K calculated by fitting a 3rd degree polynominal. The applicable conditions of ASTM-E 399-72 [5] were observed with regard to crack front straightness, length of crack, generation of the fatigue crack, 5-per cent secant method etc.

The crack propagation tests were carried out for location 3 only; again the notch was machined; two different realistic load sequences were used:

- a flight by flight sequence simulating the stresses of the lower wing surface in the wing root area of a tactical aircraft, called "TCTP spectrum" [9]. This sequence has pronounced ground to air cycles; a sample is shown in the upper half of Figure 4. One repeat period consists of 803 flights with an average of 100 cycles per flight.
- a landing gear sequence, simulating the loads acting in the X-direction, such as spin-up and spring-back on landing, taxying, braking, engine run up etc. This was called "landing gear spectrum", a sample is shown in the lower half of Figure 4. One repeat period consists of 200 flights with an average of 300 cycles per flight.

The stresses were selected such that 1 000 to 4 000 flights to complete failure of the nose landing gear strut were obtained. Crack growth was observed visually on the surface only.

Using the USAF retardation model of Willenborg et al [10] crack propagation under the landing gear spectrum was then calculated. The constants necessary for this calculation (C and n in the Forman equation [11]) were determined by three constant amplitude crack propagation tests on forgings. The K_{Ic}-values required were obtained from CT-specimens, cut from the forging near the crack location.

3. RESULTS AND DISCUSSION

The results are shown in detail in Tables 1 to 6; some results are given in Figures 5 to 10, photographs in Figures 11 and 12.

3.1 Fracture Toughness of Specimens, Fracture Toughness and Residual Static Strength of Forgings

The mean fracture toughness of CT-specimens was $\bar{K}_{Ic} = 1020\ Nmm^{-3/2}$ for the LT-direction, see Table 5, which agreed closely with literature data on this material [12, 13]. The scatter of K_{Ic} was about normal for CT-specimen taken from aluminum plate [14].

The C-shaped specimens again agreed quite well with literature data, see Table 6, on a similar type of specimen taken from a forging [13]. Scatter was high, no similar coefficient of variation having been found in a large number of fracture toughness tests [14] on aluminum. As there was not measurable difference in fracture toughness between the two fatigue crack locations (in the forging seam and beside the forging seam (see Figure 11), all valid C-shaped specimens were statistically evaluated together.

The fracture toughness of the complete nose landing gear strut for location 1, using only the valid tests as described in section 2, have a higher mean value (1375 as compared to 1020 $Nmm^{-3/2}$) and a much larger scatter ($v = 0,21$ compared to $v = 0,04$) than the CT-specimens. This means that the mean ($P_s = 50$ per cent) residual static strength of the component would have been predicted conservatively using the fracture toughness of CT-specimens taken from the forging itself. However, this conservatism is only true for probabilities of survival $P_s < 90$ per cent. At the much higher P_s values necessary for safe life parts the prediction would have been highly unconservative.

For location 3 no valid fracture toughness test was obtained with the forgings, see Table 2.

Four valid tests were possible at location 2, see Table 3, Again the mean fracture toughness was higher ($K_{Ic} = 1130$ vs. 717 $Nmm^{-3/2}$) and the scatter was also higher ($v = 0,16$ vs. $v = 0,10$) (Figure 6). The estimate of the residual static strength of the forging would have been conservative up to $P_s \leq 99,95$ per cent.

All the data discussed in the preceding paragraphs are summarized in Figure 5.

The residual static strength on net area σ_{NR} of some of the forgings (including those which had not given valid K_{Ic}-values) were extremely high, see Tables 1 to 3, surpassing the tensile ultimate of about $F_{tn} = 550\ N/mm^2$ in some cases, even for quite large cracks. No explanation can be given at the moment for these results. *)

Anyway, the load at failure was very much different for similar sizes and shapes of the crack, see e.g. Table 2: Forgings 3R2-1 and 3R3-3 had very nearly the same size and shape of crack, yet their failing load was 23 000 N and 15 700 N respectively. Again in Table 1 forgings 1R2-19 and 1R7-38 had failing loads of about 28 000 and 18 000 N.

There was no discernible difference between the residual static strength of forgings of manufacturers A, B and C. Manufacturer D (3 forgings only) lay on the lower limit of the scatter band.

*) For the calculation of the residual static strength at location 1 the formula for a curved beam in pure bending in [15] was used.

3.2 Crack Propagation

The results of the crack propagation tests are summarized in Table 4 and Figures 7 and 8. It can be seen that the scatter again was extremely large. This is true for the number of flights to failure (crack initiation plus crack propagation period) as well as the crack initiation or the crack propagation period alone, see Figure 7.

A scatter $T = N_{90}/N_{10}$ of 1 : 5,0 (landing gear spectrum) or 1 : 7,7 (TCTP-spectrum) for the crack propagation period is most unusual. The IABG has carried out many tests with similar or identical load sequences on axially loaded sheet and plate specimens of Al-Ti and Fe-alloys. In every case the scatter was much smaller than T = 1 : 2,0.

As for the fatigue life, a similar comparison is possible: The forgings gave T = 1 : 6,0 for the TCTP-spectrum. Applying the identical sequence to an axially loaded bolted joint of aluminum alloy AZ 74 resulted in T = 1 : 3,5 [9], while two types of notched specimens of 7075-T6 gave a still smaller scatter [9].

Moreover, there is no direct correlation between the number of flights to failure and the crack initiation or crack propagation period. In other words: A forging having a long fatigue life to failure does not necessarily have a long crack propagation period and vice versa. For example, see Table 4, forging 1Ri2-54 had a fatigue life of 7604 flights under the TCTP-spectrum while the crack propagation period was only 620 flights: on the other hand forging 1Ri3-49 had a fatigue life of 3620 flights and the crack propagation period was nearly the same at 640 flights: finally forging 1Ri4-12 had a very similar fatigue life at 3843 flights, but its crack propagation period was much longer at 2940 flights.

For the landing gear spectrum only two tests were carried out with identical maximum loads (30 000 N), see Table 4: the other two forgings were tested with higher and lower maximum loads respectively. Assuming a slope of 1 : 6,0 of the $\bar{\sigma}$-$\bar{N}$-curve the life of these other two forgings under a maximum load of 28 000 N can be calculated (figures in parentheses).

The corresponding crack propagation curves are shown in Figures 9 and 10. The upper end of these curves indicates failure of the forging. Figure 9 also contains the calculated crack propagation according to the Willenborg model [10], which was conservative in this case: It predicts a crack propagation life from an 1,5 mm crack to failure of 170 flights. The actual mean life of two forgings, however, was about 750 flights.

The IABG has also used the Willenborg model in another test program [16] on axially loaded sheet specimens. Under the identical load sequence it was almost exactly right for maraging steel and conservative by a factor of 1,5 for 2024-T3.

However, in several other load sequences the Willenborg model generally gave quite unconservative results: For a tactical aircraft lower wing surface load sequence it predicted, for example, a 3.6 times longer life than actually occurred in the test (material 7075-T7351) [16]. Similar findings were reported by Weissgerber et al in [17]. So the above results should not be generalized. It is planned to calculate the crack propagation under the TCTP-spectrum in 1977 and compare it to the curves given in Figure 10.

No influence of the manufacturer on crack propagation behavior could be found: The three extreme examples discussed above (1Ri2-54, 1Ri3-49 and 1Ri4-42) all came from the same forge.

The fracture surfaces of some of the forgings looked quite peculiar, see Figure 12. The forging on the left had a fatigue life of 4 400 flights, a crack propagation life of 3 510 flights and a crack initiation life of 890 flights under a maximum load in the spectrum of 28 000 N. The forging on the right (2Ri2-34) under a maximum load of 30 000 N gave 2 045, 860 and 1 185 flights respectively, see Table 4. That is, the percentages of the life spent for crack initiation and for crack propagation were grossly different. These two forgings came from manufacturers A and B. The other forgings also could be identified as to their origin by viewing their fracture surfaces: Manufacturer A's forgings always had shear type failures like 2Ri1-9, while B's forgings had the usual 90-degree failure like 2Ri2-34.

4. SUMMARY AND CONCLUSIONS

4.1 Residual Static Strength and Fracture Toughness

- The fracture toughness of complete forgings was higher in all three locations than that of specimens taken out of the forgings at these locations.

- The scatter of fracture toughness was much larger for the forgings than for the specimens. This scatter of the forgings could not be explained by the usual metallographic procedures.

- Nominally identical forgings with cracks of very similar dimensions can have grossly different ultimate failing loads.

4.2 Crack Propagation

- Crack propagation was considerably slower under a landing gear spectrum than predicted by the Willenborg retardation model. This may be due to the load sequence employed, for other sequences the Willenborg model gave unconservative results in some other test programs.

- The scatter of

  - fatigue life to failure as well as
  - the crack initiation and
  - the crack propagation period

  was extremely large for the forgings under two realistic load sequences.

- Forgings with a long fatigue life can have very short crack propagation periods and vice versa.

- The fracture surfaces and crack shapes in forgings may be highly irregular.

4.3 Use of Aluminum Forgings in Aircraft Structures

It is realized that the present program dealt only with forgings of one type, which had seen different service loads and consisted of a material no longer used in new aircraft. Therefore one should be cautious to generalize. However, until the somewhat disturbing findings have been refuted by similar test programs on other forgings, it might be advisable to consider the following remarks when designing, certificating and using aluminum forgings in aircraft

- The important forging properties determined in this test program - residual static strength, fatigue life and crack propagation life may be subject to an extremely large scatter, much larger than for sheet or plate components. In order to attain equal probabilities of survival, larger safety coefficients would therefore have to be observed for forgings than for sheet or plate components.
  For a fatigue test on a structure considering of forgings and of sheet and plate components, there obviously exists a dilemma:
  If the test is stopped at some multiple (say 4) of the required lifetime, the demonstrated structural reliability (at least in a statistical sense) is higher for the sheet and plate components than for the forgings.

- Even if an aircraft is manufactured in several countries, the important forgings should come from one supplier only.

- A long fatigue life of a forged component in test is no guarentee for a long crack propagation period. This again has obvious implications for the full scale fatigue test.
  Forgings are often used in internal structure and are therefore difficult to inspect. Every effort should be made to improve NDI techniques for such applications.

4.4 Employing Fracture Mechanics for Aluminum Forgings

- The application of fracture mechanics to aluminum forgings is difficult, to say the least. This does not reflect so much on fracture mechanics itself, but results from peculiar forging characteristics, like large scatter of properties even in one location, much more so in different locations.

4.5 Outlook

It is urgently required to test other forgings in programs which are similar to the one described here. It might then be possible to design and manufacture forgings, which do not have the undesirable characteristics reported in the present work.

5. REFERENCES

[1] Irwin, G. R.: "Crack Extension Force for a Part-Through Crack in a Plate". Journal of Applied Mechanics, Vol. 84 E, No. 4, Dec. 1962

[2] Green A. E. and J. N. Sneddon: "The Distribution of Stress in the Neighbourhood of a Flat Elliptical Crack in an Elastic Solid". Proc. Cambridge Phil. Soc. 46 (1950), pp. 159 - 164

[3] Grandt, A. F. jr. and G. M. Sinclair: "Stress Intensity Factors for Surface Cracks in Bending". ASTM STP 513, American Society for Testing and Materials, 1971, pp. 37 - 57

[4] Brown, W. F. jr. and J. E. Srawley: "Plane Strain Crack Toughness Testing of High Strength Metallic Materials". ASTM STP 410, 1976

[5] ASTM Designation: E 399-72 "Standard Method of Test for Plane-Strain Fracture Toughness of Metallic Materials" (1972)

[6] Kendall, D. P. and M. A. Hussain: "A New Fracture Toughness Test Method for Thick-walled Cyclinder Material". Experimental Mechanics, April 1972, Vol. 12 - Nr. 4

[7] Underwood, J. H., R. D. Scanlon and D. P. Kendall: "K Calibration for "C" Shaped Fracture Toughness Specimens of Various Geometries". Watervliet Arsenal, N.Y. 12189, Technical Report, April 1973

[8] Kendall, D. P., J. H. Underwood and D. C. Winters: "Fracture Toughness and Crack Growth Measurements with "C" Shaped Specimens", Watervliet, FY 72, 1973

[9] Schütz, W.: "The Fatigue Life under Three Different Load Spectra - Tests and Calculations" in: Symposium on Random Load Fatigue, AGARD-CP-118, 1972

[10] Willenborg, J., R. M. Engle and H. A. Wood: "A Crack Growth Retardation Model Using on Effective Stress Concept". AF Flight Dynamics Laboratory, TM-71-1-Fbr. (1971)

[11] Forman, R. G., V. E.Kearney and R. M. Engle: "Numerical Analysis of Crack Propagation in Cyclic Loaded Structures". Journal of Basic Eng. (1967), pp. 459-464

[12] Damage Tolerant Design Handbook, Battelle, Columbus Laboratories, MCIC - HB - 01, Dec. 1972

[13] Moore, R. L., G. E. Nordmark and J. G. Kaufmann: "Fatigue and Fracture Characteristics of Aluminum Alloy Cylinders under Internal Pressure". April 1, 1970, Alcoa Research Laboratories, New Kensington, Pennsylvania

[14] Schütz, W.: "Versuchsmethoden der Bruchmechanik", Der Maschinenschaden, Heft 5, 1975

[15] Kunz, A.: "Entwurf einer Formelsammlung". Teil 1, MPA, Stuttgart, 1970

[16] Schütz, W. and W. Oberparleiter: "Berechnung des Rißfortschrittes an Bauteilen bei veränderlichen Spannungsamplituden". IABG-Report B-TF-508, August 1976

[17] Weissgerber, D., P. Keerl and K. Sippel: "Theoretische und experimentelle Rißfortschrittsuntersuchungen für Metallstrukturen; Rißfortschritt in Kampfflugzeugbauteilen unter betrieblichen Bedingungen". MBB-Bericht UFE 1236, 1975

Table 1: Fracture Toughness and Residual Static Strength of Forgings - Location 1

Forging No	Manufacturer	Crack Area	Failing Load		Residual Static Strength on gross	Residual Static Strength on net	Stress Intensity	Fracture Toughness
		A_A [mm²]	F_{max} [N]	F_Q [N]	σ_{BR} [N/mm²]	σ_{NR} [N/mm²]	K_Q [Nmm$^{-3/2}$]	K_{Ic} [Nmm$^{-3/2}$]
1R 1-21	A	76	70 600	70 600	697	765	2 995	-
1R-2-19	B	1 034	28 350	24 250	240	642	2 430	-
1R 3-25	B	310	25 000	25 000	247	343	1 130	1 130
1R 4-29	B	208	65 700	53 700	531	667	2 420	-
1R 5-30	B	200	69 150	56 900	562	696	2 480	-
1R 6-31	C	497	29 300	28 700	283	463	1 380	1 380
1R 7-38	A	1 184	18 400	17 750	176	679	2 545	-
1R 8-41	B	310	34 800	34 800	343	488	1 620	1 620
1R 9-43	B	410	-	-	-	-	-	-
1R10-46	B	830	38 150	33 850	334	578	2 500	-

- in the last column means that a valid Fracture Toughness K_{Ic} could not be obtained

Table 2: Fracture Toughness and Residual Static Strength of Forgings - Location 2

Forging No	Manufacturer	Crack Area	Failing Load		Residual Static Strength on gross	Residual Static Strength on net	Stress Intensity	Fracture Toughness
		A_A [mm²]	F_{max} [N]	F_Q [N]	σ_{BR} [N/mm²]	σ_{NR} [N/mm²]	K_Q [Nmm$^{-3/2}$]	K_{Ic} [Nmm$^{-3/2}$]
3R1-26	A	341	51 975	48 540	387	669	1 750	-
3R2-1	A	943	23 045	23 045	186	569	1 670	-
3R3-3	D	964	15 690	15 300	117	389	1 055	-
3R4-5	A	787	25 010	24 520	192	535	1 480	-
3R5-33	B	404	39 960	38 100	302	488	1 515	-
3R6-40	D	206	37 510	37 510	289	353	995	-
3R7-36	D	1 398	10 590	10 000	76	422	1 085	-

Table 3: Fracture Toughness and Residual Static Strength of Forgings - Location 3

Forging No	Manufacturer	Crack Area	Failing Load		Residual Static Strength on gross	Residual Static Strength on net	Stress Intensity	Fracture Toughness
		A_A [mm²]	F_{max} [N]	F_Q [N]	σ_{BR} [N/mm²]	σ_{NR} [N/mm²]	K_Q [Nmm$^{-3/2}$]	K_{Ic} [Nmm$^{-3/2}$]
4R1-25	B	195	3 450	3 450	277	368	1 060	1 060
4R2-19	B	216	4 750	4 750	380	504	1 455	-
4R3-21	A	168	5 950	5 950	476	603	1 890	-
4R4-43	B	346	3 500	3 250	259	452	1 325	1 325
4R5-29	B	299	3 900	3 900	312	494	1 475	-
4R6-31	C	510	2 050	2 050	164	368	995	995
4R7-41	B	452	2 500	2 500	197	412	1 165	1 165
4R8-38	C	15	4 850	4 850	388	373	625	-
4R9-46	B	665	2 450	2 350	196	574	1 465	-

Table 4: Results of Crack Propagation Tests

Forging No	Manufact.	Max. Load of the Spectrum [N]	Max. Stress in the Spectrum [N/mm²]	Number of Flights to Failure	Number of Flights from a Crack Length of 1,5 mm to Failure	Number of Flights to a Crack Length of 1,5 mm
TCTP-Spectrum						
1Ri1-22	A	20 000 calculat.	211 (234)	3 137 (1 800)	1 980 (1 130)	1 157 (670)
1Ri2-54	B	24 000	234	7 604	620	6 984
1Ri3-49	B	24 000	234	3 620	640	2 980
1Ri4-42	B	24 000	234	3 843	2 940	903
Scatter $\overline{T}$				1 : 6,0	1 : 7,7	1 : 22,0
Landing Gear Spectrum						
2Ri1-9	A	28 000 calculat.	274 (293)	4 400 (2 950)	3 510 (2 330)	890 (620)
2Ri2-34	B	30 000	293	2 045	860	1 185
2Ri4-10	A	30 000	293	1 063	620	443
2Ri5-28	B	33 000 calculat.	322 (293)	1 910 (3 400)	870 (1 850)	1 040 (1 550)
Scatter $\overline{T} = \frac{N_{90}}{N_{10}}$				1 : 3,5	1 : 5,2	1 : 6,2

Table 5: Fracture Toughness Determined with CT-Specimens

Specimen No	Direction	Stress Intensity K_Q and Fracture Toughness K_{Ic} [Nmm$^{-3/2}$]	Manufacturer
1B1-38	L - T	992 K_{Ic}	A
1B2-38	L - T	1 059 K_{Ic}	A
1B3-19	L - T	1 284	B
1B4-29	L - T	1 360	B
1B5-25	L - T	1 002 K_{Ic}	B
1B6-30	L - T	1 315	B
1B7-41	L - T	1 023 K_{Ic}	B
K_{Ic} - arithmetic mean value	L - T	1 020 K_{Ic}	
1B8-35	T - L	773	B
1B9-21	T - L	1 013 K_{Ic}	A
1B10-46	T - L	836	B

A K_{Ic} in the third column means that a valid K_{Ic}-value according to [5] was obtained.

Table 6: Fracture Toughness, Determined with C-shaped Specimens

Specimen No	Stress Intensity K_Q and Fracture Toughness K_{Ic} $[Nmm^{-3/2}]$	Manufacturer
4B1-44S	632 K_{Ic}	C
4B3-35S	693 K_{Ic}	B
4B5- 7S	804 K_{Ic}	A
4B7-47S	657	C
4B9-48S	930	B
4B2-44N	635	C
4B4-35N	745 K_{Ic}	B
4B6- 7N	710 K_{Ic}	A
4B8-47N	403	C
4B10-48N	880	B
K_{Ic} - arithmetic mean value	717	

S = Fatigue crack in the forging seam

N = Fatigue crack beside the forging seam

A K_{Ic} in the second column means that a valid K_{Ic}-value according to [5] was obtained.

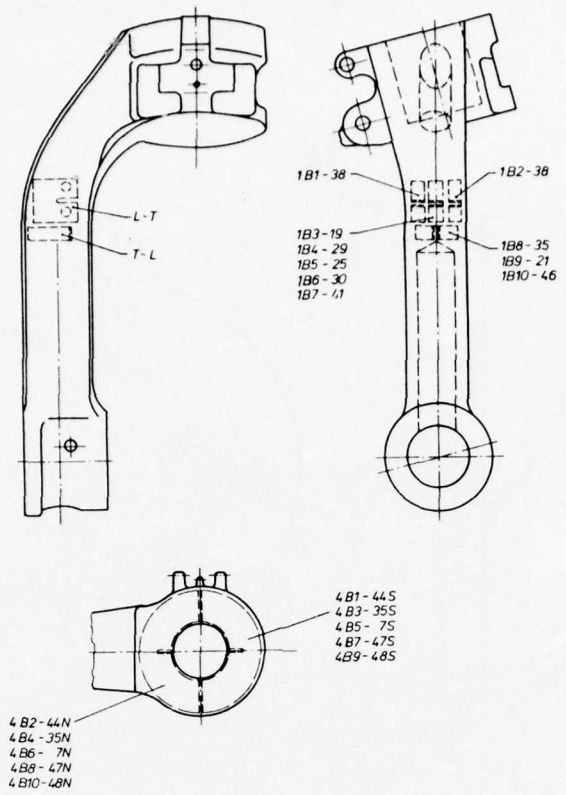

Figure 1: Nose Landing Gear Strut and Location of Fracture Toughness Specimens

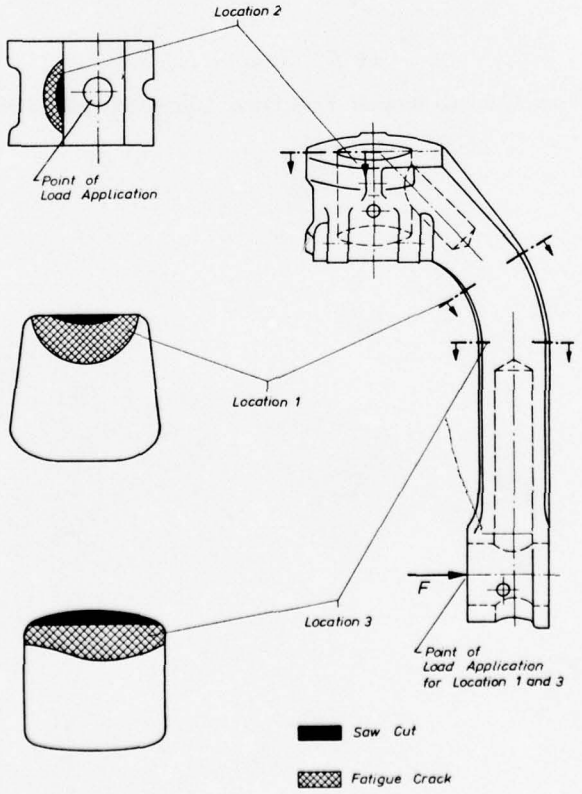

Figure 2: Artificially Induced Cracks in the Component

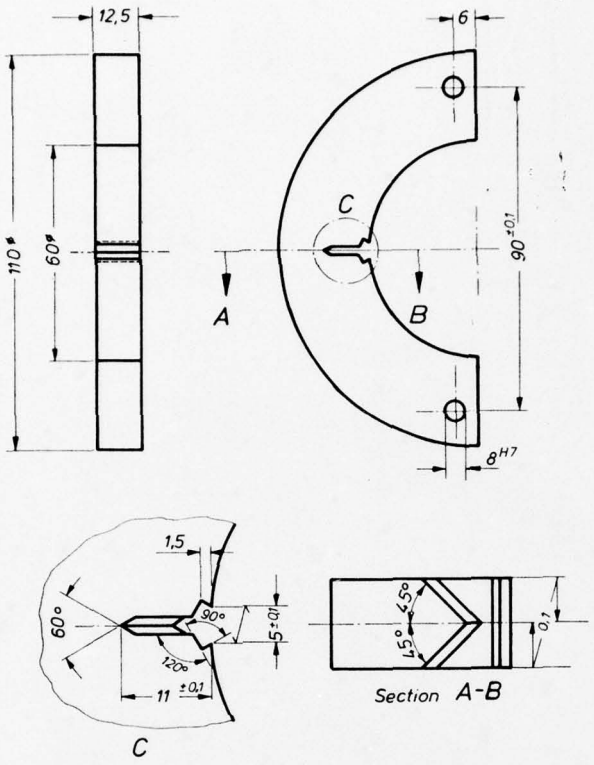

Figure 3: C-Shaped Fracture Toughness Specimen

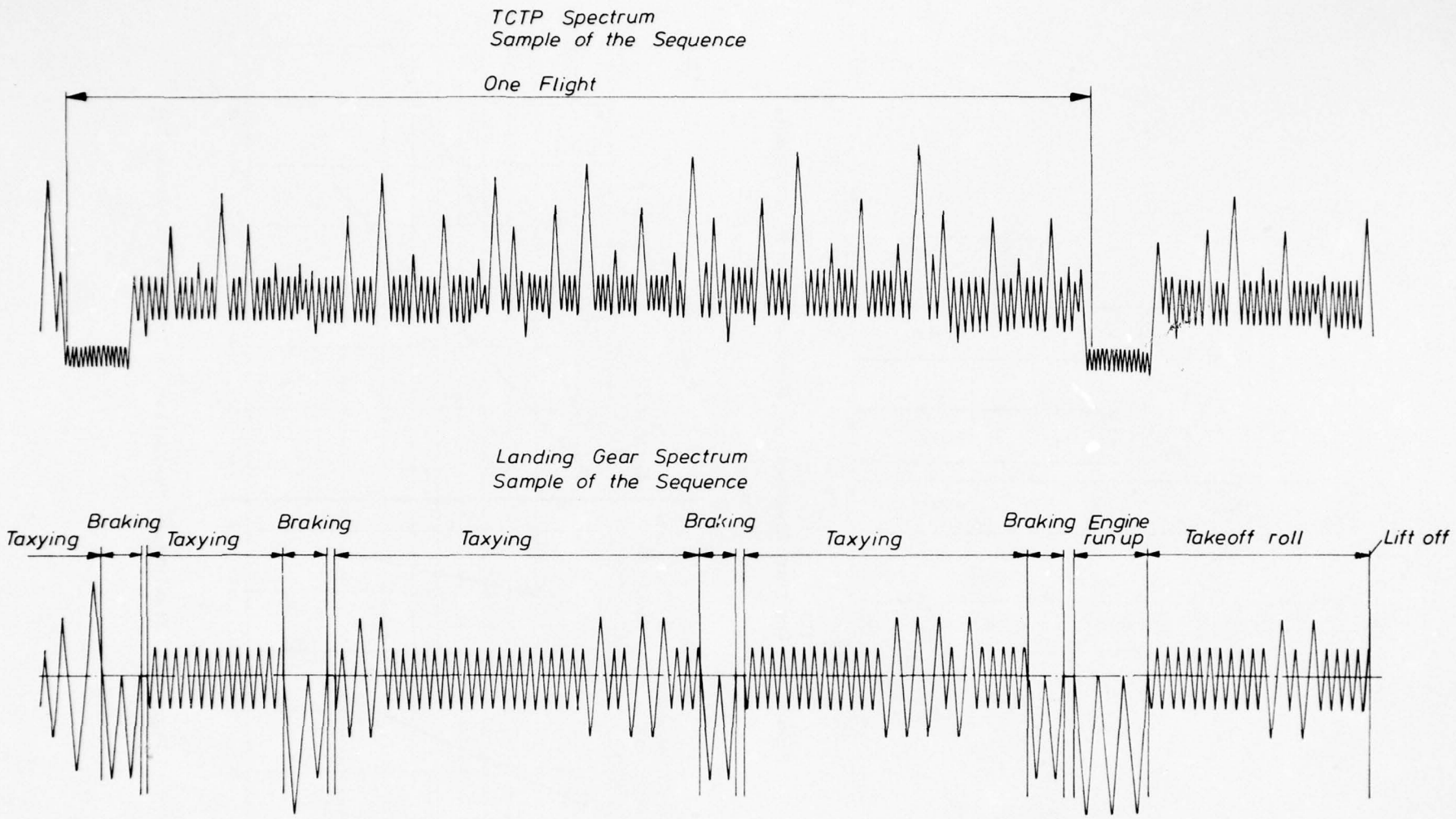

Figure 4: Samples of the Two Load Sequences Used

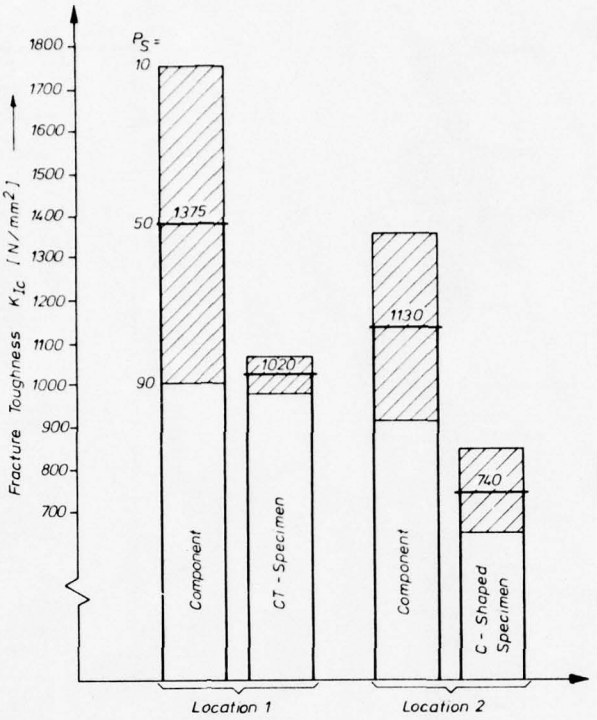

Figure 5: Fracture Toughness of Specimens and of Components

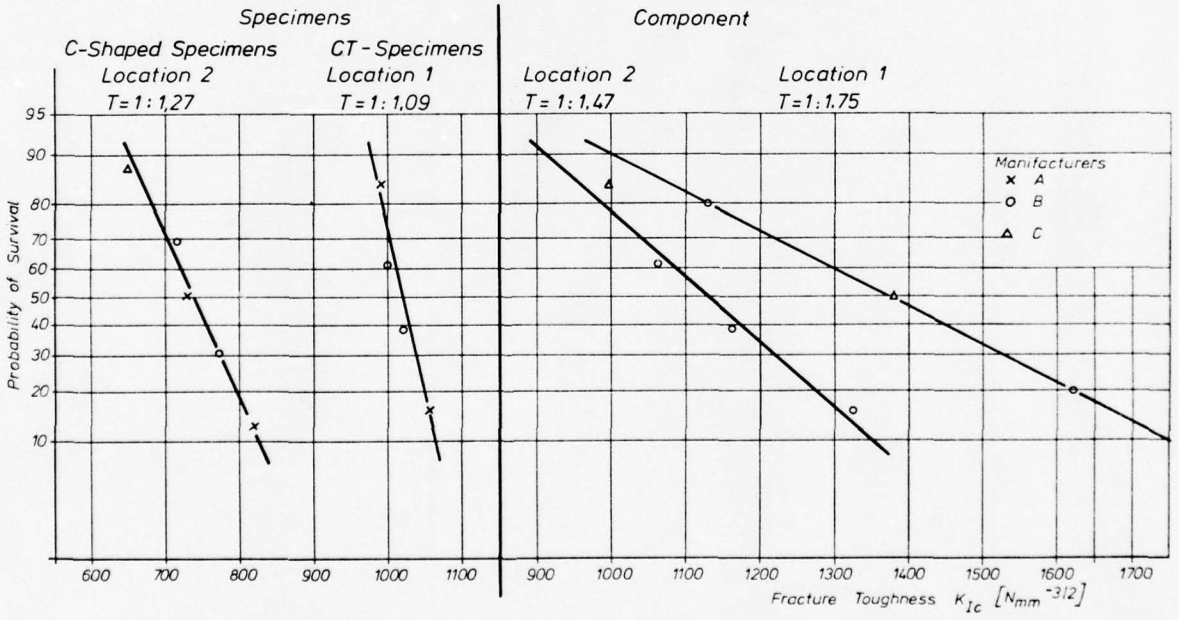

Figure 6: Statistical Evaluation of Fracture Toughness K_{Ic}

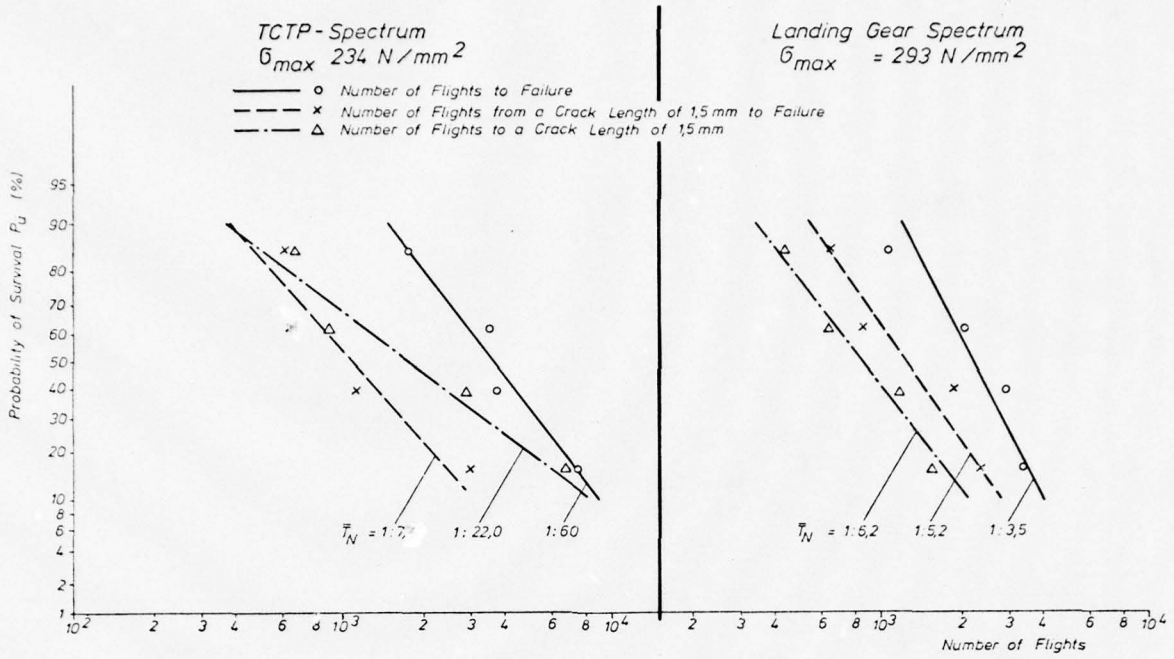

Figure 7: Statistical Evaluation of Crack Propagation Tests

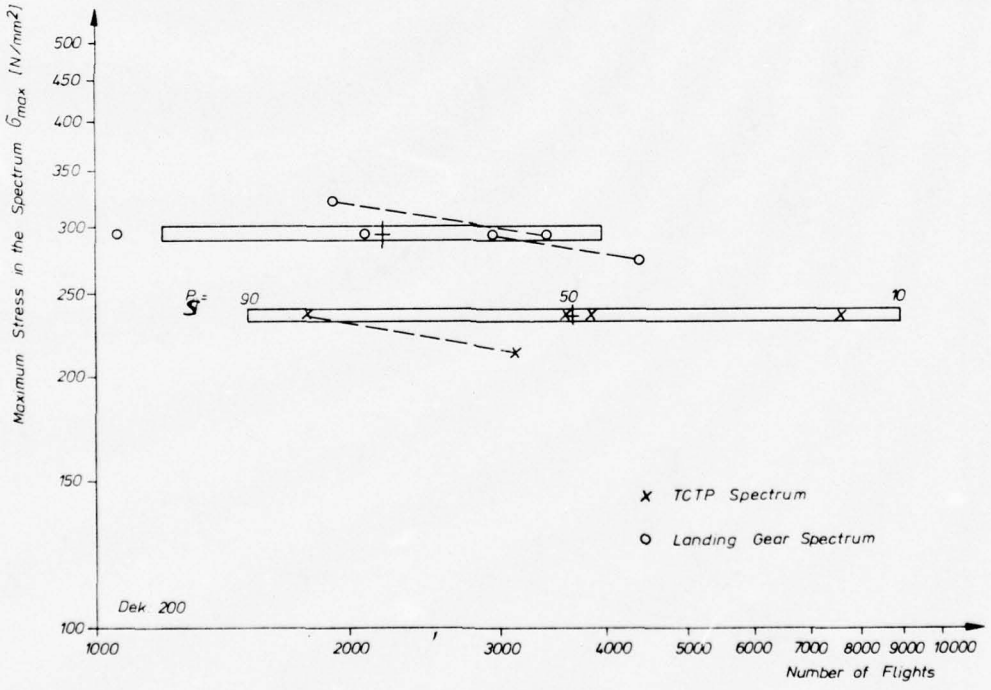

Figure 8: Fatigue Life to Complete Failure
(Crack Initiation plus Crack Propagation Period)

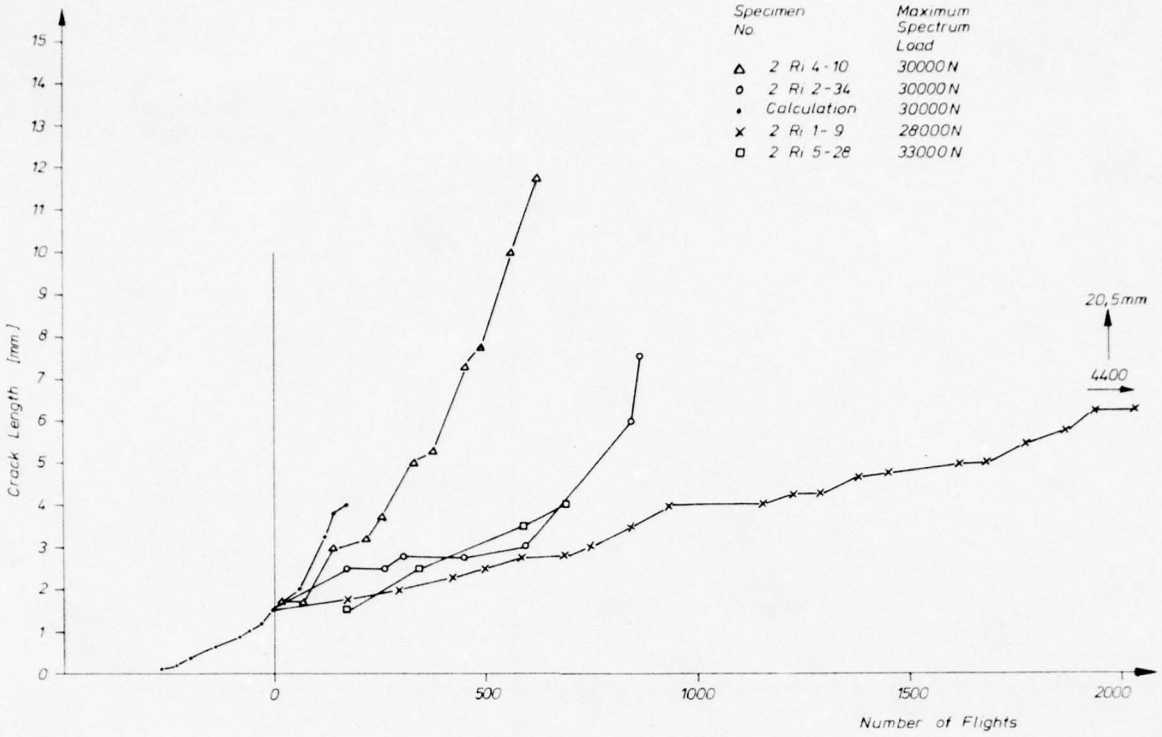

Figure 9: Crack Propagation Landing Gear Spectrum

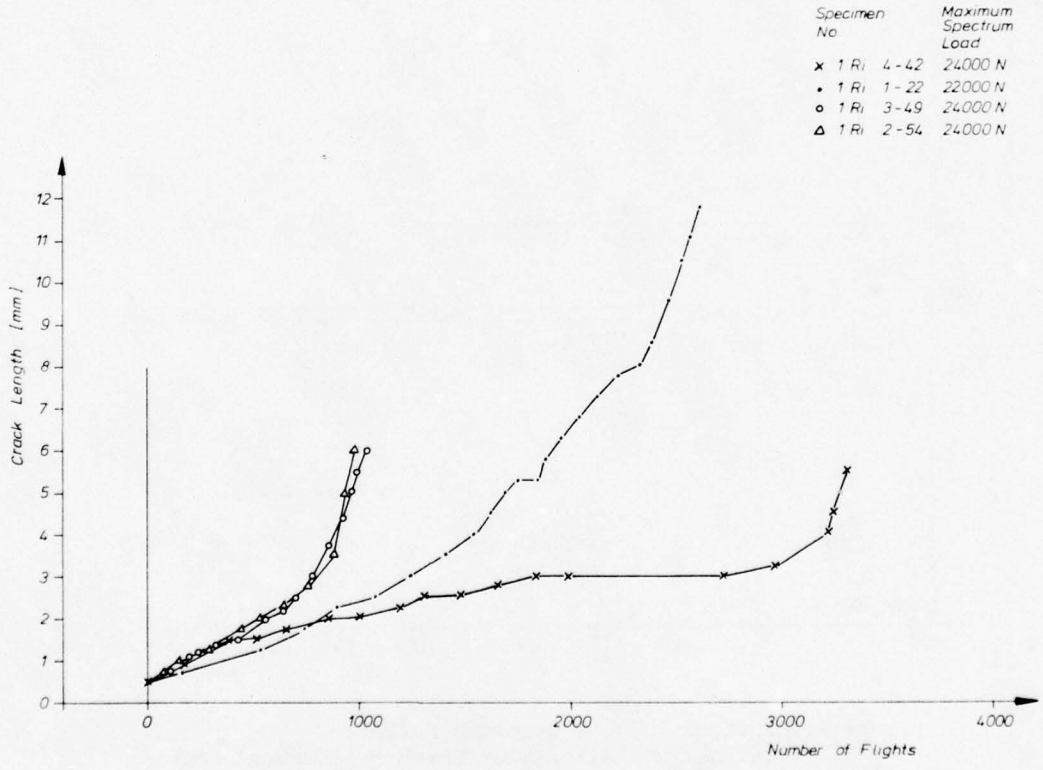

Figure 10: Crack Propagation TCTP-Spectrum

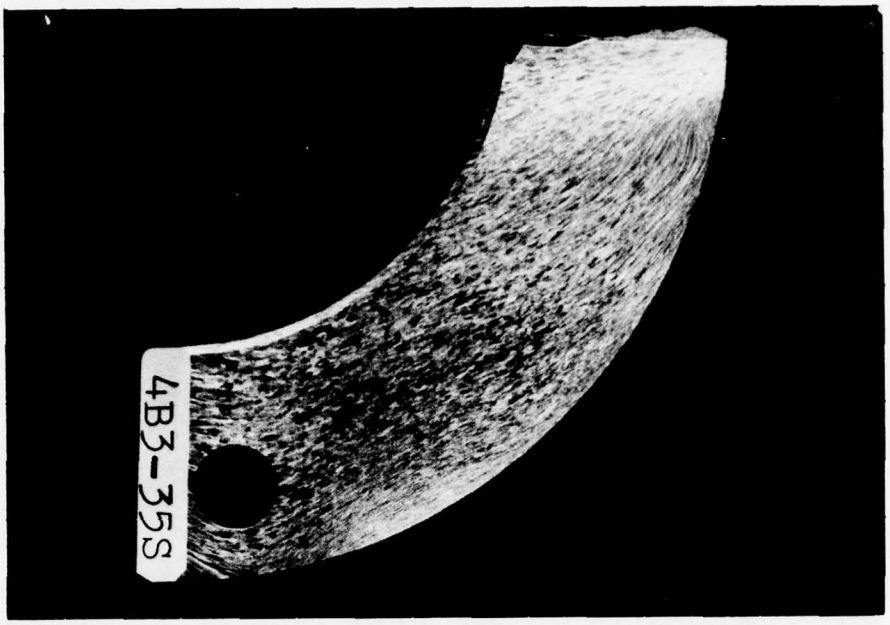

Left hand side

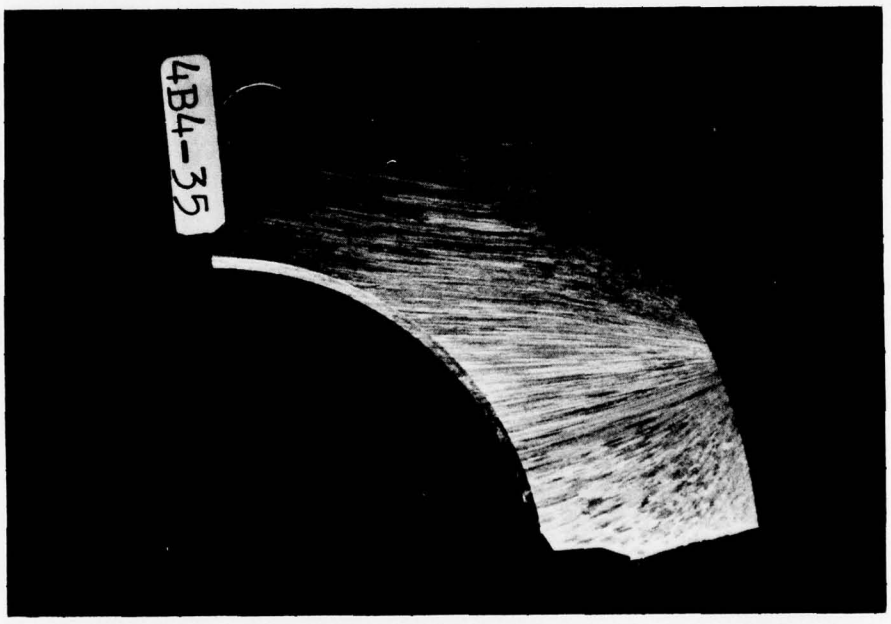

Right hand side

Figure 11: Grain Flow, Forging Seam and Location of the Fatigue Crack in C-Shaped Specimens

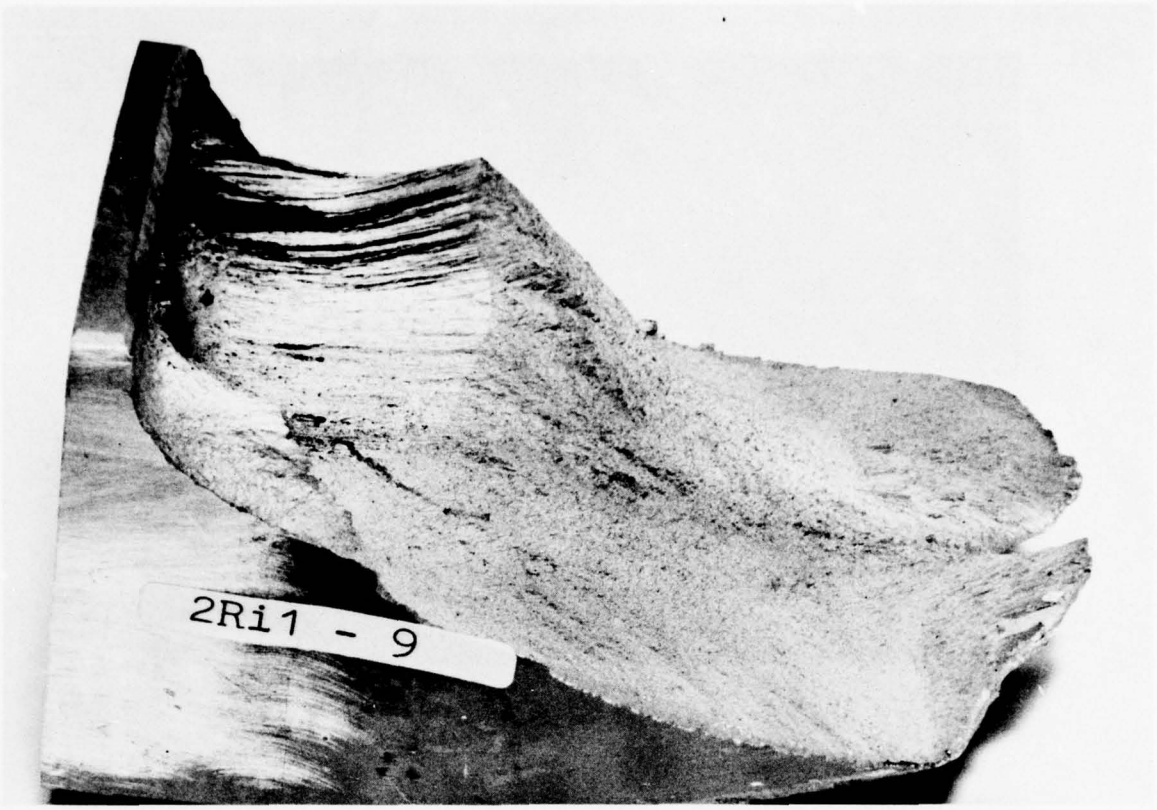

Left hand side

Right hand side

Figure 12: Fracture Surfaces of Two Forgings (Crack Propagation Tests)

CONTRIBUTED DISCUSSION

by

Dr. A.Habel
Bundesamt für Wehrtechnik und Beschaffung
Beauftragter für das Musterprüfwesen der
Bundeswehr für Luftfahrtgerät
Landshuter Allee 162 a
8000 München 19
West Germany

1. Introduction

The aim of the fatigue and fracture mechanics test on forgings of high-strength aluminum alloy presented in the paper of Dr. W. Schütz was to establish reliable and generally applicable design data on the properties of aluminum forgings in a cracked condition under static and fatigue load.

2. Durability Demonstration

To insure the airworthiness of aircraft structures and thus of forgings, it has to be demonstrated that the strength of each component is sufficient for its critical load including the required safety factor.

In the durability demonstration for components designed in accordance with the former safe-life concept, knowledge of their fatigue strength behavior was sufficient, normally using a safety factor of four to compensate for the scatter.

According to the new damage tolerance design philosophy it is, however, no longer permissible to design safety-of-flight structures using the safe-life principle, but these structures must be damage tolerant. This especially applies to single load-path structures, since these can only be designed as slow crack growth structures. Therefore, when demonstrating durability and safety of such structures, in addition to fatigue strength behavior also the behavior in the cracked condition under fatigue and static load must be known, i.e. crack propagation, critical crack length and residual static strength. Thus, these properties are much more important in the damage tolerance demonstration than in the former safe-life demonstration.

As far as the qualification of aluminum forgings is concerned, which are subject to fatigue load, it has to be clarified
- whether the data obtained reflect the behavior of the forgings so accurately and reliably as to be acceptable for a damage tolerance demonstration;
- whether the data obtained on forgings can be replaced by data obtained on specimens;
- or whether additional safety measures are required.

3. Evaluation of the Test Results

This investigation on fatigue and fracture mechanics properties of aluminum forgings in cracked condition is of fundamental importance for design and demonstration of damage-tolerant components, since in practice highly stressed forgings are often used especially for single load-path structures and since almost no data on the above mentioned properties of actual forgings are available in the relevant literature.

The question arises whether the results presented lead to fatigue and fracture mechanics data sufficiently accurate and reliable such as to be applicable to all types of aluminum forgings. Although the tests were conducted on actual forgings, it must be considered, however, that these forgings were exposed - at least in some cases - to a preloading of unknown level and frequency. As to the applicability of the results in question to forgings of other structural design, it must also be pointed out that the tests were conducted on just one type of forgings using only one type of material.

In general the results of the tests show as the prevailing characteristic a relatively high scatter of the fatigue strength properties of forgings in comparison to that of other semifinished products such as sheet metal or plates. This became apparent not only for fracture fatigue life but also for the characteristic values of the cracked condition (crack propagation, residual static strength, fracture toughness). Furthermore, it has been shown that the scatter of the fracture toughness of forgings is considerably higher than that of specimens taken from such forgings.

Without descussing the test results in detail, it can nevertheless be stated that the obtained scatter of the fatigue life is no longer covered by the safety factor of four, as usual for the safe-life concept, and even less by the reduced safety factor of two for the damage tolerance concept. In this case, however, the fatigue life was affected by the preloading in an unknown and different way. This could explain its relatively high scatter since other fatigue strength tests on aluminum forgings have evidenced a substantially smaller range of scatter.

The crack propagation behavior has also shown unusually high scatter which, again, may have been caused by an unknown preloading. Although the test show that an additionally conducted calculation of the crack propagation is in fact on the safe side, the overall result is not yet fully satisfactory, since the difference between the results obtained by calculation and those obtained by test is too great to verify agreement.

Other properties such as fracture toughness and residual strength which are not likely to have been affected by preloading show a higher scatter on forgings than on specimens taken from them. When the scatter factor of the fracture toughness found on specimens is used for forging design the result would be an unsafe component. For safety reasons it is, therefore, required that the design be based on the scatter of the forgings themselves and not on that of specimens. A workable proposition in order to be on the safe side could be provided by combining the mean fracture toughness of standard specimens with the scatter factor of the fracture toughness found for forgings.

A similar approach is feasible for the residual static strength. In this context it must be noted that, on the one hand, the scatter varies with manufacturers and that, on the other hand, there is already a considerable scatter with one manufacturer. Especially the latter fact indicates that a constant quality cannot yet be maintained by the presently employed manufacturing processes. Therefore, further efforts are required to achieve a constant quality and thus a reduction of the scatter.

4. Summary

This investigation on aluminum forgings is of fundamental importance for the design and qualification of damage-tolerant components.

The results show a surprisingly and in some cases even an alarmingly high scatter. However, the results are not yet adequate as to derive a generally applicable scatter factor for high-strength aluminum forgings. Therefore, the results must be reviewed and confirmed by further tests using new items.

In specifying safety requirements for the durability and safety demonstration of damage-tolerant components, only the scatter found on forgings as such should be applied. The scatter of specimens constitutes a safety risk, and an appropriate safety factor would have to be used in this case.

5. Recommendations

The present investigation must be supplemented by further tests on brandnew forgings covering a variety of designs and materials to obtain reliable and substantiated design data for high-strength aluminum forgings.

Even in the case of slight indications that the scatter of forgings found in the tests will be confirmed by future investigations, special measures must be taken with respect to the qualification of forgings - in particular damage-tolerant forgings - in order to determine exact figures and to compensate for the scatter of the endurance values. This could be accomplished

- either by using a general safety factor for forgings (as is already used for castings)
- or by considering the scatter of a particular forging rather than that of specimens.

Since such legal measures possibly required for safety reasons will inevitably lead to an increase in weight and thus to a decrease in the efficiency of aircraft, it is, in my opinion, in any case necessary to investigate the cause of such a high scatter. This should especially refer to the manufacturing and processing methods. The tests have also shown that in principle a reduction of the scatter is possible since the residual static strength of forgings from different manufacturers has shown different scatter. Only by reducing the scatter of fatigue and fracture mechanics properties of forgings to the order of magnitude of other semifinished products, additional safety requirements can be avoided and the quality of forgings can remain competitive with that of other semifinished products.

CONTRIBUTED DISCUSSION

by

Dipl. -Ing. Kalman Hoffer
Chief Fatigue Analysis Department
Vereinigte Flugtechnische Werke-Fokker GmbH
2800 Bremen, Germany

The various combinations of tests on finished components and test specimens taken from finished components, which are supplemented by crack propagation calculations, make this test report an important document for the development and design of similar components.

The test results are particularly valuable since hardly any component tests of this kind have been performed so far.

It will scarcely be possible, however, to make direct use of the results given in this report as it is not advisable to use the material 7075 for forgings in heat treatment condition T6. The results of this test also confirm this fact to a large extent.

STATIC RESIDUAL STRENGTH

In our opinion, the higher fracture toughness values of the forgings as against the standard test specimens (diagram, sheet 5) do not result only from the reasons stated in the report alone, but are, in our opinion, also due to the fact that

1. the stress calculation by means of the bending formula $\sigma_b = \frac{FQ \cdot a}{W}$ resulted in a value which was too high because of the larger width of the components and the plastic deformation, especially since tension and bending were superposed in the case of the standard part,

2. the variable width B of the cross section of crack position 1 cannot be accounted for in the calculation. It can be assumed that this will also lead to excessive calculated fracture values at this section.

For these reasons the fracture toughness values - in particular those for crack position 1 - cannot be considered representative, and the values of the standard test specimens are to be assumed for basic data, as indicated in the report.

Because of the considerable scatter of the forgings data a safety factor of 4 - as stated in the report - is not sufficient for forged safe-life components. It seems to be necessary to take a value of $j_{50\%} = 6.0$ as a basis for components of this kind.

CRACK PROPAGATION

The crack propagation curve for the landing gear load factor history, which was calculated on the basis of the data of the standard test specimens, shows a substantially higher crack propagation rate than the test curves. No theoretically determined crack propagation rate was stated for the TCTP wing load factor history.

Since crack propagation calculations with constant stresses and component geometries as well as corresponding test results are not available either, a quantitative statement as to the possible causes of the deviations is not possible on account of:

A. Deviations in the $K(K_{I_C})$ values resulting from the different type of loading of the component and the standard test specimens,

B. Inadequacies in the applied crack propagation determination method according to Willenberg.

The test results shown clearly indicate the serious problems of the responsible fatigue strength and/or fracture mechanics specialist who has to take decisions as to the cross section and shape of the component and the inspection intervals on the basis of these or similar test results.

The scatter determined during these tests are of particular importance, merely because the fatigue demonstration test for an aircraft in the incipient crack condition is mostly carried out on one test specimen only (full-scale fatigue test).

A decision involves considerable uncertainties because of the large scatters mentioned. These difficulties have been encountered several times in practical work recently. In the case of die forgings (main landing gear of a commercial aircraft) made of DTD 5104 the identification of the cracks occurred and the determination of the crack propagation rate and the residual strength behavior by means of a fracture mechanics calculation caused particularly great efforts both with respect to costs and work load.

It is recommendable to perform these or similar tests with forgings made of alloys subjected to those heat treatments which are often used for aircraft forgings.

APPLICATION OF FRACTURE MECHANICS TO THE F-111 AIRPLANE

W. D. Buntin
General Dynamics/Fort Worth Division
P.O. Box 748
Fort Worth, Texas 76101
USA

SUMMARY

Safe service operations of critical steel components in the F-111 aircraft are assured by analyses and tests developed using principles of fracture mechanics. A unique flaw in a major fitting which forms the inboard section of the wing caused the loss of an airplane in flight. Subsequent analytical and experimental investigations are described which thoroughly investigated the fracture characteristics of all critical steel components in the airframe. Fracture analysis tools were developed and used as essential elements in interpreting experimental data and in describing the damage tolerance of the F-111 fleet. The methodology which was evolved is compared with current airplane damage tolerance requirements.

1.0 INTRODUCTION

Critical high strength steel structural components operate in F-111 aircraft at a high level of safety. This assurance of damage tolerance is achieved through a program of fracture control. Fracture mechanics technology forms the basis of this program of analysis and testing including periodic full scale proof testing of each airplane. The F-111 fracture control program was not included as part of the original design approach but evolved as a consequence of an in-flight wing fracture which caused the loss of an airplane.

High strength steel is used in the F-111 to fabricate the wing pivot fittings, the wing carry through structure, certain of the center fuselage longerons, and the empennage carry through structure. These components are shown in Figure 1. Steel was selected as a result of trade studies including aluminum and titanium primarily because of the high density strength arrangements required in transferring relatively high airfoil loads into the fuselage within minimum space constraints. In most cases, the steel parts are formed from machined forgings and welding is used extensively in fabricating the various parts into component assemblies. The particular alloy chosen was the Ladish D6ac alloy heat treated to a tensile strength level of 220-240 ksi.

The structural integrity design and demonstration requirements specified for the F-111 included all aspects of analysis, development tests and full scale testing typical of military aircraft developed in the late 1950 and 1960 period. The essence of the structural ground test program was evaluation of durability - not a demonstration of safety. In retrospect the question of safety was rationalized on the assumption that fleet aircraft were typical in terms of damage and flaws to the full scale fatigue airframe. Testing beyond the service design requirements by a factor of 4 would account for variation in both quality and service environment. The non-destructive inspections included in the typical quality assurance programs were assumed sufficient to preclude non-typical manufacturing flaws.

Such was not the case. The following discussions describe a unique flaw that escaped a non-destructive inspection net leading to catastrophic failure. In addition, premature test failures not related per se to detail designs are also described. As a consequence of the serious questions that these events raised in regard to the integrity of the F-111 structure the fracture control program which continues in effect was developed. This program is believed to have been the first of its kind applied to an aircraft structural system and required the development of a practical methodology. The technology on which this program was based is described in the following paragraphs. A more detailed description of additional aspects of the program is given in Reference (1).

2.0 MATERIAL SELECTION FOR CRITICAL STRUCTURAL COMPONENTS

The extensive use of high strength steel in the F-111 design was unusual in comparison to most other aircraft structural systems. Approximately 33% by weight of the structural materials used in the airframe was steel. The major considerations for selection of the particular alloy were as follows:

- Maximum toughness and fatigue resistance
- Stable processing methods insensitive to normal variations
- Minimum warpage as a result of heat treatment
- Weldments which approach parent metal strength
- Alloy readily available from multiple sources
- Minimum cost

Trade studies were conducted to evaluate a number of different steel alloys including H11, 4330V modified, and Ladish D6ac alloys. The alloy which had been picked at the time of the F-111 proposal was H11, a 5% chrome steel which had been used on B-58 fittings and to a limited extent in other aircraft systems. The 4330V modified steel had been used on landing gears and other relatively small structural parts in other systems including the Grumman A2F and the McDonnell F4H as examples. The Ladish D6ac alloy was originally developed for forging die blocks specifically to overcome breakage problems. The first aerospace application was by Aerojet General for welded solid propellant rocket cases in the Minute Man Missile System. It had also been used for later versions of the Pershing and Titan missiles.

A primary requirement for the steel was satisfactory heat treat response to a process which minimized warpage. In studying the isothermal diagram for D6ac, it was noted that an unusually deep "bay" in the austenitic portion suggested that warpage could be minimized by holding a part in the temperature regime between 900°F and 1075°F without undesirable phase transformation. Further it was shown that relatively slow cooling rates would be tolerated with no transformation until the part cooled to approximately 850°F. Consequently it appeared that a modified heat treat procedure might significantly reduce warpage and such proved to be the case.

The trade studies included comparisons between the usual mechanical properties including notch sensitive tests at both -65°F as well as elevated temperatures typical of the design application. Extensive fatigue testing including both constant amplitude and spectrum loadings were conducted for the candidate materials. Stress corrosion resistance was also developed and compared using round smooth tensile specimens subjected to alternate immersion in a 5% salt solution. This series of tests showed the D6ac alloy to be more resistant than either H11 or 4330V modified to fatigue and stress corrosion cracking.

There was considerable concern in addition to the above material aspects in regard to toughness. Fracture toughness parameters were obtained by testing center hole notched tensile specimens as well as notched beam specimens. These tests were conducted at both room temperature and at -65°F for the candidate steels. The relative toughness of the alloys evaluated are shown in Figure 2. Rather than a quantitative use of the toughness data this testing provided a qualitative comparison which was included in the consideration of selecting the alloy to be used in a design. From the standpoint of toughness, the D6ac alloy proved superior and developed toughness values of K_{IC} = 60 ksi square root inch at -65°F and 80 ksi square root inch at room temperature using the aus-bay quench heat treat process and longitudinal grain properties.

The only toughness requirement in the F-111 material structural specifications was in terms of impact strength. This requirement was defined as 15 foot pounds at -65°F. The D6ac alloy was shown to meet this requirement on the basis of Charpy impact tests conducted using specimens processed in the manner typical of production parts.

The material selection program resulted in very extensive characterizations of the D6ac alloy including an unusual amount of design data with emphasis given to fatigue characterizations in the form of both constant amplitude testing and response to design spectrum loadings. Toughness evaluated in terms of the fracture mechanics parameters K_{nc} and K_{IC} was also a primary consideration, however in a qualitative sense rather than quantitative design data to be used in the design process.

3.0 FRACTURE PROBLEMS DURING TEST AND SERVICE OPERATIONS

Element fatigue tests were used extensively to investigate the response of the high strength steel to spectrum loadings in those areas where fatigue analysis was less straightforward and where the design detail characteristics were complex. Major component tests provided an evaluation beyond the element testing in that stress fields were more realistic, boundary conditions were properly simulated, and a considerably larger area was subjected to the full spectrum of design loads. In each case, examination of failed surfaces showed relatively short critical crack lengths in the steel but little or no attempt was made during these early stages to prepare failure analyses in terms of fracture mechanics.

The full scale fatigue test had completed the equivalent of 400 hours of service operations when a major failure occurred in the wing carry through box. The origin of this failure was a flaw approximately 0.10 inches deep adjacent to a bolt hole in an upstanding flange integral to the lower plate. The flange was used in the design to attach an aluminum plate which formed the rear web of the wing carry through box. Interestingly enough, the flaw occurred in a high stress region which subsequent investigations showed would probably have precipitated an early fatigue failure even though the flaw had not been present. Investigations as to the cause of this anomaly led to the conclusion that an improper application of cadmium plating and the associated electrical arc produced a crack in the material. The fatigue crack had propagated into the lower plate during the very short period of fatigue loading and failure occurred at stress levels well below the maximum stresses expected in service. The action taken at this time was to develop a gusset type fitting to be installed at the corner of the rear door installation reinforcing the upstanding steel flange. After considerable development activity, this modification to the wing carry through box was subsequently tested in fatigue well beyond the required service life.

The airframe fatigue test programs were well on their way to completion when an in-flight failure occurred on an F-111 aircraft in service. During a low altitude run over a simulated target, the left wing failed in flight causing loss of the aircraft. The load factor, speed and gross weight of the aircraft at the instant the wing separated were known to be well below design limits. An immediate investigation on-site revealed a flaw in the lower plate of the wing pivot fitting. See Figure 3. A very

thorough examination of this flaw led to the conclusion that it had developed during manufacture and had remained undetected. An analysis of the failure using the principles of fracture mechanics was very straightforward and showed stress levels consistent with the estimated load factor at the time of wing separation.

4.0 ASSURING SAFETY IN THE F-111 FLEET

The wing pivot fitting fracture which caused loss of the F-111 aircraft and, to a lesser degree, the fracture problems encountered during the test programs led to the position that fracture control of the critical steel parts in the structural subsystem was necessary. The objectives of fracture control were to insure the safe operations of the aircraft in service. The approach to development of the methodology had to take into consideration the fact that a sizeable number of aircraft were currently operational and a considerable number remained in the manufacturing program. Basically the approach was to establish an interval between inspection periods that would correspond to a very high probability that no failure would occur. Such an interval, illustrated in Figure 4, required the establishment of the following:

1. The initial size (a_i) of the assumed flaw at the beginning of the inspection period.
2. The behavior of this flaw in terms of crack growth as a function of time under service conditions of load and environment.
3. The critical size (a_c) of the flaw for service operations.

The principles of linear elastic fracture mechanics provided the basis for developing a crack growth algorithm and for determining critical flaw sizes under both proof test and in service conditions.

Initial flaw sizes, assuming that flaws do exist in the critical steel parts, had to be sufficiently small in comparison to the flaw sizes critical for service operations such that a reasonable and workable inspection program would result. Two approaches were used in establishing these initial flaw sizes - proof testing at -40°F temperatures and non-destructive inspections. Considerations of screening to flaws sufficiently small raised the question as to inspectability of the critical steel components involved. This was particularly acute in considering the aircraft which had completed the manufacturing cycle and were in service. Inspection by non-destructive inspection (NDI) techniques would require in a number of areas disassembly including removal of interference fit fasteners. The alternative was proof tests wherein such areas could be reliably screened by stress fields. That is, flaws just smaller than that which would fail the part during proof test could be safely assumed as an initial flaw size. The D6ac steel material has the basic fracture toughness properties [see Figure 7(a)] such that the lower toughness values at the -40°F temperatures selected for proof test provided initial flaw sizes in most of the areas that met the requirements for satisfactory inspection intervals.

The proof load levels were set at +7.33g's and -2.4g's at a wing sweep position equal to 56°.

There were certain areas wherein the proof testing produced relatively low stress levels that were easily accessible to non-destructive inspection techniques. In these cases NDI provided the necessary flaw size. Evaluation of inspection procedures typically used in industry were carried out. Though most of these procedures were found adequate, recommendations were made to upgrade certain of the techniques including magnetic particle and ultrasonic inspection methods. In addition, a very useful technique which has been called magnetic rubber inspection was developed in the General Dynamics laboratories and was used in certain areas. To qualitatively set an initial flaw size on the basis of NDI, it was necessary to characterize the specific procedures used for the F-111 parts in terms of curves of probability of detection vs. surface flaw dimensions at a 95% confidence level. Two such curves are shown in Figure 5. This data was established by a series of test programs including trials under production conditions by certified inspectors at General Dynamics, Sacramento Air Materiel Area (Air Force), Grumman Engineering Corporation, and other D6ac steel part suppliers.

A number of steps were evolved to determine critical flaw growth characteristics which included the following:

a. Selection of critical areas in the steel components in establishing the associated stress equations.
b. Definitions of the design service environment in terms of load, temperature, and chemical exposure.
c. Laboratory testing to provide basic fracture mechanics data.
d. Procedures for stable flaw growth analysis.
e. Experimental correlation of the flaw growth model.
f. Inspection interval calculations.

The critical parts were selected on the basis of high stress areas and critical geometries judged to be more difficult to inspect non-destructively. Critical forgings were of primary interest because of the previously discussed wing pivot fitting failure. The intervals calculated for these parts were assumed to cover the less critical areas.

The service usage spectrum was based upon mission profiles defined in terms of the usual configuration parameters such as Mach number, altitude, wing sweep, and gross weight. The spectrum also was defined in terms of thermal histories, cyclic rates and chemical environment inasmuch as these parameters were of concern as to their effect on both crack growth rates and fracture strengths of the D6ac steel alloy involved. Summaries of the service usage definition are given in Figures 6(a) and 6(b).

The basic fracture mechanics data used was developed in terms of K_{IC} and da/dn. The compact tension specimen was used primarily in developing this data. Fracture toughness (K_{IC}) of the D6ac steel is significantly a function of temperature and the heat treating process. Basic crack growth rates (da/dn) are affected by chemical environment, stress ratio, and cyclic frequency. The experiments run showed that product form, grain direction, and specimen type were of lesser importance. Examples of these data are shown in Figures 7(a) and 7(b).

Sustained load crack growth rates (da/dt) and threshold stress intensity factors (K_{ISCC}) are also established using compact tension specimens. The D6ac steel exhibits an "incubation" period defined as the time required before sustained crack growth takes place. Therefore the data was developed in the form of both incubation and failure time as a function of K_{Ii}. Subsequent investigations including tests showed that sustained loads had little or no effect on crack growth in the critical steel parts and da/dt calculations were discontinued.

The question of an analytical approach to model flaw growth presented a problem. In general such a model would make use of basic da/dn data and must predict crack size under the conditions of the design service environment. The question relative to the load interaction was the most significant aspect to be addressed.

The development of the flaw growth model and the correlating experiments are discussed in the following section.

5.0 FLAW GROWTH - ANALYTICAL AND EXPERIMENTAL

The calculation of a safe inspection interval required consideration of the problem of predicting crack growth under a sequence of varying loads in areas of differing geometry and stress level. Basic data used in the analysis is generated under constant amplitude load cycles and reduced to the form of the following equation:

$$da/dn = f(\Delta k) \tag{1}$$

where da/dn = crack size extension per cycle of load

Δk = change in stress intensity factor.

Crack growth predicted using the above equation works well if the service loading is constant amplitude. Obviously this is not the case and differences between predicted and observed growth for constant and varying amplitude load cycles were known to be very significant. Though a number of investigations were found which touched on the retardation effects of high load cycles under spectrum loading conditions, no analytical technique was readily available. Therefore, it was necessary to develop an approach which was sufficiently accurate and simple for computational purposes. The flaw growth model developed by Wheeler met these requirements (2).

Experimental data suggested the analysis procedure could be modified to include retardation effects of high loads by the addition of a retardation parameter. This parameter should have the properties of having a minimum value immediately after a high load and a maximum value at some later time increment. The parameter also intuitively should reflect the strain state at the crack tip. An equation in the following form satisfied these requirements:

$$a_n = a_{initial} + \sum_{i=1}^{n} C_{P_i} \left[da/dn = f(\Delta K_i)\right] \tag{2}$$

where $C_{P_i} = \left[\frac{R_y}{a_p - a}\right]^m$ for $a + R_y < a_p$

$C_{P_i} = 1$ for $a + R_y \geq a_p$

See Figure 8 for definition of terms.

The shaping exponent m was evaluated initially using very simple tests. Compact tension specimens with simple loadings as shown in Figure 9 indicated an m factor of approximately 1.3 would sufficiently bound the test data. Additional tests were run applying load spectra ordered in different ways, for example, low to high, high to low, which further showed that the m = 1.3 factor provided very reasonable results. A different crack configuration was tested using a surface flaw in a plate specimen and the results similar to those found using the compact tension specimen. At this point it was felt that the flaw model would be satisfactory for the fracture control program being developed and correlation of the m factor under F-111 design configurations and environment was the next step.

A series of spectrum environmental tests were run using primarily surface flaw test specimens which included the variables of:

- o environment
- o spectrum shape
- o load ordering
- o stress levels
- o compression loads
- o flaw shape
- o material properties

The test spectra were basically in two forms: flight-by-flight and block form with each block representing 200 flight hours. Both spectra were equivalent in terms of content differing primarily in the ordering of loads. Correlation of the test results indicated that the parameter m = 1.4 would conservatively form a lower bound for the F-111 design requirements. This is illustrated by the data shown in Figure 10.

The following conclusions were based on the results of the spectrum environment test program:

1. Flight-by-flight test spectra with random ordering of loads showed higher crack growth rates than the block spectrum approach.
2. Retardation characteristics were essentially the same for different peak load levels and for different overall stress levels, that is, m = 1.4.
3. Compression loads of the magnitude typical of the F-111 design had relatively little effect on crack growth test results.
4. D6ac steel alloy (220-240 ksi) appears to have greater resistance to corrosion fatigue under spectrum loadings than under constant amplitude loadings.
5. The test data indicated that sustained loads were not a significant factor in contributing to crack growth primarily because the crack would grow critical in service prior to reaching a size that produced stress intensities greater than K_{ISCC} under sustained load conditions.

The analytical and experimental work described produced a crack growth model which was then applied in the fracture control program to calculate safe inspection intervals. An example of these calculations follows:

a. Critical Part: Wing Pivot Fitting Lower Plate

Plate thickness, t = 0.281"

b. Stress Data: Maximum probable in-service, f = 95,600 psi

Proof test, f = 141,400 psi

c. Fracture Toughness: Proof Test Temp (-40°F),

K_{IC} = 36 ksi $\sqrt{in}$

In-service (+10°F),

K_{IC} = 42.5 ksi $\sqrt{in}$

d. Assumed Flaw After Proof Test:

$$a = \frac{K_{IC}^2 \left[\phi^2 - 0.212 \left(\sigma / \sigma_{ys} \right)^2 \right]}{1.21 \pi \sigma^2 M_K^2} \qquad (3)$$

where a = crack depth

ϕ = flaw shape parameter for half-penny flaw

M_K = back-face correction factor

σ = proof test field stress

$$a = \frac{(36)^2 \left[2.46 - 0.212 \, (141.4/210)^2 \right]}{3.8 \, (141.4)^2 \, (M_K = 1.0)^2}$$

$a_{initial}$ = 0.041 inches

e. Critical Size of Assumed Flaw In-Service:

$$a_{cr} = \frac{(42.5)^2 \left[2.46 - 0.212 \, (95.6/210)^2 \right]}{3.8 \, (95.6)^2 \, (M_K = 1.01)^2} \qquad (4)$$

a_{cr} = 0.124 inches

f. Calculation of Flaw Growth Time from $a_{initial}$ to $a_{critical}$:

Service Environment - (Load spectra defined in terms of stress excursions corresponding to flight and ground loads arranged in flight-by-flight and random order)

Basic da/dn Data - (Data programmed for automatic computer analysis in form of Δk versus da/dn for JP-4 fuel environment)

Crack Growth Model -

$$a_n = a_{initial} + \sum_{i=1}^{n} \left[\frac{R_y}{a_p - a}\right]^{1.4} \qquad (da/dn = f(\Delta k)) \qquad (5)$$

(Calculations programmed for automatic computer. The crack extension for each loading cycle is calculated by the above algorithm and added to the crack length prior to the particular load application)

These calculations were prepared for a total of 18 critical areas in the steel structure. A review of the resulting minimum inspection times led to the following inspection intervals for the F-111 fleet.

TAC aircraft - 1500 flight hours
SAC aircraft - 2500 flight hours

Service life monitoring procedures have shown that these inspection intervals can be extended still maintaining a high level of safety in the structural system.

6.0 COMPARISON WITH CURRENT DAMAGE TOLERANCE REQUIREMENTS

The F-111 fracture control plan developed for the critical steel structures is believed to be the first application of such procedures in providing safe aircraft structural systems. The material characterization was of necessity very thorough and investigated all of the known aspects of the D6ac steel behavior that could influence flaw growth. The application of the principles of fracture mechanics required a certain amount of ingenuity in developing a methodology leading to a sound and practical procedure of fracture control. Consequently, an extremely high level of safety has been achieved in a structural design using a high strength steel relatively brittle in comparison to the newer steel alloys available today.

It is of interest to look at the F-111 program in comparison to the current USAF damage tolerance control procedures. USAF Regulation 80-13 requires that *MIL STD 1530 be adhered to in the design of structural systems.* This standard defines the overall requirements necessary to achieve structural integrity in USAF airplanes and also specifies acceptance methods of contractor compliance. It also requires that the designs be damage tolerant in accordance with Spec MIL-A-83444, "Airplane Damage Tolerance Requirements." Damage tolerance designs are categorized into two general concepts - a) slow crack growth, b) fail safe. In either case, the presence of undetected flaws is assumed.

The current approach for safety and durability in aircraft systems design is diagrammed in Figure 11(a). Figure 11(b) describes the basic elements in the F-111 fracture control program. The basic differences arise from the fact that the F-111 work was planned and carried out after material selection and detail design was complete.

The current approach properly focuses emphasis on material selection. In the past the use of high strength materials in the push for minimum weight resulted in the use of relatively brittle materials intolerant to very small flaws. Recent emphasis in materials development has produced much tougher alloys which in themselves will produce more damage tolerant designs. However a positive plan of fracture control provides a way to safely use the less tough materials with a high degree of safety.

Detail design of the F-111 was based on the older concept of safe life as demonstrated by fatigue testing to a scatter factor of 4. The stress levels set in the structure to meet this requirement were demonstrated to be more than adequate - if no flaws are present. Such though is not the case as evidenced by the wing failure previously discussed. The fastener policy used on the F-111 in both critical steel and aluminum structure has turned out to be most satisfactory in terms of fracture control. This is also a feature of the new approach to damage tolerance in the Air Force requirements. The taper-lok interference fit bolts used in the F-111 design provide very significant improvement in reducing crack growth rates originating from holes in which these fasteners are installed.

The current approach to damage tolerance requires that both chemical and thermal environmental effects be considered. These considerations were also a significant part of the F-111 fracture control procedures in establishing the service usage spectrum. As has been pointed out, the D6ac steel alloy is susceptible to temperature extremes as far as toughness is concerned. In addition chemical environments affect crack growth rates. The possibility of detrimental chemical exposure during manufacture cannot be overlooked. Cleaning fluids, cutting coolants, etc. must be considered in a fracture control program and those that are harmful must be screened out.

The fracture analysis model used in the F-111 continues to be effective and is being employed on other programs. Other models are also available including crack closure model and the Wellenborg model. All models rely on correlation of empirical data and experimental work will continue to be necessary to verify the analytical approaches. Finite element procedures are now available for calculation of stress intensity factors as a function of crack growth through complex geometries. Work continues in developing the analysis procedures but the algorithms currently at hand can be satisfactorily used in meeting the requirements of fracture control.

The role of non-destructive evaluation in the current damage tolerance approach is two-fold. Use of non-destructive test methods during manufacture continue to screen the structural parts for flaws or defects as part of the quality assurance program. They can also be used as a basis for establishing initial flaw sizes. The current damage tolerance specifications for slow crack growth structures require that a surface flaw 0.25 inches in length be assumed in critical areas and that a corner flaw 0.05 inches in length be assumed at critical bolt holes. These requirements must be considered in the design unless the non-destructive inspection procedures can be shown to screen the structure to smaller flaw sizes. Quality control and inspection of materials and parts is a matter of degree. Therefore it is most important that non-destructive inspection capabilities be defined under production conditions in terms of probability-to-detect vs. flaw size at a high confidence level (95%). There is no question but that the F-111 could not meet the initial flaw sizes specified in the current damage tolerance criteria and that the proof test and non-destructive inspection methods would have been required to provide a satisfactory inspection interval. There is also a very real question as to the quantitative effectiveness of in-service non-destructive inspections.

In summary, fracture control will immeasurably improve structural integrity of aircraft in service. The specifics of the program will vary with the design concept. In a sense the F-111 program can be viewed as a prototype program and its success illustrates the practical addition of a very important tool in maintaining safe and reliable structural systems.

REFERENCES

1. Buntin, W. D., "Concept and Conduct of Proof Test of F-111 Production Aircraft," The Aeronautical Journal, The Royal Aeronautical Society, Volume 76, Number 472, October 1972, pp 587-598.

2. Wheeler, O. E., "Spectrum Loading and Crack Growth," Journal of Basic Engineering, Trans. ASME, March 1972.

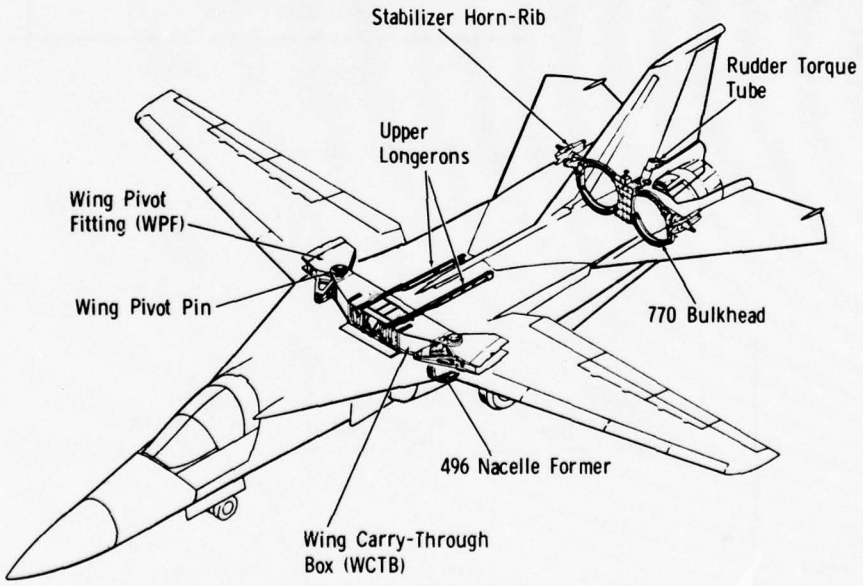

Figure 1 F-111 Critical Steel Parts

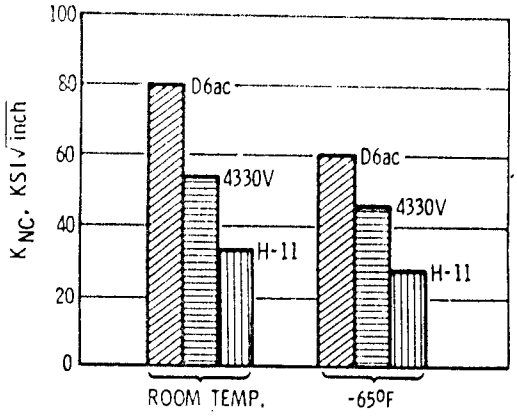

Figure 2 Steel Alloy Fracture Toughness

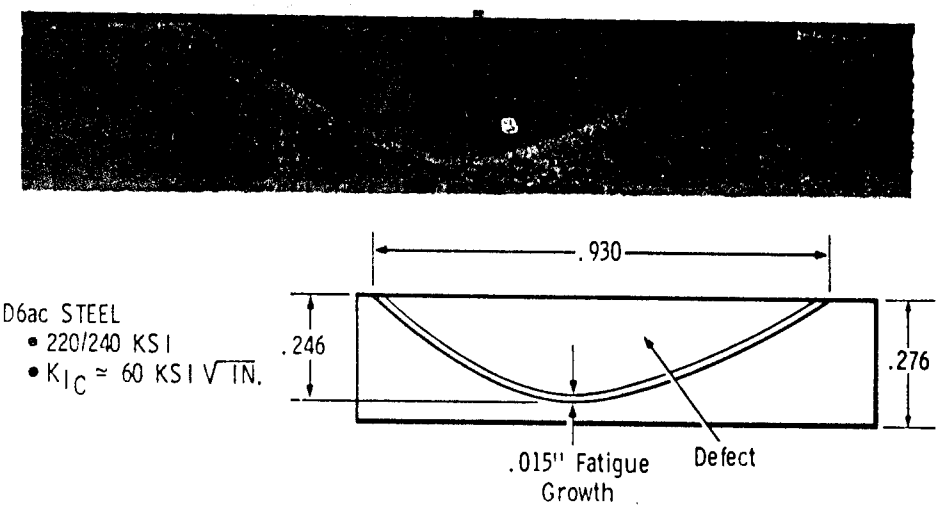

Figure 3 Wing Pivot Fitting Flaw

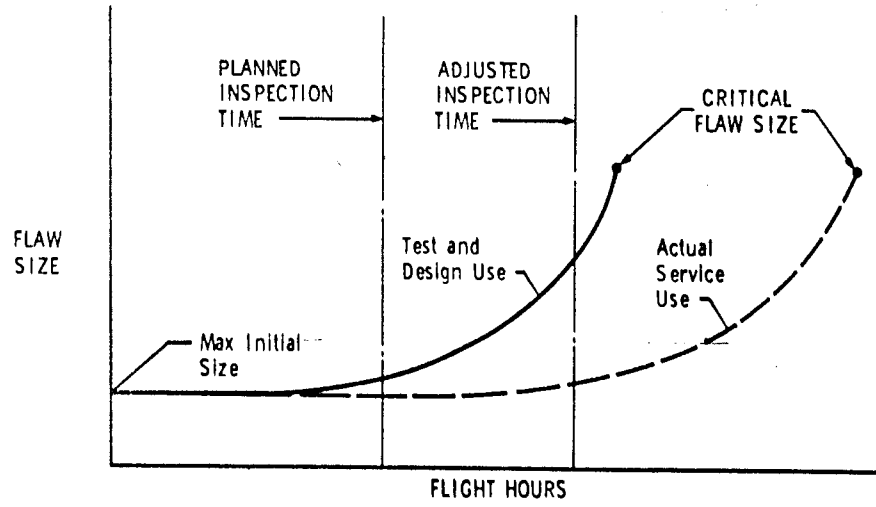

Figure 4 Inspection Interval Concept

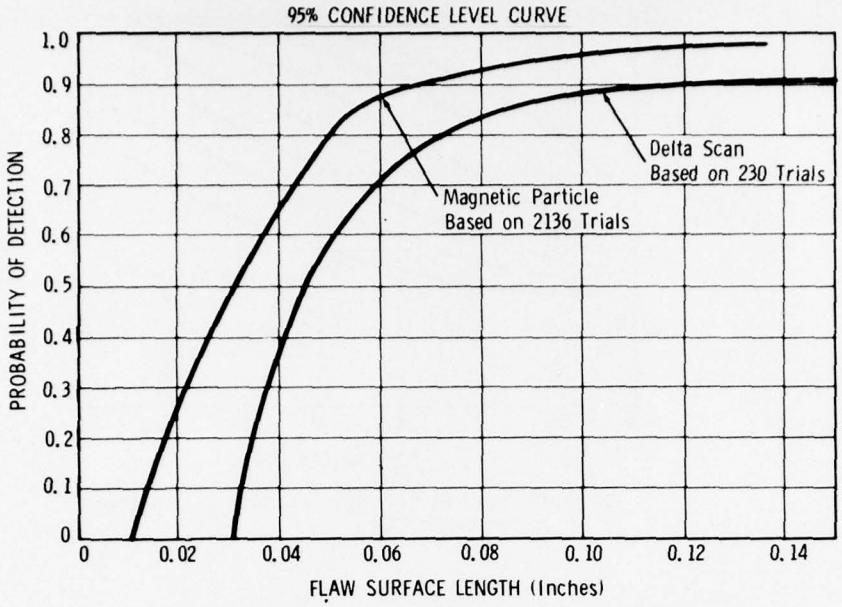

Figure 5 Non-Destructive Inspection Production Detection Capability

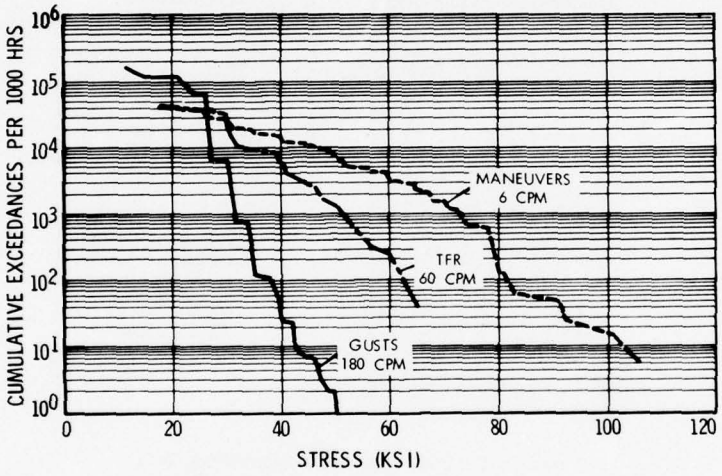

Figure 6(a) Design Service Stress Spectrum for Wing Pivot Fitting Lower Plate

FLIGHT EXPOSURE	% FLIGHT TIME
• Humidity 75%	45.8
Condensation	3.7
• Rain	.7
• Dry Air	49.8
• JP-4 Fuel	100.0 (internal)

GROUND EXPOSURE	% GROUND TIME
• Humidity - Condensation	19.7
50-75%	35.2
75-100%	34.1
• Rain	11.0
• JP-4 Fuel	100.0 (internal)

Figure 6(b) Environmental Exposure of Wing Pivot Fittings for F-111E Aircraft Based at Upper Heyford, England

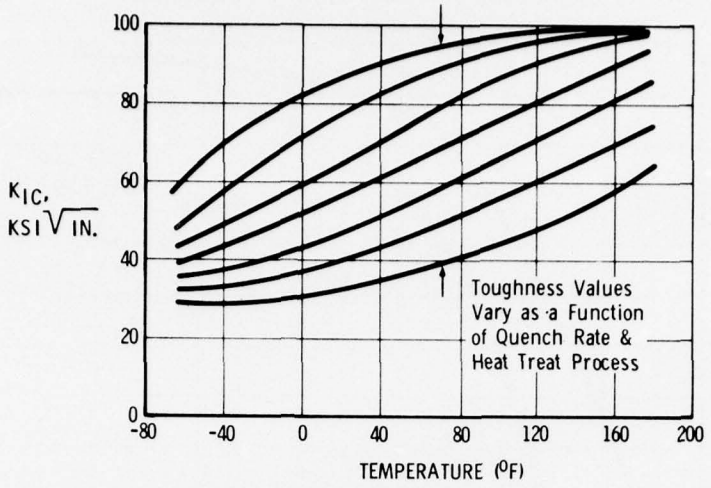

Figure 7(a) D6ac Steel Fracture Toughness as a Function of Temperature

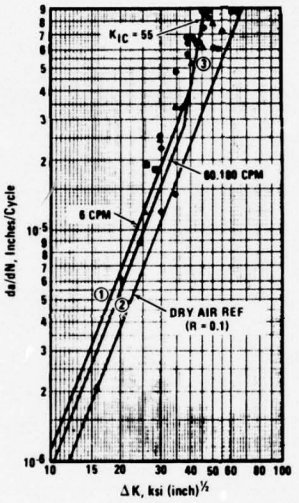

CRACK GROWTH RATE DATA

THICKNESS = 0.25 IN.

ROOM TEMPERATURE

JP-4

R = 0.1

SYM.	SPECIMEN NUMBER	H.T. METHOD	EST. K_{IC}
■	1M29(▽)	C	87
▲	1M30(▽)	C	84
●	1H28(▽)	A	95
●	2L29(▽)	E	58

ALL DATA AT 6 CPM

EQUATIONS FOR ANALYSIS CURVES
① $da/dN = 0.0028 \times 10^{-6} (\Delta K)^{2.625}$
② $da/dN = 0.0022 \times 10^{-6} (\Delta K)^{2.625}$

$da/dN = C(\Delta K)^{5.875}$

	K_{IC}	$C \times 10^{14}$
③	55	1.8129

Figure 7(b) D6ac Steel Crack Growth Rate Data

- $a_n = a_i + \sum_{i=1}^{n} C_{pi}\ [da/dN = f(\Delta K_i)]$
- $a + Ry \geq a_p$

  $C_{pi} = 1$
- $a + R_y < a_p$

  $C_{pi} = \left(\frac{R_y}{a_p - a}\right)^m$
- $\frac{da}{dN} = f(\Delta K)$

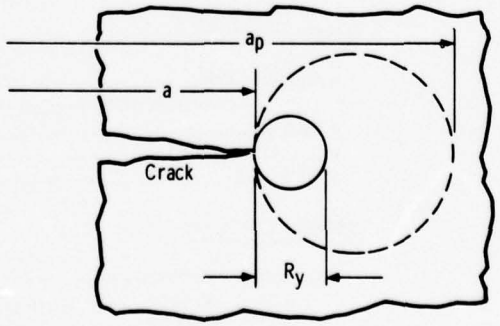

Where,

R_y = Current Yield Zone Size

$(a_p - a)$ = Distance from Crack Tip to Elastic-Plastic Interface

m = Shaping Exponent Established Experimentally

Figure 8 Analytic Flaw Growth Model Including Cp Retardation Factor

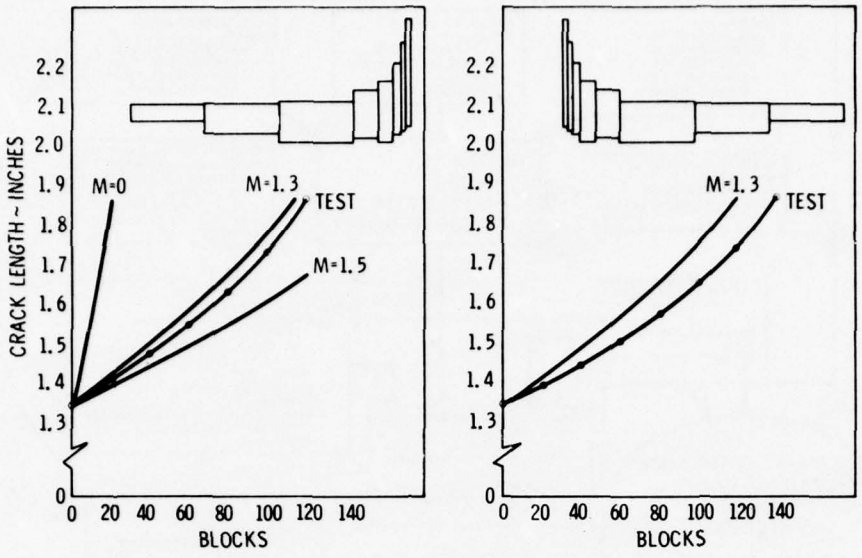

Figure 9 Analytical Correlation with Compact Tension Test Data

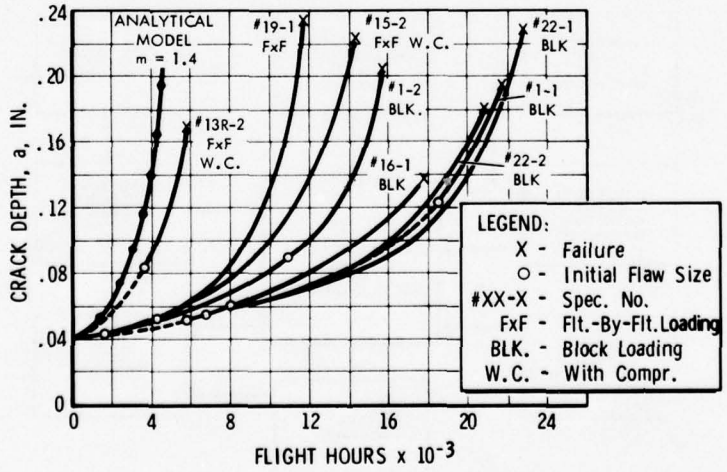

Figure 10 Surface Flaw Growth Test Results for D6ac Steel Under Spectrum Loadings in JP-4 Fuel

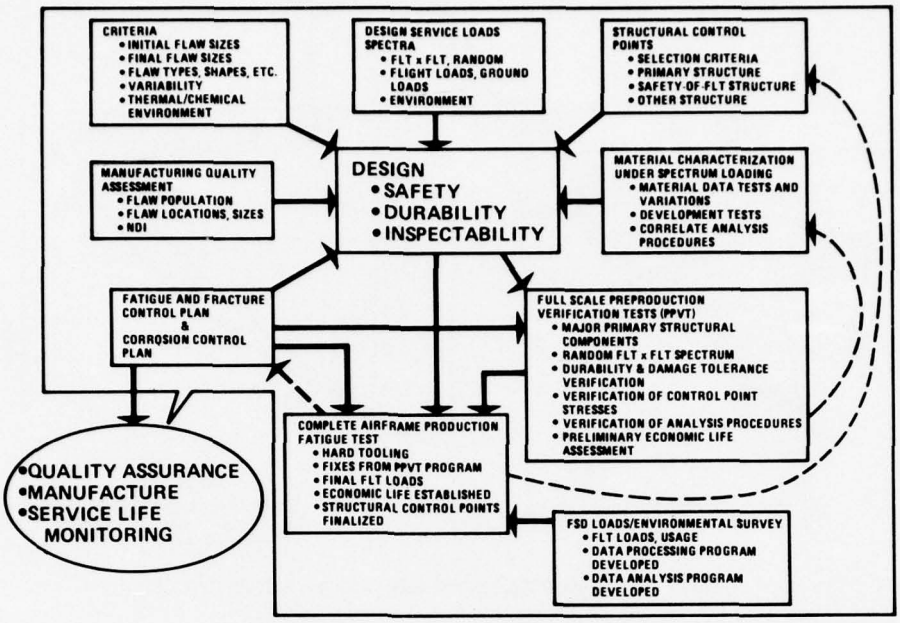

Figure 11 (a) Major Elements of Current Approach to Safe Durable Design

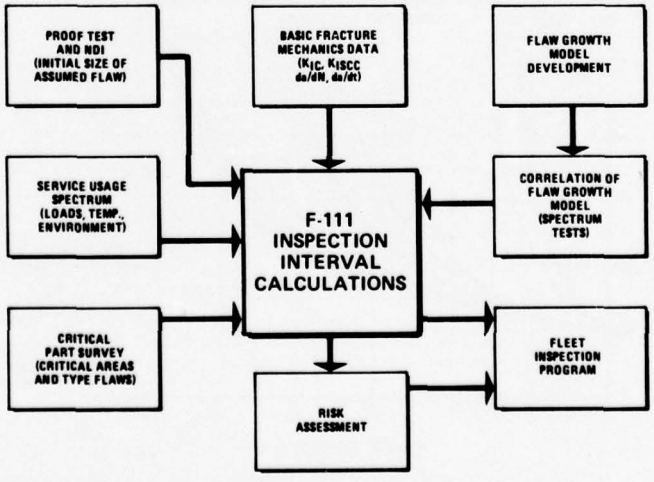

Figure 11 (b) F-111 Fracture Control

CONTRIBUTED DISCUSSION

by

J.W.Mar
Massachusetts Institute of Technology
Room 33–309
Cambridge, Massachusetts 02139
USA

The author has presented the engineering essence of the application of fracture mechanics to the F-111 airplane and he has done this very well. However there are many other 'essences' which the author has not mentioned. The other 'essences' include political and management issues which at times threatened to make the application of fracture mechanics to the F-111 airplane moot but which in the long run gave a tremendous boost to fracture mechanics. A few observations and comments may be interesting.

1. Historians always like dates. I submit the date of 22 December 1969 as the date signalling the era of fracture mechanics in the USAF. After this date, the entire Air Force hierarchy up to the military and civilian heads understood that small flaws could cause catstrophic failures. Indeed, Senators and Congressmen could and did ask knowledgeable questions about fracture mechanics. Terms such as fracture toughness, slow crack growth, scatter factors became part of the everyday vocabulary.

2. The flaw in the wing pivot fitting which began the era of fracture mechanics, up to this point in time, is a singular occurrence. All of the proof testing and other NDI have not found a similar flaw. What if this flaw had not occurred? Would fracture mechanics be where it is today? Would there be MIL STD 1530 and a MIL-A-83444?

3. The F-111A airframe has passed all of the old style fatigue tests, i.e., cyclic loading to a scatter factor of four. It has also passed all of its static structural tests.

4. The author writes "...a sizable number of the aircraft were currently operational and a considerable number remained in the manufacturing program". USAF management had to decide (a) whether or not to ground all of the airplanes and (b) whether or not to stop the production line going. (The author has many scars in his psyche because of these essences of the overall problem.)

5. The Senate was at this time also conducting hearings into the DOD management of the F-111 program. There were political pressures to cancel the program. Without fracture mechanics as the disciplinary base upon which to assess the integrity of the airframe, I am reasonably sure the program would not have survived in its present form.

6. Every item the author has listed in Fig. 11A, "Major Elements of Current Approach to Safe Durable Design", can be shown to have its roots in the structural integrity experiences of the F-111 airplane. He has only been able to touch upon the highlights. The complete story is even more fascinating.

CONTRIBUTED DISCUSSION

by

G.P.Haviland
Director of Structures and Design
B-1 Division
Rockwell International Corporation
Los Angeles, CA 90009, USA

I found Mr. Buntin's paper extremely interesting in view of the timing of his exposure as applied to the fracture mechanics discipline on the F-111 compared to my later exposure as applied to the B-1. I will explore that point further. But first, let me commend Mr. Buntin on the quality of his paper. It is comprehensive, factual, and deals with a most important phase of structural technology development during the 1969 to 1973 period.

In particular, I agree completely with the author's paragraph "...the F-111 program can be viewed as a prototype program and its success illustrates the practical addition of a very important tool in maintaining safe and reliable structural systems."

In his paper, the author makes a basic assumption which is the foundation upon which the discipline of fracture mechanics rests. He assumes that the probability of having flaws in an airframe as delivered to the customer is finite. This means that the materials chosen for fracture critical components must have crack growth characteristics which preclude reaching critical flaw size in less than one lifetime. Stated another way, the components must be damage tolerant for the life of the airframe.

The approach described by Mr. Buntin in his paper is substantially the same as that applied to the B-1 program which has fortunately taken advantage of the lessons learned on the F-111 program. For example, all of the materials selected for use on the B-1 were screened for toughness, weight and strength. The monolithic aft fuselage stabilizer support spindle fitting uses 9Ni 4Co .20C steel because of its fracture toughness and weldability. All airframe components were separated into fracture critical and non-fracture critical parts. Special inspection requirements were established and each fracture critical part was proofed by sacrificing a separate part which had been put through the same thermal and forming processes.

While the preceding has shown how the B-1, coming later in time, was able to capitalize on some of the lessons learned on the F-111, the incorporation of those lessons was far from smooth. The suppliers offered some resistance to the new requirements. Even the prime contractor resisted the new program for a time. The resistance had to be and was overcome before the fracture mechanics approach became effective. Also, in the 1970 to 1971 time period most of the people involved in calculating or testing the life of structures were fatigue oriented. They tended to look on the "new" discipline as just another way of accomplishing the same result. Gradually, the pockets of resistance in and outside of the program were won over to the ultimate benefit of the B-1.

In summary, Mr. Buntin has thoroughly described the events attending a major chronological milestone in airframe structural criteria, one which has had far reaching consequences for the B-1 program and one which will undoubtedly impact airframes of the future whether they be military or commercial. We, in the structural community are indebted to General Dynamics and Mr. Buntin for making such a significant contribution.

CONTRIBUTED DISCUSSION

by

G.E.Fitch, Jr.
Fatigue and Fracture Mechanics
B-1 Division
Rockwell International Corporation
Los Angeles, CA 90009, USA

The use of the discipline of fracture mechanics to characterize the damage tolerance of an existing design, after-the-fact, such as the F-111 is the more customary and perhaps best use of this powerful new tool. Mr. Buntin has identified the essence of the application of the procedures, in a very lucid manner, to a complex airframe fabricated from a relatively brittle steel with complex responses to processing and environmental parameters. General Dynamics, Fort Worth, has done an outstanding engineering job of isolating and therefore controlling the effects of most of those variables. This partially answers in an affirmative way one of the unresolved questions about the use of fracture mechanics in the airframe industry, i.e., "does it really enhance the safety of the airframe system?". By identifying the variables affecting strength and toughness of D6 AC steel and revising procurement and process specifications accordingly, safety on the F-111 has been improved.

In at least one other way the procedure has improved the safety status of operating the F-111. The truly critical structural elements of the airframe have been identified. By the standard fatigue "safe-life" approach the critical elements of the primary airframe may well have been those with "short" fatigue lives regardless of their importance to the integrity of the airframe. The fracture mechanics approach has succeeded in focusing attention to truly critical parts.

Because of the after-the-fact application of fracture mechanics, as Mr. Buntin points out, the discipline played no role in material selection. This introduces another important issue concerning the use of fracture mechanics, particularly when used in the design phase. Does F/M really encourage material selections which will ultimately enhance airframe safety? There has been some criticism along the line that the new philosophy damage tolerance criteria with its emphasis on crack growth from initial to critical length actually favors high-strength alloys with minimal toughness. This is due partly to the sometimes negligible impact of the critical crack length on the crack growth life of a typical airframe member. Without some attention in MIL-STD-1530 and MIL-A-83444 to independent, perhaps arbitrary constraints on critical crack length magnitude and its relation to probability of success of in-service NDI, it is difficult to frame an entirely affirmative answer to the second safety question. Industry may have to overcome its natural success oriented reluctance to acknowledge that the world of airframes is flawed at the outset and concern itself more with the all too often small differences between the initial flaw size and the critical flaw size in spite of crack growth analyses which predict adequate life. Only then can material choices be made, in the face of the ever present terrible pressure of cost/weight performance optimization, which help prevent failures before they occur rather than explain them after they occur.

NORTHROP/UNITED STATES AIR FORCE DURABILITY AND DAMAGE-TOLERANCE ASSESSMENT OF THE F-5E/F AIRCRAFT

by

S.R. Murnane, Manager, F-5 Technology Department
Northrop Corporation, Aircraft Division
3901 West Broadway, Hawthorne, California 90250

T.D. Stronge, Senior Technical Specialist
Northrop Corporation, Aircraft Division

O.B. Davenport, Airframe Division
International Fighter Systems Program Office
Aeronautical Systems Division
Wright-Patterson Air Force Base, Ohio 45433

CONTENTS

1.0 ABSTRACT

The Northrop Corporation, Aircraft Division F-5E/F air superiority fighters have successfully completed a comprehensive Aircraft Structural Integrity Program (ASIP). Although the design philosophy was based on safe-life requirements, the concepts of damage-tolerance were increasingly applied during the course of the full-scale fatigue test and in the establishment of a structural maintenance program. A summary of fatigue test failures experienced during the complete airframe flight-by-flight fatigue test is reviewed, including the application of fracture mechanics employed during resolution of these failures. Damage-tolerance analyses and specimen tests for other primary structure are discussed. State-of-the-art analytical crack growth rate predictions for flight-by-flight spectra are compared with specimen test results. Compliance of the F-5E/F airframe structure with the USAF damage-tolerance requirements is discussed, along with recommendations for the application of fracture mechanics to future aircraft design.

2.0 INTRODUCTION

The F-5E/F ASIP included a flight flutter and flight loads survey program, a static test and fatigue test program, and the analytical programs necessary to support these test programs. The primary objective of the ASIP was to ensure that the aircraft's structural design would operate satisfactorily when subjected to the conditions associated with air-to-air combat and air-to-ground weapon delivery. This paper describes only the fatigue and fracture mechanics portions of the total ASIP and discusses the USAF philosophy with respect to the application of damage-tolerance analysis. Recommendations for future aircraft design, in view of the lessons learned from durability testing and application of damage-tolerance requirements, also are presented. Definitions are contained in Section 15.0. Figure 1 shows the fatigue test setup for the F-5E complete airframe; Figure 2 is a diagram of the airframe load application scheme.

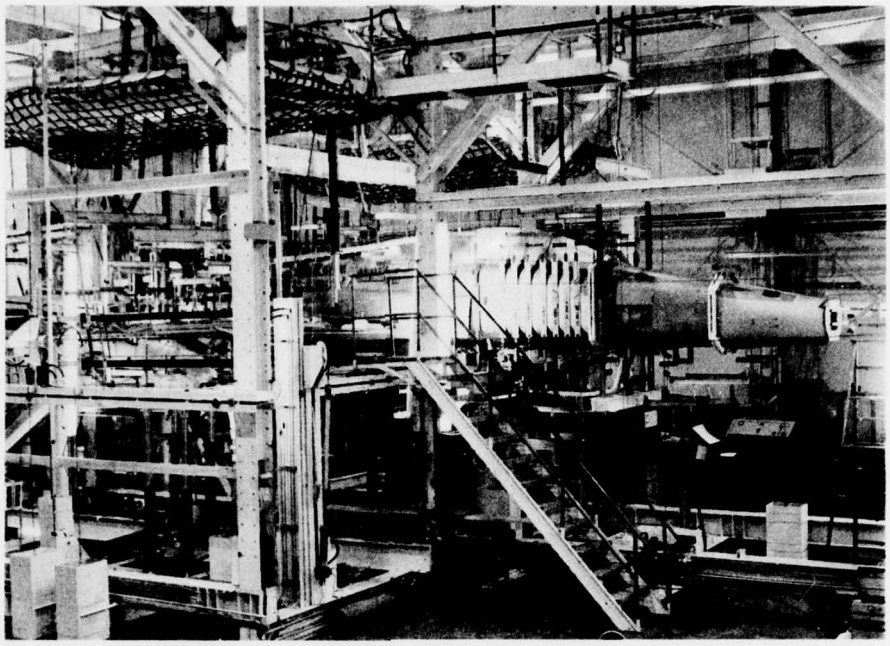

FIGURE 1. F-5E COMPLETE AIRFRAME FATIGUE TEST SETUP

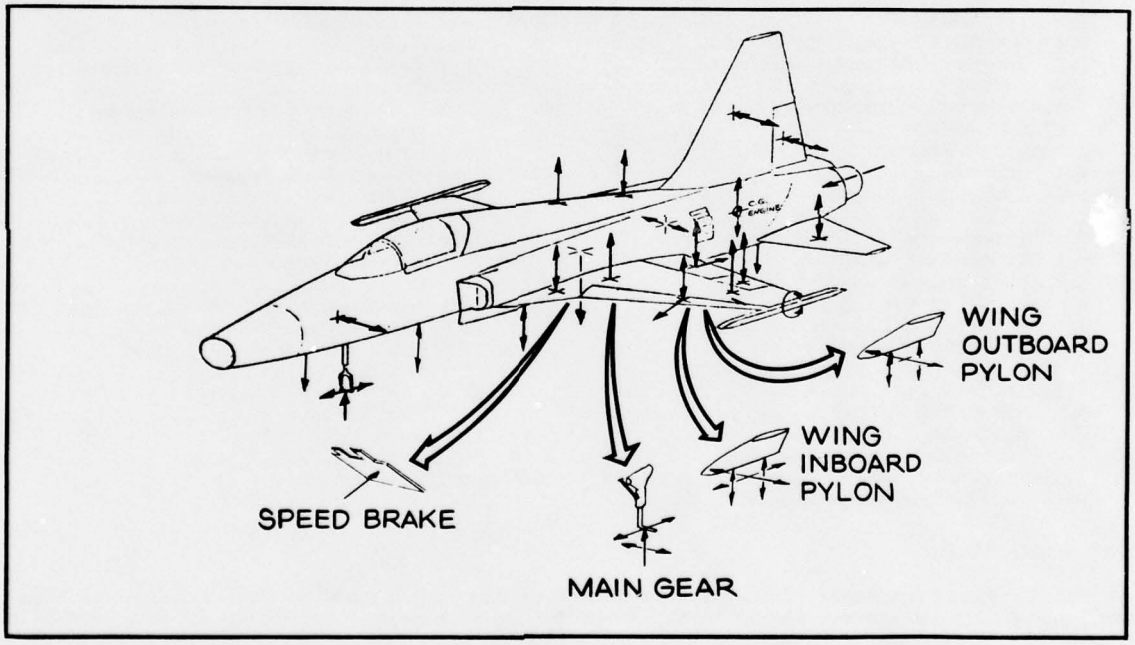

FIGURE 2. AIRFRAME LOAD APPLICATION SCHEME

3.0 REQUIREMENTS

3.1 F-5E/F Mission Requirements and Design Criteria

The F-5E and F-5F are the latest single-place and two-place aircraft in the F-5 series of lightweight, high-performance, twin-turbojet tactical fighters. A three-view diagram of the F-5E is shown in Figure 3. The aircraft's basic mission is to provide air superiority through its aerial combat capabilities. The aircraft also has a secondary mission to provide interdiction and close air support, with the capability to deliver a wide variety of ordnance. The basic structural design criteria for the F-5E and F-5F were based on the MIL-A-8860(ASG)[1] specifications and ASD TR-66-57[2] with a design safe-life goal of 4000 hours and a scatter factor of four. As the F-5E/F fatigue program was formulated during a transition period of fundamental change in the USAF ASIP philosophy, the F-5E/F ASIP was structured to meet the then-current requirements; however, as the program progressed, damage-tolerance analysis and testing were increasingly applied in the interpretation of fatigue test incidents and for subsequent redesigns. Near the conclusion of the program, the damage-tolerance and durability influence in design were virutally equivalent. The initial flaw sizes and requirements of MIL-A-83444[3] generally have been employed as the basis for determining inspection/repair requirements, with the fatigue test and subsequent analysis determining the maximum economic life.

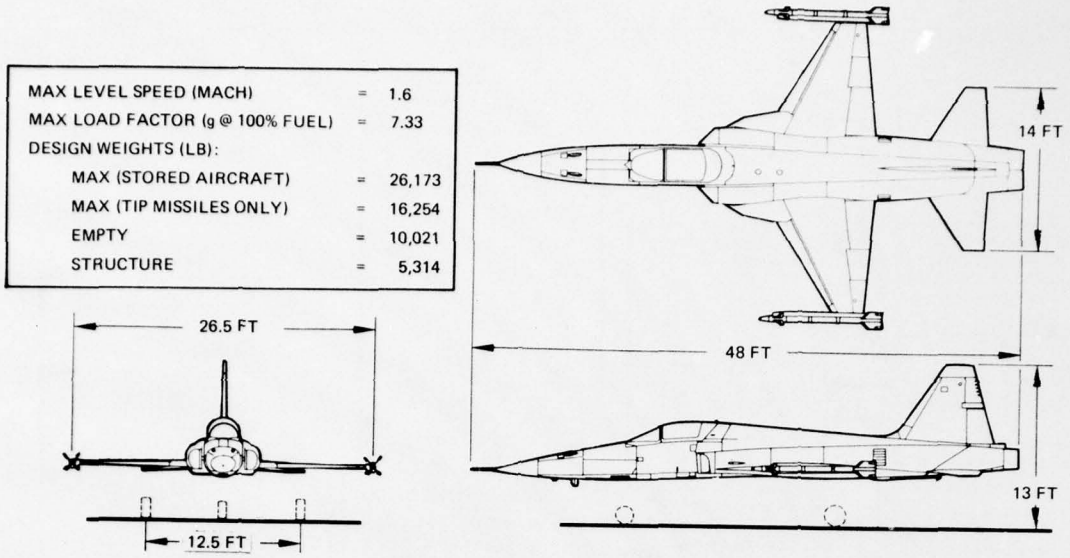

FIGURE 3. F-5E AIRCRAFT THREE-VIEW DIAGRAM

3.2 Analysis and Testing

Fatigue analysis utilizing both the Palmgren-Miner hypothesis[4] and residual stress method based on notch stress history were conducted to assess the aircraft's capability to meet the 4000-hour service life goal. These analyses were augmented by a complete airframe fatigue test conducted on a structurally complete F-5E airframe with the loading applied randomly flight-by-flight, phase-by-phase. As the test progressed, damage-tolerance analysis was conducted on each area shown to be critical during the test. With concurrent fatigue testing and production, damage-tolerance analysis provided the basis for program economies by defining inspection methods and procedures that protect flight safety and allow for use of structure with subcritical cracks. Upon conclusion of the fatigue test, a complete disassembly of the test article was conducted to detect hidden cracks. Further, a final damage-tolerance analysis, based on the test experience, the tear-down inspection results, measured flight loads, and measured stresses, is currently being conducted to provide a comprehensive structural maintenance program which will assure safety of flight throughout the economic life of the aircraft.

3.3 Economic Life and Service Life

The definition of economic life utilized in the F-5E/F development program was that point in the life of the airframe where structural damage creates an unacceptable hazard to flight, and repair costs are uneconomical compared to replacement cost of the airframe. This economic life can also be considered to be the maximum service life of the airframe, assuming that an adequate structural maintenance program is effected which will assure flight safety.

As a result of full-scale fatigue testing conducted beyond the original four lifetimes (16,000 hours) to six lifetimes (24,000 hours), the service life estimates for the F-5E/F aircraft have been increased from the required 4,000 hours to 8,000 hours for the design spectrum consisting of 85 percent air-to-air combat and 15 percent air-to-ground (85/15) missions. Other operations have different service life estimates ranging from 8,000 hours in the normal Military Assistance Program/Foreign Military Sales (MAP/FMS) roles to 2,500 hours in the DACT (Dissimilar Air Combat Training) role. (DACT is an air combat training program for USAF and allied fighter aircrews flying first-line fighters in which the F-5E/F aircraft are used to simulate the aggressor as small, smokeless, highly maneuverable aircraft.) This increase in service life takes into consideration the results of additional supporting fatigue and damage-tolerance analysis that has been accomplished, along with product improvement changes that have been incorporated in follow-on production aircraft.

3.4 Durability and Damage-Tolerance Program Flow Chart

The F-5E/F Durability and Damage Tolerance Program was conducted in three phases as shown in Figure 4: Phase I, Fatigue Test Program; Phase II, Product Improvement; and Phase III, Final Fatigue and Damage Tolerance Assessment Program. The flow chart of Figure 4 presents a pictorial representation of the overall program.

4.0 INITIAL DESIGN REQUIREMENTS FOR DURABILITY AND DAMAGE TOLERANCE

4.1 Fatigue Loads Spectra

The original durability design loads spectra requirements were formulated during the original concept studies for the International Fighter Program, later to be designated the F-5E/F. These requirements called for an aircraft to possess a high degree of durability in the air combat arena. Subsequently it was established that the mission mix

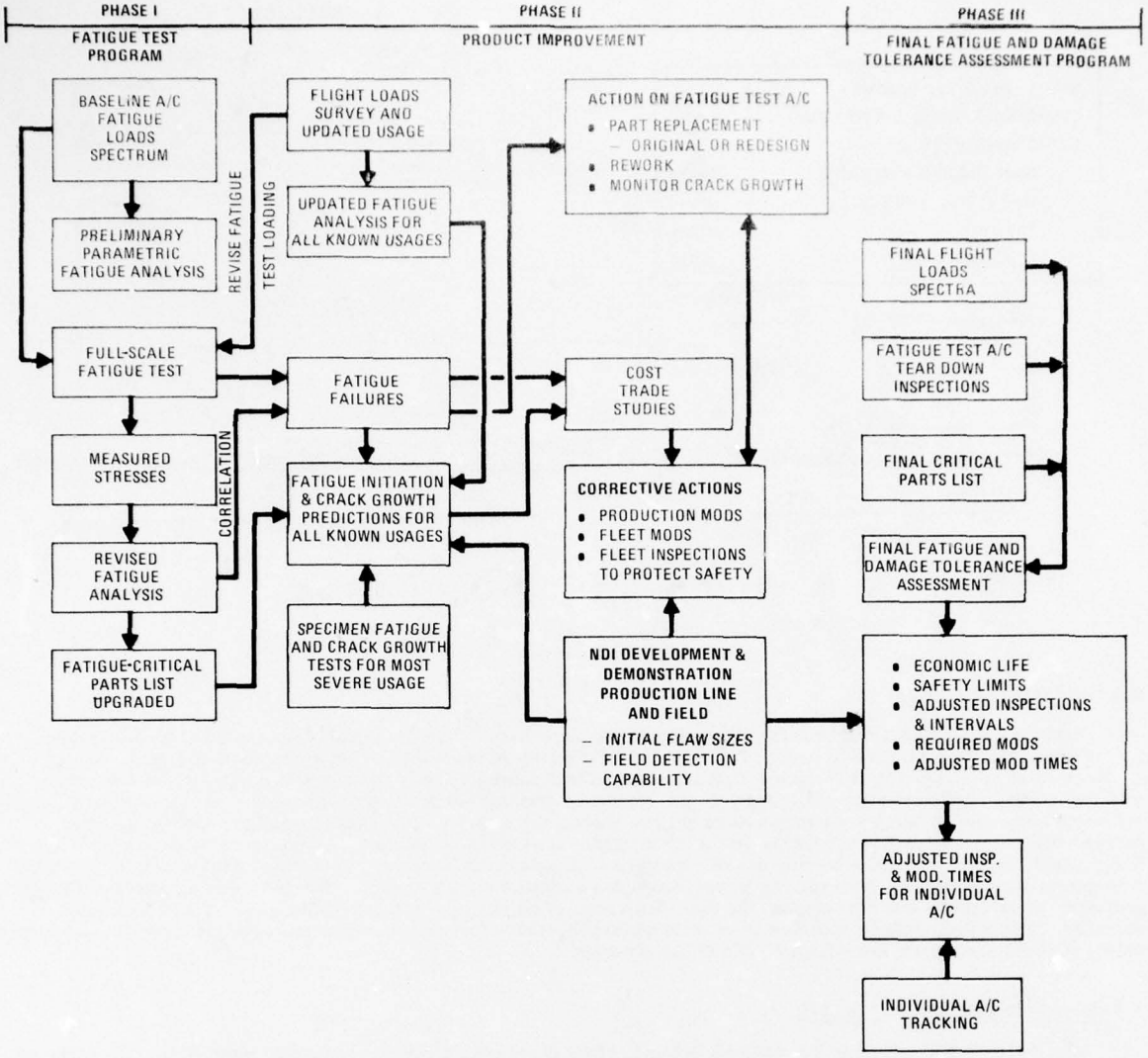

FIGURE 4. F-5E/F DURABILITY AND DAMAGE TOLERANCE PROGRAM

would be 85 percent air combat and 15 percent air-to-ground (85/15). Altitude/time distributions were coupled with the mission phase maneuver spectra for fighter aircraft from MIL-A-00866A[5] as well as other mission-related parameters, to develop the flight-by-flight, phase-by-phase load spectra. It was necessary to develop realistic loading conditions to be used in generating the fatigue load spectra for mission profiles that were representative of actual aircraft usage. An example of this is shown in Section 4 of AGARD-R-640.[6] Randomization of the flights while maintaining the normal sequence of phases, and randomizing the load occurrences within the phase, provided the best simulation of actual flight time history that could be accomplished in ground durability testing.

4.2 Service Life Objective and Target Test Life

The original design service life objective was 4000 service hours which, with a scatter factor of four, required a target test life of 16,000 hours. Subsequently, the Dissimilar Air Combat Training (DACT) usage was estimated to be as much as four times more severe than the design usage; as a result, the fatigue test program was extended for an additional two lifetimes in order to determine the maximum economic life of the airframe.

4.3 Damage-Tolerance Considerations

Although the damage-tolerance requirements of MIL-STD-1530(A)[7] had not been developed when the design of the F-5E was initiated, design concepts were employed in the original design which were beneficial from a damage-tolerance and durability standpoint. These concepts consisted of establishing a target design stress level of 4000 psi for the wing and changing the temper of the primary aluminum structural components from fully hardened to [illegible] alloys, such as 7075-T73, 7075-T76, and 7175-T73, in various sheet and wrought forms. In addition, the [illegible] leading edge flap was supported by five discrete hinges for an inherently fail-safe design. Further [illegible] of damage-tolerance during the F-5E development came from a study by Figge, et al.,[8] which utilized the [illegible] as a baseline for damage-tolerance criteria sensitivity studies. In summary, while the F-5E aircraft was not [illegible] designed to a damage-tolerance requirement, damage-tolerance features were incorporated which have contributed significantly to the airframe's success in meeting and exceeding its durability requirements and its adaptability to later application of damage-tolerance requirements.

5.0 DESIGN AND ANALYSIS

5.1 Structural Arrangement

The F-5E structural arrangement is shown in Figure 5. The fuselage is an all-metal, thin-skin, semi-monocoque structure. The metals used are conventional 7000-series aluminum, with stainless steel and titanium in the high-temperature areas of the engine bay.

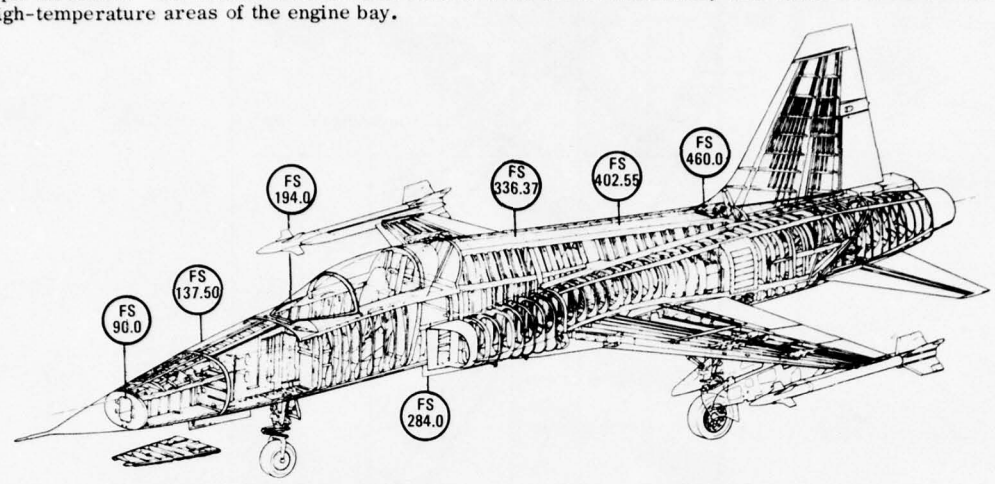

FIGURE 5. F-5E STRUCTURAL ARRANGEMENT

The wing is a multi-spar, all-aluminum structure except for steel ribs supporting the landing gear and wingtip stores. The wing was designed to be assembled in one piece from tip to tip to provide structural continuity and eliminate splices in heavily loaded members. It is attached to the fuselage at four primary attach points, located at the 15 percent and 44 percent spars, with two secondary shear ties located at the 66 percent spar. The upper and lower wing skins are both one-piece machined aluminum plate, 7075-T651 and 7075-T7351, respectively. The spars are primarily over-aged 7000-series aluminum forgings and extrusions. The ribs, except for the landing gear and wingtip ribs, are also 7000-series aluminum forgings.

The vertical stabilizer is a three-spar, multi-rib, all-aluminum structure with integrally stiffened machined skins. The main spar extends into the fuselage and transfers its load through two primary attach points.

The horizontal stabilizer is an all-movable surface, consisting of a two-cell bonded assembly composed of 7075-T6 chem-milled skins supported by full-depth aluminum honeycomb core and a central spar. A steel hinge fitting, which forms the main spar in the inboard region of the exposed planform, serves also as a carry-through member across the fuselage.

5.2 Fatigue Loads Spectra Development

The basic FMS/MAP spectrum was the first of three spectra developed for the F-5E. In 4,000 hours, there are 3,244 unique flights, of which over 2,700 flights are air-to-air missions, with air combat maneuver engagements occurring during each flight. This spectrum was utilized during the first 16,000 hours of fatigue testing. For the 8,000-hour follow-on test, two additional loading spectra were developed. The MAP Pilot Training spectrum represents 4,000 hours of foreign military pilot training. It contains 3,898 flights, of which 54 percent are air-to-air type missions, 9 percent are air-to-ground, and the remaining 37 percent are general training type missions. The spectrum for the last 4,000 hours of the fatigue test simulates Dissimilar Air Combat Training (DACT). It contains 4,028 flights, of which 72 percent are air-to-air missions and 28 percent general type missions.

The bases for the development of all three spectra are the mission profiles which provide specific durations, altitudes, speeds, weights, and configurations experienced during each phase of the mission. Structural load-producing activity within a flight is segregated into basic unique phases as shown in Figure 6.

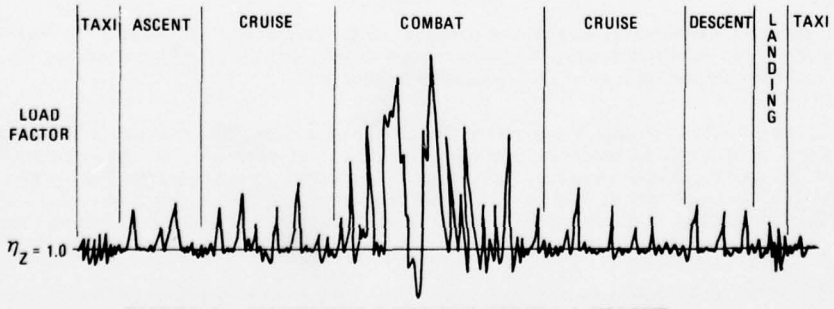

FIGURE 6. MANEUVER ACTIVITY WITHIN A FLIGHT

The time in each phase for all of the flights in a 4,000-hour period is combined with the appropriate load factor occurrence data to obtain the total load factor occurrences in each of the mission phases for the life of the airplane. The resulting composite maneuver spectra are the summation of the load factor occurrence data from the total individual mission phase load factor occurrence data. The three composite maneuver spectra are shown in Figure 7.

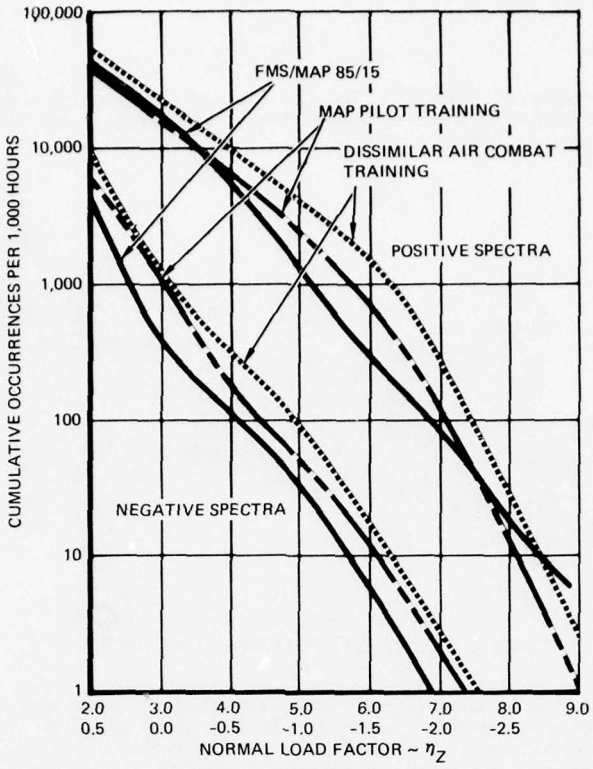

FIGURE 7. COMPARISON OF COMPOSITE MANEUVER SPECTRA

5.3 Fatigue Analysis

Stress levels used for the fuselage design fatigue analysis were derived from finite element models and tapered beam solutions. The wing and empennage stress levels were derived from tapered beam analysis. The linear cumulative damage method was used for fatigue life predictions, with quality indices derived mathematically and from component tests. This approach considers the load transfer in addition to the geometric K_t and, when the quality index is test-derived, accounts for other variables such as fastener fit, hole condition, and fretting at stress levels below the endurance limit.

5.4 Fatigue Life Predictions Prior to Start of Test

The original fatigue analysis based on calculated stresses resulted in a fatigue life prediction in excess of 16,000 hours for all primary structure. This would be a service life in excess of 4,000 hours when dividing by the normal factor of four. The most fatigue-critical location was the wing lower skin adjacent to the side of fuselage at Wing Station 30 and the 44 percent spar. The second most critical area was Wing Station 73 at the main landing gear rib at the 44 percent spar. The predicted maximum spectrum stresses were 31 KSI and 24 KSI, respectively, at these locations. The fatigue analysis yielded analytical fatigue lives of 28,000 hours at Wing Station 30 for a $K_t = 3.25$, and 84,000 hours at Wing Station 73 for a $K_t = 3.75$.

6.0 F-5E FATIGUE TEST PROGRAM

6.1 Introduction

Northrop started the structural fatigue test program on the complete F-5E airplane in March 1973. The simulation of a realistic flight-by-flight loading sequence represented a significant advancement in the state-of-the-art of fatigue testing and has resulted in a very representative fatigue test.

The F-5E Full-Scale Airframe Fatigue Test Program was successfully completed in November 1975 with the application of 16,000 hours of the basic F-5E mission spectrum, followed by 4,000 hours of MAP pilot training and 4,000 hours of the DACT mission spectrum. The residual-strength capability of the F-5E airframe structure was then demonstrated by the application, without a catastrophic failure, of over 1,000 cycles of a 9.25-g supersonic symmetrical pull-up condition to the full-scale Fatigue Test Article, which was equivalent to 110 percent of design limit load.

The results of the F-5E complete airframe fatigue test have demonstrated an estimated service life for F-5E/F aircraft, having the required modifications and ECP's incorporated, in excess of the initial 4000-hour service life design objective. A service life for the F-5E/F-5F in excess of 8,000 hours has been demonstrated for MAP/FMS aircraft used in the basic 85/15 mission role utilizing the "damage tolerance" in lieu of the "safe life" concept when the required structural maintenance and modifications are performed as scheduled. A comprehensive destructive inspection was conducted following completion of the fatigue testing. This consisted of a thorough disassembly of the airframe structure to inspect for initial flaws and to measure fatigue crack propagation.

6.2 Fatigue Test Program Objectives and Test Article Description

The four main fatigue test program objectives were to: locate fatigue-critical areas, permit early improvement of the fleet aircraft at relatively low cost, develop scheduled inspection procedures to minimize unscheduled structural maintenance, and provide test data to establish the predicted structural service life. The fatigue test article was the fifth aircraft produced and was representative of the production aircraft from a structural standpoint. The cockpit was pressurized during each flight, and the maneuvering leading and trailing edge flaps were operational. Strain gage locations were based on the results of fatigue analyses and strain gage surveys conducted on the full-scale static test airplane.

6.3 Test Spectra and Modifications

The load conditions included variations in gross weight, configuration, Mach number, and altitude as defined by the mission profiles. All of the conditions were typical of those experienced in actual flight. The load conditions included ground handling and taxi, landing, positive and negative symmetrical maneuvers, roll, yaw, and pitch maneuvers, and gust and store ejection conditions. There were thirty types of load events and over seventeen hundred discrete load conditions. The total test load events for 24,000 hours of testing approximated 1.8 million.

The original vertical tail loads spectrum was derived from aircraft response parameters recorded during four F-5A simulated air combat engagements. Cracks in the vertical stabilizer skin were discovered after 2,500 hours of testing, and a thorough review of this spectrum was performed. Special air combat flights with a loads-instrumented F-5E were flown to collect measured vertical stabilizer loads. These data indicated that the original spectrum was too severe; consequently, a revised spectrum was developed for use throughout the remainder of the test program.

Criteria utilized during the development of the follow-on fatigue test included data obtained from F-5E MAP pilot training operations at Williams AFB and from the special air combat flights. This information indicated that the maneuvering flap was actuated less often than anticipated when the original flap usage criterion was developed. During air combat usage, the flaps were actuated approximately once for every three maneuvers, as opposed to the initial assumption of once for each maneuver. The number of flap actuations was reduced accordingly during the 12,000-16,000 hour period of fatigue testing as well as during the follow-on fatigue test to reflect the actual usage data.

Comparisons of flight-test-measured flap loads and the original analytical flap loads also indicated some significant differences. Consequently, the flap loads applied during the follow-on fatigue test were revised to incorporate flight-test-measured values.

6.4 Fatigue Test Results

The critical areas established by F-5E fatigue testing following the application of 24,000 hours of simulated service usage are indicated in Figure 8. In all cases, production changes and/or in-service inspections and/or modification programs have been initiated to ensure structural integrity throughout the aircraft life.

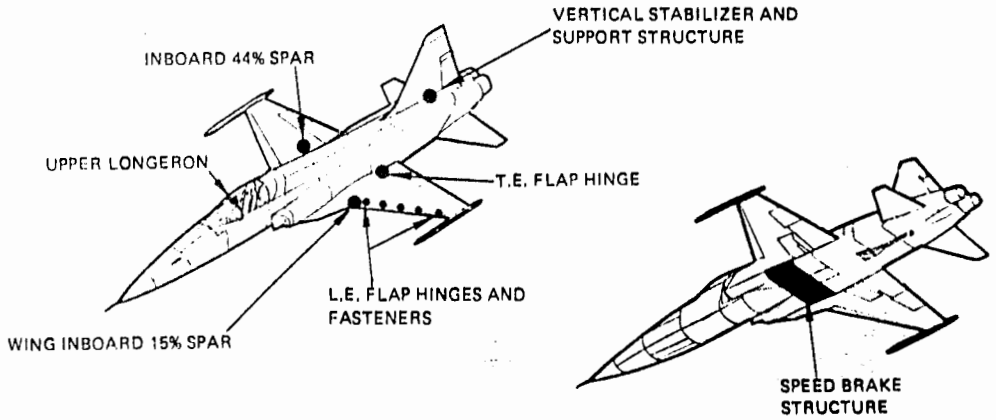

FIGURE 8. F-5E FATIGUE TEST INCIDENTS

Sections 7, 8, and 9 contain a description of some of the fatigue test results, including the production fixes and field retrofit requirements.

7.0 DESIGN CHANGES AND DAMAGE-TOLERANCE ANALYSIS OF TEST-CRITICAL AREAS

7.1 Leading Edge Flap Hinges

Early in the F-5E fatigue test program, multiple cracking was found in the leading edge flap hinges at 1400 test hours. The flap hinge arrangement, shown in Figure 9, consists of five sets of discrete hinges. Each hinge consisted of two hinge halves, with the two flapside lugs 0.2 inch thick and one wingside lug 0.5 inch thick, all made from 4340 steel at 180-200 KSI and 200-220 KSI UTS.

A damage-tolerance analysis was conducted by the USAF using linear elastic fracture mechanics theory and an initial crack of 0.020 inch through one side of the hinge pin hole. Stress concentration factors for the lugs were determined using Heywood lug data[9] for the appropriate geometries. These data were then combined with the maneuvering flap loads spectrum and da/dN fatigue crack growth data using the USAF-developed CRACKS II computer

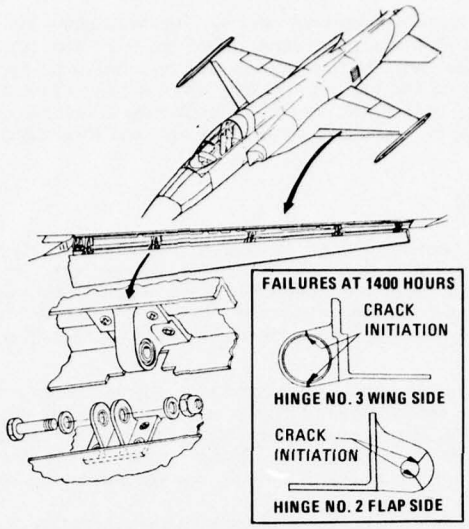

FIGURE 9. FLAP/WING HINGE ARRANGEMENT

program to develop the crack growth curves. These analyses gave crack growth lives of 240 hours for the No. 3 wing hinge and 200 hours for the No. 2 flap hinge, which, with a scatter factor of two, gave safe inspection periods of 100 hours. These inspections and intervals were implemented and prevented the development of unsafe operating conditions, thus avoiding premature aircraft grounding.

A redesign of the flap hinge system was required due to the low fatigue life and the requirement for maintaining the maneuvering flap capability. In the development of the redesigned hinges it was necessary to increase the thickness and width of the lugs to the maximum permitted by aerodynamic contours, install copper-beryllium bushings, improve surface finishes to RHR 63, shot-peen all surfaces, and increase local radii. The combined effect of these fatigue improvements has been demonstrated by component fatigue tests of the original design and the redesigned hinges, and has shown an increase in fatigue life by a factor of approximately twenty. The safe crack growth life is in excess of one design lifetime. The twenty-six aircraft that were already in service have been retrofitted with the redesigned hinges in order to ensure safety of flight and to reduce maintenance requirements.

7.2 Vertical Stabilizer

A crack was found in the root radius of the vertical stabilizer skin at 2500 test hours. Further inspection revealed a similar crack on the opposite side. These cracks were preceded by cracking of the attach angle and cracking in the fuselage frames that support the attach angles. Details of the structure are shown in Figure 10.

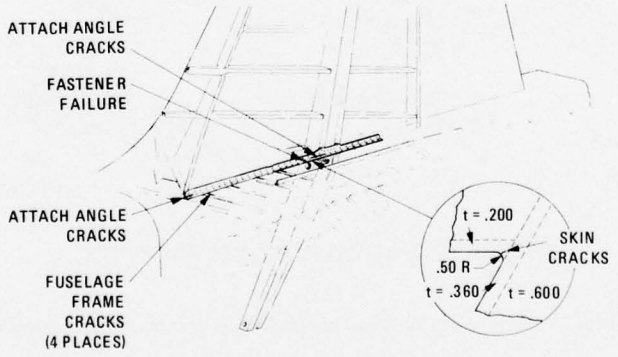

FIGURE 10. VERTICAL STABILIZER STRUCTURAL ARRANGEMENT

A review of the service history of the T-38 and F-5A/B aircraft was conducted because of the similarity in structural arrangement with the F-5E aircraft. This revealed a history of cracking in the attach angles and fuselage frames on the T-38/F-5A/B aircraft but no reports of skin cracks. Appropriate actions were initiated to provide service inspection and repair data for the F-5A/B and T-38 aircraft. One hundred and forty-nine F-5E aircraft had entered service before a redesign could be incorporated into production. The original vertical stabilizer design is being utilized until service conditions indicate replacement. A non-destructive inspection, developed to detect sub-critical cracks, has been initiated to protect the flight safety of these aircraft. A NASTRAN model of the vertical stabilizer, including the critical radius, was developed which duplicated measured strains at selected points and provided a stress concentration factor which was utilized in lieu of the Bowie factor in the crack growth analysis. This analysis gave a safe crack growth life of 700 hours for a 0.050-inch corner flaw and led to the establishment of a progressive, phased inspection program that is now in effect. In this particular case, it is estimated that the damage-tolerance approach provided an eight million dollar net program savings over a fleet-wide retrofit program. A program was

initiated for the F-5E aircraft which determined actual operating stress levels, actual load paths including secondary load paths previously assumed ineffective, and the operating loads environment. These data formed the basis for the redesign which increased the capability of the secondary load paths and removed the geometric anomalies which had precipitated the failure in the primary load path. The redesigned structure subsequently demonstrated a test life in excess of 24,000 hours for the 85/15 spectrum.

8.0 DAMAGE-TOLERANCE ANALYSIS/TESTING FOR WING STRUCTURE

8.1 Introduction

The majority of the damage-tolerance analysis conducted for the F-5E aircraft was directed at correlating analytical results with the full-scale Fatigue Test Article spectrum crack growth data in order to establish meaningful inspection intervals for those parts that had cracked. A secondary objective was verification of the crack growth model and analysis in order to analytically extrapolate the crack growth rates for different aircraft usage spectra. The regression analysis presented a problem since spectrum characteristics could not be distinguished because of the random cycle-by-cycle test loading. Striation counting, though cumbersome and expensive, was widely utilized, although many low-load cycles either did not produce striations or the striations were below the resolution of the scanning electron microscope. Where high accuracy was required, as in the wing fracture-critical areas, separate specimen tests were conducted. This permitted the segregation of crack growth from the crack-initiation period.

The data and knowledge gained from the wing specimen testing contributed greatly to an understanding of the significance and impact of the damage-tolerance philosophy and requirements. For this reason, this section of the paper will be directed solely to the wing specimen fatigue and damage-tolerance test results. Fatigue improvements realized from cold working, striation marking, and impact of hole quality on nucleation and growth patterns will be discussed.

8.2 Wing Tests

8.2.1 Reasons for Tests

Strain measurements recorded on the Fatigue Test Article wing lower skin indicated that the two critical areas, reference Figure 11, were operating at substantially higher stress levels than those used for the original fatigue analysis. A summary of the predicted and measured stresses as well as the predicted fatigue lives utilizing Miner's theory is shown below:

	Analytical Stresses		Strain Gage Data	
Skin Location	σ_{max} Ksi	Fatigue Life-Hrs	σ_{max} Ksi	Fatigue Life-Hrs
W.S. 30 ($K_t = 3.25$)	31	28000	35	12000
W.S. 73 ($K_t = 3.75$)	24	84000	39	3600

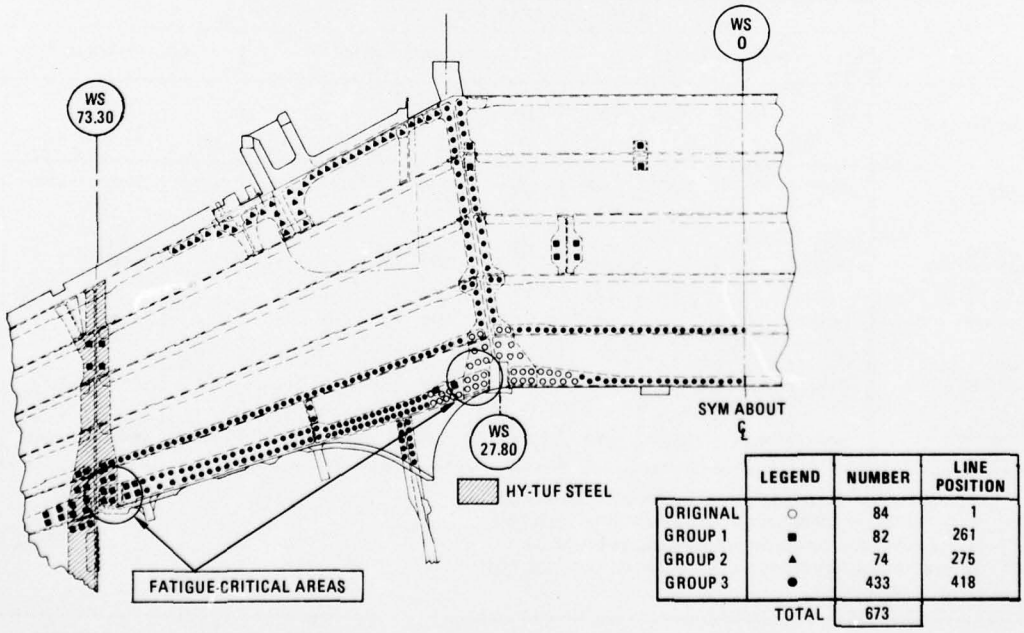

FIGURE 11. FATIGUE-CRITICAL AREAS AND COLD-WORKED HOLES FOR WING LOWER SKIN

As a direct result of the above analysis, all Group 1 holes (reference Figure 11) common to the wing lower skin and MLG rib at Wing Station 73 were cold-worked for future production. The right-hand wing of the Fatigue Test Article was cold-worked after 10,000 hours of testing, while the left-hand wing was left unmodified to further evaluate the status of aircraft delivered prior to incorporation of the cold working. A component test program was also initiated to define the actual improvement in fatigue and crack growth behavior gained from cold working (reference Para-

graph 8.2.2). The number of fastener holes cold-worked was expanded as the fatigue test program continued, to include Groups 2 and 3, both because of cracking at the spar flange fastener holes and a new requirement to utilize F-5E aircraft in a more severe Dissimilar Air Combat Training environment.

8.2.2 Description of Tests

The fatigue specimens were representative of the 7075-T73 aluminum wing skin and steel landing gear rib stack-up at Wing Station 73, as shown in Figure 12-A. Figure 12-B shows a typical test specimen.

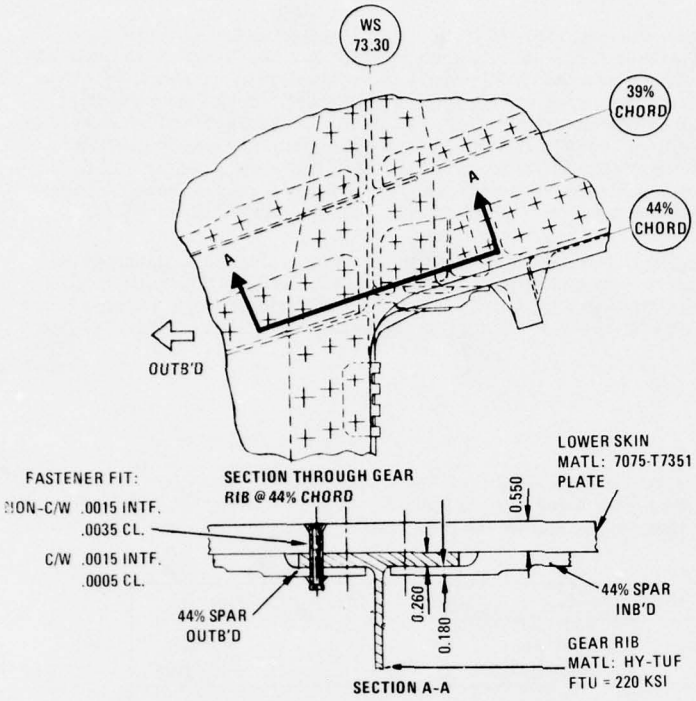

FIGURE 12-A. FATIGUE-CRITICAL LOCATION ON WING LOWER SKIN AT GEAR RIB

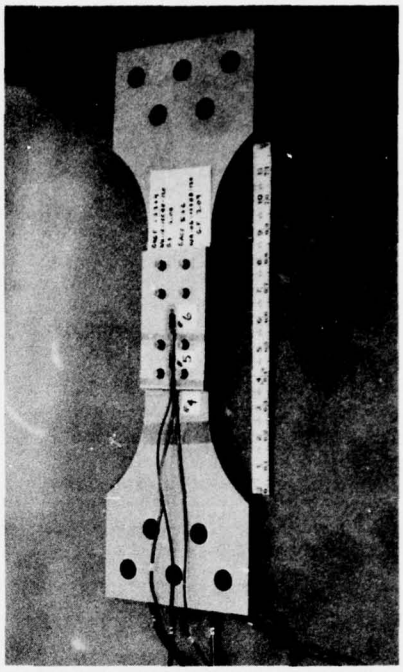

FIGURE 12-B. PHOTOGRAPH OF TYPICAL TEST SPECIMEN

	SPECIMEN TEST RESULTS (FLIGHT HOURS) – DACT SPECTRUM [4]											
	NON-COLD-WORKED				COLD-WORKED AFTER C'SK				COLD-WORKED BEFORE C'SK			
SPECIMEN NUMBER	[1] [4] 1-1	1-2	1-3	[1] 1-4	[1] 2-1	[1] 2-2	2-3	2-4	3-1	[1] 3-2	3-3	[1] 3-4
TOTAL LIFE	35550	8600	8100	6400	19600 [3]	17750 [3]	16000	15300	42900	34400	48000	31500
CRACK DETECTED (CRACK SIZE-INCHES)	11950 (.0052)			2000 (.0044)	[5]	11200 (.032)				14400 (.030)		[5]
MEASURED CRACK GROWTH	23600			4400		6550				20000		
CORRECTED CRACK GROWTH [2]	26500			6700		6800				30900		
CORRECTED TOTAL LIFE [2]	38450	8600	8100	8700		18000	16000	15300	42900	45300	48000	

[1] SPECIMENS INCORPORATED CONSTANT AMPLITUDE STRIATION MARKING
[2] CRACK GROWTH LIFE CORRECTED FOR STRIATION MARKER BANDWIDTHS
[3] FAILURE INITIATED FROM A SURFACE FLAW ADJACENT TO C'SK EXIT
[4] SPECIMEN NO. 1-1 WAS TESTED TO THE LESS SEVERE 85/15 BASIC SPECTRUM
[5] *DATA NOT YET REDUCED*

FIGURE 13. COMPARISON OF NON-COLD-WORKED AND COLD-WORKED SPECIMEN FATIGUE TEST RESULTS AT THE CRITICAL LOCATION ON THE F-5E WING (W.S. 73.0 AND 44% SPAR), REFERENCE FIGURE 12.

The cold-work system used at Northrop is the Boeing split-sleeve method, reference Figure 14, except that the mandrel expansions are higher than that used by Boeing: 0.012/0.015 inch for 0.264-in.-dia holes. All test holes were drilled, cold-worked, and reamed to nominal sizes such that the cold work expansion was 0.0135 inch. All test specimens were machined to a 125 surface finish, then shot-peened to 0.010 almen (A) intensity using 230/280 shot size prior to sulphuric acid anodizing and drilling.

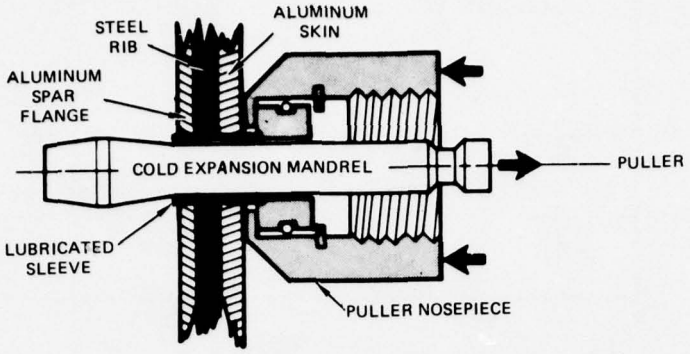

FIGURE 14. SCHEMATIC REPRESENTATION OF COLD-WORKING ALUMINUM/STEEL STACK-UP

The test spectra were identical to the flight-by-flight spectra applied to the full-scale Fatigue Test Article with all negative stresses included. Striation marker loads were applied at regular intervals since crack initiation and growth could not be monitored visually and fractographic regression had proven intractable with a random cycle-by-cycle spectrum. Striation marking consisted of applying a given number of constant-amplitude load cycles at a chosen K_{max} and R value to produce striations in the 8×10^{-8} to 5×10^{-7} inch range. The number of cycles applied should be the minimum required to produce marker widths that are detectable by the scanning electron microscope so that the impact on total fatigue life is minimal. The crack length should be known in order to control the marker widths and the K_{max} and R calculated to give the marker width required. However, as this was not feasible due to the concealed crack growth, the decision was made to apply all marks at $\sigma = 35$ ksi at $R = 0.9$. The number of marker cycles initially used was 30,000 and was reduced on subsequent tests to 5,000; the marker intervals were either 400 or 800 flights, depending on the test spectrum and whether the specimen was cold-worked. The specimens were cycled at a variable rate between 2 and 9 Hertz, with the striation marker loads applied at 6 Hertz.

8.2.3 Results

The test results are summarized in Figure 13, and crack growth plots for the striation marked specimens are illustrated in Figures 15 and 16. These plots have been corrected for the widths of the marker bands. As can be seen from Figure 16, the test crack growth for specimen No. 1-1 tested to the 85/15 basic spectrum was only 11 percent lower than the corrected growth. This specimen had 24 marks of 5,000 cycles each. Striation marks were detected as far back as a crack length of 0.004 inch for a DACT non-cold-worked specimen, whereas the first striation mark that could be detected on a cold-worked specimen occurred at 0.015 inch. This was because of the reduction in the marker load effective stress intensity, the residual compressive stresses from cold-working causing striation marker bands below a crack length of 0.015 inch to be so small as to be unrecognizable under the scanning electron microscope. The fracture faces of all test specimens are shown in Figures 17, 18, and 19.

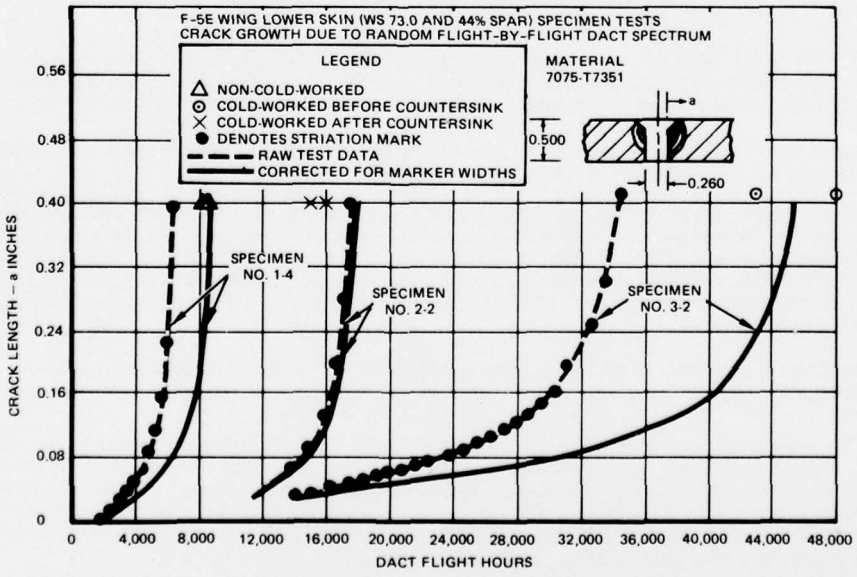

FIGURE 15. CRACK GROWTH PLOTS FOR STRIATION-MARKED SPECIMENS TESTED TO DACT SPECTRUM, REFERENCE FIGURE 11. NOTE THAT PLOTS CORRECTED FOR MARKER WIDTHS SHOW TOTAL LIVES IN GOOD AGREEMENT WITH NON-MARKED SPECIMEN LIVES.

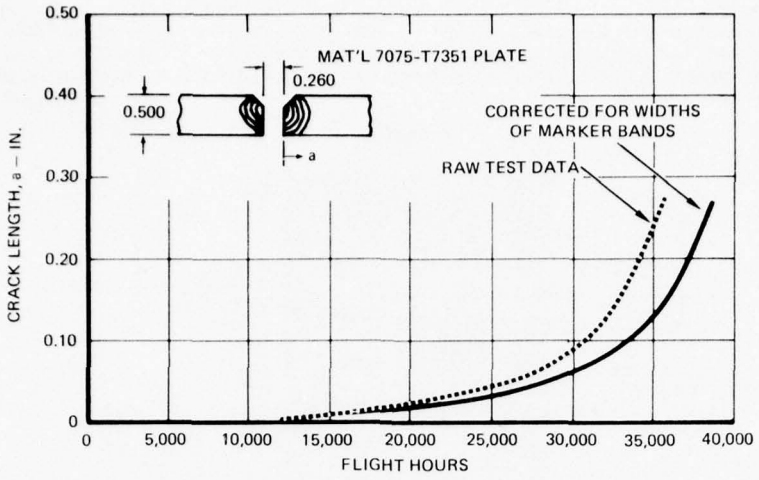

FIGURE 16. TEST RESULTS FOR NON-COLD-WORKED SPECIMEN NO. 1-1, TESTED TO 85/15 BASIC SPECTRUM; REFERENCE FIGURE 13.

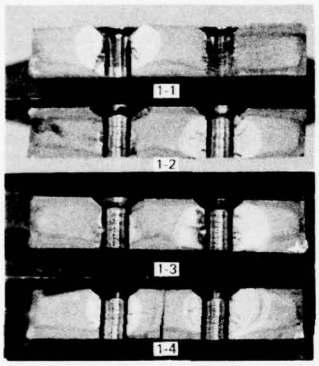

FIGURE 17. NON-COLD-WORKED SPECIMENS

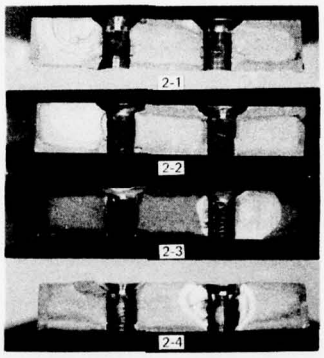

FIGURE 18. COLD-WORKED-AFTER-COUNTERSINK SPECIMENS. NOTE INITIATIONS AWAY FROM HOLES ON SPECIMENS 2-1 AND 2-2. MATERIAL NOT EFFECTIVELY COLD-WORKED AT THIS LOCATION WITH THE C'SK/CW SEQUENCE.

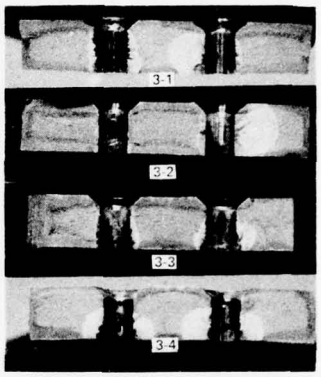

FIGURE 19. COLD-WORKED-BEFORE-COUNTERSINK SPECIMENS.

The major conclusions drawn from the test results are as follows:

8.2.3.1 - Cold-working holes in 7075-T7351 material prior to countersinking with Paragraph 8.2.2 mandrel expansion improved the total fatigue life (initiation plus crack growth) in a fighter-type environment by a factor of five. Cold-working holes subsequent to countersinking improved the total fatigue life by a factor of two.

8.2.3.2 - More than 70 percent of the total fatigue life for the 7075-T7351 material was expended in crack growth for the non-cold-worked and cold-worked specimens.

8.2.3.3 - Crack origins were multiple in nature, as shown in Figure 20, and for the non-cold-worked specimens were predominantly located between mid-thickness and the junction of the countersinking with the bore. Initiations in holes cold-worked before countersinking were more concentrated toward the faying surface. Initiations in holes cold-worked after countersinking primarily occurred in the area of the countersinking either at the hole or surface juncture, demonstrating that this region was not as effectively cold-worked and emphasizing the need for caution when using this sequence.

8.2.3.4 - Multiple fatigue initiations in the holes linked up to form common crack fronts that transitioned to through-cracks faster than corner flaws.

8.2.3.5 - The primary fatigue initiations were associated with typical production hole defects. These defects comprised helical scratches, gouges, smeared metal, and tears. The RHR values of the holes varied from 50 to 160. There was no direct relationship between RHR measurement and hole defects. Several cracks started at longitudinal scratches in the bore of the hole; the scratches were caused either by insertion of a plug gage or by the interference-fit fastener dragging small steel chips through the bore. However, it is interesting to note that the primary initiations occurred at plastically deformed smeared metal zones.

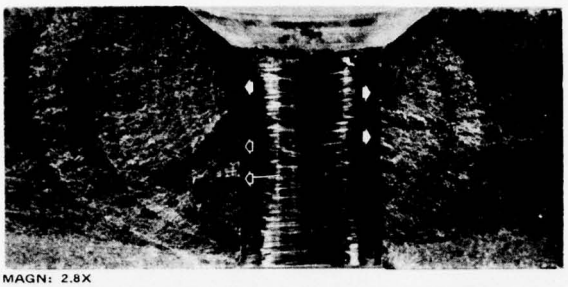

(a) SPECIMEN NO. 1-4 HOLE 1

MAGN: 2.8X

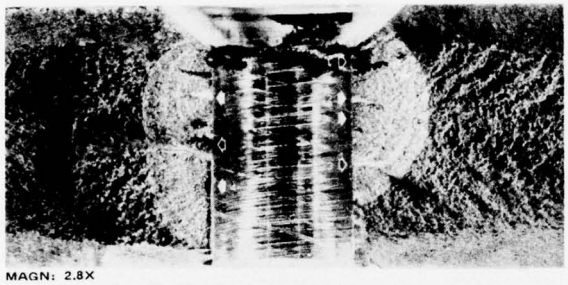

(b) SPECIMEN NO. 1-4 HOLE 2

MAGN: 2.8X

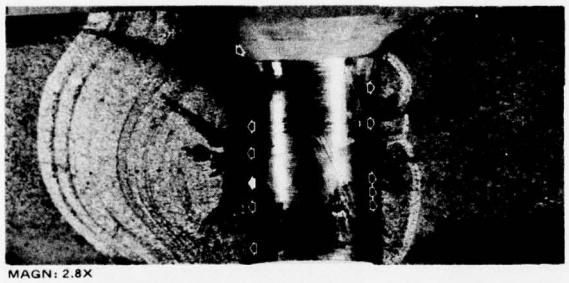

(c) SPECIMEN NO. 3-2 HOLE 1

MAGN: 2.8X

(d) SPECIMEN NO. 3-2 HOLE 2

MAGN: 2.8X

FIGURE 20. PHOTOGRAPHS ILLUSTRATE MULTIPLE INITIATION SITES. (a) AND (b) ARE NOT COLD-WORKED, REF FIGURE 17; (c) AND (d) ARE COLD-WORKED (PRIOR TO COUNTERSINK), REF FIGURE 19.

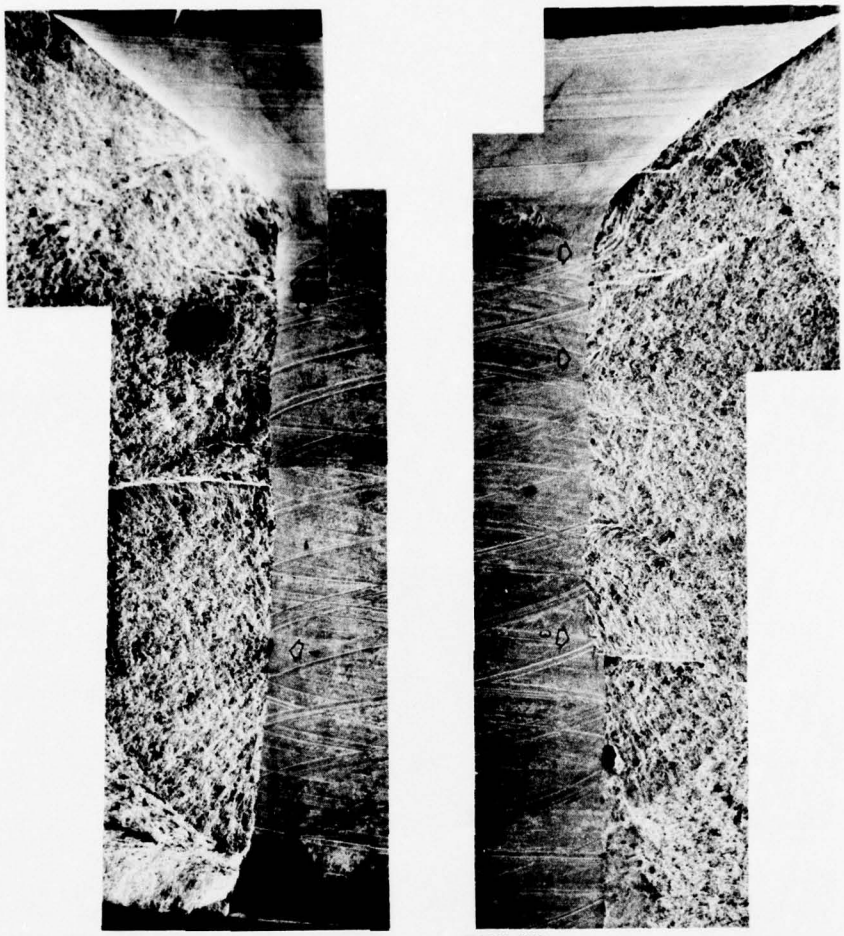

MAGN: 15X MAGN: 15X

FIGURE 21. ARROWS 1, 2, 3, AND 5 INDICATE FATIGUE INITIATIONS IN A NON-COLD-WORKED HOLE (SPECIMEN NO. 1-4, HOLE 2) AT INTERSECTIONS OF HELICAL TOOL MARKS. ARROW 4 DEPICTS A 0.002-INCH-DEEP TEAR WHICH FORMED A PRIMARY INITIATION SITE. FURTHER EXAMINATION REVEALED NO STAGE 1 INITIATION, AS STRIATIONS STARTED IMMEDIATELY FROM THE DEFECT. THE TEAR WAS PROBABLY CAUSED BY A STEEL CHIP.

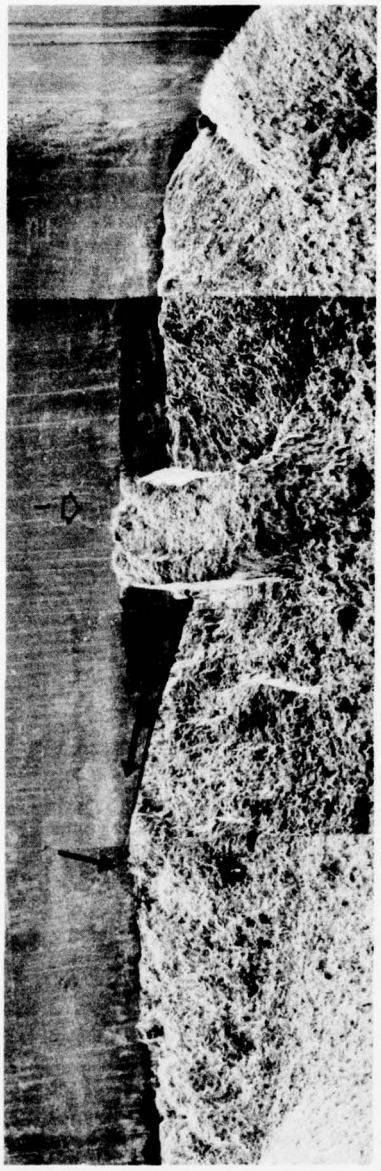

MAGN: 15X

FIGURE 22. FATIGUE CRACK INITIATING AT TOOL SMEAR. PHOTO ALSO SHOWS STRONG INFLUENCE OF REAMER WITHDRAWAL SCRATCH ON SECOND INITIATION AND SUBSEQUENT CHANGE IN CRACK GROWTH PLANE. HOLE IS COLD-WORKED (SPECIMEN NO. 3-2, HOLE 1); REF FIGURE 19.

8.2.3.6 - Striation marking proved extremely successful in facilitating segregation of crack growth from nucleation. No other striation characteristics could be detected to assist in regressing the crack growth with the random cycle-by-cycle test spectrum employed. Figures 23 and 24 depict a non-cold-worked specimen that was striation-marked at σ max = 35 KSI, R = 0.9 for 30,000 cycles at 400-flight-hour intervals. These marks are obvious to the naked eye, but later tests using 10,000 and 5,000 cycles required the use of the SEM for positive identification. The striation sizes in the marker zones varied between 2.8×10^{-8} and 3.9×10^{-8} inch for the singular crack front in the countersink of a cold-worked hole (reference arrow 1 in Figure 25), and from 4.7×10^{-8} to 6×10^{-7} inch for a crack in a non-cold-worked hole, reference Figures 26 and 27. The striation sizes quoted are obtained by dividing the width of the marker band by the number of marker cycles. The marker bands appeared as featureless zones even at 20,000 magnification, as 2×10^{-6} inch is the limiting resolution for the SEM. Striation marker bands for a specimen cold-worked prior to countersink are shown in Figures 28 and 29. In Figure 30 the arrows indicate the 24 marker bands detected in specimen No. 1-1, demonstrating a crack growth life of 38,500 hours (reference Figure 16) for a non-cold-worked hole in the 85/15 basic spectrum environment. The first marker band detected (No. 24) occurred at a crack length of 0.005 inch. Marker band No. 22 is clearly observable at 3500X in Figure 31. This mark is 0.0001 inch wide and started at a crack length of 0.009 inch.

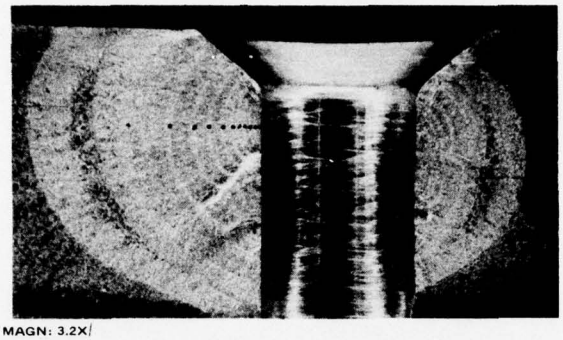

MAGN: 3.2X

FIGURE 23. STRIATION MARKER BANDS FOR NON-COLD-WORKED SPECIMEN; σMAX = 35 KSI, R = 0.9, N = 30,000 CYCLES. GROWTH BETWEEN BANDS REPRESENTS 400 FLIGHT HOURS IN THE DACT ENVIRONMENT. HOLE FINISH = 160 RHR. SPECIMEN NO. 1-4, HOLE 1, REFERENCE FIGURE 17.

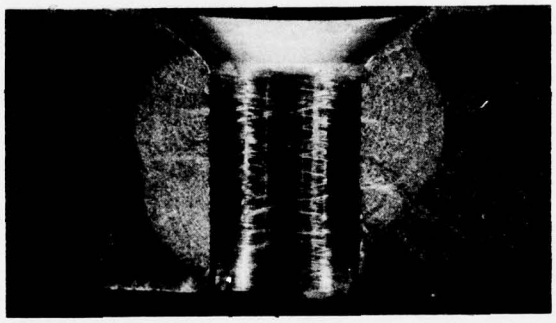

MAGN: 3.2X

FIGURE 24. ADJACENT HOLE ON SAME SPECIMEN DEPICTED IN FIGURE 23. NOTE MULTIPLE CRACK INITIATION SITES. HOLE FINISH = 130 RHR. SPECIMEN NO. 1-4, HOLE 2, REFERENCE FIGURE 17.

8.2.3.7 - The crack growth life on the F-5E wing at the fracture-critical location was demonstrated to be:

		Crack Growth Life from Fatigue-Initiated Cracks — Flight Hours	
		0.010 → Failure	0.050 → Failure
Dissimilar Air Combat Training Spectrum	Not Cold-Worked	6,200	3,500
	Cold-Worked before countersink	37,000 (Extrapolated)	25,000
85/15 Spectrum	Not Cold-Worked	23,500	9,500

The total test results, summarized in Figure 13, clearly indicate the beneficial effects of cold-working and the importance of the cold-work/countersink sequence.

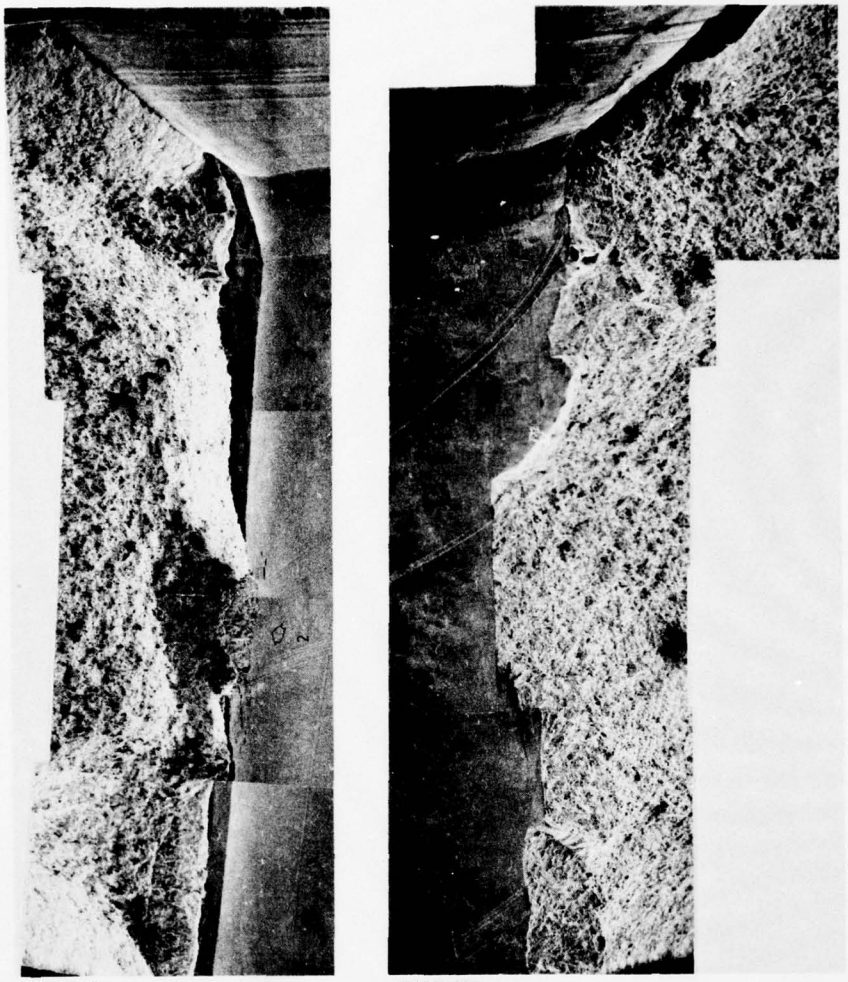

MAGN: 15X

MAGN: 15X

FIGURE 25. FATIGUE CRACKS INITIATING AT TOOL GOUGES IN COLD-WORKED HOLE WHICH ARE CAUSED BY WITHDRAWING ROTATING REAMER TOO QUICKLY. HOLE IS REAMED AFTER COLD-WORKING. SPECIMEN NO. 3-2, HOLE 2, REFERENCE FIGURE 19.

MAGN: 17X

FIGURE 26. NON-COLD-WORKED HOLE SPECIMEN NO. 1-4, HOLE NO. 1. 11 MARKER BANDS OF 30,000 CYCLES EACH, REFERENCE FIGURE 17.

MAGN: 500X

FIGURE 27. MARKER BAND NO. 11 FROM FIGURE 26 APPEARS FEATURELESS. STRIATION SIZES ARE 4.7×10^{-8} INCH. NOTE THAT STRIATION SIZE FOR FINAL MARK NO. 1 PRIOR TO FAILURE IS 6×10^{-7} INCH.

MAGN: 15X

FIGURE 28. STRIATION MARKER BANDS ON COLD-WORKED SPECIMEN NO. 3-2, HOLE 1. STRIATION SIZES FOR MARKS 25 AND 1 WERE 1.57×10^{-7} AND 5.5×10^{-7} INCH, RESPECTIVELY.

FIGURE 29. MARK NO. 5 FROM FIGURE 28. NOTE THAT MARKER BAND APPEARS STRIATIONLESS. STRIATION SIZE WOULD BE 2.8×10^{-7} INCH.

MAGN: 1000X

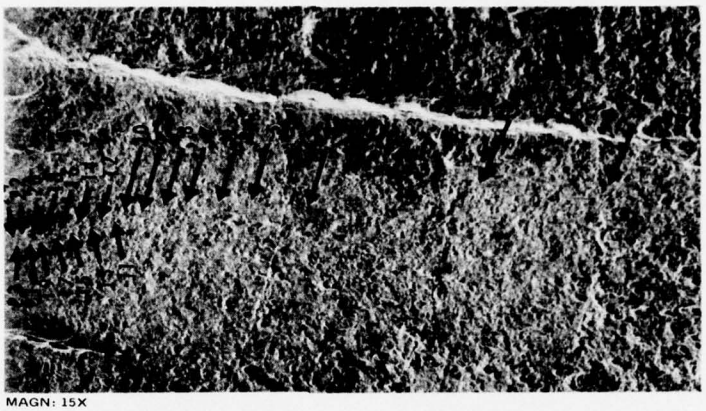

MAGN: 15X

FIGURE 30. SPECIMEN NO. 1-1 NOT-COLD-WORKED AND TESTED TO 85/15 SPECTRUM. PHOTO SHOWS 24 MARKER BANDS APPLIED AT INTERVALS OF 800 FLIGHTS.

MAGN: 3500X

FIGURE 31. MARKER BAND NO. 22 FROM FIGURE 30. ACTUAL WIDTH OF MARKER BAND IS 1×10^{-4} INCH AND WAS CREATED BY 5000 CYCLES AT σ_{MAX} = 35 KSI AND R = 0.9.

8.2.3.8 - Crack growth of similar size was observed on both sides of each hole. Cracks were always found in the adjacent holes. This is an important consideration in the assumption of continuing damage for typical fatigue-initiated cracks and indicates that when a fatigue crack breaks through to the edge of a part, the crack size on the opposite side of the hole could be of similar size. Adjacent holes drilled with the same technique would likely have similar-size cracks. The influence of a design-type single precracked flaw was not considered in these tests.

8.2.4 Test/Analysis Correlation

8.2.4.1 - Fatigue-initiation predictions were performed at Wing Station 73 and the 44 percent spar (reference Figure 11) using Miner's and residual-stress analyses. These predictions are compared with the test results for non-cold-worked specimens in the following tabulation.

Test Spectrum	Analytical Predictions of Crack Initiation $K_t = 3.75$		Specimen Test Results	
	Miner's	Residual	Test Hours at Crack Detection	Crack Size at Detection (Inch)
85/15	3,200	27,000	12,000	0.005
DACT	1,500	7,800	2,000	0.004

The results indicate that the residual stress analysis, with peak counting, produces unconservative lives, and that linear cumulative damage results in a better correlation with specimen test results.

8.2.4.2 - The results of cycle-by-cycle crack growth analyses using the test load sequence stress tape are compared with the test data in Figures 32 and 33.

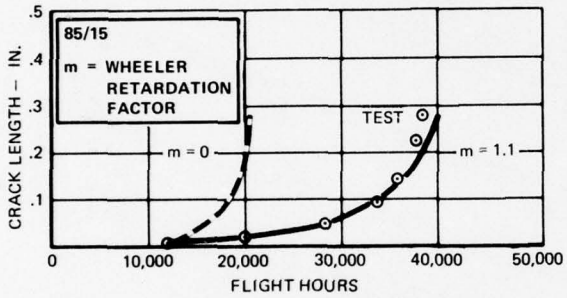

FIGURE 32. ANALYTICAL CORRELATION OF 85/15 TEST SPECTRUM CRACK GROWTH

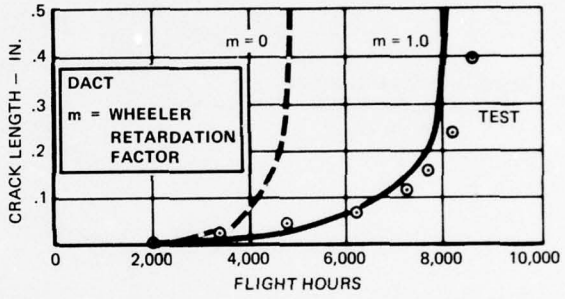

FIGURE 33. ANALYTICAL CORRELATION OF DACT TEST SPECTRUM CRACK GROWTH

The results show that a Wheeler retardation factor (m) between 1.0 and 1.1 best correlated the test data. This degree of retardation is considerably less than that observed in various other tests to block or program loading.

9.0 FINAL FATIGUE AND DAMAGE-TOLERANCE ASSESSMENT

9.1 Test-Derived Quality Indices

A visual inspection of the wing lower skin was conducted following the completion of the 24,000-hour test, and cracks were detected as shown in Figure 34. The largest crack occurred at the 39 percent spar and measured 0.9 inch long, including the hole diameter.

The test airframe was then cycled from one g to 110 percent of design limit load in order to determine the residual strength of the airframe structure. One thousand and forty-five cycles of a 9.25-g supersonic symmetrical pull-up condition were applied. At that point a pop-in was heard and the testing was terminated. The crack sizes were than remeasured, and the crack lengths are shown in Figure 35.

Fatigue-damage plots were prepared, and the demonstrated K_t at both critical locations (reference Figure 11) was determined based on the fact that cracks did not exist at either of these locations. The demonstrated K_t for the lower skin at Wing Station 30 and the 44 percent spar was 2.75, reference Figure 36. The demonstrated K_t for the lower skin at Wing Station 73 and the 44 percent spar was 2.58, reference Figure 37. Fatigue analysis for the location at Wing Station 43 demonstrated a K_t of 3.4 based on the extrapolated crack initiation. As this crack originated at a hole defect, the influence of real flaws in defining the Quality Index is apparent. The tear-down inspection of the fatigue test wing has not disclosed any cracks in the lower wing skin holes common to the steel gear rib (reference Figure 12).

If the specimen tests were representative of the wing structure and loading environment, then the specimen test results (reference Figure 13) would indicate that the left-hand wing, which was not cold-worked at this location on the fatigue test aircraft, should have had significant-size cracks at the completion of testing.

Comparison of the test specimen configuration and loading with that of the wing structure shows the following significant differences:

9.1.1 - Due to the thin wing structure, the MC/I stress gradient across the lower skin thickness is significant. The stresses at the inner surface and mid-thickness are 77 and 88 percent, respectively, of the outer-surface stresses.

The specimen stresses at mid-thickness, where the crack initiations occurred, were the same as the wing outer-surface stresses, i.e., 14 percent higher than at mid-thickness on the wing skin.

9.1.2 - The principal stress axis at this location on the wing varied between 7 and 15 degrees for flap-up conditions and between 10 and 20 degrees for flap-down conditions. This is indicative of the influence of shear stresses. Also, a biaxial tension-tension stress field exists on the wing due to the gear rib acting as an air loads redistribution member. The combined effect of shear and biaxial tension is to reduce the equivalent stress by approximately 5 percent.

From the above it is apparent that the specimen tests tended to be conservative; also, that it is extremely difficult to make specimen tests sufficiently complex to be fully representative of the actual aircraft structure.

9.2 Initial-Hole Quality Assessment Program

Northrop conducted an initial-hole quality assessment program on the F-5E in order to determine what changes would be required in current production methods and quality control procedures in order to comply with the new MIL-A-83444 specification for future designs. The results of this program showed that a large percentage of holes in the wing that were drilled with semi-automatic and fully automatic drilling machines had surface finishes in excess of 125 RHR. It was apparent that surface finish measurements of fastener holes were not being taken on the production line, and that the quality of the holes was being assessed by visual comparisons. The surface finish measurements taken during the assessment program were recorded using portable profilometers.

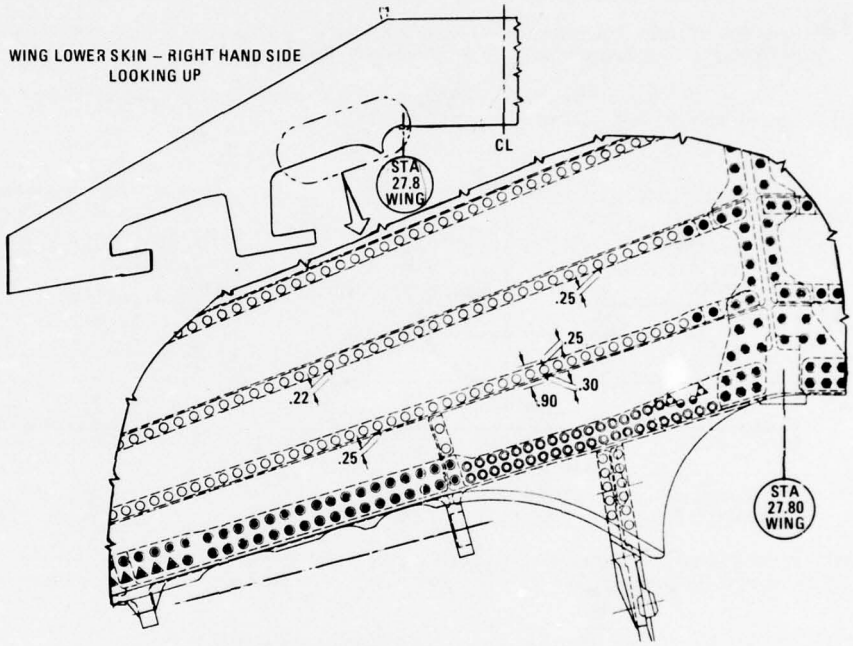

FIGURE 34. CRACK SIZES AFTER 24,000 TEST HOURS

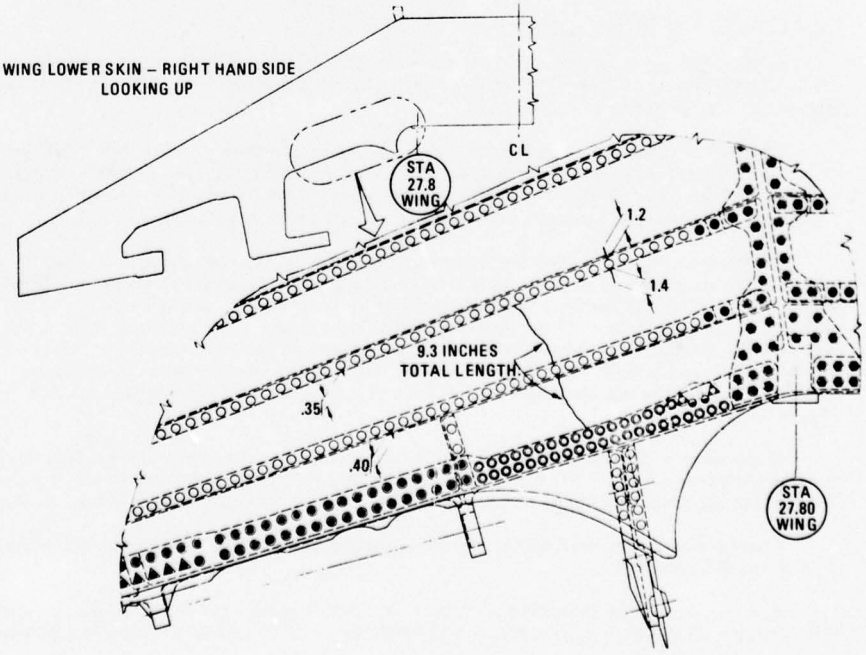

FIGURE 35, CRACK SIZES AFTER 1,045 CYCLES OF 110% DESIGN LIMIT LOAD

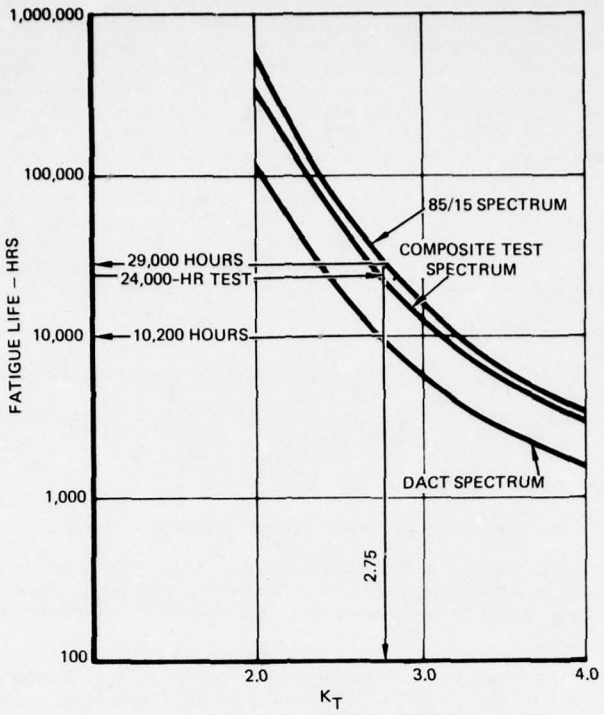

FIGURE 36. WING LOWER SKIN DAMAGE PLOTS AT W.S. 30 AND 44% SPAR

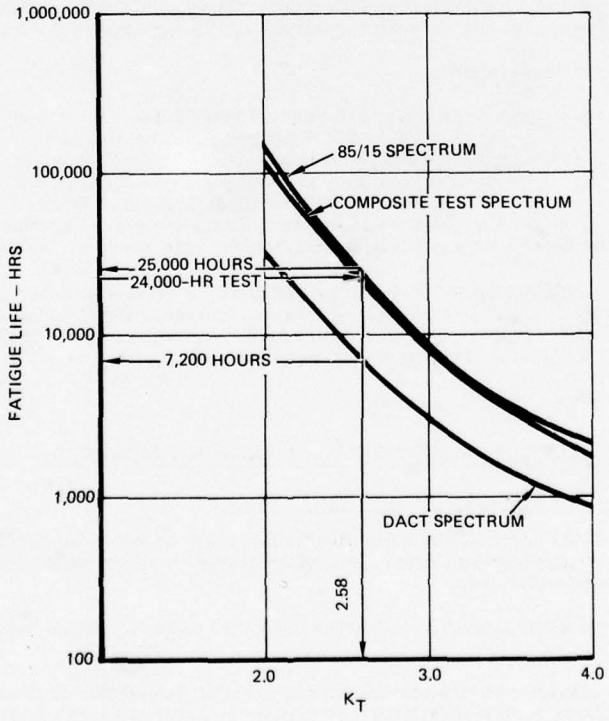

FIGURE 37. WING LOWER SKIN DAMAGE PLOTS AT W.S. 73 AND 44% SPAR

Based on the preliminary results of the initial-hole quality assessment program, an in-depth study was immediately undertaken. This resulted in revised manufacturing techniques and tooling improvements to control all possible variables, such as: drill and reamer configurations, feeds and speeds, coolants and lubricants, and tool and fixture rigidity, all in conjunction with thorough operator training and quality assurance controls. Hole finishes are now sampled quantitatively on every aircraft, and the overall result is that less than 1 percent of the holes exceed 125 RHR and these are reworked so as to meet a 125 RHR requirement. Surface finish measurements using portable profilometers have been taken on over 20,000 fastener holes in the F-5E/F wing skin and substructure.

The fundamental question that arose during this assessment program was the relationship of RHR finishes to the overall hole quality, which included hole defects such as nicks, scratches, and gouges. The general assumption was that abusive drilling and reaming, which produced high RHR finishes, would also result in hole defects. A review of all available data did verify that holes with high RHR finishes contained a higher percentage of hole defects. However, it was also found that some holes with very low RHR finishes contained some defects.

Hole defects are described as follows:

- Smeared, gouged, and torn metal caused by chatter from dull tools and lack of coolant and lubricant.
- Helical scratches caused by withdrawing spinning tool too quickly. This situation is aggravated when the feed rate is too fast, causing intersection of marks.
- Longitudinal scratches caused by withdrawing non-rotating tool.
- Tears in alum/steel stack-ups caused by steel chips withdrawn in tool flutes.

The hole quality on the full-scale Fatigue Test Article was measured, and a significant number of holes were in excess of 125 RHR. Based on the results of the Fatigue Test Article tear-down inspection following the completion of the 24,000-hour full-scale fatigue test, it was concluded that there was no direct correlation between hole roughness (RHR) and test life.

The 9.3-inch crack in the wing lower skin at Wing Station 43 and the 39 percent spar had both the primary and secondary crack initiation sites at hole defects (0.001 inch deep at primary initiation), as shown in Figures 38 and 39. Figures 40 and 41 clearly show the well-defined area of spectrum growth, as contrasted to the sporadic growth and discontinuous crack fronts resulting from the 110-percent limit design load cycles, until the crack burst from 4.1 inches to the 9.3 inches on the final load cycle. It was found that the aft edge of the crack has arrested in a fastener hole, while the forward edge had terminated between two fastener holes under the 33 percent spar. The termination of the crack at the adjacent spar indicated that a redistribution of stresses occurred which improved the residual strength of the wing.

It is apparent from the results of the Initial Hole Quality Assessment Program that hole defects do exist and contribute to early crack initiations tending to emphasize the crack growth portion of the total fatigue life. However, with a judicious selection of materials and sufficient quality assurance to justify the assumption of relatively small flaw sizes for analysis and testing, there is not a prohibitive penalty in neglecting the Stage 1 crack initiation period.

9.3 Economic Life Safety Limit Assessment

As previously defined, the economic life limit is the point where further repair is no longer economical. One measure of economic life, and that employed in the F-5E/F program, was to continuously monitor the total number of cracks found during the test, including multiple cracks and cracks in secondary structure. A large upswing in the rate at which this total changes from inspection point to inspection point indicates the approach of the limit of the aircraft's economic life. The F-5E did not reach its economic life limit in the 24,000 hours of testing; in fact, after the aircraft reached a plateau early in the test, the rate of cracking during the last 8,000 hours actually declined, reference Figure 42, even though there was a significant increase in the severity of the loading spectra being applied.

In conjunction with the establishment of the economic life limit, there are small numbers of cracks which are by nature unrepairable and which, if left unrepaired, grow to lengths which can cause a catastrophic failure within the aircraft's flight envelope. This leads to the concept of a safety limit. An example of the probable safety limit for the wing lower skin non-cold-worked holes at Wing Station 73 and the 44 percent spar based on specimen test results is shown in Figure 43.

10.0 COMPLIANCE WITH AND IMPACT OF CURRENT USAF DAMAGE-TOLERANCE REQUIREMENTS

10.1 Primary USAF Durability and Damage-Tolerance Specifications

The primary objectives of the current USAF specifications relative to durability and damage-tolerance requirements are stated below. The requirements pertaining to quality assurance and in particular to fastener holes have also been extracted from these specifications.

10.1.1 - Military Standard 1530A, dated 11 December 1975, "Aircraft Structural Integrity Program Airplane Requirements"

10.1.1.1 - The primary objective of this specification is to maintain operational readiness by identifying the potential structural problems early and defining a preventive maintenance program for orderly scheduling of inspection, replacement, or repair.

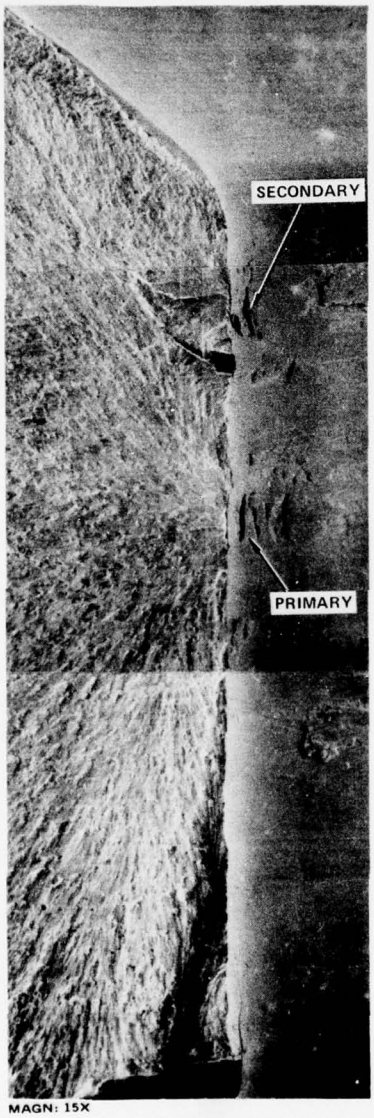

MAGN: 15X

MAGN: 68X

MAGN: 68X

FIGURE 38. PRIMARY AND SECONDARY CRACKS INITIATING FROM HOLE DEFECTS ON FORWARD SIDE OF HOLE SHOWN IN FIGURE 41. SURFACE FINISH OF HOLE MEASURED 250 RHR.

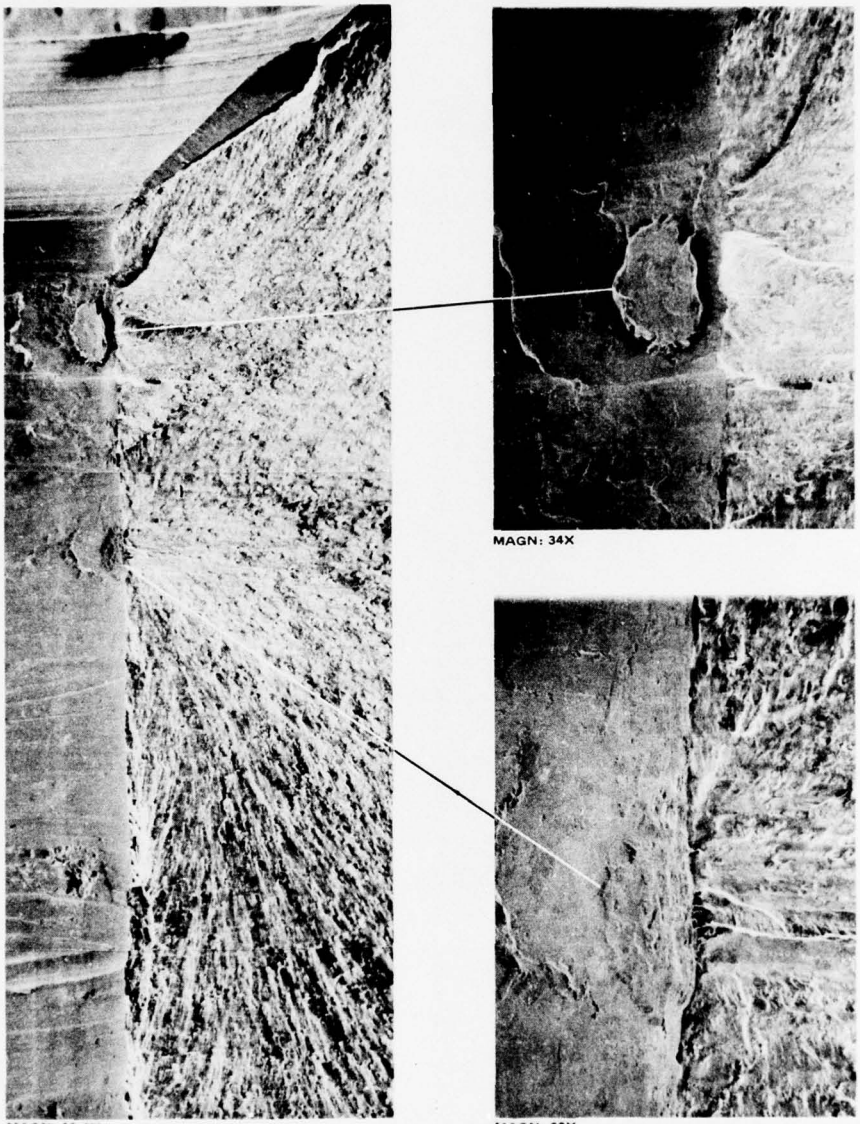

FIGURE 39. CRACK INITIATIONS FROM HOLE DEFECTS ON AFT SIDE OF HOLE SHOWN IN FIGURE 41.

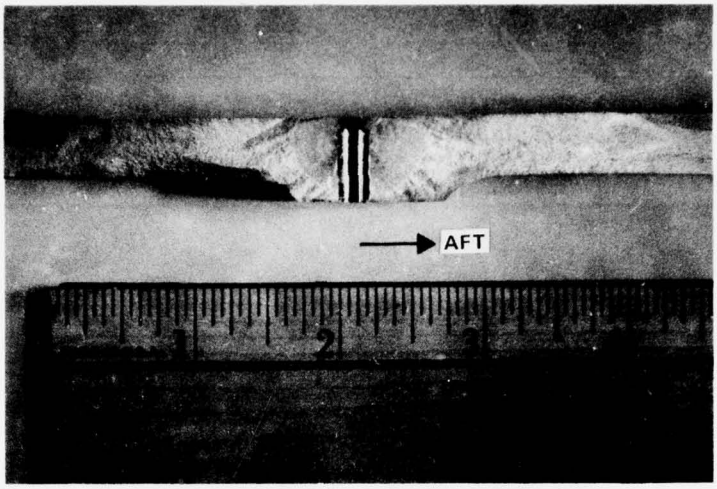

FIGURE 40. CRACK AT WING STATION 43 BETWEEN 33% AND 44% SPARS (9.3 INCHES) SUBSEQUENT TO 1045 CYCLES OF 110% LIMIT DESIGN LOAD

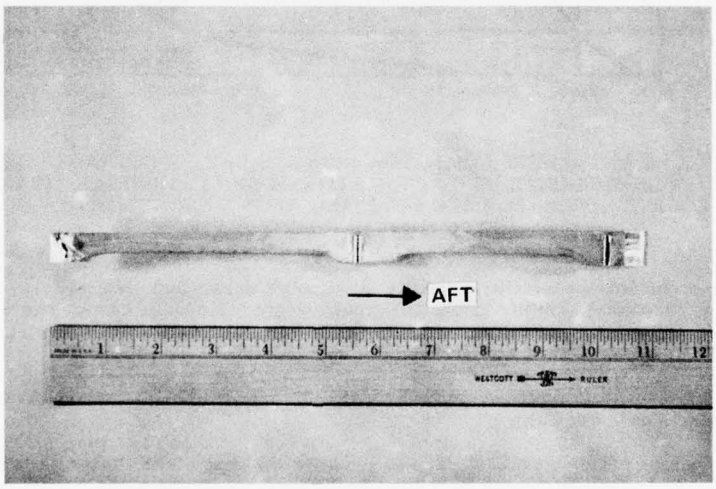

FIGURE 41. CLOSE-UP OF FIGURE 40 SHOWING TRANSITION FROM RANDOM TO CONSTANT-AMPLITUDE TEST LOADING

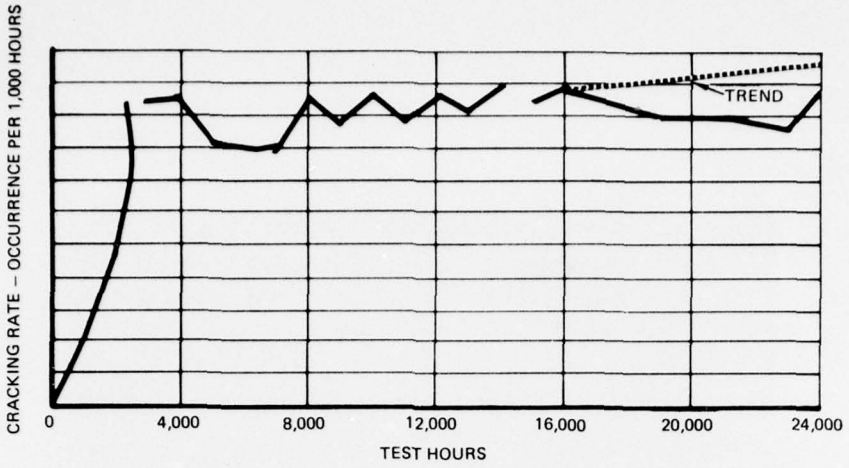

FIGURE 42. RATE OF FATIGUE CRACK OCCURRENCE VERSUS TEST HOURS FOR F-5E FULL-SCALE FATIGUE TEST ARTICLE

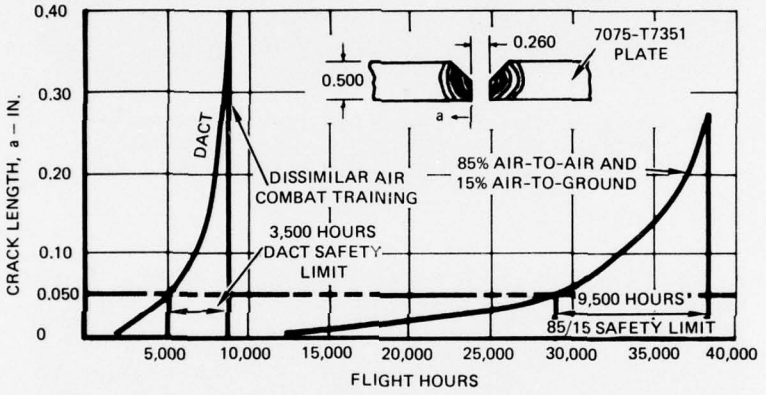

FIGURE 43. SAFETY LIMITS FOR 85/15 AND DACT SPECTRA FOR NON-COLD-WORKED HOLES AT WING LOWER SKIN FATIGUE-CRITICAL LOCATION (W.S. 73.0 AND 44% SPAR). CRACK GROWTH PLOTS ARE BASED ON SPECIMEN TEST RESULTS.

10.1.1.2 - The requirements relative to quality assurance are two-fold. Firstly, design drawings for fracture-critical parts shall identify inspection requirements. Secondly, non-destructive inspections, process control, and quality control requirements shall be established by the contractor and approved by the USAF, and shall be in compliance with MIL-I-6870 specification.

10.1.2 - Military Specification MIL-A-008866B, dated 22 August 1975, "Airplane Strength and Reliability Requirements, Repeated Loads and Fatigue"

The primary objective of this specification is to establish the analysis and testing requirements in order to minimize cracking which could result in structural failure in flight or significant maintenance problems.

10.1.3 - Military Specification MIL-A-008867B, dated 22 August 1975, "Airplane Strength and Rigidity Ground Tests"

The primary objective of this specification is the identification of ground tests required for structural evaluation of the complete airframe structure. This includes design development tests, full-scale airframe static test, and full-scale airframe durability and damage-tolerance tests.

10.1.4 - Military Specification MIL-A-83444, dated 2 July 1974, "Airplane Damage Tolerance Requirements"

10.1.4.1 - The primary objective of this specification is to establish the damage tolerance requirements in order to protect the safety of flight structure from the detrimental effects of manufacturing and processing defects through manufacturing and process controls and the use of careful inspection procedures.

10.1.4.2 - The requirements relative to quality assurance and, in particular, to fastener holes in slow-crack-growth structure, is to assume that an initial flaw size at a hole will be 0.050-inch-radius corner flaw for material thicknesses greater than 0.050 inch unless the contractor can demonstrate a better detection capability. The contractor, subject to USAF approval, can establish an initial flaw size at a hole less than the 0.050-inch radius corner flaw if the following detection capabilities can be demonstrated: Firstly, that a 90 percent probability of detection while maintaining a 95 percent confidence level can be achieved. Secondly, specifications covering the production line inspections, including production equipment and personnel, will be prepared

by the contractor and approved by the USAF delineating the requirements associated with the minimum initial flaw assumptions.

10.2 Compliance

10.2.1 - The minimum initial flaw size, as required by MIL-A-83444, Paragraph 3.1.1.1.a, for a non-cold-worked hole is a 0.05-inch-radius corner flaw for slow crack growth structure and material thicknesses greater than 0.05 inch. A smaller initial flaw size may be utilized if actual measurements are taken to insure positive detection of the smaller initial flaws supplemented by a Non-Destructive Test (NDT) demonstration program in accordance with MIL-A-83444, Paragraph 4.2, or where the fastener hole is cold-worked. One of the most controversial items in this specification is the initial flaw size to be used for design. While it is improbable that a real manufacturing defect would physically resemble a 0.05-inch-tight fatigue crack, it has been reported that defects equivalent to this size have been found in aircraft structure. (This has not been the case for the Northrop T-38/F-5 aircraft.) Although an NDT program may not be practical for all structure, it is likely that the airframe manufacturer will conduct an NDT program on the critical structure to justify the use of a smaller crack size during design, and to assure the overall quality for economic life purposes.

10.2.2 - The crack growth testing described in Section 8 for non-cold-worked specimen 1-4 tested to the DACT spectrum, reference Figures 13 and 15, demonstrated that 48 percent (3200 hours) of the corrected crack growth life (6700 hours) was expended between 0.004 inch and 0.050 inch. An NDT Program would be required to allow the use of a smaller initial flaw size than 0.050 inch and thereby make it possible to recover a significant portion of the 3200-hour crack growth life expended between 0.004 inch and 0.050 inch. The life expended to crack initiation and subsequent growth to 0.004 inch was 2000 hours, which is 23 percent of the corrected total life (8700 hours). This 2000 hours cannot be used for safety limit calculations since the associated initial flaw size by definition excludes the initiation time and subsequent growth to that size. However, this initiation and early growth period (2000 hours) can be considered in the determination of economic lives where these lives are predicted for various spectra which have not been tested and consequently have to be extrapolated from the durability test results from the baseline spectrum test. This approach consists of regressing a sizeable number of cracks from the fatigue test aircraft by fractographic methods as far as possible towards initiation. Inevitably a limit exists for this regression, usually in the order of 0.010 inch. This regression is facilitated when a block or programmed spectrum loading is applied, as the fracture face then exhibits basic spectrum characteristics. Fractographic regression for a random cycle-by-cycle spectrum requires unreasonable manpower resources on each crack unless striation marker bands are utilized. Analytical crack growth plots are then fitted to the fractographic data in order to regress the cracks to zero time. These zero-time crack lengths are then referred to as "equivalent initial flaw sizes," the operative word being "equivalent." Linear elastic fracture mechanics has very definite limitations applied to micro-crack growth, and therefore these analytical extrapolations to zero time must be considered as analytical tools and no more than a convenient method of including the initiation period in the crack growth curve. An equivalent initial flaw size based on a predetermined probability and confidence level is chosen from a statistical distribution of these equivalent flaw sizes. Crack growth analyses are then made from this flaw size for the various loads spectra in order to determine the associated economic lives. In choosing a Wheeler m value to force the crack growth curves through zero time, it must be recognized that these are really dummy m values and should not be used for predicting safety limits. The above method has merit as long as it is not misinterpreted and the derived retardation factors and material data are not used to analytically predict crack growth from real flaws, which would yield extremely unconservative results.

The damage tolerance analysis performed for the F-5E aircraft does not include any allowance for crack initiation. The safety limits quoted are based on an 0.050-inch initial flaw, in compliance with MIL-A-83444, Paragraph 3.1.1.1.a, requirement, since an NDT program justifying the use of a smaller initial flaw size had not been conducted on the F-5E/F aircraft. For aircraft that do not have the critical holes cold-worked, the safety limit for the wing based on the specimen tests and the assumed 0.050-inch initial flaw is 9500 hours for the 85/15 spectrum and 3500 hours for the DACT spectrum, reference Figure 43. For aircraft that have the critical holes cold-worked, the safety limit for the DACT spectrum is 25,000 hours, as shown in Figure 15.

10.3 Actual Impact on Design Changes

Damage tolerance had more of an impact on whether there would be a redesign of a part than it had on the actual design changes. The following steps outline the procedure used to determine if a redesign was required:

10.3.1 - Evaluation of the cracking to determine if it was meaningful or caused by a test deficiency.

10.3.1.1 - Regression of crack to point of initiation.

10.3.1.2 - Correlation of crack initiation time using fatigue and damage-tolerance analysis.

10.3.2 - Determination of the cause of the fatigue crack.

10.3.3 - Statistical study to determine how many parts will crack in service considering the various usages.

10.3.4 - Cost Trade Study — Inspection and Repair vs Redesign. The design changes normally involved removing or reducing stress concentrations, improving surface finish, and strengthening or removing redundant load paths. In some instances material changes were also made to improve fracture toughness, but the actual resizing of structure was based solely on fatigue considerations. Cold-working of fastener holes was incorporated for both fatigue and damage-tolerance considerations to preclude potential problems in the DACT environment and to enhance the damage-tolerance characteristics of the wing.

10.4 Impact of USAF Damage-Tolerance Requirements If Applied During Original Design Phase

10.4.1 Introduction

There would have been a moderate increase in overall program cost if the current USAF damage-tolerance requirements had been applied during the original design phase for the F-5E/F airplane. The implementation of the new Air Force philosophy relative to damage-tolerance analysis would have had a minor effect on the production design.

10.4.2 Fracture Control Plan

The essential aspects of this fracture control plan that would have been implemented during the original design phase for the F-5E/F airplane are as follows:

10.4.2.1 - Identification of fracture critical parts on drawings.

10.4.2.2 - Analysis and coupon testing to determine crack growth lives of critical parts.

10.4.2.3 - Modification of Purchase Orders to guarantee minimum fracture toughness properties, process controls, and inspection requirements by the supplier.

10.4.2.4 - Review and modification of production methods and process controls to minimize defect sizes on critical parts list.

10.4.2.5 - Setting up NDT program to establish initial flaw sizes that could be detected during manufacturing.

10.4.2.6 - Expanding NDI capability, methods, and procedures using latest penetrant, magnetic particle, radiographic, and ultrasonic inspection techniques to assure that flaws larger than specified sizes are detected in the critical parts.

10.4.2.7 - Preparation of damage-tolerance analysis report defining safety limits and inspection intervals for each spectrum usage.

10.4.3 Design Changes for Damage-Tolerance Compliance

10.4.3.1 - It is probable that design deficiencies such as the leading edge flap hinges would have been detected earlier in the design if damage-tolerance requirements had been applied during the original design. High-strength steel parts used on the design of the horizontal stabilizer torque tube and main spar would have been reviewed for fracture toughness and da/dN, and the heat treats would have been lowered.

10.4.3.2 - The most concentrated analysis and design effort would have been directed to the wing. The design limit stress at Wing Station 30 was 31 KSI, based on the original tapered-beam stress analysis. The maximum 85/15 basic spectrum stress at Wing Station 30 was 102 percent of the design limit stress. There were only 230 load occurrences in the 4000-hour lifetime that exceeded 80 percent of the design limit bending moment. It is apparent that when designing to 31 KSI design limit stress, there should be no fatigue or damage-tolerance problems when using the basic fatigue spectrum. This was indicated by the original fatigue analysis, and the limited crack growth analysis conducted at that time indicated extremely long lives. Later strain gage data showed that limit stress at Wing Station 30 was actually 35 KSI. If this limit stress level had been known during the original design phase when the basic fatigue spectrum was not available, then it would not have been considered acceptable from either a fatigue or damage-tolerance standpoint.

10.4.3.3 - A major potential problem was identified at Wing Station 73 when strain gages showed design limit stress levels of 42.5 KSI. The maximum basic spectrum stress was 39 KSI. Had these stress levels been known during the design phase, then local skin thickness changes would have been made from fatigue considerations alone, since Miner's prediction would have indicated a 3600-hour fatigue life. Damage-tolerance analysis made to a block simulation of the basic flight-by-flight spectra showed 2500 hours of unretarded crack growth from an 0.05 corner flaw to failure. If retardation had been considered, then the increased life would have been marginally acceptable. The inference is that fatigue analysis rather than damage tolerance would have sized the wing lower skin. In the later DACT spectrum, the maximum spectrum stresses at both critical locations increased an additional 7.5 percent above the maximum basic spectrum stresses.

11.0 FUTURE PLANS — COMPLETE DAMAGE TOLERANCE ASSESSMENT

Although the F-5E/F aircraft have completed one of the most thorough and comprehensive fatigue development programs ever conducted on a fighter aircraft, there are areas which require further development. Specifically, these areas are: increased accuracy in loads analysis through the use of flight test measured loads for all major structural components and flight conditions; an integration of these loads with current operating roles to produce accurate loads and stress spectra; a final damage-tolerance analysis of the critical areas to accurately define the safety limits; and a program of individual aircraft tracking and fleet monitoring to determine the economic life and safety limit for each aircraft. For the latter purpose, all F-5E/F aircraft owned or operated by the USAF will be equipped with a 6-level counting accelerometer, and approximately 20 percent of the USAF fleet will have multi-channel loads data magnetic tape recorders. Effort is currently underway on all of the above tasks, and the results of this effort will provide a safe aircraft out to the aircraft's maximum economic life.

12.0 RECOMMENDATIONS FOR FUTURE AIRCRAFT DESIGNS

12.1 Damage-Tolerance Versus Fatigue Analysis

Damage tolerance analysis is a logical extension of fatigue analysis and is a fundamental tool in establishing a meaningful structural maintenance program for any aircraft. It provides a guide for the selection of optimum materials and processes to provide the maximum service life and safety. However, fatigue initiation is also important, and in many instances it is undesirable to reduce the resistance to crack initiation just to obtain a high fracture toughness, K_{IC}. Such a change should consider the improvements obtained in da/dN which for most structures would be more important than K_{IC} or K_C.

Fatigue analysis in the original design phase should also continue to play a major role in sizing the structure. It is recommended that a linear cumulative damage method of analysis be utilized for this purpose.

12.2 Limitations of Damage-Tolerance Analysis

12.2.1 - The major shortcomings in the use of crack growth analysis in design are as follows:

12.2.1.1 - Stress intensity factors for structure with complex geometry and for complex crack front shapes are difficult to determine.

12.2.1.2 - Da/dN data developed for compact tension edge-cracked or center-cracked specimens are difficult to relate to each other and to differing crack configurations such as surface flaws.

12.2.1.3 - Determining the degree of retardation to be used for analysis due to deficiencies with state-of-the-art retardation models. It is obvious that there are limitations to the accuracy of a crack growth analysis. However, these limitations can be overcome to some degree with sufficient substantiating coupon and component test data. Stress intensity factors for complex geometrics should also be substantiated by constant-amplitude crack growth testing and by finite cracked element models.

Lacking any substantiating spectrum crack growth test data, analysis can be based on the assumption of no retardation since the various retardation models have been primarily substantiated against block-type programmed loading. In order to control another variable from the analysis, it is recommended that tabular da/dN test data be input to the crack growth computer program, preferably at various R values (with an appropriate interpolative routine), rather than using fitted-curve equations with R routines that can never fit the test data over the full range of ΔK — or, more particularly, over the full range of R values. The best check on the validity of any fitted crack growth equation is to use the equation to regenerate the original a-versus-N constant-amplitude test coupon data. It is suggested that the mean or 50-percent-probability da/dN data be used rather than higher-probability data (such as 90-percent or above) as such data would result in very conservative crack growth lives.

If da/dN data are not available for negative-R values and have to be extrapolated from an R = 0 plot, it is recommended that K-effective be taken as K_{max} rather than as ΔK or $K_{max}(1 - R)^m$, both of which yield conservative growth rates. The negative portion of the stress excursion does not appear to contribute to crack growth in constant-amplitude da/dN testing.

12.3 Safety Limit Goals

The economic life of the aircraft is established by the durability test of the complete airframe and the requirement is that it be greater than the design service life. There are no specific requirements for the "safety limits." These requirements are based on mutual agreement between the USAF procuring agency and the contractor. However, it is recommended that the design goal be at least two lifetimes of crack growth from a conservative initial flaw size that could be assumed to exist when the aircraft was delivered. There would not appear to be a significant weight penalty in achieving two lifetimes of crack growth with the proper material selections and operating stress levels along with good production practices and a comprehensive manufacturing NDI program. Cold-working of critical holes in areas of high local stresses should be strongly considered in order to maximize both the economic life and safety limit.

It is recommended that striation marking be utilized on the full-scale Fatigue Test Article during durability testing, as it is extremely difficult to regress crack growth for a random flight-by-flight loading, and it is undesirable to oversimplify the test spectrum just to facilitate crack regression. The stress level, R, and the number of marker cycles can be chosen or optimized in order to have an insignificant effect on total fatigue life and to ensure identifiable marks even though the marking stress will inevitably vary throughout the structure.

13.0 SUMMARY OF LESSONS LEARNED

13.1 Introduction

The purpose of this section is to summarize the lessons learned from the durability testing and the application of damage-tolerance requirements to the F-5E/F airframe. The most significant items discussed in previous paragraphs are reiterated below.

13.2 Flight Test Measured Data

The loading spectra for vertical stabilizers should be developed with care as there are few definitive load occurrence data available. A special flight loads survey program in the aircraft primary mission during air combat was conducted to develop these data for the F-5E.

Criteria utilized during the development of the follow-on fatigue test included data obtained from F-5E MAP pilot training operation at Williams AFB and from the special air combat flights. This information indicated that the maneuvering leading and trailing edge flap was actuated less often than anticipated when the original flap usage criteria were developed. During air combat usage, the flaps were actuated approximately once for every three maneuvers, as opposed to the initial assumption of once for each maneuver. Although comparisons of flight test measured leading edge flap loads indicated that the measured loads were lower, the total measured wing loads were generally higher, resulting in a reduction of the estimated service life.

The lesson learned is that the flight test measured data should be as comprehensive as possible and should be incorporated into the full-scale fatigue test loads spectrum as soon as possible, thereby reducing the possibility of experiencing unrepresentative failures or conducting the test to reduced loads that result eventually in degrading the test-demonstrated life.

13.3 Effect of Cold-Working Fastener Holes on Fatigue and Crack Growth Life

Cold-working holes in 7075-T7351 material prior to countersinking will improve the total fatigue life, initiation plus crack growth, in a fighter-type environment by a factor of five. Cold-working holes subsequent to countersinking improved the total fatigue life by a factor of two.

13.4 Advantages of Striation Marking

Striation marking proved extremely successful in facilitating segregation of crack growth from nucleation. No other striation characteristics could be detected to assist in regressing the crack growth with the random cycle-by-cycle test spectrum employed. It is recommended that striation marking be utilized on the full-scale Fatigue Test Article during durability testing.

13.5 Assumption of Continuing Damage

Crack growth of similar size was observed on both sides of each hole. Cracks were always found in the adjacent holes. This is an important consideration in the assumption of continuing damage for typical fatigue-initiated cracks, and indicates that when a fatigue crack breaks through to the edge of the part, the crack size on the opposite side of the hole could be of similar size. Adjacent holes drilled with the same technique would likely have similar-size cracks. The influence of a design-type single precracked flaw was not considered in these tests.

13.6 Initial Hole Quality Assessment Program

13.6.1 - The major question that arose during the Initial Hole Quality Assessment Program was the relationship of RHR finishes to the overall hole quality, which includes hole defects such as nicks, scratches, and gouges. The general assumption was that abusive drilling and reaming, which produced high RHR finishes, would also result in hole defects. A review of all available data did verify that holes with high RHR finishes contained a higher percentage of defects. However, it was also found that some holes with very low RHR finishes contained some defects.

13.6.2 - It is apparent from the results of the Initial Hole Quality Assessment Program that hole defects do exist and contribute to early crack initiations, tending to emphasize the crack growth portion of the total fatigue life. However, with a judicious selection of materials and sufficient quality assurance to justify the assumption of relatively small flaw sizes for analysis and testing, there would not appear to be a prohibitive penalty in neglecting the stage 1 crack initiation period in safety limit assessments.

13.7 USAF Damage Tolerance Requirements

The minimum initial flaw size, as required by MIL-A-83444, is an 0.05-inch-radius corner flaw for slow crack growth structure and material thicknesses greater than 0.05 inch. A smaller initial flaw size may be utilized, if actual measurements are taken, to ensure positive detection of the smaller initial flaws supplemented by a nondestructive test demonstration program. The testing described in Section 8.0 demonstrated that 48 percent of the total crack growth life was expended between 0.004 inch and 0.05 inch. This loss in the safety limit would justify the cost of an NDT program.

13.8 Safety Limit Goals

The economic life of the aircraft is established by the durability test of the complete airframe, and the requirement is that it be greater than the design service life. There are no specific requirements for the "safety limits." However, it is recommended that the design goal be at least two lifetimes of crack growth from a conservative initial flaw size. There would not appear to be a significant weight penalty in achieving two lifetimes of crack growth with the proper material selections and operating stress levels along with good production practices and a comprehensive manufacturing NDT program. Cold-working of critical holes in areas of high local stresses should be strongly considered in order to maximize both the economic life and safety limit.

14.0 REFERENCES

1. MIL-A-8860(ASG), "Airplane Strength and Rigidity Requirements, Repeated Loads and Fatigue," May 1960.
2. ASD TR-66-57, Air Force Aircraft Structural Integrity Program: Airplane Requirements, May 1970.
3. MIL-A-83444, "Airplane Damage Tolerance Requirements," 2 July 1974.
4. Miner, M.A., "Cumulative Damage in Fatigue," TRANS ASME, Vol. 67, 1945, page A159.
5. MIL-A-008865A, "Airplane Strength and Rigidity Reliability Requirements, Repeated Loads and Fatigue," 31 March 1971.
6. Holpp, J., and Landy, M., "The Development of Fatigue/Crack Growth Analysis Loading Spectra," AGARD-R-640, January 1976.
7. MIL-STD-1530A, "Military Standard Aircraft Structural Integrity Program, Airplane Requirements," 11 December 1975.
8. Figge, F.A, et al., "Advanced Metallic Structure Air Superiority Fighter Wing, Design for Improved Cost, Weight and Integrity," AFFDL-TR-73-52, dated June 1973.
9. Heywood, R.B., "Designing Against Fatigue of Metals," 1962.

15.0 DEFINITIONS

1. Durability. The ability of the airframe to resist cracking (including stress corrosion and hydrogen-induced cracking), corrosion, thermal degradation, delamination, wear, and the effects of foreign object damage for a specified period of time. Reference 8, paragraph 3.1.

2. Economic Life. That operational life indicated by the results of the durability test program; i.e., test performance interpretation and evaluation in accordance with MIL-A-8867 to be available with the incorporation of Air Force-approved and committed production or retrofit changes and supporting application of the force structural maintenance plan in accordance with this standard. In general, production of retrofit changes will be incorporated to correct local design and manufacturing deficiencies disclosed by test. It will be assumed that the economic life of the test article has been attained with the occurrence of widespread damage that is uneconomical to repair and, if not repaired, could cause functional problems affecting operational readiness. This can generally be characterized by a rapid increase in the number of damage locations or repair costs as a function of cyclic test time. Reference 8, paragraph 3.2.

3. Initial Quality. A measure of the condition of the airframe relative to flaws, defects, or other discrepancies in the basic materials or introduced during manufacture of the airframe. Reference 8, paragraph 3.3.

4. Damage Tolerance. The ability of the airframe to resist failure due to the presence of flaws, cracks, or other damage for a specified period of unrepaired usage. Reference 8, paragraph 3.5.

5. Slow Crack Growth Structure. Slow crack growth structure consists of those design concepts where flaws or defects are not allowed to attain the critical size required for unstable rapid propagation. Safety is assured through slow crack growth for specified periods of usage, depending upon the degree of inspectability. The strength of slow crack growth structure with subcritical damage present shall not be degraded below a specified limit for the period of unrepaired service usage.

6. Safety Limit. Crack growth time from maximum initial flaw size to critical crack length.

7. Quality Index. The effective stress concentration factor demonstrated by a test failure — derived by equating applied damage $\left(\sum \frac{n}{N} = 1.0 \text{ at crack initiation}\right)$.

CONTRIBUTED DISCUSSION

by

Prof. J.F.McCarthy Jr.
Massachusetts Institute of Technology
77 Massachusetts Avenue
Cambridge, MA 02139, USA

The subject paper is an excellent summary of the methodology to conduct a comprehensive Aircraft Structural Integrity Program (ASIP) on an existing airplane. The authors have been very candid in outlining the history of their experience in applying new Air Force criteria to a military aircraft. Their experiences should benefit those who must conduct similar programs in the future. Because of the aging fleet, concern for flight safety, and economic considerations, the Air Force is requiring other aircraft to be subjected to similar ASIP programs.

The authors lead the reader through mission requirements, design criteria, fatigue loads and spectra development, to the formulation of a comprehensive test program. A nice description is given of the test setup and the rationale behind it. Fatigue test results are summarized with the necessary design changes and damage-tolerance analyses of test-critical areas. This systematic identification of hot spots is usually known only to the contractor and the Government customer. In fact, this is the first paper in the open literature that I have seen that systematically develops real-life cases.

As with most high-performance aircraft, the wing structure of the F-5E/F is the most critical component. The fatigue-critical areas are identified with a description of the associated specimen tests and results with and without cold-worked holes. Detailed results are presented with interesting laboratory fractographic analyses of fatigue crack initiation resulting from real-world manufacturing processes. The results are similar to those experienced by other aerospace primes but which have never been systematically assembled into such a comprehensive package. The authors finally make some recommendations as to comprehensive damage-tolerance assessment programs, safety-limit goals, and future aircraft designs. Some of the conclusions are very refreshing. For example, the authors recommend that fatigue calculations be performed to define crack initiation and admit that Miner's rule is a good design tool since other methods are complex and sometimes unconservative.

Some of the surprising results of the paper include the fact that holes were found with flaws on both sides of the panel, and these cracks grew at about the same rate. Experience showed that defects tended to bunch up in an area rather than being confined to just one hole. High RHR finishes seem to aggravate cracking. With built-up aluminum/steel/aluminum panels, damage could be induced by drawing steel chips through the aluminum panels. These experiences can be very beneficial in preventing defects during manufacturing of future aircraft.

The authors have no compunction about making recommendations that are somewhat controversial. For example, they suggest that tabular da/dN data be incorporated in a computer routine rather than using fitted-curve equations, that 50-percent-probability da/dN data be used, and that K-effective be taken as K_{max}. The remarks on assumptions for initial flaw size are especially revealing.

In summary, the paper is an excellent treatise on the actual application of Air Force ASIP criteria. It will indeed provide an important contribution to the Design Manual on "Fracture Mechanics Design of Aircraft Structures" being prepared by AGARD.

CONTRIBUTED DISCUSSION

by

C.F.Tiffany
Technical Advisor, Aeronautical Systems Division
United States Air Force Systems Command
Wright-Patterson AFB, OH 45433, USA

This paper does an excellent job of describing the very comprehensive durability test program performed on the F-5E aircraft. As indicated by the authors, the aircraft was designed prior to the implementation of the current USAF Damage Tolerance Requirements specified in MIL-A-83444, and the overall structural integrity requirements specified in MIL-STD-1530A. However, Northrop did incorporate design concepts which greatly enhanced the damage tolerance of the aircraft. As indicated in the paper, this was done as a result of past experiences and a previous damage tolerance sensitivity study which Northrop performed for the Air Force.

The only apparent shortfall in the F-5E durability test program, as compared to the requirements specified in MIL-STD-1530A was with regard to test schedule. The test was somewhat late and a number of aircraft were already in service when problems were discovered during the test. This, of course, increases the cost of retrofits. Nevertheless, Northrop was able to minimize the cost impact through the development of a phased inspection program based on crack growth analyses. In fact, the authors indicated an estimated eight million dollar cost avoidance as a result of these analyses.

The authors cited a number of lessons learned during the program which seem worthy of some additional comments. I was pleased to see that in general the lessons seemed to support the MIL-STD-1530A and MIL-A-83444 requirements being imposed by the USAF on all new aircraft systems. However, the paper does imply that, since fastener hole initial flaw sizes as large as the specified .05 inch corner flaw were not found in the F-5L durability test article, perhaps the specified initial flaw size is somewhat severe. On the other hand, multiple rather than single flaws were found in the fastener holes so from this aspect the USAF damage tolerance requirements may not be severe enough.

With respect to the specified initial flaw size for slow crack growth structure, it is recognized that the probability of such an occurrence is remote, but it is not zero. Fastener hole manufacturing damage equivalent to, and in some cases in excess of, the specified .05 inch corner flaw have been observed in some past aircraft. Some examples were given in Reference 1. Also, it should be recognized that the specified quarter circular flaw shape is the most favorable shape that could be assumed (i.e., it will result in the largest slow crack growth life). For example, studies performed on the F-4 aircraft indicate that a thru-the-thickness flaw less than .03 inches in length will result in about the same slow crack growth life as the .05 inch corner flaw.

Based on these considerations and recognizing that safety of flight is dependent on there being no flaws in excess of the size assumed in design, the USAF is not yet willing to relax its current requirements. However, as the authors indicated, the current specification does allow the use of a smaller initial flaw size if it is demonstrated that the inspection procedures will preclude the occurrence of a size larger than that used in the design. I agree with the authors that the additional life achieved by use of a smaller initial flaw size does provide an incentive to the airframe manufacturer to perform an inspection demonstration.

With respect to the single rather than multiple flaw assumption, the USAF damage tolerance specification is based on the premise that all of the critical fastener holes in a given aircraft may have average to marginal quality fastener holes and that a single hole may have an initial damage as large as the specified .05 inch corner flaw. From past studies on other aircraft, it is felt that the marginal quality hole can be characterized by a .005 inch initial corner flaw. It is recognized that the worst single hole (i.e., the hole that contains the .05 inch corner flaw) also contains additional defects of a lesser size -- perhaps on the order of .005 inches. However, these lesser defects generally have negligible effect on the growth of the single large flaw and thus do not influence the slow crack growth life except in the case where the growth of the primary flaw has been terminated (e.g., by growing to a free edge). To cover this situation the damage tolerance specification, MIL-A-83444 contains requirements on continuing damage. Specifically it is stated, "When the primary damage and growth originates in a fastener hole and terminates prior to member or element failure, continuing damage shall be a .005 inch radius corner flaw emenating from the diametrically opposite side of the fastener hole at which the initial flaw was assumed to exist."

There is a recognized deficiency (or more properly an oversight) in this requirement which is intended to be corrected in the next revision to the specification. The requirement does not recognize the incremental growth of the .005 inch radius corner flaw which will have occurred up to the time that the primary damage is terminated. The specification

should read, "When the primary damage and growth originates in a fastener hole and terminates prior to member or element failure continuing damage shall be a .005 inch radius corner flaw, emenating from the diametrically opposite side of the fastener hole at which the initial flaw was assumed to exist plus the amount of growth (Δa) which occurs prior to termination of the primary damage."

REFERENCES

1. Tiffany, C. F., "The Air Force's Changing Philosophy on Structural Safety, Durability, and Life Management," presented at AIAA Structures, Dynamics and Materials Meeting in Las Vegas, Nevada, April 1974.

APPLICATION OF FRACTURE MECHANICS IN DESIGNING BUILT-UP SHEET STRUCTURES

by
H. Vlieger
National Aerospace Laboratory NLR
Amsterdam
The Netherlands

SUMMARY

Past experience has shown that during the operational life of an aircraft structure cracks or failures may arise in different structural components. In future designs the designer must be able on the one hand to restrict the occurrence of cracks by a careful detail design and on the other hand to guarantee some specified life of the aircraft if cracks nevertheless may arise. The object of this paper is to give the designer some support in this task. The attention is focussed on sheet structures.
The paper discusses briefly the different analyses that are relevant to the design of a fail-safe aircraft structure: the static strength, the crack initiation and propagation and the residual strength analyses. The main part of the paper will be devoted to the application of fracture mechanics in the crack propagation and residual strength analyses. Theoretical results of an investigation carried out at NLR in this field and verification of these results by experiments will be shown.
Finally the paper will provide some guidelines for aircraft structural applications.

1. INTRODUCTION

The task of the designer of a modern aircraft structure has been augmented as compared to that with older designs. Apart from having to meet conventional requirements regarding static strength and stiffness of the undamaged structure and buckling stability, he has to account now for the presence of cracks or damage. Depending on the design philosophy that is chosen, the designer must be able to guarantee a certain crack-free life (safe-life approach) or warrant safe operation of the aircraft with cracks being present (damage tolerant approach). In the latter case the designer is expected to be able to predict the fatigue life until final failure starting with a certain minimum (= detectable) crack length. Further he has to demonstrate that a specified load can still be carried when a certain amount of damage is present in the structure (residual strength requirement). Furthermore, if fracture instability followed by crack arrest is accepted (fail-safe structure), the designer has to show the crack arrest capability of his design.

Designing a fail-safe structure makes the greatest demands on the designer's knowledge and ability. Different analyses have to be carried out to demonstrate the airworthiness of the design, viz.: analyses of static strength, crack initiation and propagation, and residual strength. Each of these analyses will be discussed briefly in the present paper. During the discussion reference will be made to recent literature on the different subjects for the convenience of those who wish to read further.

The crack propagation and residual strength analyses will be discussed in more detail, especially with respect to fracture mechanics. The application of fracture mechanics will be focussed on the design of built-up sheet structures.

Finally the paper deals with the interrelated aspects of crack propagation, residual strength and inspection of a fail-safe design. From this the means of improving the fail-safe properties of built-up sheet structures are discussed.

2. DESIGN PROBLEMS ASSOCIATED WITH THE POSSIBLE PRESENCE OF CRACKS

2.1 Potential sources of damage

The damage that may exist in aircraft structural components can be separated into two categories, namely: defects present in the aircraft structure already when it is delivered to the customer, and damage caused during operation of the aircraft.

Defects present in new aircraft components can stem from three major sources: those existing in the mill product, those introduced during processing, and those caused by handling or assembly. Mill products can contain imperfections such as inclusions or laminations, internal defects such as cracks and porosity, and surface defects such as pits, scratches and cracks. Processing operations such as rolling, forming and machining (milling, drilling and so on) are potential defect producers because they often leave high residual stresses and stress-raising roughness. Handling operations during manufacturing and assembly can produce surface defects such as pits, scratches and cracks.

Apart from defects being present already in the new product, cracks can initiate and propagate in service for a number of reasons, e.g., as a result of improper use or maintenance, fatigue, stress corrosion, fretting corrosion and foreign object impact (turbine blade penetration, bird or hail impact).

In designing an aircraft structure the designer has to bear in mind all these potential sources of damage. Whether the existence of cracks is accepted, and if so which structural provisions have to be

taken to prevent catastrophic failure of a primary aircraft component, will depend on the design concept chosen.

2.2 Design concepts with regard to the tolerance of damage

Figure 1 gives a survey of the different structural design approaches that can be applied by the designer in order to guard against catastrophic failures as a consequence of manufacturing defects and/or service flaws. With regard to the tolerance of cracks, in principle two different design concepts can be distinguished, viz.: the safe-life concept and the damage tolerant concept.

The safe-life design concept states that the life of a component or structure is terminated when a crack occurs. It is assumed then that the structural life of the component can be predicted and the component can be replaced, repaired or retired before its predicted life expires. The life is predicted by a fatigue analysis based on a testing programme and assumed operational and loading conditions. This analysis will yield the laboratory life of the structure. The safe life then chosen is this laboratory life divided by a safety factor (or better life reduction factor) to provide for test scatter and other variables not otherwise accounted for.

The safe-life approach has the advantage that replacement of components can be scheduled and that in principle no in-service inspection is required. However, these advantages are more than outweighed by the many disadvantages, such as the difficulty of calculating the life, the large and indeterminate nature of fatigue life scatter, and the fact that accidental damage and manufacturing errors can significantly affect fatigue life. In fact, because of these shortcomings, for a number of aircraft components the safe-life concept will provide too little guarantee against unforeseen structural damage and possible catastrophic failure. This uncertainty can be reduced considerably by inserting inspections (provided the safe-life component is not hidden in an uninspectable area) or rather, by combining the safe-life approach with the damage tolerant approach.

The damage tolerant concept (see Fig.1) tolerates damaged or failed components temporarily either by providing slow growth of the damage without allowing the crack to attain a critical size required for unstable rapid propagation (slow crack growth structure), or by providing alternate load carrying members whose function it is to contain localized damage and thus prevent complete loss of the structure (multiple load path fail-safe structure), or by arranging the structural elements such that unstable rapid propagation will be stopped within a continuous area of the structure (crack arrest fail-safe structure). According to Ref.1 sufficient strength and safety of the damage tolerant structure has to be guaranteed as follows. In the case of a slow crack growth structure safety is assured through slow crack growth for specified periods of usage depending upon the degree of inspectability. The strength of this type of structure with subcritical damage being present shall not be degraded below a specified limit for the period of unrepaired service usage. In the case of a fail-safe structure safety is assured through slow crack growth of the remaining structure and detection of the damage at subsequent inspections. Strength and safety of the remaining undamaged structure shall not be degraded below a specified level for a specified period of unrepaired service usage.

The advantages of a damage tolerant structure are undoubted safety and protection against accidental damage and manufacturing errors. Its disadvantages are frequent thorough in-service inspections and the need for possible replacement (and thus grounding of the aircraft) at unscheduled periods. The reliability of a damage tolerant structure can be improved by demanding a good quality control (to reduce the chance of manufacturing defects), by using a good inspection technique and experienced inspectors (to be able to detect cracks early) and by choosing material with good crack propagation resistance.

2.3 Consequences for the designer

In practice the safe-life concept will frequently be applied in combination with the damage tolerant concept. Actually, the designer of a safe-life structure would like to be able to design a structure that is guaranteed crack-free during the entire service life of the aircraft. However, experience has taught him that by different causes, partly beyond his control (for example manufacturing defects) and despite all precautions taken, cracks sooner or later arise. Therefore, he will try to guarantee his structure for a certain crack-free life and schedule some inspections to take care of the possibility of cracking. Further, he may take some structural precautions to guard against undetected crack growth and possible fracture instability in situations where the structure is difficult to inspect.

On the other hand, the designer of a damage tolerant structure accepts the presence of cracks in his structure but wishes them to arise as late as possible in the service life, so that repairs can be limited to a minimum. Thus, apart from damage tolerance properties, he is also interested in a long crack-free life of the structure.

The foregoing signifies that the designer, regardless of which design concept he emphasizes, has to provide for a structural design with a long crack-free life and good crack propagation properties. This can be achieved by a well-considered detail design (avoidance of holes, cut-outs, sharp angles, sudden cross-sectional changes and eccentricities in components subjected to tension), by a good arrangement of structural elements, and by choosing material with good fatigue and crack propagation properties. In the case of a damage tolerant design, sufficient strength of the damaged structure is an additional requirement, so that then the fracture toughness of the damaged material is an important parameter. Finally, when a crack arises the operator must be able to detect it early, implying that the designer must provide for an accessible and easily inspectable structure.

3. ANALYSES REQUIRED FOR THE DESIGN OF A DAMAGE TOLERANT STRUCTURE

Because of the very large number of factors that must be considered, a new design is accomplished by an iterative procedure that begins with simple considerations and becomes progressively more refined and complex. This implies that the complete design procedure with its various aspects actually does not take place according to a strict scheme. However, without going too much into details, the different analyses that are required in the design phase and their effects on previously obtained results can be clearly illustrated on the basis of a flow diagram. Such a flow diagram is shown in Fig.2.

Before the proper design phase the structural lay-out of the new design, i.e. the design philosophy, the structural configuration and arrangement of structural elements, the choice of materials etc., has been fixed. Also, in the design criteria the various requirements with regard to static strength and

stiffness, crack-free life, crack propagation life, residual strength etc., have been specified. Together with the static design loads (derived from the intended operational usage) and the static material allowables (from handbooks) these data will enable the designer to come to a baseline design that meets the static requirements. Unfortunately, adequate fatigue and fracture resistance are not assured by satisfactory static strength. Therefore, supplementary analyses will be required to check whether the fatigue and damage tolerant requirements are also met. Each of these analyses, when applied to the baseline design, will provide a new design stress level (see Fig.2) dictated by the requirements of the relevant analysis. Comparison of this design stress level with that obtained in the static analysis will reveal whether the baseline design has to be resized. The final design will meet the static, fatigue and damage tolerant requirements.

In the following sections of this chapter the fatigue (or crack initiation) and the damage tolerance (or crack propagation and residual strength) analyses will be concisely reviewed. For the sake of simplicity this discussion will be mainly directed to simple sheet structures. In chapter 4 the application of fracture mechanics in the crack propagation and residual strength analyses will be discussed in more detail and applied to built-up sheet structures.

3.1 Crack initiation analysis

The commonly used analysis procedure for predicting the fatigue life to crack initiation for a certain design stress, or the design stress for a specified fatigue life, is illustrated in the flow diagram of Fig.3. The primary requisites for a fatigue analysis of a certain structural component or structural area are its expected service load experience and the behaviour of the material at critical points under these loadings.

The expected load experience of a new design is usually derived from data obtained from previous aircraft with similar flight-load profiles. Gust and manoeuvre loading statistics have been collected for many years by the NASA (Refs.2-6), and the loading statistics for military aircraft are specified in the appropriate military handbooks (Refs.7 and 8). Analyses of these data will provide information on the magnitude and frequency of occurrence of accelerations at the center of gravity of the new aircraft (Fig.3). These data have to be converted to fatigue loading spectra applicable to the areas that are considered to be critical to fatigue (e.g. the wing root region of a commercial aircraft). From these fatigue loading spectra and the geometry of the structure in a critical region (as determined in the first instance by the static strength analysis) the fatigue stress spectrum applicable to the static design stress level (see Fig.2) can be found. Assuming that at an other design stress level all stresses are factored proportionally, stress spectra for different design stress levels can be obtained. The question now is how the fatigue life of the critical area for the derived stress spectrum will depend on the design stress level.

The most common means of characterizing the fatigue behaviour of materials subjected to cyclic stresses of constant amplitude is the well-known S-N curve. Usually this curve gives the relation between the maximum stress in a cycle, S_{max}, and the fatigue life, N, at a constant value of $R = S_{min}/S_{max}$ and for a certain value of the elastic stress concentration factor K_t. Another means of data plotting provides the so-called constant life diagram, presenting constant life contours in a plot of alternating versus mean stresses. Such a diagram can be obtained by cross-plotting of a family of S-N curves found from results of tests in which mean and alternating stresses were systematically varied (K_t=constant).

In order to predict from these constant amplitude data the fatigue behaviour under spectrum (= variable amplitude) loading it is necessary to make use of a cumulative damage rule. The well-known Palmgren-Miner hypothesis is most commonly used. The Palmgren-Miner rule simply states that failure will occur when $\sum n_i/N_i = 1$, where n_i is the number of loading cycles of level S_i that is applied, and N_i is the number of cycles of stress required to cause failure at S_i (see Fig.3). In the literature results of tests on notched specimens can be found that show a fairly large variation in $\sum n/N$ values. Values smaller and larger than unity appear to occur depending on the load history parameters. A review of the effect of the different parameters on the $\sum n/N$ value can be found in Ref.9.

By converting the continuous stress spectrum of a certain design stress level into a stepped function and by using the fatigue allowables in combination with the cumulative damage rule, the design fatigue life at that design stress level can be obtained. By doing this for other design stress levels a relation between the design stress level and the fatigue life will result (see Fig.3). In the design criteria a certain design fatigue life has been specified. With this design fatigue life and the plot of design stress versus fatigue life, the design stress level dictated by the fatigue analysis ($\overline{\sigma}_{CI}$, see Fig.2) will be found. Comparing this stress level with the design stress found in the static analysis (σ_{ST}, see Fig.2) will reveal whether a redesign of the baseline has to be carried out in order to meet the fatigue life requirement.

Though the procedure outlined here describes how the fatigue life of a certain structural component can in principle be predicted, in practice this computation, and thus the computation of the fatigue design stress, appears to be a very delicate matter. One of the major problems in this respect is probably due to the fact that the $\sum n/N$ value that causes crack initiation appears to be not constant but strongly dependent on the load sequence, and the load spectrum does not give any information as to that point.

A detailed discussion of the various problems encountered in predicting the fatigue life is considered to be beyond the scope of this paper. Surveys concerning this subject are given in Refs.9 and 10.

3.2 Crack propagation analysis

Fracture mechanics usually assumes that the rate of fatigue crack growth per cycle, da/dn, is a function of the stress intensity factor range during that cycle, ΔK, and of the stress ratio, R, which is the ratio of the minimum and the maximum stress in a cycle, S_{min}/S_{max}, or

$$\frac{da}{dn} = f_R\left[\Delta K(a)\right] \qquad (1)$$

where f_R is a function dependent on the stress ratio R. The foregoing would imply that for constant amplitude tests at the same stress ratio there exists a unique relation between the crack growth rate and ΔK. Constant amplitude tests have shown that this is indeed the case. Variation of the stress ratio will yield a set of similar curves, each curve applying to a certain R-value.

Several investigators (Refs.11-13) have tried to establish empirical relations which attempt to

incorporate the effect of R, such that all constant amplitude data for a given material may be correlated by a single curve. On the basis of these empirical relations Walker (Ref.14) introduced the idea of the effective stress intensity factor range, $\overline{\Delta K}$. For a centre cracked sheet specimen $\overline{\Delta K}$ is defined as

$$\overline{\Delta K} = \alpha . \overline{S} \sqrt{\pi a} \qquad (2)$$

where α is factor accounting for panel geometry. The parameter $\overline{S}$ in Eq.(2) is the effective stress in a cycle defined as

$$\overline{S} = S_{max}(1-R)^m \qquad (3)$$

where m is an empirical constant that depends upon the material and possible the environment ($1 \geq m > 0$). Using experimental data of Ref.11 Walker showed that the crack growth rate of a given material obtained from constant amplitude tests at different R-values indeed can be represented by a single curve when it is plotted as a function of the effective stress intensity, $\overline{\Delta K}$ (see Fig.4). Values of m used in computing $\overline{\Delta K}$ were determined for best fit. The values of m found in Ref.14 were 0.5 for 2024-T3 and 0.425 for 7075-T6.

So far the discussion has been limited to constant amplitude cycling. However, the service load experience of an aircraft is by no means constant amplitude. Generally, prediction of the crack propagation properties of a new design under service loads will be obtained by integrating constant amplitude crack growth data of the pertinent material. In doing so two different approaches can be applied:

(i) Integration of constant amplitude data and making use of a linear cumulative damage rule.

(ii) Integration of constant amplitude data and using a semi-empirical cumulative damage concept.

The principle difference between both approaches is that an integration procedure using a linear cumulative damage rule does not account for interaction effects of cycles of different amplitude, whereas the semi-empirical cumulative damage concepts were developed to account for that interaction. Usually predictions using a linear cumulative damage rule lead to a conservative estimate of crack propagation life. A critical review of the different ways of crack propagation prediction, using the approaches mentioned under (i) and (ii), can be found in Ref.15.

The analysis procedure for predicting the fatigue life to failure of a cracked component as a function of the design stress level is illustrated in the flow diagram shown in Fig.5. The primary requisites are the stress spectrum of the structural component (see Fig.3), a plot of da/dn versus ΔK for the material, and the stress intensity expression for a critical crack configuration. By considering the various missions to be performed by the aircraft, from the load spectrum a flight load profile for a certain design stress level can be established. Using this flight load profile together with the stress intensity expression and the crack growth data, the crack growth rate relevant to the i-th stress cycle can be found. Integration gives the crack size, starting from a certain initial crack length, as a function of number of flight hours, for the considered design stress level. Performing the procedure outlined above for different design stress levels results in a relation between the design stress level and the number of flight hours required to propagate a crack from a certain initial value to failure. From the design fatigue life, specified in the design criteria, the allowable design stress level regarding fatigue crack propagation ($\overline{\sigma}_{CP}$, see Fig.2) will be found. Comparison of this stress level and that of the static analysis (σ_{ST}, see Fig.2) reveals whether the baseline design has to be altered to meet the specified crack propagation requirements.

3.3 Residual strength analysis

The behaviour of a sheet with a central transverse crack $2a_o$, subjected to an increasing tension stress σ, is depicted in Fig.6. The stress can be raised to a value σ_i at which the crack will start to extend slowly. This slow crack growth is stable: it stops immediately when the load is kept constant. Although the crack is larger now, a higher stress is required to maintain its propagation. Finally, at a certain critical stress σ_c a critical crack length $2a_c$ is reached where crack growth becomes unstable and sudden total fracture of the sheet results. Both slow stable crack growth and fast fracture instability occur at lower stress levels if the initial crack is longer. By testing panels with different initial crack sizes the curves labelled a and b in Fig.6 are obtained. The curve labelled c can be derived from data points of curves a and b and relates the failure stress directly to the initial crack length. This curve is of special interest to the designer because he wants to know which load can still be carried by the damaged structure when a fatigue crack of a certain size is present, and it is immaterial to him that the crack will show some slow growth prior to final failure. Curve c is denoted as the residual strength curve.

Tests have shown that the curves a, b and c, for a given thickness and panel size and for an intermediate range of crack lengths, can be represented by constant values of the stress intensity factor, viz. by $K_i = \alpha . \sigma_i \sqrt{\pi a_o}$, $K_c = \alpha . \sigma_c \sqrt{\pi a_c}$ and $K_e = \alpha . \sigma_c \sqrt{\pi a_o}$, respectively. However, for the ranges of small and large crack lengths (as compared to the panel dimensions) the constant K-curves appear to overestimate the residual strength properties. Feddersen has shown (Ref.16) that the residual strength properties for these crack lengths can be obtained by drawing two linear tangents to the intermediate range curves as shown in Fig.6. One tangent is drawn from the point $\sigma = \sigma_{yield}$ on the vertical axis, where σ_{yield} is the yield strength of the sheet material; the other tangent is drawn from the point $2a = w$ on the horizontal axis, where w denotes the specimen width. According to Ref.16 the left-hand tangency point always is at two thirds of the yield stress, independent of K, while the right-hand point of tangency is always at a total crack length of one third of the specimen width.

The foregoing implies that when the approach proposed by Feddersen is assumed, the complete residual strength curve (relating the failure stress to the initial crack length) of a sheet of a given thickness and size can be predicted from test data for which

$$\sigma_c < {}^2/_3 \, \sigma_{yield} \qquad \text{and} \qquad 2a_o < {}^w/_3 \qquad (4)$$

which means that the validity requirements for the test data are set by Eqs.(4). This means that in general a few test results will suffice to determine the complete residual strength curve for a certain panel thickness. Because the residual strength depends on thickness (with increasing thickness the

residual strength gradually decreases to the plane strain fracture toughness, K_{Ic}, see Ref.17), in the design stage the designer needs residual strength data for a range of thicknesses. Using the residual strength curve pertinent to the skin thickness applied in the baseline design, and specifying a maximum tolerable crack length, the residual strength level, $\overline{\sigma}_{RS}$, can be found. Comparison of this stress level to that obtained in the static analysis will reveal whether the baseline design meets its fail-safe requirements. The foregoing applies to an unstiffened panel. In the case where the panel is provided with stiffeners there will be an effect of the presence of the stiffeners on the shape of the residual strength diagram. This point will be discussed further in section 4.2.

4. APPLICATION OF FRACTURE MECHANICS CONCEPTS IN THE DESIGN STAGE

4.1 Discussion of application of fracture mechanics principles

In the previous chapter it was shown that in the design stage of a new aircraft fracture mechanics concepts can be applied during the fatigue crack propagation and residual strength analyses. In fracture mechanics it is usually assumed that both crack growth rate and residual strength properties are governed by the value of the crack tip stress intensity factor, K. For an unstiffened centrally cracked sheet K is defined by

$$K = \alpha . \sigma \sqrt{\pi a} \tag{5}$$

where σ is the gross stress remote from the crack, a is the half crack length and α is a factor accounting for limited panel size.

To meet stiffness and buckling requirements, in an aircraft the sheet is usually reinforced by stiffening elements. When in this type of structure a skin crack arises, the stiffeners in the region of the crack will take over some load from the skin, resulting on the one hand in a reduction of the stress intensity factor as compared to the unstiffened panel, and on the other hand in a higher local load in stiffeners and fastening elements. For any panel configuration the effectivity of this sheet-stiffener interaction will increase with decreasing distance of the crack tip to the stiffening element.

The effect of the stiffener on the stress condition at the crack tip is expressed by the value of the "tip stress correction factor", C, defined as the ratio of the stress intensity factors of the stiffened and unstiffened panel at the same crack length, or

$$C(a) = \frac{K_{stiffened}}{K_{unstiffened}} \tag{6}$$

Combining equations (5) and (6) and assuming that α equals unity, the stress intensity factor of a stiffened panel configuration can be expressed as

$$K_{stiffened} = C(a) . \sigma \sqrt{\pi a}$$

The amount of overload in the stiffener due to the presence of the crack is expressed by the value of the "stiffener load concentration factor", L, defined as the ratio of the stiffener loads occurring in the region of the crack (F_{max}) and remote from the crack (F_∞), or

$$L(a) = \frac{F_{max}}{F_\infty} = 1 + \frac{\sum_{i=1}^{n} P_i}{\sigma_{st} A_{st}} \tag{7}$$

where σ_{st} is the stiffener stress remote from the crack, A_{st} is the stiffener cross-sectional area, P_i are the fastener loads and n is the number of fastening elements per stiffener half.

It has to be remarked here that the above mentioned beneficial effect of the stiffener on the stress condition at the crack tip (i.e. $C < 1$), will occur when the panel contains a skin crack only. On the contrary, when one of the stiffeners bridging the crack has also failed then the load present in the broken stiffener will be transferred to its near-by elements, implying that the stress at the crack tip may increase significantly ($C > 1$, see Ref.18).

Assuming that the value of the stress intensity factor dictates the behaviour of the crack tip with regard to crack growth and fracture instability, it was shown in Ref.18 that the behaviour of a skin crack in a stiffened panel under cyclic loads and peak loads can be predicted from unstiffened panel data by accounting for the effect of the stiffeners as expressed by the parameter C. Because the skin crack locally entails higher stiffener loads, yielding and ultimate failure of stiffeners and fastening elements must also be accounted for in such an analysis. The procedure of computation of the residual strength and fatigue crack growth properties of cracked stiffened panels is discussed comprehensively in Ref.18. Therefore a brief description of this procedure will suffice here.

4.2 Prediction of residual strength of stiffened panels

As shown previously the stress intensity factor of the stiffened sheet can be expressed by

$$K_{stiffened} = C(a) . \sigma \sqrt{\pi a}$$

Assuming that unstable crack growth occurs when $K_{stiffened}$ attains a value equal to the plane stress fracture toughness of the unstiffened sheet, K_c ($= \sigma_c \sqrt{\pi a_c}$), then the relation between the critical stress of the stiffened sheet, σ_{sheet}, and a_c is given by the equation

$$\sigma_{sheet} = \frac{K_c}{C(a)\sqrt{\pi a_c}} = \frac{\sigma_c}{C(a)} \tag{8}$$

Equation (8) implies that the σ_{sheet}-a_c curve of the stiffened panel can be obtained by raising all points of the σ_c-a_c curve of the unstiffened panel by a factor $\frac{1}{C(a)}$ pertinent to the particular length of crack.

According to equation (7) the maximum load in the stiffener will be equal to

$$F_{max} = L(a)\ \sigma_{st} A_{st}$$

Ignoring load eccentricity and notch effects (i.e. the stress distribution over the stiffener cross-section is assumed to be uniform), failure of a stiffener will occur when the value of F_{max} of that stiffener is equal to the ultimate strength of the stiffener material, $F_{ult}(= \sigma_{ult} \cdot A_{st})$. Thus the relation between the end-stress at which the stiffener fails, $\sigma_{stiffener}$, and the crack length is given by the equation

$$\sigma_{stiffener} = \frac{\sigma_{ult}}{L(a)} \tag{9}$$

The foregoing implies that the residual strength properties of the stiffened panel will be determined by curves of the shape shown in Fig.7 by the solid lines. The lower curve dictates the behaviour of the stiffened sheet and the upper curve that of the critical stiffener (= stiffener that carries most load and thus fails first). In Fig.7 the stiffener failure curve intersects the stiffened sheet curve. It was shown in Ref.18 that in this case, after stable and unstable crack growth, failure of the panel will occur at the stress level corresponding with point A owing to failure of the critical stiffener. However, the curves do not necessarily intersect. If no intersection occurs failure of the panel will be determined by the top of the stiffened sheet curve (point B in Fig.7).

The stress level indicated by $\overline{\sigma}$ in Fig.7 has a special meaning. This stress level corresponds with point A or point B of the sheet curve, depending on the failure mode of the panel. It was shown in Ref.18 that if at any stress level below $\overline{\sigma}$ fracture instability of a skin crack might occur, then the unstably growing crack will be arrested at the adjacent stiffeners (see crack growth history for crack length a_o). For the case illustrated in Fig.7 fracture instability due to peak loads and followed by crack arrest can be expected for crack lengths between $a = \bar{a}$ and $a = a^*$. For crack lengths smaller than $\bar{a}$ fracture instability will never occur when the stress level in the structure does not exceed $\overline{\sigma}$. Thus, the stiffened panel will be fail-safe when the design stress level is chosen equal to or lower than $\overline{\sigma}$. For a more detailed discussion of the prediction of residual strength of stiffened panels the reader is referred to Ref.18.

4.3 Prediction of crack propagation in stiffened panels

To predict the fatigue behaviour of a stiffened panel with a skin crack the behaviour of both sheet and stiffeners under alternating stresses has to be considered. The crack propagation characteristics of the cracked sheet can be determined as follows. In a stiffened panel the stress condition at the crack tip will be affected by the presence of the stiffeners. Their effect on the stress intensity is expressed by the correction factor C (see Eq.(6)). Assuming that the crack growth rate is governed by the value of the stress intensity range in a cycle, ΔK, the foregoing implies that the rate of crack propagation at a certain crack length in a stiffened panel can be predicted when the relation between da/dn and ΔK of the unstiffened panel and the dependency of C on crack length are available. Having computed in this way da/dn for the stiffened panel as a function of crack length, the crack propagation curve giving the relation between the number of cycles, n, and the crack length, a, can be obtained by an integration procedure from

$$n = \int_{a_o}^{a_1} \frac{da}{\frac{da}{dn}(a)} \tag{10}$$

in which a_o is the initial skin crack length (or minimum detectable crack length) and a_1 is the maximum skin crack length that is tolerated in the structure (see Sect.5.1). In the case of a panel with intact stiffeners the value of C decreases with increasing crack length. This implies a lower stress intensity factor and consequently a retarded crack propagation. Thus an increase in fatigue life of the stiffened sheet compared with that of an unstiffened sheet can be expected.

On the other hand, due to the load concentration in the stiffeners their fatigue lives will be reduced compared to that of stiffeners in an uncracked panel. A prediction of the fatigue life of the stiffener can be made as follows. The maximum load in the stiffener (F_{max}) at a certain crack length is given in section 4.2. With increasing crack length F_{max} will increase. Having available F_{max} as a function of crack length and the crack propagation curve of the stiffened sheet, the relation between F_{max} and n can be obtained. Using this load-cycle history in combination with a cumulative damage rule and a representative S-N curve, the fatigue life of the stiffener can be determined.

The foregoing implies that the fatigue life of a stiffened panel with a crack extending across the central stiffener will be determined by curves of the shape shown in Fig.8 by the solid lines. The upper curve represents the crack propagation curve of the stiffened sheet and the lower curve the cumulative damage in the central stiffener. Assuming that the maximum tolerable damage is a two-bay skin crack and that stiffener failure occurs when $\sum n/N$ equals unity, the fatigue life of the stiffened panel will be determined by n_1 or n_2, whichever is the lower.

4.4 Comparison of predictions with test results

4.4.1 Residual strength results

Following the procedure outlined in section 4.2 the residual strength was determined for a panel configuration with five riveted Z-stiffeners with a spacing of 58 mm. The stiffener area is approximately 50 per cent of the total gross area. The material of sheet and stiffeners is 7075-T6 Alclad. The panel contains a central saw cut passing midway between two rivets. This location of the crack was chosen to

achieve arrest of the unstably growing crack between rivet holes. In this way it could be demonstrated that for crack arrest it is not mandatory that the crack tips run into blunt-shaped rivet holes but that the support of the stiffener itself will be sufficient to stop unstable crack growth.

As shown in section 4.2, the residual strength properties of a stiffened panel configuration are determined by the shape and the relative positions of the stiffened sheet residual strength curve and the stiffener failure curve, which respectively present σ_{sheet} and $\sigma_{stiffener}$ as a function of crack length. These curves can be obtained by using equations (8) and (9). In applying these equations the residual strength properties of the unstiffened panel and the dependence of C and L on crack length are required. The required relation between σ_c and a_c of the unstiffened, 2 mm thick, 7075-T6 sheet was derived from residual strength tests. For intermediate crack sizes the relation appeared to be described by $K_c = 82$ MPa.m$^{1/2}$. For higher stress levels ($> {}^2/_3 \sigma_{yield}$) and for larger crack lengths ($> {}^W/_3$) the tangents proposed by Feddersen (Ref.16) were assumed to apply. In Ref.18 it was shown that in the case of a riveted panel C and L at a certain crack length can be readily calculated when the interacting rivet forces are known. The rivet forces can be computed analytically by separating the stiffened panel and the loads on it into its composite parts and generating the equations that govern the rivet point displacements due to the different load systems. Equating the displacements in corresponding rivet points of sheet and stiffeners will yield the unknown rivet forces. To generate and solve the set of displacement equations for a riveted panel and to compute from these data C and L as a function of crack length the computer programme ARREST was developed. To account for possible yielding of rivets and stiffeners the effect of yielding of these elements on the displacement equations was incorporated in the programme. Ref.19 gives a detailed description of ARREST and of its execution in determining the residual strength diagram of cracked stiffened panels.

Using ARREST the complete residual strength diagram was determined for the above mentioned panel configuration. The results of both elastic and elastic-plastic computations are shown in Fig.9. Also shown in this figure are experimental data from residual strength tests on panels of the same configuration. The curves shown in Fig.9a are based on elastic computations and show a pronounced increase of the stiffened sheet curve when the crack tip approaches the rivet line of stiffener 1. Further, according to the central stiffener failure curve shown in Fig.9a, failure of this stiffener would occur prior to any crack growth in the sheet. This is not in agreement with the experimental results that show stable crack growth, fracture instability and crack arrest without failure of the central stiffener. The results of Fig.9a show that prediction of the residual strength properties of this panel configuration based on purely elastic computations of C and L is not possible. Apparently, due to the high load concentration in the central stiffener, yielding of rivets and stiffeners will occur at relatively low external loads. Taking into account yielding of rivets and stiffeners the curves of Fig.9b were obtained. Comparing the curves of Fig.9b with that of Fig.9a, there is a very large difference in the positions of the central stiffener failure curves, while the stiffened sheet curve of Fig.9b shows a much less pronounced increase for half crack lengths in the order of the stiffener pitch. As explained earlier in section 4.2, for the relative positions of the stiffened panel curves shown in Fig.9b, the predicted fail-safe level, $\bar{\sigma}$, is determined by the top of the stiffened sheet curve and amounts to 290 MN/m^2. Comparing the computed results of Fig.9b with the experimental data it can be concluded that there is a fairly good agreement: the instability points obtained from tests are slightly lower than predicted by the σ_{sheet}-a_c curve, while the panels that showed crack arrest failed at a stress level at least equal to the predicted $\bar{\sigma}$ level.

4.4.2 Crack propagation results

Following the procedure outlined in section 4.3 the crack propagation under constant amplitude cycling was determined for a panel configuration with five strip stiffeners at a spacing of 58 mm and a skin crack initiating from a rivet hole under the central stiffener. The strip stiffeners were attached to both sides of the sheet to avoid eccentricities. The total stiffener area was approximately 50 per cent of the total gross area. The material of sheet and stiffeners was 7075-T6.

Crack propagation in the sheet was calculated for both an intact and a broken central stiffener and for a crack passing between and through rivet holes of the adjacent stiffeners. Fig.10 presents an example of the computation procedure for the panel configuration with five intact stiffeners and the crack passing through rivet holes. It has to be remarked here that in this case the crack tips, after having reached the rivet holes of stiffeners 1, will be arrested there for a certain number of cycles. Owing to the uncertainty about the number of cycles before cracks reinitiate from the rivet holes, the arrest time was ignored in the computations.

The results of the computations are shown in Fig.11. Also shown in this figure are experimental data from crack propagation tests on panels of the same configuration. Crack growth values are plotted separately for each crack tip except for those cases where the difference in half crack length for both crack tips amounted to less than 5 mm. In those cases the average for both crack tips is plotted. No crack growth recording could be obtained when the crack tips propagated under the stiffeners. Therefore the dashed curves in this region are only estimates. The tests were discontinued when one of the stiffeners failed. To account for the above mentioned arrest in the rivet holes the predicted curve in the left part of Fig.11 was adjusted by partly shifting it upwards. The amount of shifting was adapted to the test results.

Comparing the computed results of Fig.11 with the experimental data, the agreement appears to be rather poor, particularly for half crack lengths larger than the stiffener spacing. Also shown in Fig.11 is the number of kcycles at which crack initiation and total failure of a stiffener occurred. In Ref.18 the $\sum n/N$ values of the stiffeners at stiffener failure were computed to be equal to 0.9 (for stiffener 0) and 0.4 (for stiffener 1) for panels with an intact and a broken central stiffener, respectively. The low $\sum n/N$ value in the latter case is expected because of the higher load concentration in the intact stiffeners (see Ref.18).

5. GUIDELINES FOR AIRCRAFT STRUCTURAL APPLICATIONS

5.1 Factors affecting effectiveness of a fail-safe design

The various aspects of the fail-safe problem are illustrated qualitatively in Fig.12 for a stiffened panel configuration with a stiffener spacing, s. In the first instance the means of attachment of sheet and stiffeners is immaterial. The upper and the lower diagram present the crack propagation properties

(crack length as a function of number of cycles or flight hours) and the residual strength properties (stresses at fracture instability in the sheet and at failure of the stiffener as a function of crack length). The dashed curves and the solid curves in these diagrams apply respectively to the unstiffened and the stiffened panel.

Suppose that after a certain period in service a skin crack initiates from a rivet hole under the central stiffener (indicated by n_i in the upper diagram). Assuming, in the first instance, that during the life of the structure no unstable crack growth due to peak loads will occur, then propagation of this crack with the number of cycles, n, is given by the solid curve in the upper diagram. Initially this crack will be too small to be detected during inspection. After some time it has grown to a size that allows detection ($a = a_{md}$ is minimum detectable half crack length). This crack length is attained after n_A cycles according to the upper diagram. To restrict the number of cycles between initiation and detection of a crack, an easily inspectible structure together with a reliable inspection technique applied by experienced inspectors are of paramount importance. Further, because the minimum detectable crack length still can be missed in a certain inspection, good crack propagation properties are important to limit the increase in crack length during the number of cycles to the following inspection.

Besides crack propagation and inspection requirements, the fail-safe concept demands sufficient residual strength at a certain specified maximum tolerable damage. This damage depends on the tolerable damage level that on the base of airworthiness requirements was chosen by the designer. In the case of built-up sheet structures different prescribed maximum damage levels deserve consideration, e.g.:

(i) a one-bay skin crack

(ii) a two-bay skin crack with the central member intact

(iii) a two-bay skin crack with the central member failed.

For ease of explanation the damage level mentioned under (ii) is assumed to apply here. In that case, for the relative position of sheet and stiffener curves sketched in the lower diagram of Fig.12, the fail-safe stress, $\bar{\sigma}$, and the corresponding maximum tolerable crack length, $2a_{mt}$, will be determined by the top of the stiffened sheet curve (see section 4.2). In the crack propagation diagram this crack length is attained after n_B cycles. The foregoing implies that the period that is available for crack detection during regular inspections is equal to $(n_B - n_A)$ cycles, provided no unstable crack growth occurs in this period. To obtain a long inspection interval the crack propagation properties of the sheet and the interaction of sheet and stiffeners are of primary importance. Good sheet-stiffener interaction properties, however, imply that much load is transferred from the cracked sheet to the stiffeners, so that sufficient fatigue life of the stiffeners is an additional requirement to prevent stiffener failure before n_B cycles have been reached.

So far the possibility of unstable crack growth due to peak loads was ignored. Occurrence of unstable crack growth will yield an additional complication to determining the available inspection time. The fail-safe stress level for the assumed maximum tolerable two-bay skin crack is represented in the residual strength diagram of Fig.12 by $\bar{\sigma}$. If at any stress level below $\bar{\sigma}$ fracture instability of a skin crack extending across the central stiffener occurs, then the unstably growing crack will be arrested at the adjacent stiffeners (see crack growth history of crack length a_i due to peak stress, σ_{peak}, in lower diagram of Fig.12). After crack arrest (and a possible delay in crack growth due to the peak load) the crack will propagate further by fatigue. In this case a_{mt} will be attained after n_C cycles (see upper diagram of Fig.12). Thus, owing to unstable crack growth the available inspection time will be reduced by $(n_B - n_C)$ cycles. Further, the fatigue life of the stiffeners will be reduced because they have to carry a greater load during a larger part of their life.

The problem now arises how allowance can be made for the possibility of unstable crack growth when determining the effective available inspection time. In principle fracture instability may occur at any crack length corresponding with the stress range between $\bar{\sigma}$ and σ^*, see Fig.12, although the chance of instability will of course increase with increasing crack length. The most safe approach would be to prevent fracture instability either by selecting the fail-safe stress equal to σ^* instead of $\bar{\sigma}$, or by basing the upper bound of the available inspection time on $\bar{a}$, being the smallest crack length at which unstable crack growth due to a peak load can occur, assuming that the fail-safe stress level is set at $\bar{\sigma}$. Another approach is to accept the possibility of instability, but to limit its occurrence by demanding that the σ^* level exceeds a certain percentage of the fail-safe stress $\bar{\sigma}$. Whatever approach is chosen, it will be clear from Fig.12 that at a certain required fail-safe stress level good fracture toughness properties of the skin material and good skin-stiffener interaction are important. The latter property makes demands on the stiffener fatigue properties, as explained before.

Finally it has to be remarked here that for the sake of simplicity the crack propagation curve sketched in Fig.12 assumes constant amplitude loading. In practice crack propagation in the sheet will have to be based on the pertinent load spectrum of the aircraft. Some of the specific problems that will then be encountered were discussed in Ref.15. Further, the effect of possible premature fatigue failure of a stiffener on the crack propagation and residual strength curves in Fig.12 was not considered. Figs.11 and 14 show that due to stiffener failure both the crack propagation resistance and the residual strength properties deteriorate drastically.

5.2 Improvement of fail-safe properties

A structure cannot be designed fail-safe without planning regular inspections. Therefore establishment of the inspection interval is an essential part of the fail-safe analysis. In the previous section it was shown how on the basis of the crack propagation and residual strength characteristics of the stiffened panel configuration a safe inspection interval could be predicted. Inspections are costly and time consuming. Therefore, already in the design stage one should strive for a structure that requires a minimum of inspection time and costs. In this respect the designer has to be aware of the different ways in which he can contribute. In this section different possibilities to lengthen the inspection interval and that are at the designer's disposal will be discussed. It is assumed here that the designer to the best of his ability has designed against crack initiation but that due to factors beyond his control cracks nevertheless will be present or arise in the structure (see section 2.1).

It was shown in section 5.1 that the time available for inspection, viz. $(n_B - n_A)$, at its lower bound is determined by the time that elapses between initiation and detection of the crack. Fig.12 shows that a small reduction of the minimum detectable crack length will yield a large gain in available inspection time owing to the low crack propagation rate in this range of crack lengths. This fact pleads for improved inspection techniques and experienced inspectors, but these factors are beyond the designer's scope. However,

the designer can facilitate crack detection by providing an easily inspectable structure and by indicating locations where cracks should be looked for.

Considering the crack propagation curve of the unstiffened panel in Fig.12 it can be concluded that an improvement of the crack propagation properties of the sheet material will very effectively enlarge the available inspection time. This particularly applies to the region of small crack lengths where the crack growth rate is small. Further, the available inspection time of the stiffened panel appears to increase considerably as compared to an unstiffened panel because the crack growth rate is reduced by the presence of stiffeners. The sheet-stiffener interaction is dependent on the stiffness of the attachment and in this respect it can be expected that a bonded stiffener will be more effective than a riveted stiffener. This seems to be confirmed by the test results shown in Fig.13 applying to a panel with 5 strip stiffeners (central stiffener broken) and a central crack. However, it has to be remarked here that the crack tips in the riveted panel passed between the rivets of the adjacent stiffeners. In the case where the crack tips would have run into rivet holes a considerable delay in crack growth would have occurred (see for example Fig.11, applying to a panel with 5 intact stiffeners).

It was shown in section 5.1 that unstable crack growth will reduce the available inspection time. In this respect a high value of the fracture toughness of the unstiffened sheet material will be important to reduce the chance of instability in the stiffened panel when a certain fail-safe stress level is prescribed. Further, the sheet-stiffener interaction may be important, because a good sheet-stiffener interaction may increase the ratio $\sigma^*/\bar{\sigma}$ and thus reduce the chance of instability. Whether the $\sigma^*/\bar{\sigma}$-ratio is reduced will depend on the stiffener spacing. The effect of sheet-stiffener interaction on the residual strength properties is shown in the left part of Fig.14, giving test results of bonded and riveted panel configurations with 5 strip stiffeners (central stiffener broken) and two different initial crack lengths. The bonded panels show a slightly higher residual strength. Because the high local load transfer from the sheet to the stiffeners in a bonded panel may lead to failure of the adhesive layer, two additional panels were tested with partly loose adhesive layer (each stiffener had a loose adhesive layer over a distance of 10 mm at either side of the crack line). As shown in Fig.14 the loose adhesive layer reduces the residual strength by approximately 11 %. The most striking difference between the bonded and the riveted specimens was that the bonded specimens did not show unstable crack growth.

It was shown in the foregoing that the crack propagation properties and the fracture toughness of the skin material are important parameters when considering the fail-safe properties of a stiffened panel configuration. Both properties increase with decreasing sheet thickness (Refs.17 and 20). This result has important consequences for choice of panel concepts. In particular, the fail-safe properties of the skin will be improved if laminated panels or honeycomb sandwich are employed, especially for part-through cracks in laminates and for sandwich panels with only one face sheet cracked (Ref.21).

6. CONCLUSIONS

This paper concisely reviews design analyses for demonstrating airworthiness of a fail-safe aircraft structure, i.e. static strength, crack initiation, crack propagation and residual strength analyses. The crack propagation and residual strength analyses are discussed in more detail, especially with respect to application of fracture mechanics principles and sheet structures. Theoretical results of NLR work in this field and their experimental verification are given. Further, the paper discusses the factors that influence the effectiveness of a fail-safe design and the ways in which fail-safe properties can be improved.

From the theoretical considerations and tests the following conclusions are drawn:

(i) Fail-safe aircraft structures require a long crack-free life and the guarantee that the aircraft safety is not jeopardised if, despite all precautions, cracks arise. A long crack-free life can be achieved by demanding good quality control, good detail design, and materials with excellent fatigue properties. Safety of the damaged structure can be guaranteed by striving for early crack detection during regular inspections (i.e. a good inspection technique with experienced inspectors and an accessible, easily inspectable structure), by providing good crack propagation resistance (material selection and arrangement of structural elements), and by ensuring that the structure has sufficient residual strength (good fracture toughness of the skin material, good skin-stiffener interaction, and crack stopper elements to arrest fracture instability).

(ii) Fracture mechanics satisfactorily predicts the residual strength of sheet structures, but is less successful for crack propagation. A major difficulty is that crack propagation resistance drastically deteriorates when stiffener failure by fatigue occurs, and the instant of stiffener failure cannot yet be reliably predicted. Since prediction of crack propagation is already unreliable for constant amplitude loading, a satisfactory estimate of the crack propagation life under flight loading is well beyond the state of the art.

(iii) Comparing the crack propagation characteristics of bonded and riveted panels, bonded panels are much superior when the crack path in riveted panels runs between rivets. When cracks propagate into rivet holes the riveted panels exhibit considerable additional delay in crack growth and then riveted panels seem slightly better. However, because the crack path is beyond control, bonding should be preferred.

(iv) Comparing the residual strengths of bonded and riveted panels, there appears to be negligible difference in failure stress. However, riveted panels exhibit unstable crack growth, which may considerably reduce the available inspection time, especially when the crack is arrested between rivet holes and then immediately begins further extension by fatigue. Thus, bonding again seems preferable to riveting.

(v) For the range of sheet gauges customarily used the crack propagation resistance and fracture toughness generally increase with decreasing thickness. Thus, the fail-safe properties of sheet structures will usually be improved if laminated skins or honeycomb sandwich are employed. These concepts have the additional advantage of load shedding to intact structure for part-through cracks in laminates and for sandwiches with only one face sheet cracked.

7. REFERENCES

1 Military Specification Airplane Damage Tolerance Requirements, MIL-A-83444 (USAF), 1974.

2 W.G. Walker and M.R. Copp, Summary of VGH and V-G data obtained from piston-engine transport airplanes from 1947 to 1958, NASA TN D-29, 1959.

3 Staff of Langley Airworthiness Branch, Operational experiences of turbo-powered commercial transport airplanes, NASA TN D-1392, 1962.

4 P. Donely, J.W. Jewel and P.A. Hunter, An assessment of repeated loads on general aviation and transport aircraft, Presented at the 5th ICAF symposium, Melbourne, Australia, May 1967.

5 T.L. Coleman, Trends in repeated loads on transport airplanes, Fatigue design procedures, Ed. by E. Gassner and W. Schütz, Pergamon Press, New York, 1969, pp.161-190. Also NASA TN D-4586, 1968.

6 T.L. Coleman and P.A. Hunter, Fatigue loadings on commercial transport airplanes, Airforce Conference on Fracture and Fatigue (1969), AFFDL TR-70-144 (1970), pp.123-140.

7 Military Specification Airplane Strength and Rigidity-Reliability requirements, Repeated Loads and Fatigue, MIL-A-8866 (USAF), 1960.

8 Military Specification Airplane Strength and Rigidity-Flight loads, MIL-A-8861, 1960.

9 J. Schijve, The accumulation of fatigue damage in aircraft materials and structures, Agardograph No. 157, January 1972.

10 H.F. Hardrath, Fatigue and fracture mechanics, Journal of Aircraft, Vol.8, No.3, March 1971, pp 129-142.

11 D. Broek and J. Schijve, The influence of the mean stress on the propagation of fatigue cracks in aluminium alloy sheets, NLR TR M-2111, 1963.

12 J.C. McMillan and R.M.N. Pelloux, Fatigue crack propagation under program and random loads, Fatigue crack propagation, ASTM STP 415, 1967, p.505.

13 F. Erdogan, Crack propagation theories, NASA CR-901, 1967.

14 E.K. Walker, Effects of environments and complex load history on fatigue life, ASTM STP 462, 1970, pp 1-14.

15 Various authors, Fracture Mechanics of Aircraft Structures, Ed. by H. Liebowitz, Agardograph No.176, 1973, pp 149-180.

16 C.E. Feddersen, Evaluation and prediction of the residual strength of center cracked tension panels, ASTM STP 486, 1971, pp 50-78.

17 D. Broek and H. Vlieger, The thickness effect in plane stress fracture toughness, NLR TR 74032, 1974.

18 H. Vlieger, Fail-safe characteristics of built-up sheet structures, Paper presented to the 9th ICAS symposium, Haifa, Israel, August 1974.

19 H. Vlieger and A. Sanderse, User's manual of ARREST, a computer routine for prediction of residual strength of cracked stiffened panels, NLR TR 75129, 1975.

20 D. Broek, The effect of sheet thickness on the fatigue crack propagation in 2024-T3 sheet, NLR TR M-2129, 1963.

21 R.J.H. Wanhill and G.F.J.A. van Gestel, Aluminium alloy development and evaluation for aircraft structural performance, International Meeting on Aluminium Alloys in the Aircraft Industries, Turin, October 1976.

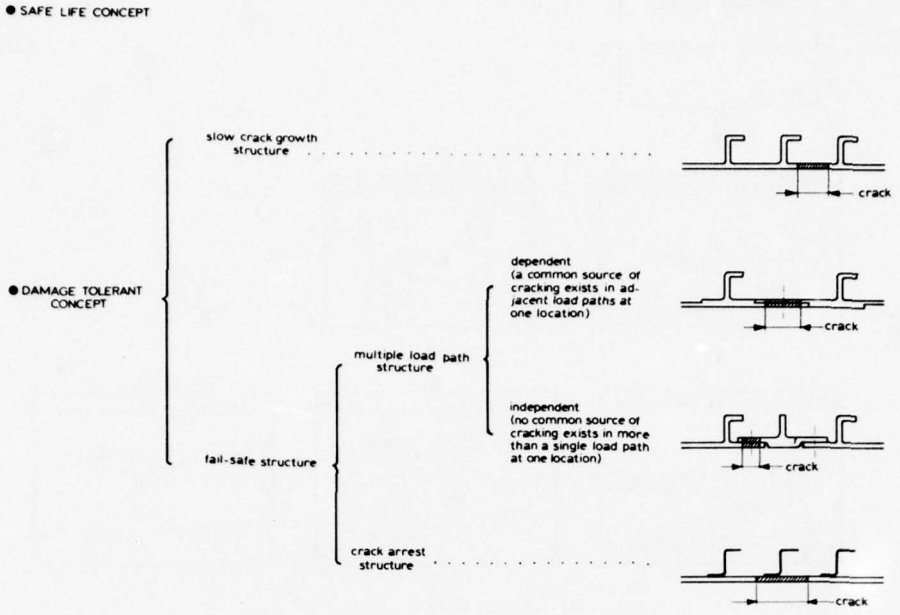

Figure 1 Survey of structural design approaches with regard to tolerance of damage

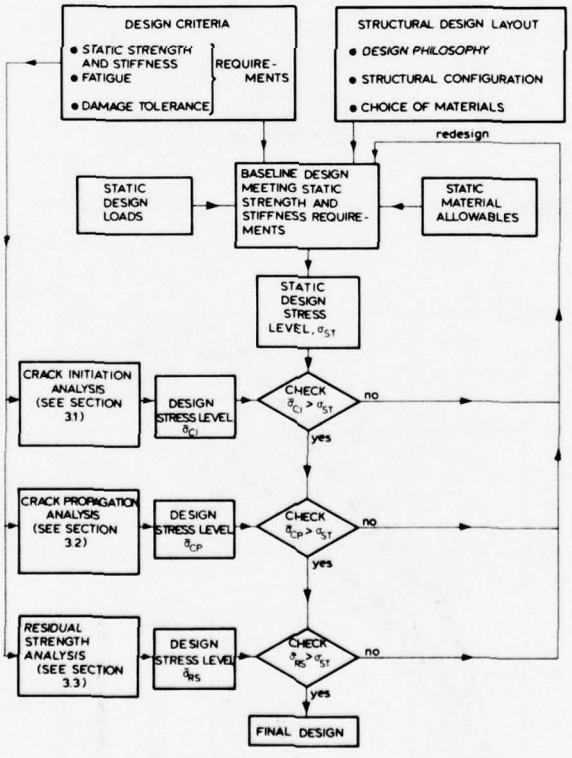

Figure 2 Flow diagram of design process of damage tolerant structure

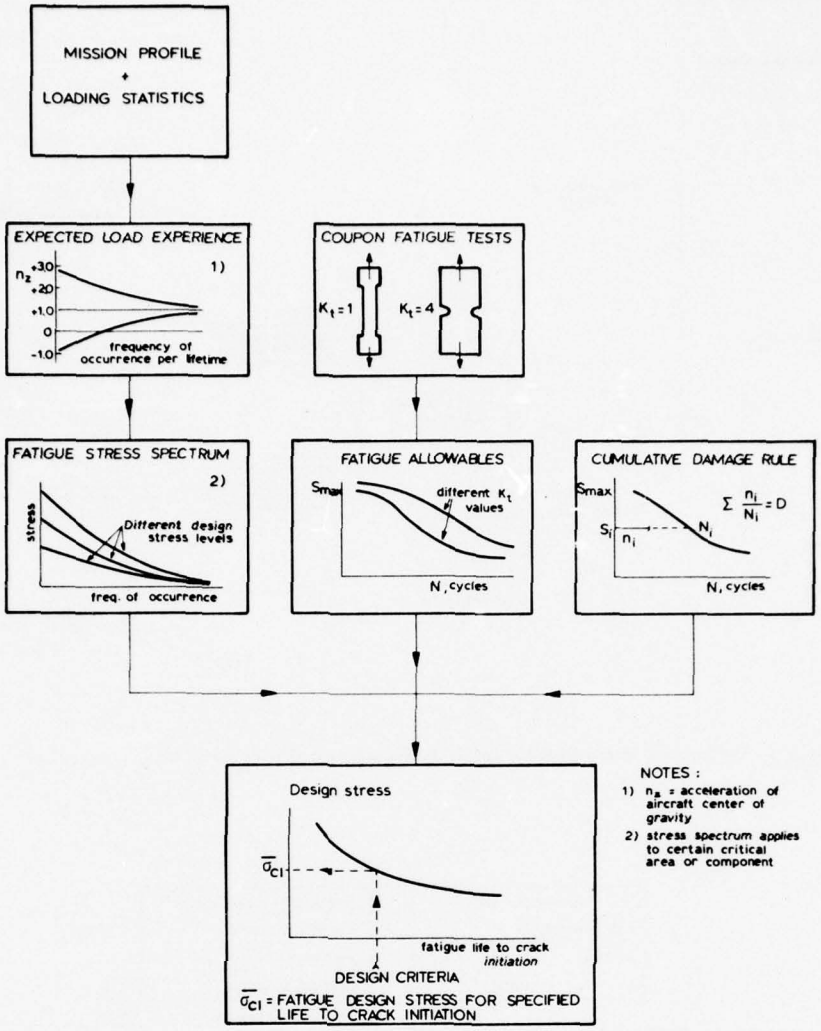

Figure 3 Flow diagram of crack initiation analysis

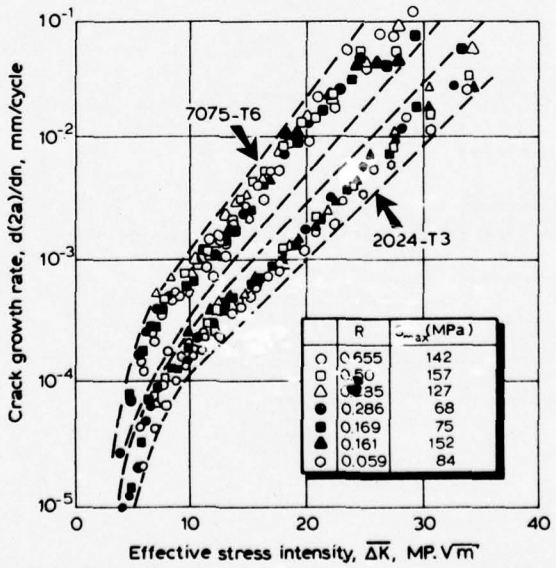

Figure 4 Crack growth rate as a function of effective stress intensity (from Ref.14)

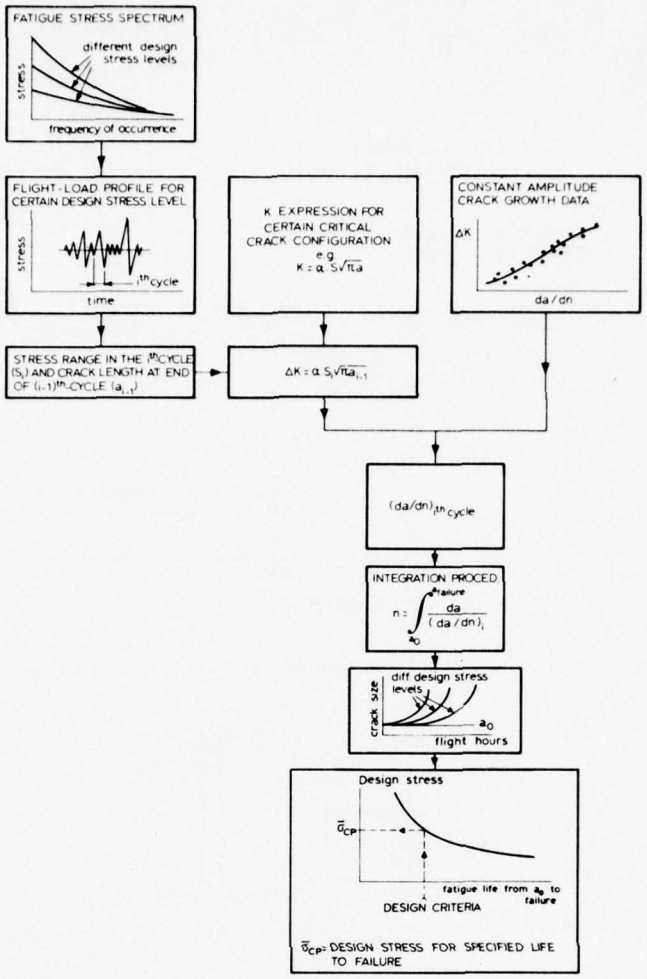

Figure 5 Flow diagram of crack propagation analysis

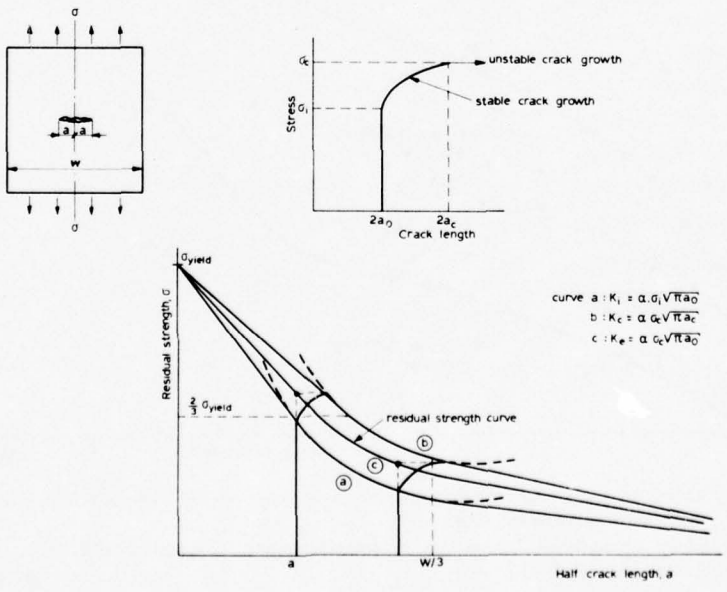

Figure 6 Residual strength diagram of unstiffened panel (schematic)

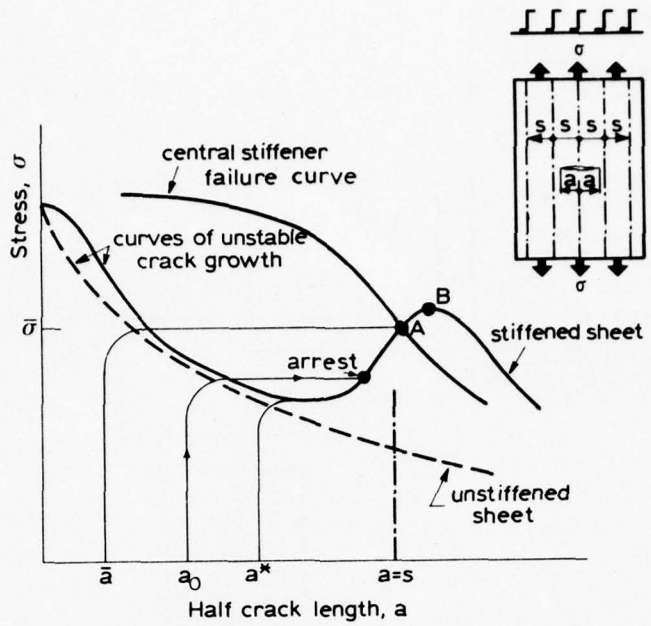

Figure 7 Residual strength diagram of stiffened panel (schematic)

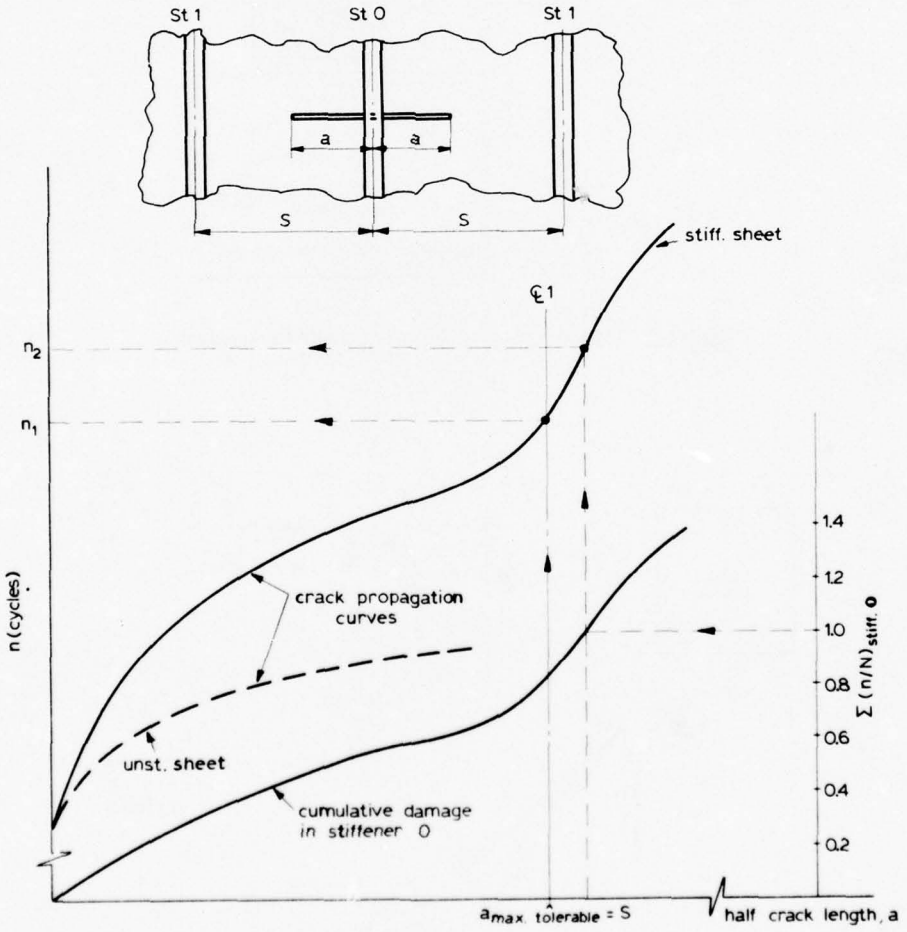

n_1 = based on max. tolerable crack length (assumed as two-bay skin crack with central stiffener intact)

n_2 = based on stiffener failure due to fatigue cycling (assumed here to occur at $\Sigma n/N = 1$)

Figure 8 Prediction of fatigue life of stiffened panel (schematic)

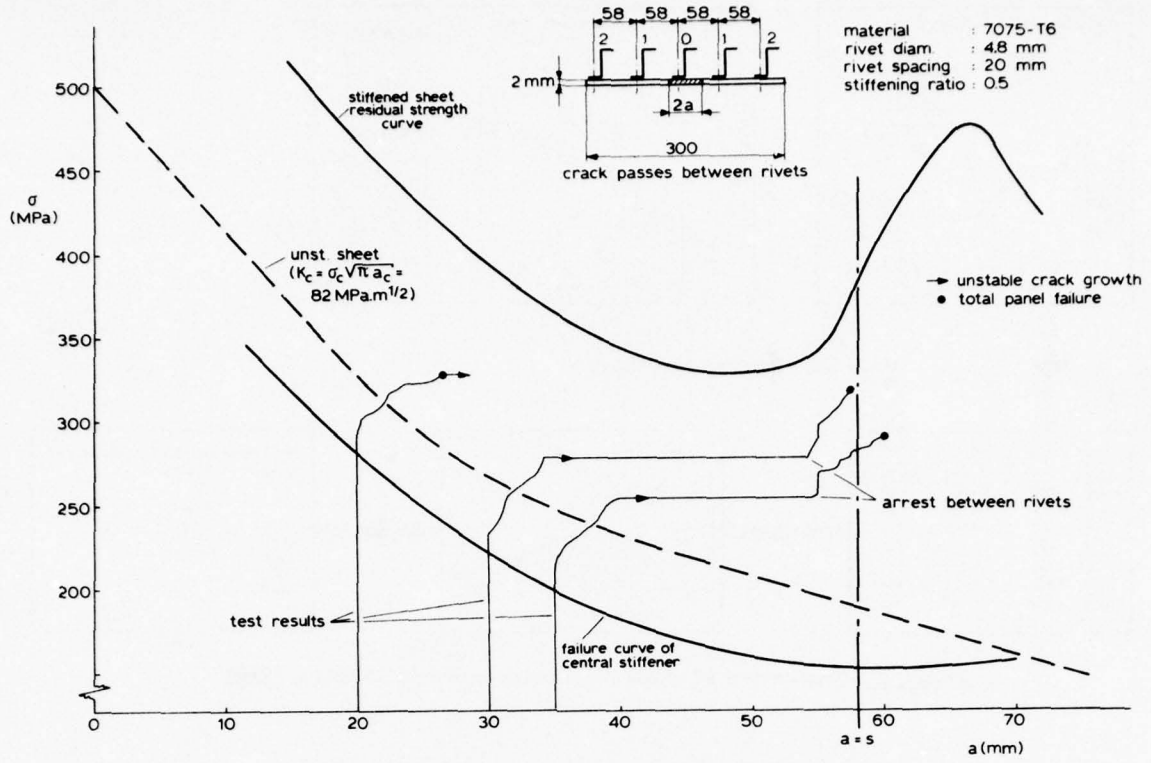

a. Results of elastic computations

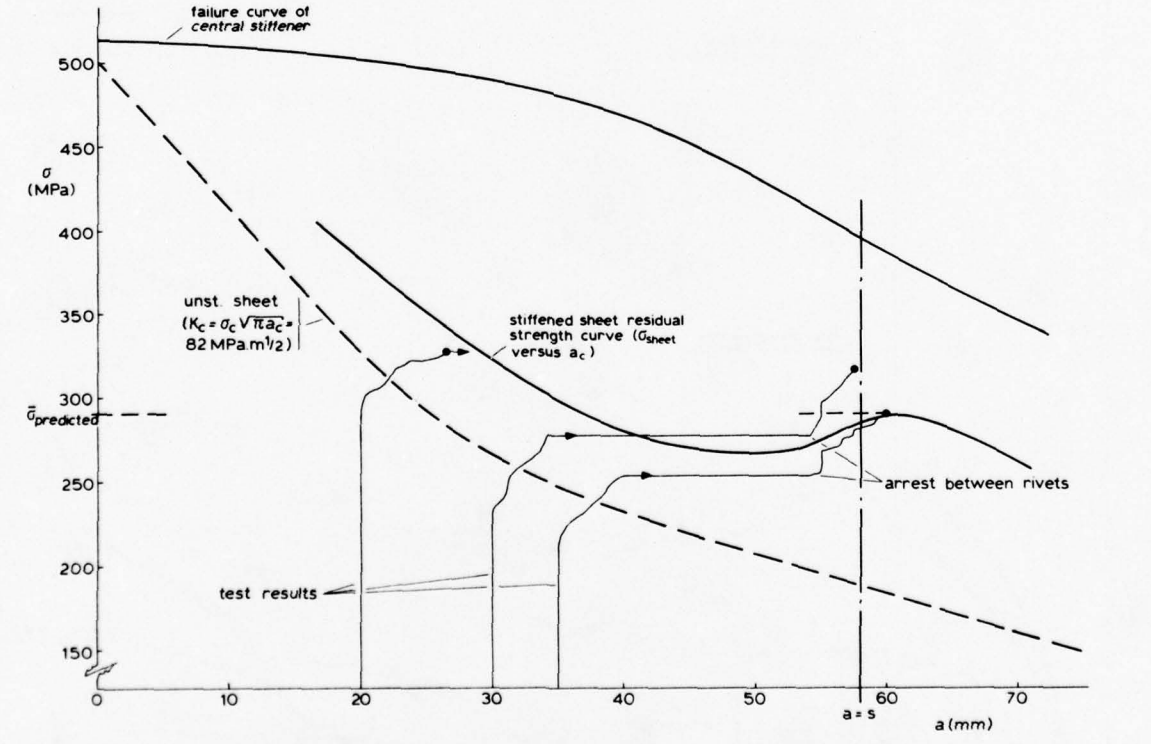

b. Results of elastic-plastic computations

Figure 9 Comparison of calculated residual strength properties of stiffened panel with test results

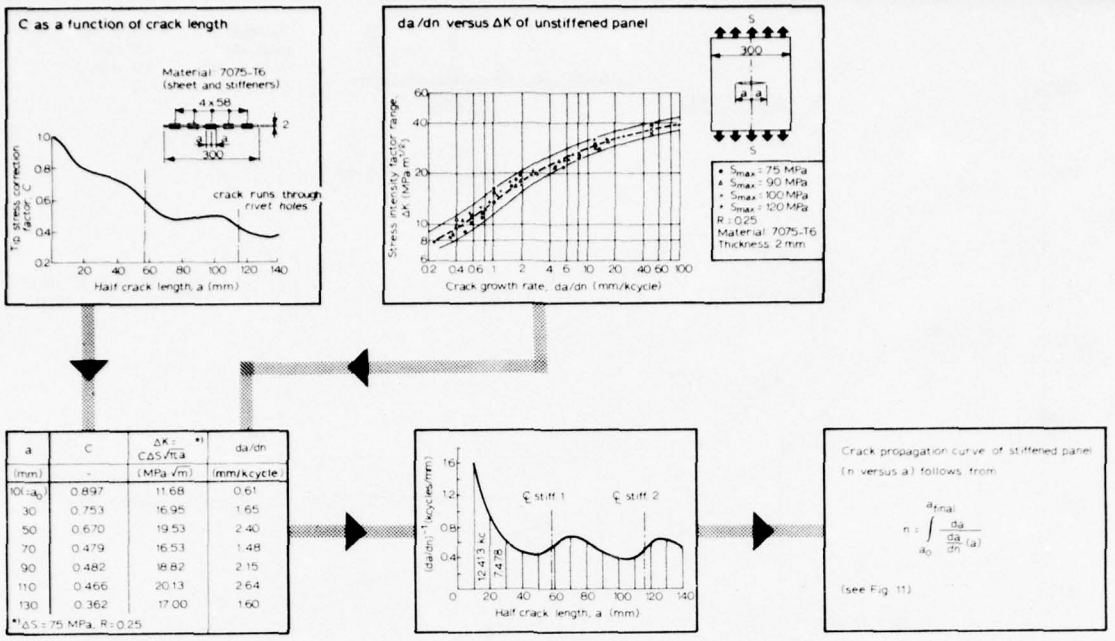

Figure 10 Computation of crack propagation curve of stiffened panel

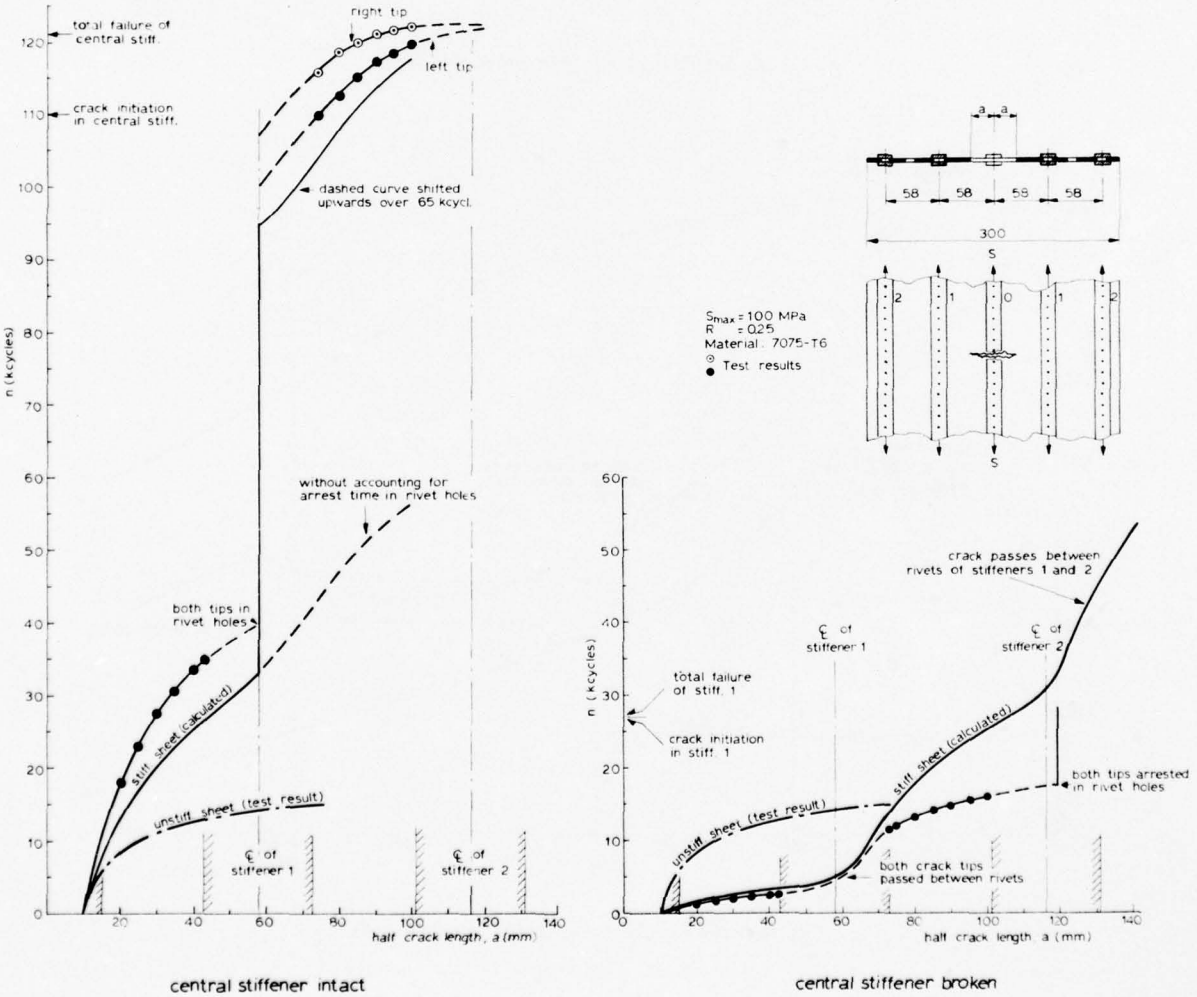

Figure 11 Comparison of calculated crack propagation curves of stiffened panels with test results

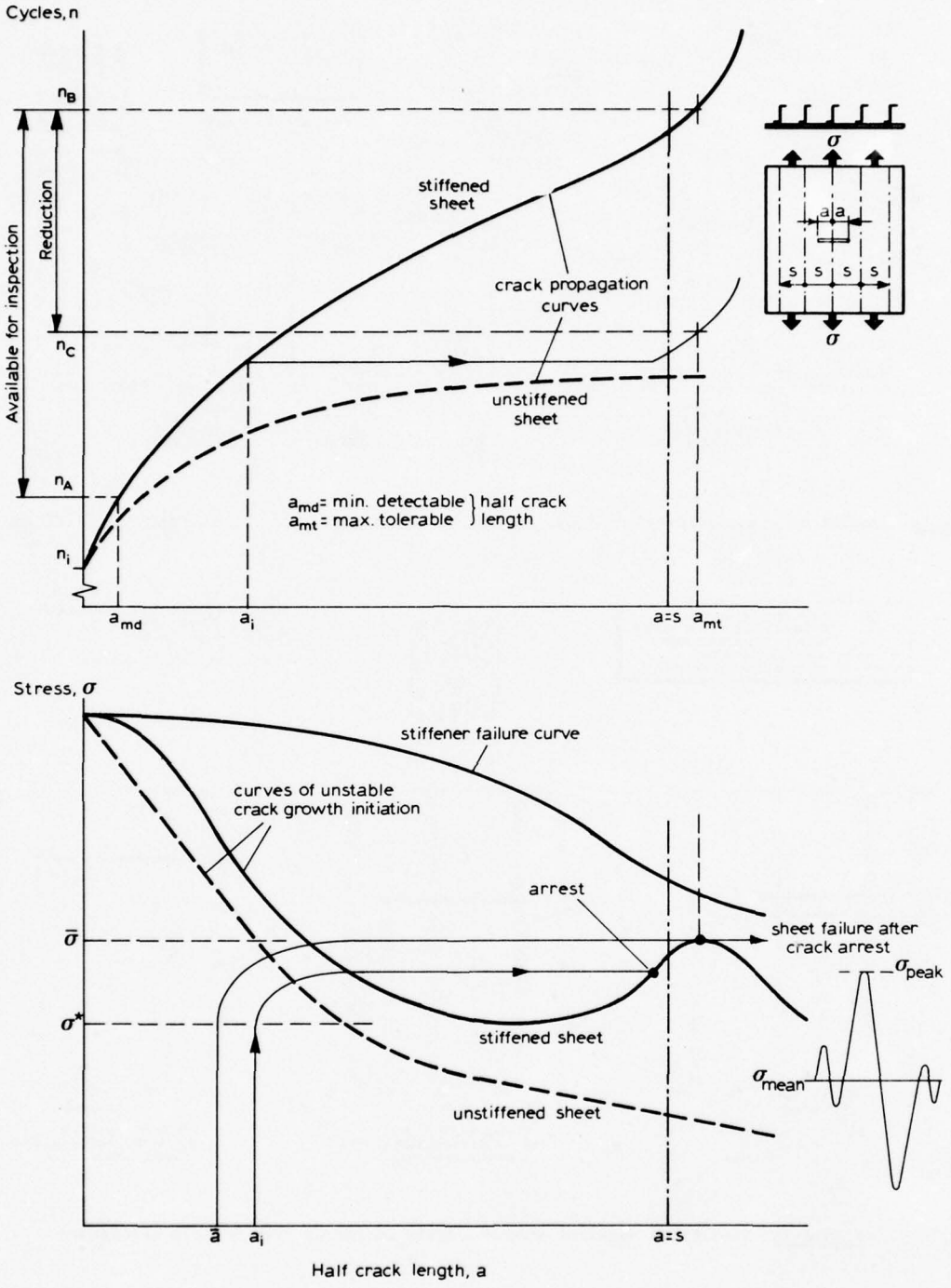

Figure 12 Various aspects of fail-safe problem

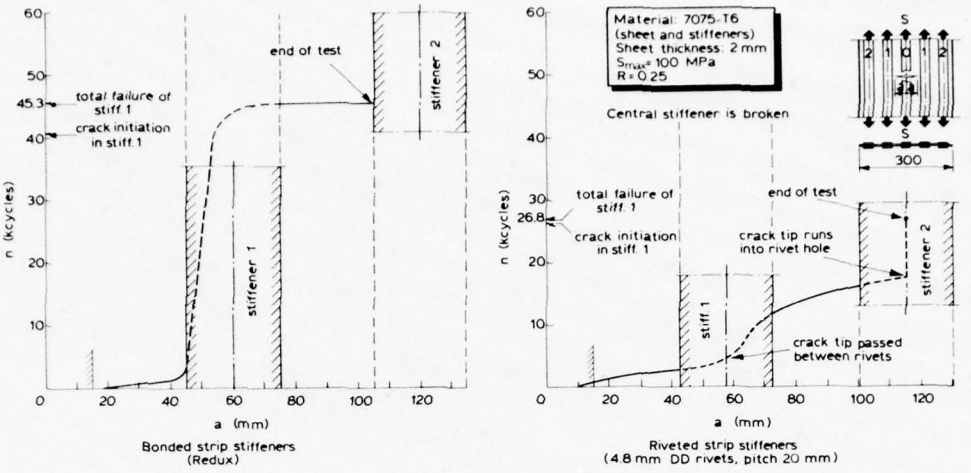

Figure 13 Results of crack propagation tests on panels with 5 strip stiffeners (central stiffener is broken)

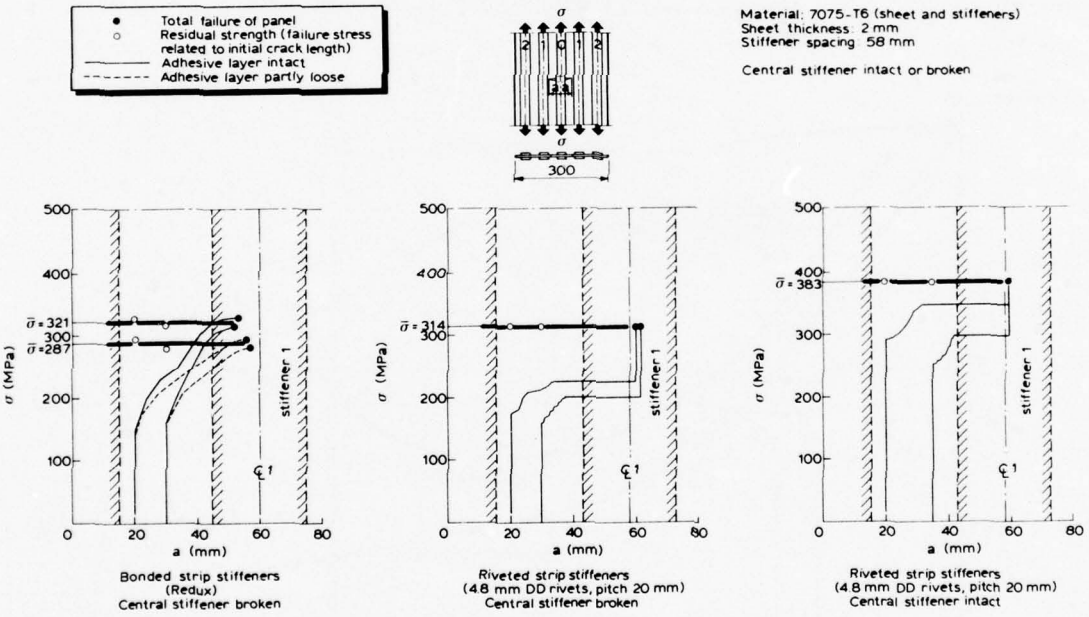

Figure 14 Results of residual strength tests on panels with 5 strip stiffeners

CONTRIBUTED DISCUSSION

by

N.F.Harpur
British Aircraft Corporation Limited,
Commercial Aircraft Division,
Filton House, Bristol BS99 7AR.
England.

In his paper the author sets out a well reasoned methodology which will serve to focus the attention of the structural designer on the role fracture mechanics principles should play in any future programme.

He begins by describing the many flaws which must be considered, be they the result of manufacture or in service use. While recognizing that manufacturing defects are potential sources of subsequent in-service fatigue damage and should be kept to a minimum by adequate inspection, I feel that a design whose integrity relies on the detection of these small defects must be very critical. I would rather see fail safety based on the larger sized damage resulting from in-service use and which are capable of being detected by normal inservice inspection.

With reference to the various approaches open to the designer I would point out that the terminology used in figure 1 does not accord with that used on civil aeroplanes. The terms "Damage Tolerant" and "Fail Safe" are, in my view, synonymous and the "slow crack growth structure" is just one solution to the fail safe problem.

The author rightly points out that the designer must provide an inspectable structure. It cannot be emphasised too often that a structure can only be deemed fail safe if damage can be detected before it reaches critical proportions.

Following examination of the design process flow diagram Fig.2 I would suggest that the flow lines be rearranged to up grade the analyses on crack initiation, crack propagation and the residual strength to have the same status as those for static strength and stiffness. This is to ensure that the results of these analyses have a more direct bearing on optimisation of the structural configuration and choice of materials.

The author briefly summarises the means of evaluating fatigue life, crack propagation rate and residual strength of structure. Although clarity is served by the simplicity of the description, certain points need to be made. For example that the fracture toughness increases with decreasing thickness is not disputed, however data (reference 1) given below show that, for certain alloys, the toughness may reach a maximum and then decrease again.

Material : Ti 6Al 4V

t in.	K_c (or K_{Ic}) Ksi $\sqrt{in}$
0.025	160
0.050	190
0.25	260
1.0	100

Further, Kc represents an upper limit to the fracture toughness at any given thickness. Indiscriminate use of Kc in for example equation 8 by inexperienced users may lead to optimistic estimates of residual strength. This problem may be avoided using the R - curve approach (reference 2).

I was pleased to see an awareness of the problems concerning the fatigue life of crack stoppers in the vicinity of a growing crack. I feel that greater attention should be paid to this hitherto neglected problem.

I also noted the discrepancy between test and theoretical crack propagation rates but, with knowledge of the data presented in reference 3, wonder how much of the difference can be attributed to scatter.

Although I appreciate the cautionary note concerning the application of peak loads during cycling and the consequent effect on evaluation of inspection intervals, certain mitigating circumstances should be mentioned. The major portion of the inspection period is obtained during the propagation at short cracks where, it is felt that intermittent peak loads will be insufficiently large to cause unstable crack growth. In other words, figure 12 tends to give a pessimistic view since the proportion of life between n_A and n_C will be larger than shown.

Although I do not dispute that bonding offers some advantages in fail safe design over rivetting I would like to see some further thought given to the optimum choice of adhesive in curved pressure shell applications where the peel strength becomes a more important parameter. On the question of unstable crack growth only occurring in rivetted panel configurations, my view is that this may be a function of test specimen configuration. Has the author achieved similar results on panels of greater stiffener pitch or on panels with stiffeners attached by more than a single row of rivets ?

Finally, I am sure there are some who would dispute that "crack propagation life under flight loading is well beyond the state of the art". Many have in the past made like statements concerning the analysis of fatigue life although the Palmgren-Miner law continues to be used. Similarly a cumulative damage sum applied to crack propagation frequently has to be used by the designer since the analysis of crack propagation rates in the service environment is one of the corner stones of the fail safe approach. It is therefore important that suitable analytic/empirical treatments are made available as soon as possible.

References.

1. Anon, "Damage Tolerant Design Handbook", Materials and Ceramics Information Center, Battelle Columbus Laboratories, Columbus, Ohio
2. Creager M. "A Note on the Use of a Simple Technique for Failure Prediction Using R-Curves". Fracture Toughness Evaluation by R-curve Methods, ASTM STP527, American Society for Testing and Materials 1973
3. Kirkby W.T. "Practical Applications of Fracture Mechanics Techniques to Aircraft Structural Problems". Paper presented at this specialist meeting.

CONTRIBUTED DISCUSSION

by

David Broek,
Battelle's Columbus Laboratories,
USA

This concise summary of damage tolerance design methodology of built-up sheet structures clearly demonstrates Mr. Vlieger's expertise in the field. Despite its limited length, the paper considers all major aspects of the methodology in general terms. Mr. Vlieger's expertise would have justified a more extensive paper in which some of the problems could have been dealt with in somewhat greater detail.

The discussion of crack initiation analysis mentions the linear accumulation of damage as being the most commonly used. It states that one of the major problems in its application is in the fact that $\Sigma n/N$ values are often substantially different from unity. It seems worth noting that recently developed methods based on a local stress-strain approach do tend to produce somewhat more accurate predictions. However, a primary cause of inaccuracies in life prediction is the inadequacy of the assumed load spectrum. Once in-flight load or strain measurements become available somewhat more reliable computations can be made for fleet monitoring purposes.

The discussion of fracture mechanics analysis of built-up structures emphasizes the analytical approach. It has been well-established now that the analytical procedure has a great versatility for parametric studies in the design stage. Its capacity to deal with stringer eccentricities is somewhat limited. This may be a restriction in the case of heavy stringer combinations.

The test data on fatigue crack propagation in stiffened panels are particularly interesting. Crack growth in the experiments turned out to be slower than predicted. The K-analysis used for this case did not include plasticity effects (fastener hole deformation). Apparently, the relatively low fatigue loads do permit an elastic analysis, because it is expected that even faster fatigue crack growth rates would have been predicted if fastener hole deformation would have been accounted for. This point would be worth further exploration.

The experiments showed considerable reinitiation times if the cracks ran into fastener holes at the stringers. It is questionable whether such long delay times can be expected in general. The stiffener spacing in the test panels was small (2.5 inches or 60 mm). This means that a two-bay crack is still a relatively small crack. In aircraft structures presently in use, stringer spacings may be as large as 7-inches (175 mm). In that case a two-bay crack will be much less affected by running into a fastener hole. Then it seems to be a safe approach to ignore a reinitiation period. Also the conclusion that bonded structures are more beneficial may have to be reconsidered for such cases. The extremely long two bay crack will carry a larger plastic zone where debonding is likely to occur, thus reducing the effectivity of the load transfer. This justifies an evaluation of the effect stiffening ratio and stringer spacing along the lines so successfully pursued by Mr. Vlieger.

The paper concludes that the prediction of crack growth under service loading is well beyond the state of the art. Reference is made to a review of prediction procedures by the discussant. Since the publication of that review, extensive new work has shown that crack growth under flight simulation loading can be predicted with reasonable accuracy. Unfortunately, here again discrepancies between the assumed and the actual load spectrum contribute more to the final inaccuracy than the analysis methodology.

The possible occurrence of fast crack growth and arrest at loads much lower than the fail safe load is discussed by Mr. Vlieger on the basis of his Figure 12. This event is indeed of great significance, and it poses a difficult problem for damage tolerance requirements. The USAF requirements for Crack-Arrest Fail-Safe structure do not permit an instability at a specified load, P_{xx}, within a certain period, t_c. This implies that the stress level $\bar{\sigma}$, (in Figure 12 of the paper) is associated with P_{xx}, and the time t_c is the crack growth period to a crack of size $\bar{a}$ (Figure 12).

In order to account for a possible instability during the fatigue crack growth period (i.e., at a crack size a_i in Figure 12) it would be necessary to make a statistical evaluation of the probability of occurrence of such an event. This would require the establishment of the probability of exceeding the instability stress σ (which varies as in Figure 12) at any crack size between $\bar{a}$ and $a = s$. Subsequently, remaining crack growth life in the case of an arrest can be determined as a function of the instability statistics. On this basis, damage tolerance requirements could set a fail safe load at a level that would give an acceptable probability of failure.

The discussion in Sec. 5.2. on the improvement of fail safe properties is very brief. Obviously, the design of a built-up sheet structure will be largely determined by other criteria than damage tolerance. If damage tolerance is an important design criterion, the designer has many parameters to work with, such as:

a. Crack growth properties
b. Toughness
c. Strength of stringer material
d. Stiffening ratio
e. Stringer spacing
f. Fastening stiffness
g. Fastener spacing.

The effects of these parameters is shown diagrammatically in Figure 1 of this discussion. The heavy lines in the figure indicate the locus of the stress level designated by $\bar{\sigma}$ in the main paper.

Figure 1a shows that an increasing stiffening ratio leads from a stringer-critical to a skin-critical design, but the stress level $\bar{\sigma}$ keeps increasing. Stringer spacing (Figure 1b) has a similar effect. However, other design criteria will set limits to these parameters.

Increasing the strength of the stringer material (Figure 1c) is only effective to the point where the design becomes skin critical. Beyond this point the stress level $\bar{\sigma}$ does not increase further.

Increasing the skin toughness (Figure 1d) leads from a skin-critical to a stringer critical design, with consistent increase of $\bar{\sigma}$.

Fastening stiffness (Figure 1e) and fastener spacing (Figure 1f) can change the design from skin critical to stringer critical with an improvement of the level of $\bar{\sigma}$. Once the structure becomes stringer critical, there is little further improvement, because the intersection of the skin-crack line and the stringer failure line stays at approximately the same stress level.

Parametric analysis of the type shown in Figure 1 can be made to optimize the structure with respect to weight-considerations and damage tolerance criteria. The analytical procedures to evaluate skin-stringer structures, to the development of which Mr. Vlieger has contributed so much, permit such parametric studies in an elegant and expeditious way. In that sense they offer great advantages over a finite element analysis.

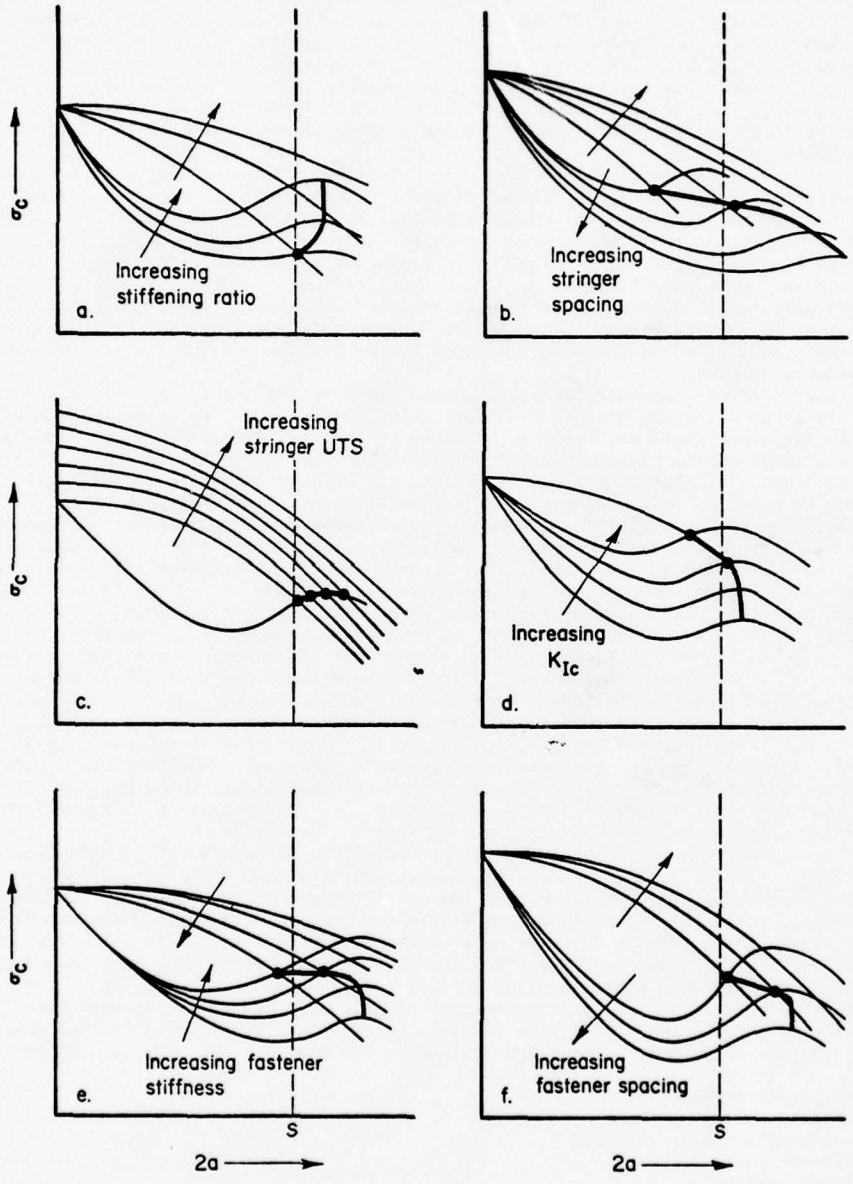

FIGURE 1. PARAMETRIC ANALYSIS FOR RESIDUAL STRENGTH OF SKIN-STRINGER COMBINATIONS

COMPARATIVE EXPERIMENTAL OBSERVATIONS AND THEORETICAL ANALYSIS OF THE PROPAGATION OF FATIGUE CRACKS

BY
Dr. G.L. De Otto
Chief Structure Engineer
Aeronautica Macchi S.p.A.
Varese, Italy

SUMMARY

The fracture sections of two primary structural elements that failed during the fatigue tests on the complete aircraft, are examined. The building-up and propagation of the cracks, the interaction effect between the various cracks, the validity of the non-destructive inspection methods (NDT) and the importance of the test load spectrum are shown by a microfractography examination of the same sections.
The assumptions on fatigue striations are verified and crack propagation experimental curves determined for an appropriate selection of the inspection intervals. The experimental propagation curves are compared to the theoretical curves calculated by the equation of Forman.

PREMISES

The MB-326 was originally designed to be employed as a basic trainer by the IAF. With the latter, Aeronautica Macchi arranged a detailed experimental programme for the investigation of the fatigue behaviour of the aircraft structures from the preliminary phases of design development in 1958.
The technical and commercial success obtained, brought the MB-326 ( ) to be adopted and operated by several foreign countries in a wide range of environments and under different load spectra (see fig. 2).
As a consequence of this, the initial fatigue test programme was supplemented to account for: the different types of role in which the different operators intended to use the aircraft; the performance increase resulting from the installation of uprated engines; the weight increase resulting from the increase of useful load.
The three fatigue tests completed by Aeronautica Macchi - in 1963 on behalf of the IAF on the MB-326 structures; in 1970 on the MB-326G structures and, finally, 1974 on behalf of the RAAF on the MB-326H structures - have allowed the ~ 600 MB-326 ( ) aircraft or so in service with the different users to reach the remarkable mark of 700,000 flying hours with no problem hindering the full utilization of the aircraft.
Besides, the continuous improvements in structure design, made possible by the large test work effected, have allowed the aircraft safe life to be extended with no appreciable changes in weight, in spite of the significant differences of aircraft utilization with the different operators compared to the original IAF service spectrum.
The development of an MB-326 ( ) version equipped with 6 underwing pylons has in fact made it possible for the aircraft to be used for training to air-to-ground and air-to-air firing with the application of very severe load spectra.
In figures 2 and 3 are given the load spectra typical of the MB-326 ( ) role, measured by the use of fatigue meters at the different users. The severity of the average load spectra of the different users can vary from 1 to 10, whilst the severity of the average load spectrum of each aircraft inside a fleet can vary from 1 to 14.
As a consequence of this, the decision taken by Aeronautica Macchi to install a fatigue meter in each aircraft not only appears to be fully justified but has also permitted an assistance service to be established with the co-operation of the users for the evaluation of the life consumed by each aircraft on the basis of the fatigue meter readings periodically taken on each aircraft.
In this way it has been possible to ensure the full utilization of the aircraft for the entire life cycle, and to concentrate the inspections into the time of the major overhauls.
From a practical point of view, this approach to the problem has materialized in the replacement of a few "safe life" components after about 3000 flying hours on MB-326 machines built in accordance with the original standard. With the design improvements introduced as a result of the varoius fatigue test campaigns carried out on parts and complete airframes, no replacement is any more required throughout the aircraft life.
The design of the critical parts has been further improved in the MB-326K (ground attack, single-seat version of the MB-326) to guarantee the aircraft a 4000-hour safe life in the ground attack role which is particularly severe from the fatigue viewpoint.
The structural standard thus achieved after 16 years of uninterrupted research, 3 fatigue tests on complete airframes and the many test on parts, has been transferred into the MB-339, the new "all-through" trainer chosen by the IAF to replace in the next five years the MB-326 in service since 1960.
Still based on the "safe life" concept for the specific purpose of taking advantage of the precious experience accumulated with the previous models, the MB-339 has been designed for a safe life of 10,000 hours of combined "basic and advanced" training, in order to offer a safe machine, free from fatigue problems.
In the frame of these studies, Aeronautica Macchi has long developed some researches on crack propagation in the fatigue critical

sections, taking advantage of the different fatigue test to failure conducted on complete airframes for the evident purpose of getting hold of the new techniques of the fracture mechanics and to study their possibilities of application and the relevant costs.
As a consequence of this, the fatigue tests on complete airframe of the new prototypes will be set up so as to permit detection and measurement of the crack propagation rate in the areas where cracks are likely to arise.

TEST RESULTS

The recent fatigue tests on the MB-326( ) complete airframe were carried out with the specific purpose of determining the curves of crack propagation in the fatigue critical sections of the fueselage center section and wing spar lower cap (figure 4) (the test was performed on a structure to an early design standard).
The fatigue test rig already available at Macchi was used for this purpose (figure 5).
By use of a pressure switch the system can apply 9 (nine) load levels for a total of 533 different manoeuvers (in flight and on the ground), corresponding to 25 flight hours.
The fatigue equipment is of very simple design and as such very reliable and unexpensive.
This equipment allows to reach load application times of ~ 2 seconds for the lowest load levels and ~ 10 seconds for the highest load levels with practically no stoppages.
The stops imposed by the necessity of inspecting the structure have been more than sufficient for the maintenance of the fatigue rig which has by now totalized more than 120,000 hours of simulated flight. During the performance of the fatigue tests, the cabin pressurization was in operation in order to reveal possible secondary effects on the cabin structure.
The cabin pressurization control was independent of the load levels.
The load distribution inside each load block was randomized as shown in figure 6.
In order to monitor the values of the loads applied to the structure, a reading of all electrical strain gauges (≃ 150) applied to the structure was taken every 10 load blocks.
On that occasion the structure remained under the load corresponding to the 7 g manoeuver for approx. 2 minutes.
The applications of these loads are visible in the fracture sections (see figures 9 and 12).
The fatigue critical sections were constantly inspected by non-destructive inspection methods to exactly determine the experimental propagation of the crack. For the steel section, the following methos were used:

a. Magnetic rubber inspection.

b. Ultrasonic method.

For the light alloy section, the inspection method essentially used was:

a. Visual inspection with the aid of a variable-focus endoscope and dye penetrants.

The magnetic rubber inspection proved to be the most accurate and effective method of crack detection and permitted to reveal crack initiation all along the lug width and growth up to conjunction in a single crack (figures 7 and 8).
In figure 8a there is shown the plot of the crack length as a function of the crack depth. This chart has been obtained by measuring the length of the crack on the hole surface and successively enlarging the hole with an oversize reamer and again measuring the new crack lengths on the surface of the hole thus obtained.
As can be seen, in their initial phase the cracks may have a lenticular propagation for which the crack length appearing on the surface may be quite different from the crack maximum length.
The endoscope has resulted a very useful means to monitor crack propagation, even if its sensitivity is much lower than that of the magnetic rubber (figure 9). The great advantage offered by the endoscope is the possibility of reaching and inspecting structures that should otherwise be considered non-inspectable.
With the aid of the periodic inspections carried out at fixed intervals and from micrographs of the fracture sections (figures 10, 11, 12, 13 and 14) it has been possible to obtain the crack propagation curves as a function of the number of applied load cycles (figures 16 and 17).

THEORETICAL CALCULATION OF CRACK PROPAGATION

After the attainment of the experimental results described in the foregoing, attention was given to the theoretical calculation of the crack propagation. The short time available did not permit to examine the problem in depth. A programme for the calculation of the crack growth was however prepared for the computer at the Computing Center of Aeronautica Macchi.
The calculation programme is based on the FORMAN formula and is practically the same as the "CRACKS" programme shown in reference (1).
No description of the calculation programme is given since it does not present any particularly significant feature. The most important points are the following:

1. The FORMAN formula is written in the form shown in figure 18 using the symbols indicated on the same figure.
2. No provision was made to evaluate the delay in crack propagation due to the plasticization of the crack front.
3. The various correction coefficients provided by the original "CRACKS" programme were not used.
4. Only the positive part of the load spectrum was considered.

A good deal of calculation was carried out with this programme in order to study the responsiveness of the same programme to the different parameters of the FORMAN equation.
In practise it has been possible to establish that the theoretical behaviour of the crack is particularly responsive to the Stress Intensity Factor, and small differences in the Stress Intensity Factor function may therefore result in big differences in the final results of the calculation, especially when such differences are in the initial calculation phase when the crack dimension has an almost null value.
In figures 20, 21, 22 and 23 are shown the results of the most significant calculations along with the experimentally determined propagation values.
In the upper left corner are given the values of the Stress Intensity Factor used in the calculation. These values have been obtained by similarity, combining the results of the curves given in the "Compendium of Stress Intensity Factors" (ref. 7). The values thus obtained have then been corrected to obtain a better approximation of the experimental crack propagation curves.
In each figure are displayed the curves of the stress intensity factor obtained from reference (7) and the curves corrected to increase the consistency of the calculation with the experimental results.
The other coefficients used in the calculation were obtained, for the 7075 T6, from the literature available for the 7075 T6, whilst for the AISI 4340, for which no data could be found, use was made of the data published for the D6 ac steel which has a composition very similar to the AISI 4340 (see figure 19).
The obtained results are encouraging but there still remains a lot to do for the reliability of this type of calculation to be improved.

CONCLUSIONS

Basing on the brief experience made at Aeronautica Macchi in the assessment of crack propagation, the following conclusions have been reached:

1. Sufficient data on the values of the coefficients to be introduced in the equation of FORMAN are not yet available.
2. The Stress Intensity Factor is the parameter that determines the crack growth behaviour, and curves capable of meeting the particular cases in a study are not eacily found.
3. The influence of negative load and plasticity must be taken into account.

From the above it is possible to infer that the study of crack propagation to be done in the design phase requires a lot of experimental work for it to be reliable.
Conversely, if adequate experimental results are available, crack propagation studies may be very helpful to determine the fatigue life variations due to load spectrum modifications.
In the future Aeronautica Macchi, through sticking to the application of the "SAFE LIFE" philosophy in its new models, is planning to go further into the determination of the "Stress Intensity Factors" for the cases covered by this study by the use of tridimensional finite elements programs (Ref. 10).
Subsequently, the programme for assessment of the crack propagation will be improved by introducing the delay due to the plasticization of the crack front caused by the high load levels.

REFERENCES

1. Robert M. Engle Jr: AFFDL-TR-70-107 – Cracks, a fortran IV digital computer program for crack propagation analysis.
2. H. Liebowitz: AGARD-AG-176 – Fracture mechanics of aircraft structures.
3. H.A. Wood: AGARD-AG-176 – The use of fracture mechanics principles in the design and analysis of damage tolerant aircraft structures.
4. J.I. Bluhm: AGARD-AG-176 – Crack propagation laws.
5. W. Schutz: AGARD-AG-176 – Experimental techniques for determining fracture toughness values.
6. W.T. Mattews: AGARD-AG-176 – Typical plain strain fracture toughness of aircraft meterials.
7. D.P. Rooke, D.J. Cartwright: Compendium of stress intensity factors.
8. R. Reid Parmerter: AFRPL-TR-76-30 – Stress intensity factors for three dimensional problems.
9. H. Tada, P.C. Paris, R. Irwin: Stress analysis of cracks handbook.
10. J. Reynen: ASME Paper No. 75-PVP-20 – On the use of finite elements in fracture analysis of pressure vessel components.

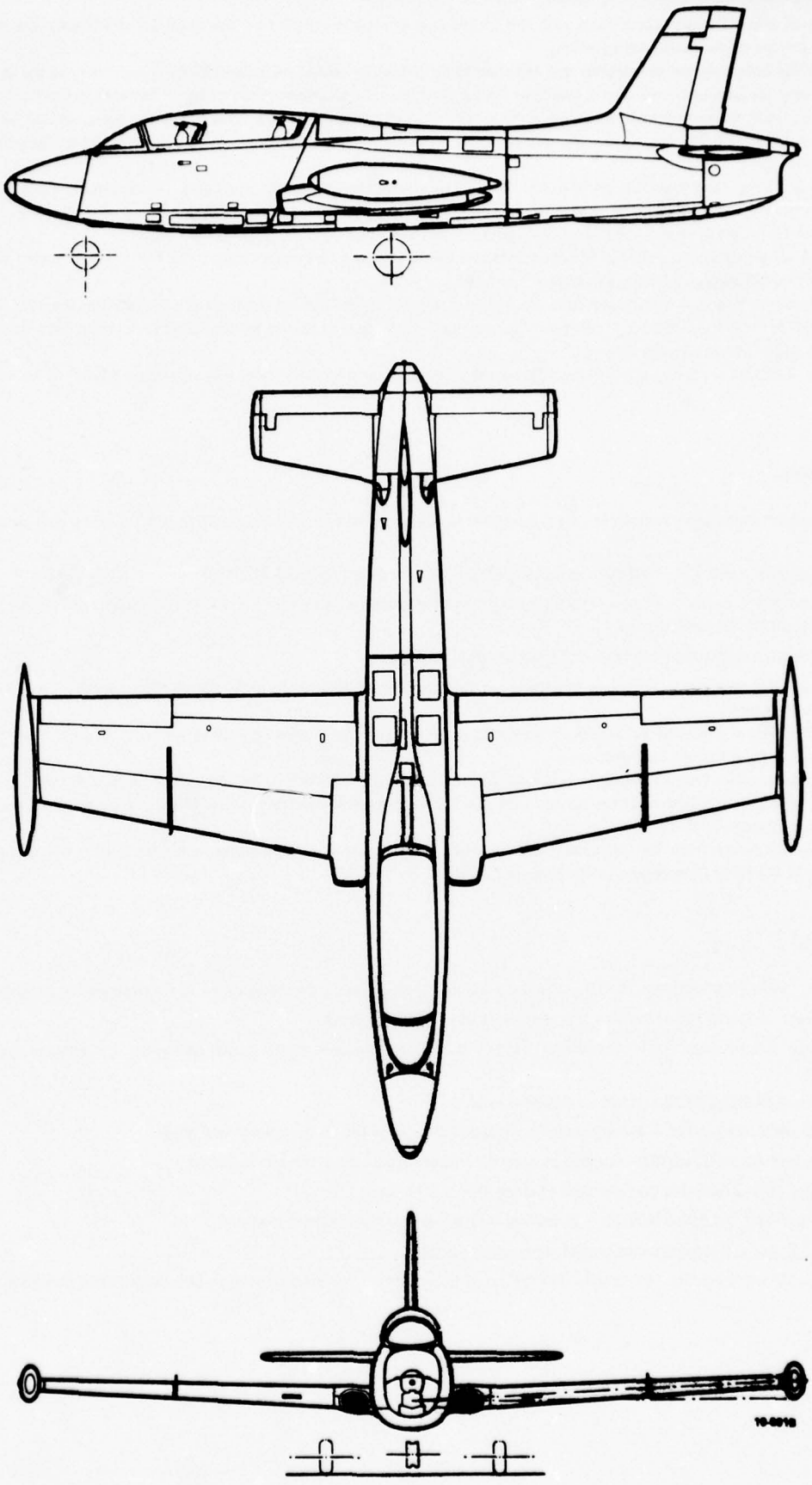

FIGURE 1. THREE-VIEWS MB-326( ) AIRCRAFT

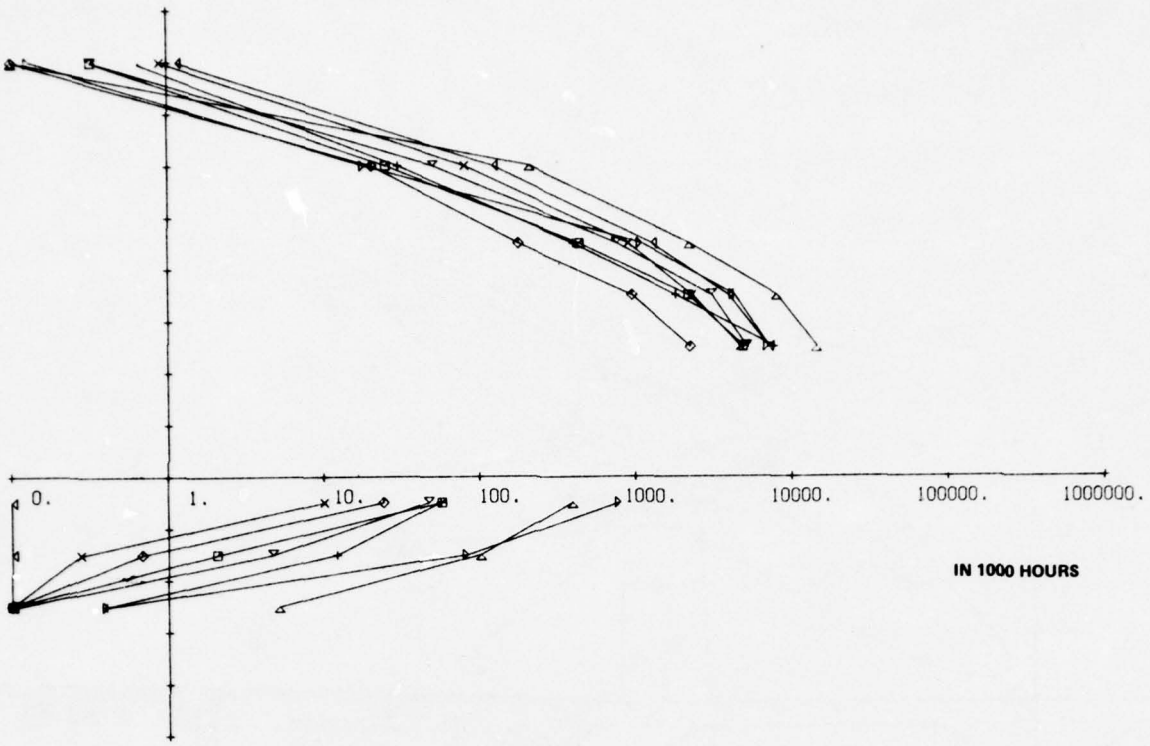

FIGURE 2. C.G. LOAD FACTOR SPECTRUMS (MEAN SPECTRUMS PER EACH FLEET IN THE WORLD)

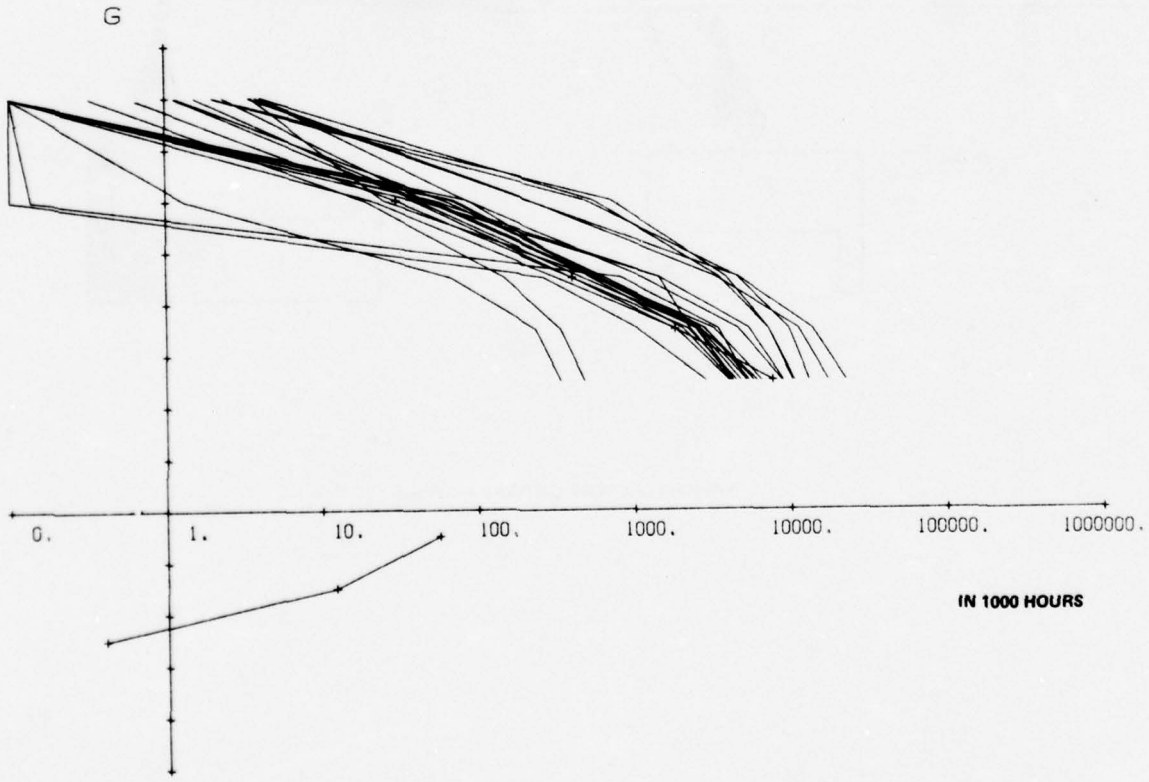

FIGURE 3. C.G. LOAD FACTOR SPECTRUMS REFERRED TO ONE FLEET (SINGLE AIRCRAFT)

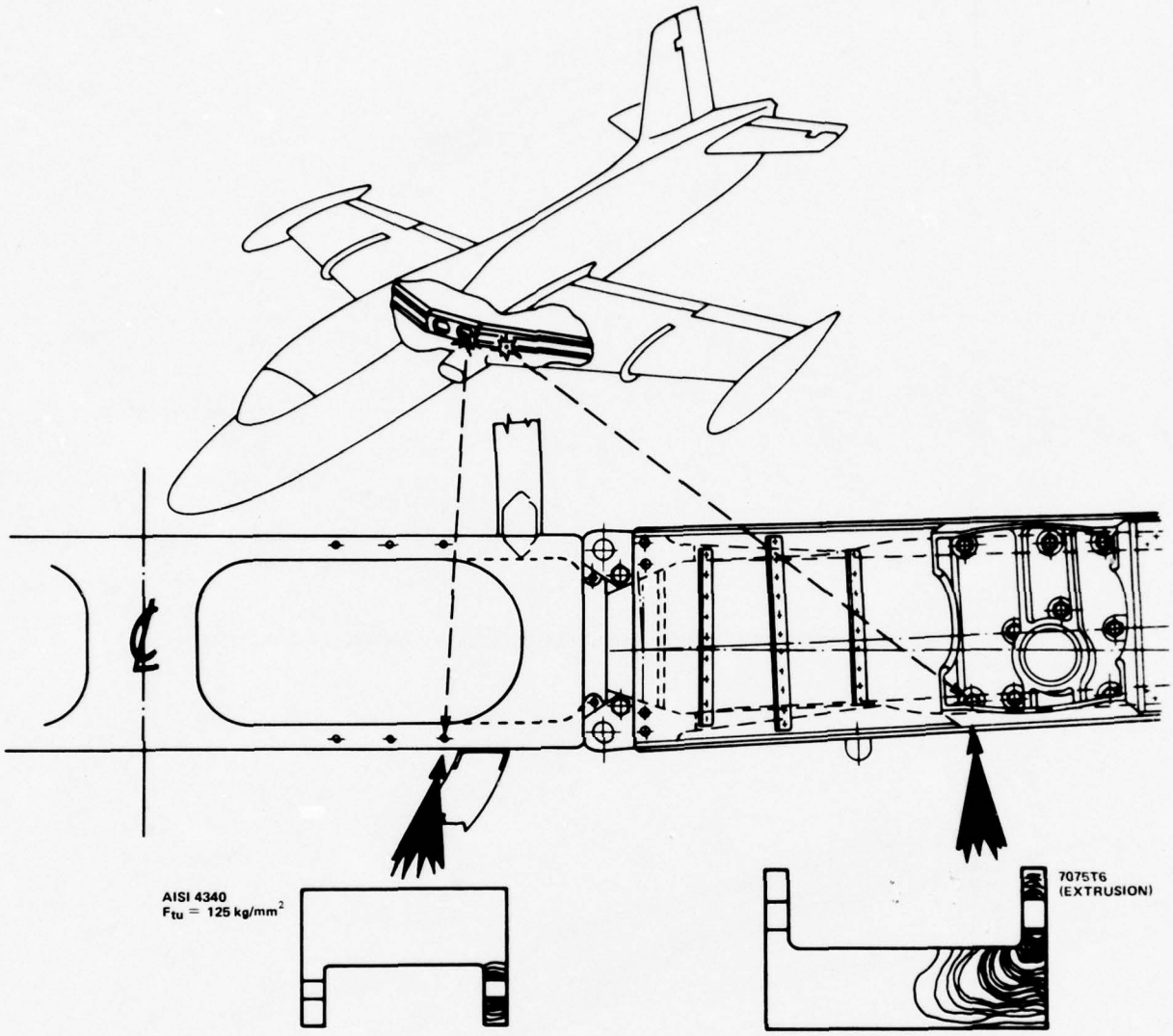

FIGURE 4. FATIGUE CRITICAL SECTIONS

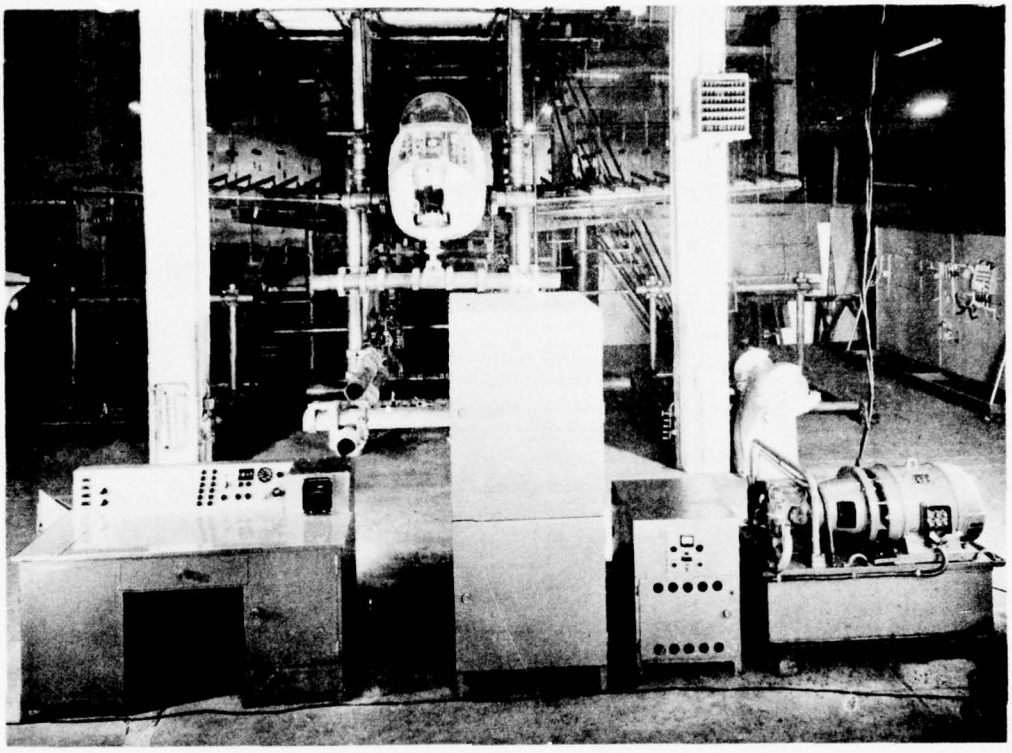

FIGURE 5. FATIGUE TEST MACHINE

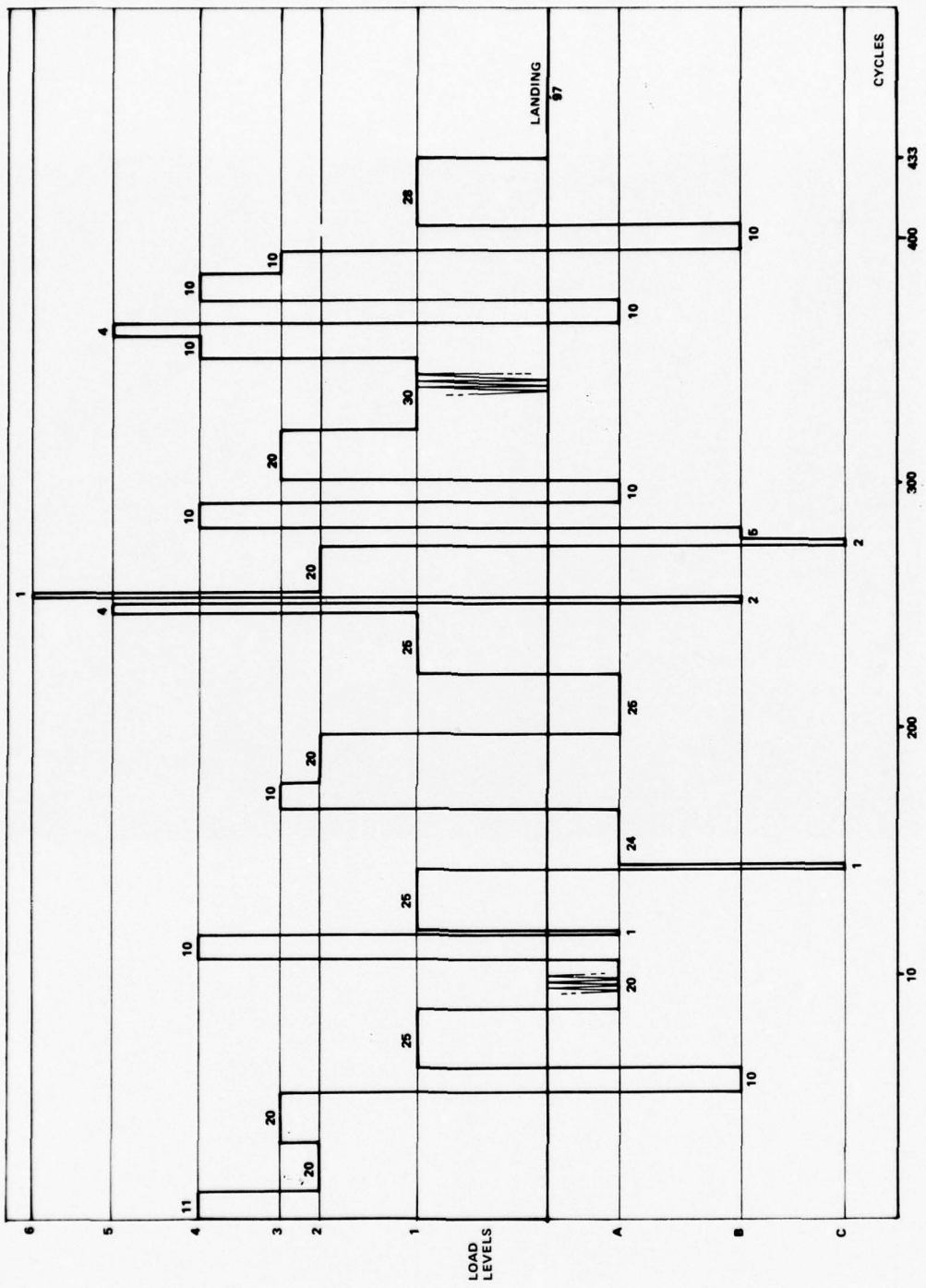

FIGURE 6. TEST LOAD PROGRAM (EQUIVALENT TO 25 FLIGHT HOURS)

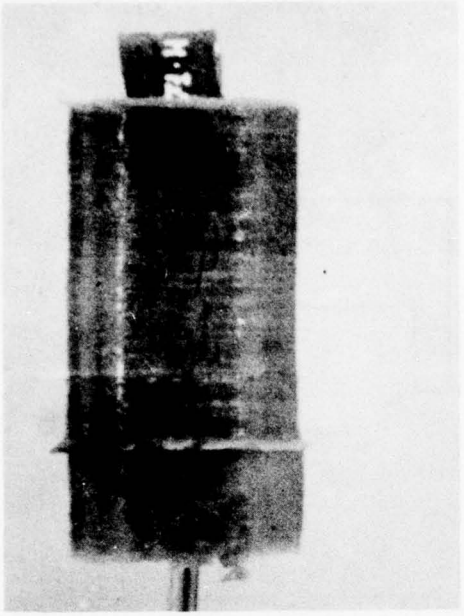

120% SAFE LIFE

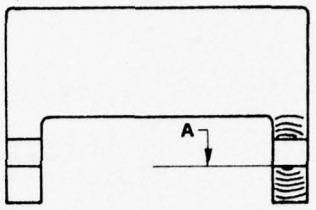

AISI 4340
F_{tu} = 125 kg/mm^2

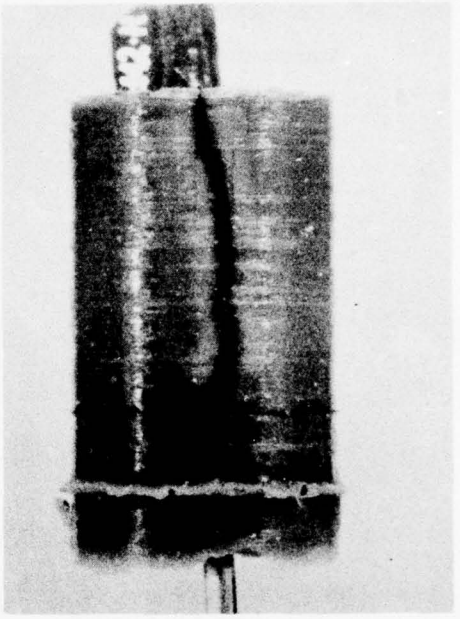

187% SAFE LIFE

147% SAFE LIFE

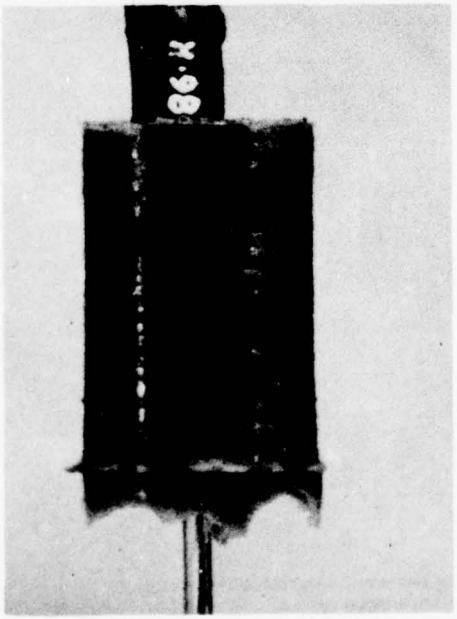

FIGURE 7. INITIATION AND GROWTH OF CRACKS IN A HOLE (SIDE A)

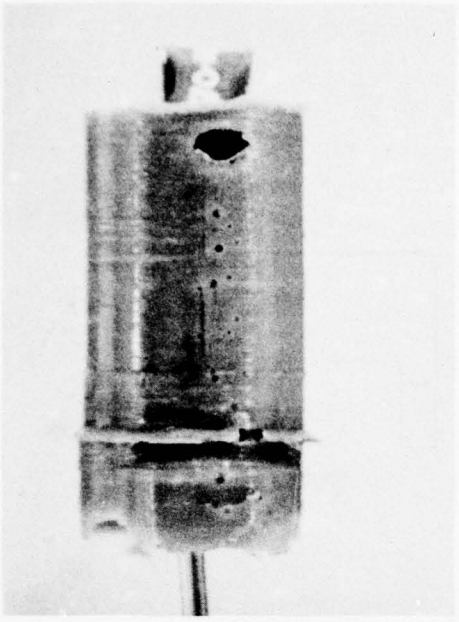

120% SAFE LIFE

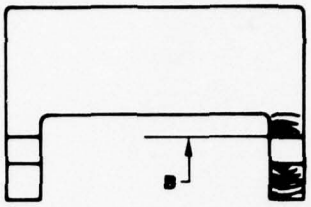

AISI 4330
$F_{tu} = 125\ kg/mm^2$

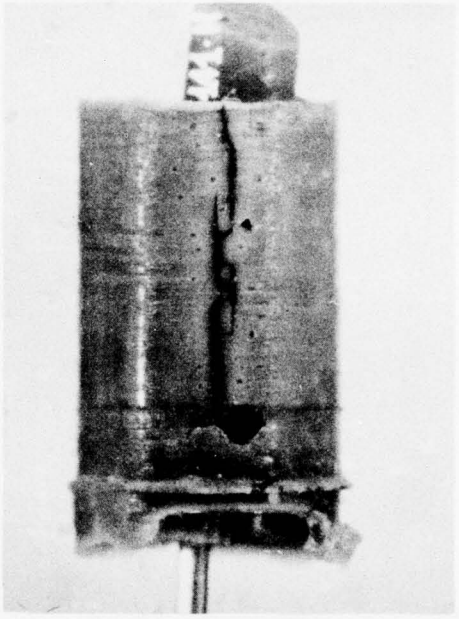

187% SAFE LIFE

147% SAFE LIFE

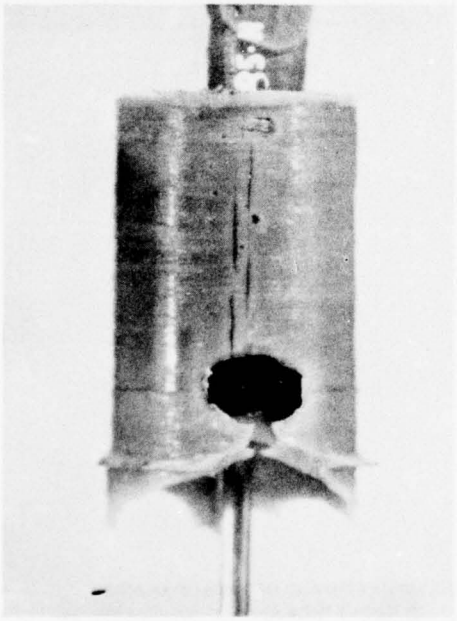

FIGURE 8. INITIATION AND GROWTH OF CRACKS IN A HOLE (SIDE B)

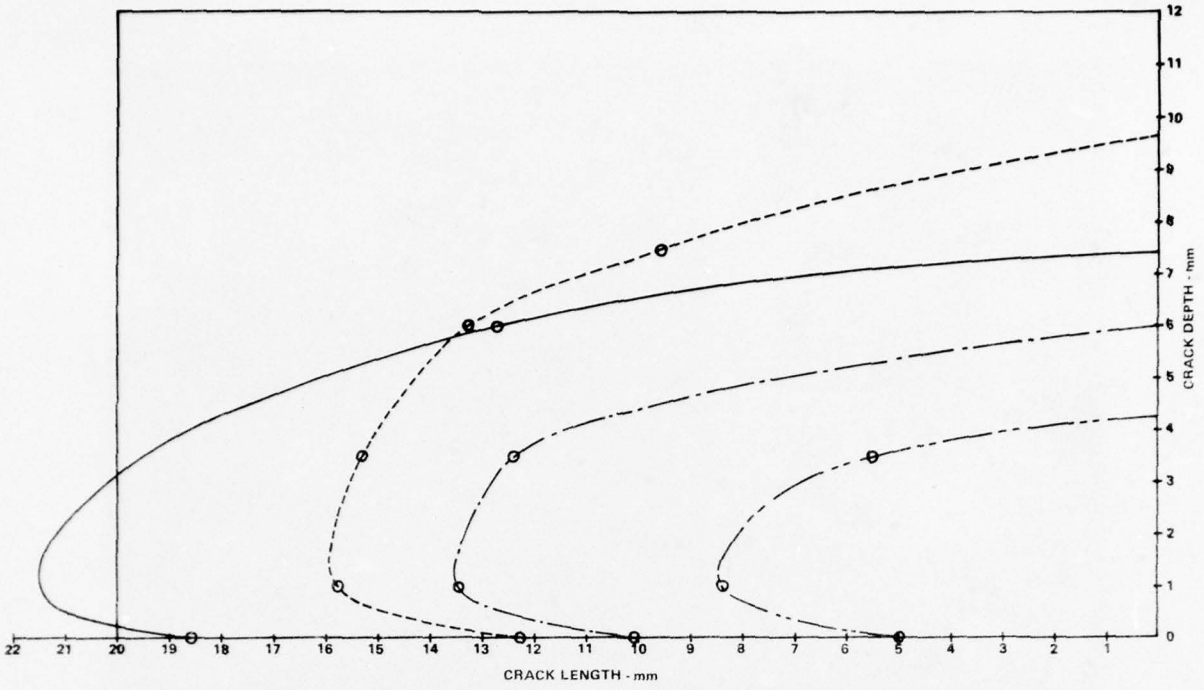

FIGURE 9

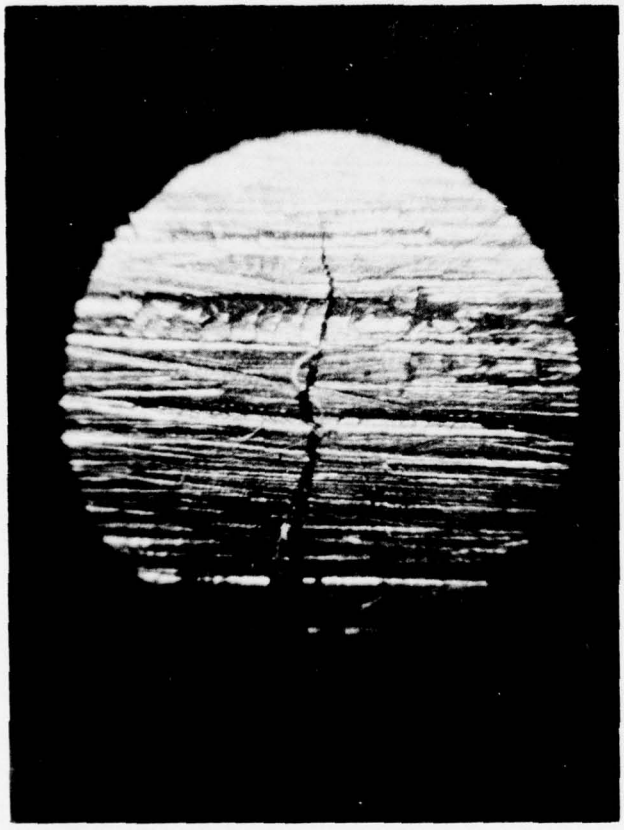

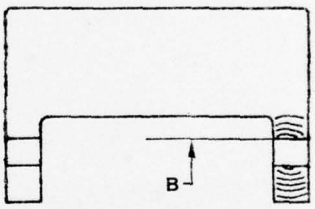

AISI 4340
$F_{tu} = 125\ kg/mm^2$

FIGURE 10. DETECTION BY ENDOSCOPE

EXTR. 7075T6

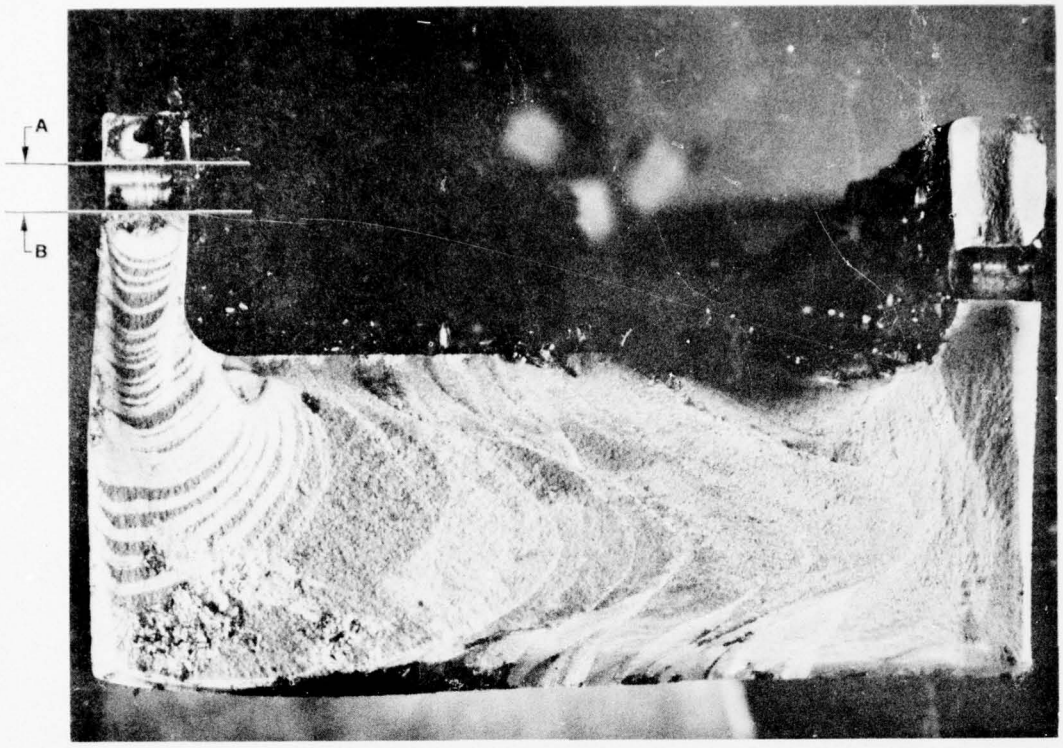

FIGURE 11. SPAR CAP MICROGRAPH

EXTR. 7075T6

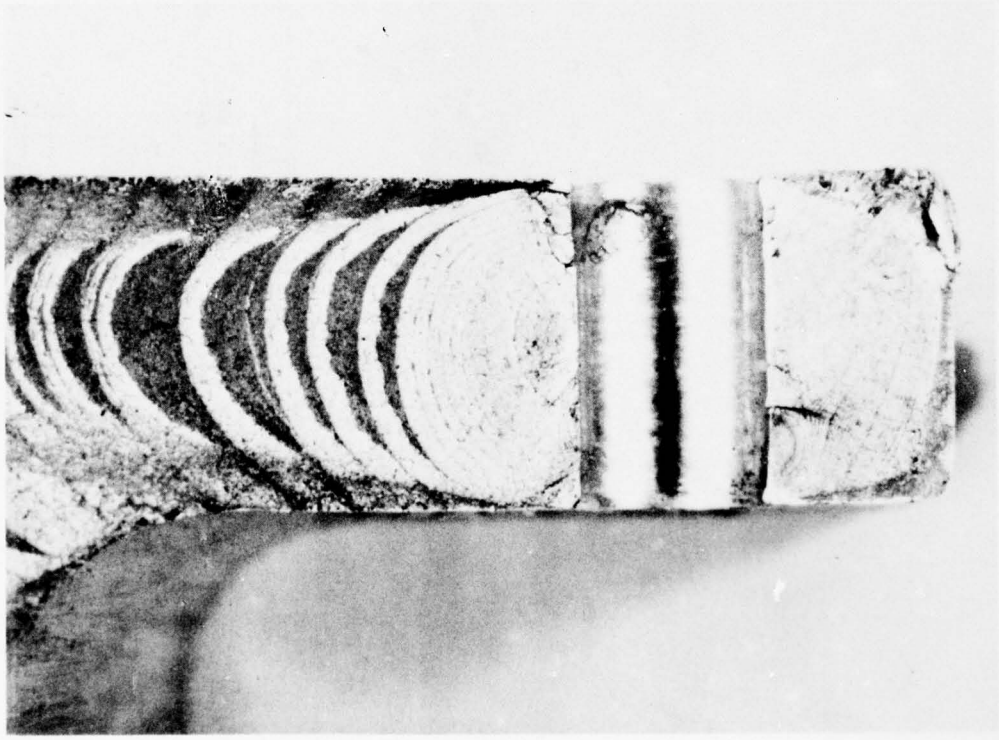

FIGURE 12. CRACK A

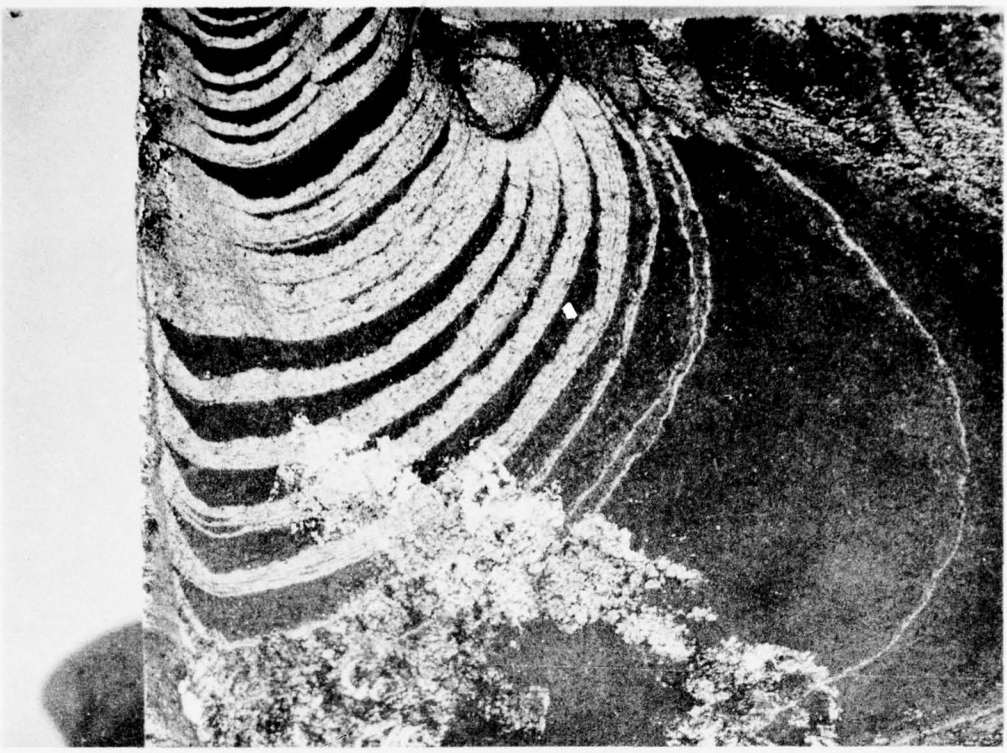

FIGURE 13. CRACK B

AISI 4340
F_{tu} = 125 kg/mm^2

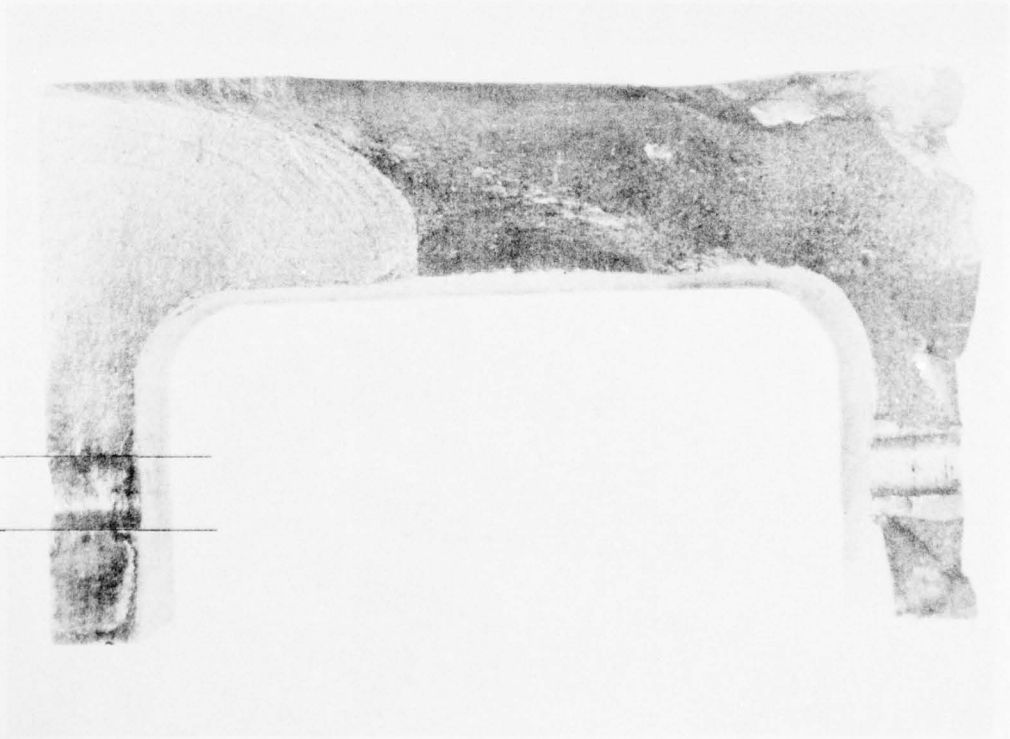

FIGURE 14. CENTER SECTION CAP MICROGRAPH

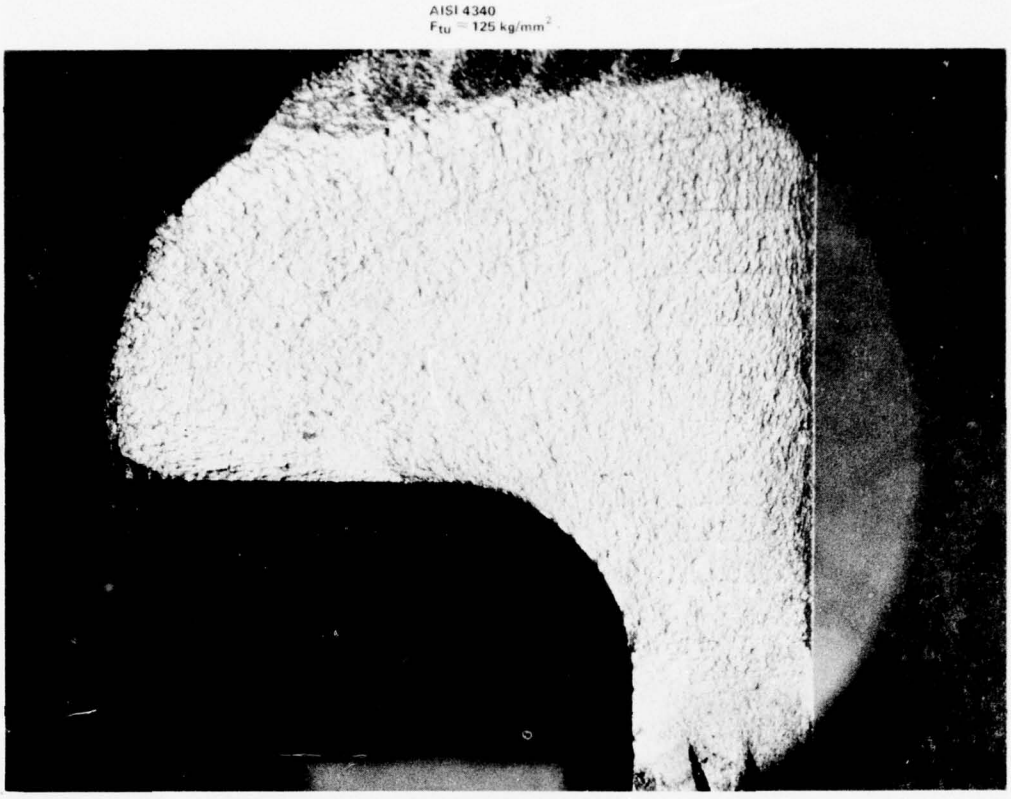

FIGURE 15. CRACK B (IMMAGNIFIED AND SPECULARLY PRINTED IMAGE)

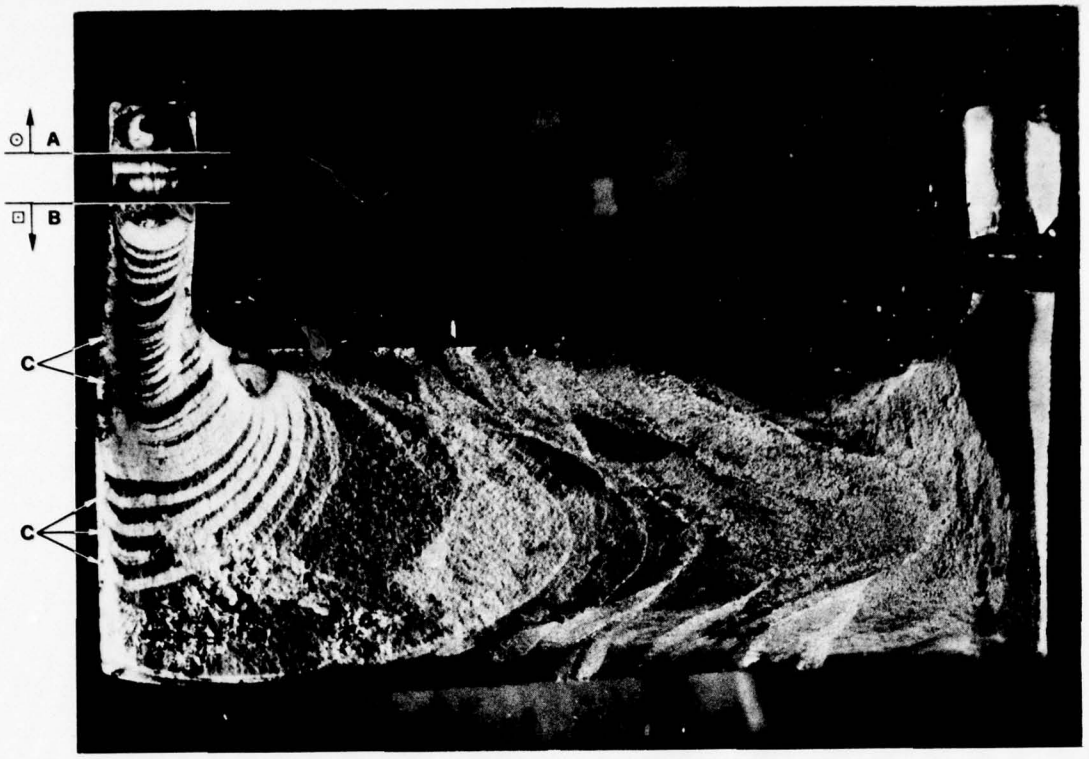

MATERIAL: 7075T6 (EXTRUSION)

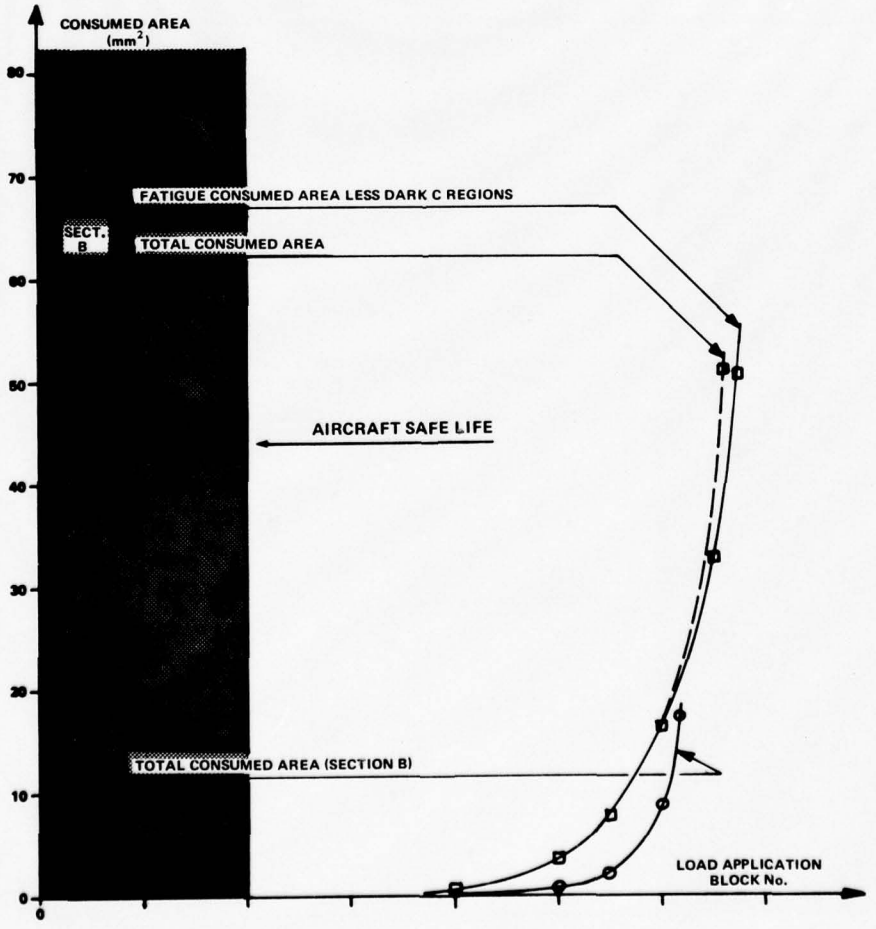

FIGURE 16

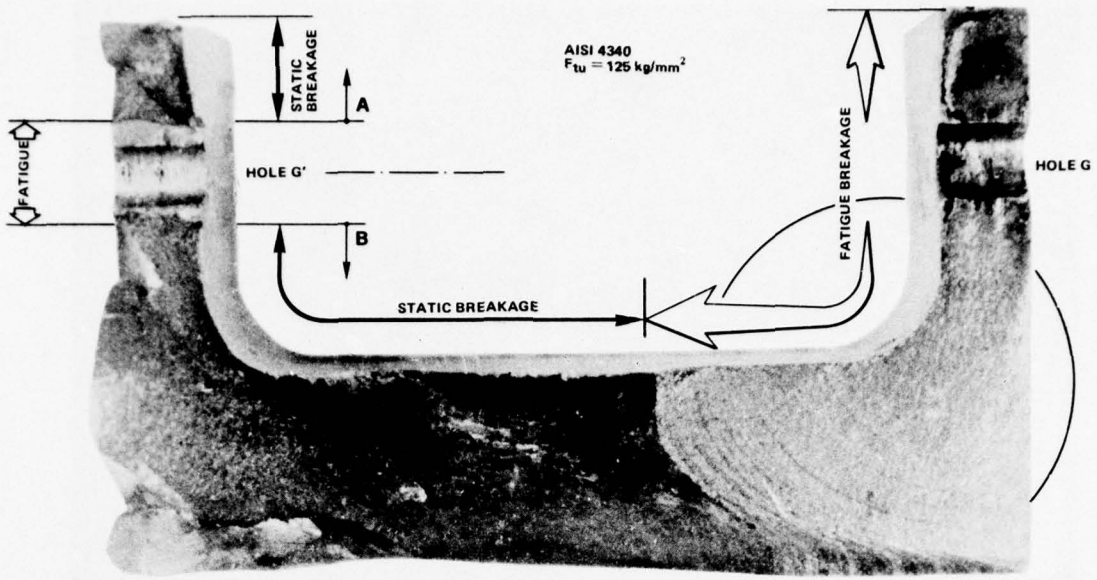
AISI 4340
F_{tu} = 125 kg/mm^2
STATIC BREAKAGE
A
FATIGUE
HOLE G'
B
STATIC BREAKAGE
FATIGUE BREAKAGE
HOLE G

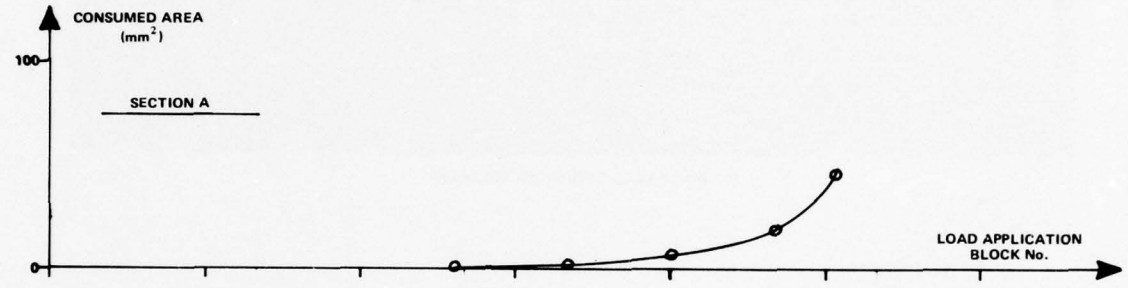
CONSUMED AREA
(mm^2)
100
SECTION A
0
LOAD APPLICATION
BLOCK No.

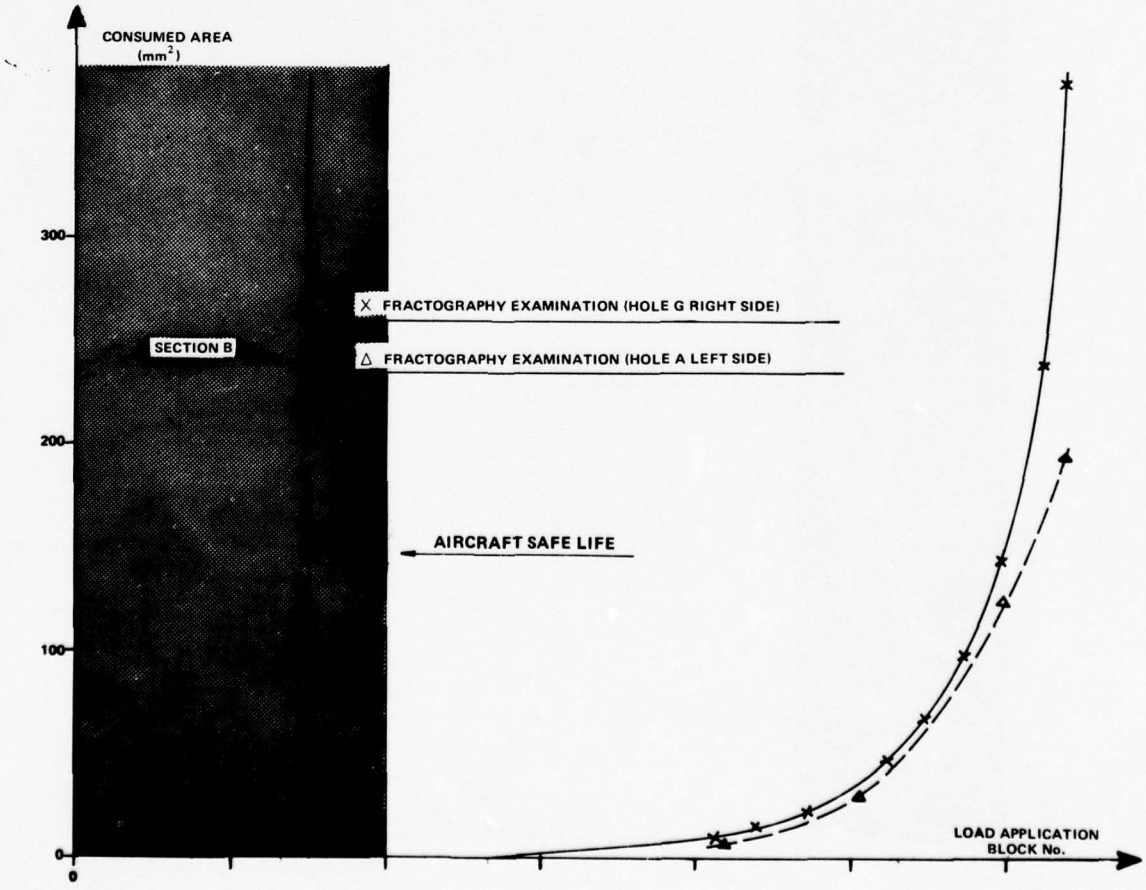
CONSUMED AREA
(mm^2)
300
200
100
0
SECTION B
X FRACTOGRAPHY EXAMINATION (HOLE G RIGHT SIDE)
Δ FRACTOGRAPHY EXAMINATION (HOLE A LEFT SIDE)
AIRCRAFT SAFE LIFE
0
LOAD APPLICATION
BLOCK No.

FIGURE 17

$$\frac{da}{dN} = \frac{c \Delta K^n}{(1 - R) Kc - \Delta K}$$

WHERE:

$$\Delta K = Ki \sqrt{\pi a \Delta\delta}$$

$$R = \sigma/\sigma_{REF}$$

$$\Delta\sigma = \sigma - \sigma_{REF}$$

WHERE:

c	= EXPERIMENTAL COEFFICIENT	–
n	= EXPERIMENTAL COEFFICIENT	–
a	= CRACK LENGTH	mm
N	= LOAD APPLICATION NUMBER	–
σ	= APPLIED STRESS	kg/mm^2
σ_{REF}	= REFERENCE STRESS	kg/mm^2
Ki	= STRESS INTENSITY FACTOR	–
Kc	= FRACTURE TOUGHNESS	kg/mm$^{3/2}$

FIGURE 18. EQUATION OF FORMAN

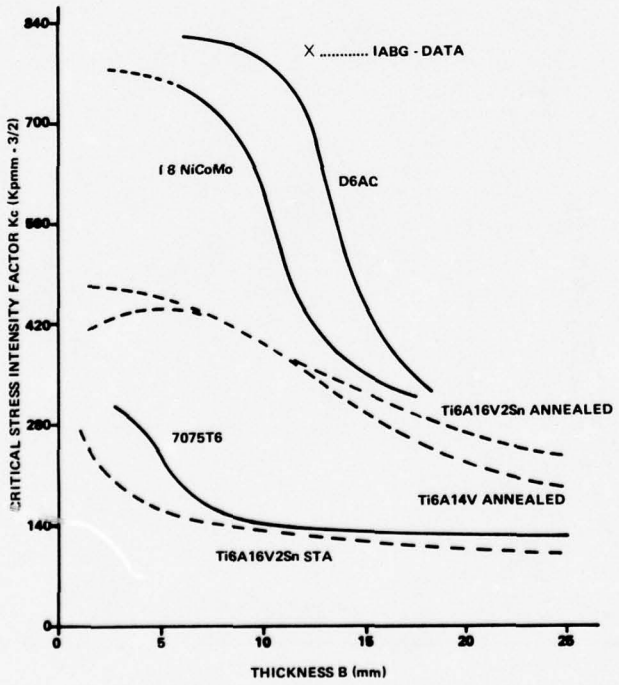

AISI 4340 (F_{tu} = 125 kg/mm^2)

$$\frac{da}{dn} = \frac{(.663) \cdot 10^{-9} \cdot \Delta K^{2.08}}{(1 - R - 791 - \Delta K}$$

7075 T6 (EXTRUSION)

$$\frac{da}{dn} = \frac{(1.) \cdot 10^{-12} \cdot \Delta K^3}{(1 - R) 168 - \Delta K}$$

FIGURE 19. CRITICAL STRESS INTENSITIES FOR SEVERAL MATERIALS AS A FUNCTION OF THICKNESS (DATA FROM IABG AND OTHERS)

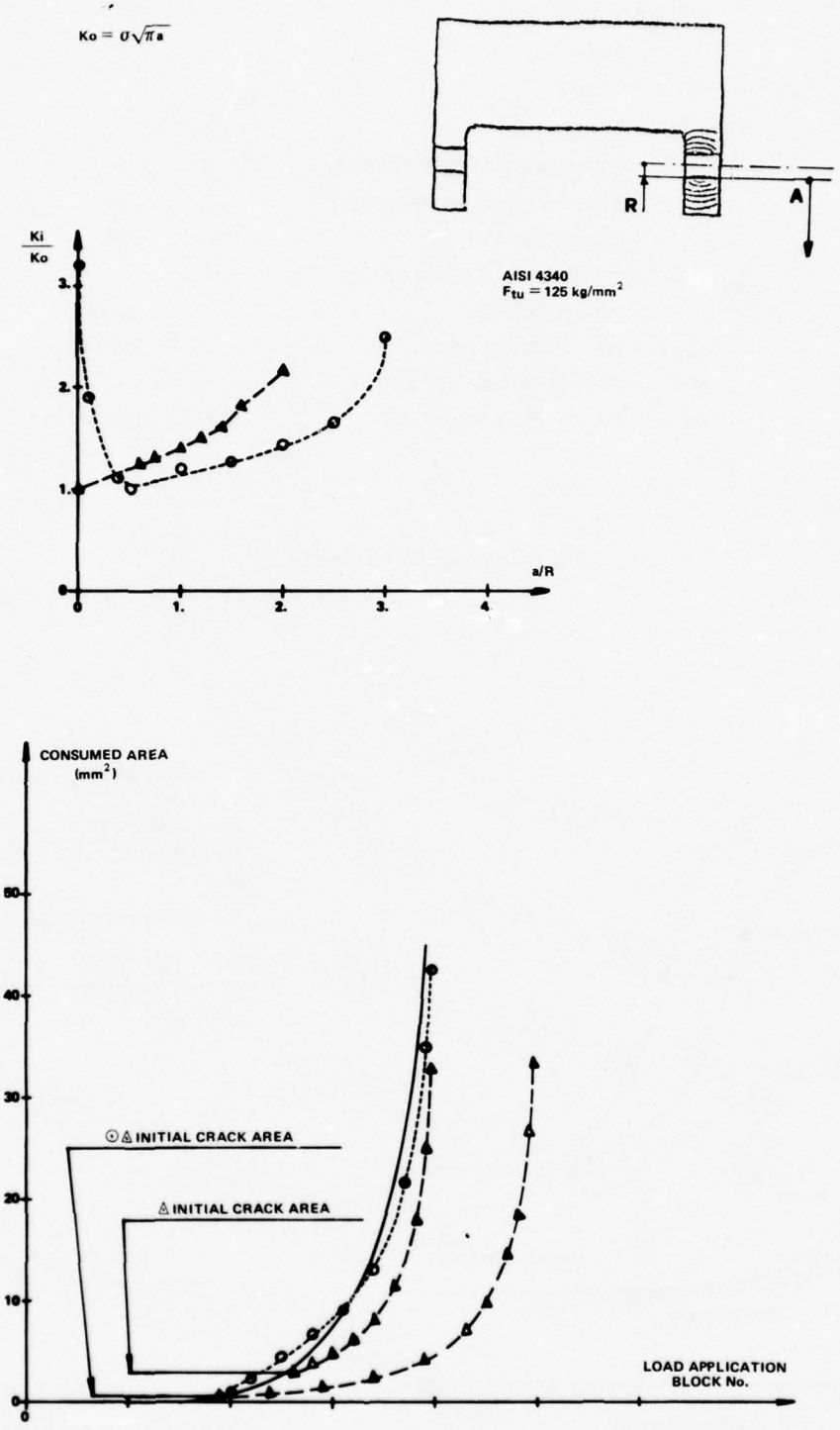
$K_o = \sigma\sqrt{\pi a}$
R
A
AISI 4340
$F_{tu} = 125\ kg/mm^2$
Ki/Ko
3.
2.
1.
0
a/R
0
1.
2.
3.
4
CONSUMED AREA
(mm^2)
60
40
30
20
10
0
⊙△ INITIAL CRACK AREA
△ INITIAL CRACK AREA
LOAD APPLICATION
BLOCK No.

FIGURE 20

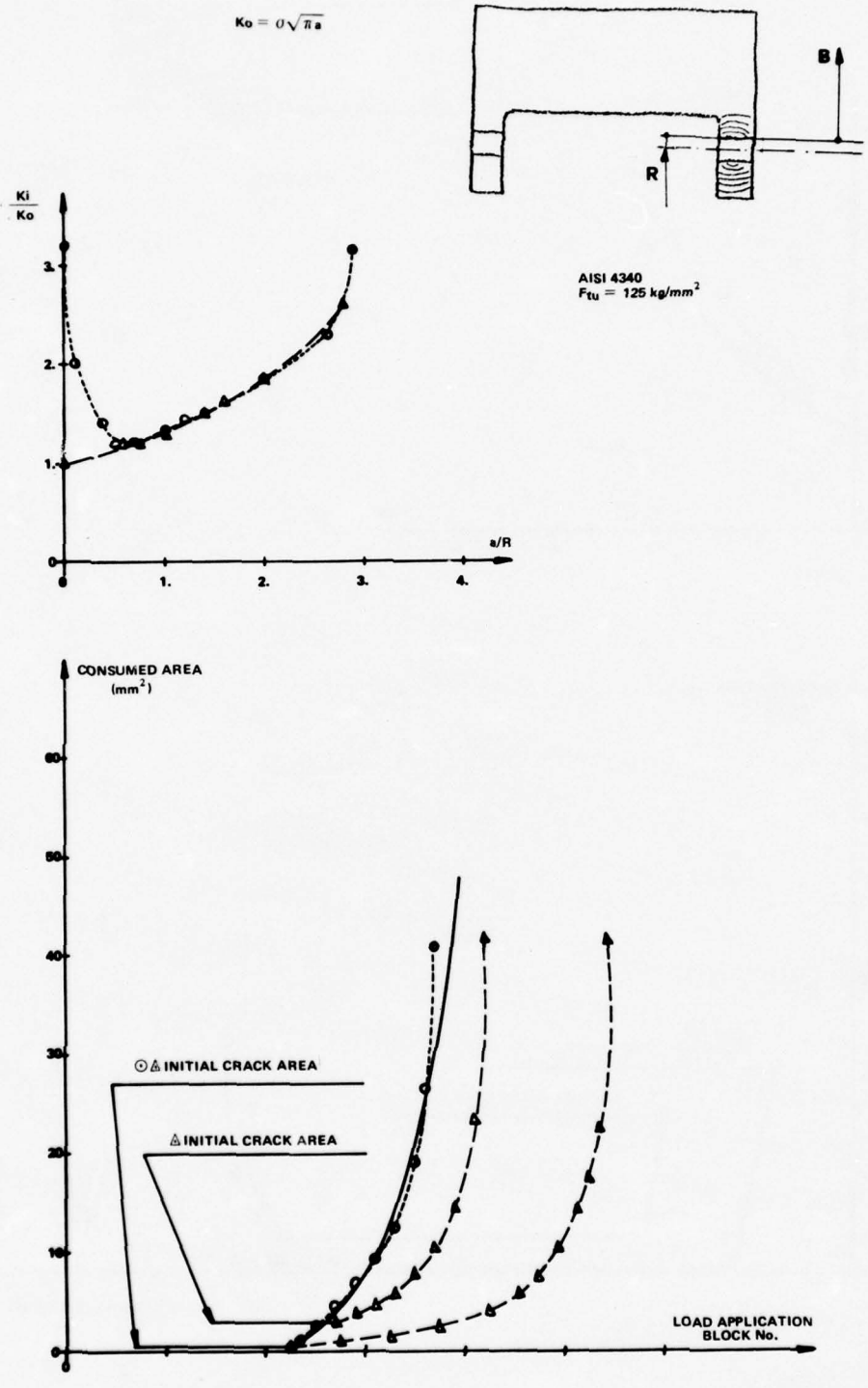
Ko = σ√πa
B
R
Ki/Ko
3.
2.
1.
0
a/R
1.
2.
3.
4.
AISI 4340
Ftu = 125 kg/mm²
CONSUMED AREA
(mm²)
60
50
40
30
20
10
0
⊙△ INITIAL CRACK AREA
△ INITIAL CRACK AREA
LOAD APPLICATION
BLOCK No.

FIGURE 21

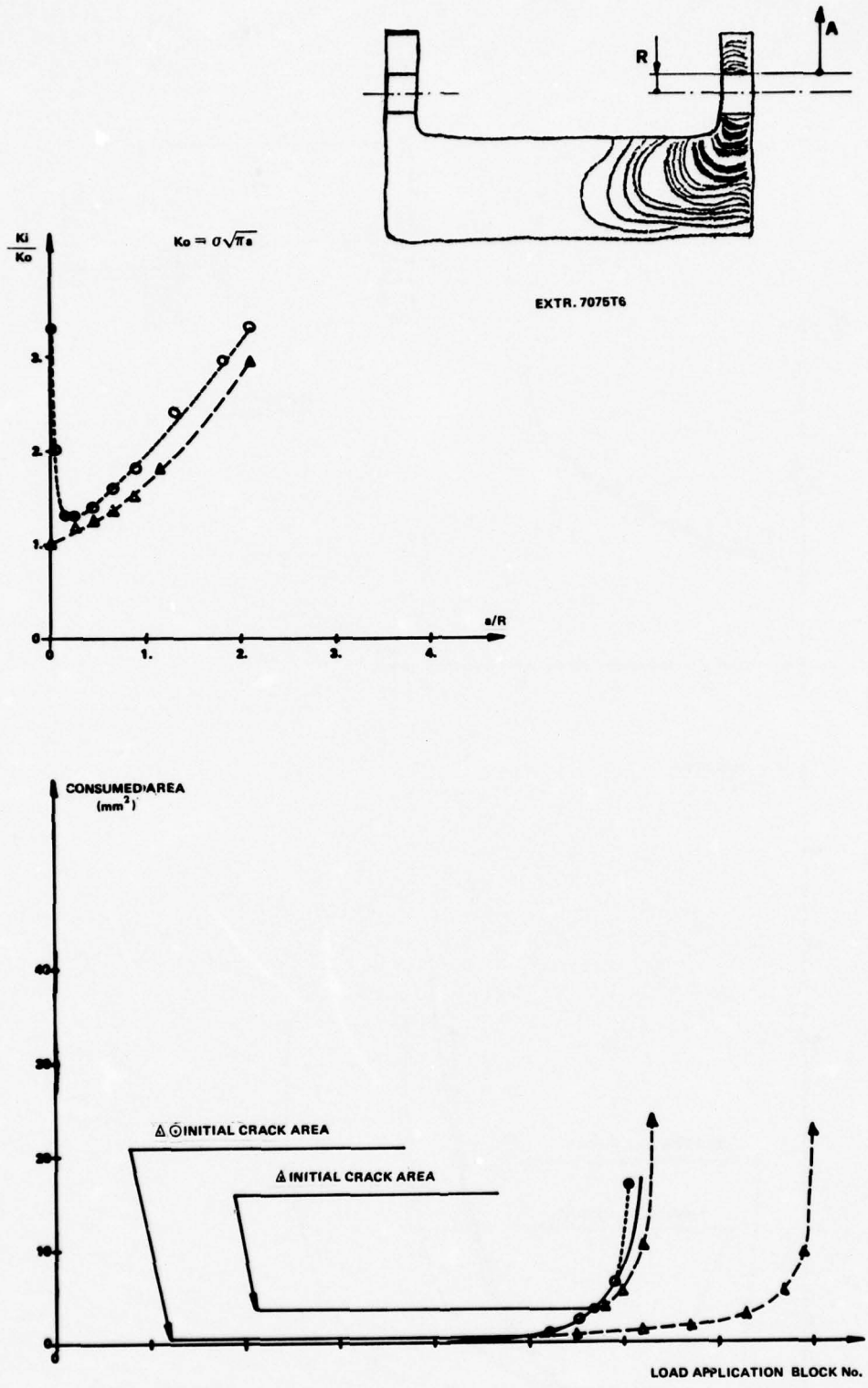
R
A
EXTR. 7075T6
Ki/Ko
Ko = σ√πa
a/R
CONSUMED AREA (mm²)
INITIAL CRACK AREA
INITIAL CRACK AREA
LOAD APPLICATION BLOCK No.

FIGURE 22

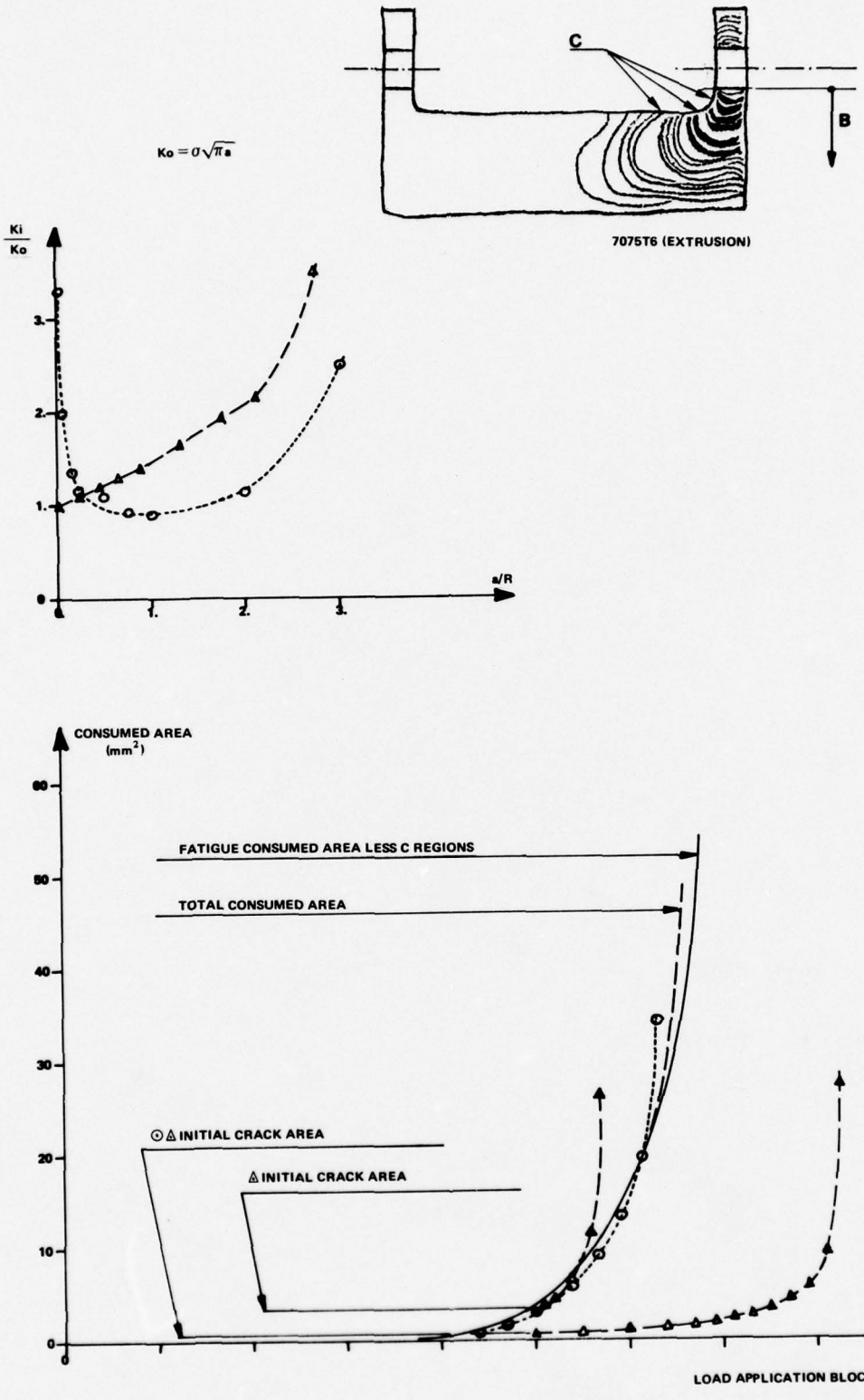
C
B
$K_o = \sigma\sqrt{\pi a}$
7075T6 (EXTRUSION)
Ki/Ko
a/R
CONSUMED AREA (mm²)
FATIGUE CONSUMED AREA LESS C REGIONS
TOTAL CONSUMED AREA
⊙△ INITIAL CRACK AREA
△ INITIAL CRACK AREA
LOAD APPLICATION BLOCK No.

FIGURE 23

FATIGUE BEHAVIOUR OF CRACKED STIFFENED PANELS

A. SALVETTI
Professor of Aircraft Construction
Istituto di Aeronautica, Università di Pisa
Via Diotisalvi, 2 - 56100 - Pisa
ITALY

SUMMARY

The investigation described in this report was undertaken to study methods of fail-safe design of aircraft structures.To this end a research was carried out with two main objectives: 1) development of methodologies to compute the crack growth under fatigue loading in stiffened structures, 2) and present minimum weight design methodologies suitable for fail-safe structures.

As far as the first question is concerned two aspects were particularly investigated namely the evaluation of the K-rate relationship in stiffened structures and the research of methodologies to correlate the stringer fatigue failures with the crack length in the sheet cover. Results on such topics based on a large set of experimental and theoretical data on cracked stiffened structures are presented.

The problem of designing minimum weight panels taking into account the fail-safe requirement was undertaken with reference to the wing lower surface structure. Using mathematical programming it was sought the optimum distribution of resisting material between sheet cover and stringers,taking into account not only the buckling phenomena connected with negative load factor flight conditions, but also the fail-safe requirement of the fail safe load for an assigned inspection interval, with given initial damage and load spectrum.

INTRODUCTION

Service catastrophic failures of important structural elements at load levels well below the allowable ones pointed out the importance of small defects, such as fatigue cracks, on the structural behaviour under static loading and suggested the design of damage tolerant structures as an expedient device against such types of failures.

In aircraft construction such a point of view is reflected in the existing air regulation and codified in the well-known fail-safe design requirements.

A first class of problems related to the design of fail-safe structures lies in estabilishing reliable and efficient inspection intervals for structures; such problem further, is closely related to the one of predicting the rate of growth of a crack in the structure under fatigue loading.

It is well known that the crack rate in a sheet of a given material under constant amplitude fatigue loading is uniquely related to the stress intensity factor (K-rate relationship) for a given stress ratio.

In the case of aircraft structures, typically made of sheet cover suitably stiffened against buckling by stringers,the problem is more involved; there are, in fact, at least two elements which combine to form the resistant cross section namely the sheet cover and the stiffeners,which interact through the fasteners. Since the cracking or the failure of such elements under fatigue loading are mutually dependent, the development of a method for evaluating the growth of a crack in such structures requires a quantitative assessment of this interaction.

A suitable approach to this problem can be based on the following points.

1) Evaluation of the crack growth rate in the sheet cover through the K-rate relationship together with a suitable theoretical method for computing the stress intensity factor in the stiffened structure.
2) Formulation of a rationale to evaluate the fatigue endurance of the stiffeners as a function of the crack length in the sheet cover and applied fatigue loading.

Another class of problem connected with the fail-safe requirement is the design of minimum weight stiffened panels taking into account the restraints on inspection intervals together with the usual restraints coming from buckling phenomena.

The purpose of the present paper is to present a set of theoretical and experimental results, obtained in the course of an investigation performed at Pisa Institute of Aeronautics, relative to the two classes of problems previously discussed.

In particular, as far as the problem of crack growth in stiffened structures is concerned, the research was confined to the investigation of riveted stiffened panels, subjected to axial loading,as they are well representative of large portion of aircraft structures which demand fail safe design. Further, being above all interested in clarifying the interaction on the crack growth of those structural elements (sheet-cover, stiffeners, fasteners)which combine to form the stiffened panel, only constant amplitude fatigue loading was taken into account.

The research developed through several steps. Computer programs were developed to evaluate the stress intensity factor and the fastener loading system; one computer program is based on the finite element method, another on the classical theory of the plane elasticity, and in both the rivets are regarded as flexible.

Being able to compute the rivet forces in a cracked stiffened panel,it was possible, on the basis of the Miner's rule and suitable S-N curves, to develop methods to evaluate the fatigue endurance of the stringers as a function of the crack length in the sheet-cover. At the same time a test program was carried out with the following main purposes:

- measurement of crack growth rate in stiffened panels;
- measurement of the crack length $\bar{l}$ in the sheet cover at which a stringer starts to crack;
- measurement of the rivet forces as functions of the crack length in the sheet cover.

To this end fatigue and static tests were performed on a large number of riveted stiffened panels (more than 70) differing in geometric shape, in dimension, in riveting and load levels.

The panels were constructed of 2024-T3 and 7075-T6 aluminum alloys. Different types of stiffener were used: strip stringers, double symmetric strip stringers, formed section stringers.

All the stringers were hand riveted:round head as well as countersunk rivets were used.

The results of such tests were used in the following ways:

- preparation of the K-rate relationship, utilizing always the theoretical K values and when disposable the theoretical-experimental K values, computed with the experimental data on the rivet forces;
- evaluation of the proposed approaches to obtain $\bar{l}$, as a function of the panel geometry and applied load
- comparison between theoretical and experimental results as far as stress intensity factor, rivet forces and stringer overloading are concerned.

The results in general provide a deeper insight in the behaviour of cracked stiffened panels showing the level of accuracy of the theoretical methods of computation, the influence of the panel geometry and the type of riveting, the limits of the rivet flexibility concept.

The experimental results demonstrated the adequacy of the proposed approaches to obtain $\bar{l}$.

As far as the second class of problems is concerned,namely the design of minimum weight fail-safe structures,the investigation was confined to the case of a stiffened panel belonging to the lower surface of a wing. In this type of structure, when fail-safe characteristics are required, it is worth investigating the optimum distribution of the resisting material between sheet cover and stringers taking into account not only the buckling phenomena connected with negative load factor flight conditions but also the fail safe requirement of holding the fail-safe load for an assigned inspection interval during which a crack, starting from a given initial dimension, propagates under a given load spectrum.

A research on this topic is in progress through the use of mathematical programming techniques; the mathematical model is based on the results on the stringer fatigue endurance found in the present investigation and on known approaches of fracture mechanics and buckling. Preliminar results on this research are presented.

CRACKED STIFFENED PANEL ANALYSIS

A first essential step to evaluate the fatigue crack growth in a stiffened panel is the development of adequate methods to obtain K and rivet forces as functions of the crack length.

Such a problem was faced developing computer programs which give,for a given cracked stiffened panel,the stress intensity factor, the rivet forces and the stringer overloading. A first computer program is based on the finite element method, (1); it results very versatile as far as the panel geometry, crack position and load conditions are concerned.

In this approach the sheet cover was idealized as an assembly of small rectangular sheets with a displacement field corresponding to a condition of elastic plane stress; the stringers as elastic beams eccentrically loaded by the axial forces applied by the fasteners.

Other computer programs were developed on the basis of well known approaches of the classical theory of the plane elasticity (complex potential and conformal mapping approach, Poe formulation).

Although the results of such computer programs are strictly applicable to unbounded stiffened panels they serve as check on the accuracy of the finite elements approach.

In all the computer programs the fasteners are regarded as flexible.

Fastener flexibility F was evaluated through an unique nondimensional parameter

$$f = \frac{FE_f d^4}{t^3} = \rho^{-1}$$

where E_f is the Young modulus of the fastener, d the fastener diameter and t the skin-stiffener thickness. f has to be evaluated experimentally with the following experimental procedure: the stiffener maximum load and rivet forces are at first evaluated as a function of f on the basis of the theoretical approach; next the same quantities are measured and by comparison with the theoretical values f is assessed. Such a procedure gives also the opportunity of controlling the hypothesis, that f does not depend on the crack length.

The computer programs can be also utilized to evaluate the stress intensity factor when the fastener force-applied load relationship is nonlinear (2).

This kind of non linearity is present when the rivet load is adequately high in relation to the hole dimensions, and depends essentially on localized plastic deformations in the zone surrounding holes, due to high bearing stresses.

The results of the computer program are given in the following form:

$$C = C(l/b,\ p/b,\ \alpha_c,\ \rho)$$

$$L = L(l/b,\ p/b,\ \alpha_c,\ \rho)$$

$$p_i = p_i(l/b,\ p/b,\ \alpha_c,\ \rho)$$

where l is the half crack length, b the stringer spacing, p the rivet pitch, α_c the reduced area ratio which takes into account the bending deformation of the stringer, (3); C, ratio between K in the stiffened and unstiffened panel, takes into account the influence of the stringers on K; L is the overload coefficient, namely the ratio of the maximum nominal stress in the stringer, computed on the basis of the beam theory, at given crack length in the sheet cover, and the same stress for zero crack length; p_i are the rivet forces.

Typical results of these computer programs are shown in Fig. 1a to Fig. 2c. More detailed results are reported in (1, 4, 5); the results of figure 2 are relative to a modification of the approach given in (6) to take into account fastener flexibility.

A mixed theoretical-experimental approach was also used to evaluate the stress intensity factor; the method is based on the measurement of all significant rivet forces Q_i in a stiffened panel and on the computation of K on the basis of the following relationship:

$$K = K^s - \sum_i K_i^r Q_i$$

where K^s, the stress intensity factor for the unstiffened panel, and K_i^r, the stress intensity factor for unit rivet force, are theoretical values.

Such an approach requires experimental data and therefore is limited in application; however its results are valuable as they are very accurate.

A THEORETICAL APPROACH TO THE EVALUATION OF STRINGER FATIGUE ENDURANCE

The crack rate in the sheet cover stiffened structures depends strongly on stringer integrity. As stringers are liable to fatigue failure when a crack propagates under fatigue loading in the panel sheet cover, a relationship between the crack length in the cover at which each stringer begins to crack and the applied load is required to evaluate the panel cracked area for a given load story.

In the case of a riveted stiffened panel, stringer fatigue failures depend on stress concentration around rivet holes caused by the combined action of the rivet forces and the applied load. As the rivet forces depend on the applied load and crack length, it is possible, in principle, for a given stiffened structure undergoing a given fatigue loading, to obtain a relationship between the applied load and the crack length in the sheet cover at which a stringer undergoes fatigue failure.

A first step in the resolution of this problem is the evaluation of the stress state in the stringers in the zones of stress concentration.

To this end two typical crack patterns are to be considered: the first is relative to a crack in the sheet cover propagating on a straight line crossing the rivet lines at the rivet holes; the second is relative to a propagation direction which crosses the rivet lines halfway between two rivets.

Therefore, with reference to the first cited crack pattern, the zones which are essentially liable to fatigue failures are those on the contours of the rivet holes where the stress resultant has the maximum value, namely the hole 0 on the crack line and the holes 1 immediately consecutive.

The stress concentration at the hole number 0 principally depends on the geometric discontinuity due to the hole; in fact the rivet is unloaded, as it lies on the crack line; diametral interference or clearance of fasteners can influence the stress concentration.

The rivet number 1 bears the maximum force among all the other rivets.

Stress concentration in these zones depends strongly on bearing stress and on the geometric discontinuities due to the lodging holes; fretting may also play an important role in starting fatigue failures in these zones.

In the case of the second crack pattern only the zones around the rivets nearest to the crack line are liable to fatigue failures; the same consideration as for the rivets number 1 are pertinent.

For the maximum stress at the hole number 0, in the hypothesis of linear elastic behaviour the following relationship holds

$$\sigma_0 = \left[K_e + \sum_{i=1}^{n} K_{i0} (p_i/A) \right] S \qquad 1)$$

where A is the stringer reduced net section area (2); K_{i0} and K_e are the stress concentration factors at the hole number 0, due respectively to the rivet force p_i.S applied to the hole number i, and to the stress S applied at the edge of the panel; Fig. 3 shows experimental results on the stress concentration factor at the hole number 0 due to a pin force applied at the hole number 1. The curve represents the boundary of a region in the p/r, r/a plane in which K is equal to the stress concentration factor due to a force applied at large distance from the hole number 0, namely K_e.

Introducing the overload coefficient $L = 1 + \sum_{i=1}^{n} p_i/A$ $_e$ taking into account the results of Fig. 3, it can be written:

$$\sigma_0 = LK_e \left[1 + \frac{p_1}{LA} \frac{K_{10} - K_e}{K_e} \right] S = L K_E^0 S \qquad 2)$$

As it results from this formula, the global stress concentration factor K_E^0 depends generally on the crack length the ratio p_1/LA.

However if the ratios p/r and r/a are chosen in such a way that $K_{10} = K_e$, K_E results independent of the crack kength, and equal to K_e.

If the crack is expected to start from a hole number 1, taking into account the results of Fig. 3, the following relationships are pertinent

$$\sigma_1 = S(K_e L + (p_1/A)\ (K_{11} - K_e) + (p_2/A)\ (K_{21} - K_e)) = LK_E^1 S \qquad 3)$$

or for adequate values of p/r and r/a

$$\sigma_1 = SK_{11}\ (p_1/A + (K_e/K_{11})\ (L - p_1/A)) \qquad 3')$$

The stress concentration factors Ke, K_{10}, K_{11} can be obtained from the literature (7) or from suitable tests.

When the stress applied at the panel ends has a mean stress S_m and an alternating stress S_a constant in value, the stress at rivets 0 or 1 has mean and alternating values given by:

$$\sigma_m = L\ K_E\ S_m \quad ; \quad \sigma_a = L\ K_E\ S_a \qquad 3")$$

where the index 0, and 1, will be omitted in favour of the compactness of writing as they are formally inessential.

Such stresses monotonically increase with the crack length since the rivet forces, for a given applied load, also increase, Fig. 1c.

With such a kind of stress variation the Miner's rule is a well grounded approach to evaluating the fatigue endurance of a stringer in the cracked stiffened panel.

In the present case the rule can be put in the following way

$$n_0/N_0 + \int_{n_\theta}^{\bar{n}} \frac{dn}{N} = 1 \qquad 4)$$

where n_0/N_0 is the fraction of the stringer life spent before crack initiation and $\bar{n}$ is the stringer endurance. Putting $N = F(\sigma_a, \sigma_m)$ and $dl/dn = f(K_a, S_m)$ where N is the endurance corresponding to the stresses σ_a and σ_m, dl/dn the fatigue crack propagation in the sheet cover and K_a the stress intensity factor relative to the crack in the sheet cover and to the stress S_a, the Miner's rule assumes the form

$$n_0/N_0 + \int_{l_0}^{\bar{l}} \frac{dl}{f(K_a, S_m)\ F\ (\sigma_a, \sigma_m)} = 1 \qquad 4')$$

where $\bar{l}$ is the crack length in the sheet cover at which a crack starts in the stringer.

It is further supposed that the stress-endurance relationship pertinent to this phenomenon can be represented by the S-N curves relative to plain specimens of the material used in the construction of the stiffened panels. This hypothesis entails negligible influence of the fretting phenomena, a topic which has been discussed in (10).

Therefore the function F can be represented, (8), for values of N in the range $N \leq 10^7$, by:

$$N = B \left\{ \frac{\sigma_a}{1 - \left(\frac{\sigma_m}{\sigma_u}\right)^m} \right\}^{-\beta} \qquad 5)$$

where B, β, m are constants depending on the material and σ_u is the ultimate tensile stress of the material.

The effective stresses for entering in such curves are proportional to the ones given by formulae 3") through an attenuation factor ξ which generally depends on the number of cycles and assumes different values for the two zones of fatigue failures (rivet 0 and 1 respectively).

The relationship 4') can be written therefore

$$n_0/N_0 + B^\beta \int_{l_0}^{\bar{l}} \frac{(\xi L\ K_E\ S_a)^\beta}{f(K_a, S_m)\left[1 - \left(\frac{\xi L\ K_E\ S_m}{\sigma_u}\right)^m\right]^\beta}\ dl = 1 \qquad 4")$$

where the appropriate value of K_E and ξ must be used in relation to the existing crack pattern.

The relationship 4") results in the possibility of obtaining $\bar{l}$ through the K-rate relationship f and the S-N curves of the plain specimens once the rivet forces and the stress intensity factor are known as a function of the crack length. Such quantities can be obtained with the aid of the computer programs discussed in the previous section. All other quantities can be obtained from the fatigue data of the material, and ξ from fatigue tests of notched specimens.

Some simplifications can be introduced in the relationship 4"): the quantity ξ can be conservatively assumed to be unity and the mean stress σ_m can be computed in the following way:

$$\sigma_m = \sigma_y - \sigma_a$$

where σ_y is the yielding stress of the material. This position, which in based on the hypothesis that yielding takes place in small zones surrounding the rivet hole, is generally correct with reference to the usual gross stress level found in aircraft because of the combined effects of tensile residual stresses due to riveting, stress concentration effects and quick increase of the rivet forces with crack length; only at small values of the crack length this position may be incorrect, but seldom this fact can introduce not negligible errors in the integral of the formula 4").

It is therefore possible to write:

$$M = n_0/N_0 + B^{\beta} \int_{l}^{\bar{l}} \frac{(L\, K_E\, S_a)^{\beta}}{f(K_a, S_m)\, [1 - (\frac{\sigma_y - L\, K_E\, S_a}{\sigma_u})^m]^{\beta}}\, dl; \qquad 4''')$$

where the parameter M, instead of 1, has been introduced for taking into account the conservative nature of the hypothesis introduced in 4''').

The outlined approach is based on several simplifications.

The fatigue behaviour of a riveted joint, in fact, is influenced not only by the stress state as described by the formulae 2) and 3) but also by residual stresses due to riveting, secondary stress systems due to bending moments introduced by rivets, types of rivets and riveting; fretting may also play an important role in the case of slow crack propagation rate and high values of n.

All these effects are not completely taken into account in the relationship 4''') and therefore it could fail to correlate satisfactorly with the experimental data.

It is therefore opportune to tackle the problem also from another point of view to obtain an alternative formulation.

The basic hypothesis of this formulation is that the fatigue behaviour of the stringer in a cracked stiffened panel can be resembled to that of dry riveted lap joints.

According to (9) the stress-endurance relationship is negligibly influenced by the mean stress, and can be put, for the range $N \leq 3.10^6$, in the form, (10):

$$N = B_{\alpha}\, \bar{S}_a^{-\alpha} \qquad 5')$$

where $\bar{S}_a$ is the alternating stress applied to the lap joint.

In the case of the stringer the stress to be used to enter in the formula 5') can be obtained from the following formula

$$\bar{S}_a = S_a\, L\, H \qquad 6)$$

where H is a parameter to be determined experimentally for taking into account possible differences between the stringer and the la joint as far as fatigue notch factors are concerned. Taking into account the formulae 5') 6') on the basis of the above said hypotheses, the Miner's rule can be written

$$\int_{l_0}^{\bar{l}} \frac{dl}{f(K_a, S_m)\, L^{-\alpha}} = (1 - \frac{n_0}{N_0})\, (H\, S_a)^{-\alpha} B_{\alpha} \qquad 4^{IV})$$

The evaluation of the proposed approaches will be performed in the following through a computation of the quantities M and H on the basis of a set of experimental data on the stringer fatigue endurance.

EXPERIMENTAL RESEARCH PROGRAM

A test program was performed with the following main purposes:

- measurement of crack growth rate in stiffened and unstiffened panels;
- measurement of the crack length $\bar{l}$ in the sheet cover at which a stringer starts to crack;
- measurement of the overload coefficient L and rivet forces in cracked stiffened panels.

To this end fatigue and static tests were performed on a large set of stiffened and unstiffened panels (more than 90 specimens) differing in geometric shape, in dimensions, in riveting and load levels. All the detailed information necessary to identify each panel is given in references (2, 3, 10). In broad outline, the panels were constructed of 2024-T3 and 7075-T6 aluminum alloys. Different types of stiffeners were used: single strip stringers, double symmetric strip stringers and Z, C formed section stringers. All the stringers were hand riveted: round head as well as countersunk rivets were used.

The formed section stringers are well representative of the current constructional practice; the rivet force offset with respect to the centroidal axis give rise to supplementary bending stresses which in the present approach are taken into account by the reduced area concept; local bending stresses (linearly varying in the thickness) may also be present in the neighbourhood of rivet holes owing to the bending moments acted by each rivet.

The double symmetric strip stringer has a stress distribution, constant in the thickness, which, on the whole, conform to the one adopted in the mathematical model relevant to cracked stiffened panels stress state computation.

The single strip stringer is lastly suitable to emphasize the role of the rivet bending moments on the stringer fatigue endurance and the stringer-sheet junction flexibility.

TEST EQUIPMENT AND PROCEDURE

All the panels were tested utilizing two axial load fatigue machines (3). A 60.000 Kg. machine was utilized for testing the Z section stringer stiffened panels and the larger unstiffened sheets; a 20.000 Kg. machine was used for the other panels. The loading was applied to the specimen fixture through hydraulic jacks and was controlled through loading cells monitoring the load with an oscilloscope in fatigue tests, with a x, y recorder in

the static tests.

The specimen fixture was attained by sandwiching the panel ends between two thick plates which were bolted and uniformly torqued to evenly distribute the clamping load. The panel ends were provided with clearance holes for the clamping bolts and with rectangular blocks, placed among the stringers, to obtain an even surface for the clamping plates. Adjustable plates were, further, provided between the grips and the panel to center the loading through the centroid of the uncracked panel.

The load applied by the clamping plates to each block was transferred by suitable devices partly to the sheet and partly to the stringers; in such a way the rivets in the zone of the clamping are practically unloaded so that unwanted fatigue failures in the clamping zones were eliminated.

In all the fatigue tests the panels were subjected to axial cyclic loading of constant amplitude.

The maximum cyclic value of the gross stress was varied in the range $5 \div 12$ Kg/mm^2, the stress ratio R in the range 0.2 - 0.6.

In each panel the crack was started through a crack raiser made with a saw cut placed in the panel center; from this cut the crack propagated approximately perpendicularly to the stringer axes. The saw cut were made to obtain the two kinds of crack pattern previously discussed.

The number of cycles required for the fatigue crack to reach various lengths as well as the crack length in the sheet at which a stringer started to crack were recorded. To obtain sufficiently accurate readings of the crack lengths, accurately spaced parallel grids were placed on the panel sheet, perpendicular to the crack propagation direction.

In the static tests the rivet forces were obtained as difference of the axial forces in the stringer cross section ahead and behind each involved rivet. The axial forces could be computed on the basis of strain measurements performed through a suitable number of strain gages placed in each involved section; details on such a procedure are given in ref. (2).

ANALYSIS OF THE RESULTS ON THE STRUCTURAL BEHAVIOUR OF CRACKED STIFFENED PANELS

All the detailed theoretical and experimental results on the cracked stiffened panels were reported in references (2, 3, 10, 11). In this paper only the main results will be summarized. The discussion of the results follows three main lines. At first the theoretical and experimental results on the rivet forces and the stress intensity factor are compared to draw some conclusions on the accuracy of the proposed theoretical approach as well as to obtain some insight into the fastener behaviour. Next some typical K-rate relationships of stiffened panels obtained from data on crack growth rate and K values from different methods are discussed; such a comparison allows to deduce some conclusions on the K-rate relationship approach as far as its application to stiffened structures is concerned. Lastly the question of the stringer fatigue endurance is considered and the validity of the proposed approaches is discussed against the stringer fatigue data.

RIVET FORCES AND STRESS INTENSITY FACTOR

A set of static tests were performed to measure the rivet forces in stiffened panels whose geometric ratios and riveting were chosen in accordance with the constructional practice; the main purposes of these tests were to obtain information on the rivet flexibility and data to compute accurately the stress intensity factor. Details of the test procedures and results are given in (2, 11). Here the main conclusions will be summarized.

Fig. 4 shows the overload coefficient L and the rivet forces P_i as a function of the crack length for a double strip stringer stiffened panel. The experimental data are shown together with the theoretical ones relative to different rivet flexibilities.

The theoretical results, based on rigid fastener approach seem to furnish a good approximation of the actual behaviour of the cracked panel at least as far as L and the more loaded rivet are concerned. This conclusion is also strengthened by comparing the results of Fig. 5 which shows the values of the coefficient C, obtained with both the rigid fastener approach and the one based on the measured rivet forces. As these results are well representative of the behaviour of the double strip stringer stiffened panels tested in the course of the present investigation, the conclusion may be drawn that the flexibility effects are negligible with this kind of stringer arrangement, at least in the range of geometry and riveting investigated.

Figures 6 and 7 are the analogues of the two previous ones but relative to a single strip stringer stiffened panel. The flexibility effects are not negligible and they seem to depend principally on the stringer sheet arrangement which implies bending moments on the rivets are present. In other words the flexibility of the rivet would seem to depend prevailingly on the rotation of the rivet in the hole enlarged by the rivet axial forces.

Fig. 8 shows analogous results for the same type of panel but fastened with countersunk rivets.

The flexibility effects are even more evident than in the previous case.

No systematic tests on the rivet forces have been performed in the case of $\mathcal{I}$ and C stringers; the measurement of axial forces with such a kind of cross section requires a great number of strain gages so that tests are costly and time consuming. Preliminary tests aimed at finding the minimum significant number of strain gages per section seem to indicate that not negligible flexibility effects are present also with these panel configurations.

The previous preliminary conclusions on the rivet forces and rivet flexibility are now object of a further experimental investigation.

The principal effort of this further research plan aims at obtaining a quantitative

assessment of the rivet flexibility. A first step in the research is devoted to ascertain if the rivet flexibility parameter f is a statistic or deterministic quantity. Fig. 9 summarizes the results obtained with three stiffened panels of the same geometry. It can be observed that experimental data do not conform to an unique set of equal theoretical ρ curves; also the same panel rivets shows different flexibility.

These differences, even if they seem not very significant in respect of global results (coefficients C and L), demonstrated the difficulty of characterizing in the computational approach the fastener system through an unique parameter.

In particular all the random effects due to riveting (interference, local yelding, friction between stringer and sheet) seem to have not negligible influence on the rivet behaviour.

FATIGUE CRACK PROPAGATION

A set of 70 fatigue tests were performed to measure the crack growth in stiffened panels. For each panel test the crack growth rate was plotted versus the stress intensity factor computed on the basis of the rigid fastener approach; when possible the K-rate relationship was also constructed with the K value obtained through the experimental data on the rivet forces. All the results are reported in detail in (2, 3, 11). Some significant results are presented in the following.

The set of figures 10 is relative to double strip stringer stiffened panels made of 7075-T6.

In each figure on the left dl/dn and K are plotted versus l; here K was computed on the basis of the measured rivet forces but it differs negligibly from the rigid fastener approach values. On the right of the figure the K-rate relationship is shown together with the K-rate relationship of an unstiffened sheet.

The results of figures 10 indicate a satisfactory agreement in the trends of the curves dl/dn versus l and K versus l; in particular the points of zero slope in the two curves are approximately coinciding, in accordance with the basic hypothesis that the stress intensity factor is the quantity which controls the fatigue crack growth in a structure.

Moreover when the results are plotted in the form of K-rate relationships, the data relative to the stiffened panels fall in a narrow band around the K-rate curve of the unstiffened sheet.

A more detailed examination of such data indicates the presence of loops in the K-rate relationships of the stiffened panels; the presence of such loops, which, at first sight, might be considered an incorrected trend, is clearly linked to the non-monotonic behaviour of K and dl/dn as functions of the crack length, and depends on possible small errors in K evaluation, particularly in the neighbourhoods of the points of zero slope, and on the scatter inherent to the fatigue crack propagation phenomenon.

Such loops, moreover, are seldom important in respect of the prediction of the crack growth rate in stiffened panels through a K-rate relationship based on data for unstiffened panels.

Figures 11 are relative to single strip stringer stiffener panels; here two curves of K versus crack length are shown: one based on K as obtained from the rigid fastener approach, the other on the K values deduced from the measured rivet forces.

As it results the rigid rivet K value gives unrealistic values of dl/dn once compared with crack growth rate in an unstiffened sheet; also the pattern of the K-rate relationship is incorrect.

On the contrary when reference to the "experimental" K value is made the K-rate relationship assumes correct values.

Fig. 12 and 13 furnish the K-rate relationships based on the "rigid rivet" K value for two typical panels: a single strip stringer stiffened panel with countersunk rivets and a $\mathcal{I}$ section stringer stiffened panel.

In the first case strong effects of rivet flexibility are present in accordance with the results of Fig. 8. The results of Fig. 13 which are well representative of all the other data obtained with panels of similar geometry, indicate that flexibility effects are present in accordance with very preliminary experimental data on the rivet force obtained in this case.

The following comments seem to be pertinent as a general conclusion of this stage of the research relative to the fatigue growth in the sheet cover of stiffened panels.

All the results clearly indicate that the K-rate relationship predicts the crack growth rate in stiffened panels with a level of accuracy satisfactory in relation to the statistical nature of the phenomenon, when the stress intensity factor is correctly evaluated.

This conclusion is worthwhile being outlined because of the following considerations: the results are important from a basic point of view since they further demostrate the soundness of the K-rate relationship approach, particularly significant because of thearather involved structural behaviour of the specimens used in the present investigation.

Such a conclusion is also important from a design point of view because all the data from unstiffened panel tests can be transferred to the stiffened structures with the aid of accurate values of the stress intensity factor.

At this stage of the research, however, no definitive conclusion can be drawn on the accuracy of the theoretical method to compute the stress intensity factor; in particular a better understanding is required of the phenomena involved with the rivet flexibility and their role in the theoretical computation methods.

STRINGER FATIGUE ENDURANCE

All the results from stiffened panels fatigue tests, where stringer fatigue failures took place, were utilized to evaluate the proposed approach to obtain $\bar{I}$. The detailed results on this topic obtained with 59 stiffened panel tests are given in (3, 10).

In broad outline the experimental values of 1, dl/dn, and the theoretical values of L and p_i were used to obtain H(the "lap joints" approach, formula 4) and M (the "stress concentration factor" approach, formula 4"'). When strong effects due to rivet flexibility were present, the experimental values of L and P_i were measured and used in the computation procedure. Two basic crack patterns were obtained in the tests, a crack crossing the junction line at a rivet hole (type I), a crack crossing the junction line in the middle between two rivets (type II).

In the following the main conclusions of such an investigation are summarized.

- "Lap - Joints" approach.

The results in terms of H coefficient obtained with this approach were analized to emphasize the influence of the main variables taken into account which are: the crack pattern, the stringer type, the rivet type, the material.

As it results from its definition H is a measure of departure of the actual stringer fatigue behaviour from that of the dry riveted lap joints; $H < 1$ indicating that the assumed S-N curve is too conservative, the opposite being true when $H > 1$.

H, furthermore, is a random variable as it is a measure of stringer fatigue endurance; therefore H lends itself to comparing the influences of the different variables only on a statistical basis. As a consequence each set of homogeneous data on H was subjected to a statistical treatment on the hypothesis that log H conforms to an extremal probability distribution. The results of such a treatment are shown in the figures from 14a to 15.

Fig. 14a shows the influence of the crack pattern which in turn influences the crack starting point in the stringer. With a crack pattern of type I systematically the crack started at the rivet number 0; this result is rather surprising since the mean loads at the two stringer cross sections corresponding respectively to the rivet number 1 and number 0 ought to be same; but a higher stress concentration is present at the rivet number 1. A possible explanation of this fatigue behaviour might be found in the presence of friction forces between sheet and stringer due to the riveting; owing to such forces the mean load should be lower at the rivet 1 than the one at the 0 rivet. Crack at the rivet number 1 could be, obviously, obtained with a crack pattern of the type II. The distributions of Fig. 14a differ above all in slope, the data relative to the rivet number 1 (lower slope) being a little more dispersed than the others.

Fig. 14b shows the influence of single and double strip stringer stiffened panels on the H distribution; only minor differences are present between the two distributions showing that the secondary bending stresses which are likely to take place in the single stripidom stringer are seldom significant.

Fig. 14c shows the influence of the rivet type: round head and countersunk type rivets are compared: no particular effect is apparent on H. In fact as far as the stringer is concerned the hole geometry is the same as well as the load application from the rivet to the stringer. Lastly Fig. 14d allows one to compare the effect of materials on H. This plot shows that 7075-T6 is more liable to fatigue failure than 2024-T3 as indicated by the higher values of H.

The figures from 14a to 14d have shown that, apart from the material, all the other variables seem to have negligible influence on the phenomenon under investigation; therefore it has been supposed that all the data relevant to a material belong to the same statistical population. Fig. 15 shows the results of such an hypothesis with respect to the material 2024-T3; the straight line has been drawn through 56 values of H which contain also the data relevant to formed stringers (zed and channel stringer). A characteristic value $H_m = 1.42$ and a median value $H_{50\%} = 1{,}32$, are found; the dispersion parameter b amounts to 14,1.

As a particular conclusion it can be observed that the reduced area concept works well since the data of formed stiffeners are in agreement with all the other data.

From the results of Fig. 15 the general conclusion can be drawn that proposed approach based on a S-N curve of the dry riveted lap joints which entails negligible influence of the mean load on fatigue works satisfactorily. In fact data obtained from different specimens but treated on the basis of the proposed approach give values of H which belong to the same statistical population.

As general conclusion relevant to this approach it can be said that the data obtained in the present investigation form an adequate basis on which the stringer fatigue endurance evaluation can be confidently based.

- Stress Concentration Factor Approach.

The values of M relevant to the crack pattern of type I, were treated on the basis of the extremal value probability distribution and the corresponding results are shown in the curve A of Fig. 16. Two orders of comments can be made as far as these results are concerned.

A first comment stems from the order of magnitude of M which is too low when compared with the expected value $M = 1$. A possible explanation of such low values is to be found in the chosen type of the $S_a - S_m - N$ curves which apply to specimens with smooth machined or polished surfaces; it is however well known that the type and the condition of the surface where cracks start are important factors in establishing the actual fatigue strength of specimens and strong reductions of strength are to be expected when there is a departure from polished surface conditions. In the present investigation the rivet hole was machined with drill and therefore severe departures from the polished surface conditions are expected to be present. The curves B and C of Fig. 17 were obtained on the assumption of a reduction of 20% and 25% respectively of the mean fatigue strength with respect to the values relevant to the polished condition, figures that are likely to be consistent with the actual surface conditions of the crack starting zones. As it results from the examination of such curves the M values are in the expected range.

Another point which deserves some attention in discussing the influence on M of the $S_a - S_m - N$ curve is the value of m, a parameter characterizing the shape of the semi-range/mean stress diagram for the material; it is not possible to ascribe a unique value of m a particular group of materials. Typical ranges of m values which can arise in practice are the following ones:

$m = 1.2 \div 1.8$ for naturally aged Al-Cu-Mg alloy
$m = 1.0 \div 1.4$ for artificially aged Al-Zn-Mg alloy

In the present investigation m = 1.2 was assumed; it respresents a mean value for the 7075-T6 alloy, but a lower bound for the 2024-T3 alloy. It is therefore useful to assess the influence of a variation in m; in the case of 2024-T3 an increase in m from 1.2 to 1.4 implies a decrease in M, in the mean, of 50%.

A second comment on the results shown in Fig. 17 is relevant to the existence of a set of data which do not belong to the expected distribution. A possible explanation of this anomaly is to be found in an incorrect evaluation of the L coefficient when the crack length is sufficiently long. In such ranges plastic deformations due to high bearing stresses are likely to take place around some rivet holes; in consequence of above the ability of the stringer in relieving the load from the cracked sheet is reduced and L assumes values lower than the ones given by the elastic analysis. As a reduction in L implies a reduction in M, since all data of the anomalus set are characterized by relatively high values of $\bar{l}$, it is likely that L computed on the basis of an elastic approach was overestimated in the range of high values of crack length, giving exceedingly high values of M.

Another set of data on M relevant to a crack pattern of type II was obtained. No statistical evaluation was done of these data as the M values are too dispersed indicating the existence of some fault in the approach. A possible explanation of this fault may be found in the global stress concentration factor to be used in evaluating M, that has the following form:

$$K_E = K_e \left[1 + \frac{p_1 A}{L} \frac{K_{II} - K_e}{K_e}\right]$$

The evaluation of K_E demands an accurate knowledge of the ratio p_1/L; this is a relative easy task when the stress state is elastic; theoretical as well as experimental methods can be used to obtain an accurate evaluation of such a ratio.

However when the bearing stress due to the load σp_1 exceeds some critical value, a redistribution of the load among the different rivets takes place with a progressive decrease of the ratio p_1/L with respect to the elastic value, with the increase of the crack length.

Further the decrease in p_1 is much greater than the decrease in L. As the value of M is sufficiently sensitive to a change in p_1/L, several M values, obtained on the basis of an elastic approach are incorrect.

As general comments to the method based on the stress concentration it can be observed that it is very sensitive to the accuracy with which such quantities as L and p_1 are determined. Evaluating such quantities on the basis of the elastic approach not negligible errors can be done.

It also requires a better characterization of the material in term of the m parameter and decrease in fatigue strength due to the actual surface conditions.

It is however worthwhile to be further investigated as it could promote a deeper understanding of the phenomenon under investigation.

MINIMUM WEIGHT DESIGN OF FAIL-SAFE STIFFENED PANELS

In the fail-safe design of the wing lower surface structures several constraints must be considered which can be summarized as it follows:

a) the damaged structure must sustain the fail-safe load for an assigned inspection interval;
b) an assigned damage (the largest crack or flaw missed in the last inspection) has to be allowed at the beginning of the inspection interval;
c) the growth of the initial damage under a given load spectrum must be allowed in assessing the residual strength of the structure and its margin of safety in respect of the fail-safe load;
d) the structure must sustain the compression loads (limit and ultimate) due to negative load factor flight conditions.

Compliance with the positive limit and ultimate loads requirements, aeroelastic requirements, crack free life requirements can give rise to further structural constraints. The purpose of the investigation carried out at the Institute of Aeronautics of Pisa University is to study stiffened panels of minimum weight taking into account essentially the constraints stated at the points a) b) c) d). The results of such an investigation are useful, it is felt, to obtain a better insight in the design problem of the wing lower surface structures and more generally of stiffened structures which demand fail-safe design.

The minimum weight approach was based on a modified penalty function methods (12). Following such an approach the absolute minimum of the function

$$\bar{W}_j = W(X) + r_j \sum_{i=1}^{n} g_i^{-1}(X)$$

must be found.

W is weight of the structure, g_i are functions that represent the constraints previously discussed, X is the vector of the state variables which individuate the structure configuration; r_y is the jth value of the penalty parameter.

As far as the constraints considered at the point d) are concerned, the g function is of the following type

$$g_i = 1 - \frac{\alpha_i Nx}{\bar{t}\sigma_b}$$

where Nx is the load per unit legth corresponding to the one g flight condition; α_i is a parameter chosen in such a way to obtain the load per unit length in the limit or ultimate load conditions; $\bar{t}$ is the mean thickness of the panel; σ_b is a buckling or crippling stress

In particular σ_b may assume the value of the local buckling stress, or the bending-torsion stringer-panel buckling stress when α_i assumes the value α_L appropriate to the limit load (non buckling design approach); the value given by the Johnson parabola is chosen when α_i assumes the value α_u pertinent to the ultimate load conditions.

All the constraint states at the points a) b) c) give rise to an unique g function of the type

$$g_i = 1 - \frac{T}{E}$$

where T is the inspection interval and E is the endurance of the structure in the conditions stated at points a) b) c). More in detail the following functional relationship is pertinent

$$E = E\ (X,\ l_o,\ \Delta Nx,\ \alpha_{FS}\ Nx)$$

where l_o is the initial damage, ΔNx is a constant amplitude fatigue loading which produces the same damage of the load spectrum, and $\alpha_{FS}Nx$ is the fail-safe load per unit length.

The computation procedure for obtaining E is the following: for a given X, starting from the initial damage l_o the growth of the crack in the sheet-cover is obtained through the Forman formula; the stringer fatigue endurance is computed with the "lap joints" approach; K and L are obtained with the Poe approach taking into account the actual geometry of the cracked structure; for each level of damage the residual strength is obtained through the usual fracture mechanics approach and the margin of safety with respect to $\alpha_{FS}Nx$ is obtained; the endurance E is obtained when this margin assumes a prescribed value.

Other constraints, which take into account upper or lower bounds on geometric dimensions, compliance with limit and ultimate loads in tension can be easily taken into account adding other g_i functions.

The detail of the numerical method and the accurate definitions of all the involved g_i functions are given in (13). Some of the results discussed in this report are shown in Fig. 17, from which the influence of the fail-safe constants on minimum weight can be appreciated.

CONCLUSIONS

A research has been carried out at the Institute of Aeronautics of Pisa pursuing the following main objectives:

- achievement of methodologies to compute the crack growth in stiffened structures;
- development of design methodologies for minimum weight fail-safe structures.

As far as the first point is concerned the main conclusions are the following ones.

- The crack growth in the sheet cover of a stiffened structure can be predicted with a good level of accuracy through the K-rate relationship of the involved material when the stress intensity factor is correctly evaluated.

  Current theoretical approaches for computing K furnish adequate results only when the fasteners behave as rigid, a situation that seems to be approached in the double strip stringer configuration.

  When strong flexibility effects are present (single strip stringer configuration, countersunk rivets) the theoretical approaches furnish unrealistic values of the stress intensity factor also because of the difficulty of introducing the actual value of the fastener flexibility in the theoretical approach.

  Researches on this question are in progress at the Institute of Aeronautics of Pisa to obtain a deeper insight on the behaviour of rivets in cracked stiffened structures.
- The statistical analysis of the data on the stringer fatigue endurance demonstrates that the "lap-joints" approach, developed in the course of the present investigation, forms an adequate basis on which the stringer fatigue endurance and its correlation with the crack length in the sheet cover can be confidently based.

  On the contrary the stress concentration approach needs, at present further investigations.
- The problem of designing minimum weight panels taking into account the fail-safe requirements has been succesfully faced through a computer program based on the penalty function method, embodying in the mathematical model results drawn from the present investigation on the stringer fatigue endurance.

REFERENCES

1 - LAZZARINO L., SALVETTI A. - A Theoretical and Experimental Research on the Fatigue Behaviour of Reinforced Shells.
ICAS Paper 70-35.

2 - SALVETTI A., FREDIANI A., GRASSI E., ROSSI F. - Theoretical and Experimental Research of the Fatigue Crack Propagation in Stiffened Panels. An Evaluation of the Paris Theory.
European Research Office Report, Contract DAJA 37-73-C-2881, London NW.1, England.

3 - SALVETTI A., FREDIANI A., GRASSI E. - Theoretical and Experimental Research on the Fatigue Behaviour of Cracked Stiffened Panels.
European Research Office Report, Contract DAJA 37-72-C-1783, London W.1 England.

4 - ROSSI F., DEL PUGLIA A. - Metodi di calcolo per lo studio di strutture irrigidite.
Paper n. 28, Istituto di Aeronautica, Università di Pisa.

5 - DEL PUGLIA A. - L'effetto degli irrigidimenti rivettati sul fattore d'intensità dello sforzo in una lamiera piana tesa e fessurata.
Paper n. 40, Istituto di Meccanica Applicata e Costruzione di Macchine, Università di Pisa.

6 - POE C.C.Jr. - The Effect of Riveted and Uniformly spaced Stringers on the Stress Intensity Factor of a Cracked Sheet.
M.S. Thesis, Virginia Polytechnic Institute, 1969.

7 - R.A.S. Data Sheets: Fatigue 65004-69020.

8 - R.A.S. Data Sheets: Fatigue E.05.02 and Fatigue E.07.03.

9 - HEYWOOD R.B. - Designing Against Fatigue.
Chapman and Hall LTD 1962, London.

10 - SALVETTI A., FREDIANI A., GRASSI E. - Fatigue Behaviour of Stringer in Stiffened Panels.
European Research Office Report, DA-ERO-124-74-G0042. London NW. 1.

11 - GRASSI E. - Researches on the Fatigue Crack Propagation in Stiffened Panels.
Istituto di Aeronautica, Università di Pisa. In preparation.

12 - CAVALLINI G., PANATTONI L. - Un metodo di calcolo per il progetto automatico di strutture di minimo peso.
Atti dell'Istituto di Aeronautica, Università di Pisa.

13 - CAVALLINI G. - Minimum Weight Design of Stiffened Panels With Fail-Safe and Buckling Constraints.
Istituto di Aeronautica, Università di Pisa. In preparation.

ACKNOWLEDGEMENTS

The author wishes to thank Ing. E. Grassi and Ing. A. Frediani for their excellent work in data reduction and friendly collaboration in report preparation.

The work was sponsored in part by the Unites States Army through its European Research Office and in part by the Italian National Research Council. The author wishes to express his thanks for this support.

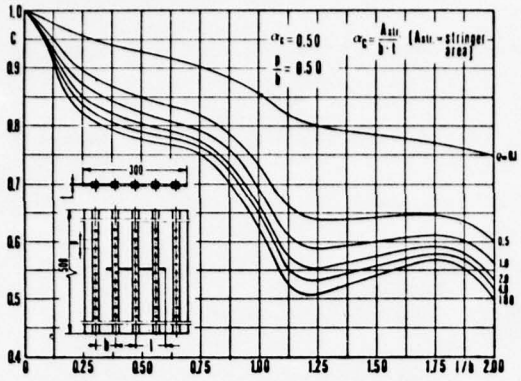

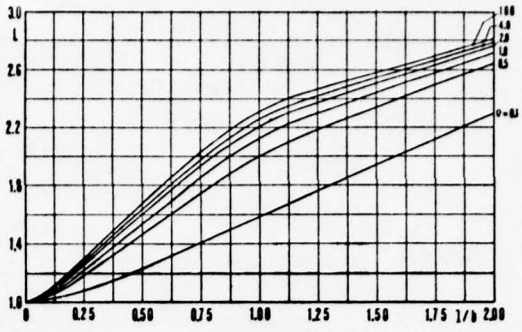

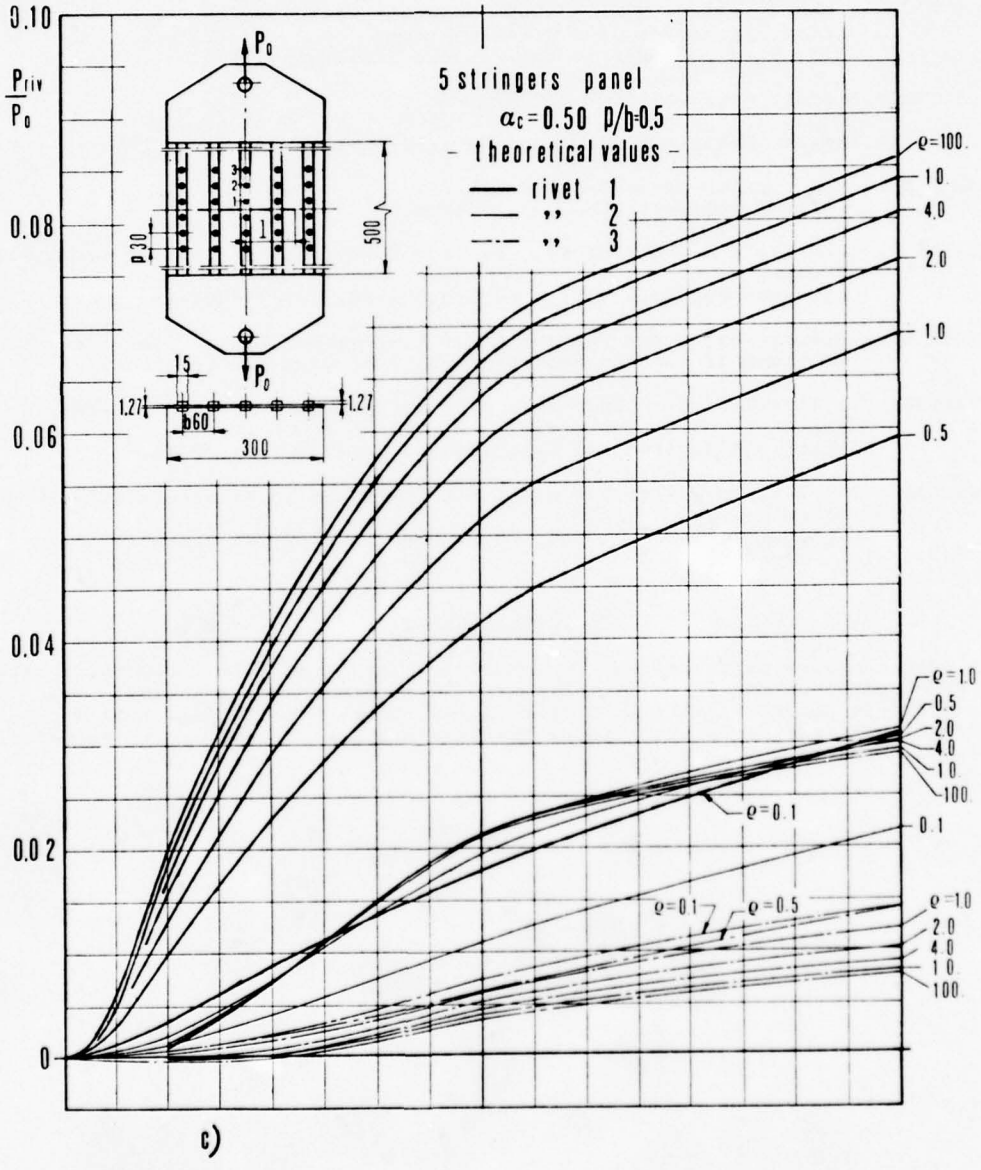

Fig. 1 - C (Fig. a), L (Fig. b), and rivet forces (Fig. c) as functions of the crack length for different rivet flexibility values (Finite Element approach).

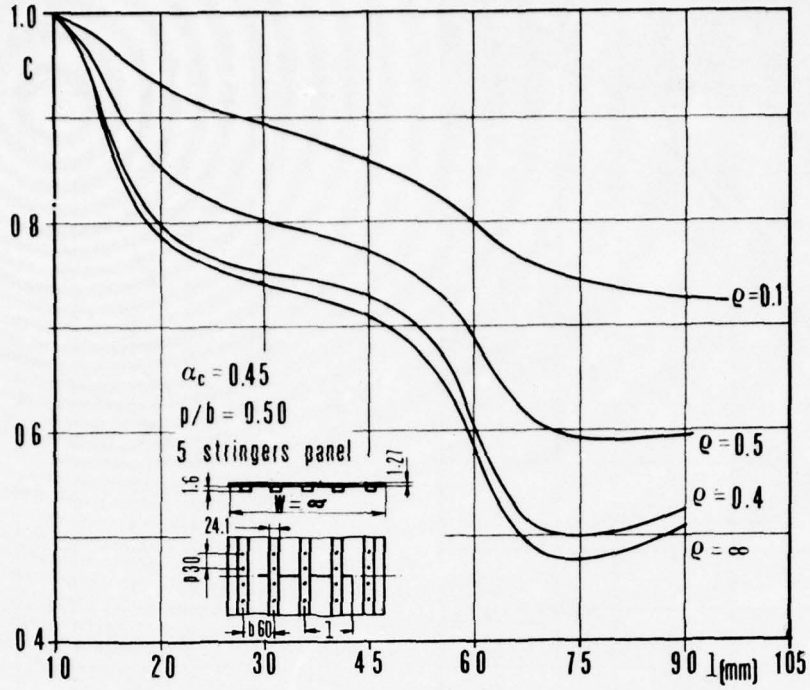

Fig. 2 - C versus crack length and rivet flexibility (Poe approach).

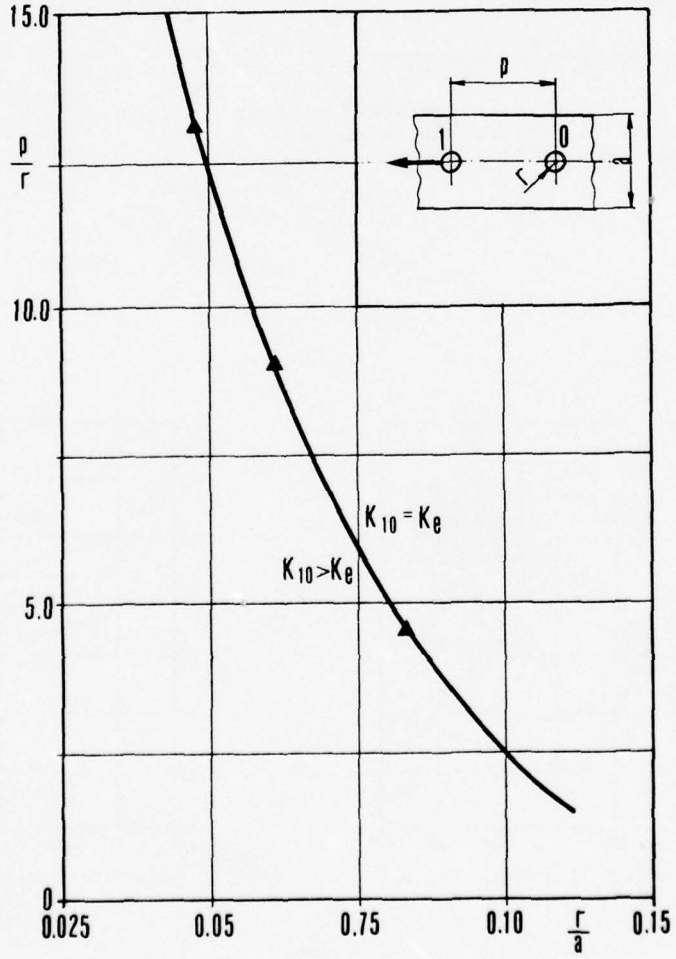

Fig. 3 - Experimental results on K_{10}.

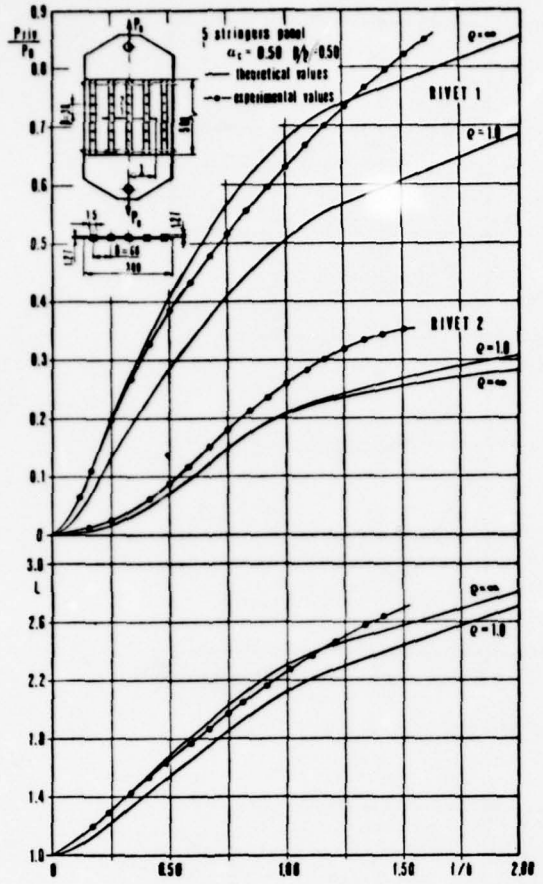

Fig. 4 - L and rivet forces versus crack length for a double strip stringer stiffened panels.

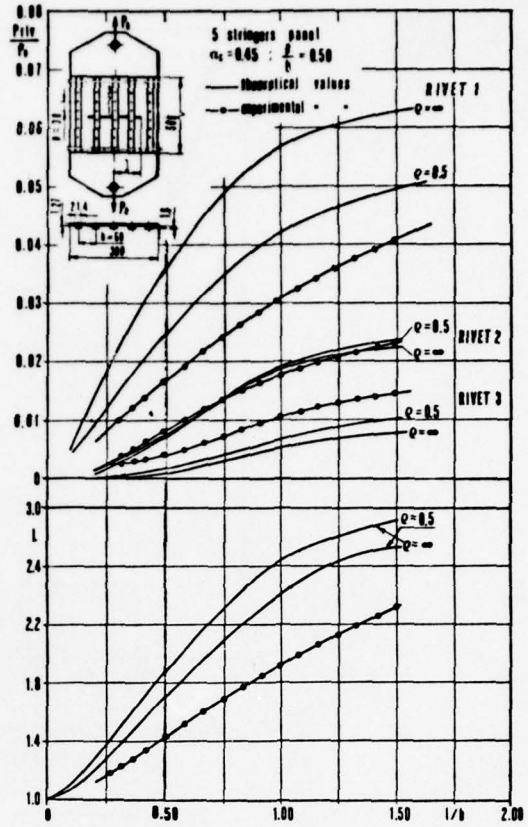

Fig. 6 - L and rivet forces versus crack length for a single strip stringer stiffened panel (round head rivets).

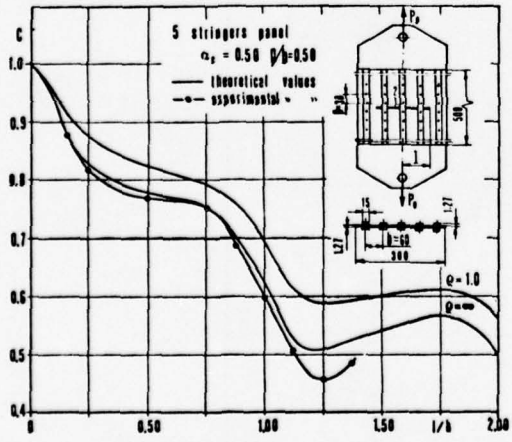

Fig. 5 - C versus crack length for a double strip stringer Stiffened panel.

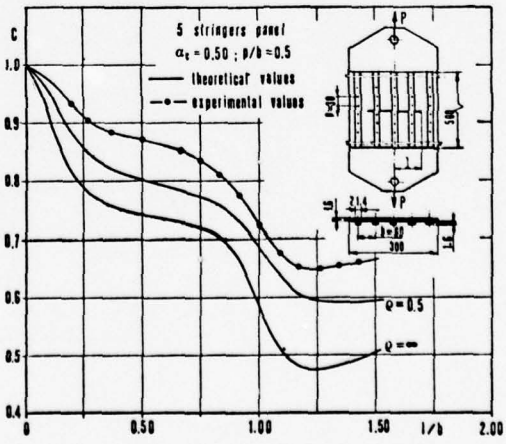

Fig. 7 - C coefficient versus crack length for a single strip stringer stiffened panel (round head rivets).

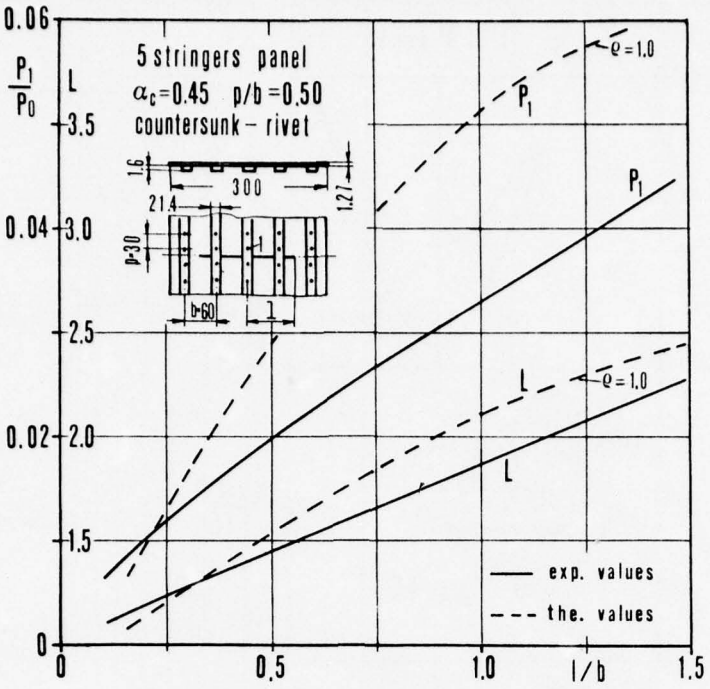

Fig. 8 - L and p_1 as a function of the crack length; experimental and theoretical values.

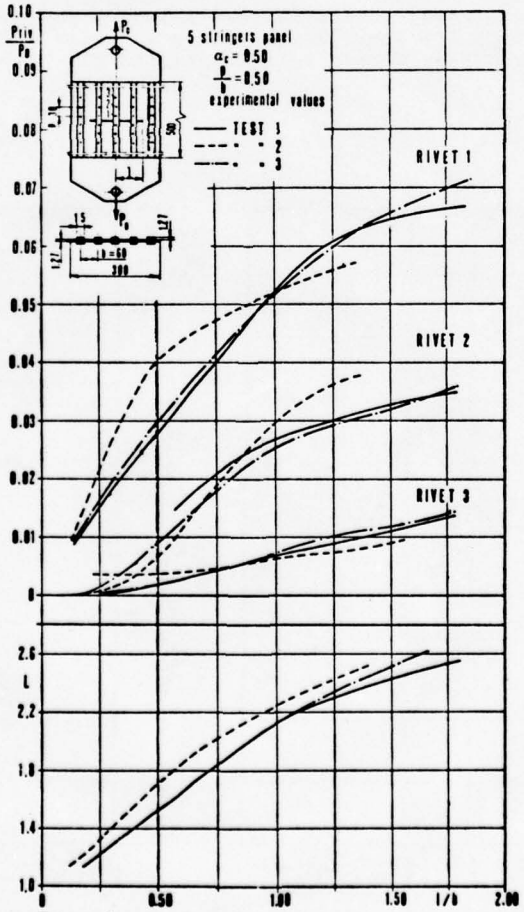

Fig. 9 - Experimental values of rivet forces and overloading coefficient L in three stiffened panels of the same geometry.

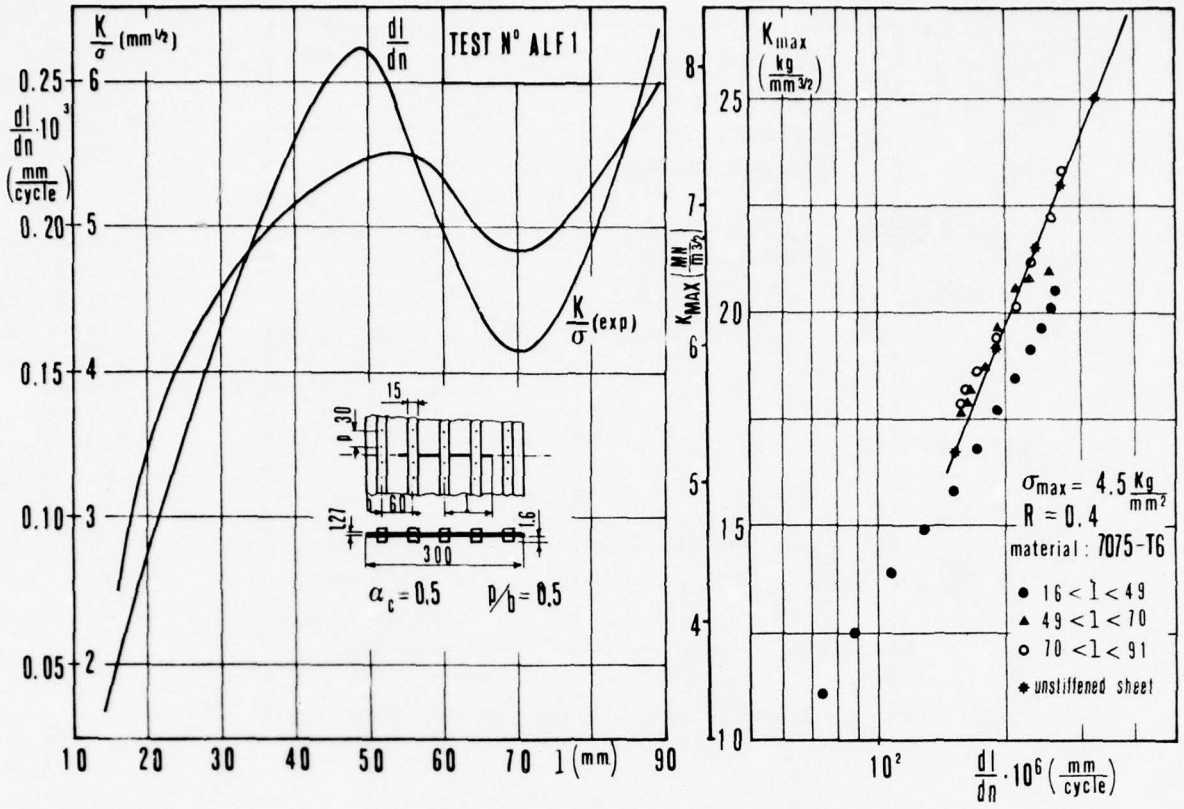

Fig. 10 - Crack growth rate, stress intensity factor per unit stress and K-rate relationships for four double strip stringer stiffened panels. Unstiffened sheet K-rate relationship is also shown for comparison purpose.

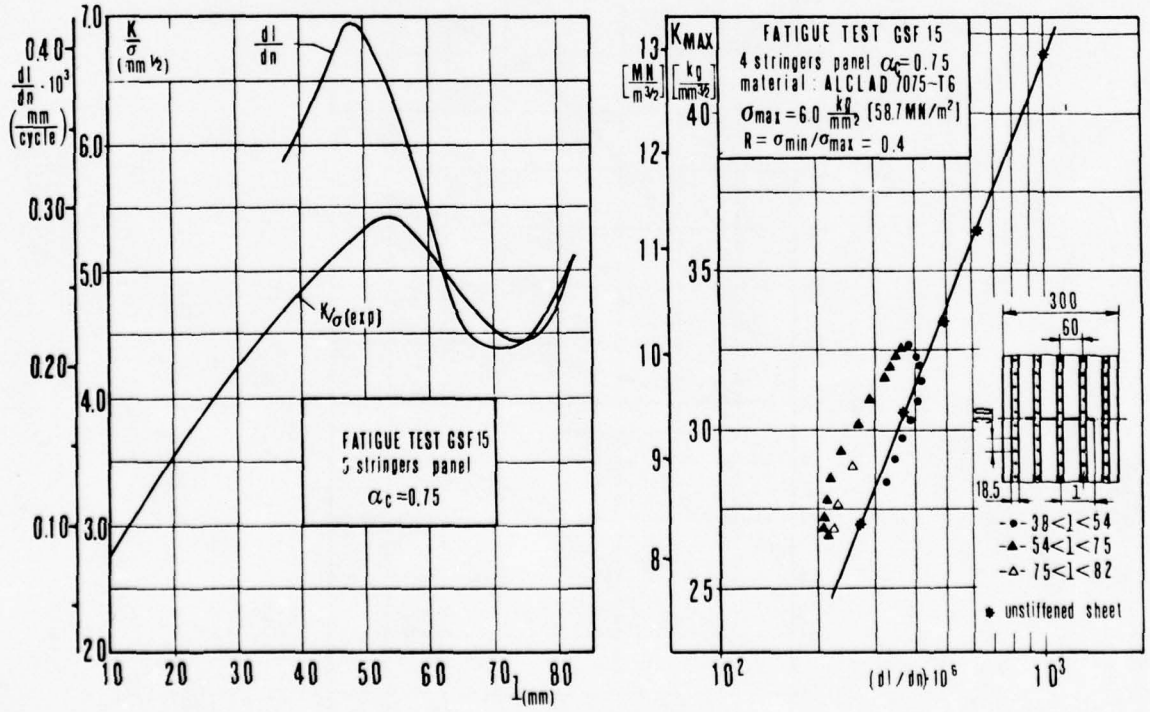

Fig. 10 - Continued.

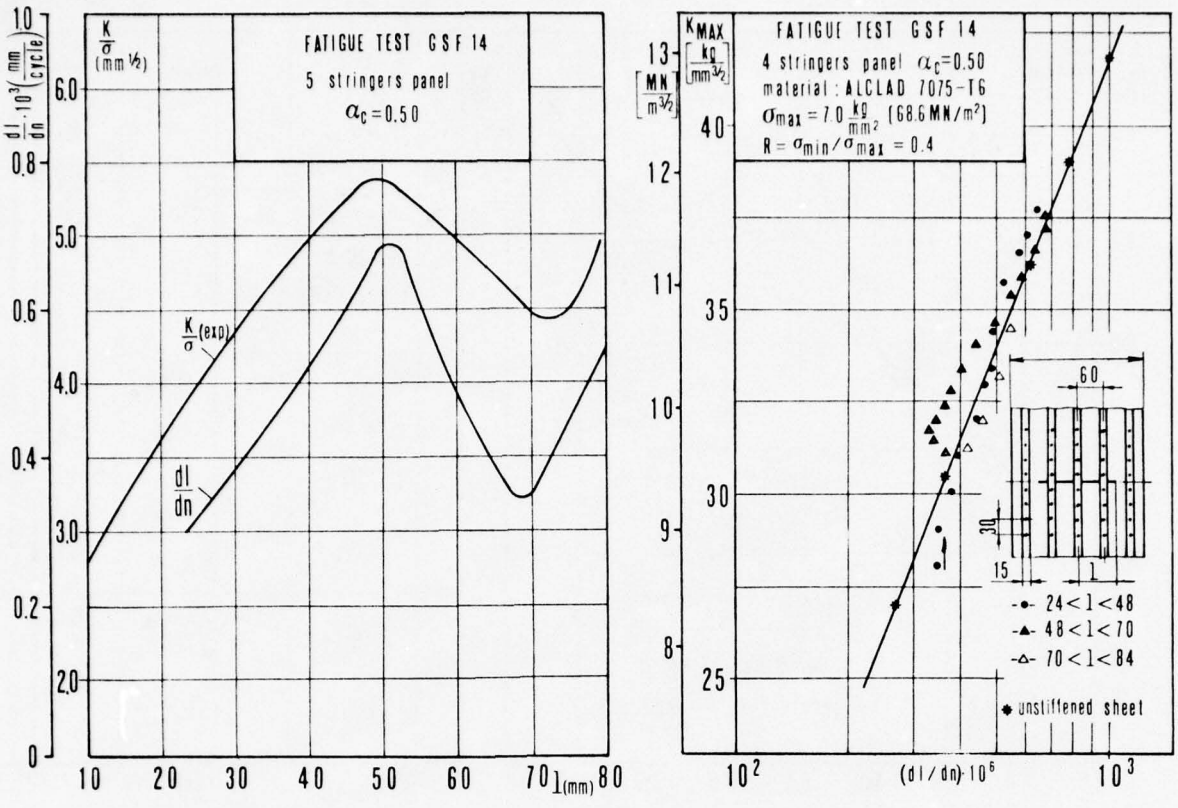

Fig. 10 - Continued.

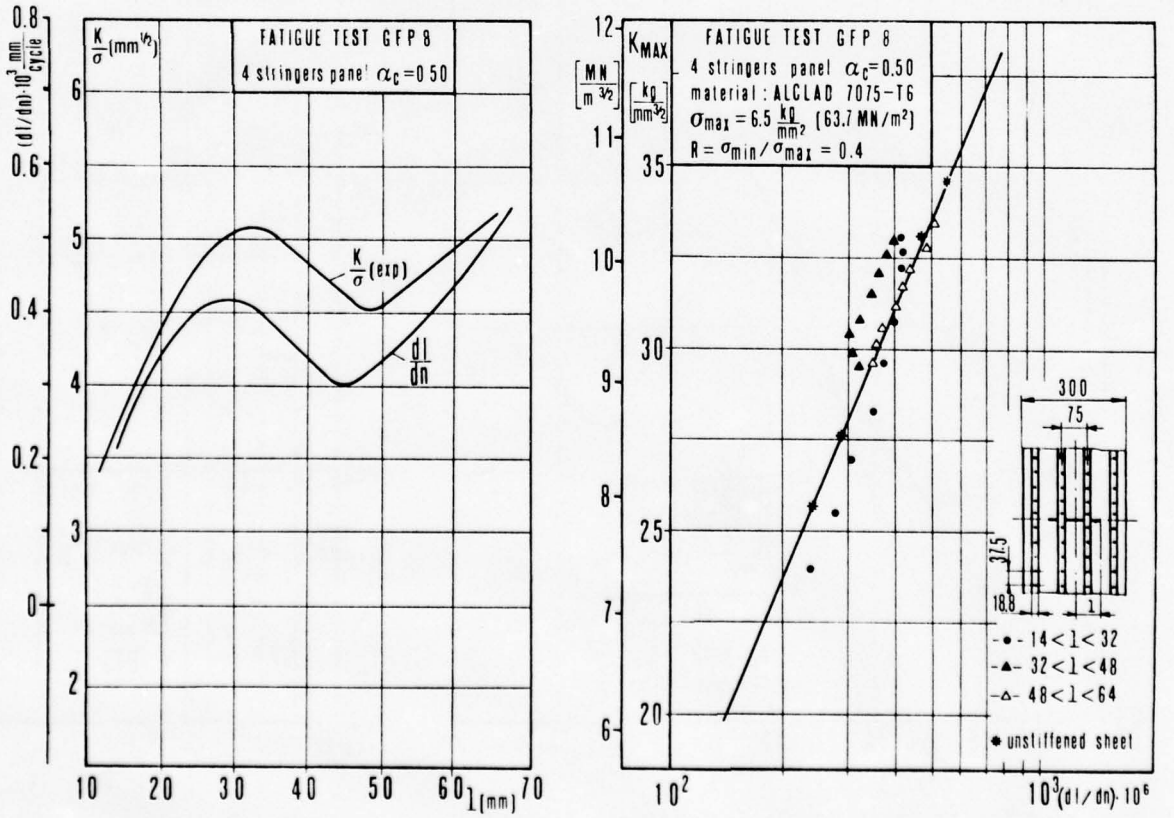

Fig. 10 - Continued.

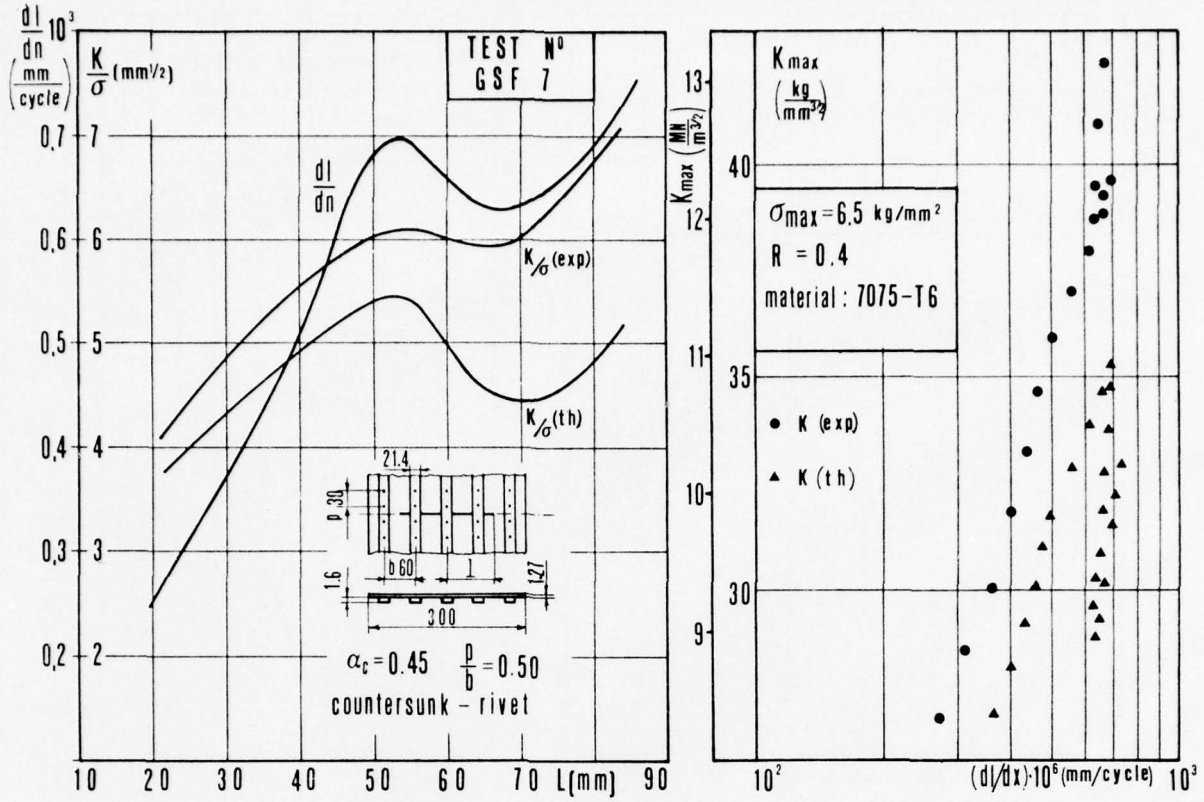

Fig. 11 - K-rate relationships for a single strip stringer stiffened panel;both rigid rivet approach (th.) and measured forces approach (exp.) has been used.

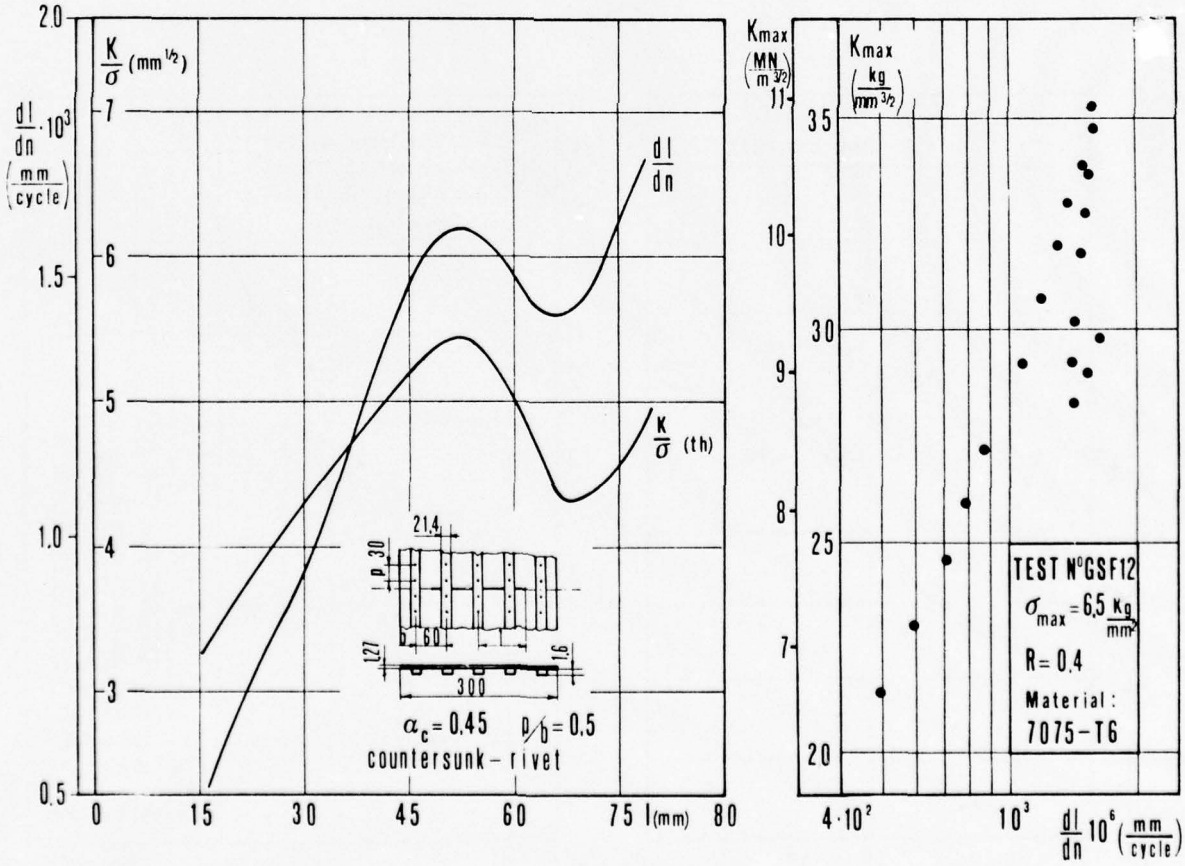

Fig. 12 - K-rate relationship for a single strip stringer stiffened panels with countersunk rivet, K was computed with the rigid fastener approach.

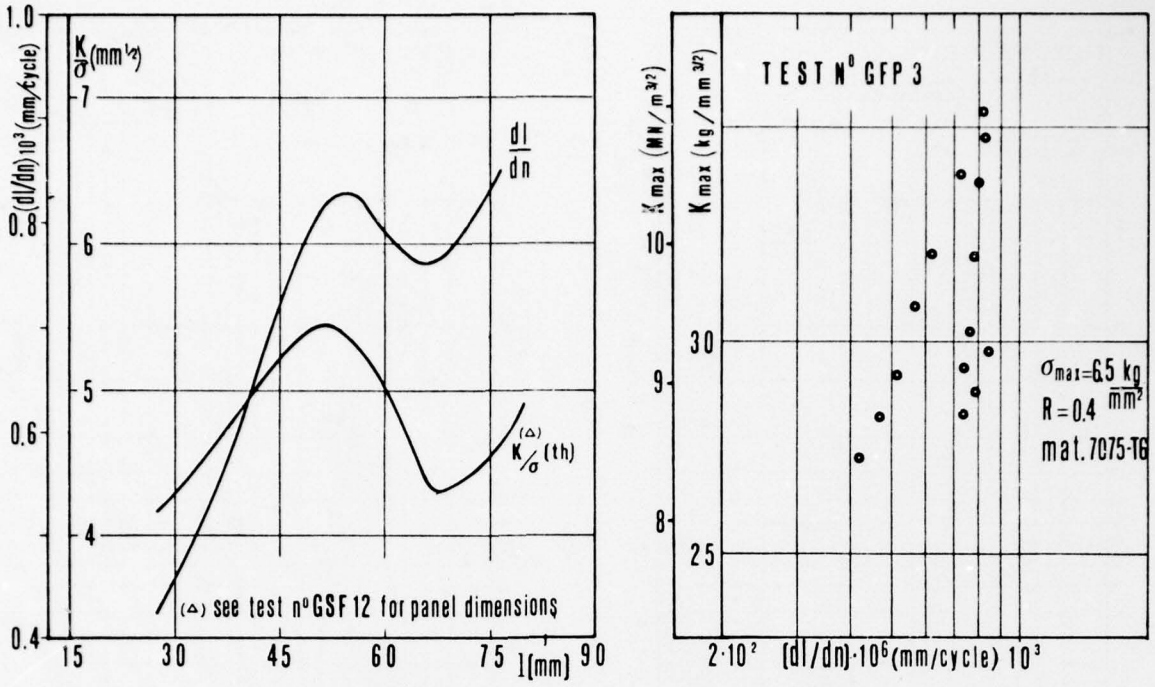

Fig. 12 - Continued.

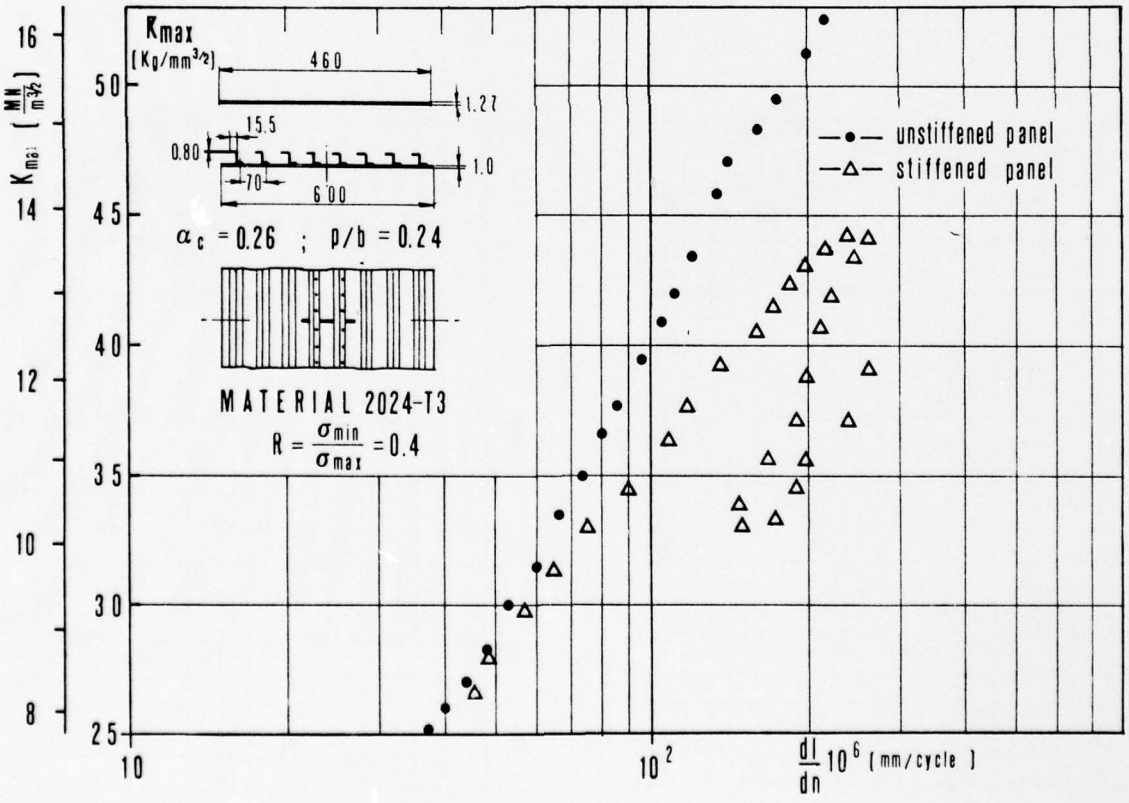

Fig. 13 - K-rate relationship for a stiffened and an unstiffened panel. K was computed on the basis of the rigid fastener approach taking into account the reduced area (2).

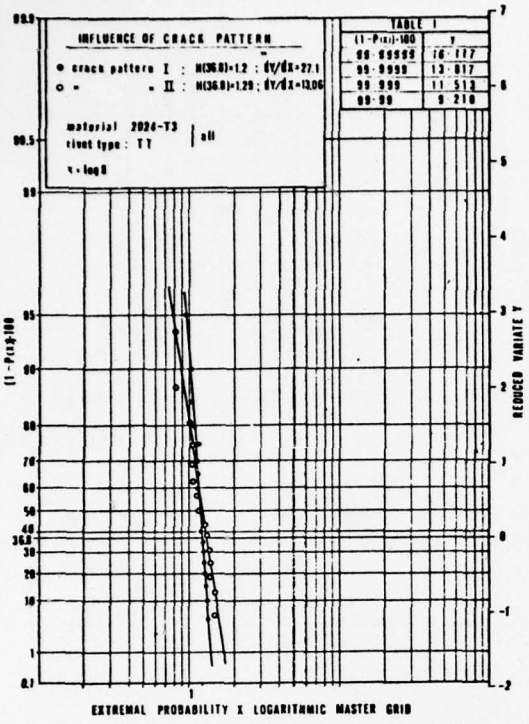

Fig. 14a - Extremal probability distribution for the random variable H. Influence of the crack pattern.

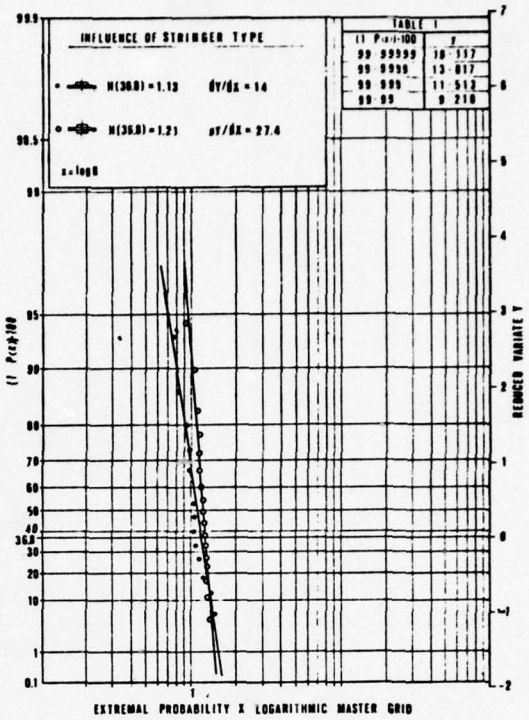

Fig. 14b - Influence of the stringer type on H distribution.

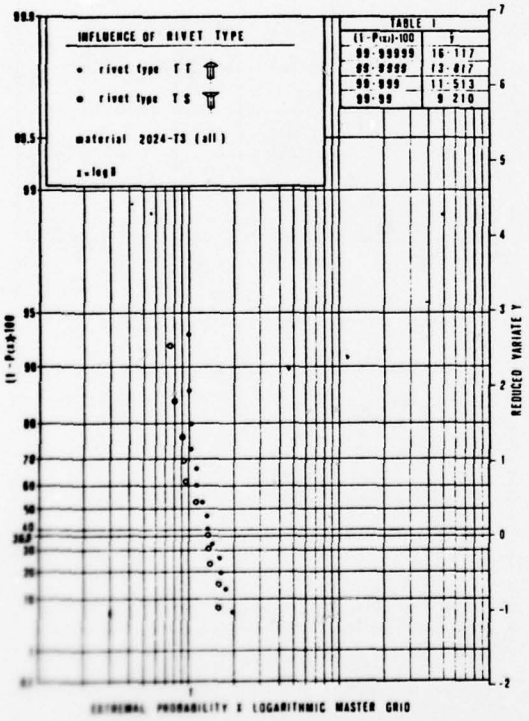

Fig. 14c - Influence of the rivet type.

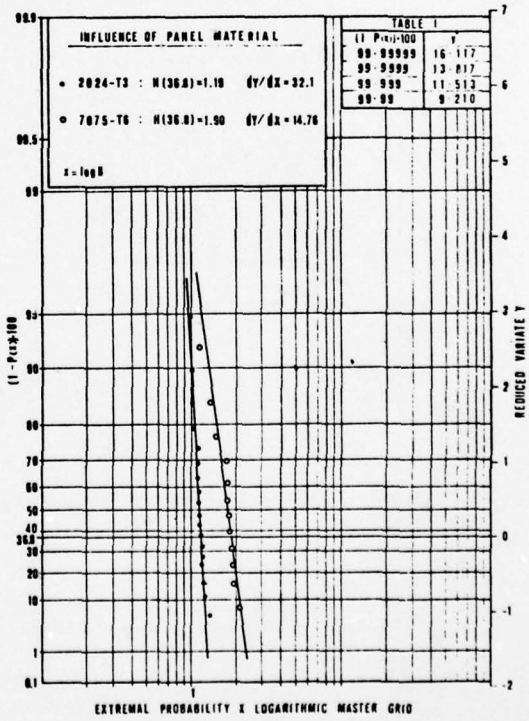

Fig. 14d - Influence of the panel material on H distribution.

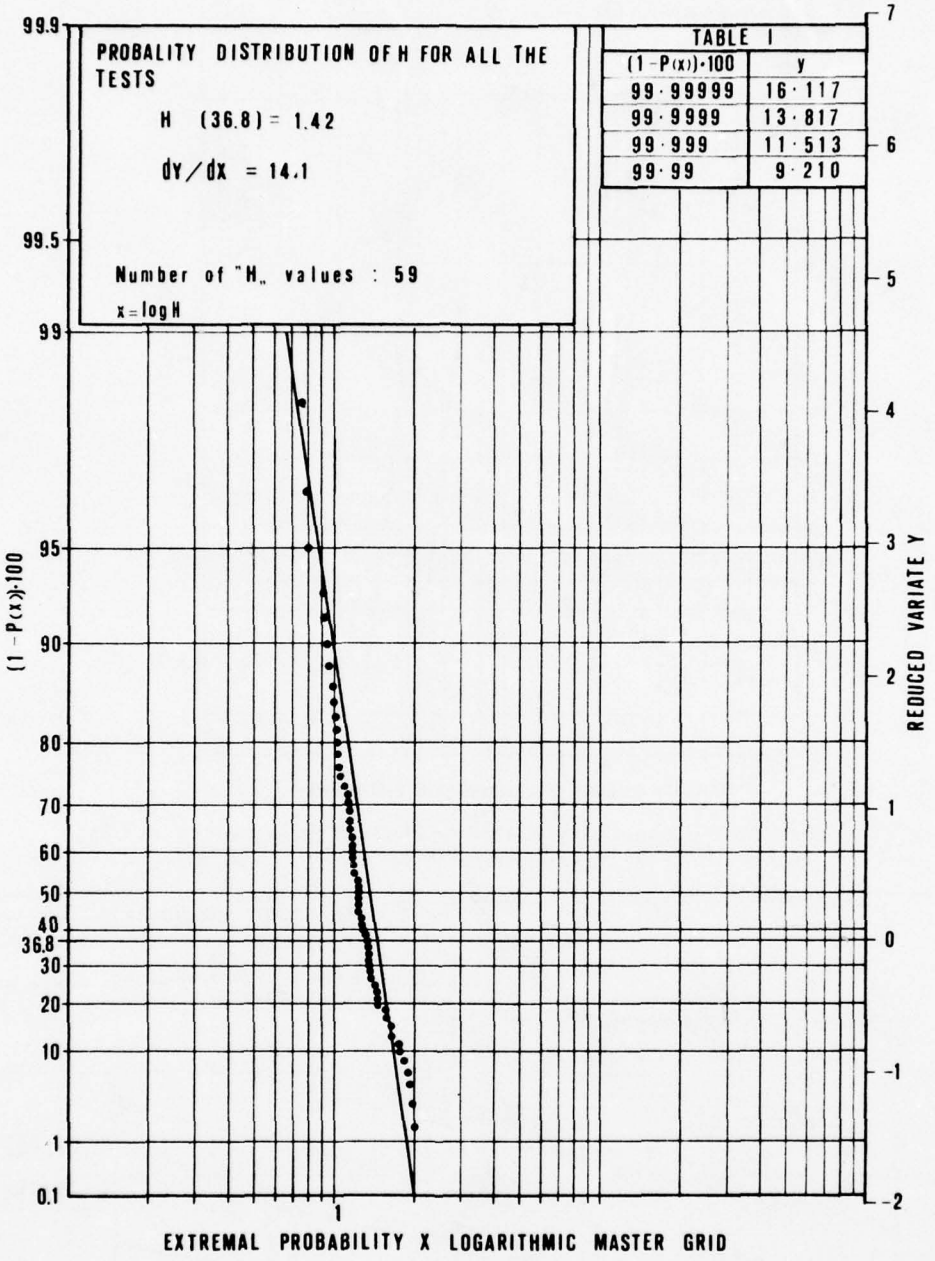

Fig. 15 - Extremal probability distribution for the random variable H as obtained from all the panels tested.

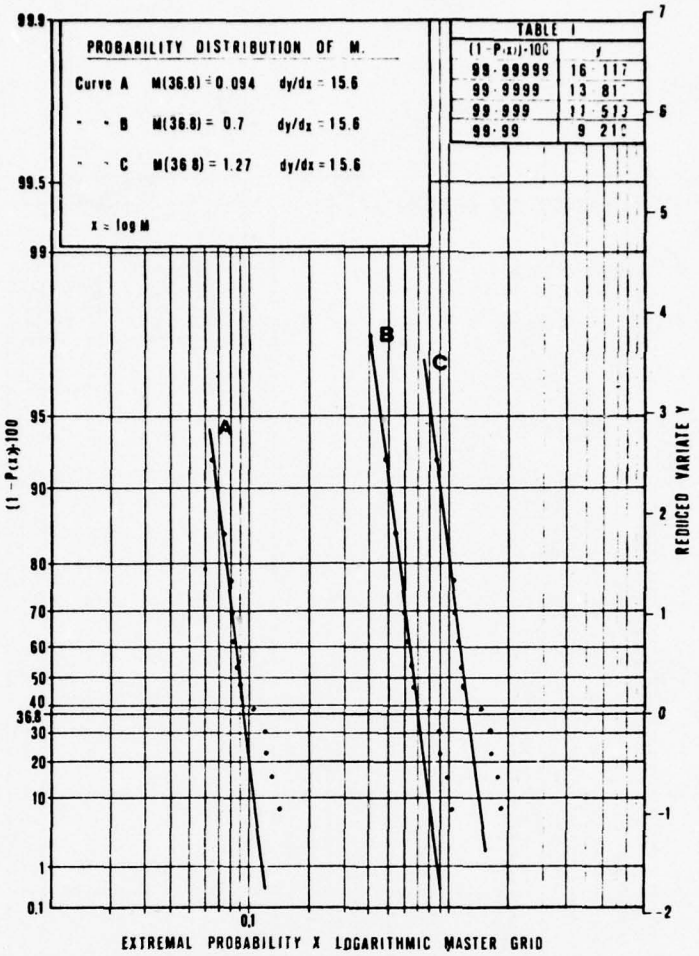

Fig. 16 - Extremal probability distributions for the random variable M, for three different the S-N curves.

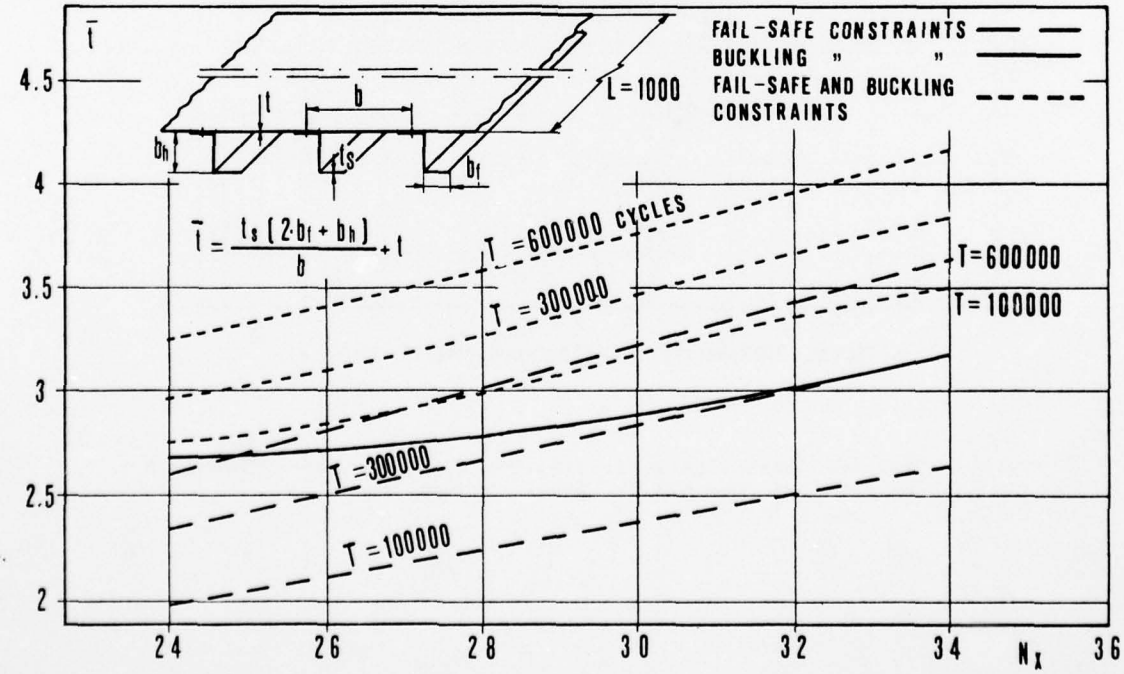

Fig. 17 - Minimum weight of stiffened panels for the panel configuration shown on the top left, and the three different kind of constraints indicate in the top right. The optimization was performed for the following values of α : α_{FS} = = 2.7, α_L = -1, α_u = -1.5 and $\Delta N_x = 0.26\ N_x$.

CONTRIBUTED DISCUSSION

by

F.I.Baratta
Mechanics Research Laboratory
Army Materials & Mechanics Research Center
Watertown, MA 02172, USA

The author and his colleagues at the University of Pisa have made significant progress in predicting crack propagation rates in cracked panels with stiffeners subjected to a fatigue environment. Two methods, one termed the "stress concentration factor", and the other, the "lap joint" approach, both utilize a mixture of theory and experiment, stress intensity computations, appropriate S-N curves combined with Minor's rule as aids in attempting to provide insight to this complex problem.

The primary difference between these two methods is that the stress concentration approach utilizes the maximum stress as a precurser to crack initiation at the rivet hole of the stiffener of a cracked panel; whereas the lap joint method presumes an analogy between the fatigue behavior in the stringer and a dry riveted lap joint.

Experimental results include the measurement of:

(a) The overload coefficient defined as the ratio of the maximum nominal stress of cracked to uncracked panel.

(b) The rivet force in cracked panels with stiffeners.

(c) Crack growth rates in stiffened and unstiffened panels.

(d) The crack length in the sheet cover at which the stringer starts to crack.

Such panels were constructed of 2074-T3 and 7075-T6 aluminum alloys. Four types of stiffeners were employed: single strip, double strip, "Z" and "C" shaped section stiffeners. Also round head and counter-sunk rivets were used.

A statistical treatment of both methods, the "stress concentration factor" and "lap joint" approach was also accomplished. In the former method fatigue endurance predictions are sensative to the accuracy of the overload coefficient and rivet load distribution, and errors arise because of the assumption of superposition when defining the maximum stress of the rivet hole. Also, better characterization of the material parameters used in the assumed S-N relationship, as well as surface finish in the rivet holes are required. Regarding the "lap joint" approach, statistical distributions based on extreme probability functions were determined for the influence of crack pattern, stringer type, rivet type and material. It was found that the only factor affecting fatigue phenomenon was the material.

Also included in this paper is a brief address aimed at minimum weight design methodologies for fail-safe structures using the experimental results from the previous work described. Such an analysis was based on modified penalty function methods, where a function was presumed and the absolute minimum of the function was found with the constraint conditions outlined.

The author's main conclusions are:

(a) If the stress intensity is accurately known, crack propagation rates in the sheet cover of a stiffened panel can be predicted with good accuracy.

(b) The stress intensity computation for rigid fasteners (double strip stiffeners) is adequate, whereas unrealistic values result with flexible fasteners (single strip stiffeners) and counter-sunk rivets.

(c) Statistical analysis of the data on stringer fatigue endurance resulting from the "lap joint" approach demonstrates that fatigue endurance and its correlation with crack length in the sheet cover can be confidently predicted; whereas the "stress concentration" approach needs to be further developed.

(d) Design of minimum weight panels accounting for fail-safe requirements has been successfully solved based on a penalty function method using stringer fatigue endurance data from the present investigation.

Regarding conclusion (c) above, in particular, the "stress concentration" factor approach, basically appears to be a sound method to further pursue. However, a formulation must include a more accurate means of defining crack initiation in the stiffener hole and this of course infers that plasticity effects must be taken into account resulting in further complexity.

The wealth of experimental data alone resulting from this program is a valuable contribution to the state-of-the-art, as well as the unique analyses presented.

CALCULATION OF STRESS INTENSITY FACTORS FOR CORNER CRACKING IN A LUG

by
R.J.H. Wanhill and C.J. Lof
National Aerospace Laboratory NLR
Amsterdam
The Netherlands

SUMMARY

Large lugs are integral to many aircraft components. They are customarily regarded as safe-life items, with consequently low design stress levels. However, safe-life design is becoming increasingly unacceptable in view of developments in damage tolerant design. Current specifications for damage tolerance recognise the potential applicability of both multiple load path and slow crack growth concepts.
One of the most important problems associated with damage tolerant design of lugs is the determination of stress intensity factors for corner flaws growing from the holes. *This paper presents results of a three-dimensional finite element analysis of such corner flaws and compares these results with experimental calibration of the effective stress intensity factor and previously suggested analytical solutions.*

INTRODUCTION

The complex, three-dimensional problem of corner flaws at holes has received considerable attention (1-7). *The problem is of more pressing interest since the USAF adoption of damage tolerance requirements* (8), for which a corner flaw at one side of a hole is one of the primary types of assumed damage (9,10). In practice, this type of flaw may be loaded either by remotely applied stresses or else by pin loading on the hole wall, the latter being of more general interest.

The present work considers the stress intensity factor for a corner flaw at *one side of a hole on a* typical aluminium alloy lug loaded by a steel pin. A three-dimensional finite element analysis of this configuration has been made, and the results are compared with experimental fatigue crack growth calibration of the effective stress intensity factor and with the previously proposed analytical solutions (1-4).

REVIEW OF PREVIOUSLY PROPOSED SOLUTIONS

Figure 1 summarises previously proposed solutions for the stress intensity factor of a corner flaw at a hole. Two solutions, figures 1a and 1c, employ the Irwin treatment for a semi-elliptical surface flaw (11) and consequently include an elliptic integral, Φ , which in the figures has been replaced by Q, the flaw shape parameter (12). The other two solutions include the Bowie relationship for a through crack at a hole(13).

All of the solutions have been derived *for remotely loaded holes.* Broek (3) *suggested* that his solution would probably apply for pin loaded holes provided that the flaw dimensions were significantly less than the hole diameter. None of the solutions includes a correction factor for finite width, and Broek's solution does not include a thickness correction. Note also that Liu's solution is for a quarter circular crack only, and that the Lockheed solution assumes that p and q are the minor and major axes of an ellipse: this assumption is not made in the Hall and Finger and Broek solutions.

The Hall and Finger solution is purely empirical, derived from fracture toughness tests where most corner flaw dimensions were equal to or greater than the hole diameters. Some of these test results were used by Liu to check his analysis (4). Broek's solution enabled fair agreement to be obtained between standard K_{I_c} results and fracture toughness estimates for remotely and pin loaded specimens with corner flaws mostly considerably smaller than the hole diameter (3). The Lockheed solution was not checked by tests.

FINITE ELEMENT ANALYSIS

The lug configuration

The lug is depicted in figure 2 with the X-Y-Z coordinate system used in the analysis. Note that the hole is eccentric with respect to the cylindrical top. Quarter circular cracks centred on a hole corner and lying in the X-Y ($\phi = 0^o$) plane have been introduced. The angle θ in the X-Y plane is defined as 0^o at the bore and $\pi/2$ at the front face.

Schematisation

Division of the cracked lug and loading pin into substructures is shown in figure 3. Most of the lug, between $\phi = \pi/8$ and $15\pi/8$, is divided by a coarse grid into 48 27-node 3-Dim elements. Between $\phi = 15\pi/8$ and $\pi/8$ there are three zones. In the wedge-shaped zones 10-node tetragonal elements are used to refine the network incrementally *over subsequent layers. For the small crack front zone* 18-node hexagonal elements are employed.

The loading pin substructure also consists of hexagonal elements, and connection with the relevant nodes in the lug substructure is radial only. This allows the coincident nodes of pin and lug to undergo tangential displacements relative to one another.

All the elements have a quadratic displacement field. Calculated stresses thus exhibit linear variation between nodes.

The computer programme

Calculations were carried out with the ASKA system (14), which is based on the finite element displacement method. The substructuring technique is well developed for this system. Hence, crack front substructure variants for different crack sizes (and shapes) are comparatively economical, despite their influence on the entire configuration.

Each analysis gave the node displacements, the stresses at element corners, and the stiffness matrices of each substructure. The node displacements and stiffness matrix of the crack front substructure were used to compute stress intensity factors according to the "Stiffness Derivative Method" developed by Parks (15).

The Stiffness Derivative Method

In linear elastic fracture mechanics the stress intensity factor is given by

$$K_I^2 = \frac{E}{1-\nu^2} \cdot G \tag{1}$$

where $G = \delta P/\delta A$ is the energy release rate, i.e. the change in elastic potential energy, δP, with change in crack surface, δA. The elastic potential energy of a body subjected to arbitrary external loading is

$$P = \frac{1}{2} \bar{u}^T [S] \bar{u} - \bar{u}^T \bar{b} \tag{2}$$

where $\bar{u}$ is the node displacement vector, $[S]$ is the stiffness matrix (of a substructure) and $\bar{b}$ is the external load vector. A small change in crack surface results in incremental changes $[\delta S]$ and $\delta\bar{u}$. For constant external load $\bar{b}$

$$\delta P = \delta\bar{u}^T [S] \bar{u} + \frac{1}{2} \bar{u}^T [\delta S] \bar{u} - \delta\bar{u}^T \bar{b} \tag{3}$$

Solution of the displacement analysis gives

$$[S] \bar{u} = \bar{b} \tag{4}$$

Thus, from (3) and (4)

$$\delta P = \frac{1}{2} \bar{u}^T [\delta S] \bar{u} \tag{5}$$

$[\delta S]$ is thus the change in stiffness resulting from crack extension, the "Stiffness Derivative". The node displacement vector $\bar{u}$ is calculated once, from $[S] \bar{u} = \bar{b}$ before crack extension.

The analysis procedure

Computation proceeds stepwise as follows:

- Analysis of the entire configuration to give displacements and stresses for all substructures. In the case of the crack front substructure these displacements and the calculated stiffness matrix $[S]$ are needed for further computation.

- A variant of the crack front substructure, a local extended crack front, is entered and a new stiffness matrix $[S^*]$ calculated. The difference between $[S]$ and $[S^*]$ is $[\delta S]$, which together with the displacement vector $\bar{u}$ (calculated in the first step) and use of equation (5) gives δP, the change in elastic potential energy for the entire configuration. Then using equation (1) a K value is calculated for the location of each displaced crack front node.

- The second step is repeated for all crack front nodes, so that the value of K along the crack front is obtained.

- For analysis of a new crack size a new crack front substructure is input. Most of the other substructures remain unchanged, whereby repetition of the first step is very economical. Thereafter the second step is repeated as above.

A local crack extension is simulated by changing coordinates of one, or more, crack front nodes. This extension must be very small ($\delta r/r < 10^{-4}$) to avoid alteration of the crackfront form.

The advantage of the stiffness derivative method is that a nodal extension changes the stiffness matrix only for those elements connected to the node and, hence, the evaluation of (5) involves little computational effort. Thus a relatively fine mesh can be used without a significant increase in computer time and cost.

EXPERIMENTAL CALIBRATION OF THE EFFECTIVE STRESS INTENSITY FACTOR

2024-T351 aluminium alloy plate, original thickness 30 mm, was chosen for fatigue crack growth calibration of the stress intensity factor. Two kinds of specimen were used. The first was a centre through-cracked panel machined to 20 mm thickness in the test section. For this configuration the stress intensity factor may be expressed as

$$K_I = \sigma \sqrt{\pi \ell \sec\left(\frac{\pi \ell}{W}\right)} \tag{6}$$

where ℓ is the half crack length and W the total width. Equation (6) is due to Feddersen (16). Owing to the substantial thickness the fatigue crack front was curved. The ℓ values measured at the surface were corrected according to A.S.T.M. E 399 (17) to take account of this curvature.

The second type of specimen conformed to the lug dimensions in figure 2. A 2 mm x 2 mm starter notch was made at one corner of the hole using a jeweller's saw. The lugs were loaded by a neat fit high strength low alloy steel pin.

Three of each specimen type were tested, using a 500 kN AMSLER pulsator with constant amplitude sinusoidal loading at a frequency of 8.3 Hz. The environment was normal air (which at the NLR signifies 40–60 % relative humidity).

Crack propagation rates were calculated from

$$\frac{d\ell}{dn} = \frac{\ell^*_{i+1} - \ell^*_i}{n_{i+1} - n_i} \tag{7}$$

where n is the number of cycles and ℓ^* the corrected half crack length for the centre through-cracked panels and the surface crack length for the lug specimens. The crack rates were related to a crack length of $(\ell^*_{i+1} + \ell^*_i)/2$.

Effective stress intensity factors for the lug specimens were obtained by assuming that at identical crack growth rates the stress intensity factors corresponding to the characteristic flaw dimensions are the same. All three lug specimens exhibited approximately quarter circular flaw growth up to ℓ^* values of 17 mm, i.e. just before failure. Thus, ℓ^* was the only flaw dimension required.

RESULTS

Analytical proposals

As mentioned earlier, none of the proposed analytical solutions, figure 1, include a finite width correction factor. It was thought that a reasonable correction factor might be that of Tada for a single edge notched specimen (18), substituting areas for lengths. Thus, for a quarter circular corner flaw:

$$F\left[\frac{\ell^*}{(W-d)/2}\right] = \sqrt{\frac{4(W-d)t}{(\pi\ell^*)^2}\tan\frac{(\pi\ell^*)^2}{4(W-d)t}} \cdot \frac{0.752 + \frac{1.01(\pi\ell^*)^2}{(W-d)t} + 0.37\left(1-\sin\frac{(\pi\ell^*)^2}{4(W-d)t}\right)^3}{\cos\frac{(\pi\ell^*)^2}{4(W-d)t}} \tag{8}$$

Equation (8) was used to correct for the finite width and thickness of the lug specimen when calculating K factors from the four solutions. The thickness correction factors of the Lockheed and Liu solutions were thus omitted, but this was not possible for the Hall and Finger solution, which presents only empirical plots in which thickness effects are automatically incorporated.

Quarter circular crack K_I/σ values for the various solutions are plotted versus ℓ^* in figure 4. Q values for the Lockheed and Broek solutions were obtained for σ/σ_y values between 0.1 and 0.2. Stress multipliers (effective K_t values) for K_{IA} in the Lockheed solution were taken, following Peterson (19), to be 3.83 for a remotely loaded hole and 5.19 for a pin loaded hole.

Figure 4 shows that K_{IA} in the Lockheed solution is much higher than the Broek and Liu K_{IA} values, which tend to fall in the same range as the Lockheed K_{IB} and K_{IC} and Hall and Finger solutions.

Finite element analysis

In a first approach of schematisation the elements were positioned with wedge apices at the crack front, and two crack sizes were analysed. These were quarter circular flaws with radii of 8.18 mm and 12.5 mm. The loading on the lug was represented by a system of prescribed displacements at the bore surface.

The stiffness derivative procedure was applied for a number of nodal points on the crack fronts, and results of the calculated stress intensity factors are shown by the solid symbols in figure 5. K_I is seen to vary smoothly along the crack front with maxima at the bore of the hole.

A second approach changed the following quantities:

- Lug loading. The steel pin was schematised to obtain a natural load distribution on the bore surface.
- Crack front elements. The elements were positioned with wedge sides at the crack front.

Two crack sizes, r = 3 mm and 10 mm were chosen. Calculated stress intensity factors are shown by the open symbols in figure 5. The data trend is similar to that for the first approach, namely a gradual decrease in K_I from the bore of the hole to the front surface. Thus, the orientation of the crack front elements is not crucial. Note that for the larger crack in the second approach there is an initial, steeper decrease in K_I away from the bore of the hole. This is probably because such a large crack encounters a wide range in stress and the schematisation allows free displacement and rotation of the lug and pin under load, unlike the first approach.

Fatigue crack growth calibration

Figures 6 and 7 present fatigue crack propagation data for centre through-cracked panels and corner cracked lugs, respectively. These data were used to obtain effective K_{Imax} values for the lug specimens, and the corresponding K_I/σ values are given in figure 4.

The best fit effective K_I/σ values agree fairly well with the Liu solution for $\ell^* \leq 12$ mm: thereafter there is wide divergence. For $\ell^* > 14$ mm the effective K_I/σ is significantly lower than all the calculated values. This is probably due to increased plasticity: shear lip formation, which retards crack growth, increased considerably towards final failure. Overall, the comparison of calculated and effective K_I/σ values is encouraging for the concept of a correction factor based on the area of cracked material compared to the original uncracked area.

Additional evidence that plasticity is having a significant influence is provided in figure 8. Here the fatigue crack growth effective K_I/σ is compared with K_{Ic}/σ values derived from Broek's measurements of pop-in and 5 % offset stresses (3). The higher the uncracked section stresses, the lower are the K_I/σ values: note especially the low values associated with net section yield.

DISCUSSION

Comparison of analytical, finite element and fatigue crack propagation determinations of K_I/σ is given in figure 9. Agreement of the results is fair and encouraging, since the methods of determining K_I/σ were very different. Including Broek's fracture toughness results shown in figure 8 there are four methods, namely

- Analytical "guesstimates", highly dependent on proper treatment of boundary conditions.
- Calculation of K_I/σ using the energy release rate relation, equation (1), and finite element analysis. Provided boundary conditions are introduced properly the method generally gives very accurate K_I determinations.
- Calculation of an effective K_I/σ assuming that the stress intensity factor controls fatigue crack propagation under constant amplitude loading. A truly elastic K_I determination, at least for larger flaw size, is ruled out by the plasticity (shear lip formation) observed for the chosen material, 2024-T351.
- Calculation of K_I/σ from fracture toughness data, assuming a unique K_{Ic} value. In addition, plasticity effects are much more pronounced than for fatigue crack propagation.

It is considered that an experimental approach to crack growth behaviour should be favoured, for the following reasons:

- It is not generally to be expected that a constant flaw shape will be maintained during crack growth, e.g. (1,20).
- Realistic loading conditions (feasible design stress levels and gust or manoeuvre spectra) and environmental effects can be studied.
- Hard to simulate effects, such as varying fit between lug and pin (including the use of bushings) and secondary bending in female lugs, can be introduced into tests.
- Data can be analysed statistically.
- Lug specimens are relatively simple, and testing of a series of specimens covering a range of characteristic dimensions is fairly inexpensive as compared to the computational costs for several substructure variants in a finite element analysis.
- Empirical-analytical formulae for prediction of crack propagation behaviour can be developed. For example, in the present work excellent agreement with the best fit fatigue crack growth effective K_I/σ is obtained for 3 mm $< \ell^* <$ 14 mm using the Lockheed K_{IC} formula and the following correction factor:

$$F\left[\frac{\pi \ell^{*2}}{2(W-d)t}\right] = 1.26 + 2.65\,\frac{\pi \ell^{*2}}{2(W-d)t} \qquad (9)$$

which is a great deal less cumbersome than equation (8).

CONCLUSIONS

A programme for evaluating the stress intensity factors of corner cracks growing from the hole in an aluminium alloy lug has shown reasonable agreement between results of different methods (analytical, finite element analysis, fatigue crack propagation tests) employing very different assumptions. An experimental approach to studying crack growth behaviour is advocated for future research.

ACKNOWLEDGEMENT

The finite element analysis was carried out under contract for the Netherlands Agency for Aerospace Programmes (NIVR).

ADDENDUM

After this paper was written, reports of two recent investigations of stress intensity factors for corner flaws at holes became available to the authors. Unfortunately, it has not been possible to discuss them, because of deadline restrictions. The investigations are:

(1) R.C. Shah, Stress intensity factors for through and part-through cracks originating at fastener holes, Mechanics of Crack Growth, A.S.T.M. STP 590, p.429, Philadelphia (1976).

(2) J.C. Newman, Predicting failure of specimens with either surface cracks or corner cracks at holes, NASA TN D-8244, June 1976.

REFERENCES

1. Lockheed Palo-Alto Research Laboratory Report LMSC-DO 80165, May 1968.

2. L.R. Hall and R.W. Finger, Fracture and fatigue growth of partially embedded flaws, Proc. Air Force Conf. on Fatigue and Fracture of Aircraft Structures and Materials, AFFDL TR 70-144, p.235, Air Force Command, Wright-Patterson AFB, Ohio (1970).

3. D. Broek, A. Nederveen and A. Meulman, Applicability of fracture toughness data to surface flaws and to corner cracks at holes, National Aerospace Laboratory Report NLR TR 71033 U, Amsterdam, January 1971.

4. A.F. Liu, Stress intensity factor for a corner flaw, Eng. Fract. Mech., 4, 175 (1972).

5. R.J.H. Wanhill, Stress intensity factor solutions for a corner flaw at a hole and their application to design, National Aerospace Laboratory Report NLR TR 73016 U, Amsterdam, January 1973.

6. R.H. Keays, A review of stress intensity factors for surface and internal cracks, Aeronautical Research Laboratories Structures and Materials Report 343, Melbourne, April 1973.

7. J.R. Snow, A stress intensity factor calibration for corner flaws at an open hole, Air Force Materials Laboratory Report AFML-TR-74-282, Wright-Patterson AFB, Ohio, May 1975.

8. Military Specification Airplane Damage Tolerance Requirements, MIL-A-83444 (USAF), July 1974.

9. H.A. Wood, The use of fracture mechanics principles in the design and analysis of damage tolerant aircraft structures, Fracture Mechanics of Aircraft Structures, AGARD-AG-176, p.19, January 1974.

10. H.A. Wood, Application of fracture mechanics to aircraft structural safety, Eng. Fract. Mech., 7, 557 (1975).

11. G.R. Irwin, Crack-extension force for a part-through crack in a plate, J. Appl. Mech., 4, 651 (1962).

12. C.F. Tiffany and J.N. Masters, Applied fracture mechanics, Fracture Toughness Testing and Its Applications, A.S.T.M. STP 381, p.249, Philadelphia (1965).

13. O.L. Bowie, Analysis of an infinite plate containing radial cracks originating at the boundary of an internal circular hole, J. Math. Phys., 35, 60 (1956).

14. ASKA Part 1 - Linear Static Analysis User's Reference Manual, Institut für Statik und Dynamik der Luft- und Raumfahrtkonstruktionen University of Stuttgart ISD-Report No.73, Revision B (1973).

15. D.M. Parks, A stiffness derivative finite element technique for determination of elastic crack tip stress intensity factors, Tech. Rep. NASA NGL 40-002-080/13, Div. of Eng., Brown University, Rhode Island, May 1973.

16. C.E. Feddersen, Contributed discussion in: Plane Strain Crack Toughness Testing of High Strength Metallic Materials, A.S.T.M. STP 410, p.77, Philadelphia (1967).

17. Standard method of test for plane-strain fracture toughness of metallic materials, A.S.T.M. E399-74, Annual Book of A.S.T.M. Standards, Part 10, p.561, Philadelphia (1975).

18. H. Tada, The Stress Analysis of Cracks Handbook, Del Research Corp., p.2.11, Hellertown, Pa. (1973).

19. R.E. Peterson, Stress Concentration Design Factors, Chapman and Hall, London (1953).

20. L.F. Impellizzeri and D.L. Rich, Spectrum fatigue crack growth in lugs, McDonnell Aircraft Co., Report MCAIR 75-006 (1975).

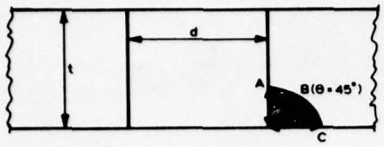

$$K_{IA} = 1.12(3\sigma)\sqrt{\frac{\pi\rho}{Q}}\sqrt{\frac{2t}{\pi\rho}\tan\frac{\pi\rho}{2t}}$$

$$K_{IB} = 1.12\sigma\left[1+\frac{1}{2}\left(\frac{d}{d+2\rho}\right)^2+\frac{3}{4}\left(\frac{d}{d+2\rho}\right)^4\right]\sqrt{\frac{\pi}{Q}}\sqrt{\frac{\rho^3+\rho^2}{2}}\sqrt{\frac{2t}{\pi}\sqrt{\frac{2}{\rho^2+\rho^2}}\tan\left(\frac{\pi}{2t}\sqrt{\frac{\rho^2+\rho^2}{2}}\right)}$$

$$K_{IC} = 1.12\sigma\left[1+\frac{1}{2}\left(\frac{d}{d+2q}\right)^2+\frac{3}{4}\left(\frac{d}{d+2q}\right)^4\right]\sqrt{\frac{\pi\rho}{Q}}$$

WHERE $\rho = \frac{p^2}{q}$ IS THE END RADIUS OF THE ELLIPSE ASSUMED TO DESCRIBE THE CRACK FRONT, AND Q IS BASED ON $\frac{p}{2q}$ USING FLAW SHAPE PARAMETER CURVES

(a) Lockheed solution (1)

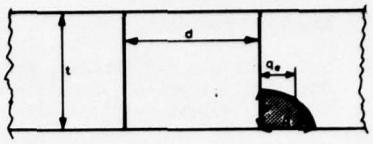

K_I IS ESTIMATED TO BE

$$K_I = 0.87\sigma\sqrt{\pi a_e}\ (\phi)$$

WHERE ϕ REPRESENTS $f\left(\frac{\ell}{r}\right)$ IN THE BOWIE RELATIONSHIP AND ℓ IS TAKEN TO BE a_e. a_e IS TO BE ESTIMATED FROM THE FOLLOWING EMPIRICAL PLOT :

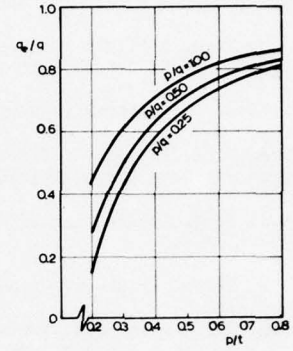

(b) Hall and Finger solution (2)

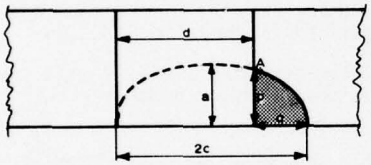

K_I WILL BE A MAXIMUM AT A, AND IS ESTIMATED TO BE

$$K_I = 1.2\sigma\sqrt{\frac{\pi\rho}{Q}}\ (\phi)$$

WHERE $\phi = \left\{\frac{p^2(d+q)^2(d-q)^2(dq)^{-1}+4p^2(d+q)^2}{4dq\left[4p^2+(d-q)^2\right]}\right\}^{1/4}$

AND Q IS BASED ON $\frac{a}{2c}\left(=\frac{p}{2\sqrt{dq}}\right)$, USING FLAW SHAPE PARAMETER CURVES

(c) Broek solution (3)

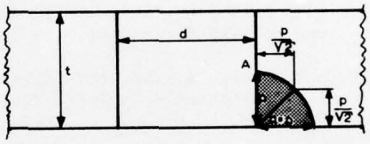

$$K_I = 1.26\,\alpha_b\sigma\sqrt{p}\ (\phi)$$

WHERE ϕ REPRESENTS $f\left(\frac{\ell}{r}\right)$ IN THE BOWIE RELATIONSHIP, ℓ IS TAKEN TO BE $p/\sqrt{2}$, AND α_b IS THE BACK SURFACE CORRECTION FACTOR TO BE ESTIMATED FROM THE FOLLOWING PLOT :

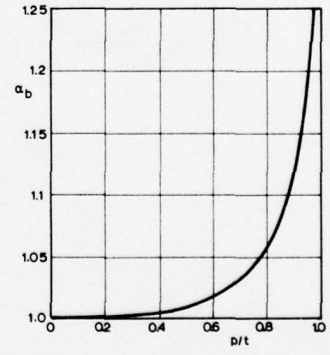

(d) Liu solution (4)

Fig.1 Proposed solutions for the stress intensity factor of a corner flaw at a hole

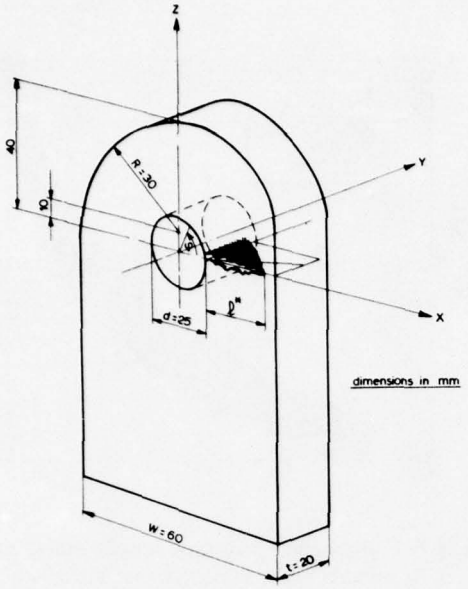

Fig.2 The cracked lug configuration

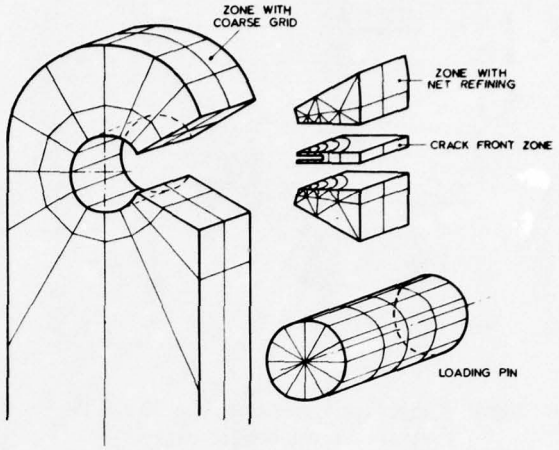

Fig.3 Schematisation of the cracked lug and loading pin

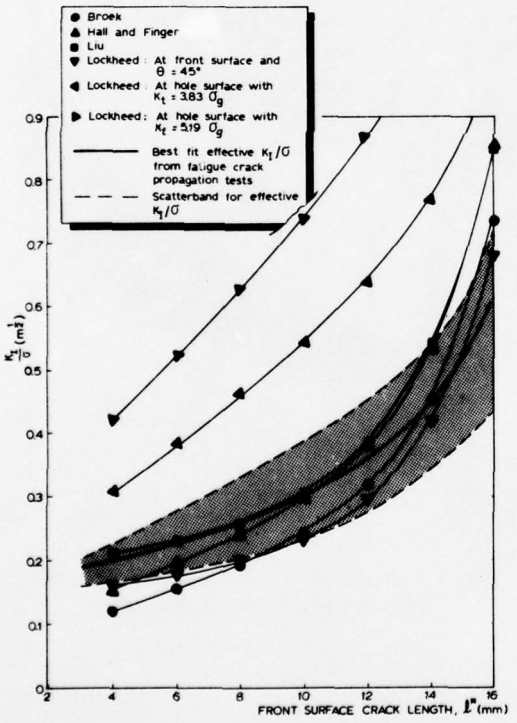

Fig.4 Comparison of analytical K_I/σ values and effective K_I/σ

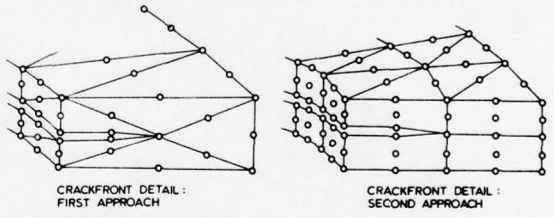

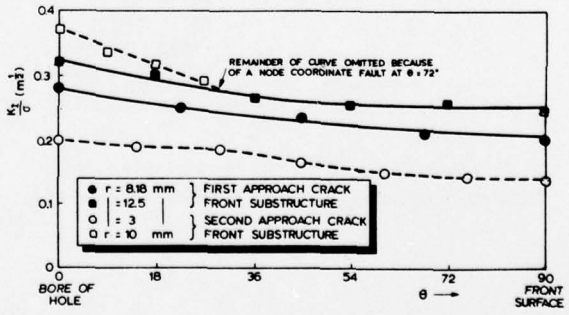

Fig.5 Results of finite element calculations of K_I along the crack fronts for quarter circular cracks (radii = l^*)

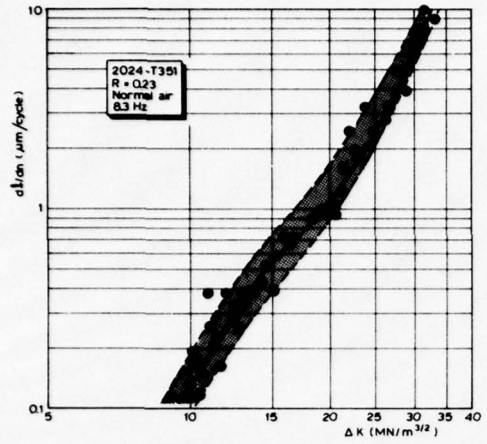

Fig.6 Fatigue crack propagation in 20 mm thick centre through-cracked panels

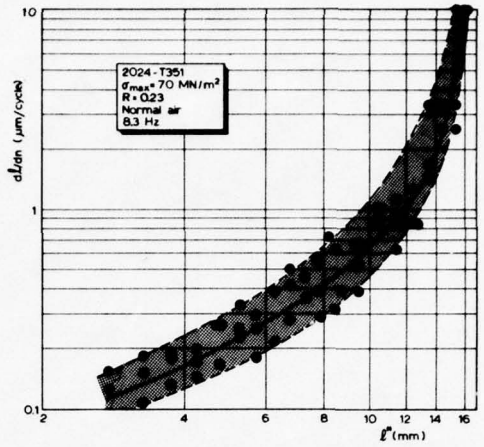

Fig.7 Fatigue crack propagation in 20 mm thick lugs containing a corner flaw at the hole

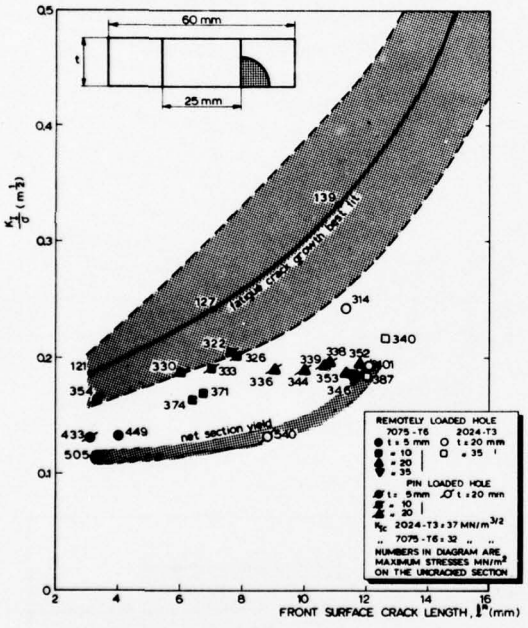

Fig.8 Comparison of fatigue crack growth and fracture toughness test results for effective K_I/σ

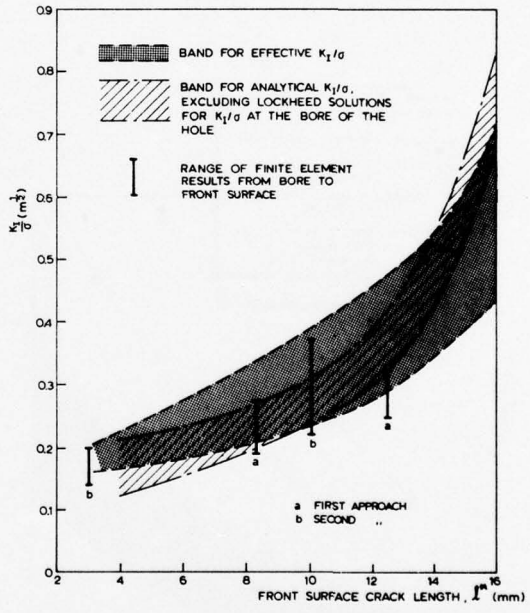

Fig.9 Comparison of analytical, finite element analyses and effective K_I/σ values

CONTRIBUTED DISCUSSION

by

D.J.Cartwright
Department of Mechanical Engineering
University of Southampton, England

The authors have tackled an important and rather difficult problem. Their treatment makes a useful contribution to existing information on stress intensity factors for corner flawed holes in tension members. Several approximate solutions are summarized and a modification to account for the finite width of the lug is proposed. Using this modification an informative comparison is made of the available solutions. The authors demonstrate that whilst there is a wide disparity between the various solutions most lie within a scatter band obtained from experimentally measuring the stress intensity factor on corner cracked, pin-loaded lugs using a fatigue crack growth rate calibration procedure. Attention is drawn by the authors to the difference between the solution of Figure 1(a) and the other solutions; it would be helpful to have the author's comments on the reasons for the differences shown. Some experimental measurements of K_I for a corner crack at a hole under external loading have been reported by McGowan and Smith[1]. They found that in most cases the existing approximate solutions tended to overestimate K_I. Have the authors considered these results in relation to their own measurements of K_I and if so how do they compare?

In the experimental determination of the stress intensity factors the authors appear to have calibrated crack growth rates for a corner-cracked, pin-loaded lug against growth rates for a center cracked panel. In the pin-loaded lug the crack growth may have occurred under mixed mode conditions whereas crack growth in the center cracked panel would have occurred under Mode I only. Some guidance on the implications of using the fatigue crack growth rate calibration procedure in such circumstances would be helpful.

The authors results from a finite element analysis of a corner cracked lug indicate reasonable agreement with their results from the fatigue crack growth measurements. It appears that the curve for $r = 3$mm with prescribed forces on the hole has been omitted from Fig. 5. There are no values of K_{II} shown for the finite element solution. Did the authors determine K_{II} in the course of their calculations and if so how did the magnitude of K_{II} compare with that of K_I. Some recent measurements on a pin-loaded lug have been made using the photoelastic frozen stress technique by Smith et al[2] in which both K_I and K_{II} were determined. This could make a useful supplement to the results of the present paper.

REFERENCES:

1. McGowan, J.J.
Smith, C.W.
Stress intensity factors for deep cracks emanating from the corner formed by a hole intersecting a plate surface.
ASTM STP 590 (1976) pp 460-476

2. Smith, C.W.
Joles, M.
Peters, W.H.
Stress intensities for cracks emanating from pin loaded holes.
Proc. of the ASTM 10th National Symposium on Fracture Mechanics.
Aug 23-25th, Philadelphia (1976) (to be published).

APPLICATION DE LA MECANIQUE DE LA RUPTURE A LA SELECTION DES ALLIAGES D'ALUMINIUM

Ière Partie

par

ODORICO Jacques
Ingénieur au LABORATOIRE CENTRAL
de la SOCIETE NATIONALE INDUSTRIELLE AEROSPATIALE,
Responsable du Service Métallurgie

-:-

RESUME

L'examen des résultats déjà acquis sur alliage léger pour les paramètres classiques de la mécanique de la rupture, mesurés en Laboratoire, à savoir K1C, KC et da/dN, met en évidence une forte dispersion. Cette dispersion probablement imputable au mode de fabrication et aux méthodes d'essai ne gêne pas quant à l'étude et à la sélection des matériaux et des traitements thermiques associés. Par contre, le calcul de durée de propagation en fatigue ou de résistance résiduelle de parties de structure d'avion avec ces valeurs de K1C, KC et da/dN parait délicat. Le développement d'essai de fatigue sur module représentatif des structures sous sollicitations complexes, proches des enregistrements des vols, semble nécessaire.

INTRODUCTION

Actuellement, nos constructions périssent ou se délabrent dans le temps pour trois raisons :

- la fatigue - la corrosion - la corrosion sous tension.

Nous exclurons de cet exposé le cas de rupture par fluage qui n'intéresse que les avions supersoniques. Ce constat nous amène à nous intéresser à des propriétés considérées maintenant comme essentielles pour garantir la sécurité, la disponibilité et la longévité des structures d'avions. Ces propriétés sont :

- la résistance statique résiduelle d'éprouvettes préfissurées en fatigue, paramètres K1C ou KC
- la sensibilité à la corrosion sous tension, dont l'importance résulte directement du mode de conception actuel des pièces structurales usinées fréquemment à partir de tôles épaisses et assemblées par des éléments de fixation à forte interférence.
- la résistance à la fatigue et plus particulièrement la vitesse de propagation des criques de fatigue, spécialement dans le domaine des vitesses moyennes et élevées (10^{-3} à 10^{-1} mm/cycle) Cette propriété est directement liée à la disponibilité des appareils et à la planification des chantiers de modification.
- la protection contre la corrosion qui commande, pour une grande part, la maintenance des structures.

Ces propriétés, sauf la dernière que nous exclurons de cet exposé, sont toutes abordables par la mécanique de la rupture.

L'objet de cette conférence sera de présenter les résultats déjà acquis pour ces différentes propriétés et les réflexions qu'ils nous inspirent quant à leur utilisation pour le choix des matériaux, la conception des structures.

RESISTANCE STATIQUE RESIDUELLE

Après une certaine durée d'utilisation sur appareil, des pièces peuvent présenter des fissures qui doivent pouvoir être détectées avant d'entrainer une rupture brutale. Il se peut, même, que certaines pièces présentent des défauts dès l'origine. La tentative est donc, dans un premier temps, de mesurer un paramètre reliable à la dimension maximale de la crique supportable pour une pièce.

Pour ce faire, nous utilisons au Laboratoire le facteur critique d'intensité de contrainte K1C dont la proportionnalité avec la taille de défaut maximal tolérable est de la forme $\left(\frac{K_{1C}}{\sigma}\right)^2 \times a$
(σ = contrainte courante).

Pour les alliages légers, de nombreuses mesures de ce paramètre ont été effectuées à l'AEROSPATIALE, en particulier sur A-U2GN (2618 A). Le tableau I donne le reflet de l'ensemble des résultats obtenus sur cette nuance à l'état T 651 sous forme de tôle épaisse laminée.

TABLEAU 1 K1C sens TL sur tôles épaisses en A-U2GN T 651

Répartition des tôles testées

Epaisseur (mm)	Nbre pour le fournisseur N°1	Nbre pour le fournisseur N°2
$25 \leqslant e < 45$	4	8
$45 \leqslant e < 65$	9	5
$65 \leqslant e < 89$	8	-
$89 \leqslant e < 114$	1	2

Total général : 37 tôles

Résultats

Fournisseur N° 1 $\overline{M}_{(K1C)} = 22{,}3$ MPa $\sqrt{m}$
$\sigma = 2{,}33$ MPa $\sqrt{m}$

Fournisseur N° 2 $\overline{M}_{(K1C)} = 19{,}1$ MPa $\sqrt{m}$
$\sigma = 1{,}11$ MPa $\sqrt{m}$

La partie la plus intéressante de ces résultats nous semble être l'écart type qui est représentatif d'une production industrielle. Afin de confirmer ces valeurs pour l'écart type, nous avons exploité dans le même esprit les résultats publiés dans " DAMMAGE TOLERANCE BOOK ", exploitation résumée dans le Tableau 2.

TABLEAU 2

K1C Sens TL sur tôles épaisses en alliage léger				
Alliage	Etat	Nbre de valeurs	$\overline{M}$ MPa$\sqrt{m}$	$\overline{M}$ MPa$\sqrt{m}$
2014	T 651	25	23,1	1,55
2214	T 651	10	35	1
2214	T 651			
	SP 417	15	32,3	2
2024	T 851	37	22,1	1,4
2124	T 851	43	26,8	2,85
2124	T 851			
	SP 417	60	26,9	2,8
2618	T 651	52	20,9	1,9
7050	T7365I	16	31,3	2,5
7075	T 651	19	23,9	1,7
7075	T 7351	19	27,6	2,9
7075	T 7651	40	25,7	2,8
7475	T 651			
	SP	13	38,5	2,65
7475	T 7351			
	SP	17	41,3	2,7

Il ressort de ce tableau que la valeur de l'écart type est effectivement de l'ordre de

$$2 \text{ à } 2{,}5 \text{ MPa } \sqrt{m}.$$

Ceci revient à dire que, pour une fabrication d'une nuance et d'un type de demi-produit, les valeurs K1C à atteindre seront comprises entre

$$\overline{M} - 5 \text{ MPa } \sqrt{m} \quad \text{et}$$

$$\overline{M} + 5 \text{ MPa } \sqrt{m}$$

ce qui fait une dispersion de l'ordre du tiers de la valeur moyenne. Cette dispersion est probablement imputable en partie à la conduite de l'essai, mais si cette conduite est très pointue, le comportement des pièces dans le cas de chargement complexe en service risque d'être également très dispersé. Pour la part la plus importante, cette dispersion est à relier à la fabrication actuelle de demi-produits qui n'est pas suffisamment gelée ou pas suffisamment maîtrisée.

Dans le cas de pièces épaisses, si un Bureau d'Etude voulait prendre en compte cette notion de longueur critique de crique, il devrait, semble-t-il, choisir une valeur à ($\overline{M} - 2\sigma$). Dans ce cas, l'ordre de grandeur des défauts limites tolérables pour une forme géométrique très simple en fonction de la nuance est donnée au Tableau 3.

TABLEAU 3

Ordre de grandeur des défauts Limite tolérable (en sens TL)		
Nuance	$\overline{M}_{(K1C)} - 2\sigma$ MPa$\sqrt{m}$	$2a = \frac{2}{\pi} \cdot \frac{(K_{1c})^2}{\sigma^2}$ * (mm)
A-U2GN T 651	17,5	11,5
7075 T 7351	21,8	17,8
7475 T 7351 SP	35,9	42
A-U4G1 T 351 (2024)	30	34

* σ = 130 MPa ce qui correspond à la contrainte maximale d'un cycle F - 0,1 F amenant une rupture par fatigue en 200.000 cycles avec un Kt = 5,3

Les valeurs très théoriques de 2 a ainsi obtenues sont pauvres, hormis pour le 7475 et le 2024. Il faut en déduire que le meilleur choix métallurgique est, en général, insuffisant pour garantir des ruptures brutales. La vraie garantie reste, pour les pièces épaisses, dans un dimensionnement correct vis-à-vis de l'initiation en fatigue et dans des choix technologiques permettant le blocage des fissures éventuelles au cours de la propagation.

En fait, sur avion, les épaisseurs en cause sont généralement inférieures à celles permettant d'obtenir un K1C et le paramètre à utiliser est alors le KC. Pour ce paramètre, il ne nous a pas été possible de déterminer des valeurs moyennes et des écarts types. Peu de résultats sont disponibles et, de plus, ils sont très différents d'un Laboratoire à l'autre. Ces écarts mettent en cause probablement la conduite des essais mais aussi le fait que le KC doit être très sensible à ces conditions d'essais.

Le tableau 4 donne quelques résultats obtenus au LABORATOIRE CENTRAL de l'AEROSPATIALE.

TABLEAU 4

Valeur de KC à 20°C sur tôle d'alliage léger (éprouvette IRWIN)

Nuance	Epaisseur (mm)	Fréquence (HZ)	en fatigue: F - 0,1 F (MPa)	Longueur de fissure à rupture (mm)	KC fatigue (MPa$\sqrt{m}$)	KC statique (MPa$\sqrt{m}$)
A-U2GN T 65I	I,4	3I,5	I00	III,5	50	52 pour une épaisseur de 1 mm
		3I	I40	89	58	
		24,5	I80	84	71	
	2	26,5	I00	9I,5	43	
		27,5	I40	82,8	55	
		27	I80	79,5	69	
	3	24	I00	II6,5	52	48 pour une épaisseur de 3 mm
		27,5	I40	I05	66	
		25,5	I80	85,5	72	
	5	27	I00	9I,I	42	
		8,5	I40	88,3	58	
		8,5	I80	73,5	65	
A-U4G1 T 3	I,6	24	I00	III,2	50	69 pour une épaisseur de 2 mm
7075 T 735I	2	22,5	I00	II8,8	53	85
		24	I00	I25	59	
	4	30	I00	I25	59	80
		30	I00	I28	60	
	6	26	I00	I25	59	87
		26	I00	I25	59	

On peut noter dans ce tableau les écarts significatifs obtenus entre les valeurs du KC fatigue et celles du KC statique, les premières étant très sensibles à la contrainte maximale du cycle.

Finalement, les déterminations de K1C ou de KC sur éprouvette avec une méthode d'essai précise est d'un intérêt évident pour comparer en Laboratoire des traitements thermiques d'une même nuance en prenant soin de le faire sur un même et seul demi-produit. Pour comparer des nuances ou des fournisseurs entre eux, la déterminationde pré-paramètres K1C ou KC est également très intéressante à condition de travailler sur un échantillonnage suffisant.

Maintenant, au niveau conception, les résultats obtenus au stade éprouvettes de Laboratoire sont, en général, pauvres ou dispersés, ce qui implique que le simple choix du métal et de son traitement thermique n'est pas suffisant pour se garantir de rupture brutale sur appareil.

RESISTANCE A LA PROPAGATION DES CRIQUES EN FATIGUE

Lorsque des fissures apparaissent dans une structure, l'idéal serait de prévoir de façon quantitative quelle sera leur évolution au cours des cycles successifs de chargement. Cette connaissance permettrait d'estimer la durée de vie résiduelle de la construction en cause avant que ces fissures n'atteignent la dimension critique qui ferait courir des risques de rupture catastrophique. En fait, cette tentative correspond à deux recherches : - celle des seuils de détection sûrs des méthodes de contrôle non destructives - celle de la détermination des vitesses de propagation des criques en fatigue.

Sur le premier point, il faut rappeler que le seuil sûr de détection d'une méthode de contrôle non destructive fait intervenir une notion de probabilité de découverte qui dépend, à la fois de la méthode, des sous-ensembles sur lesquels elle est appliquée et du personnel qui l'applique.

Des résultats ont déjà été publiés, notamment aux Etats-Unis. Pour notre part, des études sont en cours pour essayer de chiffrer cette " probabilité " de détection pour différentes tailles de défaut sur un type d'éprouvette donné, mais nous ne possédons pas encore de résultats présentables.

Pour le second point, la détermination des vitesses de propagation des criques en fatigue, nous avons abordé le problème au stade Laboratoire. Nous utilisons des éprouvettes IRWIN ou ASTM et nous traçons les courbes $da/dN = f(\Delta K)$. Dans le même esprit que pour le K1C et le KC, nous avons essayé de regrouper suffisamment de résultats pour aborder l'aspect statistique de cette caractéristique.

Tout d'abord le Graphique N° 1 regroupe des essais sur les nuances A-U2GN T 6, 7075 T 73, A-U4SG T 6, A-U4G1 T 3 et 7475 T 73. La première remarque qui s'impose est que, hormis le 7475 et peut-être l'A-U4G1, les autres nuances donnent des résultats semblables. Les résultats que nous allons exposer sur A-U2GN sont donc transposables à ces autres nuances.

Nous avons regroupé dans les tableaux 5 et 6 les résultats obtenus sur A-U2GN T 6 pour, respectivement : les tôles minces - les tôles épaisses.

TABLEAU 5

Vitesse de propagation de criques en fatigue sous charge sinusoïdale (R = 0,1)

Tôle	Type éprouv.	Epaisseur (mm)	Fréquence (Hz)	Valeur de ΔK (MPa$\sqrt{m}$) pour da/dN = 10^{-3} mm/cycle	Valeur de ΔK (MPa$\sqrt{m}$) pour da/dN = 10^{-2} mm/cycle	Valeur de daN (mm/cycle) pour ΔK = 20 MPa$\sqrt{m}$	Valeur de daN (mm/cycle) pour ΔK = 32 MPa$\sqrt{m}$
1	Irwin	1,6	25	20,5	33	$9,9.10^{-4}$	9.10^{-3}
				20,2	33,6	$9,9.10^{-4}$	$8,9.10^{-4}$
2	Irwin	5	20	22,6	33	$5,8.10^{-4}$	$8,8.10^{-3}$
				20,8	31,5	$6,3.10^{-4}$	$1,3.10^{-2}$
	ASTM	5		18,1	28,1	$1,4.10^{-3}$	$2,8.10^{-2}$
				19	31,2	$1,1.10^{-3}$	1.10^{-2}
	Irwin	1,5	20	17,5	30,6	$1,4.10^{-3}$	$1,2.10^{-2}$
				20,1	34,5	$9,6.10^{-4}$	$7,3.10^{-3}$
3	Irwin	3	0,1	21,5	30,5	$8,7.10^{-4}$	$1,3.10^{-2}$
			1	19,6	30,7	$1,2.10^{-3}$	$1,1.10^{-2}$
			25	20	33,8	1.10^{-3}	8.10^{-3}

TABLEAU 6

Vitesse de propagation de criques en fatigue sous chargement sinusoïdal (R=0,1)

Tôle	Epais. tôle (mm)	Type éprouv.	Epais (mm)	Fréquence (Hz)	Valeur de ΔK (MPa$\sqrt{m}$) pour da/dN = 10^{-3} mm/cycle	Valeur de ΔK (MPa$\sqrt{m}$) pour da/dN = 10^{-2} mm/cycle	Valeur de daN (mm/cycle) pour ΔK = 20 MPa$\sqrt{m}$	Valeur de daN (mm/cycle) pour ΔK = 32 MPa$\sqrt{m}$
1 Fournis. (A)	50	Irwin	1,6	25	18	26,9	$2,4.10^{-3}$	$2,7.10^{-2}$
					19,4	29,8	$1,3.10^{-3}$	$1,4.10^{-2}$
2 Fournis. (A)	30	Irwin	1,6	25	18,5	30,3	$1,2.10^{-3}$	$1,5.10^{-2}$
					18,2	31	$1,4.10^{-3}$	1.10^{-2}
3 Fournis. (B)	45	Irwin	1,6	30	20,3	28,9	$9,8.10^{-4}$	$1,9.10^{-2}$
					19	32,1	$1,2.10^{-3}$	$9,9.10^{-3}$
4 Fournis. (B)	45	Irwin	1,4	30	19,7	31,9	1.10^{-3}	1.10^{-2}
					20,6	33	9.10^{-4}	$8,5.10^{-3}$
5 Fournis. (B)	45	Irwin	2	30	18,2	31,2	$1,6.10^{-3}$	$1,1.10^{-2}$
						36,4		$5,7.10^{-3}$
6 Fournis. (B)	30	Irwin	3,2	30	24	36,3	$8,4.10^{-4}$	5.10^{-3}
					23,6	35,9	9.10^{-4}	$5.10.10^{-3}$

Malgré le faible nombre de résultats, nous avons calculé les valeurs moyennes et les écarts types associés. Il ressort de cette exploitation que, sur A-U2GN T 6, en chargement sinusoïdal (R = 0,1) la vitesse varie comme suit :

- sur tôles minces à $\Delta K = 20$ MPa$\sqrt{m}$

$5{,}2.10^{-4} \leqslant da/dN \leqslant 2{,}1.10^{-3}$ mm/cycle , dans 95% des cas

à $\Delta K = 32$ MPa$\sqrt{m}$

$5{,}5.10^{-3} \leqslant da/dN \leqslant 2{,}2.10^{-2}$ mm/cycle, dans 95% des cas

- sur tôles épaisses à $\Delta K = 20$ MPa$\sqrt{m}$

$6{,}5.10^{-4} \leqslant da/dN \leqslant 2{,}4.10^{-3}$ mm/cycle , dans 95% des cas

à $\Delta K = 32$ MPa$\sqrt{m}$

$38.10^{-3} \leqslant da/dN \leqslant 2{,}8.10^{-2}$ mm/cycle , dans 95% des cas.

De la même façon, il faudrait examiner des résultats de mesure de vitesse en cyclage sinusoïdal en faisant varier la contrainte statique et le rapport contrainte dynamique sur contrainte statique. La variation de ces deux paramètres de chargement fait varier très sensiblement (du même ordre de grandeur ou plus qu'un changement de nuance) les vitesses de propagation.

D'autres facteurs tels que le mode de chargement et l'environnement influent encore sur la mesure de vitesse que l'on peut faire en Laboratoire. Par exemple, le passage du sinusoïdal simple au sinusoïdal plus quelques surcharges peut changer fondamentalement les résultats. Pour illuster l'importance du spectre de chargement, nous avons porté sur le graphique N° 2 les résultats obtenus sur éprouvettes en 606I T 6 sollicitées sous différents chargements complexes. Finalement, il s'avère que cette mesure de vitesse sur éprouvettes de Laboratoire est dispersée pour des conditions d'essais figées et, de plus, très sensible à ces conditions d'essais. Ceci ne met pas en cause l'intérêt de ces mesures pour des choix de matériaux mais n'autorise pas les Bureaux de Calcul à utiliser les valeurs obtenus pour la conception.

RESISTANCE A LA CORROSION SOUS TENSION

La recherche de l'immunité totale vis-à-vis de la corrosion sous tension a commandé, ces dernières années, les principaux développements dans le domaine des alliages légers. Nous disposons, à l'heure actuelle, de nuances et surtout de traitements de simple ou double revenu amenant à un état légèrement sur-revenu nous garantissant de ce type de ruine. Dans le cadre du Laboratoire, nous développons à la fois des essais sur éprouvettes non fissurées et sur éprouvettes pré-fissurées (KISCC). Le tableau 7 regroupe quelques valeurs de KISCC obtenues sur différents alliages légers sous forme de tôles épaisses laminées à charge ou déformation imposée constante.

TABLEAU 7

Matériau	Etat	Milieu	KISCC MPa$\sqrt{m}$
A-U2GN (2618 A)	T 351 + 4 h./190°C	1	6,3
	T 651 (T 351+19 h./190°C)	1	8,5
A-U4GI (2024)	T 351	1	6,3
		2	8,5
A-U4SG (2014)	T 651 (T 351+15 h./170°C)		9,5
	T 651 (T 351+10 h./177°C)		8,6
A-Z5GU (7075 français)	T 651	1	7,3
	T 7651	1	17-20
	T 7351	1	18-22
7075 (provenance USA)	T 651	2	7,6
	T 7651	2	22
	T 7351	2	24

(1) Solution A3 : essai en immersions-émersions alternées (10 mn - 50 mn)

(2) Solution à 3,5 % de NaCl avec mouillage de l'échantillon trois fois par jour

Pour ce paramètre, il n'est pas possible de dégager des valeurs de dispersion vu le peu de résultats.

Par contre, il existe deux classes de produit : les insensibles et les sensibles, pour le sens le plus défavorable, c'est à dire le travers court. Dans les autres sens, la tenue est toujours nettement supérieure, ce qui donne une possibilité d'emploi, même pour les nuances dites sensibles.

Finalement, la mesure de ce paramètre KISCC en Laboratoire permet d'établir un classement relatif des alliages entre eux. Par contre, pour la conception et contrairement au phénomène de fatigue, il nous semble que le simple choix de la nuance, associé à quelques précautions de dessin pour ne pas trop contraindre continument le métal en sens travers court, garantit des risques d'initiation et de propagation des criques en corrosion sous tension.

TENUE A L'INITIATION DE CRIQUES EN FATIGUE

Nous ne développerons pas ce point qui, sur le plan expérimental sur éprouvette de Laboratoire et sur sous-ensemble, est parfaitement défini. Nous voudrions seulement attirer l'attention sur les essais d'éprouvette de Laboratoire comprenant des lignes de fixation. Ce type d'essai apporte, à notre sens, un complément aux essais plus classiques d'éprouvette entaillée conduisant au tracé d'un diagramme de GOODMAN. La ligne de fixation est un cas fréquent sur appareil et le lieu privilégié des initiations de criques. Dans une ligne de fixation, la fabrication, même très bien conduite, conduit à des écarts de chargement entre les différents trous et les différentes fixations. Dans le choix d'une nuance, il faut prendre en compte son pouvoir d'accomodation géométrique au niveau des trous pour annuler les écarts de contrainte.

Le graphique N° 3 regroupe quelques résultats et met en évidence cette adaptation géométrique.

CONCLUSION

Nos résultats nous amènent à penser qu'actuellement les processus de fabrication ne sont pas suffisamment adaptés ou suffisamment précis pour garantir la reproductibilité des caractéristiques utilisées en mécanique de la rupture. Un contrôle systématique de ces paramètres en réception pourrait permettre de faire un tri après avoir vérifié que la dispersion sur un même produit n'est pas excessive. A notre avis, cette solution étant très onéreuse, elle ne doit être appliquée qu'exceptionnellement.

Pour le choix d'une nuance et de son traitement thermique associé, la mesure des paramètres K1C, KC et da/dN que nous pratiquons permet un premier classement. Par contre, nous avons constaté que le tracé des courbes $da/dN = f(\Delta K)$ est un essai peu sélectif. A notre avis, ce test de propagation est nettement insuffisant. Le manque de sélectivité de ce test par rapport à ce que nous avons pu constater sur appareil est lié principalement au mode de chargement nettement trop simplifié. Nous développons en complément des essais de propagation à chargement sinusoïdal incluant périodiquement des surcharges. Ce type d'essai dont les résultats détaillés vous seront exposés dans la conférence suivante met en évidence les possibilités de freinage ou de blocage des fissures suivant les nuances. Nous commençons également à développer des essais d'écrouissage cyclique pour apprécier l'évolution des caractéristiques mécaniques du métal au sein de la zone plastique, caractéristiques mécaniques qui peuvent être supérieures ou inférieures à celles du métal initial.

Pour la conception nous ne pensons pas que le seul choix d'une nuance et de son traitement thermique associé soit suffisant pour nous garantir des propagations de criques à vitesse excessive en fatigue. De même, nous ne pensons pas que les valeurs de vitesse de propagation et de facteur d'intensité de contrainte critique déterminé en Laboratoire sur éprouvette de Laboratoire puissent permettre au Bureau d'Etude d'effectuer des calculs de durée de fonctionnement de structure comportant des fissures; La procédure que nous appliquons actuellement dans ce but passe par des essais de module ou partie de structure aux formes réelles sollicitées suivant des spectres très proches de ceux enregistrés en vol. La durée de vie d'une structure fissurée dépend essentiellement des phases de ralentissement ou de blocage de la crique et dépend essentiellement des choix technologiques de construction et du type de spectre de charge rencontré.

Graphique N°1.

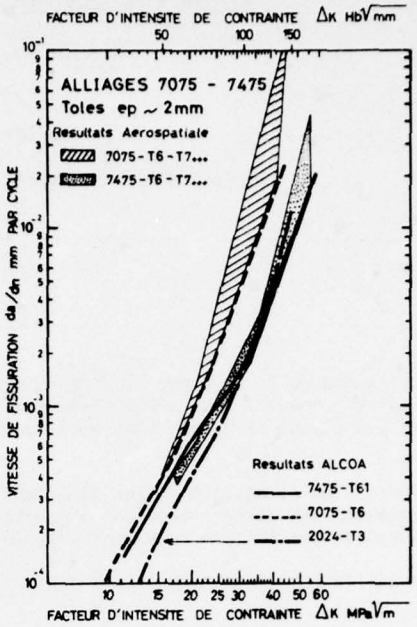

Graphique N°2.

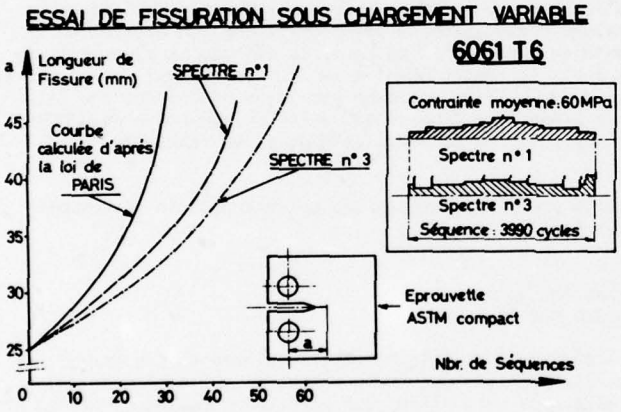

Graphique N°3.

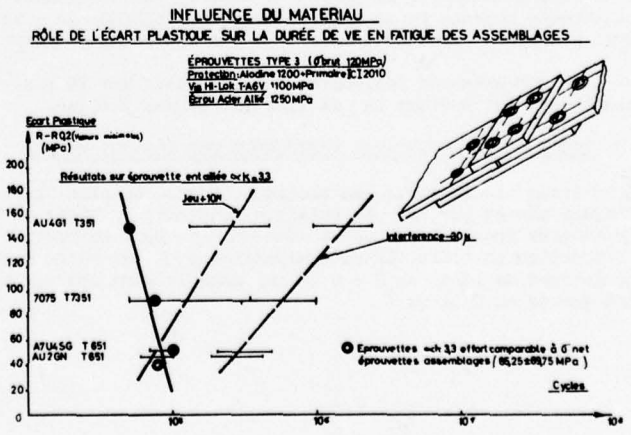

APPLICATION DE LA MECANIQUE DE LA RUPTURE A LA SELECTION DES ALLIAGES D'ALUMINIUM

2ème Partie : Résultats

par

BATHIAS Claude
Ingénieur au LABORATOIRE CENTRAL
de la SOCIETE NATIONALE INDUSTRIELLE AEROSPATIALE

-:-

RESUME

Comme suite à l'exposé de J. ODORICO, nous faisons le point des trois approches faites sur la mécanique de la rupture mises en oeuvre pour sélectionner les alliages d'aluminium et déterminer leur comportement en service. Les principaux résultats sont exposés et discutés en même temps que les moyens d'investigation :

- la détermination standard de KC et de da/dN
- la fissuration par fatigue sous des rapports de charges différents
- la fissuration par fatigue sous amplitude de charge variable

L'influence de l'environnement n'est pas abordé ici.

INTRODUCTION

Les produits de faible épaisseur mis en oeuvre dans l'Industrie Aéronautique sortent pratiquement toujours du cadre où la mécanique linéaire des ruptures s'applique couramment. La rupture par instabilité et la fissuration par fatigue des plaques minces en alliage d'aluminium se développent dans un domaine où la déformation plastique à fond de fissure est importante. Quoi qu'il en soit, la méthode la plus utilisée actuellement pour sélectionner les matériaux vis à vis du comportement à la fissuration est fondée sur le facteur d'intensité de contrainte calculé dans le mode I. Cette approche permet de déterminer des critères de rupture et des lois de comportement. Nous présentons dans ce qui suit les résultats du LABORATOIRE CENTRAL de l'AEROSPATIALE pour les trois types d'alliages les plus utilisés dans nos fabrications : l'A-U4GI, l'A-Z5GU et l'A-U2GN.

Comme il a été dit par J.ODORICO, notre méthodologie pour la sélection des matériaux et la détermination de leurs propriétés en fissuration passe par trois étapes qui sont :

- l'étude de KC
- l'étude de la fissuration sous sollicitation uniforme
- l'influence des surcharges sur la propagation des fissures.

Nous attachons une égale importance à l'incidence des caractéristiques métallurgiques et des paramètres mécaniques sur le comportement des matériaux à la fissuration. Les trois étapes de cette méthodologie n'ont pas le même intérêt pour sélectionner les alliages, mais elles nous paraissent également utiles pour déterminer les propriétés à prendre en compte dans le calcul des structures. C'est plutôt sous ce dernier aspect que sous le premier que le sujet est développé.

S'il est vrai que l'étude standard de la vitesse de fissuration par fatigue n'est pas une approche sélective pour prévoir le comportement des matériaux, c'est qu'elle ne tient pas compte de la réalité des sollicitations de service. Il suffit de simuler les conditions de fonctionnement en jouant par exemple sur la contrainte moyenne ou la modulation de l'amplitude du cycle pour rendre ce moyen d'investigation efficace tant au plan du choix des matériaux que sur celui du comportement en service.

Après avoir présenté rapidement nos résultats sur la résistance résiduelle, nous ferons une revue détaillée des études entreprises sur la fissuration par fatigue.

ETUDE DE LA RESISTANCE RESIDUELLE DES PLAQUES MINCES

Nous avons étudié, pour les alliages légers les plus utilisés, comment la rupture se produit dans des plaques minces portant une entaille centrale. En dépit de leurs imperfections, les deux critères K1C et KC restent le fondement de notre méthodologie pour déterminer les propriétés des matériaux à la rupture par fissuration instable. La détermination de KC est faite dans des plaques de 600 x 200 mm avec une fissure de fatigue de longueur $2a = 66$ mm, dans le sens travers long. La composition chimique des alliages étudiés est donnée au Tableau I.

La mise en charge de l'éprouvette ainsi fissurée est faite sur une machine hydraulique de traction 100 Tonnes en commandant la vitesse de montée en charge. Le calcul du KC est effectué à l'aide de la formule suivante, dans laquelle on tient compte de la correction de largeur définie de DIXON :

$$K_c = \left[1 - \left(\frac{2a}{W}\right)^2\right] - \frac{1}{2} \times \sigma\sqrt{\pi a}$$

σ est pris pour étant la contrainte moyenne pleine tôle au moment de la rupture, 2 a est la longueur de la fissure au moment de la rupture.

Pour chaque nuance essayée, nous avons déterminé, dans quelques cas, la valeur de KC au début de la propagation de la fissure. Ces essais complémentaires, associés à un enregistrement photographique de la rupture, nous ont permis de préciser le comportement des matériaux. Les résultats obtenus présentés dans les figures I à 3 vérifient bien que les courbes représentatives de KC en fonction de l'épaisseur présentent un maximum vers les faibles épaisseurs. Ce maximum est atteint pour une épaisseur d'environ 3 mm pour les alliages dans l'état T 6 ou T 4. Un écrouissage de la tôle entre trempe et revenu a pour effet d'aplatir la courbe.

Une étude systématique des cassures a montré que la chute du KC vers les épaisseurs croissantes correspond à la transition contrainte plane - déformation plane. Une exception : l'A-Z5GU T 735I, lequel se rompt toujours en cisaillement jusqu'à l'épaisseur de 10 mm et ne présente pas de maximum marqué pour les tôles minces. Son excellent niveau de résistance résiduelle (80 MPa$\sqrt{m}$) est donc grosso modo indépendant de l'épaisseur du produit.

Sans entrer dans le détail du processus de rupture des plaques minces fissurées, il est intéressant de noter que la propagation stable de la fissure qui précède l'instabilité est longue de plusieurs millimètres dans l'A-U2GN T 65I alors qu'elle est très courte dans l'A-Z5GU T 735I où le bout de fissure s'émousse avant qu'il n'y ait propagation. Ces différences se retrouvent dans l'écart qui existe entre le KC à la rupture brutale et le KC au début de la propagation. Ce dernier est plus faible que le premier. Il est d'environ 25% pour l'A-U2GN T 65I , 15% pour l'A-U2GN T 6 et l'A-U4GI T 35I , 10% pour l'A-Z5GU T 65I et 5% pour l'A-Z5GU T 735I. (Tableau 2).

En toute rigueur, on est tenté de considérer le KC au début de la propagation pour être parfaitement à l'abri de la rupture, mais il faut souligner que même cette valeur est encore plus élevée que le K1C déterminé selon la Norme. De ces résultats, il apparait qu'en produit de faible épaisseur, les alliages étudiés se classent, par rapport à la valeur de KC maxi, de la façon suivante :

- A-Z5GU T 735I 85 MPa $\sqrt{m}$
- A-U4GI T 4 75 MPa $\sqrt{m}$
- A-Z5GU T 6 75 MPa $\sqrt{m}$
- A-U4GI T 35I 68 MPa $\sqrt{m}$
- A-U2GN T 6 65 MPa $\sqrt{m}$
- A-Z5GU T 65I 60 MPa $\sqrt{m}$
- A-U2GN T 65I 55 MPa $\sqrt{m}$

ETUDE STANDARD DE LA FISSURATION PAR FATIGUE

Les essais de fissuration par fatigue sont effectués dans des éprouvettes compactes dont le paramètre W = 75 mm et dans des éprouvettes plates à entaille centrale lorsque l'épaisseur est inférieure à 5 mm. A épaisseur égale, on ne note pas d'influence du type d'éprouvette sur les résultats. Sauf indication contraire, la fissure se propage dans la direction TL. Dans les études standard de la fissuration par fatigue, les essais sont conduits avec un rapport R voisin de zéro sous une sollicitation sinusoïdale uniforme. L'écart entre deux courbes représentatives de la relation de PARIS n'a de signification que par rapport à la dispersion des essais. Généralement, pour étudier l'influence d'un paramètre, on s'est fondé sur trois essais, quelquefois cinq.

Entre plusieurs essais du même type, on observe une dispersion qui est habituellement inférieure à un rapport 2 pour des vitesses comprises entre 10^{-4} mm/cycle et 10^{-1} mm/cycle. Un écart entre deux courbes n'est donc considéré comme significatif que si la vitesse de fissuration diffère au moins d'un facteur 2 pour un K donné. Si on tient compte de la dispersion, l'influence de nombreux paramètres, y compris la composition chimique des alliages, sur la vitesse de fissuration est souvent faible à l'échelle de la représentation graphique, en particulier pour les vitesses en régime établi entre 10^{-5} et 10^{-3} mm/cycle (FIGURE 4). Les écarts se creusent pour les vitesses élevées, mais alors les critères K1C et KC semblent mieux adaptés dans ces circonstances pour choisir les matériaux, eu égard à la difficulté des mesures des grandes vitesses de fissuration.

I°- Influence de la direction de la fissure par rapport au laminage

Dans l'A-U2GN T 65I, on n'a pas trouvé d'influence de la direction de la fissure par rapport au laminage. Les essais ont été effectués sur des éprouvettes de 1,6 - 2 et 3,2 mm d'épaisseur. Il semble donc que l'écrouissage cyclique à fond de fissure détruise l'effet de la texture. On pourrait trouver là une explication au fait que la propagation brutale d'une fissure est sensible à la direction de propagation par rapport au laminage, alors que la fissuration par fatigue ne l'est pas.

2°- Influence de l'épaisseur de l'éprouvette

L'influence de l'épaisseur a été étudiée sur l'A-U2GN T 65I et l'A-Z5GU T 735I pour des épaisseurs comprises entre 1 mm et 8 mm (FIGURES 5 et 6). Les résultats obtenus ne sont pas aussi clairs que ceux connus pour la détermination du facteur critique KC parce que la vitesse de fissuration est, à la vérité, assez peu affectée par l'épaisseur de l'éprouvette. Toutefois, on remarque pour les deux alliages que :
- pour les fortes épaisseurs 8 et 5 mm, la vitesse de fissuration est plus grande que pour les faibles épaisseurs
- l'épaisseur optimale pour laquelle la vitesse est la plus faible est de l'ordre de 2 à 3 mm.

3°- Influence de la fréquence

L'influence de la fréquence a été étudiée sur des éprouvettes en A-U2GN T 6 de 1,6 mm d'épaisseur entre 0,1 et 30 Hz (FIGURE 7). Dans cette gamme de fréquence, on ne note pas d'influence de la fréquence de la vitesse de propagation de la fissure. Nos résultats sont en accord avec ceux que l'on peut relever dans la littérature /1/. Généralement, dans les alliages légers et même dans les aciers, on ne trouve ni d'influence de la fréquence entre 0,1 et 50 Hz, ni d'influence de la contrainte nominale sur la vitesse de fissuration lorsque les essais sont faits à la température ambiante et en l'absence d'un effet d'environnement.

4°- Influence de la température (FIGURE 8)

Nos résultats d'essais obtenus sur l'A-U2GN T 6 montrent que, jusqu'à 200°C, la vitesse de fissuration décroît légèrement lorsque la température augmente dans le domaine limité entre 10^{-3} et 10^{-2} mm/cycle. Entre 10^{-2} et 10^{-1} mm/cycle, la température n'a pas d'influence. Des essais effectués aux fréquences de 0,1 et 25 Hz n'ont pas permis de mettre en évidence une influence de la fréquence dans les essais à chaud. Les résultats montrent que l'A-U2GN est particulièrement apte à résister à la propagation des fissures de fatigue à température élevée, ce qui n'est pas le cas des alliages non revenus comme d'A-U4GI T 3. Des expériences faites au M.I.T sur l'A-U4GI T 3 montrent qu'à 135°C la vitesse de fissuration est plus élevée qu'à la température ambiante. L'écart se creuse encore si la température atteint 240°C. /2/

5°- Influence de la pureté des alliages de la série 7000

La composition chimique a une influence plus ou moins marquée sur la fissuration par fatigue. La pureté en silicium et en fer des alliages de la série 7000 a, par contre, une influence assez nette sur les vitesses de fissuration supérieures à 10^{-4} mm/cycle. Autour de 10^{-2} mm/cycle, on observe un écart d'un ordre de grandeur entre les résultats obtenus sur un 7075 et un 7475. Ce dernier alliage présente alors les meilleures caractéristiques à la fissuration par fatigue de tous ceux de sa catégorie.

INFLUENCE DU RAPPORT R SUR LA FISSURATION PAR FATIGUE

Le rapport de charge R = K min / K max est un des paramètres qui, avec l'effet des surcharges, nous parait le plus utile à considérer pour déterminer le comportement des matériaux en service vis à vis de la fissuration par fatigue. Cette question a été abordée avec des sollicitations de quatre types (FIGURE 9)à l'aide d'éprouvettes compactes de 5 mm d'épaisseur et d'éprouvettes à entaille centrale de 5 et I,5 mm d'épaisseur.

I°- Résultats obtenus sur éprouvettes compactes

On observe que toute variation de R est accompagnée par une modification des coefficients C et m de la loi de PARIS (FIGURES 10 à 16). Dans les configurations du type A, la vitesse de fissuration à Δ K donné augmente avec R compris entre 0,01 et 0,5. Lorsqu'une partie du cycle est en compression, pour R = 0,3, on n'observe pas d'effet notable si on ne considère que la partie positive de l'amplitude du facteur d'intensité de contrainte Δ K.

Dans les configurations du type B, le rapport R est constamment voisin de zéro et on devrait, en principe, trouver des courbes confondues quelle que soit la charge maximale du cycle, ce qui est seulement vérifié pour des vitesses de fissuration de l'ordre de 10^{-3} mm/cycle. A l'exception de l'A-U2GN pour lequel les résultats sont quasiment confondus à la dispersion près, on trouve que, dans le domaine des vitesses supérieures à 10^{-2} mm/cycle, la vitesse augmente avec la charge maximale du cycle. Puisque le facteur d'intensité de contrainte maximale K max est, dans ce cas, égal à Δ K, il ne peut y avoir d'effet du paramètre K max mais seulement de la charge maximale. Cet effet se traduit par une augmentation substantielle du coefficient m de la loi de PARIS avec la charge maximale appliquée initialement à l'éprouvette. Pour les longueurs de fissure les plus grandes, l'amplitude de la déformation plastique cyclique en avant de la fissure est importante : elle pourrait expliquer les écarts observés.

Dans les configurations du type C, on observe encore que la vitesse de fissuration augmente, à Δ K donné, lorsque R augmente de 0,5 à 0,75. Le coefficient m augmente avec R de telle sorte que, pour des vitesses de l'ordre de 10^{-4} mm/cycle, on ne remarque pas d'influence de R bien que K max soit très différent d'un cas à l'autre. Ainsi, pour ces faibles vitesses et pour un facteur d'intensité de contrainte moyen suffisamment élevé, la fissuration ne parait dépendre que de Δ K.

Les configurations du type D sont les seules où le coefficient m décroît lorsque R augmente. Néanmoins, à Δ K donné, la vitesse de fissuration augmente avec R. La variation de m pourrait être attribuée, comme dans les configurations B, à la grande amplitude de la déformation plastique cyclique, m diminuant avec cette dernière.

Pour chaque configuration, les alliages étudiés réagissent avec des différences qui peuvent être mises en évidence pour un ΔK commun. La valeur de 15 MPa$\sqrt{m}$ convient bien pour des vitesses de fissuration de l'ordre de 10^{-3} mm/cycle. On trouve alors des facteurs sur la vitesse de 10 et de 20 lorsque R passe respectivement de 0,01 à 0,5 et de 0,01 à 0,75 pour l'A-U2GN T 6 alors qu'ils ne sont que de 6 et de 10 avec les mêmes valeurs de R pour l'A-U4G1 T 3 et l'A-Z5GU T 73.

2°- Résultats obtenus sur éprouvettes à entaille centrale

Les résultats obtenus avec des éprouvettes plates à entaille centrale sont très similaires à ceux obtenus avec des éprouvettes compactes. A la dispersion près, l'influence du rapport R sur la vitesse de fissuration est retrouvée pour les éprouvettes d'épaisseur 1,5 mm et 5 mm. On note que l'influence du rapport R a tendance à être plus importante sur les éprouvettes les plus épaisses.

Les coefficients m de la loi de PARIS sont un peu plus grands dans les éprouvettes de 5 mm. L'influence de l'épaisseur reste toujours très modeste par rapport à celle de R. A l'exception de l'A-U2GN, on observe toujours une influence de la charge initiale sur les résultats des configurations du type B. Nous avons calculé pour un ΔK de 50 MPa$\sqrt{m}$ que la contrainte maximale dans la section restante est de l'ordre de 500 MPa pour la configuration 4, alors qu'elle n'est que 250 MPa pour la configuration 6. Il n'est donc pas surprenant de trouver dans ces conditions, une influence de la charge maximale lorsque cette dernière conduit à une déformation plastique généralisée.

3°- Discussion

Les résultats obtenus avec les deux types d'éprouvettes sont cohérents. L'accord des deux méthodes est particulièrement bon pour les rapports R élevés. Dans cette étude, nous nous sommes efforcés de faire varier R de plusieurs façons. En général, lorsque R augmente de 0 à 0,75, la vitesse de fissuration augmente, à ΔK donné, dans le domaine des vitesses compris entre 10^{-4} et 10^{-2} mm/cycle. Les coefficients C et m de la loi de PARIS sont simultanément affectés sans qu'aucune règle précise puisse être dégagée. Lorsque R augmente, le coefficient m peut augmenter ou diminuer selon la configuration du cycle.

L'augmentation de R entraine, évidemment, une augmentation de K max pour un ΔK donné et, comme nous le verrons plus loin, une augmentation de K max a tendance à provoquer des ruptures statiques qui accélèrent la vitesse de fissuration pour les ΔK élevés. Par conséquent, le rapport R et le coefficient m devraient augmenter ensemble. S'il n'en est pas toujours ainsi, c'est qu'un autre facteur intervient. Cet autre facteur pourrait être la charge maximale appliquée initialement à l'éprouvette. En effet, dans les configurations du type B, R , K max et K min sont constants pour un ΔK donné et on observe néanmoins une augmentation du coefficient m avec la charge maximale liée essentiellement à une accélération de la vitesse au-delà de 10^{-2} mm/cycle.

Dans les éprouvettes plates à entaille centrale, on vérifie, à ΔK donné, que m augmente, soit lorsque la charge initiale augmente, soit lorsque la contrainte dans la section restante de l'éprouvette diminue. Ces deux situations sont souvent concomitantes.

Dans les configurations du type D, où la charge moyenne est constante, K max varie moins que dans les configurations A et C lorsque R varie. Il s'ensuit que dans la configuration 10, K max est 1,5 fois plus grand que dans la configuration 11, alors qu'il est deux fois plus grand à ΔK identique dans la configuration 2 que dans la configuration 1 et ceci pour des R donnés. L'influence de K max liée au déclenchement des ruptures statiques sera donc moins marquée dans les configurations D que dans les configurations A et C. Par contre, les variations de contrainte dans la section restante sont plus importantes dans les configurations D. Par exemple, dans les éprouvettes plates à entaille centrale, pour ΔK : 25 MPa$\sqrt{m}$, la contrainte dans la section restante est de 160 MPa dans la configuration 11 ; elle est de 400 MPa dans la configuration 10 et de 250 MPa dans la configuration 1.

Ces considérations tendent à expliquer que la pente de la droite représentative de la configuration 10 est plus faible que celle de la configuration 11 à cause de la déformation plastique importante qui se développe dans le premier cas pour les ΔK élevés.

En conclusion, il apparait que deux effets antagonistes s'exercent sur le coefficient m : l'un est R ou K max, l'autre est la contrainte dans la section restante de l'éprouvette ou bien la charge initiale appliquée. L'accroissement de R accélère la fissuration en favorisant des processus de rupture statique. Celui de la contrainte dans la section restante introduit un ralentissement lorsque le métal peut se consolider sous déformation cyclique, traduisant ainsi l'influence de l'histoire de la fissuration.

L'A-U2GN T 6, le moins ductile des trois matériaux essayés, est le moins sensible à l'effet de charge, mais il est, en revanche, le plus sensible à l'effet de K max.

Dans la limite de nos essais, il semble que l'effet de la charge n'intervienne que dans le domaine des fortes vitesses et que sur le coefficient m ; alors que R influe simultanément sur m et sur une translation de la courbe de PARIS. De ce fait, c'est le paramètre R qui exerce la plus grande influence sur la vitesse de fissuration, l'effet de charge n'étant à considérer que comme une correction supplémentaire .

Des observations microfractographiques montrent que, pour un rapport R voisin de zéro ou négatif, le faciès de la cassure est strié jusqu'à des vitesses de l'ordre de 10^{-3} mm/cycle. Lorsque le rapport R augmente à 0,5 et 0,75, le pourcentage de plages striées diminue pour faire place à des plages de cupules. La vitesse microscopique est, dans ces conditions, différente de la vitesse macroscopique, laquelle augmente à cause de la formation des cupules.

4°- Vérification de la relation de FORMAN

Bien que plusieurs relations aient été proposées pour rendre compte de l'influence de R sur la vitesse de fissuration, c'est celle de FORMAN qui a, actuellement, le plus de crédit :

$$\frac{da}{dN} = \frac{C'\Delta K^n}{(1-R)K_c - \Delta K}$$

Une discussion très complète de la validité de ces relations est donnée par SJ.MADDOX [3]. Nous trouvons que nos résultats expérimentaux sont approximativement en accord avec la relation de FORMAN pour des valeurs de R comprises dans un domaine de variation restreint. En prenant pour KC une valeur proche de K max, lorsque da/dN tend vers l'infini, on trouve pour les trois alliages étudiés les relations suivantes :

- pour l'A-U2GN T 6 $\quad \frac{da}{dN} = \frac{6,5.10^{-7}(\Delta K)^{4,12}}{(1-R)\,60 - \Delta K}$

- pour l'A-U4GI T 3 $\quad \frac{da}{dN} = \frac{5,6.10^{-6}(\Delta K)^{2,94}}{(1-R)\,70 - \Delta K}$

- pour l'A-Z5GU T 73 $\quad \frac{da}{dN} = \frac{1,7.10^{-5}(\Delta K)^{2,66}}{(1-R)\,80 - \Delta K}$

Une des difficultés que nous avons rencontrée dans l'établissement de la relation de FORMAN est le choix de KC.

5°- Résultats antérieurs

Des travaux antérieurs [4-5] avaient déjà montré la forte influence de R sur la vitesse de fissuration des alliages légers à haute limite d'élasticité par opposition aux alliages à faible limite d'élasticité et aux aciers au carbone. GUNN, HUDSON et PEARSON [4-5] trouvent un effet de R sur les coefficients C et m de la relation de PARIS pour les alliages A-U4GI, A-Z5GU et A-U2GN. BROEK et SCHIJVE ne trouvent un effet que sur le coefficient C [6].

A la lumière de notre étude, il semble effectivement que pour certains types de sollicitation (le type A par exemple), seul le coefficient C soit affecté, mais, dans le cas général, C et m le sont simultanément. Conformément aux résultats de PEARSON, nous trouvons que l'alliage le moins ductile, l'A-U2GN, est le plus sensible aux variations de R.

INFLUENCE DES SURCHARGES SUR LA FISSURATION PAR FATIGUE

Les sollicitations réelles en service sont généralement non uniformes. Il est bien connu que le cumul linéaire des dommages en fatigue ne convient qu'aux faibles variations de sollicitation. Chaque fois qu'il y a succession de cycles dont les amplitudes sont très différentes, le cumul de dommage n'est pas linéaire. Un cas particulièrement représentatif des conditions de service est celui de la propagation d'une fissure de fatigue sous une sollicitation comportant des surcharges.

Dans la mesure où la vitesse de fissuration est très perturbée par l'application d'une surcharge, nous attachons une grande importance au comportement des matériaux ainsi sollicités.

Le ralentissement de la fissure après application d'une surcharge a été attribué [7-8-9] à la formation d'une zone plastifiée importante due à la surcharge et aux conséquences qui en découlent : formation de contraintes résiduelles de compression, réduction du Δ K effectif, émoussement de la fissure. Plusieurs modèles ont été proposés en s'appuyant sur l'hypothèse que la propagation de la fissure est ralentie tant que la zone plastifiée initiale est entièrement inscrite dans la zone plastifiée due à la surcharge. Nous avons cherché à vérifier le bien fondé de cette hypothèse en étudiant simultanément la vitesse de fissuration et l'étendue de la zone plastifiée à fond de fissure. Par ailleurs, nous nous sommes efforcés de mettre en évidence les mécanismes microscopiques mis en jeu.

Les résultats donnés ici portent sur l'étude de la zone plastifiée, sur la relation entre la longueur de la fissure affectée et le diamètre de la zone plastifiée, sur l'influence de la modulation des surcharges, sur le mécanisme microscopique et sur la comparaison du comportement des alliages en fonction de leurs traitements thermiques.

I°- Procédure expérimentale

Les essais de fatigue sont effectués sur une machine asservie, pilotée par un calculateur PDP II, sous sollicitation sinusoïdale, à 1 hertz sauf exception. Le rapport R est maintenu à 0,01. Les éprouvettes sont du type compact avec W = 75 mm et B = 10 mm. L'alliage A-U4G1 T 35I a une limite d'élasticité de 320 MPa ; l'A-U2GN T 65I revenu I9 h. à I90°C ou sous revenu I0 h. à I90°C a une limite d'élasticité de 400 MPa. La vitesse de fissuration est mesurée en surface à l'aide d'un microscope mobile de grossissement 30. La vitesse microscopique est déterminée au microscope électronique sur répliques.

2°- Mesure de la zone plastifiée

La zone plastifiée par la surcharge est mise en évidence à la surface de l'éprouvette soigneusement polie électrolytiquement, par éclairage en lumière rasante et observation en lumière diffractée. La mesure des dimensions de la zone plastifiée est faite sur clichés photographiques sans difficulté notable. Conformément au modèle théorique, la zone plastifiée est constituée de deux ailes dont la dimension r_y perpendiculaire à la fissure est approximativement donnée par la relation d'IRWIN :

$$r_y = \frac{1}{2\pi}\left(\frac{\Delta K}{Re}\right)^2$$

Dans la direction de propagation, r_x vaut à peu près le quart ou le cinquième de r_y . Pour l'A-U4G1, les valeurs de r_y calculées et mesurées coïncident à 20% près. Pour l'A-U2GN, les valeurs mesurées sont supérieures aux valeurs calculées. Quel que soit l'alliage, on trouve que le nombre de surcharges appliquées a une faible influence sur la dimension mesurée de r_y .

Pour un faible facteur d'intensité de contrainte, on peut considérer que r_y est constant pour une à cent surcharges consécutives. Pour des facteurs d'intensité de contrainte plus élevés, le rayon r_y mesuré augmente un peu entre une et dix surcharges mais on le trouve constant pour cinquante et cent surcharges. Ces différences peuvent être dues à la saturation de la déformation plastique. Les deux ailes de la zone plastifiée forment un angle de 40 à 60° avec le plan de la fissure, cet angle étant le plus petit pour les surcharges les plus fortes.

3°- Mesure du ralentissement de la fissure pour une surcharge

Lorsque le taux de surcharge $\frac{\Delta K \text{ pic}}{\Delta KC}$ augmente, on observe une augmentation de la longueur de fissure et du nombre de cycles affectés par le ralentissement, ainsi qu'une diminution de la vitesse minimale observée au cours du ralentissement. La longueur de fissure affectuée a' est, en général, inférieure au diamètre $2\,r_y$ mesuré, sauf pour l'alliage A-U4GI où il peut y avoir coïncidence pour les surcharges élevées . Ces derniers résultats sont en accord avec ceux de RW.HERTZBERG [7] .

La longueur de fissure affectée est toujours supérieure à la dimension de la zone plastifiée dans la direction de propagation. Pour l'A-U4GI, a' vaut 70 à 100% de $2\,r_y$. Pour l'A-U2GN, a' vaut environ 75% de $2\,r_y$ quel que soit le taux de surcharge (FIGURES 17 à 19). Nous avons relevé une influence de la fréquence sur le processus de ralentissement. A la fréquence de 10 Hertz, la longueur de fissure et le nombre de cycles affectés augmentent alors que la taille de la zone plastifiée est inchangée. A 0,1 hertz nous observons le phénomène inverse.

4°- Influence du nombre de surcharges et des modulations

Pour un taux de surcharge donné, si on multiplie le nombre de surcharges consécutives, le nombre de cycles affectés croît alors que la vitesse minimale au cours du ralentissement décroît. On observe alors dans les deux cas une asymptote qui apparait entre 10 et 50 surcharges (FIGURE 20).

La longueur de fissure affectée a' augmente sensiblement avec le nombre de surcharges, de façon à ne s'étendre que sur 25% de la dimension $2\,r_y$ mesurée pour les surcharges les plus élevées. Il apparaît donc que a' augmente moins vite que $2\,r_y$. Ces observations, ajoutées à celles sur l'influence de la fréquence, montre qu'il n'existe pas, en général, de ralation simple entre le diamètre de la zone plastique et la longueur de la fissure où il y a ralentissement. Cependant, pour chaque configuration, on trouve un rapport constant entre ces deux dimensions.

Nous avons enfin essayé des surcharges modulées en dix ou vingt cycles dans l'A-U4GI. Pour un taux de surcharge de 1,5 la modulation n'apporte pas de modification notable sur le ralentissement. Pour un taux de surcharge de 2, des surcharges égales consécutives sont nettement plus efficaces que des surcharges modulées.

Il ressort de nos essais que le taux de surcharge et la valeur nominale de la surcharge sont les paramètres prédominants du processus de ralentissement. La fréquence, le nombre de surcharges, la modulation, sont des paramètres moins importants. L'influence de l'épaisseur de l'éprouvette n'a pas été étudiée.

5°- Aspect microscopique du processus de retard

Dans des éprouvettes de 10 mm d'épaisseur, la fissure est plane. L'application d'une ou plusieurs surcharges produit une déchirure en forme de croissant comme indiqué dans la FIGURE 21. La progression de la fissure au centre de l'éprouvette est très supérieure à celle prévue par la loi de PARIS. En revanche, à la surface de l'éprouvette, la fissure reste bloquée. La déchirure est constituée à l'échelle microscopique de cupules et, de ce fait, la fissure est émoussée au centre de l'éprouvette.

Par observations micrographiques, nous avons mis en évidence que la fissure reste complètement arrêtée, après la surcharge, au sommet de la déchirure, mais elle continue à se propager dans les ligaments compris entre la déchirure et la surface jusqu'à ce que le front de la fissure rattrape sa forme initiale. Le ralentissement est donc essentiellement lié à la zone plastifiée qui se développe à la surface de l'éprouvette et aux conséquences qui en résultent.

6°- Comparaison des deux alliages

Pour un Δ Ko initial de l'ordre de 12 MPa$\sqrt{m}$, le ralentissement dû aux surcharges est en moyenne comparable dans l'A-U4Gl et l'A-U2GN sous-revenu. Il est moindre dans l'A-U2GN revenu. Toutefois, on bloque pratiquement la fissure pour un taux de surcharge de 2,3 dans l'A-U4GI, ce qui n'est pas possible pour l'A-U2GN. Pour un même taux de surcharge, on observe que, lorsque Δ K pic augmente, la vitesse minimale diminue et le nombre de cycles affectés augmente pour l'A-U4GI. C'est l'inverse pour l'A-U2GN. Mais pour ces deux alliages, la longueur de fissure affectée augmente.

La conclusion la plus importante qui ressort de cette étude des alliages A-U4GI et A-U2GN est que le processus de ralentissement des fissures de fatigue par application de surcharges est lié à la déformation plastique à fond de fissure et à la surface de l'éprouvette mais qu'il n'existe pas de relation simple entre le diamètre de la zone plastifiée et le ralentissement. Ce dernier semble dépendre en plus de la ténacité, de la consolidation cyclique du métal, de la déformation plastique cyclique. Ces paramètres qui jouent sur les contraintes résiduelles et le Δ K effectif doivent être pris en compte pour exprimer correctement ce phénomène.

CONCLUSIONS

Nous avons passé en revue les principaux résultats obtenus par trois approches fondées sur la mécanique de la rupture pour sélectionner les alliages d'aluminium et déterminer leur comportement en service. Tous les résultats présentés paraissent utiles mais certains d'entre eux semblent insuffisants. En particulier l'essai standard de fissuration par fatigue ne conduit pas à la discrimination réaliste et nécessaire pour la détermination optimale du comportement des structures fissurées.

C'est pourquoi une simulation des conditions de service en tenant compte du rapport de charge des variations d'amplitude nous paraît indispensable. Ces investigations sont complétées, en général, par l'étude de l'influence de l'environnement, corrosion sous tension ou fatigue-corrosion, cette dernière étant la plus représentative des sollicitations des structures aéronautiques.

BIBLIOGRAPHIE

/1/ GT. HANN -R.SIMON Metallurgical Control Of Fatigue Crack Growth In High Strength Aluminium Alloys AFML - TR 72-48 May 1972

/2/ K.ERHARDT - A.WILSON - RM.PELLOUX - M.GRANT Mechanism Of Fatigue Crack Propagation In Aluminium Alloys AFML - TR 71-109 May 1971

/3/ SJ.MADDOX The Effect Of Mean Stress On Fatigue Crack Propagation A Literature Review Int. Jour. Of Fract. Volume 11 June 1975 - Page 389

/4/ NJ. GUNN Fatigue Cracking Ratis and Residual Strengths of Eight Aluminium Alloys RAE Technical Report 64.824, Octobre 1964

/5/ S.PEARSON The Effect of Mean Stress on Fatigue Crack Propagation in Half-Inch Thick Specimens of Aluminium Alloy RAE Techn.Report 68297 - 1968

/6/ D.BROEK and J.SCHIJVE The Influence Of The Mean Stress On The Propagation of Fatigue Cracks In Light Alloy Sheet - Aircraft Engineering - March 67, page 10

/7/ RW.HERTZBERG and WJ.MILLS The Effect Of Sheet Thickness On Fatigue Crack Retardation in 2024 T 3 Aluminium Alloy Eng. Fract. Mech. 75 Vol. 7 pages 705-711

/8/ J.SHIJVE Prediction of Fatigue Crack Propagation in Aircraft Materials Under Variable Amplitude Loading Rep. VTH 193 - DELFT UNIVERSITY March 75

/9/ WD. DOVER - NF.BOUTLE Crack Closure Of Positive Stresses During Random Load Fatigue Crack Growth - Journ. of Strain An. Vol. II, N° 01, 1976, pages 32-38

TABLEAU I : Composition chimique des alliages

	Cu	Mg	Ni	Mn	Cr	Si	Fe	Ti	Zn
A_U4G1	4,4	1,45	_	0,6	_	0,09	0,22	_	0,05
A_U2GN	2,4	1,63	1,13	0,05	_	0,1	1,13	0,11	0,07
A_Z5GU	1,52	2,55	_	0,04	0,22	0,14	0,21	0,05	5,88

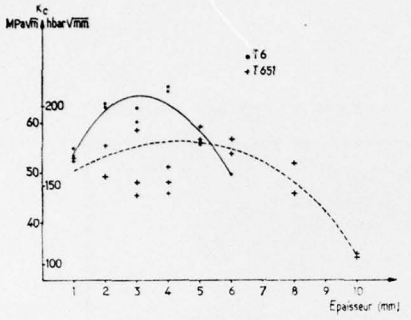

Fig.1 Alliage A_U2GN

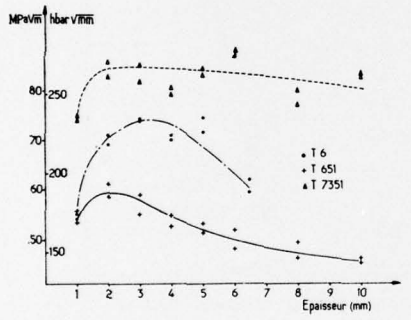

Fig.2 Alliage A_Z5GU

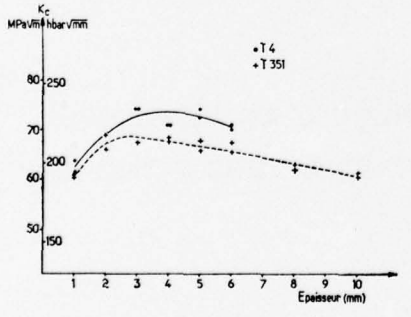

Fig.3 Alliage A_U4G1

TABLEAU II : Influence de la propagation stable sur la détermination de Kc, Eprouvette type Irwin.

Nuance	Etat	Epaisseur (mm)	Kc MPa $\sqrt{m}$ au début de la propagation stable	Kc MPa $\sqrt{m}$ a la rupture brutale
A_U2GN	T 6	1	44	53
		2	55	64
		3	51	60
		3	57	63
		6	41	50
A_U2GN	T 651	8	36	52
		8	36	46
A_Z5GU	T 651	6	50	52
		6	45	48
		8	39	49
		8	43	46
		10	42	46
A_Z5GU	T 7351	8	78	79
A_U4G1	T 351	8	54	63
		8	52	62

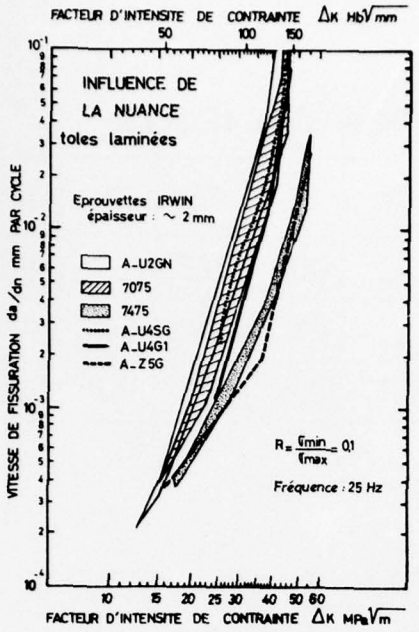

Fig. 4 : Comparaison des vitesses de fissuration de plusieurs alliages d'aluminium

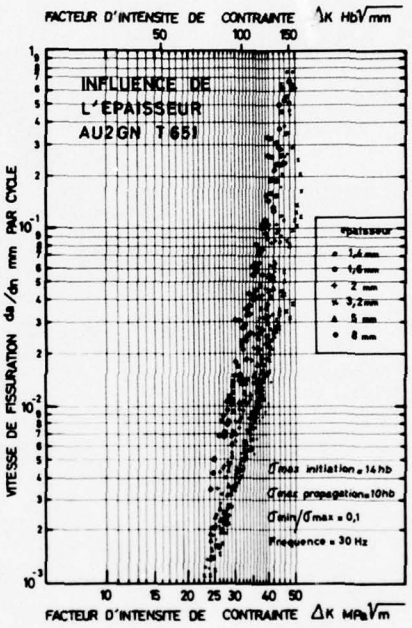

Fig. 5 : Influence de l'épaisseur sur la vitesse de fissuration de l'AU2GN

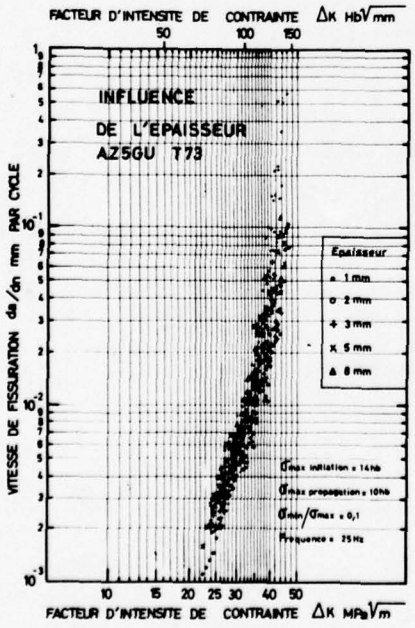

Fig. 6 : Influence de l'épaisseur sur la vitesse de fissuration de l'AZ5GU

Fig. 7 : Influence de la fréquence sur la vitesse de fissuration

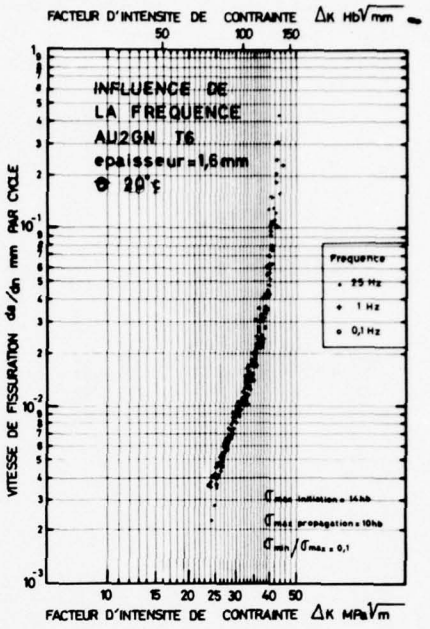

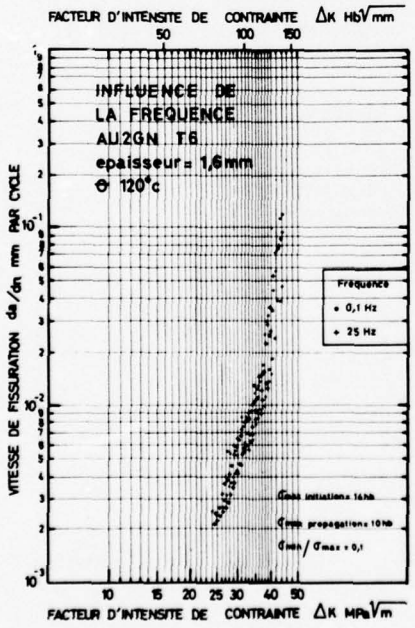

Fig. 8 : Influence de la température d'essai sur la vitesse de fissuration

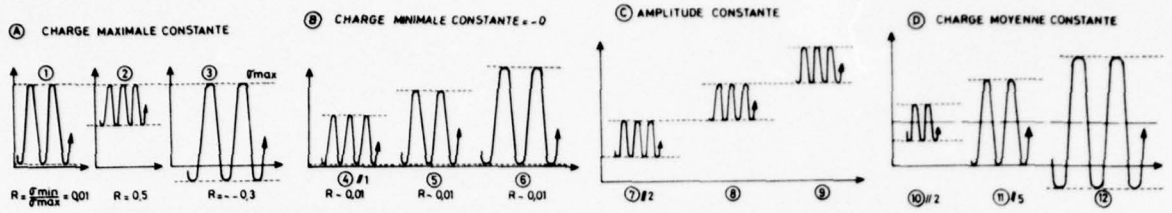

Fig.9: Différents types de sollicitations

Fig.10

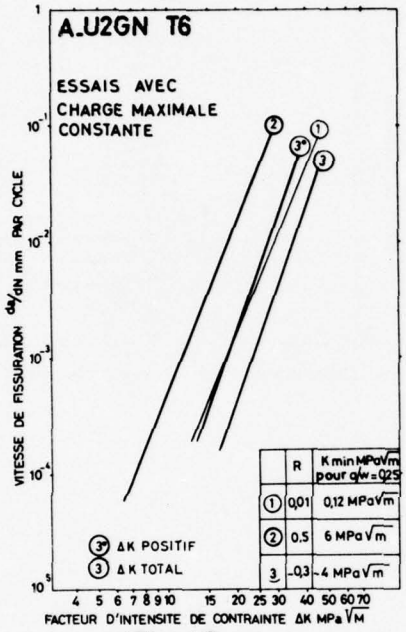

Fig.11

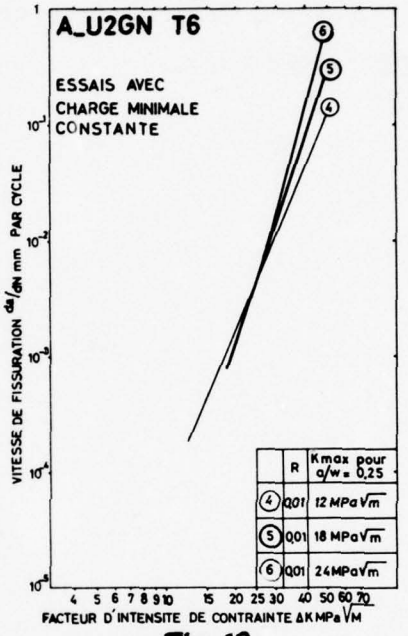

Fig.12

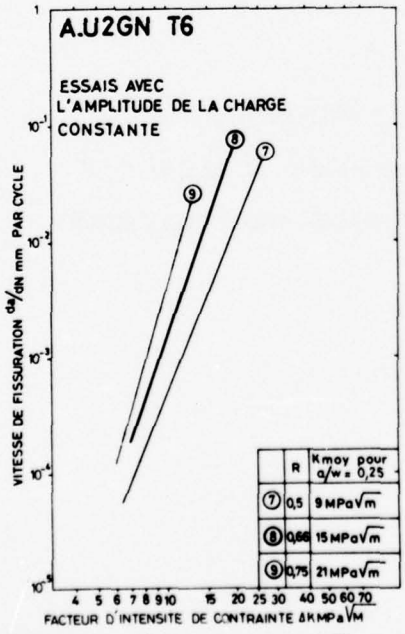

Fig.13

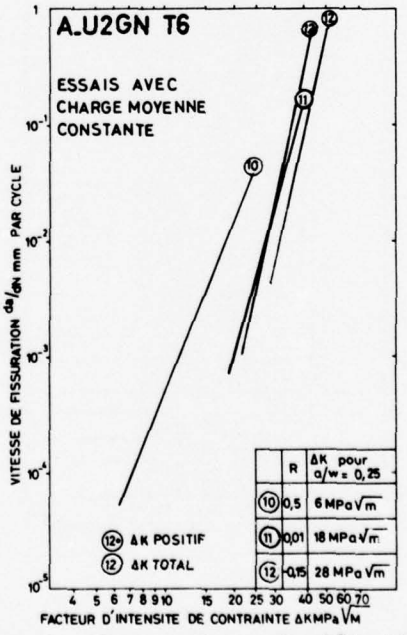

Influence du rapport R sur la vitesse de fissuration de l'A_U2GN

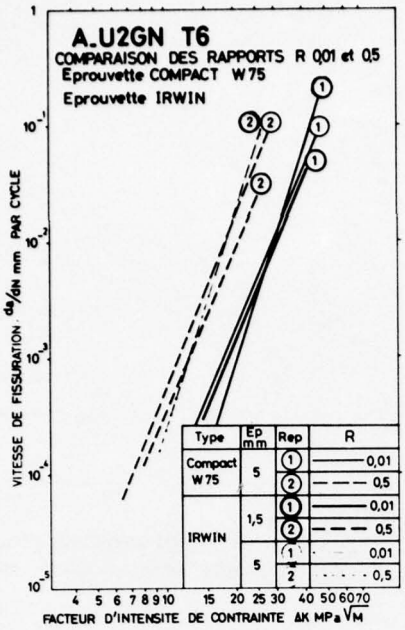

Fig.14 : Influence du rapport R dans deux configurations d'essai sur la fissuration de l'A_U2GN

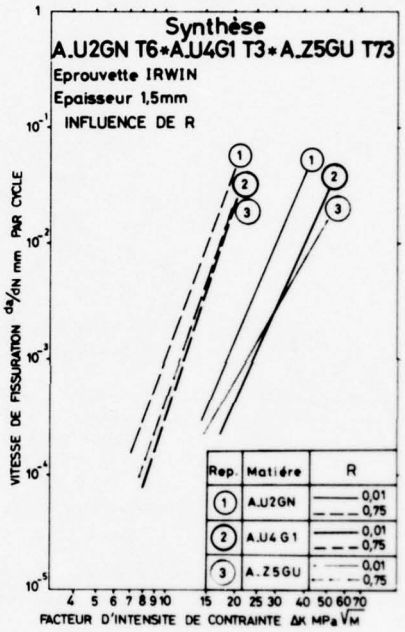

Fig.15 : Comparaison des vitesses de fissuration de trois alliages d'aluminium (B = 1,5 mm)

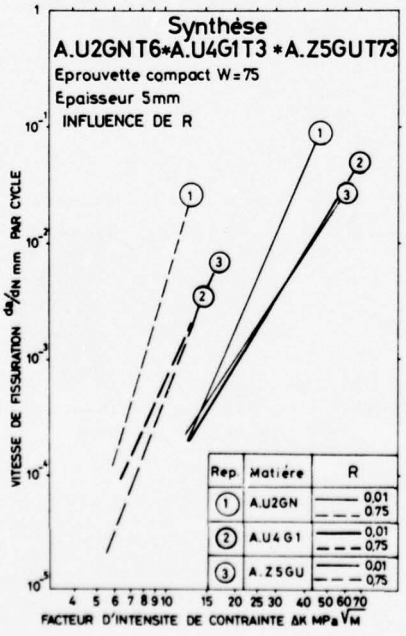

Fig.16 : Comparaison des vitesses de fissuration de trois alliages d'aluminium (B = 5 mm)

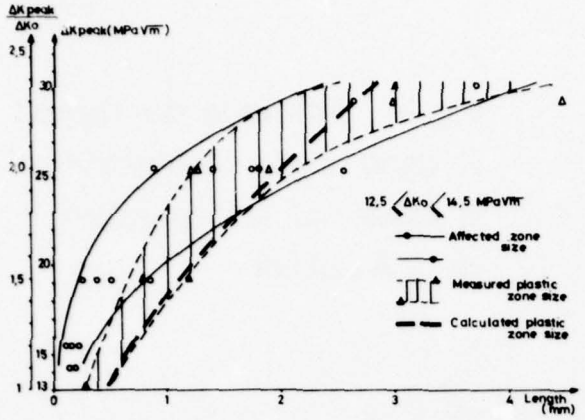

Fig17 CORRELATION BETWEEN AFFECTED ZONE SIZE AND PLASTIC ZONE SIZE IN 2024 ALLOY

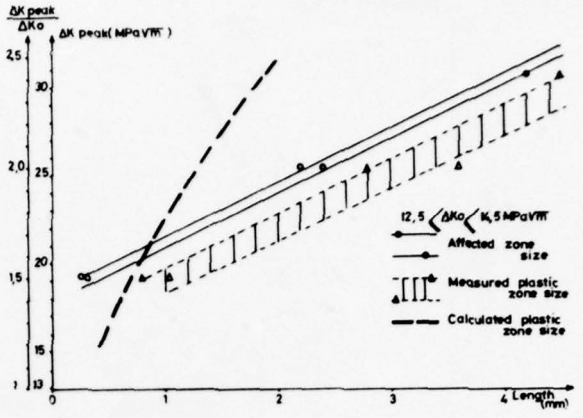

Fig18 CORRELATION BETWEEN AFFECTED ZONE SIZE AND PLASTIC ZONE SIZE IN PEAK AGED RR 58

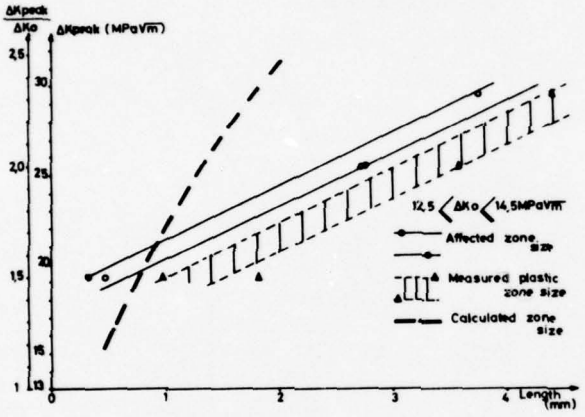

Fig19 CORRELATION BETWEEN AFFECTED ZONE SIZE AND PLASTIC ZONE SIZE IN UNDER AGED RR 58

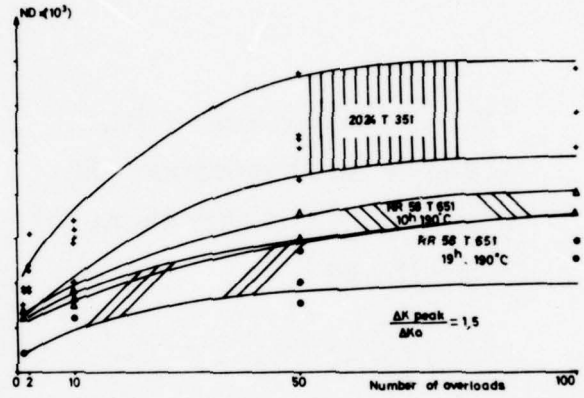

Fig20 EFFECT OF NUMBER OF OVERLOADS ON CYCLES OF DELAY

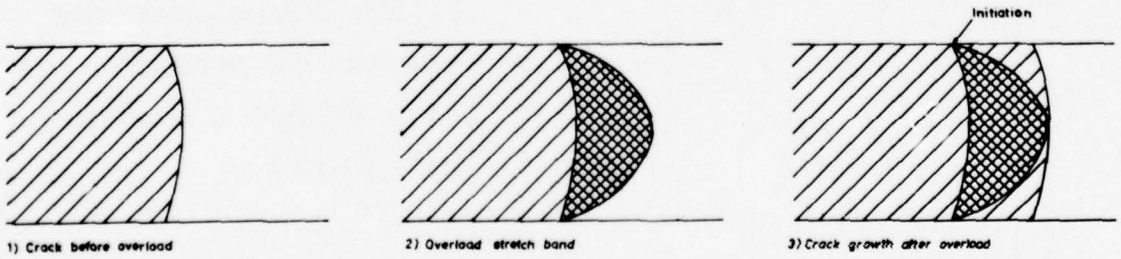

Fig21 MODEL ILLUSTRATION CRACK GROWTH BEFORE AND AFTER OVERLOAD IN PLANE STRAIN CONDITION

EXPOSE CONTRIBUE

par

W.Barrois
Ingenieur en chef militaire de l'Air (retraite)
42, rue Larmeroux, 92170 Vanves, France.

Le sujet traité concerne la possibilité de choisir un alliage d'aluminium pour la fabrication d'une structure d'avion en s'appuyant sur les résultats des essais simples élémentaires effectués en laboratoire.

La communication de Mr. Bathias correspond à une étude systématique effectuée dans les laboratoires de la Société Aérospatiale à Suresnes pour mettre en évidence les paramètres gouvernant le taux de fissuration en fatigue et la résistance statique résiduelle d'éprouvettes planes minces comportant une entaille centrale s'étendant dans la direction du travers long et, pour les épaisseurs supérieures à 5 mm, le comportement en fatigue d'éprouvettes "compactes" avec une fissure se propageant aussi dans la direction du travers long. Il est regrettable que la cas de la fissure sollicitée par une traction perpendiculaire dirigée selon le travers court n'ait pas été étudié pour des éprouvettes compactes relativement minces découpées dans des tôles épaisses en A-U2GN.

Dans l'étude de la résistance statique résiduelle des tôles fissurées, le meilleur résultat est obtenu avec l'alliage A-Z5GU-T7351 (7075-T7351) pour lequel aucune diminution de résistance n'est constatée pour les fortes épaisseurs, jusqu'à 10 mm. La valeur de $K_{Ic} = 85$ Mpa$\sqrt{}$ m a été déterminée d'après la longueur de la fissure avant l'application de la charge et la valeur de cette charge pour la rupture.

En fatigue, l'influence du rapport $R = S_{min}/S_{max}$ du cycle sur le taux de fissuration a été étudiée pour l'alliage A-U2GN dans les quatre cas de valeurs constantes de (A) la charge maximale, (B) la charge minimale, (C) la variation $S_{max} - S_{min}$ et, (D) la charge moyenne. Dans le cas (B), l'effet de R n'apparaît que pour les grandes vitesses de fissuration lorsque la région non encore fissurée de la largeur de l'éprouvette est soumise à des contraintes élevées, même loin du front de fissuration.

L'effet des surcharges et de leur répétition sur le taux de fissuration en fatigue a été étudié pour les alliages A-U4G1-T351 (2024-T351) et A-U2GN-T651 dans les deux cas du revenu normal de 19 h à 190°C et du sous revenu de 10 h à 190°C. Le processus améliorateur des surcharges est lié aux déformations plastiques créant des contraintes résiduelles de compression aux extrémités de la fissure dans un domaine non encore fissuré. Les essais de Mr. Bathias montrent un meilleur comportement de l'alliage A-U4G1 ce qui rejoint le classement relatif de l'A-U4G1 et de l'A-U2GN en résistance statique résiduelle. Dans ce case encore, l'étude de comportement d'éprouvettes compactes tendues dans la direction du travers court et prélévées dans des tôles épaisses aurait permis de compléter les connaissances sur l'action des surcharges. En effet, dans les structures réelles, le travers court est parfois sollicité en traction par suite des excentricités dans les assemblages et une surcharge améliorant le comportement en fatigue des régions de la structure où l'on connaît le signe des contraintes pourraît entraîner une rupture locale dans une région où le travers court serait tendu.

L'étude des effets de la fréquence des chargements et de la température des essais sur des éprouvettes en alliage d'aluminium A-U2GN-T6 n'a pas montré d'influence notable de ces paramètres pour le domaine

$$0{,}1 \text{ Hz} \leqslant f \leqslant 30 \text{ Hz}, \quad 25°\text{C} \leqslant \theta \leqslant 200°\text{C}.$$

Il convient de noter que les effets de la fréquence et de la température pourraient être plus marqués pour les structures des avions dans les conditions du service, c'est-à-dire pour le domaine:

$$1 \text{ cycle/heure} \leqslant f \leqslant 30 \text{ Hz} \quad \text{et} \quad -30°\text{C} \leqslant \theta \leqslant +30°\text{C}.$$

Ceci nous conduit aux diverses conclusions de la communication de Mr. Odorico. Pour des tractions effectuées dans la direction du travers long et des tôles épaisses en alliage d'aluminium A-U2GN-T651 (2618 A) avec 37 éprouvettes prélevées dans des tôles d'épaisseur variant de 25 à 114 mm, les valeurs de K_{Ic} étaient:

Fournisseur 1 Moyenne $\overline{M}(K_{Ic}) = 22{,}3$ MPa$\sqrt{}$ m écart quadratique moyen $s(K_{Ic}) = 2{,}33$ MPa$\sqrt{}$ m
Fournisseur 2 " 19,1 " " " 1,11 "

L'auteur propose d'utiliser la valeur $\overline{M} - 2s$ comme base pour définir la longueur limite tolérable de la fissure comme

$$2a = (2/\pi)\left(\frac{\overline{M} - 2s}{\sigma}\right)^2$$

où $\sigma = 130$ MPa . Même en écartant les réserves de l'auteur sur les différences entre les conditions des essais de laboratoire et les conditions plus complexes des structures en service, les longueurs de fissure ainsi déterminées ne sont pas des longueurs tolérables mais des longueurs correspondant à une probabilité de rupture encore trop élevée. Ces longueurs sont à considérer comme les valeurs critiques pratiques des longueurs atteintes par les fissures après leur propagation pendant la durée entre deux inspections successives, les longueurs initiales étant suffisantes pour que les fissures soient détectées en principe à la première inspection. De plus, les valeurs de K_{Ic} ne concernent que les fissures académiques dans les régions de répartition connue des contraintes ou le dessinateur a vérifié que le travers court du matériau n'était pas sollicité en traction. Pour le régions où le travers court est tendu les valeurs admissibles de K_{Ic} seraient beaucoup plus faibles et il ne peut être question de longueurs détectables de fissures. Tout au plus, si l'on disposait d'essais de laboratoire dans la direction du travers court et dans un environnement représentatif des conditions en service, on pourrait envisager de définir une dimension des défauts de fabrication suffisamment petite pour que la croissance de ces défauts pendant toute la durée d'utilisation de la structure ne puisse conduire à un danger de rupture significatif. Cela renforce l'opinion de l'auteur selon laquelle la sélection du métal et de son traitement thermique ne peut s'appuyer sur les essais simplifiés de laboratoire pour garantir l'absence des ruptures en service et que des essais de développement sur des éléments de structures à l'échelle grandeur sous des spectres de chargement représentatifs permettraient mieux de juger le choix du matériau et de son traitement.

Il convient de souligner ici que le dessinateur croit souvent éviter de faire travailler le métal dans la direction du travers court mais que les excentricités existant dans les assemblages et les répartitions non calculables des contraintes dans les pièces mécaniques de formes complexes entraînent souvent l'existence de contraintes de traction inprévues dans des directions quelconques par rapport au fibrage bien que la masse de métal soit sollicité par des contraintes connues dans des directions non dangereuses. On pense ici que les valeurs de K_{Ic} dans la direction du travers court constituent la donnée principale du problème de la résistance des structures usinées dans des tôles épaisses ou dans des pièces de forge où l'usinage coupe les fibres.

On s'associe pleinement aux conclusions de l'auteur sur l'intérêt des essais d'assemblages rivés ou boulonnnés, même dans le cadre du choix du matériau et de son traitement thermique. Cependant, on pense que le maximum de connaissances utilisables par le Bureau d'Etudes serait apporté par des études détaillées de chaque cas de rupture locale apparaissant dans les essais statiques et dans les essais de fatigue à l'échelle grandeur ainsi que de chaque cas d'endommagement de la structure en service.

INFLUENCE OF ENVIRONMENT AND PRODUCTION PROCESSES ON THE CRACK PROPAGATION BEHAVIOR OF UNSTIFFENED SHEET

by
K.H. Rendigs
Materials and Processes Development Department
Vereinigte Flugtechnische Werke-Fokker GmbH
2800 Bremen, Germany

SUMMARY

Practical tests to determine the fracture behavior of unstiffened sheet under environmental and production process influences were carried out in order to give information on how far fracture toughness properties established under normal laboratory conditions can be transferred into practice.

Crack propagation properties, K_c values and residual strength σ_c were established on clad 2.0 mm thick sheet of aluminium alloy 2024 in naturally aged condition at a stress level of $\sigma_m \pm \sigma_a = 88.3 \pm 39.2$ N/mm^2 and under environmental and production process influences. The environmental influences examined were the following:

- normal laboratory conditions
- continual wetting with artificial sea water

The production process influences examined were as follows:

- stretching with a total amount of stretch forming of 13 and 16 % respectively;
- a bonding cycle simulated in the "delivered" condition and
- stretching with a total amount of stretch forming of 13 % with following bonding cycle.

The test results show that

- the influence of artificial sea water on the material examined was very small;
- due to the stretching there was an improvement of the crack propagation properties not expected in this order of magnitude;
- smaller values regarding the K_c data and the residual strength σ_c under environmental and production process influences were established than in the delivered condition;
- the bonding process regarding crack propagation behavior in a stretched condition leads to lower values compared to the delivered condition, and
- hardly any influence of the bonding process on the K_c- and residual strength values was noticed.

INTRODUCTION

In order to be able to demonstrate the fail-safe properties and economical inspection intervals required nowadays by the certification authorities both for military and civil aircraft, mathematical predictions of the crack propagation and residual strength behavior of critical components are necessary.
The characteristic data necessary for this are a.o. dependent on the material, component geometry, production processes and environmental influences. Although this fact is known, there are hardly any tests available. This test program is designed to be a first contribution to the investigation of this field.

A reliable prediction of the propagation of cracks is necessary for the following reasons:

- material loading with combat aircraft is so high that cracks can propagate very quickly under certain circumstances. An assessment of the crack propagation rate as well as of the critical crack length is therefore absolutely necessary.
- for reasons of increased efficiency it is imperative to establish a maximum service interval within which a possible damage does not endanger the structural strength.
- for low-cost structures the knowledge of crack behavior is a basic requirement. An economical overall result can be obtained only through reliable definition of maximum permissible manufacturing faults.

TASK AND AIMS

Tests on unstiffened sheets will show how far fracture toughness properties established under normal laboratory conditions can be transferred into practice when environmental and production process influences are included.
The aims of this task were to determine the

- crack length as a function of the number of cycles $2l = f(N)$,
- crack propagation rate as a function of the stress intensity factor

$$\frac{d(2l)}{dN} = f(\Delta K)$$

- residual strength σ_c and
- fracture toughness K_c

on unstiffened clad sheet of aluminium alloy 2024 T3 (thickness = 2 mm) under environmental and production process influences.

MATERIAL

The test material (clad sheet 2024 T3, 2 mm thick) was supplied by the Aluminium Company of America (Alcoa). The dimensions and the Lot-no. are as follows:

2.0 x 1200 x 2500 mm

Lot-no. 442-901

The chemical composition of the basic material and of the cladding of 2024 (3.1364) is taken from the Alcoa certificate and is comprised in the following table:

	Basic Material	Cladding
Copper	3.8 - 4.9 %	max. 0.05 %
Magnesium	1.0 - 1.2 %	-
Manganese	0.3 - 0.9 %	max. 0.05 %
Silicon	max. 0.50 %	max. 0.55 %
Iron	max. 0.50 %	-
Zinc	max. 0.25 %	-
Chromium	max. 0.10 %	-
Others, each	max. 0.05 %	max. 0.03 %
Others, all	max. 0.15 %	-
Aluminium	remainder	99.45 %

The static tensile strength values (average) of 2024 T3, established from three specimens each in L and LT direction, are listed in the following table:

$\sigma_{0.2}$ N/mm^2		σ_B N/mm^2	
L	LT	L	LT
393	344	475	469

Data on heat treatment applied during the program at VFW-Fokker in accordance with Luftfahrtnorm [1] for 2024 (3.1364) are as follows:

- solution heat treatment (salt bath): 495 $\pm$ 5°C/20 min soaking time/quenching in water 40°C max.
- naturally aged to T42a : 96 h min. after stretching (annealing, 10 % pre-stretching, solution heat treatment, 3 % post-stretching)
- naturally aged to T42b : 96 h min. after stretching (annealing, 10 % pre-stretching, solution heat treatment, 6 % post-stretching)
- annealing (O) : 410 $\pm$ 10°C/2 h soaking time/furnace cooling at a rate of 30°C max./h to 250-200°C, then air cooling.

TEST SCOPE

The test procedure comprised the determination of fracture-toughness characteristics on 2 mm thick, clad sheet of aluminium alloy 2024 under environmental and production process influences.

In order to manufacture the stretched test specimens necessary to carry out the test program a total of three sheets with the dimensions 2.0 x 1000 x 2000 mm were subjected to a stretch forming process. All three sheets were pre-stretched by 10 %, two of these post-stretched by 3 % and one by 6 %. Six L and six LT specimens with a total amount of stretch forming of 13 % and three L and three LT specimens with a total amount of stretch forming of 16 % were required.

Crack propagation tests were carried out on center notched flat specimens (see Fig. 1) at a stress level of $\sigma_m \pm \sigma_a = 88.3 \pm 39.2$ N/mm^2 and afterwards the residual strength data of the specimens were determined. Three L and three LT specimens each were tested in the delivered condition under laboratory conditions in order to obtain the basic values.

Furthermore, three specimens in L direction, which were in the delivered condition, were tested under continual wetting with artificial sea water.

Three specimens each were tested at a stress level of $\sigma_m + \sigma_a = 88.3 \pm 39.2$ N/mm^2 under the following production process influences:

- stretching with a total amount of stretch forming of 13 and 16 %, sampling in L and LT direction (12 specimens)
- simulated bonding process with sheet in the delivered condition, sampling in L direction (3 specimens)
- stretching with a total amount of stretch forming of 13 % and a subsequent simulated bonding process, sampling in L and LT direction (6 specimens).

FORM AND PREPARATION OF TEST SPECIMENS

Center notched flat specimens (see Fig. 1) were used for the tests. The definition of the direction is as follows:

L = sampling parallel to direction of rolling
LT= sampling transverse to direction of rolling

The blanks required for preparation of the specimens were cut with plate-shears. Contouring of the specimens was done by milling.
The typical manufacturing procedure of a stretch forming process consisting of the following was chosen: annealing - pre-stretching - solution heat treatment - post-stretching and ageing.

One particular difficulty was encountered during the stretch forming process due to the requirement for a uniform amount of stretch forming across the whole test sheet. This requirement had to be fulfilled under any circumstances in order to obtain comparable test results. Prior to stretch forming all sheets were therefore printed with a screen, which consisted of squares with an edge length of 100 mm. After the stretch forming program had been carried out this screen was measured and the specimen position plan was established with the following premise: uniformity of amount of stretch forming of all specimens. The sheets were stretch formed in direction of rolling. Stretch forming was carried out as follows:

- annealing of all sheets
- free pre-stretching of all sheets by approx. 10 %
- 20 min solution heat treatment for all sheets
- post-stretching of two sheets across a stretch forming block by approx. 3 % and one sheet by approx. 6 %.

Subsequently, all sheets were naturally aged.

The influence of chemical surface pre-treatment together with the temperature load occurring in a maximum of 5 permissible bonding cycles [2] on crack propagation and residual strength behavior of 2024 was examined. The bonding process, however, was simulated. The bonding process is briefly described as follows:

- Alkaline degreasing 80°C/15 min in accordance with FH 2-5.0020 [3]
- Alkaline etching 35°C/3 min in accordance with FH 2-5.0110 [4]
- Pickling 65°C/30 min in accordance with FH 2-5.0108 [5]
- Spray-rinsing with fully desalinated water (susceptance less than 10 µ Siemens) approx. 10 min
- Drying of sheets in an air-circulating oven of 50°C/30 min
- Priming with BR 227 by means of a spray pistol in accordance with FH 1-9.5703 [6]
- Drying of primer at 100°C/60 min
- Simulation of 5 bonding cycles with FM 96 [2]. Each cycle began at room temperature. The temperature was increased linearly in 90 min up to 180°C. This temperature was held for 60 min with subsequent air cooling.
- All specimens were heated in an air-circulating oven at one time.

TEST PERFORMANCE

Center notched flat specimens (see Fig. 1) were used for the determination of the crack propagation behavior, the residual strength σ_c and the fracture toughness K_c of 2024. All crack propagation tests occured at a stress level of $\sigma_m \pm \sigma_a = 88.3 \pm 39.2$ N/mm^2. For the test performance a fully electronic universal testing machine (static load 20 Mp and dynamic load 10 Mp), Instron Modell 1251, was available. The test frequency was 30 Hz with sinusoidal load in the load-controlled range. In order to determine the residual strength σ_c the testing machine was operated display-controlled.
The test performance was similar to ASTM-E-399-72 [7] and ASTM STP 410 [8] as follows:
The specimens were fatigue pre-cracked to a crack length of 2l = (0.45 - 0.55) x specimen width (B). The crack length was plotted in the usual way versus the number of cycles. As there were different cycle numbers up to the begin of crack propagation due to the non-uniform manual notching, an initial crack length of 4 mm was chosen for the plotting. Subsequently, the specimens were loaded to fracture in order to determine the residual strength σ_c and the fracture toughness K_c.
The test performance under laboratory conditions proceeded as described above.

TEST PERFORMANCE UNDER ARTIFICIAL SEA WATER

The tests with artificial sea water were carried out under continual wetting of the crack tip. The artificial sea water was prepared in accordance with Fed. Test Method Std. No. 151a Method 812 [9] . The composition of the sea water remained constant throughout the test as it was not used again.

TEST EVALUATION

Evaluation of the test results was carried out with the help of a computer program. The following was established:

- the K_c value in accordance with the Feddersen equation [8] .

$$K_c = \frac{P_{max}}{W \cdot B} \sqrt{\frac{\pi \cdot l}{\cos \frac{\pi \cdot l}{W}}}$$

where

K_c = critical stress intensity factor
P_{max} = max. load during static testing
W = specimen width
B = specimen thickness
l = half the crack length (fatigue)

- the crack propagation rate in accordance with the Forman equation [10, 11] :

$$\frac{d\ (2l)}{dN} = \frac{C \cdot (\Delta K)^n}{(1-R)\ K_c - \Delta K}$$

where

2 l = crack length (fatigue)
N = number of cycles
ΔK = stress intensity range
R = stress ratio σ_u/σ_o

as well as the magnitudes C and n occurring in the Forman equation (Tab. 1).

The residual strength σ_c was calculated according to the following formula:

$$\sigma_c = \frac{P_{max}}{(W-2l)\ B}$$

Symbol explanation see above.

TEST RESULTS

INFLUENCE OF ENVIRONMENT ON CRACK PROPAGATION CHARACTERISTICS, FRACTURE TOUGHNESS K_c AND RESIDUAL STRENGTH σ_c

Fig. 2 shows the two arithmetical mean curves of 2024 T3, tested in L direction under laboratory conditions and under continual wetting with artificial sea water. This figure indicates that material 2024 T3 has only a slightly lower resistance to crack propagation when it is continually wetted with artificial sea water. A reduction of the cycle number by about 3700 was determined at a crack length of 2l = 60 mm so that the cycle number existing in LT direction was almost reached (Fig. 3).

Fig. 8 permits a comparison of the crack propagation rates of 2024 T3 (delivered condition) under laboratory conditions and under continual wetting with artificial sea water. It was established that the crack propagation rate increased only slightly when the material was continually wetted with artificial sea water. As can be seen from fig. 9, a substantial influence of the sampling direction on the crack propagation rate could not be determined either.

Tab. 1 summarizes the data necessary to calculate the critical stress intensity factor K_c and the K_c values established, the Forman constants C and n as well as the residual strength values σ_c . The scatter of the Forman constants, which assumes considerable proportions in some cases, is to be attributed to deficiencies in the computer program. At present this program is being modified as it is to be included in the HSB [12] .
The K_c and σ_c mean values determined under laboratory conditions and with artificial sea water are listed in the following table:

Parameter	K_c (kpmm$^{-3/2}$)		σ_c (N/mm^2)	
	L	LT	L	LT
Laboratory conditions	229	209	343	312
Artificial sea water	227	-	339	-

It can be seen from this table that the K_c and σ_c values measured under artificial sea water correspond to those established under normal laboratory conditions.

INFLUENCE OF PRODUCTION PROCESSES ON CRACK PROPAGATION CHARACTERISTICS, FRACTURE TOUGHNESS K_c AND RESIDUAL STRENGTH σ_c

INFLUENCE OF STRETCH FORMING

The crack propagation curves of the stretched specimens and those of the "as delivered" specimens are combined in fig. 4. This figure and the following table show that

2 l (mm)	cycle x 10^4					
	2024 T3 Delivered condition		2024 T42a 10 % pre-stretched solution heat treated 3 % post-stretched		2024 T42b 10 % pre-stretched solution heat treated 6 % post-stretched	
	L	LT	L	LT	L	LT
20	4.87	4.55	8.56	6.70	8.68	6.00
30	5.60	5.19	9.70	7.46	9.81	6.80
40	5.94	5.60	10.45	8.04	10.40	7.20
50	6.12	5.73	10.88	8.30	10.75	7.40
60	6.25	5.84	11.12	8.46	10.95	7.51

- the crack propagation characteristics of 2024 T42a and T42b are the same in L direction when the total amount of stretch forming is 13 or 16 %,
- at a total amount of stretch forming of 16 % and a crack length of 2l = 60 mm in LT direction the cycle number falls short of that for a total amount of stretch forming of 13 % by 9500 cycles,
- the difference in the cycle numbers between the specimens tested as delivered and after stretch forming amounts to about 47900 cycles in favor of the stretched specimens in L direction and at a crack length of 2l = 60 mm and that
- in LT direction at a crack length of 60 mm the cycle number increases by 16700 cycles when the total amount of stretch forming is 16 % and by 26200 cycles when the total amount of stretch forming is 13 % as compared to the values found for the "as delivered" specimens, this influence being due to stretch forming.

Fig. 10 permits a comparison of the specimens tested as delivered with those tested after stretch forming with respect to their crack propagation behavior. It can be concluded from this comparison that

- the crack propagation rate in L direction is in any case lower than in LT direction,
- the crack propagation characteristics are particularly favorable at a total amount of stretch forming of 13 % in L direction and that
- the most unfavorable crack propagation characteristics were found up to a stress intensity range of ΔK = 77 kpmm$^{-3/2}$ in the delivered condition in LT direction.

Tab. 1 shows the K_c values established, the Forman constants C and n as well as the residual strength values σ_c .

The following table summarizes the K_c and σ_c mean values established under laboratory conditions and after stretch forming.

It can be seen from this table that the stretch forming process causes a slight reduction in the fracture toughness values as compared to the delivered condition. The residual strength σ_c shows the same tendency.

Parameter	K_c (kpmm$^{-3/2}$)		σ_c (N/mm^2)	
	L	LT	L	LT
2024 T3 (delivered condition)	229	209	343	312
2024 T42a (10% pre-stretched 3% post-stretched	211	187	316	279
2024 T42b (10% pre-stretched 6% post-stretched	224	194	333	288

INFLUENCE OF A BONDING PROCESS

Fig. 5 and the following table permit a comparison of the crack propagation curves for the delivered condition, for delivered condition + simulated bonding process and for a 13 % stretching + simulated bonding process.

2 l (mm)	cycle x 10^4					
	2024 T3 Delivered condition		2024 T3 Delivered condition + bonding process		2024 T42a 10 % pre-stretched, solution heat treated, 3 % post-stretched + bonding process	
	L	LT	L	LT	L	LT
20	4.87	4.55	4.28	-	6.59	5.53
30	5.60	5.19	4.79	-	7.61	6.34
40	5.94	5.60	5.23	-	8.25	6.75
50	6.12	5.73	5.39	-	8.61	6.95
60	6.25	5.84	5.51	-	8.81	7.06

It can be seen from this comparison that the cycle number for 2024 in the delivered condition (T3) in L direction has decreased by 7400 cycles after the simulation of the bonding process at a crack length of 2 l = 60 mm. The cycle number for the stretched specimens, in contrast, has increased by 25600 cycles in L direction and by 12200 cycles in LT direction at a crack length of 2 l = 60 mm as against the delivered condition. However, a reduction in the cycle numbers at a crack length of 2 l = 60 mm by 23100 cycles in L direction and 14000 cycles in LT direction has occurred as against a total amount of stretch forming of 13 % in the "unbonded" condition (Fig. 6 and Fig. 7).

Fig. 11 permits a comparison of the crack propagation behavior of 2024 in the delivered condition + bonding process and with a 13 % stretch forming + bonding process. As expected, the stretched specimens have the lowest crack propagation rate in L direction whilst the specimens in the delivered condition + bonding process show a higher crack propagation rate than the specimens in the delivered condition as the stress intensity range increases. The crack propagation curve of the stretched and "bonded" specimens from the LT direction was added to this figure for information. It becomes apparent that an increase in the crack propagation rate can be expected when the stress intensity range exceeds 70 kpmm$^{-3/2}$.

Tab. 1 summarizes the K_c values established, the Forman constants C and n as well as the residual strength values σ_c and the values necessary to establish these data.

The K_c and σ_c mean values established are compared in the following table:

Parameter	K_c (kpmm$^{-3/2}$)		σ_c (N/mm^2)	
	L	LT	L	LT
2024 T3 (delivered condition)	229	209	343	312
2024 T3 + bonding process	226	-	338	-
2024 T42a 10 % pre-stretched 3 % post-stretched + bonding process	225	199	330	297

This comparison shows that the bonding process exerts only a minimum influence on 2024 T3 with respect to the K_c value and the residual strength σ_c. As far as the K_c value is concerned, this applies also to 2024 T42a (13 % total amount of stretch forming), whilst the negative influence on the residual strength values is a little more pronounced.

COMPARISON OF THE INFLUENCE OF ENVIRONMENT AND PRODUCTION PROCESS ON THE CRACK PROPAGATION BEHAVIOR

The following is a presentation of the test results established for 2024

- in the delivered condition (T3) tested under laboratory conditions and under continual wetting with artificial sea water respectively,
- at a total amount of stretch forming of 13 % or 16 %,
- in the delivered condition + simulation of a bonding process and
- with a 13 % stretch forming + simulation of a bonding process.

CRACK LENGTH AS A FUNCTION OF THE CYCLE NUMBER

Fig. 6 contains a comparison of the crack propagation curves for 2024, tested in the delivered condition T3, with a total amount of stretch forming of 13 and 16 % (T42a and T42b) under continual wetting with artificial sea water, in the delivered condition + bonding process and with a 13 % stretch forming + bonding process. Sampling was carried out in L direction. It can be seen from this figure that

- the crack propagation behavior deteriorates slightly under continual wetting with artificial sea water,
- an enormous improvement in the crack propagation resistance - by a factor of almost 2 when compared to the delivered condition - can be achieved by a total amount of stretch forming of 13 or 16 %,
- the crack propagation resistance of 2024 T3 is reduced by the influence of a bonding process and
- the favorable crack propagation characteristics achieved by stretch forming are reduced by about 50 % at a total amount of stretch forming of 13 % with a subsequent simulated bonding process. However, the cycle number for a crack length of 2 l = 60 mm exceeds that for the delivered condition by 25600 cycles.

Fig. 7 shows the crack propagation behavior of 2024

- in the delivered condition T3,
- with a 13 % or 16 % stretch forming (T42a) or (42b) and
- with a 13 % stretch forming + bonding process.

Sampling was carried out in LT direction. It can be seen from this figure that

- the crack propagation resistance is in any case increased by the production process influences investigated,
- the most favorable crack propagation characteristics are achieved at a total amount of stretch forming of 13 % whilst the cycle number reached at 16 % stretch forming and a crack length of 2 l = 60 mm falls short of that reached with a 13 % stretch forming by 9500 cycles, and
- the improvement in the crack propagation characteristics achieved by stretch forming is reduced by 50 % by the bonding process simulation in the case of the material stretched by 13 %. However, the cycle number still exceeds that for the delivered condition by 12200 cycles at a crack length of 2 l = 60 mm.

CRACK PROPAGATION ACCORDING TO FORMAN

Fig. 12 and 13 show the crack propagation rate $\frac{d\ (2l)}{dN}$ which was established according to Forman and is plotted as a function of the stress intensity range ΔK for 2024 T3, T42a and T42b under environmental and production process influences.

Fig. 12 contains the crack propagation curves of 2024 in L direction

- in the delivered condition T3,
- in the delivered condition under continual wetting with atificial sea water,
- with a total amount of stretch forming of 13 % and 16 % (T42a or T42b) and
- with a 13 % stretch forming + bonding process.

It can be seen from this figure that

- only a slight increase in the crack propagation rate as against the delivered condition was measured as a result of the simulated bonding process and the continual wetting with artificial sea water,
- there is a substantial reduction in the crack propagation rate after stretch forming as compared to the unstretched condition over the entire stress intensity range ΔK investigated and
- the positive influence on the crack propagation rate achieved by stretch forming is reduced by the subsequent bonding process simulation; the results obtained, however, were still much better than those for the delivered condition.

Fig. 13 shows the crack propagation curves of 2024 in LT direction, which were established according to Forman,

- in the delivered condition T3,
- with a total amount of stretch forming of 13 % and 16 % (T42a or T42b) and
- with a 13 % stretch forming + bonding process.

2024 behaves in about the same way with all parameters. The comparison of the samples stretched by 13 % with those subjected to the bonding process after having been stretched by 13 % illustrates the negative influence of the bonding process on the crack propagation behavior. When the stress intensity range ΔK increases, the crack propagation rate increases as well.

FRACTURE TOUGHNESS K_c AND RESIDUAL STRENGTH σ_c

In fig. 14 the fracture toughness and residual strength mean values of 2024 are plotted as a function of the relevant test parameters. The data and their scatter values are to be taken from tab. 1. This comparison shows that

- the most unfavorable values exist at a total amount of stretch forming of 13 %,
- in all cases investigated the reduction in the fracture toughness and the residual strength values, which is caused by the stretch forming, is larger in LT than in L direction and
- a slight increase in fracture toughness and residual strength data by the simulation of a bonding process can be observed in the case of the specimens which were stretched by 13 %.

REFERENCES

[1] LN 29850 "Wärmebehandlung von Aluminium" Normenstelle Luftfahrt Entwurf

[2] FH 1-9.5802 Fertigungshandbuch VFW-Fokker "-Klebstoffe-Klebstoff FM-96"

[3] FH 2-5.0020 Fertigungshandbuch VFW-Fokker "Reinigen von Teilen aus Al- und Mg-Legierungen, alkalisch"

[4] FH 2-5.0110 Fertigungshandbuch VFW-Fokker "Beizen von Teilen aus Al und Al-Legierungen alkalisch"

[5] FH 2-5.0108 Fertigungshandbuch VFW-Fokker "Beizen von Al-Legierungen vor dem Kleben (Pickling Verfahren)"

[6] FH 1-9.5703 Fertigungshandbuch VFW-Fokker "-Anstrichstoffe - Primer BR-227"

[7] ASTM E 399-72 "Standard Method of Test for plane-strain fracture toughness of metallic materials"

[8] ASTM STP 410 "Plane-strain crack toughness testing of high strength metallic materials"

[9] Fed. Test Method Std. No. 151a Method 812, 17. Juli 1956

[10] Forman, R.G., Kearney V.E. und Engle, R.M.: "Numerical Analysis of Crack Propagation in Cyclic-Loaded Structures", The American Society for Mechanical Engineers ASME Paper No. 66 WA/Met. 4 (1966)

[11] Leis, H. und Schütz, W. "Bewertung neuer Flugzeugbauwerkstoffe mit den Methoden der Bruchmechanik", Luftfahrttechnik-Raumfahrttechnik Nr. 10 Okt. 1970

[12] HSB, Handbuch Struktur Berechnung; IASB

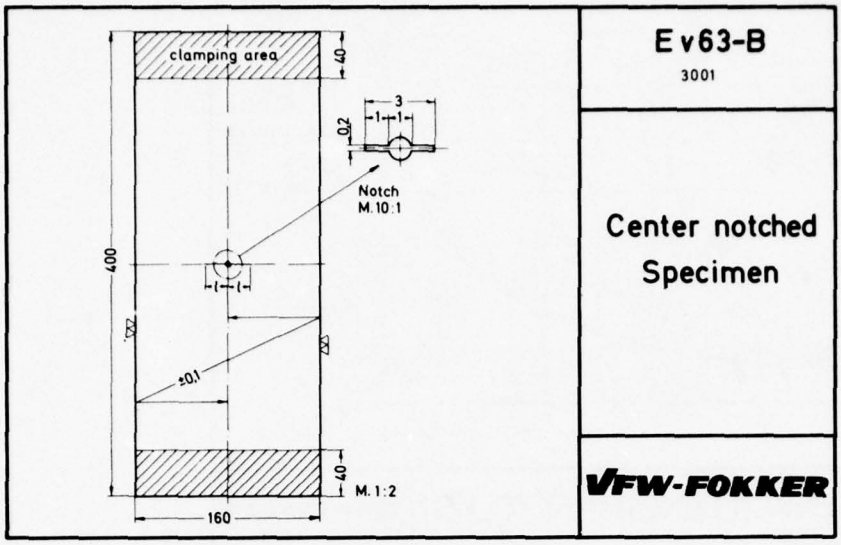

Fig. 1

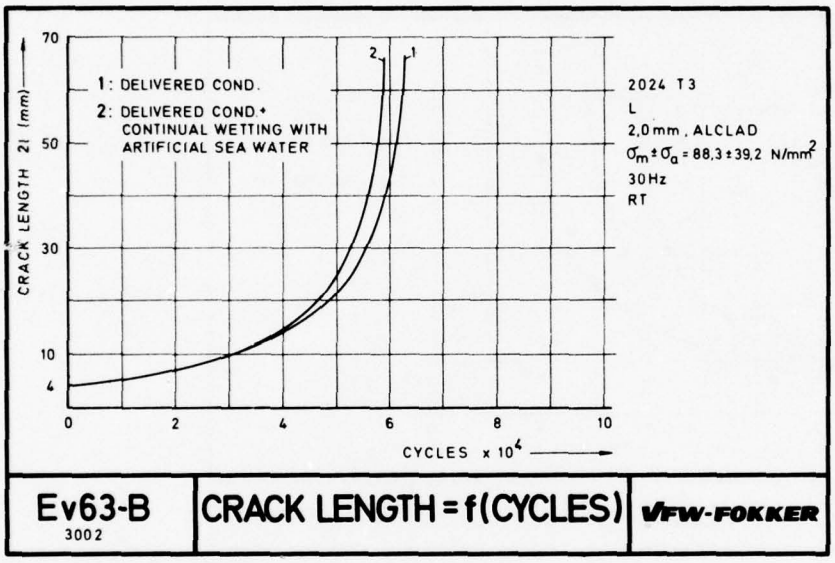

Fig. 2

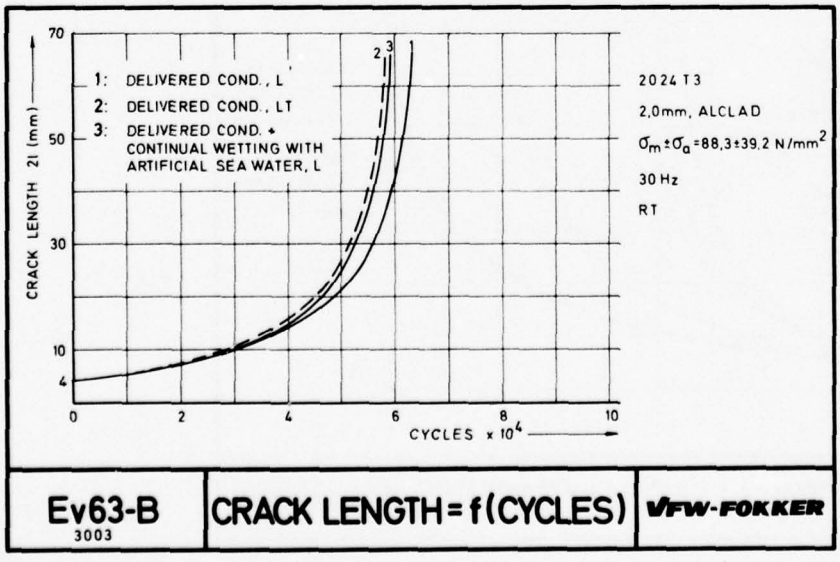

Fig. 3

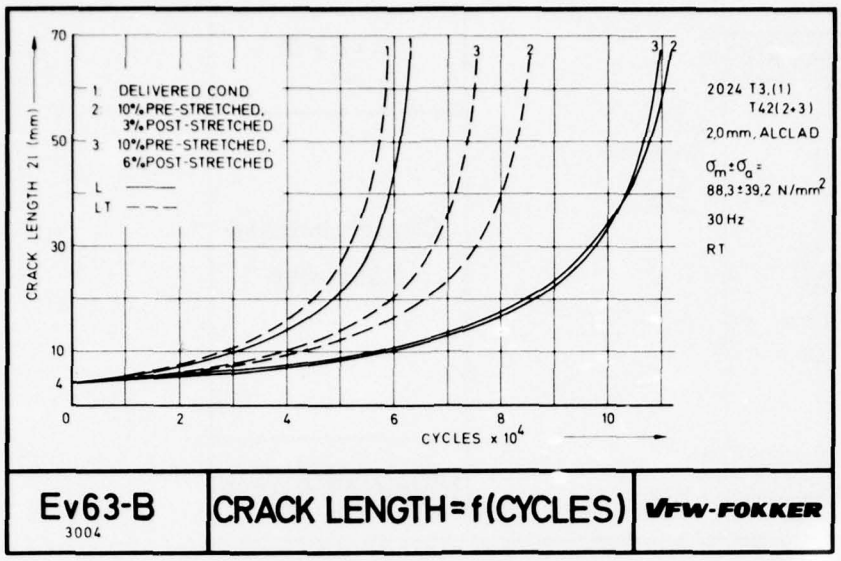

Fig. 4

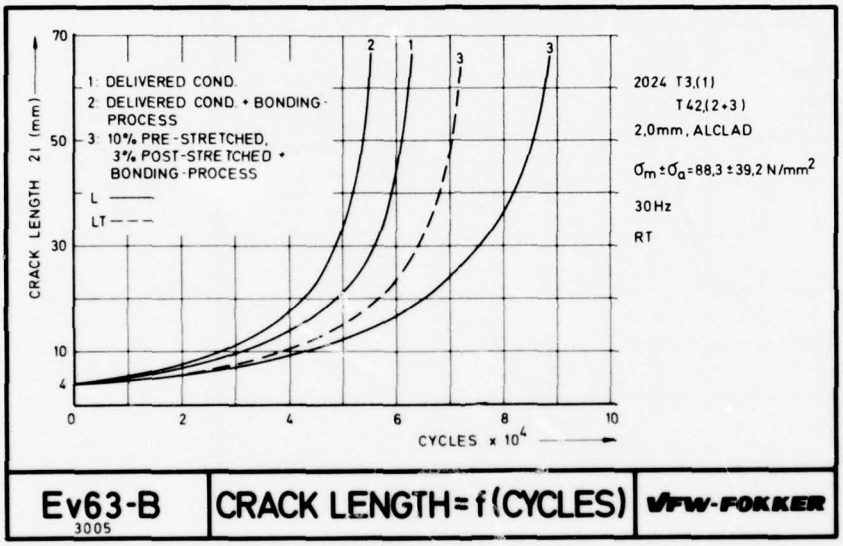

Fig. 5

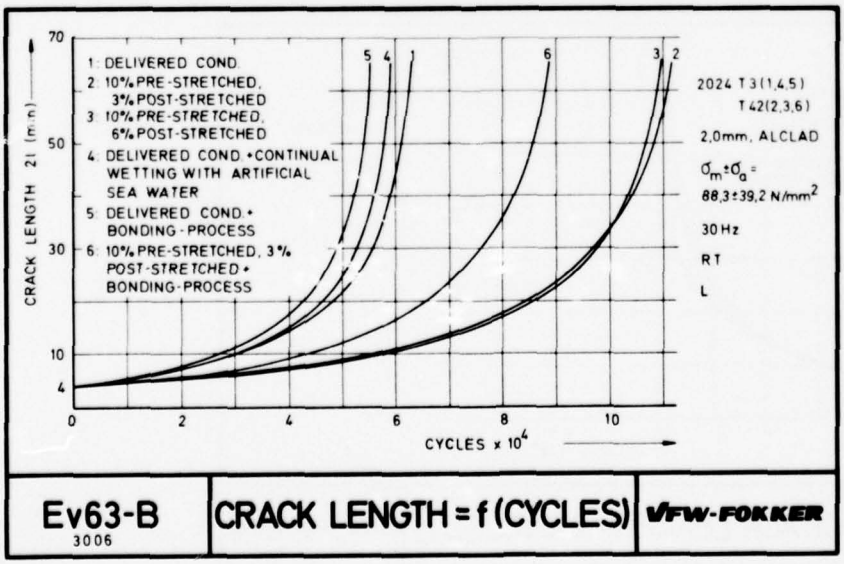

Fig. 6

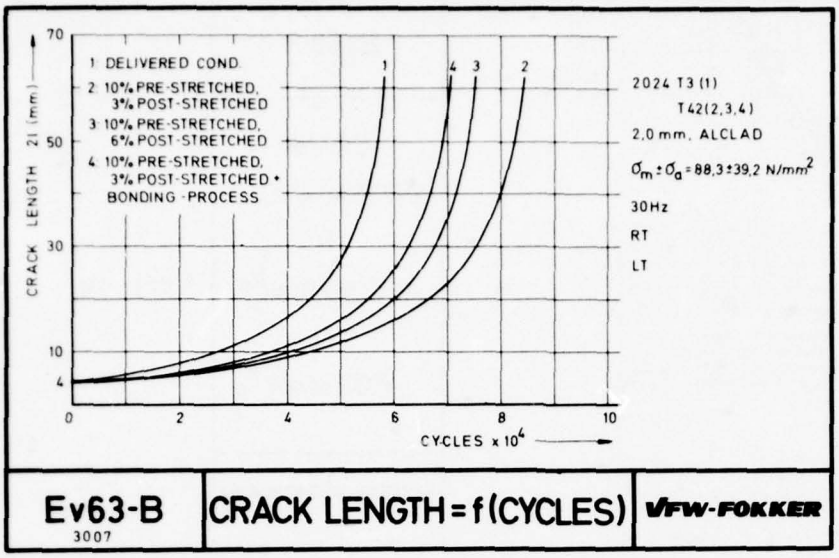

Ev63-B 3007	CRACK LENGTH = f (CYCLES)	VFW-FOKKER

Fig. 7

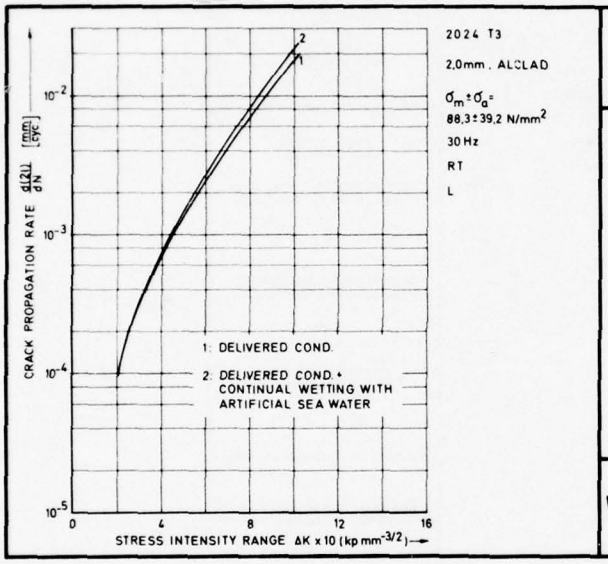

Ev63-B 3008
CRACK PROPAGATION IN ACCORDANCE TO FORMAN
VFW-FOKKER

Fig. 8

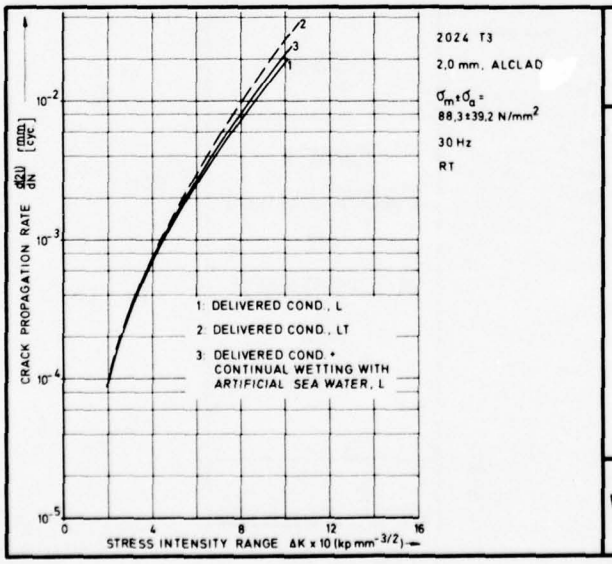

Ev63-B 3009
CRACK PROPAGATION IN ACCORDANCE TO FORMAN
VFW-FOKKER

Fig. 9

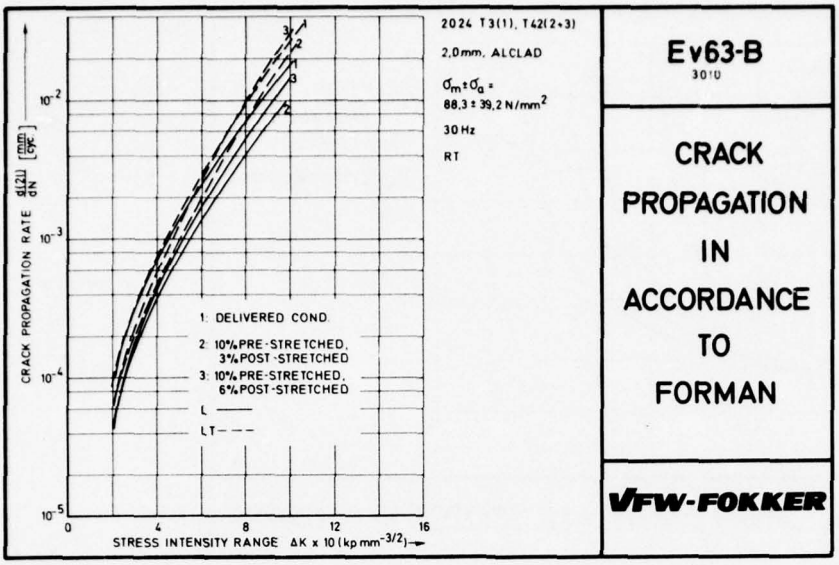

Fig. 10

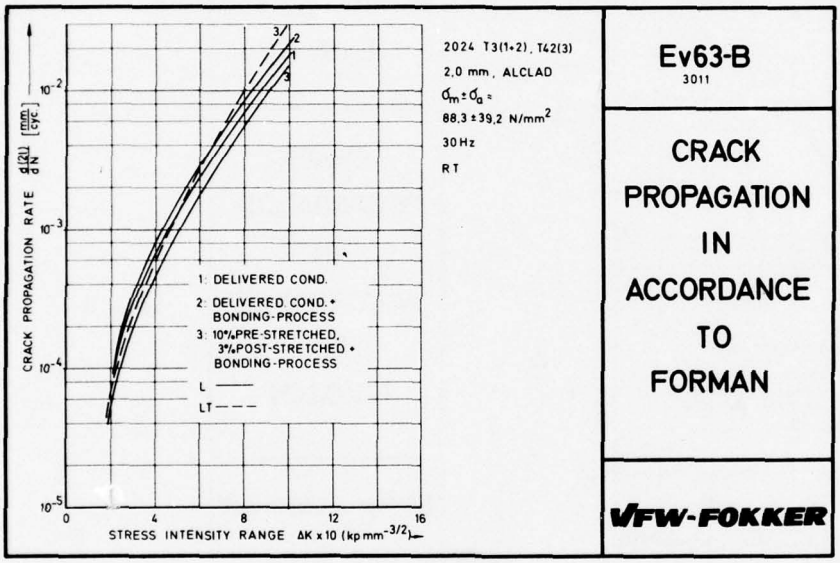

Fig. 11

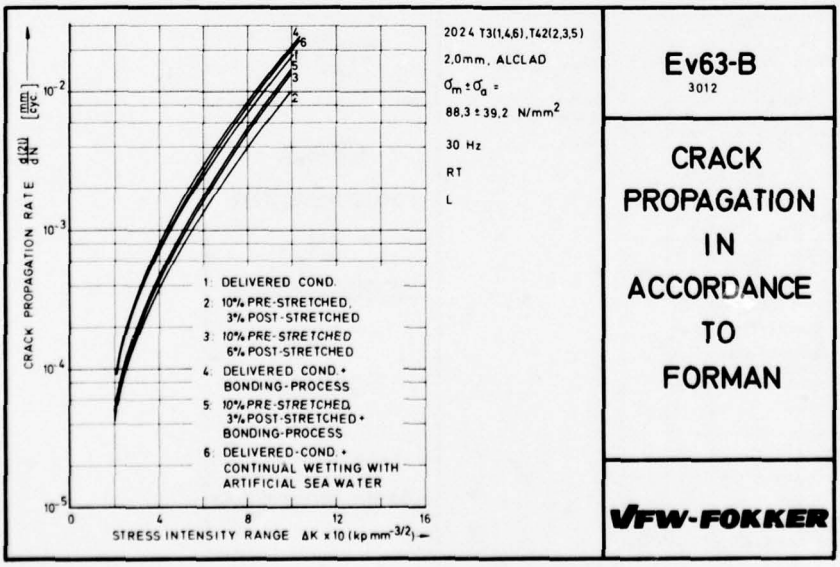

Fig. 12

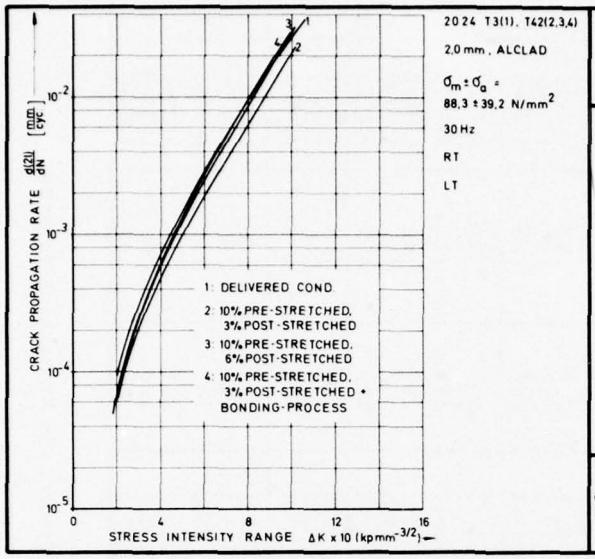

Ev63-B
3013

CRACK PROPAGATION IN ACCORDANCE TO FORMAN

VFW-FOKKER

Fig. 13

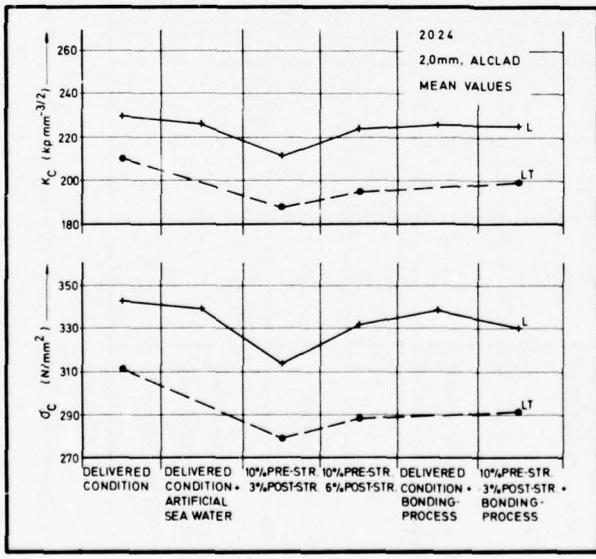

Ev63-B
3014

K_C, σ_C = f (ENVIRONMENT AND PRODUCTION PROCESSES)

VFW-FOKKER

Fig. 14

Spec.	Parameter	Sampling	$\sigma_m \pm \sigma_a$ (N/mm^2)	F_{max} (daN)	W (mm)	B (mm)	l (mm)	σ_c (N/mm^2)	K_c (kpmm$^{-3/2}$)	C x 10^{-5}	n
1		L	88,3 ± 39,2	6020	160	2,00	37,0	343	230	6,8200	2,5067
2		L	"	6050	"	"	36,4	344	228	5,4980	2,5537
3	Delivered	L	"	6140	"	"	36,1	342	230	3,3994	2,6858
4	Condition	LT	"	5480	"	"	36,9	312	209	8,2965	2,4466
5		LT	"	5430	"	"	36,5	306	205	1,0175	2,9625
6		LT	"	5500	"	"	37,6	318	213	1,6695	2,8745
7		L	"	5870	"	"	37,7	340	227	2,3564	2,7993
8	Artificial	L	"	6110	"	"	36,2	342	229	3,2119	2,7259
9	Sea Water	L	"	5990	"	"	36,2	335	226	5,7832	2,5720
10		L	"	5140	"	"	36,9	314	210	3,0504	2,5202
11	10% pre-stretched	L	"	5240	"	"	36,2	315	211	2,1741	2,6293
12		L	"	5180	"	"	37,1	318	213	1,9457	2,6392
13	3% post-stretched	LT	"	4630	"	"	36,4	279	187	2,8010	2,5691
14		LT	"	4480	"	"	37,2	275	185	2,0965	2,6504
15		LT	"	4620	"	"	37,2	284	190	4,4449	2,4302
16		L	"	5380	"	"	37,4	337	226	1,3359	2,7873
17	10% pre-stretched	L	"	5380	"	"	36,5	330	222	2,1038	2,6768
18		L	"	5380	"	"	36,7	332	223	5,1973	3,0491
19	3% post-stretched	LT	"	4580	"	"	37,1	285	192	5,3040	3,0758
20		LT	"	4640	"	"	37,0	288	194	8,2738	2,9351
21		LT	"	4610	"	"	37,5	290	195	3,1976	2,6049
22		L	"	6000	"	"	36,8	340	228	6,4139	2,5530
23	Bonding-process	L	"	5820	"	"	37,8	338	226	2,6741	2,7849
24		L	"	5820	"	"	37,1	336	225	2,8431	2,7623
25		L	"	5480	"	"	37,1	321	225	1,2227	2,8456
26	10% pre-stretched	L	"	5550	"	"	36,1	333	223	7,4600	2,9734
27	3% post-stretched	L	"	5550	"	"	36,6	337	226	4,3469	2,5327
28	+ bonding-process	LT	"	4830	"	"	37,2	297	199	3,0351	2,6354
29		LT	"	4810	"	"	37,7	299	200	1,2223	3,4889
30		LT	"	4740	"	"	37,5	294	197	2,6595	2,6683

TABLE 1 : Fracture Toughness Values of 2024 under Influence of Environment and Production Process

CONTRIBUTED DISCUSSION

by

Dr. Karl O.Sippel
Messerschmitt-Bölkow-Blohm GmbH
Aircraft Division
Postfach 801160
8000 München 80, Germany

Cold forming without or in connection with certain heat treatments as well as temperature application in connection with certain production processes such as bonding are routine processes applied to sheets in aircraft manufacture. Although it is obvious that such processes tend to influence the grain structure, the atomistic condition and, also the type and distribution of precipitates, as for example in age-hardening aluminium alloys, such influences on the material properties have been analysed only to a small extent. In specifications, they are only taken into account in so far as they have an influence upon the static strength values. Therefore, it is encouraging to learn that this complex of problems has been taken up in this place, particularly with respect to the crack propagation behaviour which, as a result of growing demands for damage tolerant design, is gathering momentum.

The test results reveal that stretch forming has a strong influence upon the crack propagation behaviour. In this connection, it seems to be of little effect when solution heat treatment is followed by 3% or 6% forming. The major influence is presumably caused by the 10% stretch forming of the material in the annealed condition, followed by solution heat treatment. Cold forming of such a high degree in connection with a subsequent solution heat treatment, which is not carried out every day, very probably entails recrystallization and formation of coarse grain. Appropriate grain structure investigations would be desirable in this instance. Similar examinations made by VFW on behalf on MBB, concerning other 2024 T3 sheets showed that 3% and 6% cold stretching without subsequent solution heat treatment results in the crack propagation behaviour progressively deteriorating with a higher degree of stretch forming. Thus, for completeness sake, it would be interesting to have additional tests performed on sheets, which, prior to being solution heat treated, were stretched only be 3% or 6% rather than 10%.

The slight, or in the case of the stretched samples somewhat pronounced, deterioration in the crack propagation behaviour after application of five bonding cycles and heating to 180°C is probably attributable to the transition from the naturally aged condition to an artificially aged condition. In this case, a condition will presumably be obtained which will settle between the naturally aged condition and the artificially aged condition which is normal for the 2024 alloy. In this range, the 2024 alloy is said to be particularly susceptible to corrosion. It would be therefore be interesting to analyse the general corrosion behaviour of the 2024 alloy after bonding treatments of that kind.

The practical application of the results of crack propagation tests performed in a laboratory corrosive environment is somewhat problematic. These results should only be used for comparative considerations. The results obtained are bound to depend very much on the frequency used in the test. The frequency selected in the present case was apparently so high that corrosive influences failed to show any practical effect.

It is not astonishing that the residual strength was not affected by the presence of a corrosive medium. This is apparently due to the fast progress made by the stable and unstable crack propagation. The other test parameters also fail to clearly influence the residual strength. This might be attributable to the fact that the applied stresses in the residual cross section are partially above or at least close to the limit of 0.8 times the yield strength which usually must not be exceeded for valid K_c-value determinations.

Finally, it should be pointed out that similar tests ought to be performed to include sheets of other aluminium alloys. Such tests would provide evidence permitting a substantially better selection of sheet materials for a specific application.

CONTRIBUTED DISCUSSION

by

D.Munz
German Aerospace Research Establishment (DFVLR)
5000 Köln 90, Germany

For a fail-safe design the fatigue crack propagation behavior and the residual strength have to be known. Because of the many influencing parameters, the prediction on fatigue crack propagation rate or fatigue life for a component in service from laboratory tests with simple specimens is very difficult. To obtain a good approximation of the real material behavior, the effects of the following parameters should be known:

load history (mean load, frequency, random load effects),
environment,
stress state (multiaxial loading, plane stress - plane strain),
material variation due to processing and manufacturing.

In the paper of K. H. Rendigs it was tried to find out the effect of some of these parameters on the aluminum alloy 2024. Following are some comments on the results:

a) Environmental effect
Overviewing the literature concerning the environmental effect on fatigue crack propagation it can be found that for some materials there is an effect especially at high crack growth rates and for others there is an effect especially for low crack growth rates. Aluminum alloys belong to the second group of materials. [1 - 3]. Only the threshold ΔK_{th}, below which there is no crack growth, can be independent of the environment. In contrast to this normally observed behavior, Rendigs has found the same crack growth rate in air and under continual wetting of the crack tip with artificial seawater at low crack propagation rates and a small increase in the seawater environment at high crack propagation rates. Possibly the wetting procedure, not specified in the paper, is different from test where the specimen is immersed in the liquid environment.

b) Effect of stretching
It has been known, since the fundamental work of Krause and Laird [4], that a deformation between quenching and ageing (thermomechanical treatment) can be beneficial to the fatigue behavior. For practical applications of thermomechanical treatment it is important to know the effect of parameters such as amount of stretching, time between quenching and stretching or ageing temperature on the fatigue behavior. In the paper of Rendigs the effects of two different amounts of stretching were investigated. After a prestretch of 10 % and solution heat treatment, a poststretch of 3 % and 6 % was performed. Compared to the unstretched material, a reduction of crack propagation rate was found. The 3 % stretch yields a somewhat lower crack propagation rate than the 6 % stretch. This is in agreement with previous results obtained by Broek and Bowles [5], who have found that a 1 - 3 % stretch gives optimum properties.

c) Fracture toughness and residual strength
The fracture toughness determination was not performed according to ASTM E 399 as claimed in the paper. K_c was determined from the maximum load and the initial crack length, not taking in account the crack propagation during the loading up to P_{max}. Therefore the effects of the different thermomechanical treatments should be the same on P_{max} and σ_c. This is in contrast to a statement made in the paper.

The slight reduction in residual strength due to the stretching is astonishing. Broek and Bowles [5] have found an increase. Their materials,however, were not prestretched.

Additional remarks

For a prediction of the fatigue life in service additonal tests are necessary:

a) The fatigue crack propagation under random load condition should be investigated for the different treatments and environments. A comparison of different materials by tests with constant amplitude and with varying amplitude can result in a different ranking of the materials [6].

b) Especially in corrosive environment, but also in air, the frequency can influence the crack propagation behavior [2].

c) Corrosion fatigue behavior can be very important. Therefore the astonishing result of no effect of salt solution at low crack propagation rates should be confirmed by additional tests.

References

[1] W. E. Krupp, D. W. Hoeppner, E. K. Walker: Crack propagation of aluminum alloys in corrosive environments. In Corrosion Fatigue, Chemistry, Mechanics and Microstructure, National Association of Corrosion Engineers 1972, p. 468.

[2] H. L. Marcus, J. C. Williams, N. E. Paton: The influence of gaseous environments on corrosion fatigue. In Corrosion Fatigue, Chemistry, Mechanics and Microstructure, National Association of Corrosion Engineers 1972, p. 346.

3 J. Schijve, W. J. Arkema: Crack closure and the environmental effect on fatigue crack growth, Report VTH-217 of the Delft University of Technology 1976.

4 A. R. Krause, C. Laird: A critical investigation of the factors controlling the long-life fatigue properties of aluminum alloys. Mat. Sci. Engng. 2 (1968), 331.

5 D. Broek, C. Q. Bowles: The effect of cold deformation and ageing on fatigue crack propagation and residual strength of 2024 sheet material. Report NLR TR 69048 U (1969).

6 R. J. Bucci: Spectrum loading - a useful tool to establish the role of microstructure in fatigue crack growth resistance of metal alloys, Tenth National Symposium on Fracture Mechanics, Philadelphia 1976.

PROOF-LOAD TESTING ON 300 M STEEL

by

Wolfgang Geier, Dipl.-Ing.
Material and Fatigue

and

Karl O. Sippel, Dr. Ing.
Head of Department Material and Fatigue

MESSERSCHMITT-BÖLKOW-BLOHM GMBH
Aircraft Division
8000 München 80, P.O.Box 801160
W-Germany

SUMMARY

As a result of the fundamental considerations made on the Proof-Load Procedure, general conditions for its basic applicability may be defined.

It has been established that the procedure is sufficiently safe for use if the maximum operational load is limited or the safe crack growth interval is considered to be a statistical value.

The test results proved that the safe crack growth interval can be determined theoretically.

The examination of the specific proof-load parameters provided new information on the effects and influence of the test parameters on crack propagation and residual strength. The rate of crack propagation decreases with increasing proof-load in relation to the operational load and with the proof-load interval becoming smaller. The proof-load conditions being constant, the permissible interval for the transport aircraft load spectrum is greater than that for the combat aircraft load spectrum.

The experimental examination of the Proof-Load Procedure was performed using the material 300 M exclusively. Further experiments are necessary to determine to what extent the information gathered can be applied to other materials and load spectra.

In order to guarantee a crack length range large enough to measure the influence of the specific proof-load parameters on crack propagation it was necessary to perform the crack propagation tests on a very low stress level due to the very low fracture toughness of the steel 300 M. Future tests also will take into consideration a stress level adequate to the ultimate strength of the candidate material.

1. PURPOSE OF THE PROOF-LOAD PROCEDURE

Based on the assumption that cracks in structural parts cannot be avoided, crack propagation investigations are required to prove damage tolerance or to determine reasonable inspection intervals.

The incipient crack length is essential for the calculation of crack propagation; this crack length is supposed to represent the largest possible crack that, caused for example during manufacture or installation, can be overlooked in the acceptance test. The extent of the detectable crack depends on the crack test procedure and on the accessibility of the component. Test procedures such as x-ray, ultrasonic, magnaflux testing etc. have so far been used by quality assurance or for subsequent inspections.

Recently, proof-load tests have been introduced as a non-destructive crack test procedure /1/. Compared to conventional procedures, the proof-load test has the advantage that cracks beyond a certain length, i.e. cracks being equal to, or longer than the critical crack length under proof-load, are safely detected, because in this case, the component will be destroyed.

2. FUNCTIONING OF THE PROOF-LOAD PROCEDURE

If a component or even the entire structure is subjected to a proof-load, which does not result in destruction, this means that, with adequate reliability, a critical crack can be excluded for those areas under tensile stress. The critical crack length theoretically determined from the proof-load and the fracture toughness is used as the incipient crack length for further crack propagation investigations (see Fig. 1). As can be seen from Fig. 1, the proof-load must exceed the maximum operating load. The larger this difference, the larger the approved proof-load interval. The proof-load test and the subsequent limited operation of the component - safe crack growth interval = proof-load interval - can be repeated until a possible crack existing in the component becomes unstable.

The proof-load interval can also be increased by overcooling the component during the test. However, this is only possible with materials which exhibit a decrease in fracture toughness at low temperature.

3. PROOF-LOAD TESTING IN AIRCRAFT CONSTRUCTION

Although proof-load testing as a means of crack testing in connection with the crack propagation life study is fairly new in aircraft construction, there are already a few cases which have become known.

3.1 Proof-Load Test of F-111 Aircraft

One of the first and, probably one of the most spectacular cases was the proof-load test on the F-111 A performed by General Dynamics /2/. About 325 complete aircraft were submitted to static loads of 7.33 g to -2.4 g in a refrigerating chamber at -40°F. During the test three aircraft failed due to cracks in the lower base plate and in the left-hand horizontal stabilizer fitting. The reason for this test was the crash of a F-111 A of the USAF in December 1969 during a training flight. The left wing separated in flight due to a flaw in the lower plate of the wing pivot fitting although the load factor was well below design limits. A thorough examination of the part was made in General Dynamics and Air Force laboratories. Metallurgical study led to the conclusion that the flaw had been generated during the manufacturing process and had not been detected during inspection.

3.2 Proof-Load Test of B-52 Aircraft

Proof-load testing and its suitability as an inspection method for aircraft was discussed at the AGARD Meeting held in Ankara in October 1975 /3/.

On this occasion it was stated that 78 B-52 aircraft had been subjected to the proof-load test. During the tests, defects occurred on small components only. The cost for the proof-load test is only about one tenth of the conventional inspection cost.

3.3 Proof-Load Test MRCA-Tornado Aircraft Component

Another example of proof-load testing is the testing of a major component of the MRCA-Tornado prototype. This test gave rise to the following systematical investigation.

Due to the difficult access to this component, the proof-load test is employed as an additional test for prototype and pre-series aircraft. In this test, the component is subjected to tensile stress until the limit load is reached. Since, despite crack testing, cracks in this component could not be fully excluded, the proof-load test now provides the possibility of forecasting a safe crack growth interval.

4. TEST PROGRAMME

For the application of the proof-load procedure, the following questions arise:

- What influence have the proof-load level, the proof-load holding time, and the proof-load interval on the crack propagation behaviour?
- How can the optimum proof-load interval or the safe crack growth interval be determined?
- What influence has the load spectrum on the safe crack growth interval?
- What are the general conditions which on principle are to be fulfilled for the application of the proof-load procedure?

In order to clarify these questions, such factors as the proof-load level, the holding time, and the interval as well as the load spectrum have been investigated for various parameters (see Fig. 2).

The material selection as well as the determination of the maximum operating load of $\sigma_o = 250$ N/mm^2 for the flight-by-flight crack propagation tests with and without proof-loads were closely related to the tests which were required to determine the safe crack growth interval for the MRCA Tornado by means of the proof-load tests.

The brittleness of the material results in extremely small critical crack lengths when using loads appropriate to the strength of the material.

Compared with the ultimate strength of the material which is approximately 2100 N/mm^2, the operating load used for the following tests seems to be unrealistic.
Since it was the relative influence of the proof-load parameter and the principle of the procedure which were the main subjects of the test - and not the results as such - the relatively low proof load proved to be suitable for taking measurements in a sufficiently large crack length area.
It is assumed that the relations to be expected at this low stress level are generally transferable to higher stress levels.

A study of aluminium alloy performed to determine the influence of the stress level on the permissible proof-load interval had already revealed that the interval decreases with increasing stress level. In this test, the ratio of proof-load to maximum operation load remained constant. This is due to the fact that the ratio of the critical crack length under maximum operating load to that under proof-load does not depend upon the stress level; however, the difference between both critical crack lengths and, consequently, the interval decreases with increasing stress level.

It can be assumed that, particularly in the case of materials with extreme brittleness such as the high-strength 300 M steel, the permissible proof-load interval could at a very high stress level decrease to such an extent that this procedure is no longer economical. This consideration was another reason to select the relatively low stress level for the basic investigation.

The c.g. acceleration spectra used are a typical combat aircraft spectrum and the standardized transport aircraft spectrum (see Fig. 4). While the transport aircraft spectrum comprises mainly gusts and take-off and G.A.G. load cycles, the combat aircraft spectrum consists almost entirely of maneuvering loads.

A centre crack specimen was used for the tests. The crack starting notch was produced by electric discharge. The crack propagation tests were performed in the Laboratorium für Betriebsfestigkeit in Darmstadt using a process-computer controlled $\pm$ Mp hydraulic ram of Messrs. Schenk.

5. TEST RESULTS

In general the result of the experimental investigation of the proof-load procedure regarding the influence of this specific parameters on the crack propagation behaviour can be rated as positive.

5.1 Crack Propagation and Retardation Caused by Proof-Loads

It is well known that single peak loads, exceeding considerably the maximum spectrum load, spread into a flight-by-flight load sequence may cause a delay in fatigue crack propagation. However, it is easy to understand that with increasing proof-load frequency a point could be reached beyond which a further increase of the proof-load frequency adversly affects the fatigue crack propagation life. Within the here investigated combinations of proof-loads and proof-load frequency which might be of practical interest no adverse effects have been found (see Fig. 5/9). Even with a relatively high proof-load of $1.45\bar{\sigma}_o$ and an extremely short interval of 200 flights the crack propagation life in the combat aircraft spectrum was quadrupled.

After the application of the proof-load, short cracks exhibited a considerable delay in propagation (see Fig. 5). Near the critical crack length however, the proof-load exhibited a considerable increase in crack propagation as revealed by the dark striations on the pictures of the fracture planes in Fig. 6.

The application of the proof-load tests within the investigated parameter range, resulted in a general improvement of the crack propagation behaviour. For the time being, this applies only to the 300 M material and to the two spectra investigated.

5.2 Proof-Load Holding Time

During the investigation of the proof-load holding time, no influence on crack propagation behaviour could be realized. While on the majority of the specimens crack propagation became unsteady during, or immediately after reaching the full proof-load, fracture occurred on some specimens after a proof-load holding time of approximately 10 secs only. This may be attributed to the fact that the crack length present at the beginning of the proof-load test may be somewhat smaller, equal to, or somewhat larger than the critical crack length under proof-load. Providing that the crack length is equal to, or larger than, the critical crack length, the fracture occurs either at, or shortly prior to, reaching the full proof-load. On the other hand, the critical length under proof-load can be reached by a gradual crack propagation under constant load (= creeping). An extended proof-load holding time would, therefore, also cover cracks which are slightly smaller than the critical crack length under proof-load. This means that the procedure has an improved reliability. Therefore, a minimum holding time of the proof-load of 15 secs is recommended for the 300 M material.

5.3 Successive Proof-Loads

By means of several successive application of the proof-loads, the retardation effect should be intensified and those cracks, which are somewhat smaller than the critical crack length under proof-load, should be detected. The three successive proof-loads applied at the end and/or beginning of the proof-load interval had no effect on crack propagation and residual strength. Since these tests have been performed with one proof-load level and one proof-load interval only, this procedure, i.e. multiple proof-loading, cannot be fully evaluated. For this purpose, further tests would be required.

5.4 Influence of Load Spectrum on Proof-Load Interval

The proof-load tests with the transport aircraft spectrum resulted in a considerably longer life when compared with the combat aircraft spectrum. The crack propagation retardation was so great that, with a proof-load interval of 2000 flights and a proof-load of $1.3\bar{\sigma}_o$, the crack propagation under operational load came to a halt. The retardation effect which differs greatly from spectrum to spectrum may be explained as follows:

As is generally known, the retardation increases within a certain crack range when performing crack propagation tests under constant load amplitude with single peak loads, when these single peak loads become greater and more frequent in relation to the constant amplitude load. When transferred to the load spectrum as a criterion for the retardation, this ratio requires that the spectrum load level should be equal to the constant amplitude load. When "equal" is understood in relation to the contribution of the load spectrum towards damage, which in this case is crack propagation, the load spectrum level that, according to Miner rule, makes the greatest contribution towards total damage would be the most suitable. Investigations revealed that this level is about 2/3 to 3/4 of the maximum spectrum load /4/. A comparison between the proof-load and the load level of both spectra , in relation to the same number of flights, shows that the number of the load cycles within this level is considerably higher in the combat aircraft spectrum than in the standard transport aircraft spectrum (see Fig. 4). With the proof-load intervals, being equal, the load level of the combat aircraft spectrum, that causes considerable damage, would comprise load cycles approximately 20 times as many as the standard transport aircraft spectrum. Therefore, the crack propagation retardation, caused by the proof-load, has a greater effect with the standard transport aircraft spectrum than with the combat aircraft spectrum.

6. Predetermination of the Safe Crack Growth Interval

The predetermination of the safe crack growth interval (= proof load interval) for a certain flight-by-flight load sequence and for a certain proof-load level has already been described at the beginning. In general, the flight-by-flight crack propagation curve from which the proof-load interval is derived can be determined experimentally or by means of a crack propagation calculation, for example after Forman (see Fig. 7/8). A comparison of the proof-load intervals which have been determined after both methods shows that the crack propagation curve obtained experimentally results in a proof-load interval which is 2 to 5 times greater than the proof-load interval obtained with the Forman equation. This difference, which varies with the load spectrum and the level of the proof-load, is to be attributed to the crack propagation calculation after Forman, which does not consider any delay effects. The length of the proof-load interval appears to be also dependent on the spectrum. Compared with the combat aircraft load spectrum, the standard transport aircraft load spectrum results in proof-load interval being 2 to 3 times longer when applying the crack propagation curve determined by experiments.

For a certain proof-load the length of the proof-load interval depends on the slope of the crack propagation curve in the interval range. Various flight-by-flight crack propagation tests /5/ indicate that the slope of the crack propagation curve is influenced by the type of the load spectrum in this range. It can be assumed that the slope of the curve will become flatter with increasing retardation which, in turn, is dependent on the type of the load spectrum.

7. PRACTICAL HINTS FOR DETERMINATION OF THE PROOF-LOAD INTERVAL

As a result of this investigation and, particularly, as a result of the proof-load investigation specifically performed for the MRCA-Tornado aircraft, practical hints for the determination of a safe proof-load interval are given in the following pages.

As already mentioned at the beginning, the flight-by-flight crack propagation curve as well as the critical crack length under proof-load and under maximum operational load are required to determine the interval.

The two critical crack lengths represent the upper and lower limits of the crack propagation curve, from which the interval is derived, taking the scatter of material and load level into account.

7.1 Scatter of Fracture Toughness

Since the interval depends largely on the incipient crack length calculated from fracture toughness and proof-load stress factors, the material scatter relative to the facture toughness must be specially considered.

If, e.g. the fracture toughness of the material used for the component is somewhat higher than that which was used to determine the interval, the interval of the component is on the unsafe side as concerns the actual admissible interval. This may lead to failure of the component under operational load within the proof-load interval. Thus the higher fracture toughness and consequently the longer the critical crack length under proof-load are to be assumed the safer is the interval. The fracture toughness value that is exceeded with a probability of only 10^{-3} can be deemed to be sufficiently safe; i.e., in order to calculate the critical crack length under proof-load, the fracture toughness value with a probability of exceedance of 0.1 % will be used.

7.2 Scatter of the Crack Propagation Curve

The scatter of the load and the crack propagation, e.g. the crack propagation retardation effect of the material, influence the slope of the crack propagation curve and thus also the value of the admissible interval.

The steeper the slope of the crack propagation curve is in the area of the interval the more the interval decreases.

The slope is very much affected by the load spectrum and, to a certain degree, also by the retardation effect of the material. In general, flight-by-flight load sequences with relatively low peak loads (truncation) which are, however, rather frequent cause a steep slope of the crack propagation curve and thus a shorter interval.

A decrease in the retardation effect through truncation during flight operations and the entailing decrease of the interval result in a certain risk that can be covered as follows.

If the flight-by-flight crack propagation curve is calculated by means of a crack propagation model which does not take the retardation effect into account as is the case in the Forman equation, this risk is excluded in most cases. A safety factor is not necessarily needed any longer, provided there are no uncertainties in the input data for the calculation.

If a flight-by-flight crack propagation curve is used which has been obtained by means of tests, the load scatter must be taken into account by allowing for a safety factor frequently choosen to be 2.
Prior to the proof-load test, it should always be checked whether the proof-load interval is of sufficient length in order to guarantee that the test procedure can be carried out economically.

8. FUNDAMENTAL PRINCIPLES CONCERNING THE APPLICABILITY OF THE PROOF-LOAD PROCEDURE

Finally, some fundamental principles concerning the applicability of proof-load procedure shall be discussed taking the static airframe design into consideration.

As mentioned before, the safe crack growth interval increases with the increasing difference between the proof-load and the maximum operational load. This difference is a decisive factor for the applicability and cost effectiveness of the proof-load procedure. In the following, an answer shall be given to the questions:
Up to what limit may the proof-load be increased in respect of the most important design values and what are the limiting factors?

8.1 Definition of Frequently Used Terms

First, however, it seems to be necessary to clarify some terms which are frequently used in this connection, such as

maximum operation load

limit load

safe load

ultimate load and

reserve factor.

"Safe load" means a load value which is likely to occur during the life of an aircraft, and its structure must be such as to withstand that load. The safe load is identical with the limit load, and when multiplied by the factor 1.5, it is called ultimate load.

When dimensioning leight-weight constructions, the value of ultimate strength to ultimate stress shall be 1. In order to ensure for example the required fatigue life or the stability of the structure, in most cases this ratio is greater than 1. This ratio is then called 'reserve factor'!

As far as the maximum operating load is concerned, a quantification can only be made in connection with a probability of occurrence which is derived from an extreme value distribution.

8.2 Premises for Proof-Load Application

As the maximum operating load is a statistical value and may, therefore, under certain circumstances, reach or even exceed a fixed proof-load, the question arises whether the proof-load can, in principle, be applied. The application of the proof-load procedure under the above mentioned condition - i.e. the maximum operating load must be smaller than the proof load - would only be possible, if the maximum operating load would be limited. This would not necessarily lead to restrictions in flight operations, especially not in the case when the proof load is allowed to be much greater than the limit load.

The proof load limit is reached, if plastic deformations can be expected, which, for example, would result in a change in the geometry. For components without reserve of strength it can be assumed that this limit for proof-load is reached when the limit load is exceeded by 1.2 to 1.3 times. It depends on the reserve factor to what extent the limit load can be exceeded by the proof-load.

It would, however, be more realistic to have a proof-load philosophy that does not provide for the maximum operating load being limited. This could be realized by assuming that the maximum operating load which is subject to a certain distribution is a statistical value. Consequently, the upper limit of the crack propagation area and thus the proof load interval itself are also subject to the same distribution.

9. REFERENCE

/1/ Mil Spec 84 444

/2/ W.D. Buntin:
Concept and Conduct of Proof Test of F-111 Production Aircraft;
Aeronautical Journal Oct. 1972

/3/ M.D. Coffin and C.F. Tiffany:
New Air Force Requirements for Structural Safety, Durability and Life Management; A/AA Paper N. 75-781

/4/ W. Schütz und H. Zenner:
Schadensakkumulationshypothesen zur Lebensdauervorhersage bei schwingender Beanspruchung; Zeitschrift für Werkstofftechnik, 4. Jahrgang, Heft 1 (1973) Seite 25 - 33.

/5/ D. Weisgerber und P. Keerl:
Theoretische und experimentelle Rißfortschrittsuntersuchung für Metallstrukturen (Rißfortschritt in Kampfflugzeugbauteilen unter betrieblichen Bedingungen), ZTL 1975

10. ACKNOWLEDGEMENT

The work was supported by the Ministry of Defence of the F.R.G.

$$l_c = \left(\frac{K_{Ic}}{\sigma_{PL}}\right)^2 \frac{1}{C \cdot \pi}$$

l_c = Critical Crack Length
K_{Ic} = Fracture Toughness
σ_{PL} = Proof-Load Stress
C = Stress Intensity Magnification Factor
σ_{max} = Maximum Operation Stress

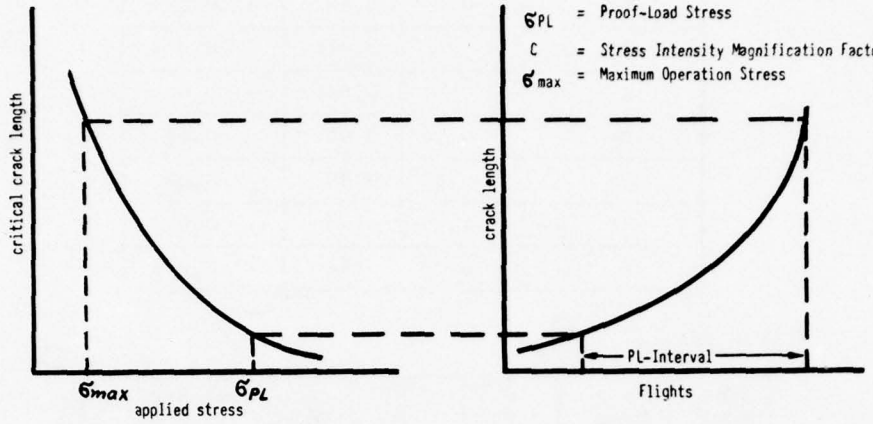

Fig. 1 : Determination of Proof-Load Interval Depending on Maximum Operation Stress, Proof-Load Stress and Flight-by-Flight Crack Propagation Curve

Material used: high-tensile steel 300M

Specimen No.	Load Spectrum	Max. Load Spectrum Stress in N/mm²	Proof Load		
			Interval (Flights)	Level σ_{PL}/σ_o	Holding Time (sec)
1/2/3	Constant Amplitude	225,6	-	-	-
4/5	Fighter Aircraft Spectrum	250,1	-	-	-
6/7/12	"	"	200	1,3	15
13	"	"	200	1,3	0,1
8/9/10	"	"	2000	1,3	15
11	"	"	2000	1,3	0,1
15/16	"	"	1000	1,3	15
14	"	"	1000	1,3	0,1
17/37	"	"	1000	1,45	15
18/19/20	"	"	2000	1,3	300
21/22/23	"	"	2000	1,45	15
24/27	"	"	200	1,15	15
25/26	"	"	600	1,15	15
32/35	"	"	2000	1,3x3	15
38/39	"	"	200	1,45	15
29/34	Standard E.F.P.-Transporter	"	-	-	-
30	"	"	2000	1,3	15
31	"	"	2000	1,15	15

Fig.2 Test Programme

Chemical Composition

Constituents	%		Tolerance
	min	max	
C	0,40	0,45	+ 0,02
Si	1,45	1,80	± 0,05
Mn	0,65	0,90	± 0,04
P	--	0,010	+ 0,005
S	--	0,010	+ 0,005
Cr	0,70	0,95	± 0,05
Mo	0,35	0,45	± 0,03
Ni	1,65	2,00	± 0,05
V	0,05	--	- 0,003

Static Values

σ_B N/mm^2	$\sigma_{0,2}$ N/mm^2	δ %	ψ %	K_c N/mm$^{3/2}$ S = 5 mm	K_{Ic} N/mm$^{3/2}$
2102	1734	8,76	40,66	2200	1226

The tensile tests were carried out to DIN 50145 by using the probe B 6 30 DIN 50125, and heat treatment was carried out to specification M 360 of Rotax Ltd., London.

Fig. 3 : Material 300 M, Chemical Composition and Static Values

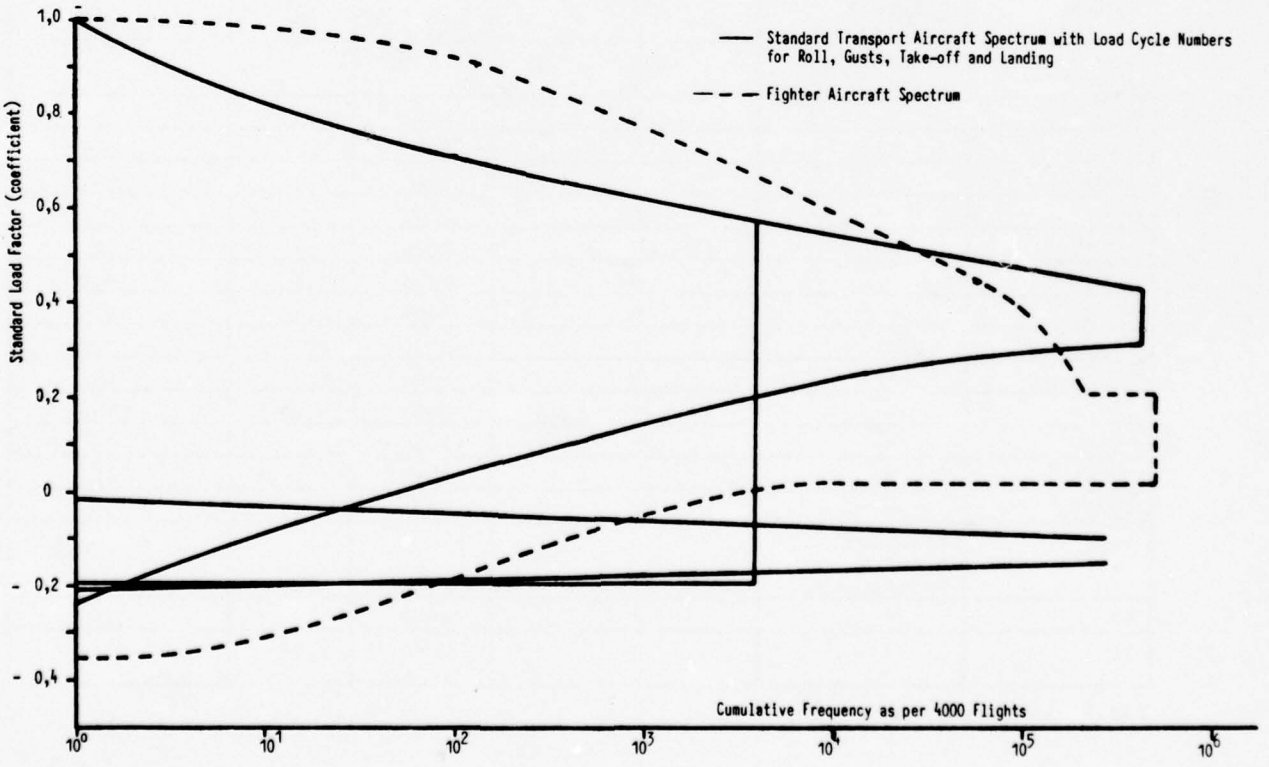

Fig. 4 : Load Spectra

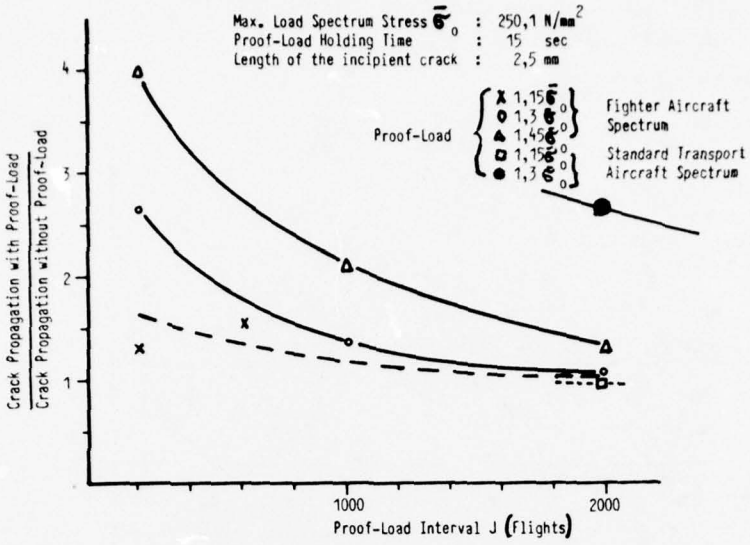

Fig. 5 : Influence of Proof-Loads and Proof-Load Intervals on the Flight-by-Flight Crack Propagation Behaviour for Fighter Aircraft Spectra and Standard Transport Aircraft Spectra

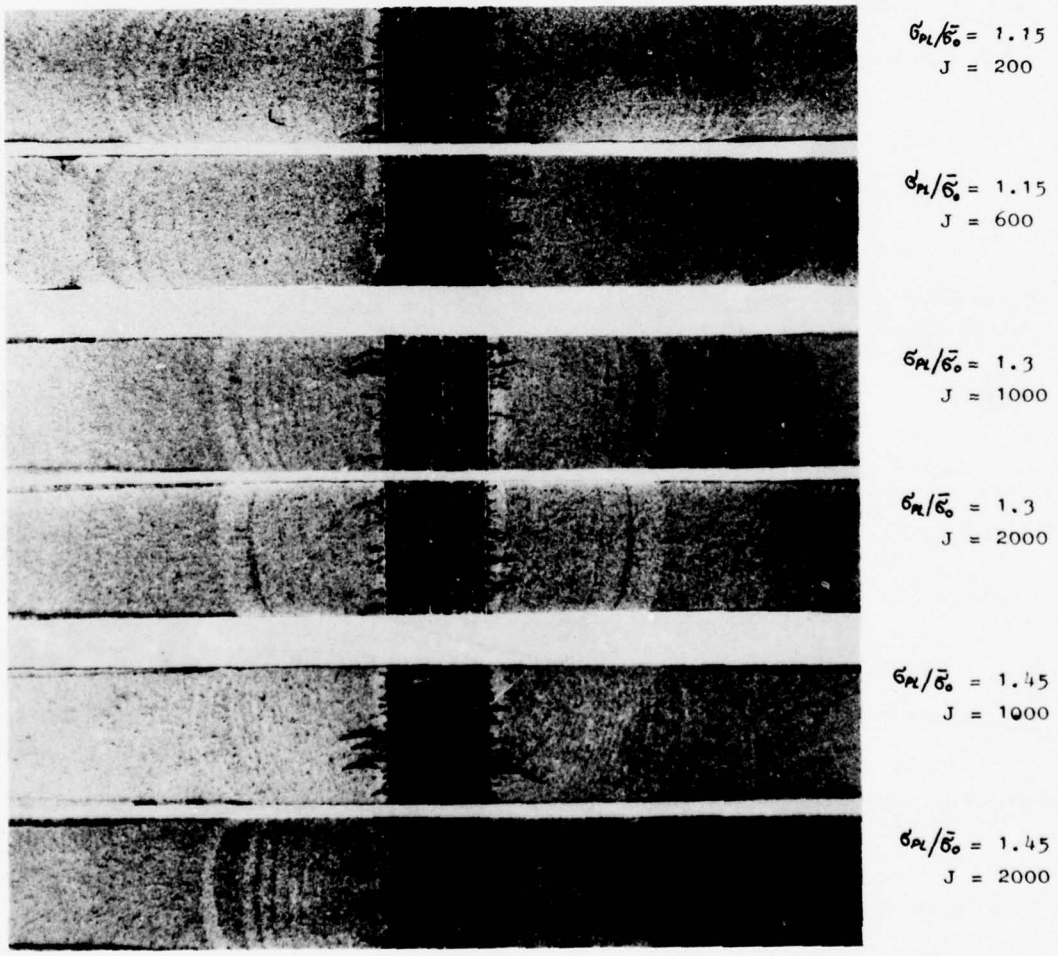

Fig. 6 : Surfaces of Fracture of the Crack Propagation Specimens, Taking the Proof-Loads and the n_z-Fighter Aircraft Spectrum As Operating Load

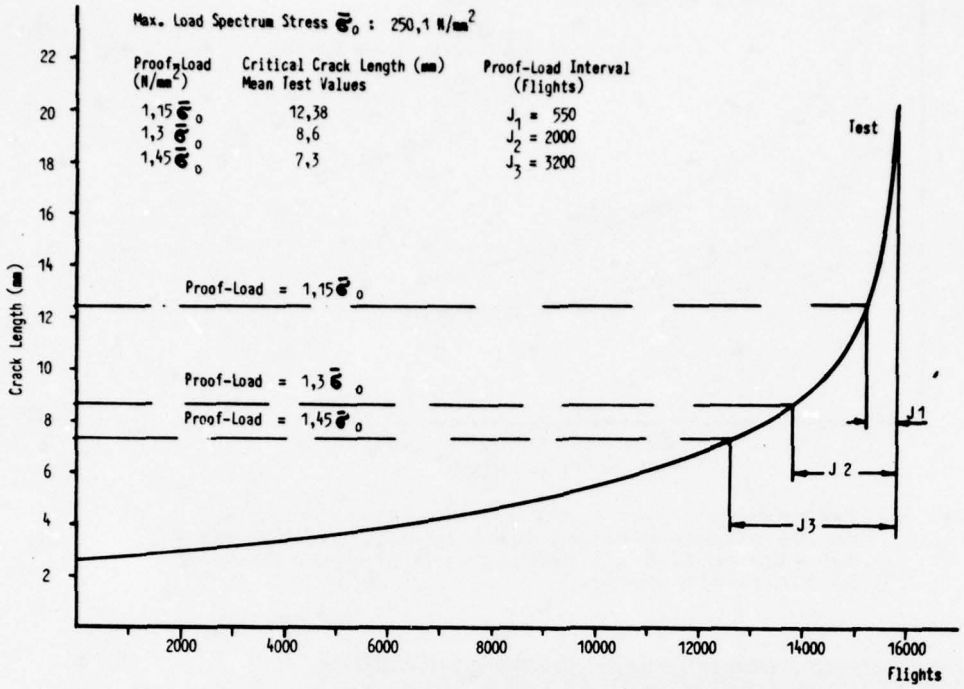

Fig. 7 : Proof Load Intervals Derived from Flight-by-Flight Crack Propagation Tests

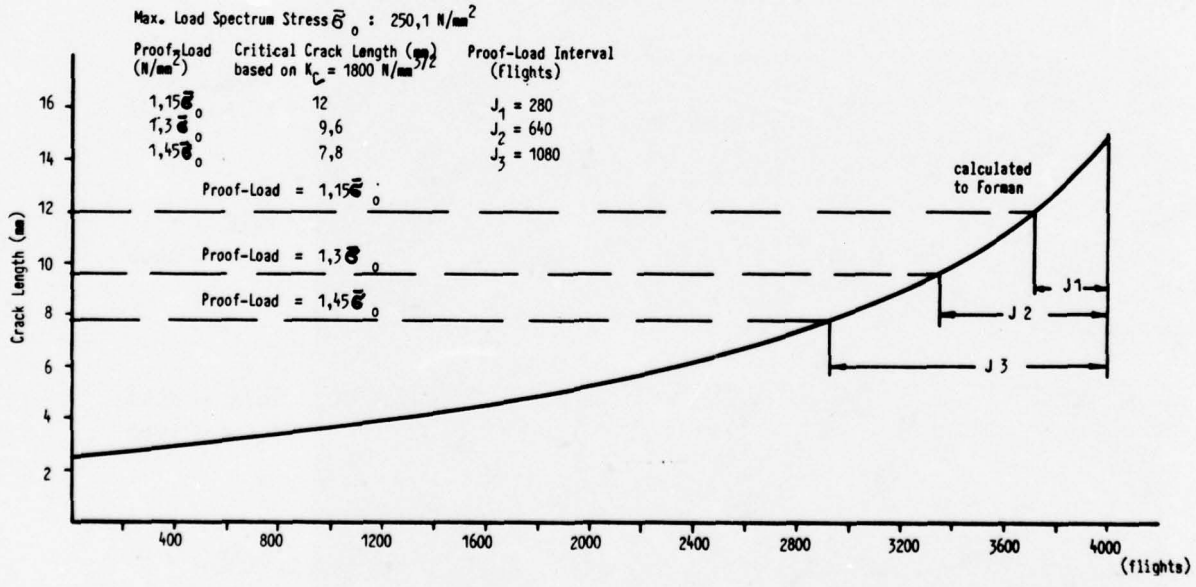

Fig. 8 : Proof Load Intervals Derived from Crack Propagation Calculation after Forman

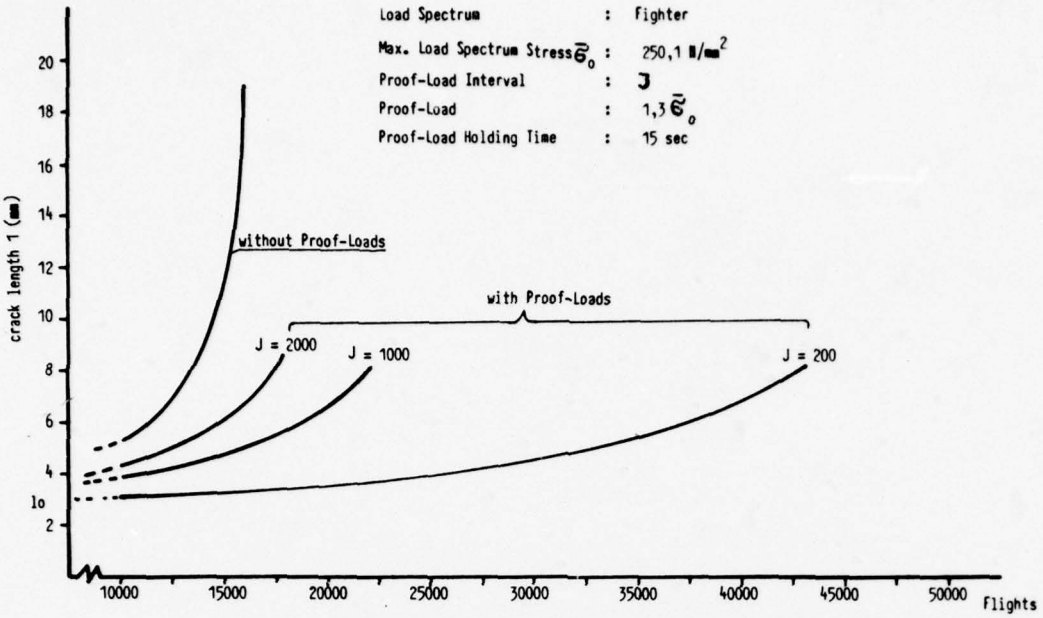

Fig. 9 : Influence of Proof-Load and Proof-Load Holding Time on Crack Propagation Retardation under Flight-by-Flight Load Sequence

CONTRIBUTED DISCUSSION

by

Dr. -Ing. Walter Schütz
Industrieanlagen-Betriebsgesellschaft mbH
Einsteinstrasse, 8012 Ottobrunn, Germany

1. INTRODUCTION

At first sight, proof load testing seems to be a simple and reliable NDI-method; on second thought, however, a number of questions become apparent:

- How high should the proof load be, compared with the (at best) statistically known service loads?
- How long a time should it be held?
- What effect will the proof load have on subsequent fatigue life? } if the part did not fail
- How large a crack can still be present after the proof load considering the scatter of fracture toughness? } if the part did not fail
- How long a fatigue life is really assured (i.e. when must the next proof load be applied), considering
  - the unknown scatter of service loads and
  - the unknown scatter of fatigue crack propagation properties?

  This is probably the most difficult question.
- As it is not possible to stress all components of a complete structure to the same percentage of limit or ultimate in a proof load test, different crack sizes will be present in different parts of the structure. (Even if they are of the same material and have been designed to identical stresses.)

Thus it is obvious that a large number of expensive tests will have to be carried out before relying on proof testing for the structural integrity of aircraft structures and components.

On the other hand, it is well known that the USAF has auccessfully used proof load testing for its F-111 and B-52 fleets. To this discussant's knowledge no thorough investigation of the various parameters as discussed above has been published in the open literature; it may, however, be assumed that the USAF did not embark on the F-111 proof testing program without previous large scale laboratory investigations.

2. RESULTS AND DISCUSSION

As proof testing is also to be employed on some components of the MRCA Tornado tactical aircraft, a test program on ultra high-strength steel 300 M was carried out by MBB and is described in the paper discussed. Most of the problems mentioned above have been investigated for this material; therefore this work is an important contribution to our knowledge on proof load testing.

One is immediately struck by the extremely low fracture toughness of 300 M, which at K_{IC} = 1226 N/mm$^{3/2}$ is hardly equal to that of a modern aluminum alloy like 7475-T73; this is somewhat surprising, as the landing gears of many civil transport aircraft have been manufactured from this material for years.

The crack propagation behaviour was extremely unfavourable as well, see FIG 9 of the paper: At a maximum spectrum load of less than one eighth of tensile ultimate, the crack propagation life was about 16 000 flights under a fighter load sequence. An aluminum alloy like 2024-T3 will give a similar crack propagation life at a maximum spectrum load of about one third (!) of ultimate. So, proof load or no proof load, this discussant would draw the conclusion to drop this unfavourable material immediately.

Anyway the tests have shown that

- the higher the proof load, the longer the allowable proof load interval
- the proof load interval depends to a larger degree on the load spectrum applied: At identical proof loads of 1,3 · σ_{max} of the load spectrum, the proof load interval is much longer under a transport aircraft load sequence than under a fighter sequence
- the higher the number of proof loads applied, the slower is the crack propagation.

The paper also contains a general discussion on how to overcome the problem of scatter of fracture toughness and crack propagation properties, without, however, giving the necessary constants like standard deviation necessary for a numerical calculation. These constants can only be obtained by a large number of expensive tests.

3. CONCLUSIONS

The work described in the paper shows how a modern proof load testing program must be carried out: Reliance is placed on complex, i.e. flight-by-flight-tests, and not on calculations alone. Work of this kind should be continued on other typical materials.

CONTRIBUTED DISCUSSION

by

W.D.Buntin
General Dynamics/Fort Worth Division
P.O. Box 748
Fort Worth, Texas 76101
USA

The subject paper presents an interesting investigation of the proof load procedure in providing a safe operating interval for aircraft structure. The material used is a martensitic steel designated 300M and considered to be relatively brittle in terms of toughness. In general the questions investigated are indeed basic to the applicability of proof testing in assuring fracture control and, in part, parallel the more important technical aspects conducted in the investigation described in Reference 2 of the subject paper.

The related investigation of the proof load program of the F-111 aircraft which is mentioned in the paper can be updated. A total of 521 complete aircraft were proof tested under the conditions described as Phase I of that program. Only two aircraft sustained failure during these proof tests and they were repaired and returned to service. In general the F-111 proof testing continues to be viewed as a very effective method of fracture control and a second round of testing designated as Phase II has begun in Air Force laboratories in Sacramento, California.

In general, the technical conclusions are felt to be well taken. The paper states that the relations developed using the relatively low stress levels are assumed to apply at higher levels which raises interesting questions about stress level effects. Notwithstanding the rationale for the stress level assumption, further experimental work at higher stress levels would be interesting for the purpose of verifying these assumptions. The question of variability of fracture toughness in the structural material is also well taken. Toughness will undoubtedly be a factor of processing as well as part thickness and this must be recognized in developing proof test programs. Additional questions which might be of interest include cyclic rate and environmental effects on crack growth. The 300M steel is known to be reasonably resistant to stress corrosion cracking relative to other steels in its class; however, the question should be investigated before being put aside.

The paper also properly points out that analytical methods (for example, Forman's equation) which do not account for retardation effects in crack growth rates can be con-

servative. A number of retardation schemes have been developed in crack growth analysis procedures and it would be interesting to see how the 300M material responds.

A final comment -- the paper quite properly cautions against applying specific results from these particular investigations to other materials used in structural design. Stress level effects, material forms, environmental effects, material properties, etc. will require experimental investigation for the specific design problem. The purpose of the subject paper, however, was to establish the concept including certain general relations and indeed this has been done well.

PANEL DISCUSSION TO SPECIALIST MEETING ON FRACTURE MECHANICS DESIGN METHODOLOGY

by

David Broek

Battelle's Columbus Laboratories, U.S.A.

On a multitude of occasions during this meeting, engineers expressed their reluctance to accept the results of damage tolerance analysis because of its presumable inaccuracy. This pertains in particular to crack-growth computations and to a lesser extent to residual strength calculations. Admittedly, the analysis procedures have shortcomings and further developments are required. However, the accuracy of the analyses should be judged against the background of the level of accuracy that can reasonably be expected from any engineering analysis. Furthermore, the inaccuracies due to the analysis procedure should be clearly distinguished from those due to the data input, since the combination of the two constitutes the accuracy of the final result. If the inaccuracy in the input data predominates in the end result, the inadequacies of the analysis become of secondary importance.

To consider the accuracy of an engineering analysis, the classical static strength analysis of the new (undamaged) structure will be taken as an example. In this analysis, the modulus, the yield strength, and ultimate tensile strength of the material are usually considered as reliable data input. Nevertheless, in setting the design allowables a substantial margin is taken with respect to the values actually observed. The static strength analysis is considered a sophisticated design tool. Yet, when it comes to the full-scale test of the complex structure, it turns out that the difference between the actual static strength and the calculated strength can easily be as much as 10 percent. (In this respect, it should also be recognized that the structure fails at only one place) In view of this descrepancy and in view of possible misjudgment of the maximum loads, a substantial safety factor is taken on the calculated strength.

It is difficult to understand why a damage tolerance analysis is demanded to have a better accuracy then a conventional static strength analysis. It was shown during this meeting that the residual strength of cracked complex structure can be predicted within about 10 precent also. This proves the adequacy of the analysis at least for those applications. It was also shown at this meeting (W. Schütz) that in some cases the residual strength of a forged component can be largely different than predicted. However, this was due to the inconsistency of the properties of the material, rather than due to inadequate analys. Obviously, in the case discussed by Dr. Schütz, a residual strength test could not give more reliable information than an analysis, nor would a more sophisticated analysis improve the prediction.

The accuracy of fatigue-crack-growth computations has been questioned even more during this meeting. The available retardation models for the prediction of fatigue-crack growth under variable amplitude (or flight simulation) loading do lack a sound physical basis, but the Wheeler model for example, seems to contain the right parameters. Some of the models have adjustable constants, which make them suitable for many applications.

Figure 1 shows experimental data of flight simulation tests based on a fighter spectrum. The load history consisted of 100 flights separated by ground-air-ground cycles. There were four different missions and eight different flight types. The series of 100 flights was repeated. Also shown in Figure 1, are crack-growth curves that were calculated on the basis of various retardation models, by means of a cycle-by-cycle integration on a CDC-6400 computer. In some cases, average baseline crack-growth data ($da/dN = f(\Delta K)$) were used, in other cases upper bound data were used. Finally, the results are shown of a linear integration (i.e., no retardation considered).

Figure 1, indeed, suggests that the computations are inaccurate and that almost any crack-growth life prediction can be attained. The Wheeler model contains an adjustable constant m, that relates the retarded crack-growth rate after an overload to the unretarded or linear crack-growth rate, through

$$\left(\frac{da}{dN}\right)_{\text{linear}} = \left(\frac{\text{Maximum extent of previous plastic zone}}{\text{Current plastic zone size}}\right)^{m} \left(\frac{da}{dN}\right)_{\text{retarded}}.$$

The linear da/dN for a given cycle is obtained from the baseline data (material-da/dN data). The retarded rate is found by taking the ratio of plastic zones to the power m and multiplying with the linear da/dN. The results shown in Figure 1 are for various values of m (1.4, 1.8, 2.2).

By selecting the proper value of m for a given spectrum, the model can be adjusted to give more accurate results. Figure 2 shows the ratio of predicted life and test life (N_{pred}/N_{test}) as a function of m for a fighter spectrum. The data are for various spectrum variations and various crack-growth intervals. When using average data, a value of m = 1.4 seems to give the best results for this spectrum and this material.

After such an adjustment of the model, more accurate predictions can be made as shown in Figure 3 for a titanium alloy. The effect of spectrum variations as brought about by a change in design stress can be predicted very well. The same is true for other minor spectrum variations. Once the model is adjusted, it can be used reasonably well for a variety of problems associated with the same general spectrum shape and the same material.

Figure 4 shows some statistics on the accuracy of the predictions. Again, a variety of spectrum shape variations, crack-growth intervals, and two materials are included. Apparently, the majority of the predictions is within about 20 percent of the actual life, which is extremely good for fatigue predictions.

However, in this case again, the accuracy of the predictions is affected more by the input data than by the analysis procedure. Part of those input data are the baseline da/dN properties, but to some extent their effect was included already in the data presented. Of more importance are the spectrum and the stresses. Small spectrum variations or small discrepancies in the stresses may have a significant effect on crack growth, as can be appreciated from Figure 3. If the stress analysis is 10 percent off, the predicted crack-growth life may be 40 percent off (if the crack-growth rate roughly varies with the fourth power of ΔK). It was also found that small variations in the spectrum can easily account for a factor of 2 in crack-growth life.

Against this background, the anomalies in the crack-growth-prediction method per se, become of secondary importance. A further sophistication of this method would not largely improve the end-result if the accuracy of the input data is not improved.

Another source of anomalies not yet mentioned is the crack geometry. The crack-growth computation has to assume a certain initial flaw shape. Depending upon the flaw configuration, the crack-growth life can vary largely. An improved crack-growth-prediction method would not eliminate this problem.

Apparently, reasonable crack-growth predictions for flight-by-flight loading can be made provided the input data are reliable. During the progress of the design, the input data gradually become better defined. In the early design stages, their accuracy is low. Nevertheless, computed crack-growth information can be used in a comparative way in parametric studies, to evaluate the relative crack-growth performance resulting from certain design changes.

At the time of component testing and full-scale testing, some actual crack-growth information becomes available. On the basis of these data the models can be adjusted and subsequently all predictions for other cases and other locations can be updated. As a consequence, these predictions have approximately the same accuracy as the experimental data.

When in-flight spectrum measurements become available, a final updating of the crack-growth predictions can be made. At that time, a final safety-factor on crack-growth life can be taken to establish inspection intervals. (It is emphasized that safety factors anywhere else in the computations, i.e., on cyclic stresses or on baseline data, do not permit evaluation of the margin of safety; moreover the margin of safety will be different for different configurations. Taking a safety factor on the final outcome of the computation is the only way to factor all computations to the same extent.) The effects of different aircraft usage can also be evaluated. In particular, the problem of the occurrence of high loads can be analyzed, since also the effects of spectrum truncation and clipping can be adequately predicted with a well-adjusted crack-growth model.

Crack-growth computations may be costly, because of the long computer times involved. However, for the application to specific cases much more efficient computation routines can be followed, permitting the use of desk computers or even pocket calculators.

Present-day knowledge of fracture mechanics and modern stress-analysis techniques permit the prediction of damage tolerance (crack growth and residual strength) of most of the airplane structure. The techniques still have shortcomings. Also, the data required as input to the analysis do not always have the desirable accuracy. However, shortcomings can be pointed out in the guesswork associated with any new design. In general, designing is a projection in the future of past experience, using more or less approximate models for stress analysis and estimating the unknowns. Confidence in the design procedures is based upon experience and apparent adequacy in the past. The magnitude of the applied safety factors reflects the degree of confidence.

Hence, the shortcomings of damage tolerance analysis can hardly be an excuse for postponing the application to design, although the lack of past experience asks for some caution. In the absence of experience, some confidence in the methodologies can be obtained from an application to existing designs, where a comparison with service behavior can be made directly. Otherwise, confidence can only be built by accumulating experience through cautious application.

On a few occasions during this meeting, damage-tolerance analysis was almost categorically rejected as inadequate. The alternative is to rely entirely on tests. However, tests suffer from some of the same inadequacies (i.e., spectrum input, material variability). Of course, tests will always be necessary (even static strength is demonstrated by experiment), but tests provide information for a few cases only. A combination of analysis and tests allows evaluation of other critical locations with the possibility of updating the results. Damage-tolerance analysis does have shortcomings. It is not yet generally applicable. Research will continue to improve the procedures. However, postponing application of the present technology - until these new developments materialize - is no longer justified.

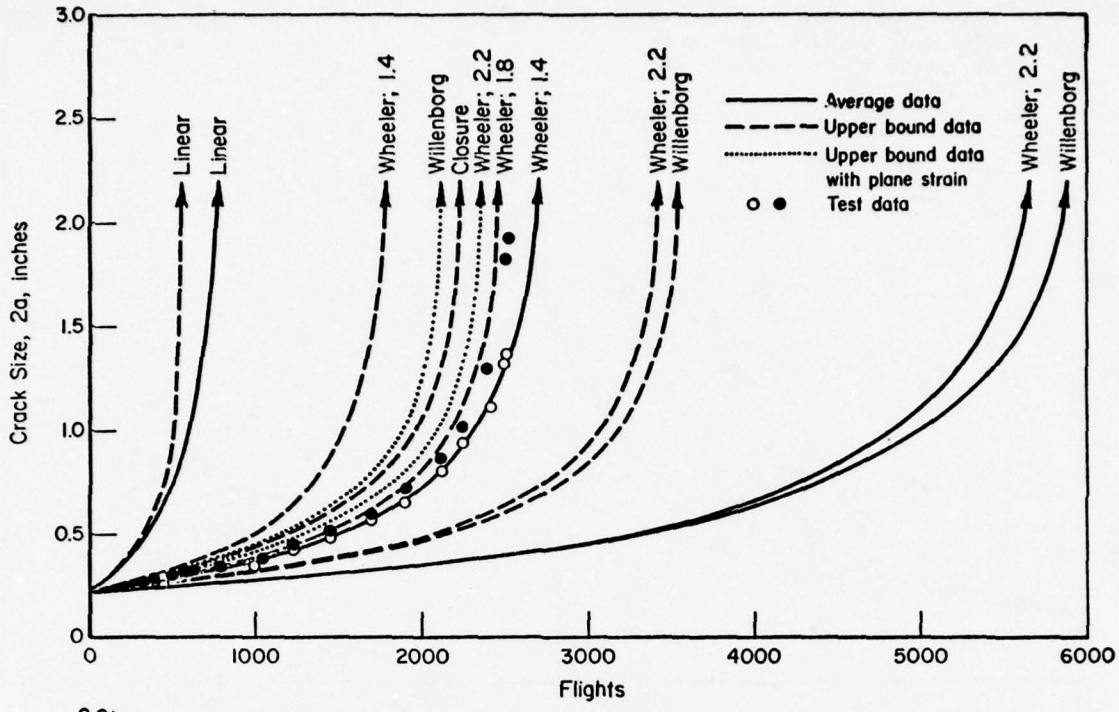

FIGURE 1. PREDICTION OF CRACK GROWTH WITH VARIOUS MODELS. 7075-T72 Aℓ

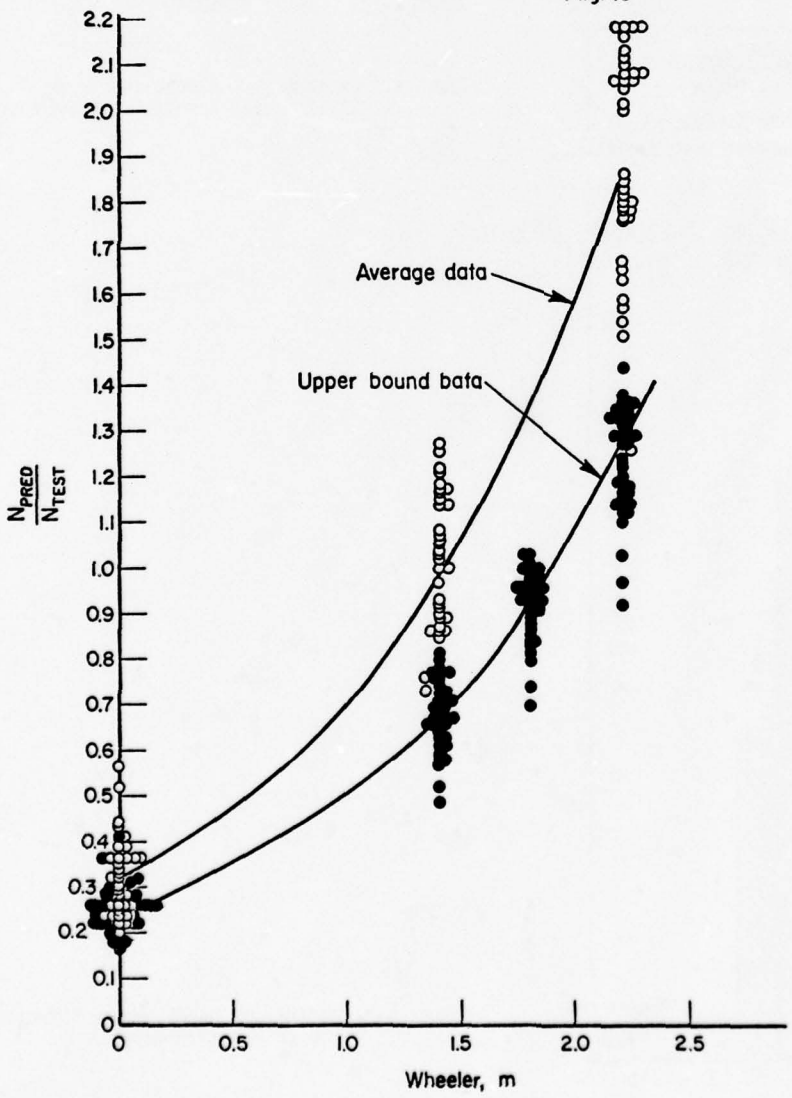

FIGURE 2. VARIATION OF PREDICTION AS A FUNCTION OF RETARDATION EXPONENT M.

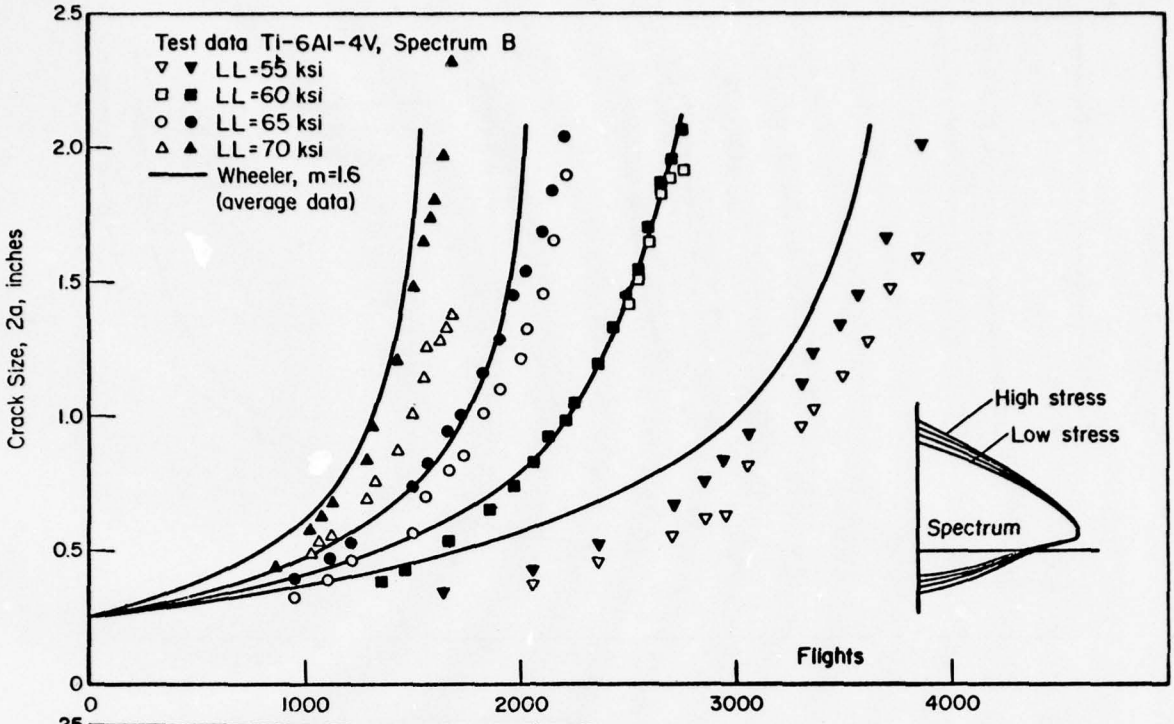

FIGURE 3. CRACK GROWTH PREDICTIONS WITH AN ADJUSTED MODEL. EFFECT OF DESIGN STRESS

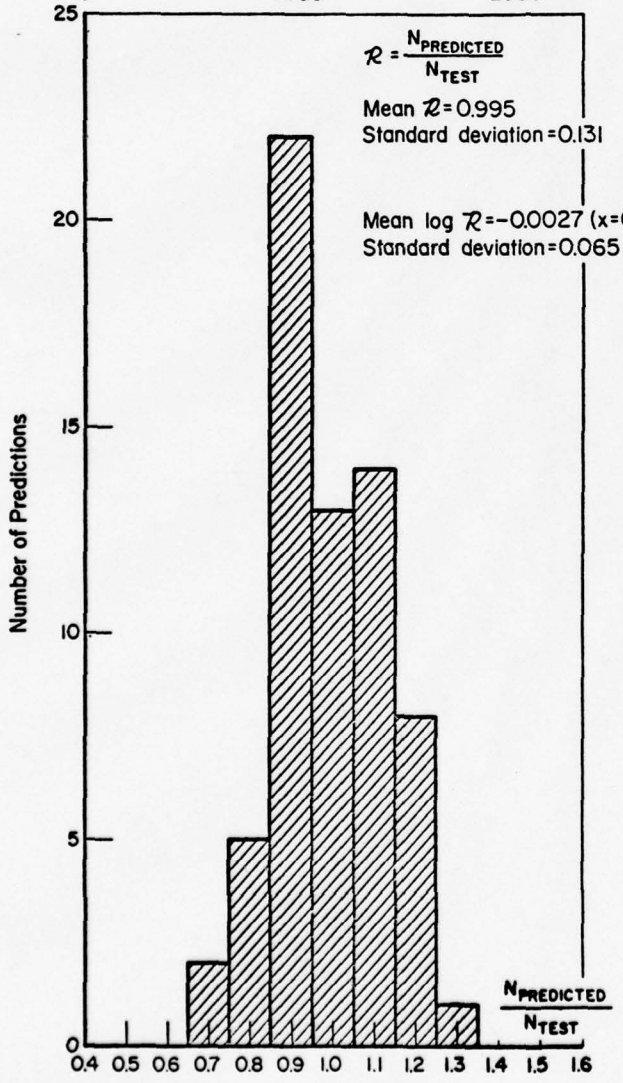

FIGURE 4. ACCURACY OF CRACK GROWTH PREDICTION WITH AN ADJUSTED MODEL.

DAMAGE TOLERANCE AND DURABILITY ASSESSMENTS OF UNITED STATES AIR FORCE AIRCRAFT

by
M. D. Coffin, C. F. Tiffany and R. Bader
Wright-Patterson Air Force Base, Ohio 45433
United States

SUMMARY

The United States Air Force is pursuing a program to conduct damage tolerance and durability assessments of "in-service" aircraft to assure structural safety and economic life management. The F-4C/D assessment serves as a classic example to illustrate the objectives, the approach, and the results desired. The assessment was conducted by a team of McDonnell Aircraft Company and Air Force personnel. The general methodology associated with the accomplishment of the technical tasks is presented and discussed. The modification and inspection program resulting from this assessment is described.

1. INTRODUCTION

Since the 1969/70 time period, there have been significant changes in the Air Force philosophy for achieving structural safety and durability in military aircraft. These changes were strongly motivated by serious structural problems which were encountered in several new system development programs as well as severe cracking problems in older "in-service" aircraft. A critical examination was made of the entire "cradle to the grave" cycle of aircraft development, procurement and life management. From this evolved a new consistent policy and appropriate requirements which are documented through military specifications to ensure enforcement (Ref 1). These new structural requirements are being used in the development of new Air Force aircraft such as the F-16.

For the older "in-service" aircraft, the approach to implementation of the intent of the new philosophy is to perform damage tolerance and durability assessments. These assessments are accomplished in the light of present day technology improvements in the areas of fracture mechanics, stress analysis, loads and dynamic analysis, fatigue analysis, non-destructive inspection, and materials engineering. Specifically, the goals of these assessments are to:

A. Determine the inspections required to protect the safety of the structure and when they should be accomplished.

B. Obtain overall visibility as to the probable future cost obligations for structural maintenance and modifications.

C. Predict the probable economic life limits of the aircraft, and

D. Determine life extension options as may be appropriate or necessary.

This body of information is vital for the conduct of life management programs and for effective force structure and budgetary planning. Such assessments have been completed on a number of aircraft with others either in progress or being initiated as described below.

Other than a structural recovery program which was performed on the F-111 in 1970 and 71, the first significant structural safety and durability assessment was initiated on the C-5A as a result of cracking problems encountered in full-scale testing plus the in-service failure of an engine pylon. This independent review effort involved a team of approximately one hundred contractor and Air Force structures engineers working for about one year at the Lockheed-Georgia plant. As a result of this study, life estimates of the structures were obtained, inspection procedures established, and nine different life extension plans were developed. These plans involved various usage changes, load reduction schemes, and structural modifications. Overall budgetary cost estimates were also developed for each plan to assist in the selection and to provide the Air Force visibility as to its probable future cost obligations. From the nine plans, one involving a load alleviation system, fuel management, and a downstream structural modification was selected.

Since this effort on the C-5A, similar but somewhat smaller efforts have been completed on the F-4C/D and F-4E(LES) aircraft and are nearing completion on the A-7D aircraft. Assessments are in progress on the C-141, F-5E and the AWACS aircraft. Also, one is being initiated on the T-38 series aircraft and planned for the A/T-37 aircraft. In addition, similar efforts, but much more limited and shorter in duration, were employed to assess the status of the B-52D and KC-135 forces and to arrive at a number of possible solution options. On the B-52D the selected option involved proof testing of each aircraft followed by a major structural modification. As in the F-111, a proof test was used as an inspection technique on the B-52D. Because of the large number of fasteners requiring inspection, proof testing on the B-52D was found to be about one-tenth as expensive as individual fastener hole eddy current inspections. A program of inspections plus a major reskinning wing modification is being implemented for the KC-135 force.

The damage tolerance and durability assessment on the F-4C/D aircraft serves as a classic example of the approach, so it has been selected to illustrate the technical methodology used in these assessments.

The overall program was divided into seven separate assessment tasks. The interrelationships of these tasks are shown in Figure 1.

In Task 1, the structurally critical areas of the aircraft were identified. In Task 2, stress spectra were developed for each critical area. In Task 3, initial "as-manufactured" quality of the F-4 was established. These three tasks developed the necessary background information and methodology required for subsequent tasks. In Task 4 a baseline or "average" F-4 aircraft was evaluated. A baseline or average aircraft was defined as an aircraft flying "standard" missions with "average" usage. Economic limits, safety limits and the inspection intervals were developed for this baseline aircraft. In Task 5, these methods were applied to determine the economic limits, safety limits and inspection intervals for each individual aircraft by tail number. These limits and intervals will be described and defined later. The sixth task included determining and evaluating the structural modifications required to extend the life of the F-4 force to 8000 hours. Finally, in the seventh task, the preliminary costs and schedules were developed along with actions necessary to implement results of the study.

2. IDENTIFICATION OF CRITICAL AREAS

The primary considerations in identifying the structural critical areas are (a) the impact of failure, (b) type of structure, and (c) degree of criticality as depicted by Figure 2. The full-scale fatigue tests and force experience, if available, along with analyses were used to determine those areas which were most critical on the F-4. As an example of the approach, an area would be most critical item if (1) failure would impair flight, (2) is slow crack growth or monolithic type structure, and (3) the critical flaw sizes are small and are not inspectable. At the other extreme, if an area was of minor economic impact to repair, was fail-safe or multiple load path type structure, had large critical flaw sizes and was inspectable, we would classify that item as a noncritical area. Most items are not clearly either most critical or noncritical and require engineering judgment for evaluation. In the study over a hundred areas were initially screened for their criticality. Fifty areas were investigated in detail. Eleven areas were classified as being noncritical, leaving thirty-nine areas identified as critical either from a safety or a durability (economic) aspect.

Figure 3 depicts the general areas of concern listed by major structural assembly; the wing, the fuselage, and the empennage. For the wing, there had been evidence of cracking at holes in the lower surface and internal structure. Also, cracks had been found in the wingfold rib area including the aft lower locking lug area. The wing is monolithic type structure and is categorized as slow crack growth design. The critical crack sizes are generally small and the structure is not inspectable without disassembly. For the fuselage, cracking had occurred at holes in the skin and internal structure, particularly in the fuel cell floor area. The engine mounts had exhibited cracks and failures. The fuselage is generally multiple load path fail-safe design structure, fail-safe design. The critical crack sizes are generally small; however, the fuselage is more inspectable than the wing. Other than early service problems with the horizontal stabilator, the empennage had been relatively trouble free.

3. STRESS SPECTRA DEVELOPMENT

Counting accelerometer and multi-channeled (VGH) data from force aircraft formed the basis for developing stress spectra required for the F-4 evaluation. These data were used to determine mission usage and severity of usage. The N_Z exceedance per thousand hours versus load factor for air-to-air, air-to-ground and nontactical missions for the F-4 are shown in Figure 4. From these data, a baseline exceedance curve was developed. VGH data, flight load survey data and strain survey data from full-scale fatigue tests were used to convert the load factor data into stress exceedance curves. From the stress exceedance data, the baseline stress exceedance curves were developed. These exceedance data were formatted into flight-by-flight stress spectra hours involving 730 unique flights per 1000 hours. These baseline flight-by-flight spectra were developed for 19 locations on the aircraft, then interpolated for the other 20 locations, in order to give stress spectra for the 39 critical areas.

In addition, spectra representing past usage were developed for (a) an air combat maneuvering (ACM) training spectrum, (b) a non-ACM training spectrum, (c) a Southeast Asia spectrum, (d) a reconnaissance (RF) Southeast Asia spectrum, and (e) an RF training spectrum. In addition, the sensitivity of the baseline spectra to usage variations was evaluated. Examples of variations included a substitution of air-to-air for air-to-ground, a look at the air base having most severe usage, and an evaluation of hard landing effects.

Table 1 shows the relative flaw growth life of the past usage spectra in relation to the baseline spectrum. The relative flaw growth life shown in the ratio of the flaw growth life for the past usage spectrum divided by the flaw growth life for the baseline spectrum. In particular, these lives are the crack growth life from an initial crack of .01 inches to .03 inches. The ACM base life is slightly less than the baseline life. The Southeast Asia life is also less than the baseline life even though the Southeast Asia load factor frequency curve was less severe than the baseline (See Figure 5). This is because the average weights of the aircraft during the Southeast Asia missions were

much higher and thus were more damaging. Both RF-4C spectra have longer life than the baseline spectra life.

4. INITIAL QUALITY ASSESSMENT

The next task was a determination of the initial "as-produced" quality of the F-4 aircraft. A Navy full-scale fatigue test article formed the basis for the initial quality assessment. This structure was manufactured in the middle 1960's and was felt to be representative of the quality of the C&D model production aircraft. In teardown inspections, the location of cracks was determined and the final flaw sizes in the aircraft were measured. These fracture surfaces were examined by optical and electron fractography and, knowing the test load spectrum, were "traced back" to assist in determining the flaw sizes at the beginning of the test. These cracks were tracked back as far as possible and then extrapolated by analysis to time zero to determine the equivalent initial flaw size for each location. An equivalent initial flaw size distribution was then determined. These data were then analyzed statistically to assist in determining the initial flaw sizes for use in the economic and safety limit analyses. (See Figure 6)

Figure 7 shows an example of a measured fracture surface and the analytical extrapolation to determine the equivalent initial flaw size at time zero. The Navy full-scale fatigue test completed 11,800 hours of testing. For this example, the flaw size at the conclusion of testing was about .06 inches. The flaw growth curve for this crack was tracked by optical fractography to about 4000 hours of testing and a flaw size of about .01 inches. This flaw growth curve was matched by analysis and then analytically extrapolated back to time zero leading to a determination of an equivalent initial flaw of about .0022 inches. All of the equivalent initial flaws used in the analysis were obtained by this procedure.

A total of 104 cracks in the full-scale fatigue test article were analyzed in this manner. These data were then used to establish the cumulative probability versus the equivalent initial flaw size as shown in Figure 8. Of the various statistical distributions evaluated, the Johnson S_U distribution appeared to give the best fit. The 95% confidence line is also shown. This plot indicates that an equivalent initial flaw of .01 inches or larger could be expected to be found in one out of every 1000 fastener holes. An initial equivalent flaw of .02 or larger could be expected to be found in one out of every 435,000 fastener holes and an initial flaw of .03 or larger could be expected to be found in one out of every 40,000,000 fastener holes.

In selecting the initial flaw size used in the safety limit analysis, the initial flaw size must be selected sufficiently large such that it is unlikely that critical holes in operational aircraft contain initial flaws greater than that selected, but must not be selected so large as to result in premature aircraft modification times, thus limiting total aircraft life.

For the durability assessment, the initial flaw size used in economic limit analyses must be representative of a marginal, but not worse, quality hole in critical areas of the airframe and be sufficiently large such that most holes can be repaired by a single oversizing at the predicted economic limit.

The sizes selected have a dominant bearing on when inspections and modifications must be made. Figure 9 depicts these considerations.

Figure 10 illustrates the selection of initial flaw sizes for operational limit predictions. For example, if .005 inches were selected as the equivalent initial flaw for the economic limit prediction, we would expect one out of every ten fastener holes to have cracks larger than the economic repair size at the predicted repair time. This would result in an unacceptably large number of fasteners requiring nonstandard repair. If a .01 size equivalent initial flaw was selected, it would be expected to be exceeded once in every 1000 fastener holes. If the aircraft has about 5000 critical holes on it, we would then expect five fastener holes per aircraft to have cracks larger than the standard economical repair size at the predicted modification time. This appears to be a much more acceptable situation and thus .01 was selected as the equivalent initial flaw size for the economic limit prediction analyses.

If .02 inches for the equivalent initial flaw size were selected for the safety considerations, we would then expect that one out of 80 aircraft would have a flaw equal to or greater than the .02 value at the time of manufacture. This, we feel, is unacceptable from a safety standpoint. Therefore, the .03 inch equivalent initial flaw size was selected for the safety limit predictions. We would expect that one out of every 40,000,000 fastener holes or approximately one in 8000 aircraft would have a flaw of this size or greater. In relating to the force of about 1800 F-4 aircraft, it is unlikely that any individual F-4 aircraft would contain a flaw equal to or greater than .03 at the time of manufacture.

5. BASELINE AIRCRAFT ASSESSMENT

The baseline aircraft was defined as a typical F-4C/D with no major structural modifications. The baseline spectrum was as previously defined. In order to properly categorize actions, it was necessary to establish several key definitions. The safety limit was defined as the time beyond which the risk of failure is considered to be unacceptable if no preventative actions are taken. Two safety limits are defined,

Class I and Class II. An area is classified as a Class I safety limit if a single failure can result in the loss of an aircraft. For example, if a crack propagates from a fastener hole in the lower wing skin, it is most likely that the airplane will be lost. The action required for an aircraft exceeding a Class I safety limit is to stop flying and inspect, repair and/or modify the aircraft as soon as possible. Depending upon the individual location and situation, flight under severe restrictions may be permitted in lieu of grounding the aircraft.

An area or location is defined as a Class II safety limit if more than a single event is required to cause loss of the aircraft, however, it must be recognized that it is possible that these events could occur within a short usage period. An example of a Class II safety limit would be the fracture or failure of a fuel cell floor. For example, the floor must fracture, then the bladder must be ruptured to spill fuel and then the fuel must ignite in order for the potential loss of the aircraft to occur. The action required is to perform inspections as frequently as necessary to protect flight safety and to implement repairs or modifications as soon as possible.

The economic limit is defined as the most opportune time for repair or modification of the structure.

The inspection interval is defined as the period of usage equal to one-half of that required to attain the safety limit.

Figure 11 depicts considerations other than the equivalent initial flaw necessary for the calculation of the safety limit, the economic limit and the inspection interval. Severe conditions were chosen for the calculation of the safety limit and the inspection interval. .03 inches was assumed for the initial flaw, and the flaw shape was assumed to be a through crack at a fastener hole. The environment selected was water and air or water and fuel dependent upon the location on the airframe. Flight-by-flight flaw growth analysis, including spectrum retardation effects, was used.

For the economic limit calculations, average or normally expected conditions were selected. An .01 initial flaw size and a corner or "thumbnail" shape crack typical of what is normally to be expected were chosen. The environment chosen was air or fuel dependent upon the location. Similarly, flight-by-flight flaw growth analysis, including spectrum retardation effects, was used.

Figure 12 outlines the overall analysis verification procedures. As seen in the figure, the flaw growth analysis procedure was verified by predicting the results of element tests that were conducted under a flight-by-flight loading sequence. Crack growth retardation effects were included in the flaw growth analysis procedure. The analysis procedure was also used to predict the crack growth from the pylon hole on the F-4E (LES) full-scale fatigue test. Correlation with the crack growth curve obtained after the pylon hole area was cut out of the aircraft and the flaw growth curve traced was excellent. This same crack growth analysis procedure was then used to calculate the safety limits, the economic limits and the inspection intervals for the F-4C/D aircraft.

6. OPERATIONAL LIMITS

Tables 2, 3 and 4 list the resulting operational limits for the baseline aircraft. The economic limit, inspection interval and safety limit are given in terms of baseline flight hours. These baseline or average hours are not necessarily representative of any specific aircraft in the force but represent the hours associated with average or nominal mission mix and severity of usage. Table 2 lists the locations in slow crack growth structure and Tables 3 and 4 list the location in fail-safe structures. The individual aircraft assessment is discussed in the next section.

Shown in Table 2 are the locations which are classified as a Class I safety limit. The items are listed in increasing order of flight hours for the lower wing skin. The wing-fold rib is a separate item, but also defined as a Class I safety item. The box beside each item indicates when the area should be modified. If an area requires fastener removal for inspection, then the inspection time becomes the modification time. This is because the expense required to remove a fastener for inspection is a major portion of the total expense required for modification.

Tables 3 and 4 list the Class II safety limits. Some areas identified have a very low number of flight hours for both the inspection interval and the safety limit. Those areas which have been subjected to force wide inspections, modifications or repairs are identified by asterisks. The fuselage station 303 bulkhead is an example of an area of high economic impact. If that area is not repaired prior to cracking beyond the standard oversized fastener, it would require major structural rework or replacement. The cost to replace the bulkhead would be many times that required to just repair the fastener holes in the bulkhead.

As a result of this study, several actions were initiated immediately such as inspection programs and interim repairs to address the indicated problem areas of most immediate concern.

7. INDIVIDUAL AIRCRAFT ASSESSMENT

The next task involved the assessment of the individual aircraft and development of a method to adjust the economic and safety limits and inspection intervals based on actual aircraft usage. The approach used is outlined in Figure 13.

The counting accelerometer data forms the basis for determining the condition of the individual fleet aircraft. A damage index, which is a measure of flaw growth, is established for each critical area. Also, for each critical area an allowable damage index is established. The inspection or modification should then be accomplished when the actual aircraft damage index for a particular control area is equal to or less than the allowable damage index. It is not suggested that the modifications need be accomplished at the specific time indicated as this could result in excessive operational down time. However, the procedures developed will allow logical groupings of modifications or inspections.

8. DETERMINATION OF DAMAGE INDICES

The program to track the individual aircraft is outlined in Figure 14. Data available on an aircraft tail number basis includes the location where the aircraft flew, the load factor exceedance counts from the counting accelerometer and the flight hours. At a particular location, an N_Z stress relationship can be determined dependent upon the usage spectra flown. From this relationship the number of stress level counts per month, for example, can be determined. From analysis and experimental results, flaw growth curves at this same location can be determined from flight-by-flight spectra. Illustrated are the economic limit flaw growth curves for two past usage spectra and the baseline spectrum. From these data stress versus number of cycle curves for the .01 to .03 inch flaw growth curves can be developed as shown. From these curves the allowable counts at each stress level for the corresponding past usage spectra can be determined. From the number of stress counts per month and the allowable counts at each stress level, the amount of damage per month can be calculated. This can be summed over the usage of the aircraft to determine the total damage on an individual aircraft basis.

Because of the different calculated limits at each of the critical areas, it is necessary to do these calculations for each critical area. There are 39 critical locations, three limits required, and approximately 1800 aircraft in the fleet, which could, thus, result in an excessive computational workload.

Thus, the question arose, "Can the damage index computed at one location on the aircraft be used to predict flaw growth characteristics at other locations?" The study team determined that for the safety and economic limit calculations there was a small band of scatter for all critical locations when the results were normalized as shown in Figure 15. Likewise, for the range of spectra examined, the scatter was small. From this result, it was concluded that the flaw growth could be scaled from location to location and also among spectra.

This study finding was, of course, very significant in the reduction and interpretation of fleet tracking data. Since the flaw growth data can be scaled from location to location and from spectra to spectra, only one damage index need be calculated per aircraft. The point selected called the control point was the lower wing skin at butt line 44 (B.L. 44). The allowable damage index was chosen equal to unity to correspond to 3900 baseline flight hours, which is the economic limit at that location. The allowable damage indices for all other critical locations in the structure are then the ratios of the baseline operating limits (hours) or inspection intervals (hours) to 3900 hours. The fraction of life (or inspection interval) used at any location at any point in time is the ratio of the aircraft damage index to the allowable index for the specification location. For example:

$$\frac{\text{Aircraft index} = .3}{\text{Allowable index} = .6} \times 100 = 50\% \text{ of life or interval has been used.}$$

Table 5 lists the allowable damage indices for the Class I safety limits.

9. DEVELOPMENT OF THE TRACKING PROGRAM

The damage index for each individual aircraft was determined using available counting accelerometer data and the procedures discussed. The aircraft that exceeded the damage index allowables for critical areas were identified by tail number. In general, problem areas predicted by the tracking program correlated with service experience.

At the time of the study, the survey established, for example, that several aircraft had exceeded the Class I safety limit for a specific location on the wing (the pylon hole). An inspection program for this area was immediately initiated for the specifically identified aircraft. The results of these inspections tended to verify predictions and corrective repairs were made.

Those aircraft exceeding the Class II safety limits were also identified by tail number. Those aircraft exceeding the economic limits and/or the inspection intervals were programmed for inspection, repair and/or modification at the earliest opportunity.

An overall program of inspection, modification, and repair for the entire fleet was developed by projecting damage indices based on anticipated usage.

10. MODIFICATION OPTIONS

The baseline and individual aircraft assessments identified when and where the modifications were needed. In this section the selection of the preferred modifications and the rationale leading to their selection are discussed. Some possible major alternatives to the preferred modifications are briefly discussed and then the operational limits of the modified aircraft are determined.

Figure 16 indicates that modifications can be classed in three general categories: (a) the fastener system, (b) local reinforcement, and (c) part replacement.

Three options were considered for the fastener system. The first, an oversize ream with a straight shank clearance fit fastener which is typical of the original manufacture on the F-4. The second option considered an oversize ream with a tapered interference fit fastener. The third option considered an oversize ream with a cold work life improvement process in the hole and a straight shank fastener.

For the part replacement class, the options considered were identical design and a redesigned part within the geometric constraints of the subject part.

The cold work process was selected for fastener holes and is described briefly: The inspection of the hole is accomplished and then an oversize ream is used to clean up the hole. This process is repeated until there is no indication of any cracks in the hole. Then, an oversized mandrel is pulled through a thin wall split bushing in the fastener hole. This process introduces beneficial compressive residual stresses. After the hole expansion, a light ream is accomplished to clean up the hole. The principal application of the cold work process is on the wing. The reasons for selection of the cold work process are: (1) It is highly effective in retarding crack growth if any cracks should remain in the fastener holes, (2) it permits the use of straight shank fasteners, (3) it is tolerant to minor process errors and (4) it is considered to be cost effective.

Figure 17 depicts experimental results to illustrate the benefits of the cold work process in the fastener holes. Crack depth is plotted against test hours. The fastener hole is cold worked at the time of modification representing the retrofit on fleet aircraft. It is the intent to remove all cracks at the time of this retrofit. In the element tests some cracks were intentionally left in holes to determine their crack growth behavior after cold working. It can be seen that with even a crack of approximately .04 inches growth did not occur during additional cycling. In some cases, element tests were run to well over 100,000 hours of baseline usage with little or no crack growth. Thus, it was felt that the cold work process does, in fact, fix the fastener holes.

During manufacture the aluminum parts on the F-4 are anodized for protection. While this coating is very thin, it is also brittle. This brittle coating cracks under stressing and thus cracking starts at locations on corners or edges of the plates as illustrated in the example. This cracking starts at time zero and continues, although it is not the predominant mode of cracking until after the fastener holes are fixed. Applying the criteria for the safety limit calculation at the time of modification of the fastener holes, and then plotting the corner crack growth curve to failure, we obtained a life that is sufficient to achieve over 8000 hours of baseline usage for the F-4. Inspections will be required for the corner or edge cracking as indicated.

The stringer #1 area at fuselage station 359 is chosen as an example of the location requiring local reinforcement. There are two baseline configurations as illustrated. On the later F-4C and F-4D models, a short angle reinforcement was installed. In test, cracks had been found emanating from the fastener holes and the plate nut rivet holes as shown in Figure 18.

Figure 19 illustrates the rationale generally applied in arriving at the selection of the local reinforcements for the F-4. Option 1 was to cold work the bolt holes only, however, cracks do occur in the rivet holes and this approach was rejected. Option 2 is to cold work the bolt and the rivet holes, however, it was found that the minimum rework required removed too much material and this approach was rejected also. Option 3 would be to redesign the stringer, eliminate the rivet holes, and cold work the bolt holes. However, the stringer extends the full length of the fuselage and this would be an extensive and expensive replacement. This option was also rejected. Option 4 was selected, which reduced the stress levels through local reinforcement as shown in Figure 19.

The wingfold rib is selected to typify the part replacement category. See Figure 20. Full-scale test and service experienced had indicated cracking at bolt and plate nut inlet holes. While the bolt holes are inspectable with the rib on the aircraft, the inspection of the plate nut rivet holes requires disassembly.

The options considered for the wingfold rib were similar to those described for stringer #1. See Figure 21. The option selected was to redesign the wingfold rib, eliminate the plate nut rivet holes by attaching the plate nuts in an alternate manner and cold working the bolt holes.

Table 6 lists the preferred modifications for the critical areas. Most of the items on the lower wing skin are fastener hole critical areas and the preferred modification is identified as the cold work process. The pylon holes and the drain holes are recommended to be fixed by cutting out a local area and installing a steel press fit bushing. The B.L. 100 area had previously been modified with Taper Lok fasteners. This area has sufficient life provided that it is inspected for edge or corner cracking. The 29% stiffener area is a stiffener on the lower wing skin and this stiffener attaches to a span-wise shear web. This area was thought to be inspectable only with a major tear down of the wing and thus would be very expensive. However, feasibility inspections indicated that this internal area can be inspected through the lower surface of the lower wing skin to determine if cracks exist. Other modifications are as shown in Table 6 and consist of part replacement, fastener changes, fastener hole cold working and local reinforcement.

Two major alternatives were considered as possible candidates rather than the many local modifications required. The first was a complete new inner wing torque box. However, it was determined that the cost of the new inner wing greatly exceeds the cost of all the preferred modifications, therefore, that alternative was rejected. The other major alternative considered was the installation of a steel strap along the main spar. However, this modification, while it does fix the main spar area, does not fix seven other items on the wing or provide a life greater than the preferred modifications. Thus, an additional cost would be incurred without fixing all the areas, therefore, this approach was rejected. For the fuselage the only practical approach available because of its construction was to incorporate the preferred modifications.

11. OPERATIONAL LIMITS OF THE MODIFIED AIRCRAFT

With the incorporation of the identified preferred modifications at the proper time, the economic and safety limits of the F-4C/D and RF-4C force should equal or exceed the desired 8000 hours of equivalent baseline usage in all critical areas. If we consider the RF aircraft only, then all RF's are expected to achieve 8000 hours of operational usage. For the C's and D's, it is anticipated that 80% of the C's and D's would achieve 8000 hours of operational usage. The remaining 20% of the C's and D's, which are currently being subjected to severe usage, will require special considerations -- either early retirement or rotation to a base of less severe usage.

In addition, post-modification inspections will be required in certain critical areas. Most of the areas requiring inspection are in the wing and are for edge or corner cracking along the trailing edge.

The modifications identified have been determined based on analysis and element testing. Final verification of the modifications identified is being accomplished on a full-scale fatigue test.

Budgetary cost and modification schedule estimates were developed and actions required of all Government agencies involved in the F-4 program were identified. The program is now being implemented.

12. CONCLUSIONS

As direct results of the damage tolerance and durability assessment, actions were taken to protect the safety of the F-4 force and to develop a modification and life extension program to minimize excessive downstream repair costs.

The program of inspections and modifications for the entire F-4C/D force will provide the desired goal of 8000 hours of baseline usage. Additionally, it established quantitatively that severe usage can significantly reduce the lifetime of an aircraft, a fact not fully appreciated by all Air Force planners.

The assessment provided the best approach and much of the detailed methodology currently being used in the performance of damage tolerance and durability assessments of other Air Force operational aircraft.

13. REFERENCES

Coffin, M. D., Tiffany, C. F., "New Air Force Requirements for Structural Safety, Durability, and Life Management," Journal of Aircraft, Vol 13, No. 2, Feb 1976, pp 93-98.

TABLE 1

Relative usage severity

SPECTRUM	RELATIVE FLAW GROWTH LIFE
BASELINE	1.0
ACM BASE	.85
NON-ACM BASE	1.10
S.E.A.	.94
RF-4C S.E.A.	1.33
RF-4C TRAINING	1.8

TABLE 2

Operational limits – slow crack growth structure

ITEM	ECONOMIC LIMIT	INSPECTION INTERVAL	CLASS I SAFETY LIMIT
LOWER WING SKIN @ PYLON HOLE	N/A	2850	5700
@ BL 44	3900	4500	9000
@ MLG TRUNNION	5500	4550	9100
@ BL 70	5500	4850	9700
@ BL 132.50	4900	5600	11200
@ FWD MLG RIB	7000	5500	11000
@ CENTERLINE	5650	20200	40400
@ BL 100	SEE MODIFIED AIRCRAFT ASSESSMENT		
@ FWD SBA RIB	*7000*	*7100*	*14200*
@ TORQUE RIB	7450	7550	15100
@ 29% STIFFENER	N/A	7700	15400
@ FRONT SPAR	9400	12850	25700
@ DRAIN HOLE	N/A	10300	20600
@ WINGFOLD	11000	14200	28400
WINGFOLD RIB	6900	4000	8000

TABLE 3

Operational limits – slow crack growth structure

ITEM	ECONOMIC LIMIT	INSPECTION INTERVAL	CLASS II SAFETY LIMIT
OUTER WING, AFT LOCKLUG	N/A	600	1200
STABILATOR	N/A	750	1500
FUEL CELL NO. 6 FLOOR	N/A	900	1800
FUEL CELL NO. 5 FLOOR	N/A	1000	2000
FUEL CELL NO. 4 FLOOR	N/A	1650	3300
FUEL CELL NO. 4 COVER	N/A	2250	4500
FUEL CELL NO. 4 SIDEWALL	N/A	2500	5000
F.S. 303 BULKHEAD	2600	2850	5700
SKIN AT FS 493 SPLICE	13000	4200	8400
OUTER WING, LOWER SKIN	4800	6600	13200
FUEL CELL NO. 3 FLOOR	N/A	13500	27000
FIN FINGER PLATES	>100,000	44500	89000

TABLE 4

Operational limits - fail safe structure

ITEM	ECONOMIC LIMIT	INSPECTION INTERVAL	CLASS II SAFETY LIMIT
UPPER TANGENTIAL LINK	N/A	$a_{cr} < .03$	$a_{cr} < .03$
TURTLEBACK DOOR @ FS 335	950	2450	4900
FWD. UPPER ENGINE MT. (TENSION)	N/A	1175	2350
TURTLEBACK DOOR @ FS 359	2000	6300	12600
FORWARD ENGINE MT BACK UP	N/A	2150	4300
TURTLEBACK DOOR @ FS 303	2800	7750	15500
STRINGER NO 1 @ FS 359 (EARLY F-4C)	5200	3500	6600
STRINGER NO 1 @ FS 359 (F-4C, F-4D)	6200	4100	8200
MAIN SPAR @ BL 132.50	4500	4200	8400
FUSELAGE SKIN @ FS 303	6900	4400	8800
STRINGER NO 1 @ FS 303	8400	6500	13000
CENTERLINE RIB	7300	12800	25600
TURTLEBACK DOOR @ FS 351	10200	13000	26000

TABLE 5

Allowable damage indices

ITEM	ECONOMIC LIMIT	INSPECTION INTERVAL	CLASS I SAFETY LIMIT
LOWER WING SKIN @ PYLON HOLE	N/A	0.73	1.46
@ BL44	1.00	1.15	2.30
@ MLG TRUNNION	1.41	1.17	2.34
@ BL 70	1.41	1.25	2.50
@ BL 132.50	1.26	1.44	2.88
@ FWD MLG RIB	1.80	1.41	2.82
@ CENTERLINE	1.45	5.17	10.34
@ BL 100	SEE MODIFIED AIRCRAFT ASSESSMENT		
@ FWD SBA RIB	1.80	1.82	3.64
@ TORQUE RIB	1.91	1.94	3.88
@ 29% STIFFENER	N/A	1.98	3.96
@ FRONT SPAR	2.41	3.29	6.58
@ DRAIN HOLE	N/A	2.64	5.28
@ WINGFOLD	2.82	3.64	7.28
WINGFOLD RIB	1.77	1.03	2.06

TABLE 6

Selection of preferred modifications

ITEM	PREFERRED MODIFICATION
LOWER WING SKIN	
@PYLON HOLE	INSTALL PRESS FIT BUSHING
@BL44	COLD WORK
@MLG TRUNNION	COLD WORK
@BL70	COLD WORK
@BL132.50	COLD WORK
@FWD MLG RIB	COLD WORK
@CENTERLINE	COLD WORK
@FWD SBA RIB	COLD WORK
@TORQUE RIB	COLD WORK
@29% STIFFENER	INSPECT
@FRONT SPAR	-
@DRAIN HOLE	INSTALL PRESS FIT BUSHING
@WING FOLD	COLD WORK
WING FOLD RIB	REPLACE, COLD WORK
UPPER TANGENTIAL LINK	REPLACE, NEW MATERIAL
TURTLE BACK DOOR @ FS335	TAPER LOKS
FWD UPPER ENGINE MT (TENSION)	NEW COMPRESSION MOUNT
TURTLE BACK DOOR @ FS359	REWORK HOLES
FORWARD ENGINE MT BACK-UP	REINFORCE STRUCTURE
TURTLE BACK DOOR @ FS303	REWORK HOLES
STRINGER NO 1 @ FS359 (EARLY F4C)	ADD STRAPS
STRINGER NO 1 @ FS359 (F4C, F4D)	ADD STRAPS
MAIN SPAR @ BL 132.50	COLD WORK
FUSELAGE SKIN @ FS303	REWORK
STRINGER NO 1 @ FS303	ADD STRAPS
CENTERLINE RIB	INSPECT
TURTLE BACK DOOR @ FS351	ADD DOUBLERS
OUTER WING, AFT LOCKLUG	REPLACE WITH STEEL LUG
STABILATOR	INSTALL STRAP
FUEL CELL NO 6 FLOOR	CORRUGATED
FUEL CELL NO 5 FLOOR	ALUMINUM
FUEL CELL NO 4 FLOOR	REINFORCEMENT
FUEL CELL NO 4 COVER	
FUEL CELL NO 4 SIDEWALL	
FS 303 BULKHEAD	GAPPED BOLTS, TL'S
SKIN @ FS 493 SPLICE	INSTALL FITTING, COLD WORK
OUTER WING, LOWER SKIN	COLD WORK
FUEL CELL NO 3 FLOOR	-
FIN FINGER PLATES	-

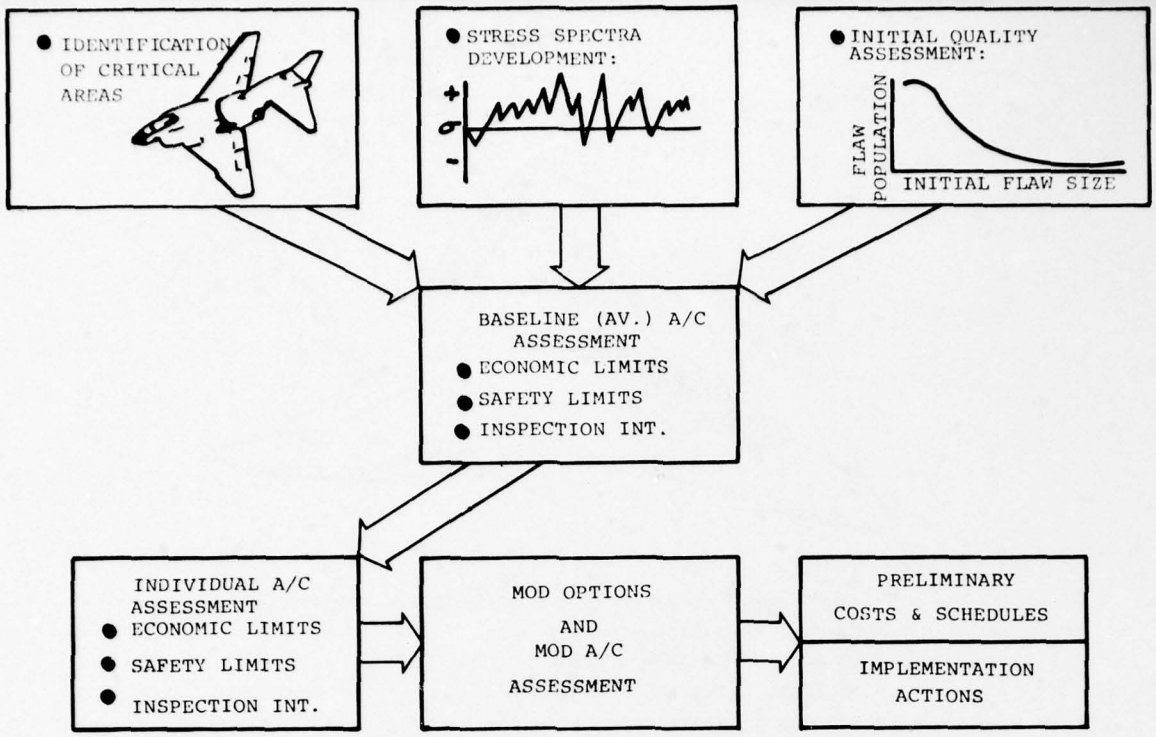

Fig.1 Assessment tasks

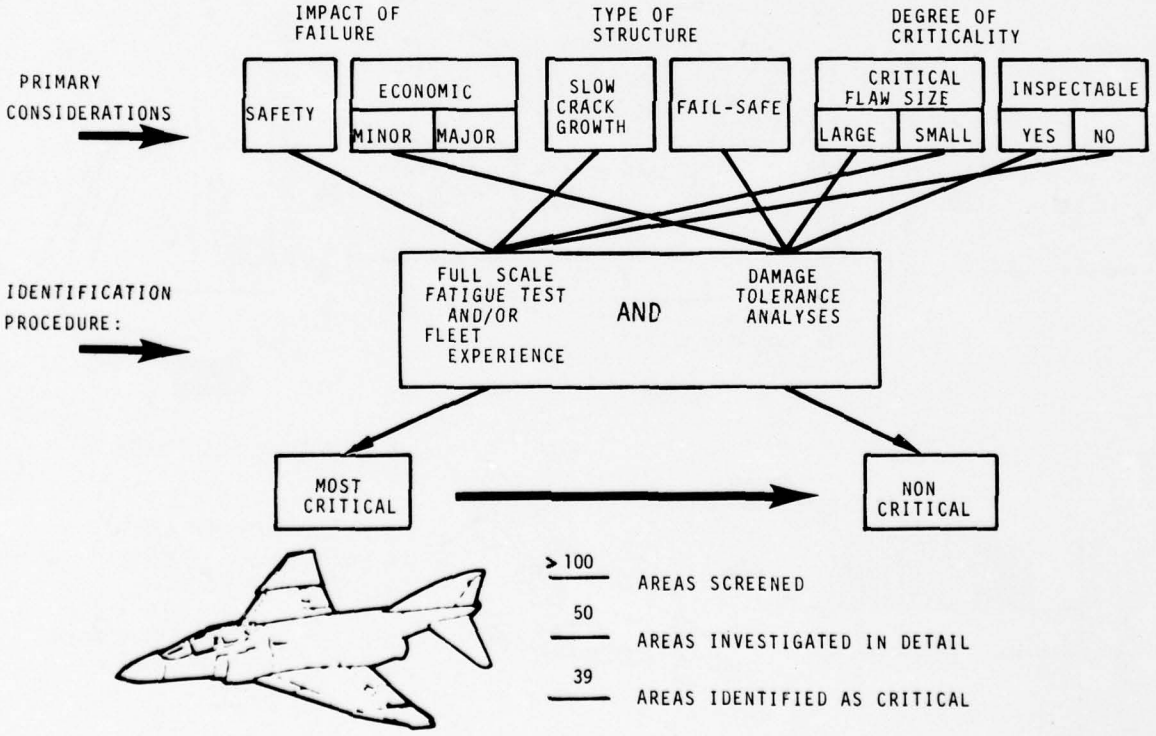

Fig.2 Identification of critical areas

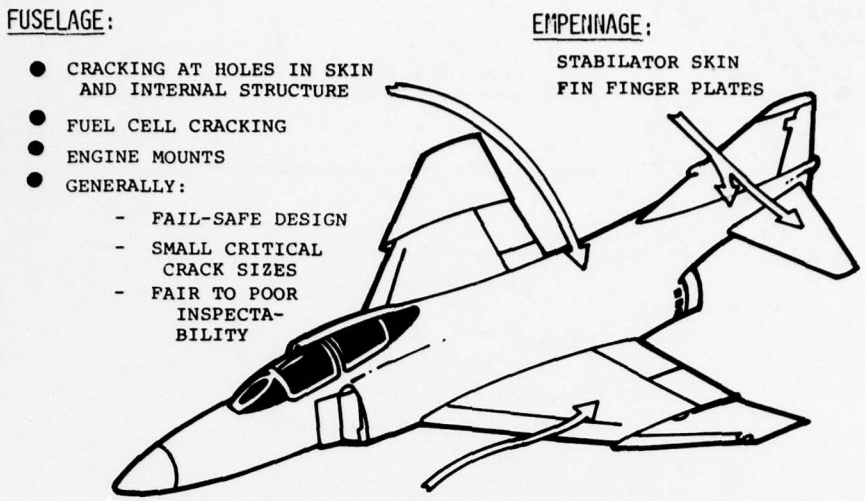

Fig.3 General areas of concern

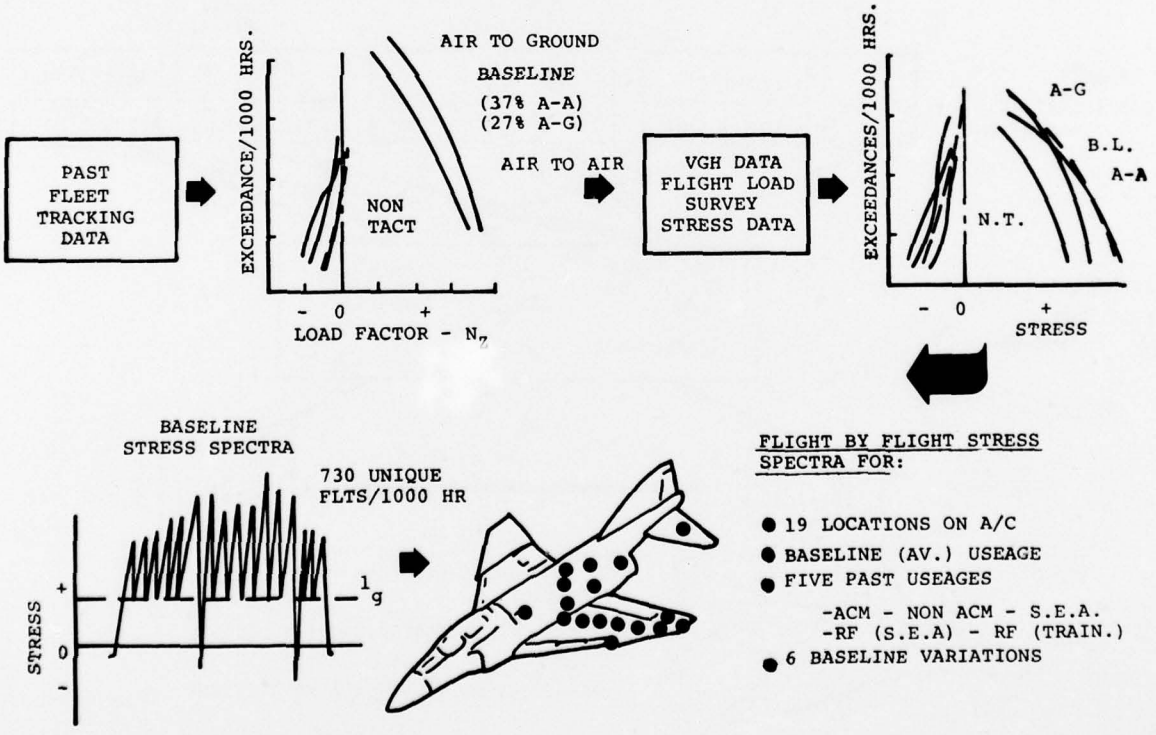

Fig.4 Stress Spectra Development

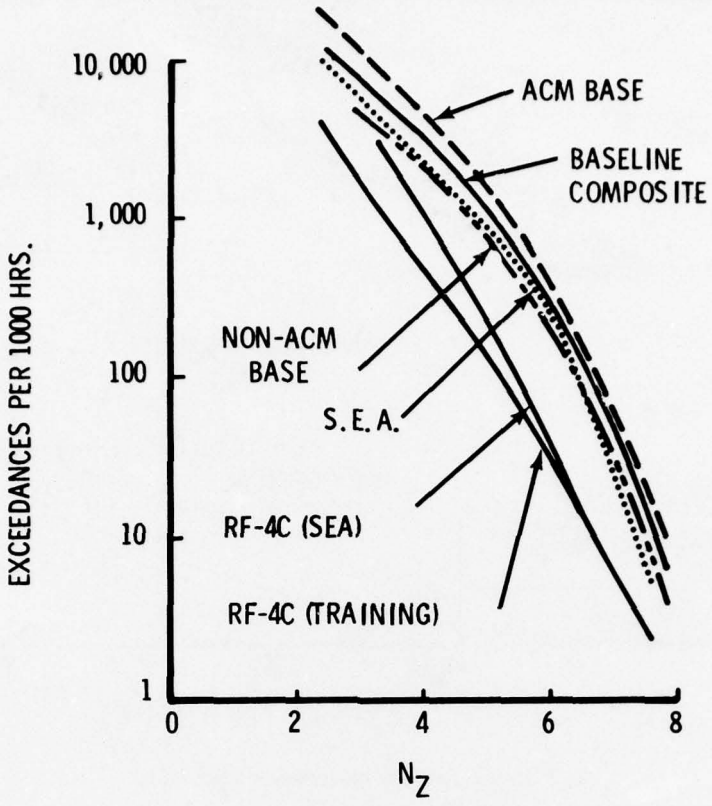

Fig.5 Load factor frequency data (past usage)

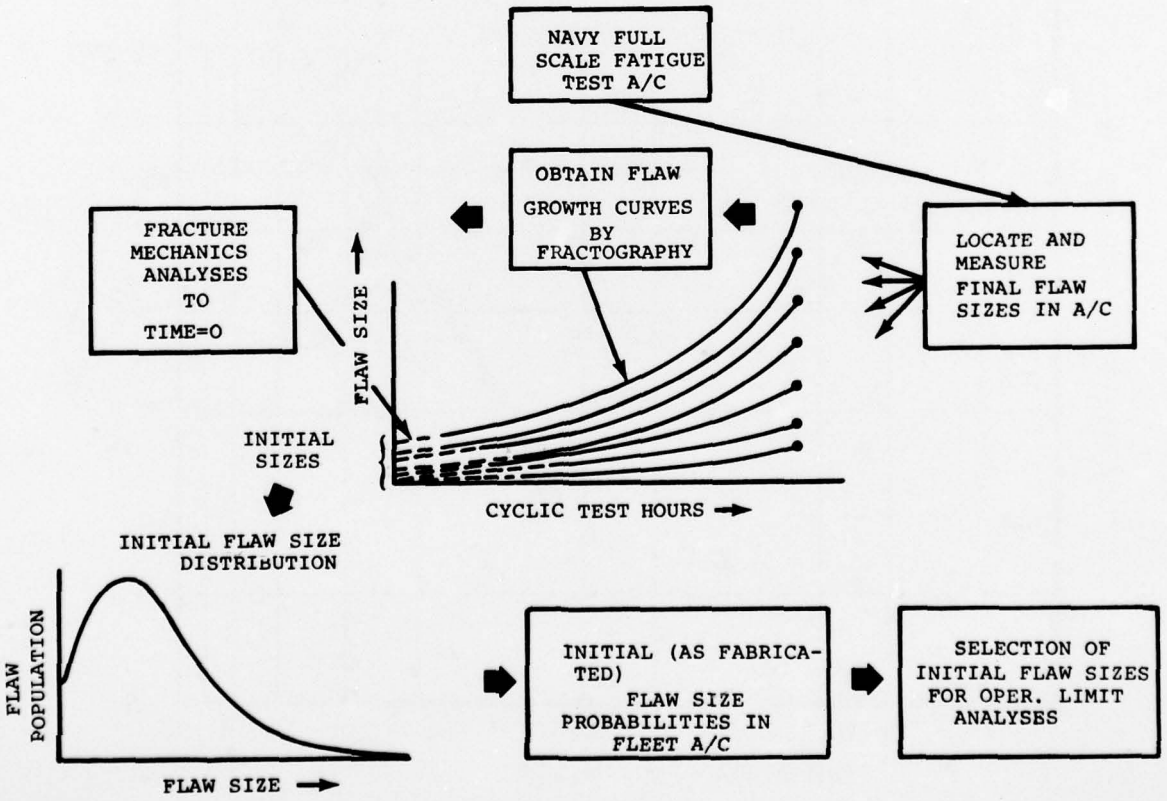

Fig.6 Initial quality assessment

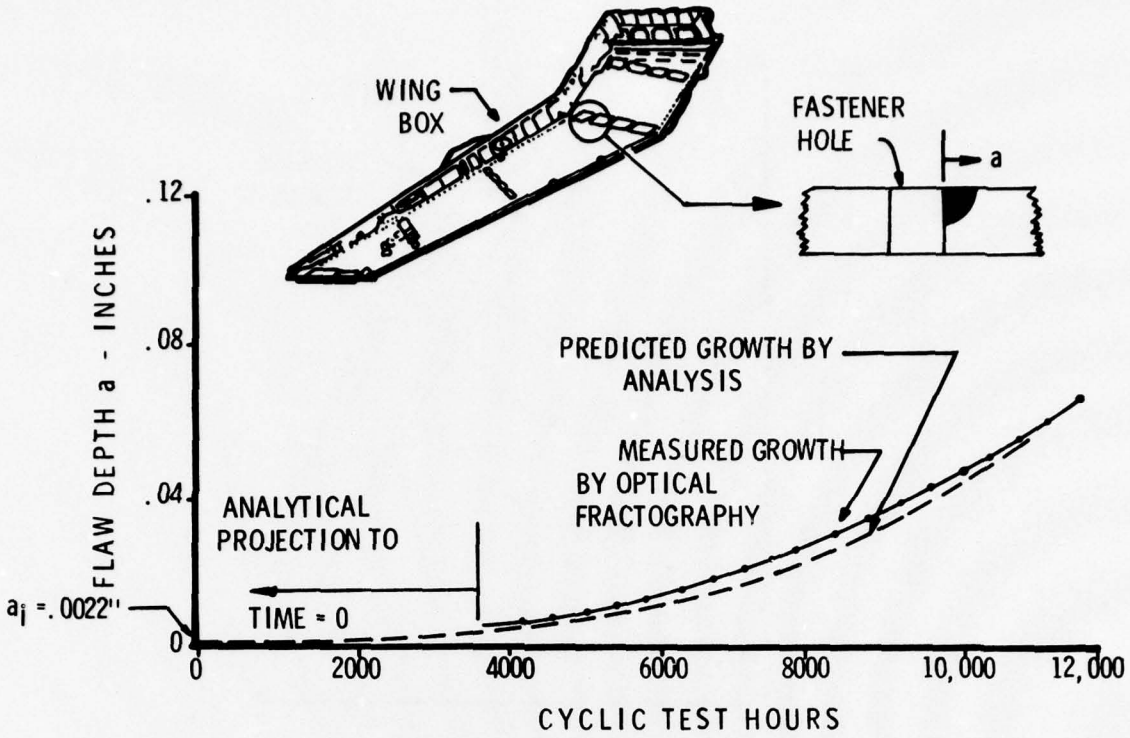

Fig.7 Initial flaw size determination (example)

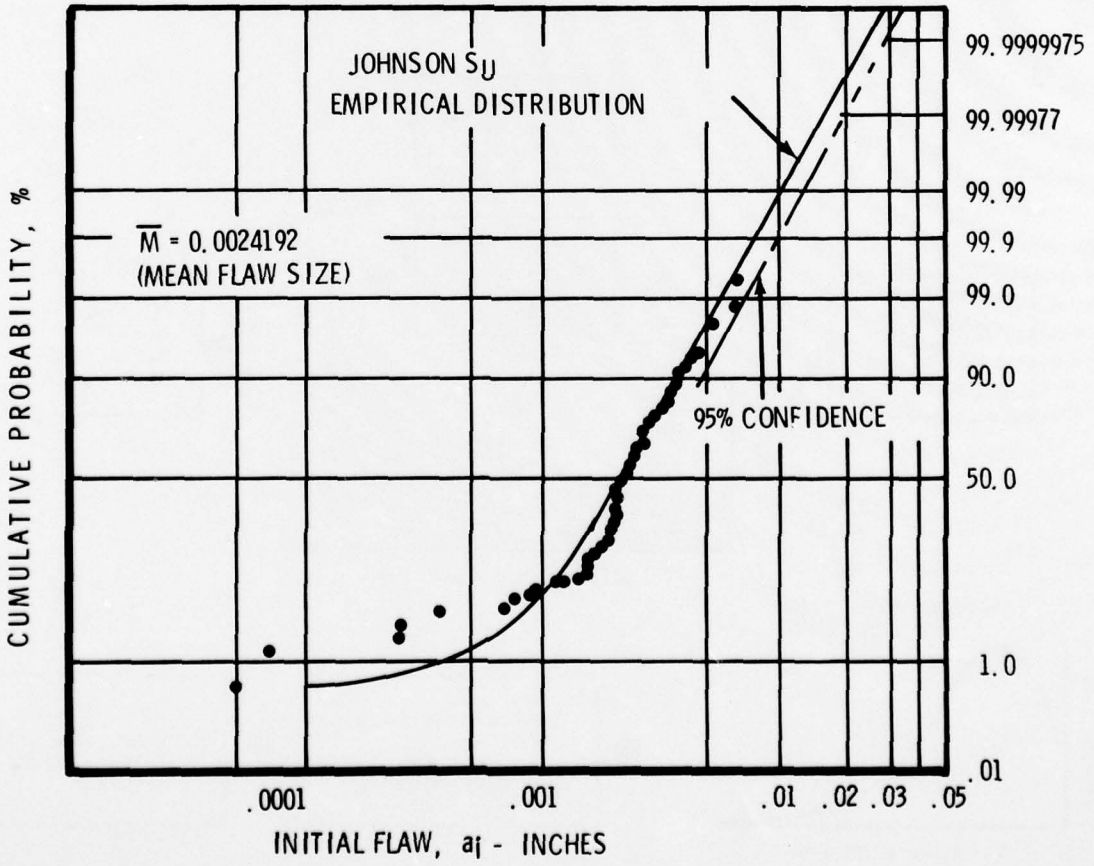

Fig.8 Initial flaw size probabilities

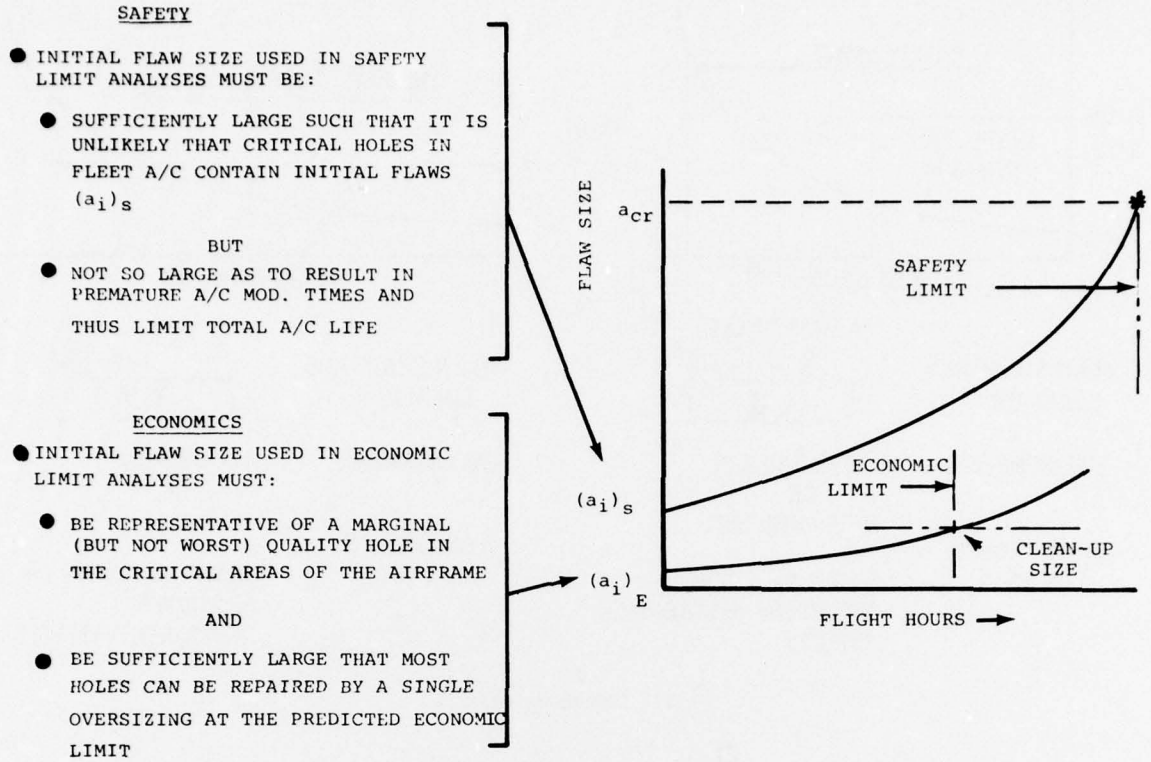

Fig.9 Philosophical considerations in selection of initial flaw sizes

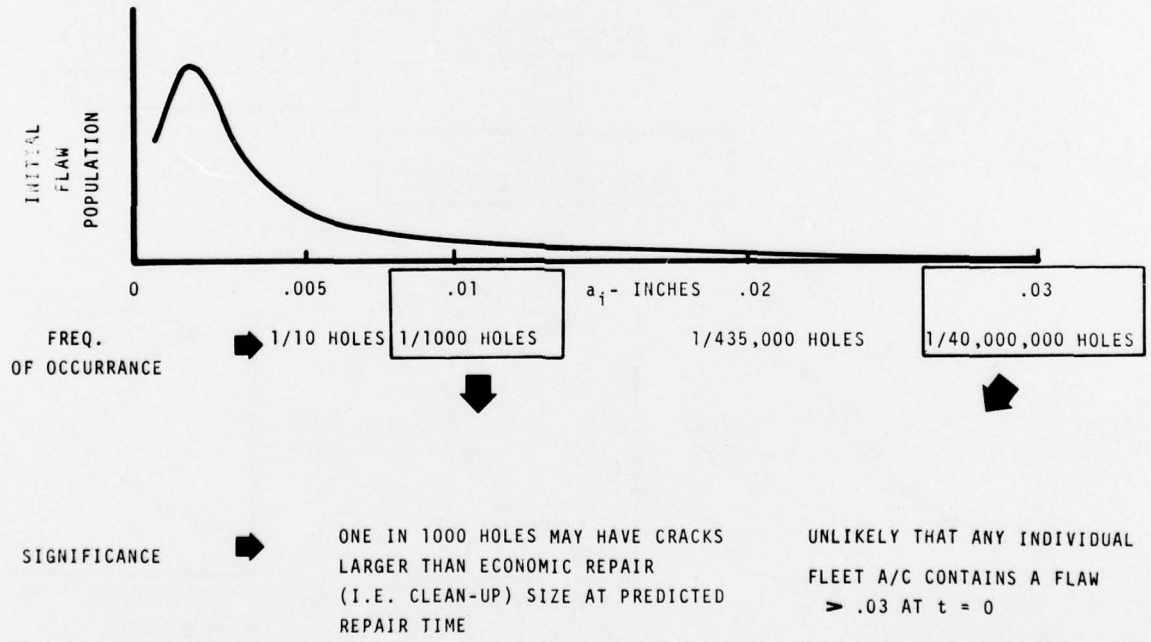

Fig.10 Selection of initial flaw sizes for operational limit predictions

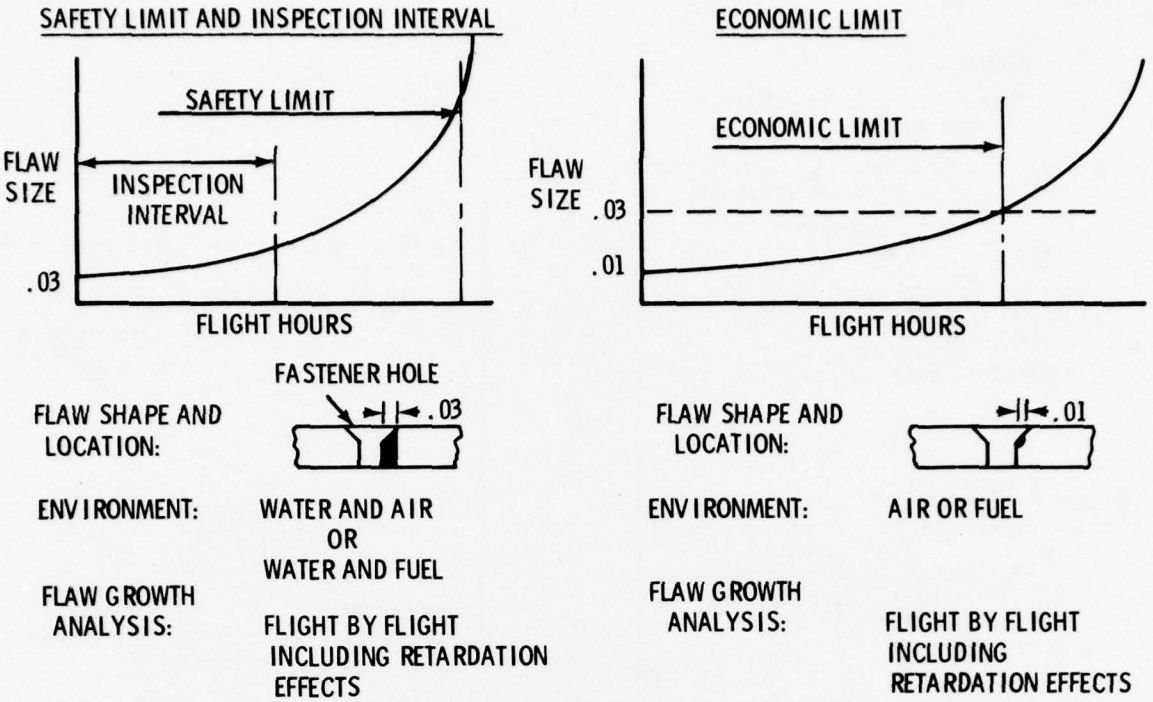

Fig.11 Calculation of limits

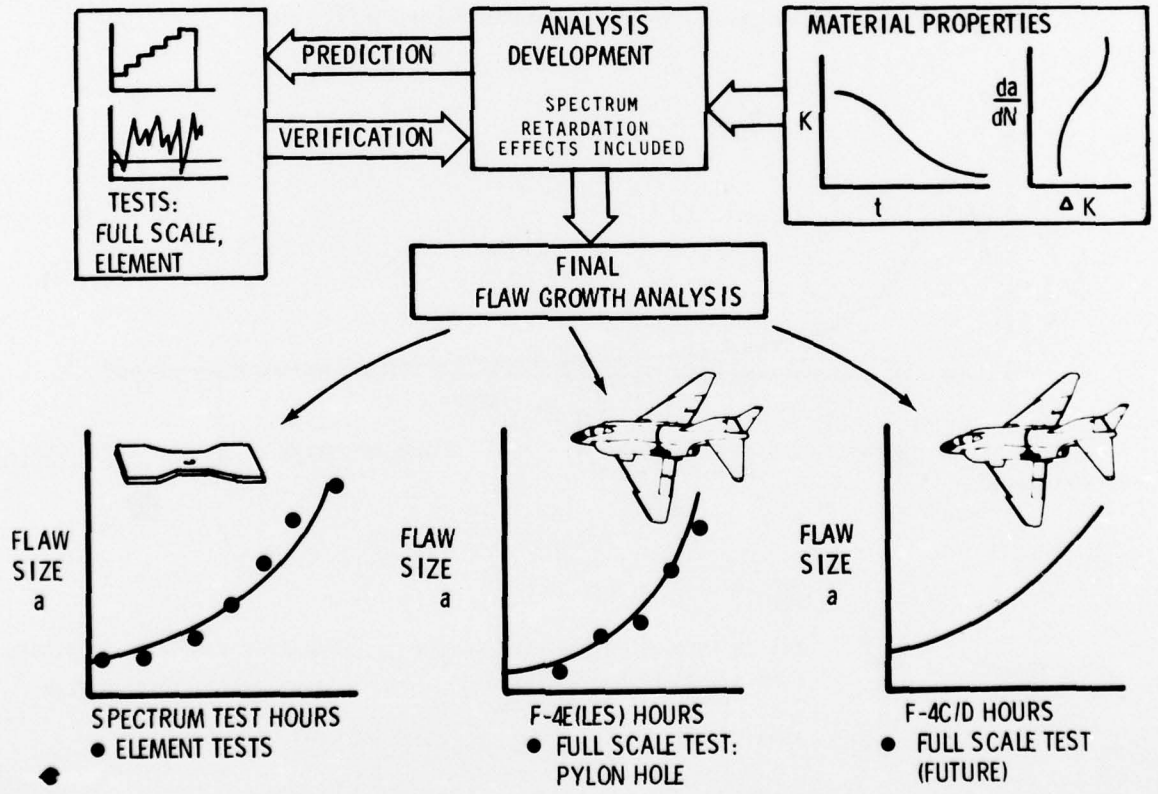

Fig.12 Verification of analysis procedures

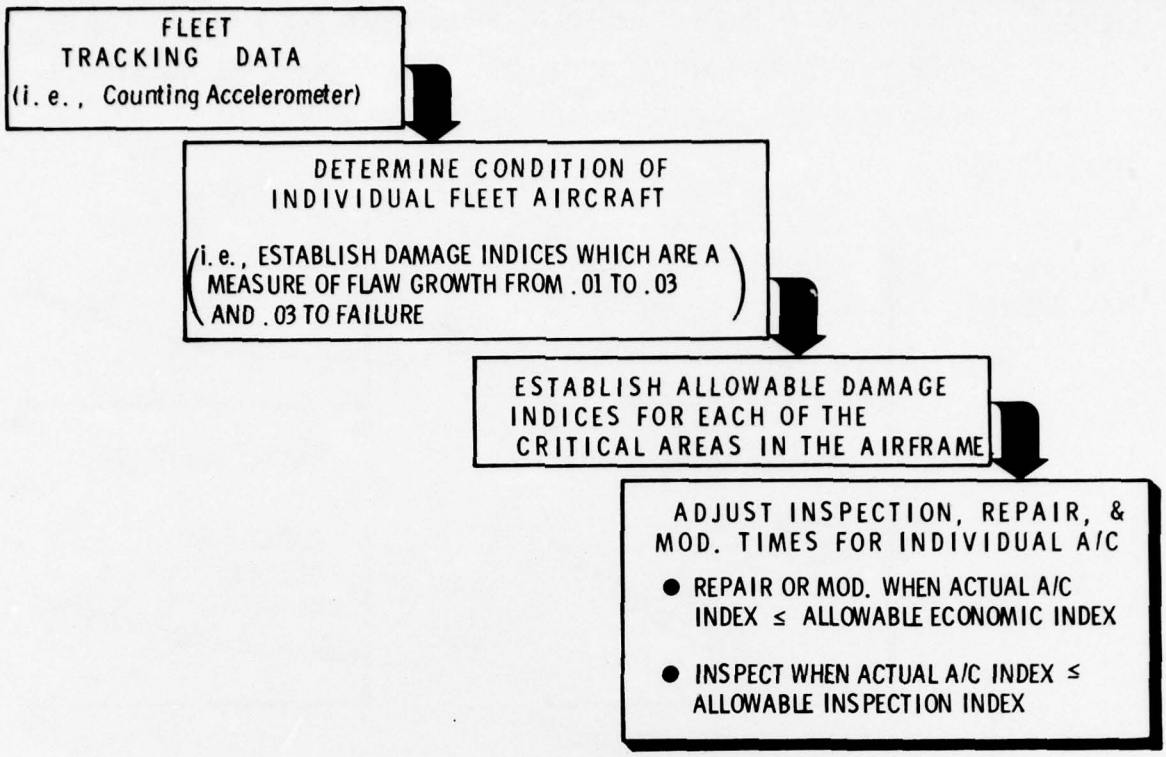

Fig.13 Individual aircraft assessment

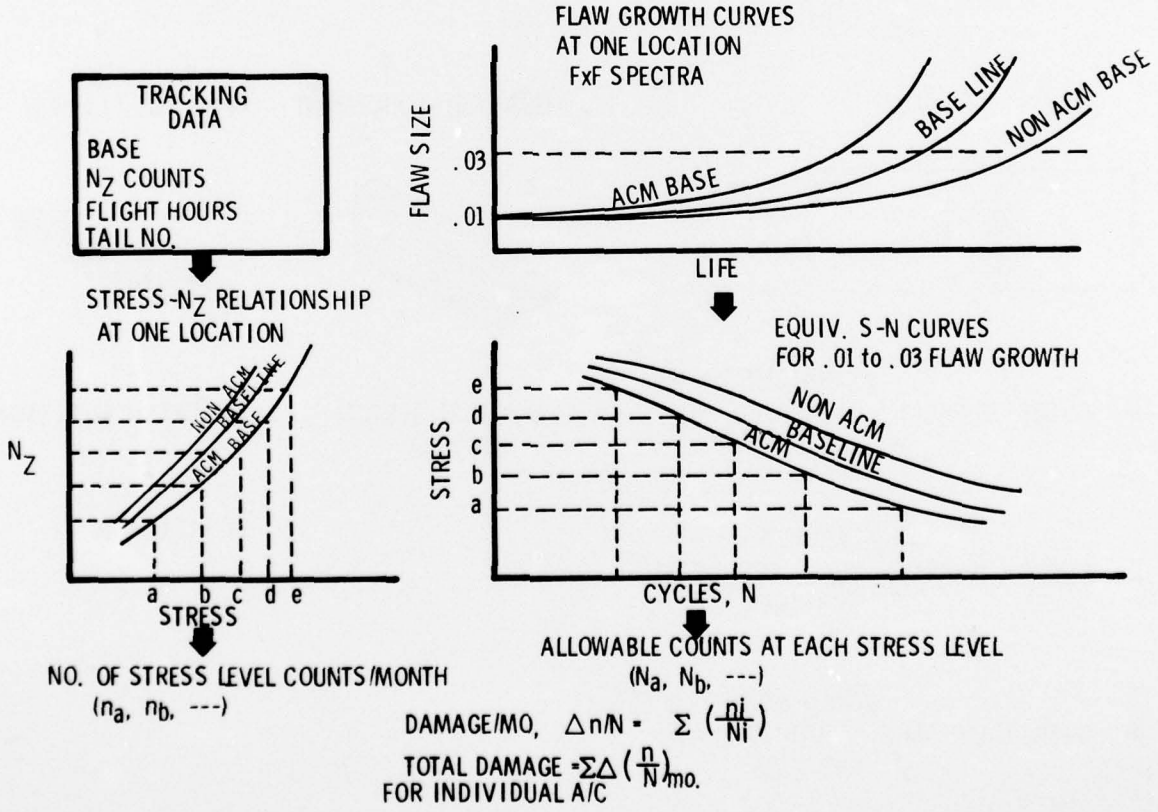

Fig.14 Determination of damage indices in individual aircraft

PROBLEM: CAN THE DAMAGE INDEX COMPUTED AT ONE LOCATION ON THE AIRCRAFT BE USED TO PREDICT FLAW GROWTH AT OTHER LOCATIONS, OR DO WE NEED TO COMPUTE DAMAGE INDICES FOR EVERY CRITICAL LOCATION?

STUDY FINDING:

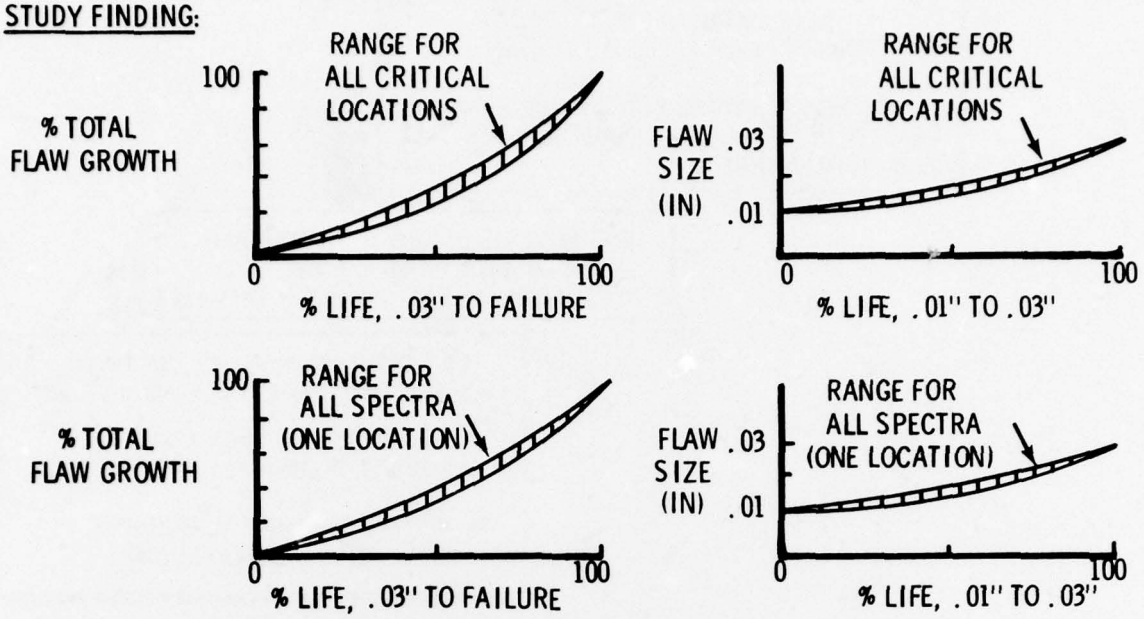

CONCLUSION: FLAW GROWTH CAN BE SCALED FROM LOCATION TO LOCATION, (AND ALSO AMONG SPECTRA)

Fig.15 Determination of damage indices

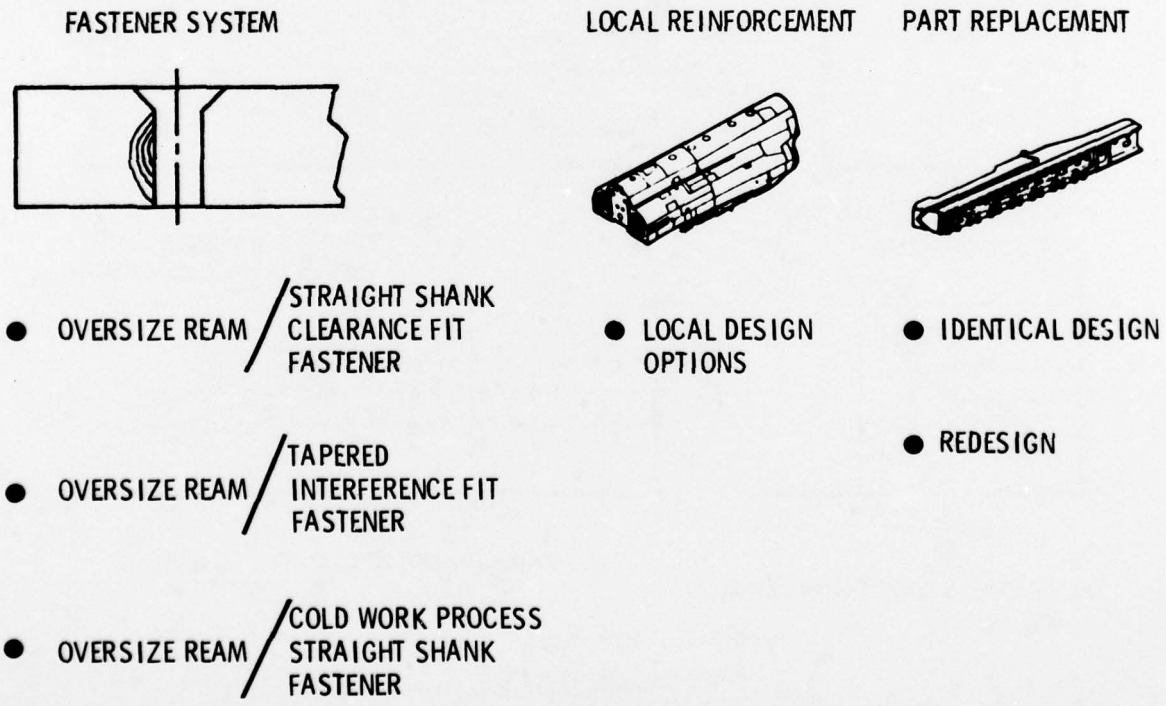

Fig.16 Examples of local modifications options

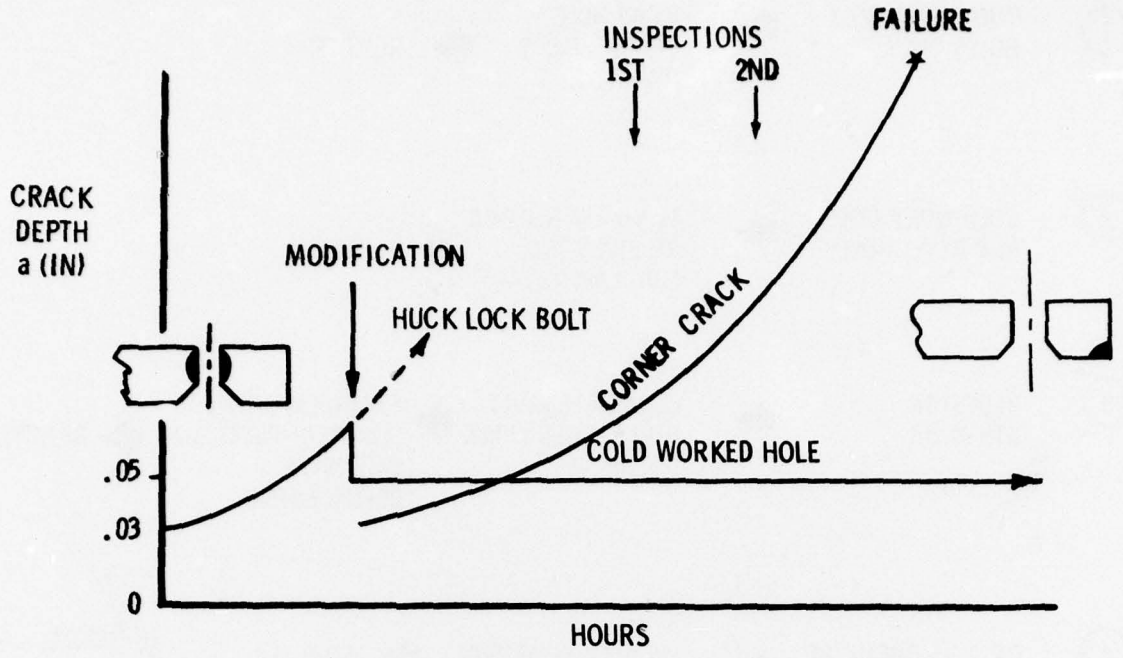

Fig.17 Operational limits after retrofit cold work

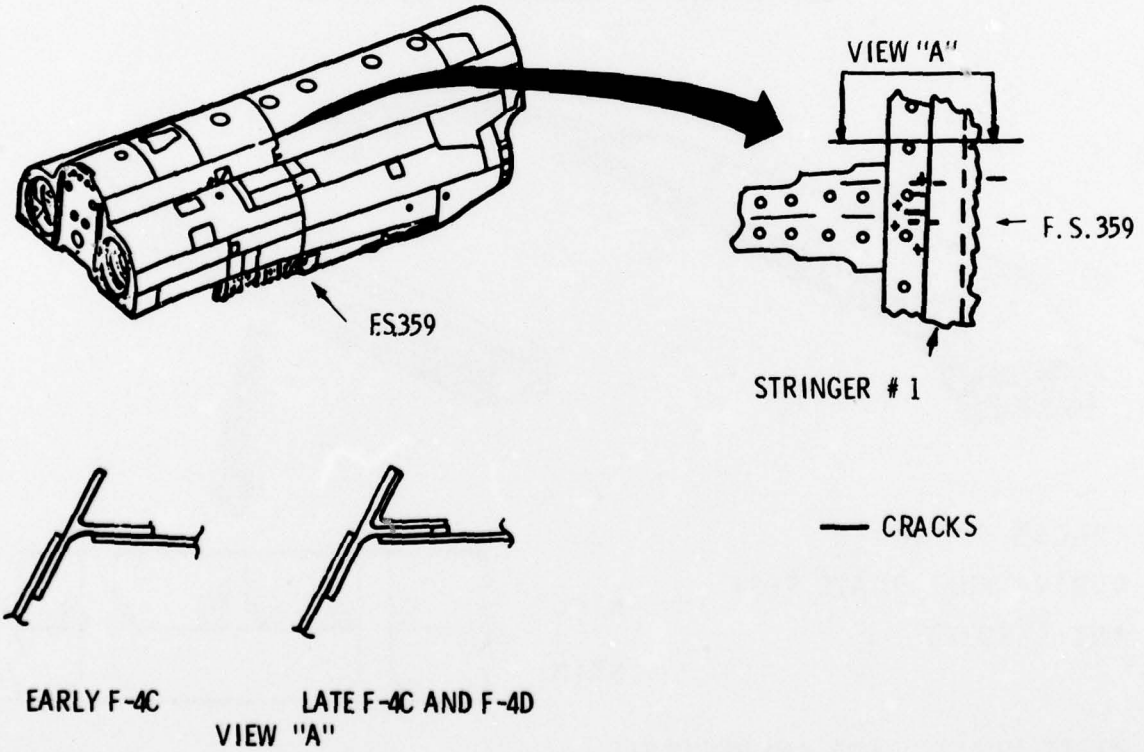

Fig.18 Local reinforcement – stringer No.1

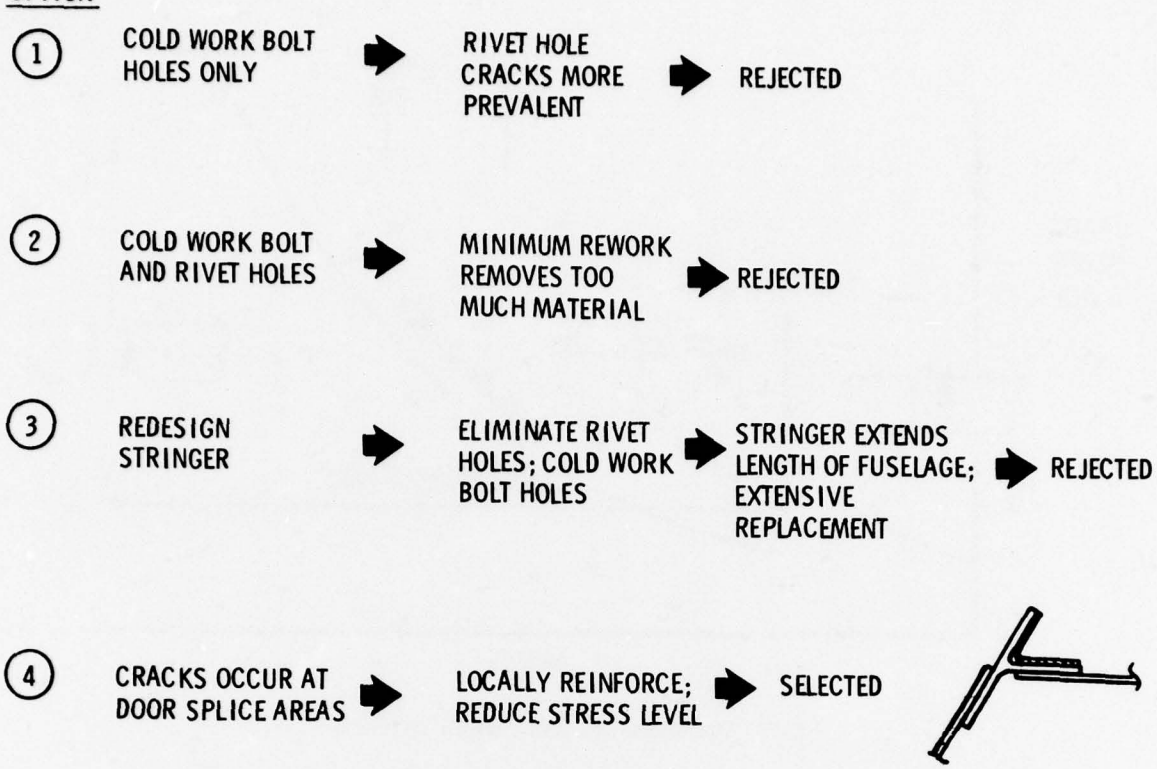

Fig.19 Rationale for local reinforcement of stringer No.1

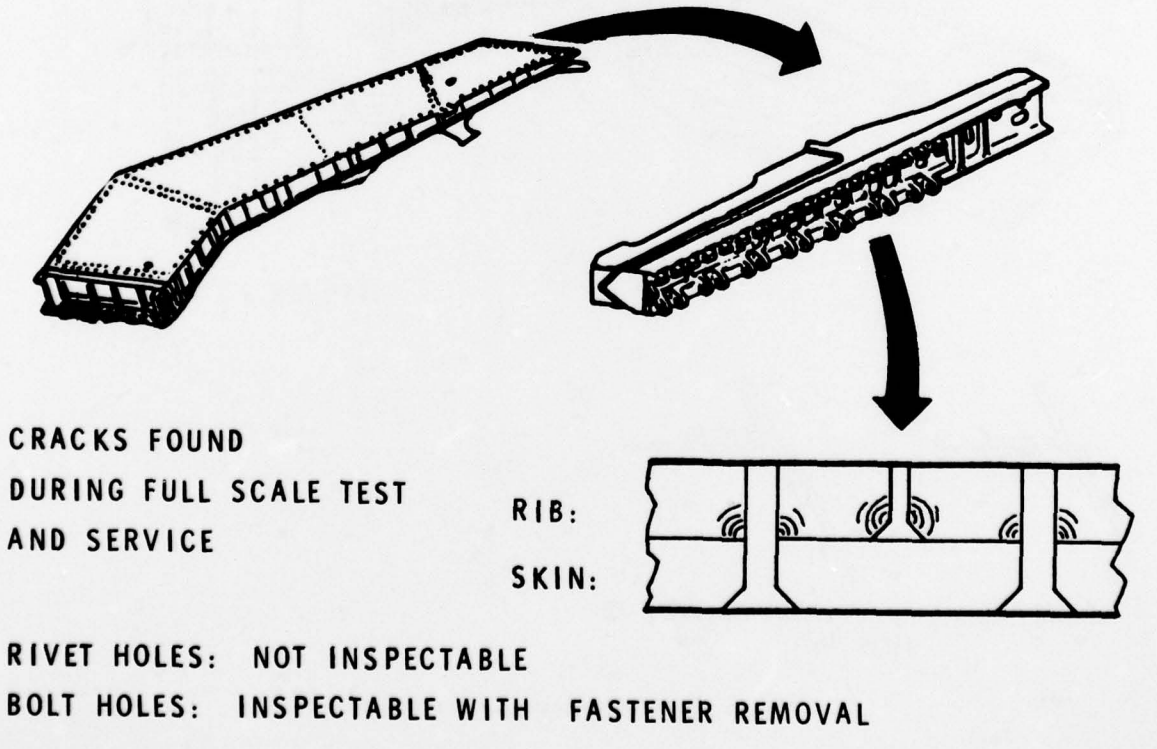

Fig.20 Part replacement – wing fold rib

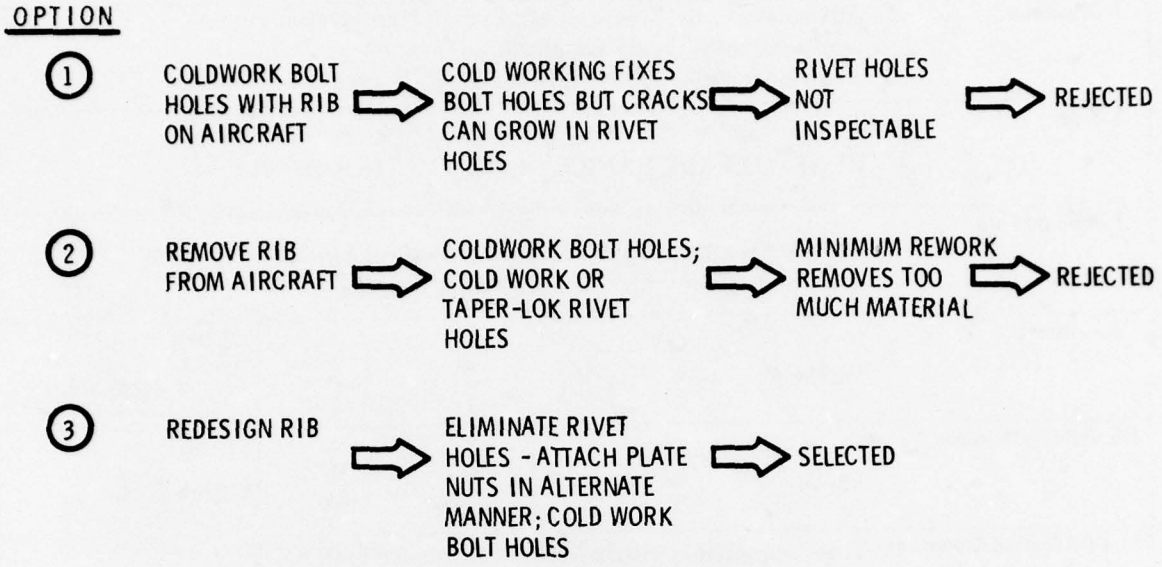

Fig.21 Rationale for replacement of wing fold rib

(9) Conference proceedings.

REPORT DOCUMENTATION PAGE

1. Recipient's Reference	2. Originator's Reference	3. Further Reference	4. Security Classification of Document
	(14) AGARD-CP-221	ISBN 92-835-1090-X	UNCLASSIFIED

5. Originator Advisory Group for Aerospace Research and Development
North Atlantic Treaty Organization
7 rue Ancelle, 92200 Neuilly sur Seine, France

6. Title (6) FRACTURE MECHANICS DESIGN METHODOLOGY.

7. Presented at The 43rd Meeting of the AGARD Structures and Materials Panel held in London, UK on 28–29 September 1976.

8. Author(s)	9. Date
Various	(11) Feb[redacted]77
10. Author's Address	**11. Pages**
Various	(12) 278 273 p.

12. Distribution Statement This document is distributed in accordance with AGARD policies and regulations, which are outlined on the Outside Back Covers of all AGARD publications.

13. Keywords/Descriptors

Fracture properties	Aerospace engineering	Crack propagation
Fracturing	Nondestructive tests	
Design criteria	Aircraft	

14. Abstract

Many problems in the aerospace field that are concerned with new high-strength materials, flow susceptibility, stress corrosion, non-destructive testing, fractographic material examination, crack propagation and residual strength aspects of the fatigue of aircraft structures, and brittle fracture, require that fracture mechanics concepts be made available to the engineer and designer The purpose of this Meeting was to present examples of how fracture mechanics is used in the design of aircraft structures and their components. In addition to practical examples being emphasized, gaps of knowledge required by the designer were identified. The presentations and subsequent discussions will provide a contribution to the Design Manual on 'Fracture Mechanics Design of Aircraft Structures' being prepared by AGARD.

Papers and other contributions presented at the 43rd Meeting of the AGARD Structures and Materials Panel held in London, UK on 28–29 September 1976.

CDB 400 043

AGARD Conference Proceedings No.221
Advisory Group for Aerospace Research and Development, NATO
FRACTURE MECHANICS DESIGN METHODOLOGY
Published February 1977
278 pages

Many problems in the aerospace field that are concerned with new high-strength materials, flow susceptibility, stress corrosion, non-destructive testing, fractographic material examination, crack propagation and residual strength aspects of the fatigue of aircraft structures, and brittle fracture, require that fracture mechanics concepts be made available to the engineer and designer. The purpose of this Meeting was to present examples of how fracture mechanics is used in the design of aircraft

P.T.O.

AGARD-CP-221

Fracture properties
Fracturing
Design criteria
Aerospace engineering
Nondestructive tests
Aircraft
Crack propagation

AGARD Conference Proceedings No.221
Advisory Group for Aerospace Research and Development, NATO
FRACTURE MECHANICS DESIGN METHODOLOGY
Published February 1977
278 pages

Many problems in the aerospace field that are concerned with new high-strength materials, flow susceptibility, stress corrosion, non-destructive testing, fractographic material examination, crack propagation and residual strength aspects of the fatigue of aircraft structures, and brittle fracture, require that fracture mechanics concepts be made available to the engineer and designer. The purpose of this Meeting was to present examples of how fracture mechanics is used in the design of aircraft

P.T.O.

AGARD-CP-221

Fracture properties
Fracturing
Design criteria
Aerospace engineering
Nondestructive tests
Aircraft
Crack propagation

AGARD Conference Proceedings No.221
Advisory Group for Aerospace Research and Development, NATO
FRACTURE MECHANICS DESIGN METHODOLOGY
Published February 1977
278 pages

Many problems in the aerospace field that are concerned with new high-strength materials, flow susceptibility, stress corrosion, non-destructive testing, fractographic material examination, crack propagation and residual strength aspects of the fatigue of aircraft structures, and brittle fracture, require that fracture mechanics concepts be made available to the engineer and designer. The purpose of this Meeting was to present examples of how fracture mechanics is used in the design of aircraft

P.T.O.

AGARD-CP-221

Fracture properties
Fracturing
Design criteria
Aerospace engineering
Nondestructive tests
Aircraft
Crack propagation

AGARD Conference Proceedings No.221
Advisory Group for Aerospace Research and Development, NATO
FRACTURE MECHANICS DESIGN METHODOLOGY
Published February 1977
278 pages

Many problems in the aerospace field that are concerned with new high-strength materials, flow susceptibility, stress corrosion, non-destructive testing, fractographic material examination, crack propagation and residual strength aspects of the fatigue of aircraft structures, and brittle fracture, require that fracture mechanics concepts be made available to the engineer and designer. The purpose of this Meeting was to present examples of how fracture mechanics is used in the design of aircraft

P.T.O.

AGARD-CP-221

Fracture properties
Fracturing
Design criteria
Aerospace engineering
Nondestructive tests
Aircraft
Crack propagation

structures and their components. In addition to practical examples being emphasized, gaps of knowledge required by the designer were identified. The presentations and subsequent discussions will provide a contribution to the Design Manual on "Fracture Mechanics Design of Aircraft Structures" being prepared by AGARD.

Papers and other contributions presented at the 43rd Meeting of the AGARD Structures and Materials Panel held in London, UK on 28–29 September 1976.

ISBN 92-835-1090-X

tures and their components. In addition to practical examples being emphasized, gaps of knowledge required by the designer were identified. The presentations and subsequent discussions will provide a contribution to the Design Manual on "Fracture Mechanics Design of Aircraft Structures" being prepared by AGARD.

Papers and other contributions presented at the 43rd Meeting of the AGARD Structures and Materials Panel held in London, UK on 28–29 September 1976.

ISBN 92-835-1090-X

structures and their components. In addition to practical examples being emphasized, gaps of knowledge required by the designer were identified. The presentations and subsequent discussions will provide a contribution to the Design Manual on "Fracture Mechanics Design of Aircraft Structures" being prepared by AGARD.

Papers and other contributions presented at the 43rd Meeting of the AGARD Structures and Materials Panel held in London, UK on 28–29 September 1976.

ISBN 92-835-1090-X

structures and their components. In addition to practical examples being emphasized, gaps of knowledge required by the designer were identified. The presentations and subsequent discussions will provide a contribution to the Design Manual on "Fracture Mechanics Design of Aircraft Structures" being prepared by AGARD.

Papers and other contributions presented at the 43rd Meeting of the AGARD Structures and Materials Panel held in London, UK on 28–29 September 1976.

ISBN 92-835-1090-X

AGARD

NATO OTAN

7 RUE ANCELLE · 92200 NEUILLY-SUR-SEINE

FRANCE

Telephone 745.08.10 · Telex 610176

DISTRIBUTION OF UNCLASSIFIED AGARD PUBLICATIONS

AGARD does NOT hold stocks of AGARD publications at the above address for general distribution. Initial distribution of AGARD publications is made to AGARD Member Nations through the following National Distribution Centres. Further copies are sometimes available from these Centres, but if not may be purchased in Microfiche or Photocopy form from the Purchase Agencies listed below.

NATIONAL DISTRIBUTION CENTRES

BELGIUM
Coordonnateur AGARD – VSL
Etat-Major de la Force Aérienne
Caserne Prince Baudouin
Place Dailly, 1030 Bruxelles

CANADA
Defence Scientific Information Service
Department of National Defence
Ottawa, Ontario K1A OZ2

DENMARK
Danish Defence Research Board
Østerbrogades Kaserne
Copenhagen Ø

FRANCE
O.N.E.R.A. (Direction)
29 Avenue de la Division Leclerc
92 Châtillon sous Bagneux

GERMANY
Zentralstelle für Luft- und Raumfahrt-
dokumentation und -information
Postfach 860880
D-8 München 86

GREECE
Hellenic Armed Forces Command
D Branch, Athens

ICELAND
Director of Aviation
c/o Flugrad
Reykjavik

ITALY
Aeronautica Militare
Ufficio del Delegato Nazionale all'AGARD
3, Piazzale Adenauer
Roma/EUR

LUXEMBOURG
See Belgium

NETHERLANDS
Netherlands Delegation to AGARD
National Aerospace Laboratory, NLR
P.O. Box 126
Delft

NORWAY
Norwegian Defence Research Establishment
Main Library
P.O. Box 25
N-2007 Kjeller

PORTUGAL
Direccao do Servico de Material
da Forca Aerea
Rua de Escola Politecnica 42
Lisboa
Attn: AGARD National Delegate

TURKEY
Department of Research and Development (ARGE)
Ministry of National Defence, Ankara

UNITED KINGDOM
Defence Research Information Centre
Station Square House
St. Mary Cray
Orpington, Kent BR5 3RE

UNITED STATES
National Aeronautics and Space Administration (NASA),
Langley Field, Virginia 23365
Attn: Report Distribution and Storage Unit

THE UNITED STATES NATIONAL DISTRIBUTION CENTRE (NASA) DOES NOT HOLD STOCKS OF AGARD PUBLICATIONS, AND APPLICATIONS FOR COPIES SHOULD BE MADE DIRECT TO THE NATIONAL TECHNICAL INFORMATION SERVICE (NTIS) AT THE ADDRESS BELOW.

PURCHASE AGENCIES

Microfiche or Photocopy

National Technical
Information Service (NTIS)
5285 Port Royal Road
Springfield
Virginia 22151, USA

Microfiche

Space Documentation Service
European Space Agency
10, rue Mario Nikis
75015 Paris, France

Microfiche

Technology Reports
Centre (DTI)
Station Square House
St. Mary Cray
Orpington, Kent BR5 3RF
England

Requests for microfiche or photocopies of AGARD documents should include the AGARD serial number, title, author or editor, and publication date. Requests to NTIS should include the NASA accession report number. Full bibliographical references and abstracts of AGARD publications are given in the following journals:

Scientific and Technical Aerospace Reports (STAR),
published by NASA Scientific and Technical
Information Facility
Post Office Box 8757
Baltimore/Washington International Airport
Maryland 21240, USA

Government Reports Announcements (GRA),
published by the National Technical
Information Services, Springfield
Virginia 22151, USA

Printed by Technical Editing and Reproduction Ltd
Harford House, 7–9 Charlotte St, London W1P 1HD

ISBN 92-835-1090-X